Universitat Autònoma de Barcelona

The evolution of semicircular canals in anthropoid primates: Phylogenetic implications for Miocene catarrhines

Alessandro Urciuoli

Institut Català de Paleontologia
Miquel Crusafont

Universitat Autònoma de Barcelona
Facultat de Ciències
Departament de Biologia Animal, de Biologia Vegetal i d'ecologia

The evolution of semicircular canals in anthropoid primates:

Phylogenetic implications for Miocene catarrhines

Alessandro Urciuoli

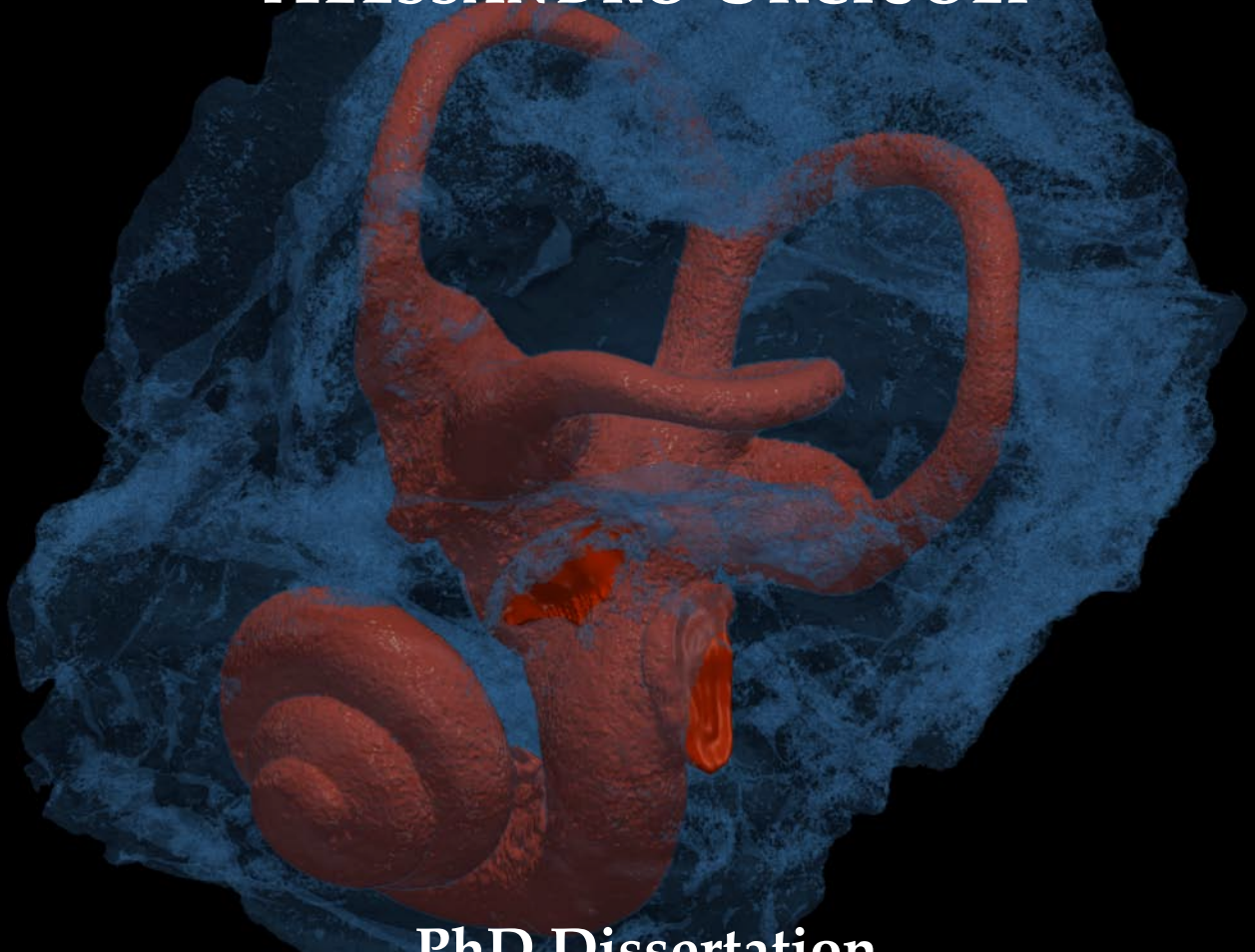

PhD Dissertation

Universitat Autònoma de Barcelona
PhD Programme in Biodiversity

2021

Supervisors
Dr. Salvador Moyà-Solà
Dr. David M. Alba

Institut Català de Paleontologia
Miquel Crusafont

Universitat Autònoma de Barcelona
Facultat de Ciències
Departament de Biologia Animal, de Biologia Vegetal i d'Ecologia

The evolution of semicircular canals in anthropoid primates:

Phylogenetic implications for Miocene catarrhines

ALESSANDRO URCIUOLI

PhD Dissertation

PhD Programme in Biodiversity

2021

Supervisors: Salvador Moyà-Solà

David M. Alba

Institut Català de Paleontologia
Miquel Crusafont

Universitat Autònoma de Barcelona
Facultat de Ciències
Departament de Biologia Animal, de Biologia Vegetal i d'Ecologia

The evolution of semicircular canals in anthropoid primates:

Phylogenetic implications for Miocene catarrhines

Dissertation submitted by **Alessandro Urciuoli** to the PhD Programme in Biodiversity, Department of Animal Biology, Plant Biology and Ecology, in fulfillment of the requirements for obtaining the degree of Doctor by the Universitat Autònoma de Barcelona with International Doctoral Research Component, and elaborated under the supervision of:

Dr. Salvador Moyà Solà, ICREA at Institut Català de Paleontologia Miquel Crusafont and Unitat d'Antropologia Biològica (Departament de Biologia Animal, de Biologia Vegetal i d'Ecologia), Universitat Autònoma de Barcelona.

Dr. David Martínez Alba, Institut Català de Paleontologia Miquel Crusafont, Universitat Autònoma de Barcelona.

Signed in Bellaterra, on February 11th, 2021:

Dr. Salvador Moyà-Solà	Dr. David M. Alba	Alessandro Urciuoli
Supervisor	Supervisor & Tutor	PhD Candidate

Index

Abstract

Catarrhine primates originated in Africa by the Oligocene. They include the crown group—cercopithecoids (Old World monkeys) and hominoids (apes and humans)—plus several extinct lineages from the Miocene of Africa and Eurasia. The phylogenetic relationships of many extinct catarrhines remain controversial due to the incomplete and fragmentary nature of their fossil record, coupled with abundant homoplasy and mosaic evolution. The identification of anatomical areas less prone to homoplasy is thus crucial for providing additional phylogenetically informative characters to infer the phylogeny of extinct catarrhines. Based on previous research, the morphology of the bony labyrinth semicircular canals (SCs) of the inner ear was considered promising in this regard. The present dissertation thus aimed to explore the utility of the semicircular canals for phylogenetic inference among extant and extinct anthropoids, with emphasis on particular Miocene catarrhines.

Specific aims include: (1) testing the suitability of different three-dimensional geometric morphometric (3DGM) approaches; (2) quantifying the phylogenetic signal embedded in SC morphology and identifying characters amenable to cladistic analysis; and (3) testing competing phylogenetic hypotheses for European Miocene catarrhines (pliopithecoids and hominids). The methods rely on microcomputed tomography scans and landmark-based standard 3DGM, as well as an innovative deformation-based (landmark-free) alternative approach. Shape data were analyzed by means of bivariate (allometric) regressions and multivariate analyses (between-group principal component analysis), coupled with phylogenetically-informed methods (phylomorphospace with ancestral node reconstruction, cladistic indices), metrics of phylogenetic signal (Pagel's λ and Blomberg's K), and cluster analysis.

The results are provided in three separate published articles, which are subsequently discussed in relation to current literature and with regard to prospects for the future. The first article analyzes patterns of SC shape variation in extant catarrhines and tests its utility for making phylogenetic inferences in extinct hominoids. The remaining two articles build upon such results to test alternative phylogenetic hypotheses in the pliopithecoid *Epipliopithecus* and the dryopithecine apes *Hispanopithecus* and *Rudapithecus*. The following conclusions are reached:

(1) Deformation-based 3DGM adequately captures SC shape variation and eliminates biases of standard 3DGM that depend on the subjective design of the landmarking protocol.

(2) SC shape embeds strong phylogenetic signal and discriminates among major anthropoid clades and even extant major hominoid genera, thus being potentially useful to test phylogenetic hypotheses for extinct taxa.

(3) The reconstruction of ancestral morphotypes enables the definition of several characters of the SCs potentially synapomorphic for crown catarrhines, crown

hominoids, and crown hominids. The latter are most distinctive due to their stout volumetric proportions.

(4) The SC morphology of the pliopithecoid *Epipliopithecus* confirms the widely held view that this taxon is most parsimoniously interpreted as a stem catarrhine more derived than propliopithecoids, rather than a hominoid (as suggested by some recent studies).

(5) The enigmatic ape *Oreopithecus* displays a mosaic of primitive and derived SC features suggestive of a stem hominoid status coupled with the independent acquisition of some hominid synapomorphies.

(6) The SC morphology of the dryopithecines *Hispanopithecus* and *Rudapithecus* confirms they are distinct great ape genera, but does not conclusively favor a stem hominid vs. hominine status, because African apes are largely plesiomorphic as compared with the more derived orangutans.

(7) As a general conclusion, as the first study devoted to the study of SC morphology among anthropoids by means of deformation-based 3DGM, this dissertation confirms the potential of this anatomical area for phylogenetic inference in Miocene catarrhines. Future lines of research should focus on extending this research to other internal structures (cochlea and middle ear ossicles) to further contribute with additional characters to formal morphology-based cladistic analyses of extant and fossil catarrhines.

Acknowledgments

Funding. This dissertation has been possible thanks to a predoctoral grant of the Formación de Personal Investigador (FPI) programme (BES-2015-071318), within a R&D project of the Agencia Estatal de Investigación (CGL2017-82654-P, AEI-EU FEDER) with Salvador Moyà-Solà and Raef Minwer-Barakat as principal investigators). The research performed has also been funded by R&D project CGL2016-76431-P (AEI/FEDER EU, with David M. Alba and Daniel DeMiguel as principal investigators), and the Generalitat de Catalunya (CERCA Programme, and consolidated research groups 2017 SGR 86 and 2017 SGR 116 GRC).

Data access and infrastructures. Some computations were performed at the CALMIP supercomputing center (Toulouse, France; grant number 2016-[P1440], to the AMIS Laboratory, Paul Sabatier University of Toulouse, France) and in the Barcelona Supercomputing Center (Barcelona, Spain; grant number BCV-2020-1-0008, to Josep Fortuny.

The following people and institutions granted access to the CT scans of extant and fossil comparative material: Ursula Göhlich (Naturhistorisches Museum of Wien, Austria); Martin Dockner (Vienna μCT-Lab, Austria);. Wilhelm Wimmer (University of Bern, Switzerland); Loïc Costeur (Naturhistorisches Museum of Basel, Switzerland); Lorenzo Rook (Università degli Studi di Firenze, Italy); Jose Braga (Paul Sabatier University of Toulouse, France); Timothy Ryan (Pennsylvania State University, USA); Fred Spoor (Natural History Museum of London, UK); Richard Kay (Duke University, Durham, USA); Sergio Almécija (American Museum of Natural History, New York, USA); Lauren Gonzales (University of North Texas, Denton, USA); Erik Seiffert (University of Southern California, Los Angeles, USA); the Max Plank Institute for Evolutionary Anthropology (Leipzig, Germany); the American Museum of Natural History (New York, USA); the Museum of Comparative Zoology (Harvard University, Cambridge, USA); the Division of Fossil Primates of the Duke Lemur Center (Duke University, Durham, USA); the Evolutionary Studies Institute (University of the Witwatersrand, Johannesburg, South Africa); and the European Synchrotron Radiation Facility (Grenoble, France).

Professional acknowledgments. I would like to express my deepest gratitude to my supervisors Salvador Moyà-Solà and David M. Alba, not only for their guidance throughout all these years, but also for their warm hosting almost seven years ago, when I first arrived at the Institut Català de Paleontologia (ICP) as an Erasmus student, slightly disoriented, yet full of expectations about a career in paleontology. I

am in debt to Salvador for trusting me the PhD grant linked to his project as well as for teaching me, with his own example, that a researcher should always follow their intuition, guided by curiosity and eagerness for discovery. In turn, I might try to summarize my gratefulness to David in just one word and thank him for everything, yet it would still represent an underestimation. I do not know if I would ever be able to repay him for the incredible amount of effort and dedication that he has invested on me through time. Nonetheless, I will surely do my best to put it to good use by trying to constantly grow as a researcher.

Besides my supervisors, I would like to thank a number of brilliant researchers who, during my scientific training, helped me to stay on the best possible path with their guidance and suggestions. My first thought goes to Lorenzo Rook: without him, I would not have even been able to start my journey in the realm of paleontological and paleoanthropological research, so thank you for giving me the chance of working in the field I always dreamed of. I am also most grateful to Daniel DeMiguel, who helped and supported me from the very beginning and on a daily basis during the elaboration of my master thesis. I also thank Dani for the good time spent together, for the Sunday vermouths, for teaching me that one must have "criterio" in approaching life challenges, and for gifting me with the honor of your friendship. My profound gratitude also goes to Clément Zanolli, not only for representing a guiding light in the development of this dissertation and a most valuable friend, but also for hosting me during my research stay in the Paul Sabatier University of Toulouse. I particularly thank Clément for the countless hours spent together discussing about, literally, every possible aspect of life in science.

I am also grateful to the following researchers, who contributed in a number of different ways to the writing and development of the chapters included in this dissertation: Sergio Almécija, for his always constructive corrections and suggestions; Amélie Beaudet, for helping me with the scans of *Australopithecus* and with the ancestral state reconstructions; Jean Dumoncel, for his invaluable technical help; Marta Pina, for her reviews and support; Masato Nakatsukasa and Naoki Morimoto, for their valuable comments and for the chance of studying *Nacholapithecus*; David Begun, for his advice on hominoid evolution and for providing access to the material of *Rudapithecus*.

I would like to thank as well Assumpció Malgosa (coordinator of the PhD Programme in Biodiversity of the UAB), as well as the members of the monitoring committee of my dissertation (Emmanuel Serrano Ferrón, Iolanda Álvarez Cobo and Maria Constenla Matalobos), for their guidance throughout the process. I also thank the following researchers for accepting to participate in the evaluation committee of my dissertation: Lorenzo Rook, Ignacio Martínez, Loïc Costeur, Josep Fortuny, and Isaac Casanovas-Vilar. In this regard, Lorenzo Rook and Loïc Costeur deserve

particular mention for having written the reports necessary to request the international mention.

Multiple experienced and postdoctoral researchers from the ICP further deserve to be acknowledged for the supervision provided to me and other PhD students thanks to their wisdom and experience: Marc Furió, Joan Madurell-Malaperia, Àngel Luján, Judit Marigó, Juan Abella, Carmen Nacarino-Meneses, Víctor Fondevilla, Soledad de Estaban-Trivigno, Raef Minwer-Barakat, and Júlia Arias-Martorell. I also extend my gratitude to all the personnel (past and present) of the ICP for their endless support, in particular: Jordi Galindo and Josep M. Robles, for curating the specimens; Xènia Aymerich, Marina Rull, for the preparation of the fossil remains; Pere Figuerola, for the dissemination of my research outputs; Enric Menéndez, Mónica Vincent, Laila Pilgren, and Maria Pérez, for their assistant with the grant bureaucracy; Mireia Manjón, for being an irreplaceable support in troubling times; Josep Torres, for providing support with the scripts; Sergio Llácer, for the marvelous segmentations; Manel Llenas and Manel Méndez, for the fundamental help during excavations; and Pepi, for helping me keeping a nice and tidy office.

A special thanks goes to my colleagues Florian Bouchet, Sílvia Jovells-Vaqué, Guillem Orlandi-Oliveras, Guillem Pons-Monjo, Leonardo Sorbelli, Rafel Matamales-Andreu, Chabier De Jaime-Soguero, Sharrah McKenzie, Víctor Vinuesa, Teresa Calderón, Saverio Bartolini Lucenti, Andrea Villa, and Omar Cirilli: without you all, this journey would have not been worth the same. Thank you for your happiness, for sharing with me the burden of the hard times, and for all the moments we spent together.

Personal acknowledgments. At the personal level, I would like to thank all of my friends, old and new, spread all over several European countries: thanks for your encouragement, it did really make the difference! Particularly, I feel beholden to my Peruginian fellas Andrea (aka Ferro), Giacomo, Terry, Ludo, Riccardo, Peppe, Franco, Alessandra, Jacopo, and Mauro. You have my total affection and, despite the distance, I have been always feeling you at my side! To my lazy-crazy flat mate Marco, you have become a part of my life that will never fade out. Thanks to the "cani" of Barcelona Andrea (aka Pilgrims), Anton Giulio, and Dario, companions of endless nights. My gratitude to Laura and Lavinia for always been there when I most needed them. Thanks to Quique for sharing these last months of thesis writing with me in the apartment. To all the fellas of the UAB volleyball team, thanks for helping keep my mind in balance. Eventually, thanks to my Toulousain "colocs" David, Sevan, and Catty for hosting me and showing me around Toulouse.

I would like to express as well my gratitude to my family (in the quite extended Italian meaning of the term) for the support I have always received and for the freedom they gave me in the making of my choices. Above all, I would like to thank

my mother Rita, who bequeathed me the curiosity for all living (and not-so-living-anymore) beings and for their evolution, and my father Stefano, from whom I inherited the passion for technology and learned how to think rationally; my achievements are also yours. Eventually, I am very grateful to my grandmothers: Iva, who thought and still thinks that my main task has been searching for teeth (how accurate, indeed); and Nietta, who always pushed me to move one step forward.

One last and special mention is for Andrea, who has always been at my side during, possibly, the most intense and challenging experience of my life. Thank you for your patience, advice, and infinite hours spent together in front of a screen just to reassure each other with our own presence. Thanks for your trust in me and in my personal growth, for your essential support that pushed me over any obstacle that I faced, and, especially, for inspiring me to be a better person. You are my today and my future, you are my everything.

Chapter 1:
Introduction

Chapter 1. Introduction

1.1. Catarrhine evolution

1.1.1. Extant catarrhines

Primates are a moderately diverse mammalian order (>400 extant species) that inhabits a plethora of different habitats—mostly across the tropical regions of Africa, Madagascar, Asia and South America—and shows diverse behavioral adaptations (Fleagle, 2013). The earliest crown primates (or euprimates) are recorded at about the Paleocene/Eocene boundary (56 Ma) across western North America, western Europe, Africa and Asia (Bloch et al., 2007; Silcox, 2008). They are divided into two suborders: the Strepsirrhini (lemurs and lorises) and the Haplorrhini (tarsiers and simians). In turn, haplorrhines are divided into two infraorders: the Tarsiiformes (tarsiers) and the Simiiformes or Anthropoidea (simians, i.e., monkeys, apes, and humans). Two extant anthropoid clades are recognized, normally distinguished at the parvorder rank: the Platyrrhini (New World monkeys) and the Catarrhini; the latter are in turn subdivided into two superfamilies: Cercopithecoidea (Old World monkeys) and Hominoidea (apes and humans).

Catarrhines are named after their downward pointing nostrils, from the Ancient Greek 'κατά' ('kata', meaning down) and 'ῥινός' ('rhinos', nose). Their extant members are characterized by several synapomorphies that distinguish them from platyrrhines (e.g., Harrison, 1987, 2013; Fleagle, 2013): loss of the third premolars; frontal-sphenoid contact separating the parietal from the zygomatic; tympanic bone forming a tubular and fully ossified external auditory meatus; and lack of entepicondylar foramen in the distal humerus.

Cercopithecoids. Old World monkeys are currently much more diverse than hominoids, including ca. 130 species from Africa and Asia classified in two subfamilies (Cercopithecinae and Colobinae; Groves, 2001; Fleagle, 2013). Their body mass broadly ranges from very small arboreal species (~1 kg for *Miopithecus talapoin*) to the mostly terrestrial baboons and mandrills (weighting as much as 50 kg). All cercopithecoids share a bilophodont molar occlusal morphology, characterized by the presence of two transverse crests, which allow them to process low quality food items, such as unripe fruits and leaves (Temerin & Cant, 1983). Regardless of whether they occupy a terrestrial or arboreal niche, cercopithecoids possess a pronograde body plan. Colobine monkeys (also known as leaf-monkeys) are currently restricted to Asia

and characterized by a large, complex, and ruminant-like stomach, useful for processing a cellulose-rich diet (Davies & Oates, 1995; Fleagle, 2013). Smaller than other cercopithecoids (4–15 kg; Fleagle, 2013), colobines are mainly arboreal quadrupeds and leapers (Hunt, 2018) and show some amount of sexual dimorphism (Fleagle, 2013; Hunt, 2016). Cercopithecines, in turn, are mostly distributed in Africa (except for macaques, also found in Eurasia), possess large cheek pouches, and are highly sexually dimorphic (especially papionins; Fleagle, 2013).

Hominoids. Extant hominoids represent the remnants of a much more diverse group that radiated during the Miocene (see Section 1.1.3). Two extant families are included: the small bodied hylobatids (gibbons and siamangs) and the larger hominids (great apes and humans). They widely range in size, from ca. 4 kg in gibbons to >200 kg in male gorillas (Fleagle, 2013). With the exception of modern humans, hominoids are restricted to the tropical forests of Africa (chimpanzees, bonobos and gorillas) and southeast Asia (hylobatids and orangutans). Among other features, hominoids share a bunodont dentition (with rounded cusps), long forelimbs, lack of an external tail, and a suite of postcranial adaptations collectively known as the orthograde body plan.

The small-bodied hylobatids are the most speciose hominoid family and have a southeastern Asian distribution (Reichard et al., 2016). Based on morphological, cytological, and molecular evidence (e.g., Napier & Napier, 1967; Stanyon, 2013; Carbone et al., 2014), they are considered the sister group of hominids. Four major allopatric lineages of gibbons and siamangs are currently recognized as distinct genera: *Symphalangus*, *Hoolock*, *Nomascus*, and *Hylobates* (Reichard et al., 2016). They possibly diverged during a short amount of time, which does not allow to conclusively resolve their internal phylogenetic relationship, not even based on nuclear DNA (Carbone et al., 2014). Overall, hylobatid species are a fairly homogenous in their morphology. They are small-bodied (5–11 kg) and display low sexual dimorphism (although sometimes they are dichromatic). Their molars are simple, with low cusps and broad foveae, adapted to a frugivorous diet. They display a globular braincase, large and well-spaced telescopic orbits, a low zygomatic root, and a short face with distinct midfacial prognathism (Shea, 2013). While they are in several respects more plesiomorphic (monkey-like) that hominids (e.g., they retain ischial callosities), their appendicular skeleton is extremely specialized for performing acrobatic locomotor behaviors such as ricochetal brachiation—such as extremely elongated forelimbs (the longest among primates relative to body size; Fleagle, 2013), and slender and curved digits.

Hominids share many anatomical features with hylobatids, most of them related with orthogrady and suspensory behaviors, yet they are much larger and display several distinctive skeletal traits (Fleagle, 2013; Hunt, 2016). Extant hominids are

classified in four different genera, which comprise eight species and several subspecies (Fleagle, 2013; Hunt, 2016; Nater et al., 2017). With the exception of humans (cosmopolitan), the three allopatric species of *Pongo* (*Pongo pygmaeus*, *Pongo abelii*, and *Pongo tapanuliensis*) are the only hominids inhabiting Asia. Conversely, the two species of *Gorilla* (*Gorilla gorilla* and *Gorilla beringei*) and the two species of *Pan* (*Pan paniscus* and *Pan troglodytes*) are restricted to the forests of equatorial Africa. Despite their marked differences in skeletal anatomy, great apes and humans display a number of shared derived features—such as a high zygomatic root, a large nasoalveolar clivus, and extensive maxillary sinus, and the absence of subarcuate fossa in adults. They also display overlap between the premaxilla and the palatine process of the maxilla (although the pongine and hominine conditions differ markedly and might be homoplastic).

Orangutans display a marked canine and body size sexual dimorphism (~36 kg and ~78 kg for females and males, respectively; Fleagle, 2013) and are quite distinctive from other hominids. They display supraorbital costae (instead of a supraorbital torus), orbits higher than broad, a narrow interorbital region, a procumbent premaxilla that considerably overlaps the maxilla, an airorhynchous cranial configuration, a concave face, and wrinkled molar enamel. Postcranially, they possess very elongated forelimbs and a hook-like hand with long fingers and a short thumb, specialized for quadrumanous suspensory behaviors, vertical climbing and orthograde clambering (Almécija et al., 2007, 2009). Gorillas are also very dimorphic in body size (~70–90 kg and up to 200 kg for females and males, respectively; Fleagle, 2013) and canine size, and the males have much more developed ectocranial structures (supraorbital torus as well as sagittal and nuchal crests). Their molar occlusal morphology displays a higher relief as an adaptation to a folivorous diet. Like chimpanzees and bonobos, they move quadrupedally by means of knuckle walking, but unlike in the former their digits are not elongated as compared to the thumb. Chimpanzees and bonobos are much smaller than gorillas (33–46 kg and 45–60 kg for females and males, respectively; Fleagle, 2013). They resemble gorillas in cranial morphology, but display much less developed sagittal and nuchal crests. Their hands are elongated as in orangutans, and they more frequently engage in arboreal behaviors than gorillas. The two species of *Pan* differ in minor anatomical details (and bonobos are less sexually dimorphic) and more markedly in the sociosexual behavior and diet. Finally, modern humans (*Homo sapiens*) differ from great apes by displaying extensive adaptations for committed terrestrial bipedalism (e.g., long hindlimbs, short and broad pelvis, a non-opposable hallux, and the presence of two arches in the foot; Bramble & Liebermann, 2004; Harcourt-Smith, 2015), a very enlarged globular neurocranium (e.g., Wood & Collard, 1999; Holloway, 2008, 2015), and an orthognathous face with a reduced masticatory apparatus and a protruding chin. The foramen magnum is more anteriorly located than in great apes, as

consequence of basicranial flexion, due to adaptation for bipedalism. The hand proportions and other morphological details are suitable to perform refined manipulative behaviors (such as pad-to-pad precision grasping; Almécija & Alba, 2014; Almécija et al., 2015). Dentally, humans are characterized by reduced canine sexual dimorphism and the loss of the upper canine/lower premolar honing complex, reduced molar size, thick enamel, and the frequent absence of third molars.

1.1.2. Stem catarrhines

Oligocene stem catarrhines from the Afro-Arabia. Based on molecular data, platyrrhines and catarrhines diverged by the middle Eocene (~40–44 Ma; Chatterjee et al., 2009; Springer et al., 2012), although the oldest putative catarrhines—the oligopithecids—are not recorded until the latest Eocene in Afro-Arabia (~34 Ma; Seiffert et al., 2010; Seiffert, 2012). Oligopithecids are considered stem anthropoids by some authors (e.g., Harrison, 2013), but despite the retention of very plesiomorphic features for anthropoids (e.g., low encephalization and unfused mandibular symphysis; Seiffert, 2012) they already show some catarrhine synapomorphies in the cranium (loss of the second premolar and third premolars sexually dimorphic in size; Seiffert, 2012) and postcranium (Seiffert et al., 2000; Seiffert & Simons, 2001).

Somewhat more derived stem catarrhines, the propliopithecids (frequently also elevated to superfamily rank; e.g., Harrison, 2013), are recorded in more recent deposits of the Fayum in Egypt (Simons, 1987, 1995; Seiffert, 2006, 2012; Simons et al., 2007) by the early Oligocene (~30 Ma; Rasmussen, 2002; Seiffert, 2006), when various lineages of stem anthropoids (parapithecids and proteopithecids) still persisted (Seiffert et al., 2005, 2010; Harrison, 2013). Three propliopithecid genera (*Propliopithecus, Moeripithecus*, and *Aegyptopithecus*) are normally distinguished (Seiffert et al., 2010; Seiffert, 2012). They are characterized by small body size (4–8 kg, depending on the species; Fleagle, 2013), strong sexual dimorphism (at least in *Aegyptopithecus*; Simons et al., 2007), and several catarrhine synapomorphies (loss of the second premolar, presence of a honing complex between upper canine and the lower third premolar, and reduced postglenoid foramen). At the same time, the retention of more plesiomorphic features (annular external auditory meatus, broad and ascending wing of the premaxilla, and distal humerus with entepicondylar foramen and large dorsal epitrochlear fossa) denote their basal status, preceding the divergence between cercopithecoids and hominoids (Harrison, 1987; 2013; Simons et al., 2007; Seiffert et al., 2010).

Saadanius is another putative stem catarrhine, known exclusively on the basis of a cranium from the latest early Oligocene of Saudi Arabia (Zalmout et al., 2010). It differs from propliopithecids by the possession of a tubular ectotympanic (Zalmout et al., 2010), which is synapomorphic of crown catarrhines. Together with its large body

size, this feature has been used to advocate a more derived status for *Saadanius* than for both propliopithecids and pliopithecoids (see below), placing it in a monotypic superfamily of its own (Zalmout et al., 2010). However, the cladistic analysis provided by the latter authors recovered an earlier branching of *Saadanius* compared with pliopithecoids (which lack a tubular ectotympanic), suggesting that the condition of the former taxon might represent an independent acquisition from that of crown catarrhines. Most authors have interpreted that, from the plesiomorphic condition displayed by stem anthropoids and propliopithecids (annular ectotympanic), the complete tubular ectotympanic of crown catarrhines evolved from a partially ossified intermediate condition such as that found in pliopithecoids (e.g., Szalay & Delson, 1979; Andrews et al., 1996). Nevertheless, given that the small ectotympanic of both the stem cercopithecoid *Victoriapithecus* (Benefit & McCrossin, 1997) and the stem hominoid *Ekembo* (Napier & David, 1959) does not protrude laterally and displays a small V-shaped notch, it is not inconceivable that the tubular ectotympanic evolved to some extent independently in cercopithecoids and hominoids (Begun, 2002a, 2015; 2017; Alba et al., 2015a). Therefore, the phylogenetic significance of this feature regarding the purportedly more derived status of *Saadanius* toward crown catarrhines compared with propliopithecids remains to be confirmed. On the other hand, more recent cladistic analyses have recovered *Saadanius* as a stem cercopithecoid more primitive than *Victoriapithecus* (Nengo et al., 2017; Gilbert et al., 2020a).

Miocene small-bodied catarrhines from Africa. The phylogenetic relationships of small-bodied catarrhines from the Miocene of Africa are even more controversial, as they are complicated by their high diversity and the paucity of remains available for most taxa. At least three genera are considered closely related and customarily grouped into a single family (the dendropithecids), recorded from early to middle Miocene of East Africa: *Micropithecus*, from the early to middle Miocene of Kenya and Uganda (~20–15 Ma; Harrison, 1988, 1989, 2002, 2010; Pickford et al., 2010); *Dendropithecus*, from the Early Miocene of Kenya and Uganda (~20–17 Ma; Le Gros Clark & Thomas, 1951; Harrison, 1988; Pickford et al., 2010); and *Simiolus*, from the early to middle Miocene of Kenya (~17.5–12.3 Ma; Leakey & Leakey, 1987; Pickford & Kunimatsu, 2005; Harrison, 2010; Rossie & Hill, 2018). Although some authors have questioned the monophyly of the group (Rae, 1999; Nengo et al., 2017; Rossie & Hill, 2018; Gilbert et al., 2020a), dendropithecids (sometimes elevated to superfamily rank; e.g., Harrison, 2010) are generally considered a clade, interpreted as either stem catarrhines sister to proconsulids + crown hominoids (Harrison, 1987, 1988, 2002, 2010, 2013; Stevens et al., 2013), or as basal-most hominoids (Rae, 1999; Zalmout et al., 2010; Alba et al., 2015a; Begun, 2015; Rossie & Hill, 2018) perhaps showing

proconsulid (Harrison, 1988; Rae, 1997; Begun, 2015) or nyanzapithecid (Rose et al., 1992; Singleton, 2000; Rossie & Seiffert, 2006; Rossie & Hill, 2018) affinities.

Several other small-bodied catarrhine genera (*Limnopithecus*, *Lomorupithecus*, *Kalepithecus, Kogolepithecus*, *Iriripithecus*, and *Karamojapithecus*) are recorded in the early and middle Miocene of Africa (e.g., Harrison, 1988, 2010, 2013; Pickford et al., 2010; Cote et al., 2016). Unfortunately, most of them are known from fragmentary material, which complicates deciphering their phylogenetic relationships. The cladistic analysis by Gilbert et al. (2020a) recovered *Limnopithecus* as a dendropithecid most closely related to *Dendropithecus* (albeit these authors did not recover the monophyly of the family). Based on currently available evidence, is likely that small-bodied catarrhines from Africa do not constitute a monophyletic clade, but a paraphyletic assemblage of more or less derived stem catarrhines and maybe some stem hominoids. However, no clear phylogenetic links have been thus far established with either pliopithecoids or hylobatids (see below), which must have originated from African ancestors in the early Miocene.

Pliopithecoids. After being isolated in Afro-Arabia for a long time, catarrhines are first recorded in Eurasia by pliopithecoids from the early Miocene of China (~18–17 Ma; Harrison and Gu, 1999; Begun, 2002a; Harrison, 2013). Although their ancestry is unknown, the fact that Eurasia was devoid of catarrhines during the Oligocene and earliest Miocene suggests an African origin for the group (Harrison, 1987, 2013; Begun, 2017). They probably dispersed into Eurasia before the Langhian transgression, through the intermittent land corridor that connected Africa with Eurasia during the closure of the Tethys Seaway ~19 Ma (Harzhauser et al., 2007; Harrison, 2013). Due to superficial similarities in the cranial morphology, several authors initially suggested a phylogenetic link with hylobatids (e.g., Hürzeler, 1954; Zapfe, 1958, 1961; Simons & Fleagle, 1973). However, during the last decades pliopithecoids have generally been considered a clade of stem catarrhines (Delson & Andrews, 1975; Ciochon & Corruccini, 1977; Fleagle, 1984; Harrison, 1987, 2005, 2013; Andrews et al., 1996; Begun, 2002a, 2017). This is consistent with their retention of a number of plesiomorphic features for crown catarrhines (such as the incomplete ossification of the external auditory meatus, the presence of an entepycondilar foramen in the distal humerus, and the single hinge-like carpometacarpal joint in the thumb; Zapfe, 1961; Szalay and Delson, 1979; Harrison, 1987, 2005; Andrews et al., 1996; Begun, 2002a, 2017). Based on several recent cladistic analyses (Zalmout et al., 2010; Stevens et al., 2013; Nengo et al., 2017; Gilbert et al., 2020a; but see Alba et al., 2015a), pliopithecoids would precede the cercopithecoid-hominoid split but postdate the branching of propliopithecids, as indicated by the presence of a partially ossified ectotympanic (see discussion above). Taking into account that cercopithecoids and hominoids diverged ~25–30 Ma (Steiper & Young, 2008; Wilkinson et al., 2011; Springer et al., 2012), this phylogenetic position

would imply a long ghost lineage of at least 12–14 Myr for pliopithecoids (Begun, 2017).

Pliopithecoids were widely distributed across Eurasia from the early to the late Miocene, with multiple genera that may provisionally be arranged into four different families (Harrison and Gu, 1999; Moyà-Solà et al., 2001; Begun, 2002a, 2017; Harrison, 2005, 2013; Alba et al., 2010a; Alba & Moyà-Solà, 2012; Alba & Berning, 2013; Sankhyan et al., 2017; Harrison et al., 2020): dionysopithecids (*Dionysopithecus* and *Platodontopithecus*), krishnapithecids (*Krishnapithecus*), pliopithecids (*Pliopithecus* and *Epipliopithecus*), and crouzeliids (*Plesiopliopithecus*, *Barberapithecus*, *Anapithecus*, *Egarapithecus*, and *Laccopithecus*). The taxonomic rank and systematic arrangement of these groups is not settled and varies among authors (e.g., see Alba et al., 2010a; Alba & Moyà-Solà, 2012; Begun, 2002a, 2017; Harrison, 2013), which is not surprising given that most genera are known by fragmentary dental material—with the notable exception of *Epipliopithecus*. This seriously hampers our understanding of the internal phylogenetic relationships of pliopithecoids as well as their status relative to other stem catarrhines and dendropithecids. Rossie & MacLatchy (2006) proposed *Lomorupithecus*, from the early Miocene of Uganda, as an African pliopithecoid (see also Rasmussen et al., 2019; Gilbert et al., 2020a). However, this hypothesis has not gained acceptance (Alba et al., 2010a; Harrison, 2010; Pickford et al., 2010) and *Lomorupithecus* is generally considered a dendropithecid by most authors (Harrison, 2013).

1.1.3. Fossil crown catarrhines

Fossil cercopithecoids. The first ~10 Myr of Old World monkey evolution, from the divergence with hominoids until the split of the two living subfamilies (the colobines and cercopithecines; see Section 1.1.1) sometime in the early to middle Miocene (20–14 Ma; Raaum et al., 2005; Perelman et al., 2011; Springer et al., 2012; Pozzi et al., 2014), are poorly known. Only a few cercopithecoid partial mandibles and isolated teeth are known before 19 Ma (Pilbeam & Walker, 1968; Stevens et al., 2013; Rasmussen et al, 2019). The oldest specimen dates to the late Oligocene (25.2 Ma) and consists of a partial mandible with m3 ascribed to *Nsungwepithecus* from Tanzania (Stevens et al., 2013). By the late early Miocene of Africa, stem cercopithecoids are moderately diverse, with five genera known from dentognathic remains (*Alophe*, *Prohylobates*, *Victoriapithecus*, *Noropithecus*, and *Zaltanpithecus*; Locke et al., 2020). *Victoriapithecus*, from the early to middle Miocene, is by far the best known (including thousands of specimens from middle Miocene deposits but just a few from the early Miocene; Benefit, 1999; Pickford et al., 2003; 2019). *Victoriapithecus* was a small-bodied (3–5 kg; Harrison, 1989) frugivorous terrestrial monkey (Benefit & McCrossin, 2010). It possessed several extant cercopithecoid derived characters in

craniofacial and postcranial morphology, and incompletely bilophodont molars (Benefit, 2000; Benefit & McCrossin, 1997, 2010). In addition, it retained a number of plesiomorphic features relative to crown cercopithecoids (more closely resembling both of propliopithecoids and pliopithecoids), coupled with some similarities with extant and extinct hominoids (Benefit, 1993, 1994, 1999, 2000; Benefit & McCrossin, 1997, 2010). *Victoriapithecus* and other stem cercopithecoids have traditionally been allocated to a distinct family, the Victoriapithecidae (von Koenigswald, 1969; Benefit 1987, 1993), which nevertheless is most likely paraphyletic (Leakey et al., 2003; Miller et al., 2009; Stevens et al., 2013; Rasmussen et al., 2019). To avoid this problem, the recently described basal-most cercopithecoid *Alophe* was left unassigned to family (Rasmussen et al., 2019).

Several molar occlusal features—degree of bilophodonty (incipient vs. patent lophs), tuberculum sextum development, and presence/absence of crista(id) obliqua—provide some hints about the phylogenetic relationships of early and middle Miocene stem cercopithecoids (Rasmussen et al., 2019). The available record indicates that bilophodonty evolved in a mosaic fashion from a generalized stem catarrhine occlusal pattern similar to that of propliopithecids (Benefit, 1999; Miller et al., 2009; Rasmussen et al., 2019). Columnar buccal cusps and the median buccal cleft evolved first, together with the buccolingual alignment of the four main cusps in two (mesial and distal) pairs. The more or less complete development of the loph(id)s (transverse shearing crests) characteristic of the bilophodont occlusal pattern followed, preceding the complete loss of the crista obliqua and m1–m2 hypoconulids (Rasmussen et al., 2019). The original selection pressures that led to the emergence of the bilophodont occlusal pattern are unclear. Traditionally considered a folivorous adaptation (i.e., for shearing leaves; Kay & Hylander, 1978; Szalay & Delson, 1979), the emergence of bilophodonty was subsequently reinterpreted as an adaptation for the consumption of hard fruits and seeds based on middle Miocene victoriapithecids (Benefit, 1999, 2000). The dental morphology of more plesiomorphic early stem cercopithecoids (particularly *Alophe*) suggest that the precursor of bilophodonty was indeed an adaptation to frugivory with some sclerocarpic component, but that the truly bilophodont pattern evolved later possibly as an adaptation to folivory. (Rasmussen et al., 2019).

Victoriapithecids went extinct toward the end of the middle Miocene (~12 Ma; Benefit & McCrossin, 2010), but the divergence among crown cercopithecoids dates back to ~20 Ma (Raaum et al., 2005)—implying that the first modern cercopithecids appeared in Africa well before the oldest crown cercopithecoid fossils currently known (~12.5 Ma; Rossie et al., 2013). The earliest known crown member is an indeterminate colobine from the late middle Miocene of Kenya (12.5 Ma; Rossie et al., 2013), followed by the colobine *Microcolobus* (9.5–9.0 Ma; Benefit & Pickford, 1986; Jablonski & Frost, 2010). Colobines are also the first cercopithecids recorded out of

Africa; in particular, *Mesopithecus* is first recorded in Europe at least by ~8.5 Ma and subsequently throughout Eurasia (Koufos, 2006; Alba et al., 2015b), where it lasted until the Early Pleistocene (~2.3 Ma; Alba et al., 2015b). It remains unsettled whether *Mesopithecus* is a member of the Asian colobine clade (Presbytina; Groves, 2000; Jablonski, 2002) or a stem colobine (Alba et al., 2015b; Frost et al., 2015). The much younger (1.9 Ma) *Cercopithecoides williamsi* is the oldest secure African colobine (Colobina; Frost et al., 2015), although older members of this clade possibly date back to 3.8–3.5 (Harrison, 2011) or even ~5–4 Ma (Leakey et al., 2003).

Cercopithecines are not recorded until the late Miocene of Africa. The molecular data suggest an early late Miocene divergence (~11.0–10.3 Ma; Roos et al., 2019) between the Cercopithecini and Papionini. The oldest cercopithecine (Papionini indet.) has been recovered from the Chorora Formation in Ethiopia (~8.5–8 Ma; Suwa et al., 2015; Katoh et al., 2016), while the undoubted (stem) papionin "*Parapapio*" *lothagamensis* is recorded slightly thereafter in Kenya (7.4–5.0 Ma; Leakey et al., 2003; Jablonski & Frost, 2010). In turn, a single guenon molar from Abu Dhabi (8–6.5 Ma) represents the earliest occurrence of cercopithecins (Gilbert et al., 2014). While the latter have always been restricted to Afro-Arabia, papionins (macacinans and papioninans) are also found in Eurasia (e.g., Delson, 1974; Köhler et al., 2000; Alba et al., 2014, 2015b; Roos et al, 2019). Macacinans are first recorded in northern Africa during the late Miocene (7.0–5.0 Ma; Delson, 1975, 1980; Szalay & Delson, 1979; Benefit et al., 2008) and in Europe during the latest Miocene (~5.5 Ma; Köhler et al., 2000; Marigó et al., 2014; Alba et al., 2014), roughly coinciding with the divergence between African and Asian macaques (Roos et al., 2019). It is uncertain whether macaques dispersed into Eurasia across Gibraltar or the Middle East (Gilbert et al., 2014; Alba et al., 2015b), but their dispersal roughly coincided with the Messinian Salinity Crisis (Alba et al., 2014, 2015a), being subsequently recorded throughout Eurasia. Papioninans are mostly recorded in East and South Africa during the Plio-Pleistocene (Jablonski & Frost, 2010), but extinct geladas (*Theropithecus*) also dispersed into Eurasia during the Pleistocene (Delson, 1993; Gilbert et al., 1995; Hughes et al., 2008; Belmaker, 2010; Roberts et al., 2014; Roos et al., 2019).

Fossil stem hominoids. There is universal consensus that hominoids originated in Africa, but the phylogenetic relationships among fossil hominoids, as well as the status of some taxa as stem catarrhines vs. stem hominoids, are still a matter of debate (e.g., Harrison, 2010; Alba, 2012), leading to diverging systematic schemes for the group (e.g., Harrison, 2010, 2013; Alba, 2012; Begun, 2015; Gilbert et al., 2020b). Besides the two families of crown hominoids (Hylobatidae and Hominidae), three families of stem hominoids (of questionable monophyly)—sometimes distinguished only at the subfamily rank (Nengo et al., 2017; Gilbert et al., 2020a)—may be distinguished (Gilbert et al., 2020b): Proconsulidae, Nyanzapithecidae, and Afropithecidae. There

might be a fourth family of stem hominoids (Pliobatidae; Alba et al., 2015a), depending on the phylogenetic interpretation of *Pliobates* (see below).

Hominoids are first recorded in the Oligocene of Kenya (28–24 Ma) by dentognathic material assigned to *Kamoyapithecus* (Leakey et al., 1995a; Hammond et al., 2019) and an indeterminate nyanzapithecine (Hammond et al., 2019), as well as in the late Oligocene of Tanzania (25.2 Ma) by *Rukwapithecus* (Stevens et al., 2013). The scarce material available for *Kamoyapithecus* precluded until recently confirming its purported hominoid affinities (Leakey et al., 1995a; Zalmout et al., 2010; Alba, 2012; Begun, 2015), being alternatively interpreted by some as a stem catarrhine (Harrison 2010, 2013; Zalmout et al., 2010; Stevens et al., 2013). However, its canine morphology was recently shown to indicate close affinities with the proconsulid *Proconsul* (Hammond et al., 2019). In turn, *Rukwapithecus*, which is similarly known based on dental material, appears somewhat more derived by displaying similarities with the early Miocene nyanzapithecid *Rangwapithecus* (Stevens et al., 2013). The meager evidence available for Oligocene hominoids therefore suggests an early divergence between proconsulids and nyanzapithecids. Despite their similar antiquity, recent cladistic analyses suggest that proconsulids constitute the basal-most clade of stem hominoids, sister to the clade including nyanzapithecids together with afropithecids and crown hominoids (Nengo et al., 2017; Gilbert et al., 2020a).

Proconsulids include two genera (*Proconsul* and *Ekembo*) with multiple species each early Miocene localities of Kenya and Uganda (22.5–17 Ma; Peppe et al., 2009; Harrison & Andrews, 2009; Harrison, 2010; McNulty et al., 2015). Until recently (McNulty et al., 2015), they were all subsumed within a single genus (*Proconsul*), with the exception of some authors than distinguished a different genus (*Ugandapithecus*; Senut et al., 2000; Pickford, 2002; Pickford et al., 2009), generally considered a junior synonym of *Proconsul* (Harrison, 2010; McNulty et al., 2015). *Samburupithecus*, from the late Miocene of Kenya (~9.5 Ma; Pickford et al., 1984; Ishida & Pickford, 1997), has been sometimes considered a stem hominine (e.g., Ishida et al., 1984; Andrews, 1992), but most likely it is a late surviving proconsulid (Begun, 2001, 2013, 2015; Alba, 2012; Harrison, 2010, 2013). Proconsulids retain a number of plesiomorphic features compared with crown hominoids (Begun, 2015), such as a short premaxilla that does not overlap the hard palate, a generalized dentition with well-developed molar cingula, and a short tubular ectotympanic with a deep V-shaped notch in the external margin. As in all primates except hominids and some large-bodied cercopithecoids and lemurs, proconsulids possess a large and deep subarcuate fossa (Spoor & Leakey, 1993). They also display a mosaic of primitive (monkey-like) and derived (hominoid-like) postcranial features, overall indicative of a pronograde body plan compatible with generalized arboreal quadrupedalism and powerful-grasping cautious climbing (Rose, 1983, 1997; Kelley, 1997; Ward, 1993, 1997, 2015; Ward et al., 1993; Walker, 1997; Harrison, 2010; Daver & Nakatsukasa, 2015). Although some authors have considered

proconsulids in a broad sense to precede the cercopithecoid-hominoid divergence (Harrison, 2010), their hominoid status is best shown by the lack of an external tail (Ward et al., 1991; Nakatsukasa et al., 2003). They are medium- to large-bodied (10–50 kg; Ruff et al., 1989; Rafferty et al., 1995), display a lower degree of encephalization than great apes (in the range of extant hylobatids; Walker et al., 1983; Begun & Kordos, 2004; Alba, 2010), and apparently displayed a somewhat slower life history than cercopithecoids (Kelley, 1997, 2004; Kelley & Smith, 2003; Smith et al., 2003).

Nyanzapithecids are more diverse than proconsulids and span a wide temporal range, from the late Oligocene (25.2 Ma, *Rukwapithecus*; Stevens et al., 2013) to the late Miocene (9.9–9.8 Ma, Nyanzapithecidae indet.; Kunimatsu et al., 2017)—or even later (8.3–6.7 Ma; Rook et al., 2011) if the late Miocene ape *Oreopithecus*, from the Tusco-Sardinian paleobioprovince (see below), is a nyanzapithecid, as long suggested based on dental similarities (Harrison, 1986) and as further confirmed by most recent cladistic analyses (Nengo et al., 2017; Gilbert et al., 2020a). Besides *Oreopithecus*, they currently include six genera (*Rukwapithecus*, *Rangwapithecus*, *Mabokopithecus*, *Turkanapithecus*, *Xenopithecus* and *Nyanzapithecus*), comprising a minimum of ten species (Harrison, 2010; Pickford et al., 2010; Stevens et al., 2013; Kunimatsu et al., 2017; Nengo et al., 2017). They are medium-sized catarrhines (ca. 10–15 kg for male individuals; Harrison, 2010; Fleagle, 2013), although males of *Oreopithecus* would have exceeded 30 kg (Jungers, 1987). Nyanzapithecids share a distinctive dental morphology (Harrison, 2013; Nengo et al., 2017) and—based on *Nyanzapitecus* and *Turkanapithecus*—display some cranial similarities with hylobatids. These are interpreted by some as homoplastic (Nengo et al., 2017), although they could alternatively reflect the primitive condition for crown hominoids (Alba et al., 2015a). A juvenile cranium of *Nyanzapithecus* from the middle Miocene of Kenya (~13 Ma; Nengo et al., 2017) does not show the semicircular canal morphology of hylobatids, characterized by large radii (see Sections 1.2 and 1.3), although such configuration might have evolved much latter in time. *Nyanzapithecus* also displays a fully ossified external acoustic meatus—much more extant-catarrhine-like than in *Ekembo*—whereas it is too damaged in *Turkanapithecus* (Leakey & Leakey, 1986a). Currently, there is no information available about the development of the subarcuate fossa. The postcranial morphology suggests that nyanzapithecids were above-branch, pronograde quadrupeds broadly similar to proconsulids, perhaps with some suspensory adaptations but without specific adaptations to hylobatid-like brachiation (Langdon, 1986; Nengo & Rae, 1992; Rose, 1993, 1994; Ward, 1997a; Harrison, 2010; Nengo et al., 2017).

Oreopithecus, from the late Miocene (8.3–6.7 Ma; Rook et al., 2011) of the Tusco-Sardinian Paleobioprovince, deserves particular mention. This genus is well known on the basis of craniodental and postcranial remains (Gervais, 1872; Hürzeler, 1951, 1954, 1958; Delson, 1986; Harrison, 1986; Sarmiento, 1987; Szalay & Langdon, 1986;

Rook, 1993; Clarke, 1997; Harrison & Rook, 1997; Köhler & Moyà-Solà, 1997; Moyà-Solà & Köhler, 1997; Moyà-Solà et al., 1999; Rook et al., 1999, 2004; Almécija et al., 2014; Hammond et al., 2020). Nevertheless, the phylogenetic relationships of *Oreopithecus* have long been proved controversial (Delson, 1986), being alternatively considered a cercopithecoid (Szalay & Delson, 1979), a hominoid (Straus, 1963; Sarmiento, 1987), a relative of African nyanzapithecids (Harrison, 1986), a hominid of uncertain affinities (Alba, 2012), a dryopithecine (Moyà-Solà & Köhler, 1997; Harrison & Rook, 1997), or even a hominin (Hürzeler, 1954). The peculiar occlusal morphology of *Oreopithecus* has been interpreted as an adaptation for folivory (Ungar & Kay, 1995; Ungar, 1996), but microwear data suggest a more eclectic frugivorous diet (DeMiguel et al., 2014). Its cranial morphology has been interpreted as plesiomorphic for crown hominoids (Harrison, 1986; Begun et al., 1997; Begun, 2002b, 2013, 2015) or secondarily derived (Moyà-Solà & Köhler, 1997; Alba et al., 2001). The postcranium, in turn, is highly derived (modern hominid-like); some features have been interpreted as indicative of terrestrial bipedalism (Straus, 1963; Köhler & Moyà-Solà, 1997; Rook et al., 1999; Moyà-Solà et al., 2005a)—in agreement with the possession of human-like hand proportions for refined manipulation (Moyà-Solà et al., 1999, 2005a; Almécija et al., 2014)—while other authors have emphasized vertical climbing (Hammond et al., 2020) and suspensory adaptations (Jungers, 1987; Harrison, 1991; Harrison & Rook, 1997; Susman, 2004; Begun, 2007; Deane & Begun, 2008; Russo & Shapiro, 2013). Recent cladistics analyses supported the view that *Oreopithecus* is a late-surviving nyanzapithecid (Nengo et al., 2017; Gilbert et al., 2020a), which would imply a substantial amount of homoplasy given its postcranial similarities with hominids.

Among the families of stem hominoids, afropithecids are most difficult to interpret. Recent cladistic studies (Nengo et al., 2017; Gilbert et al., 2020a) have recovered them as paraphyletic, with *Equatorius* being more derived than proconsulids but sister to the clade including the remaining stem hominoids + the crown group, and *Morotopithecus* and *Afropithecus* being successive sister taxa to nyanzapithecines, within a clade of stem taxa sister to the crown group. On the other hand, other authors have considered that afropithecids are more derived than nyanzapithecines and even included *Equatorius* as a stem hominid (Ward et al., 1999; Ward & Duren, 2002; Cameron, 2004; Andrews & Kelley, 2007; Alba, 2012). Besides *Equatorius*, *Afropithecus*, and *Morotopithecus*, two additional genera (*Heliopithecus* and *Otavipithecus*) probably belong to this family (Ward et al., 1999; Andrews & Kelley, 2007; Alba, 2012; Begun, 2013, 2015). Other taxa currently considered stem hominids, such as *Griphopithecus* and *Nacholapithecus*, or even *Kenyapithecus*, have been sometimes considered afropithecids as well (Cameron, 2004; Moyà-Solà et al., 2009a; Casanovas-Vilar et al., 2011). However, they are treated here as kenyapithecine hominids following Alba (2012). Afropithecids are recorded from the early to the middle Miocene (~20–13 Ma) of Kenya, Uganda, Namibia and Saudi Arabia (Pilbeam,

1969; Andrews et al., 1978; Leakey & Leakey, 1986b; Andrews & Martin, 1987; Watsink, 1989; Anyonge, 1991; Conroy et al., 1992; Leakey & Walker, 1997; Singleton, 2000). *Morotopithecus* has been considered a junior synonym of *Afropithecus* (Pickford, 2002; Patel & Grossman, 2006; Harrison, 2010), but differences in cranial morphology suggest they are distinct (MacLatchy et al., 2000; Alba, 2012; Begun, 2015; Deane, 2017). They were medium- to large-bodied (similar to proconsulids; Andrews, 1992; Conroy et al., 1992; Leakey & Walker, 1997; Gebo et al., 1997) and possibly relied on a more sclerocarpic diet than proconsulids (Deane, 2017). Their postcranial morphology is less well known than for proconsulids, but it is generally similar to that of the latter. The only exception is *Morotopithecus*, which displays some evidence indicative of an orthograde body plan (Sanders & Bodenbender, 1994; Gebo et al., 1997; MacLatchy, 2004; Nakatsukasa, 2008; MacLatchy et al., 2019), although this is generally considered an independent acquisition from that of crown hominoids (Sanders & Bodenbender, 1994; Gebo et al., 1997; MacLatchy, 2004; Young & MacLatchy, 2004; Alba, 2012; MacLatchy et al., 2019). Although some authors have favored that hominids evolved from afropithecids (Moyà-Solà et al., 2009a; Alba, 2012), *Morotopithecus* and *Afropithecus* still display a primitive nasoalveolar morphology (Begun & Gülec, 1998; Nakatsukasa & Kunimatsu, 2009; Alba, 2012; Begun, 2015).

Finally, pliobatids are a monotypic family erected on the basis of *Pliobates*, from the middle/late Miocene of the Iberian Peninsula (~11.6 Ma; Alba et al., 2015a). *Pliobates* displays a previously unknown combination of crown hominoid synapomorphies coupled with more pleasiomorphic features resembling dendropithecids and more primitive stem catarrhines, as well as some specific similarities with hylobatids (Alba et al., 2015a). Cranially, *Pliobates* combines a short and incompletely ossified tubular ectotympanic with a hylobatid-like short face with a distinct muzzle, telescopic orbits, and an encephalization degree below that of hominids (Alba et al., 2015a). In the postcranium, *Pliobates* shows numerous hominoid synapomorphies in the forelimbs—related to increased forearm pronation-supination at the elbow joint and enhanced rotation and ulnar deviation capabilities at the wrist—coupled with more plesiomorphic (stem catarrhine-like) features (Alba et al., 2015a). This combination has been functionally related to above-branch cautious climbing coupled with some adaptations to suspensory behaviors (Alba et al., 2015a). A cladistics analysis recovered *Pliobates* as a stem hominoid more derived than proconsulids, thus being interpreted as a late-surviving European offshoot of a stem hominoid lineage of African origin (Alba et al., 2015a). Alternatively, *Pliobates* has been recovered as a pliopithecid by some cladistic analyses, mostly due to the lack of a fully ossified external acoustic meatus (Nengo et al., 2017; Gilbert et al., 2020a; see also Benefit & McCrossin, 2015). If *Pliobates* were a stem hominoid, it would imply a crown hominoid last common ancestor (LCA) more hylobatid-like (in terms of body

size and cranial morphology) than previously assumed (Alba et al., 2015a; Grabowski & Jungers, 2017). If *Pliobates* is instead a pliopithecoid, then it shows a remarkable amount of postcranial homoplasies with crown hominoids (more so than atelids; Alba et al., 2015a). It is however noteworthy that *Pliobates* shows much greater similarities in dental morphology with dendropithecids than with pliopithecoids (Alba et al., 2015a), leading to the alternative hypothesis that it might be a late-occurring European dendropithecid. Even if this would imply a considerable amount of parallel evolution with crown hominoids, the phylogentic status of dendropithecids as stem hominoids vs. stem catarrhines is not settled (see above), so the same applies to *Pliobates*.

Crown hominoid origins. Africa was an island continent separated from Eurasia by the Tethys Seaway at least until ~19 Ma (Seiffert, 2012; Begun et al., 2012), when the emergence of an intermittent land-bridge between Africa and Eurasia allowed faunal exchange (Harzhauser et al., 2007). This route enabled the dispersal of pliopithecoids into Eurasia (see above) and, shortly thereafter, that of hominoids. Hylobatid ancestors possibly dispersed into Eurasia by the same time, but their origins (see Section 1.1.1) remain elusive due to their scarce Miocene record (Harrison, 2016; Gilbert et al., 2020a). Molecular data suggests that hylobatids diverged from hominids ~20 Ma (Perelman et al., 2011; Springer et al., 2012; Finstermeier et al., 2013; Pozzi et al., 2014). However, they are not recorded until the middle Miocene (*Kapi*; 13.8–12.5 Ma, Pakistan; Gilbert et al., 2020a) and the late Miocene (*Yuanmoupithecus*; ~9.0–7.0 Ma, China; Pan, 2006; Harrison, 2016), and only two additional extinct hylobatid genera (*Bunopithecus* and *Junzi*) have been described from the Pleistocene and Holocene, respectively (Ortiz et al., 2015; Turvey et al., 2018). It is unknown from what African taxa hylobatids might have evolved. Decades ago, pliopithecoids were considered as broadly ancestral to hylobatids due to superficial similarities in cranial and postcranial morphology (e.g., Hürzeler, 1954; Zapfe, 1958, 1961; Simons & Fleagle, 1973), but this hypothesis is no longer tenable (e.g., Zalmout et al., 2010; Stevens et al., 2013; Nengo et al., 2017; Gilbert et al., 2020a). Hylobatids probably evolved from a dendropithecid or proconsulid ancestor that dispersed from African during Mid-Miocene Climatic Optimum (Barry et al., 1995; Alba et al., 2015a; Gilbert et al., 2020a,b).

The hominid fossil record is much more abundant than that of hylobatids, but uncertainties persist regarding the phylogenetic status of the oldest hominoid remains recorded from Eurasia. They consist of a partial tooth of cf. *Griphopithecus* from Engelswiess, Germany (16.5–16.0 Ma; Heizmann & Begun, 2001; Casanovas-Vilar et al., 2011). Given the scarce morphology preserved, it can only be asserted that thick-enameled large hominoids were present in Europe by this time. Larger samples including both *Griphopithecus* and *Kenyapithecus* (Alpagut et al., 1990; Begun, 1992a, 2002b; Begun et al., 2003; Kelley et al., 2008a,b) are not recorded until somewhat later

(~14 Ma) in Turkey (Casanovas-Vilar et al., 2011). There is consensus that *Kenyapithecus*, also recorded in Kenya by ~14 Ma, is probably a stem hominid (Harrison, 1992, 2010; Ward et al., 1999; Kelley et al., 2002, 2008a,b; Ward & Duren, 2002; Andrews & Kelley, 2007; Alba, 2012; Pugh, 2020). Some authors have included this genus, together with other middle Miocene hominoids from Africa (*Nacholapithecus*, and even *Equatorius*) and Eurasia (*Griphopithecus*), in a single subfamily (Kenyapithecinae) of hominids (Alba, 2012), characterized by thick enamel like afropithecids. However, the hominid status of these other genera is much debated (Harrison, 2010; Begun, 2015; Nengo et al., 2017; Gilbert et al., 2020a). According to Alba (2012), kenyapithecines would include the equatorins (*Equatorius* and *Nacholapithecus*) and the kenyapithecins (*Griphopithecus* and *Kenyapithecus*). Cameron (2004) made a similar distinction but included these tribes (and even the afropithecids) within the Dryopithecinae instead of the Kenyapithecinae.

Kenyapithecines are broadly similar in size to proconsulids, from which they differ in craniodental morphology, while their postcranium is similarly indicative of a pronograde body plan (Alba, 2012; Begun, 1992a, 2002b, 2015). *Nacholapithecus*, from the middle Miocene of Kenya (~14.9–14.7 Ma; Nakatsukasa & Kunimatsu, 2009), displays a couple of crown hominid synapomorphies in the cranium (overlap between the maxilla and the premaxilla, and loss of the subarcuate fossa), but retains a pronograde body plan similar to that of proconsulids and afropithecids except for some features indicating a greater emphasis on forelimb-dominated behaviors such as climbing (Kunimatsu et al., 2004, 2019; Ishida et al., 2004; Nakatsukasa & Kunimatsu, 2009; Takano et al., 2020). Similarly, the cheek teeth of *Equatorius* (~16.0–14.5 Ma, Kenya; Ward et al., 1999) resemble those of the Eurasian *Griphopithecus* but are generally considered to warrant allocation into distinct genera (Ward et al. 1999; Kelley et al. 2000; Ward & Duren 2002; contra Begun 2000, 2002b; Benefit & McCrossin 2000), while its postcranium denotes generalized arboreal quadrupedalism and largely resembles that of proconsulids (Begun, 1992a, 2002b, 2013, 2015; McCrossin & Benefit, 1997; Ward et al., 1999; Ward & Duren, 2002; Allen & McCrossin, 2007). While the phylogenetic status of *Griphopithecus* from Central Europe and Turkey (~14.5–11.5 Ma; Casanovas-Vilar, et al. 2011a) is more uncertain, *Kenyapithecus* from the middle Miocene of Kenya (~14 Ma; Andrews & Walker, 1976; Pickford, 1986; Andrews et al., 1996; Begun, 2002b; Kelley et al., 2008a,b) and Turkey (~14.5–14.0 Ma; Casanovas-Vilar et al., 2011) appears more derived than afropithecids due to the possession of a high zygomatic root, which is a crown hominid synapomorphy (Pickford, 1986; Harrison, 1992, 2010; Andrews, 1996, 2019; Ward et al., 1999; Kelley et al., 2002, 2008a,b; Andrews & Kelley, 2007; Alba, 2012; Begun, 2013, 2015; Pugh, 2020).

Soon thereafter kenyapithecines are first recorded in Turkey, both pongines and dryopithecines are recorded in Asia and Europe, respectively. Persisting uncertainties about the phylogenetic relationships of dryopithecines have led to opposite views on

the origins of the great ape and human clade—e.g., compare Moyà-Solà & Köhler (1993, 1995) and Alba (2012) with Begun et al. (2012) and Begun (2013, 2015). It is thus currently uncertain if there was a single large-bodied ape dispersal from Africa into Eurasia, if pongines and dryopithecines share a Eurasian last common kenyapithecine ancestor, and especially whether dryopithecines are the siter clade of pongines or ancestor or stem hominines (see below).

Fossil hominids from Eurasia. Pongines include the extant orangutans (*Pongo*) and at least five extinct genera (*Sivapithecus*, *Ankarapithecus*, *Khoratpithecus*, *Indopithecus, Gigantopithecus*, and, maybe, *Lufengpithecus*; Alba, 2012; Begun, 2015). While some of them are monotypic, others (*Sivapithecus*, *Khoratpithecus*, and *Lufengpithecus*) include multiple species (Ji et al., 2013; Begun; 2015; Chaimanee et al., 2019). These extinct taxa are customarily considered pongines based on geography and the possession of purported pongine craniodental synapomorphies displayed by extant orangutans. The most evident pongine synapomorphy, shared by *Pongo*, *Sivapithecus*, *Ankarapithecus* and *Khoratpithecus*, relates to their subnasoalveolar morphology, which is characterized by a long and procumbent premaxilla that considerably overlaps with the palatine processes of the maxillae, generally resulting in a smooth subnasal floor (e.g., Begun & Güleç, 1998; Kelley, 2002; Begun, 2015; Chaimanee et al., 2019). *Ankarapithecus* from Turkey (~9.8 Ma; Ozansoy, 1965; Alpagut et al., 1996; Kappelman et al., 2003) is considered the most basal pongine due to a more plesiomorphic configuration of the premaxilla (Begun & Güleç, 1998; Begun, 2015). In turn, *Khoratpithecus* (~12.4–6.0 Ma, South East Asia; Chaimanee et al., 2004; Coster et al., 2010; Jaeger et al., 2011) has been interpreted as the sister taxon of *Pongo* based on the morphology of the mandible, although the configuration of the premaxilla suggests a more distant relationship than in the case of *Sivapithecus* (Chaimanee et al., 2019).

Sivapithecus is known by more abundant material (Andrews & Cronin, 1982; Pilbeam, 1982; Ward & Pilbeam, 1983; Kelley, 1988, 2002; Pilbeam et al., 1990; Kappelman et al., 1991; Ward, 1997b; Barry et al., 2002, 2013; Madar et al., 2002; Morgan et al., 2015) from the middle and late Miocene of India and Pakistan, customarily assigned to three species that range from 12.7 to 8.5 Ma (Barry et al., 2002, 2013; Kelley, 2002), aside from some Nepali material tentatively ascribed to this genus (Andrews & Tekkaya, 1980). The similarities between *Sivapithecus* and extant *Pongo* in craniodental morphology are extensive, including an airorynchous cranium, tall and narrow orbits, and a narrow interorbital space—besides the long, horizontal and procumbent premaxilla that considerably overlaps the hard palate and configures a smooth subnasal floor (Ward & Pilbeam, 1983; Ward & Brown, 1986; Brown & Ward, 1988; Ward, 1997b; Kelley, 2002; Begun, 2015). Paradoxically, *Sivapithecus* displays a more primitive postcranial morphology consistent with a pronograde body plan

(Pilbeam et al., 1990; Madar et al., 2002; Morgan et al., 2015), and its molars lack the characteristic enamel wrinkling of orangutans that is present in *Lufengpithecus* (Schwartz 1997; Begun, 2015). Two of the largest primates ever recorded (200–300 kg in males; Fleagle, 2013; Zhang & Harrison, 2017) are also included in the Ponginae: the late Miocene *Indopithecus* (~8.9–8.6 Ma, India; Cameron, 2003; Pillans et al., 2005) and the much younger *Gigantopithecus* (~2.0–0.3 Ma; China, Vietnam, and Thailand; Zhang et al., 2014; Zhang & Harrison, 2017). *Gigantopithecus* is generally considered to be derived from *Indopithecus*, which might indicate a phylogenetic link with *Sivapithecus*. This would be consistent with the results of a paleoproteomic analysis based on >2.0 Ma *Gigantopithecus* remains, which confirmed its pongine status and indicated an early divergence from orangutans at ~12–10 Ma (Welker et al., 2019). The Chinese *Lunfengpithecus* (~10–6 Ma; Harrison, 2002; Kelley, 2002; Qi et al., 2006; Alba, 2012; Begun, 2015) has also been included in the Ponginae, but during the last decade the monophyly of the taxon has been questioned and a stem hominid status considered more likely (Kelley & Gao, 2012; Chaimanee et al., 2019; Gilbert et al., 2020b; Pugh, 2020). At present, it is uncertain whether *Lufengpithecus* is a pongine more basal than others, a dryopithecine, or a hodgepodge of species belonging to different clades.

Almost contemporaneously with the Asian forms, dryopithecines—here distinguished as a subfamily (Dryopithecinae; Casanovas-Vilar et al., 2011; Alba, 2012; Andrews, 2019), but alternatively recognized as a tribe (Dryopithecini; Begun, 2009, 2010, 2013, 2015)—are first recorded in Europe (France and Spain, ~12.5–11.2 Ma; Casanovas-Vilar et al., 2011; Alba et al., 2013, 2017). There is universal consensus that dryopithecines are great apes (i.e., hominids) more derived than kenyapithecines (Moyà-Solà & Köhler, 1993, 1995, 1996; Moyà-Solà et al., 2004, 2009a,b; Begun, 2009, 2010, 2015; Alba et al., 2010b; Casanovas-Vilar et al., 2011; Alba, 2012; Begun et al., 2012; Nengo et al., 2017; Gilbert et al., 2020a,b). However, despite being represented by cranial and postcranial material, dryopithecines still defy a coherent systematic placement within the Hominidae. This is due to uncertainties about their phylogenetic relationships with extant and other extinct great apes. The supposed lack of hominids in the late middle to late Miocene of Africa and the recognition of some purported hominine synapomorphies has led some authors to advocate a Eurasian origin of the African ape and human clade and their subsequent dispersal back to Africa in the late Miocene (Begun et al., 1997, 2012; Begun, 1992a, 2001; 2002b, 2009, 2010, 2013, 2015, 2017; Begun & Nargolwalla, 2004). Alternatively, based on the recognition of purported pongine synapomorphies, other authors advocated a stem pongine status for dryopithecines (Moyà-Solà & Köhler, 1993, 1995; Köhler et al., 2001a). A third hypothesis is that dryopithecines are stem hominids preceding the hominine-pongine divergence (Andrews, 1992; Moyà-Solà et al., 2004, 2009a,b; Alba, 2012; Alba et al., 2015b; Nengo et al., 2017; Gilbert et al., 2020a). It has been argued that dryopithecines

could have evolved from earlier kenyapithecines (Moyà-Solà et al., 2009a; Alba, 2012), but this scenario is compatible with the various phylogenetic hypotheses discussed above. From a biogeographic viewpoint, the possibility remains that hominines locally evolved in Africa from middle Miocene kenyapithecines, while dryopithecines and pongines independently evolved as vicariant sister taxa from other kenyapithecine ancestors in Eurasia (Alba, 2012). Under such scenario, dryopithecine would be stem pongines in cladistic terms despite lacking most of the syanpomorphies currently recognized for this group.

Nine dryopithecine genera may be recognized, being classified in three tribes following Alba (2012): the middle Miocene genera (*Pierolapithecus*, *Dryopithecus*, and *Anoiapithecus*) would belong to the Dryopithecini, whereas the early late Miocene (Vallesian) genera (*Hispanopithecus* and *Rudapithecus*) would be included within the Hispanopithecini, and the later Miocene (Vallesian to Turolian) genera (*Ouranopithecus* and *Graecopithecus*) into the Ouranopithecini. *Danuvius*, recently described by Böhme et al. (2019), is intermediate in age (close to the middle/late Miocene boundary at 11.6 Ma) between dryopithecins and hispanopithecins, but more similar in dental and postcranial morphology to the hispanopithecins (D. M. Alba, pers. comm.), and thus being included here in the latter family. Finally, the taxonomic identity and phylogenetic affinities of the late Miocene ?*Udabnopithecus* (8.1–7.7 Ma; Georgia; Gabunia et al., 2001), sometimes included in *Dryopithecus* (Gabunia et al., 2001; Agustí et al., 2020), are uncertain.

Dryopithecins appear slightly less derived than hispanopithecins in dental morphology (Moyà-Solà et al., 2009a,b; Alba et al., 2010b; Alba, 2012; Begun et al., 2012; Pérez de los Ríos et al., 2012; Begun, 2015). *Dryopithecus* was the first fossil ape ever discovered (Lartet, 1856) At present, it includes cranial and postcranial material from the middle Miocene (~12.4–11.2 Ma; Casanovas-Vilar et al., 2011; Alba et al., 2019) of France, Austria and Spain (Lartet, 1856; Gaudry, 1890; Harlé, 1898, 1899; Depéret, 1911; Mottl, 1957; Mein, 1986; Begun, 2002a; 2009, 2015; Moyà-Solà et al., 2009a; Alba, 2012; Begun et al., 2012; Alba et al., 2013; Pérez de los Ríos et al., 2013). *Dryopithecus* is a large-bodied hominid (44–50 kg; Moyà-Solà et al., 2009a; Alba et al., 2011) that differs from other dryopithecins in facial morphology (Moyà-Solà et al., 2009a; Alba, 2012), including some similarities with gorillas that might be symplesiomorphic. The postcranium of *Dryopithecus* is not very well known (Pilbeam & Simons, 1971; Moyà-Solà et al., 2009b; Almécija et al., 2012; Pina et al., 2019), being suggestive powerful grasping above-branch quadrupedalism and cautious climbing without evidence of an orthogade body plan. With an age of 12.0 Ma (Moyà-Solà et al., 2009b; Casanovas-Vilar et al., 2011; Alba et al., 2017) and an estimated body mass of ~43 kg (for males; Susanna et al., 2014), *Pierolapithecus* from Spain displays an overall hominid-like facial morphology (Moyà-Solà et al., 2004; Alba, 2012). This genus further displays the oldest evidence of an orthograde body

plan in multiple anatomical regions (broad and shallow thorax, short and ventrally located lumbar spine, long and stout clavicle, patellar morphology; Moyà-Solà et al., 2004, 2005b; Alba, 2012; Pina et al., 2014; Ward, 2015a) despite the lack of specific adaptations to suspensory behaviors (Moyà-Solà et al., 2004, 2005b; Almécija et al., 2009; Alba et al., 2010c; contra Begun & Ward, 2005; Deane & Begun, 2008, 2010; Begun et al., 2012). Overall, postcranial evidence for *Pierolapithecus* indicates a forelimb-dominated locomotor repertoire with a significant component of vertical climbing but further retaining powerful-grasping adaptations for above-branch quadrupedalism (Moyà-Solà et al., 2004, 2005b; Almécija et al., 2009; Alba et al., 2010c; Alba, 2012). In turn, *Anoiapithecus* (12.4–12.0 Ma, Catalunya, Spain; Alba et al., 2017) differs from other dryopithecins by the possession of a very orthognathous face and a distinct canine morphology (Moyà-Solà et al., 2009b; Alba, 2012; Alba et al., 2013), further combining several hominid synapomorphies with more plesiomorphic features resembling kenyapithecines. Some authors have raised doubts about the distinction at the genus rank of *Pierolapithecus* and *Anoiapithecus* from *Dryopithecus* (Begun, 2002b, 2007, 2009, 2010, 2015), but they are considered distinct here given multiple differences in craniodental morphology (Moyà-Solà et al., 2004, 2009a,b; Alba, 2012; Pérez de los Ríos et al., 2012; Alba et al., 2013).

Hispanopithecins include *Hispanopithecus* from Spain (~10.5–9.6 Ma), *Rudapithecus* from Hungary (10.0–9.8 Ma), and probably *Danuvius* (11.6 Ma) from Germany (Casanovas-Vilar, et al. 2011; Alba et al., 2019; Böhme et al., 2019). With a body mass of ca. 17–31 kg, *Danuvius* displays an orthograde body plan with suspensory adaptations (Böhme et al., 2019), but no adaptations to bipedalism (Williams et al., 2020; contra Böhme et al., 2019). *Hispanopithecus* is well known on the basis of dental (Villalta & Crusafont, 1944; Crusafont Pairó & Hürzeler, 1969; Begun et al., 1990; Harrison, 1991; Begun, 1992b; Golpe Posse, 1993; Alba et al., 2012a,b), cranial (Moyà-Solà & Köhler, 1993, 1995) and postcranial (Moyà-Solà & Köhler, 1996; Almécija et al., 2007; Alba et al., 2012c; Susanna et al., 2014; Pina et al., 2012) remains. Although *Hispanopithecus* was formerly considered a junior subjective synonym of *Dryopithecus* (Simons & Pilbeam, 1965; Szalay & Delson, 1979; Harrison, 1991; Golpe Posse, 1993; Andrews et al., 1996; Begun, 2002b), a distinct genus status is currently granted by most authors (Moyà-Solà et al., 2009b; Begun, 2009, 2013, 2015; Alba, 2012; Alba et al., 2012a,b,c; Marigó et al., 2014; Susanna et al., 2014). *Hispanopithecus* shows several hominid synapomorphies in the cranium (e.g., loss of subarcuate fossa; Moyà-Solà & Köhler, 1993, 1995; Begun, 1994; Köhler et al., 2001a,b) and clear adaptations to suspensory behaviors (Moyà-Solà & Köhler, 1996; Almécija et al., 2007; Alba et al., 2010c, 2012a; Alba, 2012; Pina et al., 2012; Susanna et al., 2014), although it still retained some features functionally related to above-branch quadrupedalism (Almécija et al., 2007; Alba et al., 2010c, 2012a). *Rudapithecus*, from the late Miocene of Hungary (10.3–9.8 Ma; Casanovas-Vilar et al., 2011) is well known

based on craniodental and postcranial remains (Kordos, 1987; Begun, 1988; 1992a,b, 1993, 1994, 1995, 2002b, 2009, 2015; Begun & Kordos, 1993; Kordos & Begun, 1997, 2001a,b; Gunz et al., 2020). Formerly included in *Dryopithecus* (e.g., Begun & Kordos, 1993; Kordos & Begun, 1997; Begun, 2002b) and in *Hispanopithecus* (e.g., Almécija et al., 2007; Moyà-Solà et al., 2009b; Casanovas-Vilar et al., 2011; Alba, 2012; Alba et al., 2012a,b), both genera are here considered distinct following most recent publications (e.g., Begun, 2015).

Ouranopithecins are recorded from the late Miocene (Vallesian, ~9.6–7.0 Ma; Koufos, 2006) of Greece, Bulgaria and Turkey. Two genera are included: *Ouranopithecus* and *Graecopithecus*. They are characterized by large size (~110 kg for male individuals of *Ouranopithecus*; Begun, 2002b; 2007, 2009, 2015; Begun et al., 2012; Fleagle, 2013) and by the hyperthick molar enamel, the latter interpreted as an adaptation to a sclerocarpic diet (Begun & Kordos, 1997; Begun, 2002b, 2007, 2009, 2013, 2015; Begun et al., 2012). *Ouranopithecus* from Greece (de Bonis & Melentis, 1977, 1978; Begun, 2013, 2015; Koufos et al. 2016), Bulgaria (Spassov & Geraads, 2008; Spassov et al., 2012) and Turkey (Güleç et al., 2007) has been interpreted as early hominin by some authors (e.g., de Bonis & Koufos, 1993, 1994; de Bonis et al., 1998; Koufos & de Bonis, 2004), but cladistic analyses have recovered *Ouranopithecus* at most as a stem hominine (Begun et al., 1997; Begun, 2001, 2002b, 2005, 2007), being generally classified along with other dryopithecines (Alba, 2012; Begun et al., 2012; Begun, 2013, 2015). *Graecopithecus* from Greece (von Koenigswald, 1972; Begun, 2002b, 2009; Begun et al., 2012; Böhme et al., 2017; Fuss et al., 2017) has been considered as a senior synonym of *Ouranopithecus* (e.g., Smith et al., 2004) or as a nomen dubium (Koufos & de Bonis, 2005; Alba, 2012). Recent evidence (Fuss et al., 2017) confirms previous views (Begun, 2002b, 2007; Koufos & de Bonis, 2005) that *Graecopithecus* is best considered distinct genus, but does not substantiate its claimed hominin affinities (Benoit & Thackeray, 2017; contra Fuss et al., 2017).

Fossil hominids from Africa. In the late Miocene, the African fossil record is almost devoid of hominoids, especially if compared to the panoply of European forms during the same time interval. Only *Chororapithecus* from Ethiopia (~8.0 Ma; Suwa et al., 2007, 2015; Katoh et al., 2016) and *Nakalipithecus* from Kenya (9.9–9.8 Ma, Kenya; Kunimatus et al., 2007) are recorded. *Chororapithecus* has been considered a possible early member of the gorilla clade based on some dental similarities with extant gorillas and overall large size (Suwa et al., 2007). In turn, the similarly large-sized *Nakalipithecus* has been linked to *Ouranopithecus* (Kunimatsu et al., 2007; Morita et al., 2017). However, the material available for these genera is too scarce to reach any definitive conclusions.

Soon thereafter, the earliest putative hominin genera are recorded in the latest Miocene of central and eastern Africa: *Orrorin* (~6.0 Ma, Kenya; Senut et al., 2001),

Sahelanthropus (ca. 7.0–6.0 Ma, Chad; Brunet et al., 2002, 2005; Zollikofer et al., 2005 Macchiarelli et al., 2020), and *Ardipithecus* (5.7–4.3 Ma; Ethiopia; White et al., 1994, 2009; Haile-Selassie, 2001; Haile-Selassie et al., 2004). Given that molecular data suggest that the divergence between the *Pan* and humans occurred ~9–7 Ma (e.g., Moorjani et al., 2016), these forms are crucial for our understanding the early evolution of hominins. *Sahelanthropus* has been interpreted as a hominin based on basicranial and canine morphology (Brunet et al., 2002; Zollikofer et al., 2005; Guy et al., 2005), but alternatively interpreted as an African ape (Wolpoff et al., 2002), and its postcranial morphology is not particularly indicative of bipedalism (Macchiarelli et al., 2020; contra Brunet et al., 2002). In contrast, the femur of *Orrorin* more clearly denotes bipedalism (Pickford et al., 2002; Galik et al., 2004; Almécija et al., 2013). The more complete postcranial remains of *Ardipithecus* from the Pliocene (White et al., 2009; Lovejoy et al., 2009a,b,c,d) are also indicative of at least some degree of terrestrial bipedalism (as shown by the morphology of the pelvis), but combined with arboreal cautious climbing and certainly much less committed to terrestriality than in australopiths (as shown by the retention of an abducted hallux in *Ardipithecus*; White et al., 1994; Simpson et al., 2019). In craniodental morphology, *Ardipithecus* shows hominin syanpomorphies in the basicranium as well as reduced canines that evince the loss of the canine honing complex (Lovejoy, 2009; Suwa et al., 2009a,b; White et al., 2009; Kimbel et al., 2014).

While there are no unquestionable fossil remains of chimpanzees until ~0.5 Ma (McBrearty & Jablonski, 2005), abundant remains of hominins have been recovered from the Plio-Pleistocene of Africa, belonging to two genera of australopiths (*Australopithecus* and *Paranthropus* spp.; e.g., Wood & Constantino, 2007; Berger et al., 2010; Wood & Schroer, 2013; Kimbel, 2015) and multiple species of *Homo* (e.g., Antón et al., 2014; Berger et al., 2015; Collard & Wood, 2015; Schrenk et al., 2015; Kimbel & Villmoare, 2016; Wood & Boyle, 2020). *Australopithecus* includes at least six species (Boyle & Wood, 2020; but see Collard & Wood, 2015) from the Plio-Pleistocene (~4.4–1.9 Ma; Boyle & Wood, 2020) of East Africa, South Africa, and Chad (e.g., Leakey et al., 1995b; Brunet et al., 1996; Asfaw et al., 1999; Berger et al., 2010; Hammond & Ward, 2013; Simpson, 2013; Kimbel, 2015; Kimbel & Villmoare, 2016). The four species included in *Paranthropus* have a slightly younger range (~3.7–0.9 Ma; Boyle & Wood, 2020) and their remains have been collected from eastern Africa and South Africa (Wood & Constantino, 2007; Wood & Schroer, 2013). The postcranial morphology of both australopith genera is clearly adapted to bipedal locomotion, despite the retention of some primitive features indicative of some terrestrial abilities (Ward, 2013, 2015b). In contrast, australopiths retain a modest brain capacity, only slightly larger than that of great apes (Holloway, 2008, 2015; Alba, 2010; Almécija & Sherwood, 2017), and show a very specialized masticatory apparatus with megadont molars (Ward, 2015b). As currently conceived, *Australopithecus* is in all probability

paraphyletic (Wood & Constantino, 2007; Wood & Schroer, 2013), and even the monophyly of *Paranthropus* has been questioned (Wood & Schroer, 2013), although cladistic analyses consistently recover them as a monophyletic group (Strait et al., 1997; Mongle et al., 2019).

Homo is not recorded until the latest Pliocene (~2.8 Ma, Ethiopia; Villmoare et al., 2015), being by far the most speciose hominin genus—even if the validity of multiple of its species, distributed throughout the Pleistocene and Holocene (Boyle & Wood, 2020), is questionable. Initially restricted to Africa, multiple *Homo* species dispersed out of Africa into Eurasia at different times, although *H. sapiens* is the only species that reached a worldwide distribution (Boyle & Wood, 2020). At present, the diagnoses of the earliest species ascribed to *Homo* is contentious (e.g., Tattersal & Schwartz, 2009; Schrenk et al. 2015; but see Collard & Wood, 2015). Humans display adaptations to committed terrestrial bipedalism, a degree of encephalization clearly higher than great apes, and reduced molar size (e.g., Kimbel, 2009). In addition, humans are characterized by the purposive production of stone tools (Almécija & Sherwood, 2017) in relation to the habitual consumption of meat (Milton, 1999; Foley, 2001), being characterized by a specific human predation pattern that includes the exploitation of large animal carcasses (Thompson, et al., 2019). However, the first species to clearly display a modern human-like bipedalism and a higher degree of encephalization than australopiths is *Homo erectus* s.l. (e.g., Spoor et al., 1994; Antón, 2003; Rightmire, 2004; 2013; Alba, 2010). This species appears in Africa ~1.9 Ma (Boyle & Wood, 2020) and, soon thereafter, it is recorded outside of Africa, as attested by the ~1.8 Ma fossils from Dmanisi (Georgia; e.g., Lordkipanidze et al., 2013). Additional species of *Homo* are recorded since the late Early Pleistocene (e.g., Boyle & Wood, 2020). However, there is consensus that anatomically modern humans (*H. sapiens*) originated in Africa (Stringer, 2002)—with the earliest remains dating back to ~300 ka in Morocco (Hublin et al., 2017) and the oldest remains out of Africa being documented ~200 ka (Hershkovitz et al., 2018).

1.2. The primate vestibular system

1.2.1. General morphology

The vestibular system is possibly one of the most ancient vertebrate sensory systems (Retzius, 1881, 1884; Engström et al., 1966; Wersäll & Bagger-Sjöbäck, 1974; Lowenstein & Saunders, 1975; Curthoys et al., 1977; Igarashi et al., 1981). It is housed in the bony labyrinth of the inner ear together with the hearing organs—namely, the cochlear, the vestibular, and the tympanic ducts. The mammalian vestibular system is

composed, bilaterally, by endolymph-filled membranes: the three semicircular ducts[1] (anterior, lateral, and posterior), which capture angular accelerations; and the otolith organs (the saccule and the utricle), which detect linear forces and gravity, respectively. In turn, the osseous labyrinth consists of a set of consecutive cavities encapsulating the ducts and the sacs of the vestibular system (Fig. 1). The labyrinth comprises the three canals (named after the duct therein), the common crus (a shared segment between the anterior and posterior canals), and the bony vestibule; the latter

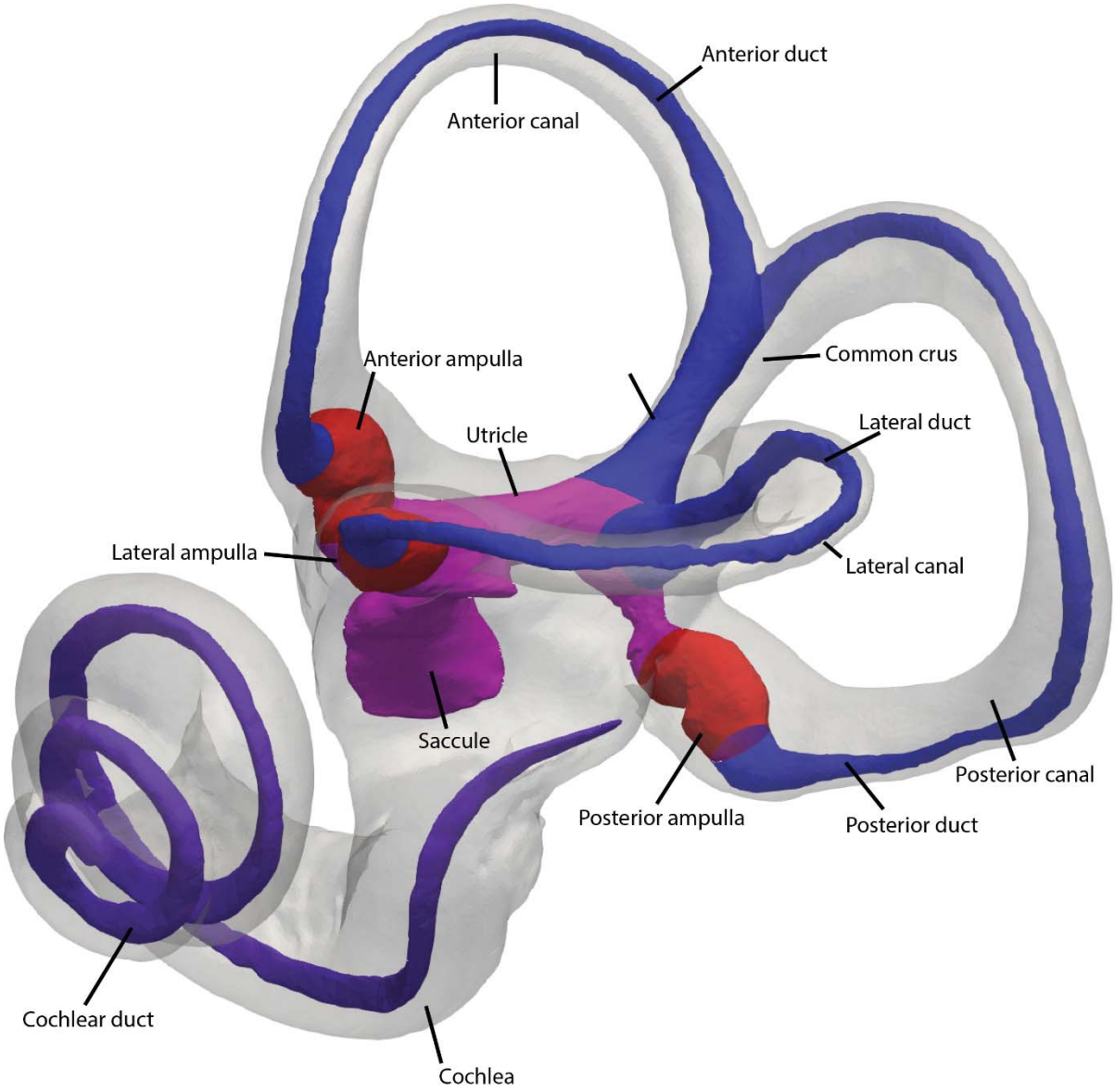

Figure 1. 3D model of the human inner ear. The bony labyrinth (shaded) loosely surrounds the membranous semicircular ducts (blue), the cochlear duct (purple) and the sacciform organs (fucsia).

[1] Based on the definition by the International Anatomical Nomenclature Committee (1983), we use 'semicircular canal' for the bony structure, and 'semicircular duct' for the membranous duct found inside the canal.

is divided into the spherical recess inferiorly (which contains the utricle) and the elliptical recess superiorly (which houses part of the saccule). The membranous labyrinth is totally immersed in the perilymphatic fluid and is suspended within the osseous labyrinth, to which it is anchored (and, hence, also to the temporal bone) by fine trabecular bone filaments (Rabbitt et al., 2004). Each semicircular duct is formed by a slender portion and by the associated ampulla, an enlarged structure containing the sensory organs: the crista ampullaris and the cupula. The crista ampullaris is a crest-like ridge of the ampullary wall that protrudes into the lumen of the ampulla and is covered with a sensory epithelium formed by hair cells. In turn, the cupula embeds the cilia of the hair cells. The semicircular canals closely mirror the path and size of the ducts, which are tacked against the outer margin of the latter (Blanks et al., 1975; Spoor, 1993; Clarke, 2005; Hullar, 2006; Ifediba et al., 2007). The ducts, however, occupy a variable amount of canal volume, inversely proportional to the size of the animal (Igarashi et al., 1981, 1986; Ramprashad et al., 1984; Hashimoto et al., 2005), thus preventing to reliably infer the radius, volume, and lumen cross-sectional area of the ducts from their bony encasing (Curthoys et al., 1977; Ramprashad et al., 1984).

Due to their high mineralization, petrosal remains are common in the fossil record—often being well preserved even in very crushed specimens (e.g., Rook et al., 2004; Benoit et al., 2013). Therefore, they provide a wealth of morphological data amenable to paleobiological inference from either a functional or a phylogenetic viewpoint (e.g., Spoor, 1993; Spoor et al., 2007; Lebrun et al., 2010, 2012; Ni et al., 2010; Wu et al., 2014; Mennecart et al., 2017). Indeed, together with the external morphology of the temporal bone—which is very informative from a phylogenetic perspective (e.g., Van Kampen, 1904; Van Der Klaauw, 1931; MacPhee, 1981)—the shape of inner ear can be used to identify fossil species even in the lack of associated remains (Benoit et al., 2013; Braga et al., 2013). The otic capsule (i.e., the bony labyrinth) possesses the additional advantage of being stable from an ontogenetic viewpoint, due to its ossification in early prenatal stages (between the 17th and the 19th week of gestation in humans; Jeffery & Spoor, 2004) and the lack of subsequent remodeling during development (Curthoys, 1982; Dechesne et al. 1986; Jeffery & Spoor, 2004). This enables a straightforward comparison between juveniles (or even infants) and adults.

1.2.2. Function of the vestibular system

The vestibular system provides vertebrates with the ability of detecting and controlling their own motion in the environment (Highstein, 2004), being fundamental for navigation (Fitzpatrick et al., 2006; Valerio & Taube, 2016), motor coordination (Owen & Lee, 1986; Berthoz, 1991; Mergner et al., 1997) and spatial awareness (Angelaki & Cullen, 2008). These functions are fulfilled by means of complex interactions between the vestibular system and the proprioceptors of several muscles,

which generate the vestibulo-ocular and vestibulocollic reflexes (serving to stabilize the gaze and head motion through movement; Berthoz & Pozzo, 1988; Bronstein, 1988; Pozzo et al., 1990; Dunbar et al., 2004, 2008; Highstein, 2004; Cox & Jeffery, 2008; Rabbitt, 2019), as well as the vestibulospinal reflexes (contributing to the maintenance of posture; Allum & Honegger, 1998; Allum et al., 1998; Creath et al., 2008).

From a macromechanical perspective, the semicircular ducts work as inertial sensors, responding to angular accelerations and parsing the acceleration vector into three components—each carried by a canal nerve and transmitted to the central nervous system through the eighth cranial nerve (e.g., Yamauchi et al., 2002; Chang et al., 2004; Rabbitt et al., 2004; Rabbitt, 2019). When the head undergoes angular accelerations, the endolymph adjacent to the membranous ducts moves jointly with them and with the cranium, whereas the fluid in the center of the duct lumen shows a velocity lag due to momentum conservation. This causes the displacement of endolymph within the semicircular ducts and a corresponding deformation of the cupula—which is captured and traduced by the hair cells into a spike train modulation in the afferent nerves (Yamauchi et al., 2002). The movement of the endolymph along the ducts can be described by the general expression for momentum conservation of an incompressible fluid, based on Newton's second law, and can be linked to cupular volume displacement. Considering a simplified model restricted to the single toroid loop identified by one semicircular canal, cupular displacement is governed by the mass of the moving endolymph, the damping of the fluid's movement, and the cupular stiffness, following a second-ordinary differential equation. Thus, the amount of endolymph mass and the damping are inversely proportional to the integrated and squared integrated local area of the duct cross-section, respectively (Rabbitt et al., 2004; Rabbitt, 2019). As a direct consequence, the direction of the mechanical response is dominated by the orientation of the slender portion of the ducts (Rabbitt et al., 2004; Rabbitt, 2019). The interactions among the ducts have been described by increasingly sophisticated models (Oman et al., 1987; Van Buskirk, 1987; Damiano & Rabbitt, 1996; Rabbitt, 2019), also considering the interaction of all three canals at the same time (Rabbit, 1999; Ifediba et al., 2007). Based on these models, it is also possible to link cupular deformation to the rotation of the head (i.e., angular head velocity), and to define the two different (slow and fast) time constants. The slow time constant (τ_1) is approximated by the ratio of cupular stiffness and movement damping, while the fast time constant (τ_2) roughly corresponds to the quotient between the damping of the movement and the mass of the displacing endolymph. Both govern the reaction of the system to a stimulus. Specifically, τ_2 determines how rapidly the cupula deforms after an impulse occurring at time $t = 0$, while τ_1 governs the following phase of slow recovery to zero. Notably, τ_1 is relatively insensitive to uniform changes in the size of the ducts, while τ_2 is directly proportional to the cross-sectional duct area.

On the basis of these constants, two contrasting (the slow-sensitive and the fast-sensitive) hypotheses have been proposed. Based on the assumption that larger animals have slower head movements, Jones and Spells (1963) asserted that large animals have large sensitive canals to detect slow head movements, while small animals have minute and less-sensitive canals to prevent overstimulation caused by rapid head accelerations occurring during fast movements. According to these fundaments of the slow-sensitive hypothesis, the frequency spectrum of head movements would be the most important factor driving the evolution of canal and duct morphology. Hence, evolutionary changes in the canal radius of curvature (R), in the ductal radius, and in their shape, would be determined by the need to match the resulting time constants with the head movement frequency range typical of a species (Muller, 1999). Hence, the absolutely larger canals of larger animals may achieve a downward shift in frequency range to accommodate for their presumably slower and lower-frequency head movements (Jones & Spells, 1963; Howland, 1973). In contrast, empirical studies indicate that fast-moving animals display, on average, a larger radius of curvature than slower taxa of similar body mass. This pattern was first discovered by Gray (1908) on the small semicircular canals of sloths, and is found in many other vertebrate groups, such as birds (Tanturri, 1933; Turkewitsch, 1934; Hadziselimovic & Savkovic, 1964; Money & Correia, 1972; Ramprashad et al., 1986), carnivorans (Grohé et al., 2016, 2018; Schwab et al., 2019), rodents (Bhagat et al., 2020), and primates (Matano et al., 1985, 1986; Spoor & Zonneveld, 1998; Spoor et al., 2007). Based on this evidence, the fast-sensitive hypothesis argues that 'agile' animals (i.e., showing acrobatic or very rapid locomotion repertoires) require larger, and thus more sensitive, canals to detect fine differences in their rapid head accelerations.

Neither of the aforementioned hypotheses entirely explains the correlation between observed locomotor behaviors and semicircular canal size and shape. Malinzak (2010) challenged both hypotheses and proposed that the main selection pressure on the shape of the semicircular canals is the orientation of the axes of mean sensitivity. This so-called 'fast-accurate' hypothesis postulates that stimuli occurring along specific directions and around definite axes are best interpreted by the vertebrate brain. As consequence of how the movement is presented to the central nervous system by the vestibular afferent nerves, the brain would most accurately quantify angular velocities occurring about specific axes of mean sensitivity (Malinzak, 2010). Thus, selection would act to align the axes of mean sensitivity with those of habitual rotations experienced by the animal, consequently enhancing fitness. Stemming from this hypothesis, Malinzak et al. (2012) further linked locomotor modes to the deviation from orthogonality of the canals: species with more orthogonally oriented canals would be more proficient to process head accelerations of greater magnitude and coming from any direction, thus allowing a more agile locomotor repertoire. Such assumption, however, does not take into account the mechanical

coupling of the anterior and posterior canals (and ducts) in the common crus—which alters the overall sensitivity of the system—or the amplification or compensation of the neural discharge occurring in the vestibular afferents (Muller & Verhagen, 1988). It is noteworthy that the relative orientation of the vertical canals modulates the sensitivity for pitch and roll head movements. Particularly, it is higher for accelerations occurring about the pitch axis when the anterior and posterior canals form an obtuse angle, and when they are of different shape and size (Muller & Verhagen, 2002a,b,c)—two conditions that are often found in species frequently engaging in fast suspensory behaviors (Le Maître et al., 2017; Gonzales et al., 2019).

Independently from the controversial interpretation of the mechanics and function of the vestibular apparatus—which is outside the scope of this dissertation—the two aforementioned time constants are possibly the only proxy for measuring the balancing capabilities of particular species. Unfortunately, experimental values for these constants, which require very complex biophysical models, are known for very few primate species, such as humans (Oman et al., 1987; Muller & Verhagen, 2002a,b,c; Rabbitt et al., 2004; David et al., 2016), squirrel monkeys (Rabbitt et al., 2004; David et al., 2016), and macaques (David et al., 2016). However, it is reassuring that improvements in staining techniques, which permit the fixation of the fragile duct membranes (Metscher, 2009), coupled with the increasing resolution of CT scans, have recently enabled a preliminary inspection of the vestibular system morphology in 25 mammal species (including 13 primates) and thus offer the prospects for inferring the value of the time constants also in fossil taxa (David et al., 2019).

1.2.3. The evolution of semicircular canal morphology: state of the art

Studies of inner ear morphology can be traced back to the 19th century, with the seminal work of Hyrtl (1845) on the comparative anatomy of the mammalian middle and inner ear, based on the casts of the air-filled cavities of macerated temporal bones. Nevertheless, except for a few descriptive analyses of the great ape inner ear published toward the end of the 19th century and most of the 20th century (Denker, 1899a,b; Berg, 1903; Gray, 1907, 1908; Altmann & Vermes, 1933; Takahashi, 1976), the inner ear morphology of most primates and mammals remained understudied until about three decades ago. Advances in computed tomography techniques—in particular, the advent of microcomputed tomography (μCT), which currently allows a very high resolution even for sizable remains—and the increase of the available facilities for digital imaging at a reduced cost provided a brand new non-destructive approach to explore the structures concealed inside extant and fossil specimens. The consequent increasing interest in inner anatomy has been dramatic and virtual

paleontology has flourished during the last 25 years (see reviews in Balzeau et al., 2010; Weber & Bookstein, 2011; Cunningham et al., 2014; Sutton et al., 2016). Inner ear structures, in particular, gained a considerable amount of attention. Spoor (1993) was the first to explore, by means of CT scanning, the labyrinthine morphology of fossil hominins as well as to analyze human inner ear anatomy from a phylogenetic and paleobiological perspective (Spoor et al., 1994; Spoor & Zonneveld, 1998; Spoor et al., 2003). Following these pioneering studies, several research lines arose during the 2000s. These may be distinguished based on their scope (inferring locomotion, understanding ontogeny, and reconstructing phylogenetic affinities) or on methodological grounds (use of standard morphometrics based on linear measurements vs. three-dimensional geometric morphometrics [3DGM]).

Habitat preferences. Changes in semicircular canal morphology have been used to trace some major adaptive shifts in vertebrate evolution, especially during the transition from terrestrial to aquatic life in various tetrapod clades. In particular, the changeovers experienced by crocodylomorphs (during the Mesozoic) and cetaceans (by the Eocene) are among the best documented in the fossil record (Thewissen et al., 2001; Motani, 2009) and have been investigated from the perspective of semicircular canal shape. This is because, in addition to pervasive changes in the appendicular skeleton, adaptation to the aquatic environment also implies a rearrangement of the axial skeleton. Among others, the neck progressively shortens and loses mobility, thus directly affecting the vestibulocollic reflex efficiency (Ketten, 1992; Spoor & Zonneveld, 1998). This is the most plausible cause of the patent atrophy of the canals in both whales and crocodylomorphs, where they appear much smaller than what expected based on body mass (Spoor & Zonneveld, 1998; Spoor et al., 2002; Ekdale, 2013; Schwab et al., 2020) and brain size (Spoor, 1997; Spoor & Zonneveld, 1998). However, the tempo and mode of these evolutionary processes in cetaceans and crocodylomorphs appear quite different. A vestigial vestibular system is already present in the earliest crown cetaceans, thus preceding postcranial adaptations (Spoor et al., 2002). In contrast, the reduction of the canals was more progressive in crocodylomorphs, possibly as a consequence of a more gradual reduction of neck length (Schwab et al., 2020).

Ecological niches are also linked to semicircular canal shape to some extent. For example, among lungless salamanders (Plethodontidae) it is possible to discriminate between species inhabiting complex microhabitats—which possess robust and highly curved semicircular canals, suggesting enhanced vestibular senses—from cave specialists—where the vestibular system appears much reduced, possibly hinting at relaxed selection pressures on the vestibulo-ocular reflex (Capshaw et al., 2019). Similarly, the fossorial caecilians exhibit a great reduction of the semicircular canals (as compared to other amphibians), coupled with a unique elaboration of the sacculus

(Maddin & Sherratt, 2014). Despite the presence of a strong phylogenetic signal (and the doubtful results obtained for lacertid lizards; Vasilopoulou-Kampitisi et al., 2019), canal shape could be used to distinguish among different ecomorphs in *Anolis* lizards (Dickson et al., 2017) and squamate reptiles as a whole (Palci et al., 2017), as well as to trace the numerous emergences of aerial descent behaviors in this order (Boistel et al., 2011). The morphology of the semicircular canals is also related to ecological niches among other groups. Hence, it is possible to distinguish between semiarboreal (Pfaff et al., 2017) and semiaquatic (Grohé et al., 2016) carnivorans, due to differences in canal size and shape; fossorial squirrels from arboreal and gliding squirrel species, with the latter displaying different canal proportions and larger diameters overall (Pfaff et al., 2015); between arboreal and terrestrial opossums, the latter displaying smaller lateral canals (Sánchez-Villagra & Schmelzle, 2007; Schmelzle et al., 2007); and between pelagic and coastal porpoises (but not odontocetes as a whole; Costeur et al., 2018) by means of canal orientation (Racicot et al., 2016). It has also been demonstrated that semicircular canal size may reflect hunting strategies in carnivorans, with species using pounce and pursuit predation showing larger canals (Grohé et al., 2018) than pursuit or opportunistic feeders (Schwab et al., 2019).

Locomotor inferences. Several researchers have attempted to infer the function of the vestibular system exclusively based on bony labyrinth morphology, to gain insight into the paleobiology of extinct animals. The first and most widely used method for predicting locomotion relies on the correlation between semicircular canal radius and duct sensitivity (see Section 1.2.2). In different vertebrate groups, the correlation between canal radius and body mass displays a negative allometric relationship (Jones & Spells, 1963; Spoor & Zonneveld, 1998; Spoor et al., 2007). By taking this size-scaling relationship into account, several comparative studies have shown (e.g., Gray, 1907, 1908; Tanturri, 1933; Turkewitsch, 1934; Hadziselimovic & Savkovic, 1964; Money & Correia, 1972; Matano et al., 1985, 1986; Schmelzle et al., 2007), albeit not without criticism (e.g., Hopkins, 1906; David et al., 2010; Malinzak, 2010; Malinzak et al., 2012; Rae et al., 2016; Benson et al., 2017), that fast-moving animals possess larger radii (particularly that of the lateral canal) than their slower counterparts. Within primates, hominids possess smaller semicircular canals than expected based on body size, which has been related to their overall slow and deliberate locomotion (Spoor & Zonneveld, 1998; Spoor et al., 2007). Despite sharing with great apes the possession of small canals overall, *H. sapiens* displays particularly large vertical canals relative to the lateral. This discrepancy was used to trace the emergence of bipedalism in the hominin lineage (Spoor et al., 1994), as the size of the anterior and posterior canals would have played a critical role in stabilizing the body while moving bipedally. Albeit with some criticism (Graf & Vidal, 1996), Spoor et al. (1994) found that *Homo erectus* was the oldest hominin displaying modern human-

like semicircular canal proportions, whereas both *Paranthropus* and *Australopithecus* retained a great ape-like condition—thereby suggesting that australopiths would have been less committed to habitual terrestrial bipedalism than *Homo*.

Canal radius has also been used to reconstruct the evolution of locomotion in many primate clades (Walker et al., 2008; Silcox et al., 2009; Ni et al., 2010; Ryan et al., 2012) by relying on the six 'agility categories'—ranging from very slow (for sluggish and cautious species, showing small canal radii) to very fast (in the case of swift and acrobatic taxa, possessing enlarged radii)—defined by Spoor et al. (2007). Based on these analyses, many Paleocene and Eocene primates (with the exception of notharctid adapiforms), based on their relatively small radius, have been interpreted as fairly slow-moving species showing a lesser amount of leaping behaviors than most other primates (Silcox et al., 2009). In turn, the plesiomorphic condition for anthropoids was reconstructed as slow and deliberate, as already displayed by the earliest stem anthropoids *Parapithecus* and *Apidium*, contrasting with the fast and agile locomotion inferred for the basal stem anthropoid *Proteopithecus* and stem platrryhines as a whole (Ryan et al., 2012). A medium to slow locomotion would have been retained by the stem catarrhines *Catopithecus* and *Aegyptopithecus*, as well as by the more advanced stem catarrhine *Saadanius*. In contrast, the crown catarrhine LCA, the stem hominoid *Ekembo*, and the stem cercopithecoid *Victoriapithecus* were inferred as capable of a more agile and jerky locomotion (Ryan et al., 2012). The results for *Victoriapithecus* are concordant with the locomotor behaviors displayed by extant cercopithecoids, but the agile locomotion inferred for *Ekembo* contrasts with its postcranial morphology, indicating that it rather engaged in powerful-grasping arboreal pronograde quadrupedalism and cautious climbing and clambering (Ward et al., 1991, 1993; Ward, 1993, 2015; Kelley, 1997; Walker, 1997; Nakatsukasa, et al., 2004; Dunsworth, 2006; Daver & Nakatsukasa, 2015). Ryan et al. (2012) recovered a markedly slow locomotion for the analyzed Miocene hominoids (namely, *Hispanopithecus*, *Rudapithecus*, and *Oreopithecus*), which was related to their postcranial adaptations for below-branch suspensory behaviors (Begun, 1992a; Ward, 2015a). Based on the purported relationship between canal radius and agility, it is noteworthy that the evidence provided by semicircular canals is inconclusive as to whether the hominoid LCA possessed large semicircular canals (indicative of agile locomotion) like *Ekembo* and hylobatids—implying that hominids subsequently evolved smaller canals due to the adoption of a slower locomotion—or whether it was a slow-moving species with small canals (with the condition of hylobatids representing a secondary reversal to the stem hominoid condition; Ryan et al., 2012).

Aside from canal radius, an experimental study conducted on 11 strepsirrhine species found a strong correlation between canal orthogonality (defined as the overall deviation from 90° among angles between canals of one side of the head) and log-transformed agility scores. This correlation also holds for mammals as a whole (Berlin

et al., 2013) and has been purportedly proposed as a much more reliably proxy than canal radius for inferring agility. Hence, swift-moving species would possess more orthogonally oriented canals, capable of processing angular accelerations from any direction with constant accuracy (Malinzak et al., 2012). The latter authors found a greater range canal orientation variability in slow-moving species, as confirmed by 3DGM analyses of strepsirrhine and platyrrhine primates (Perier et al., 2016; Gonzales et al., 2019). Their increased variation could be a consequence of relaxed selection pressures as a result of the less demanding (in terms of accuracy) cautious locomotor behaviors performed by these species (Billet et al., 2012).

Although the use of 3DGM techniques has become widespread in paleoanthropology (see reviews in Adams, Rohlf, & Slice, 2013; Gunz & Mitteroecker, 2013), very few analyses (mostly limited to strepsirrhines and platyrrhines) have used them to investigate the relationship between semicircular canal shape and locomotion (Perier et al., 2016; Gonzales et al., 2019). This might be a consequence of the complex three-dimensional morphology of the canals, which hinders the precise definition of many homologous landmarks. A comparative study including three extant apes (namely, *G. gorilla*, *P. pygmaeus*, and *P. troglodytes*), the hylobatid *Hylobates lar*, and modern humans concluded that semicircular canals can be used to distinguish hominoid species based on their positional behaviors (Le Maître et al., 2017). However, in that study the various species show considerable overlap in shape—probably due to the very limited number of landmarks used—and each locomotor type is represented by one or two species only, making it impossible to discern whether the observed differences are actually due to locomotion.

Based on the assumption that the lateral canal would be held horizontal to most efficiently record rotational head movements occurring in that plane (Schoenemann, 1906; Girard, 1923; Ledebkin, 1924; de Beer, 1947; Van Der Klaauw, 1947; Dujim, 1951; Vidal et al., 1986)—as in this position the sensory hair cells of the semicircular canal and its associated ampulla would result perpendicular to it (Fitzpatrick et al., 2006; Graf & Klam, 2006; Hullar, 2006)—its orientation has been used as a proxy for inferring 'at rest' and 'alert' head postures. Despite some inconsistencies documented in the same studies, this relation was taken for granted by numerous authors and has been largely used to reconstruct head posture in extinct species (e.g., Spoor et al., 1993; Witmer et al., 2003; Hullar, 2006; Sereno et al., 2007), leading to lively discussion on various topics such as the evolution of hominin bipedalism (Benoit-Gonin & Lafite-Dupont, 1907; Fitzpatrick et al., 2006). In the last decades, various studies criticized such a relation in different vertebrate groups (e.g., Witmer et al., 2008; Araújo et al., 2017; Benoit et al., 2017; Coutier et al., 2017) and observed that there is a considerable amount of deviation in both mammals (~20–30° upward pitching; de Beer, 1947; Vidal et al., 1986; Schellhorn, 2018) and birds (between −15° and 50°; Dujim, 1951; Marugán-Lobón et al., 2013). A very recent experimental analysis conducted on a large sample

of ungulates identified a loose correlation between neutral head posture and lateral canal orientation, while diet (browsing vs. grazing), presence/absence of head-butting behavior, and phylogeny would be more tightly related to neutral head posture (Benoit et al., 2020). The orientation of the lateral canal would rather be influenced by how the head is maintained in motion, thus discouraging the use of lateral canal orientation for neutral head stance inferences.

Evolutionary constraints. The ossification of the otic capsule is well known, especially in humans (e.g., Bast, 1942; Jeffery & Spoor, 2004), marsupials (Sánchez-Villagra & Schmelzle, 2007) and ruminants (Mennecart & Costeur, 2016). However, the evolutionary constraints that affect the final shape of the semicircular canals are still a matter of debate. Several studies hypothesized that the spatial constraints imposed by brain size, as well as basicranial length and orientation, largely affect labyrinthine morphology (Spoor et al., 1994; Hublin et al., 1996; Spoor & Zonneveld, 1998; Jeffery & Spoor, 2004; Jeffery et al., 2008). Indeed, brain growth and development appear as one of the most relevant factors influencing basicranial morphology, especially in the midline flexion (Ross & Ravosa, 1993; Jeffery & Spoor, 2002) and petrous pyramid orientation (Dean, 1988). Such proposals are in line with the association found between the orientation of the cranial base and that of the labyrinth in the sagittal plane among mammals (e.g., Villemin & Beauvieux, 1934; Delattre, 1951; Fenart & Deblock, 1973) and with the basicranial morphology of humans (Spoor & Zonneveld, 1998). Hence, the coronally rotated petrous pyramid and labyrinth could be related to the highly flexed human basicranium, and the consequent need to accommodate a very large brain in a relatively short cranial base (Spoor, 1997; Spoor & Zonneveld., 1998). The overall size of the cranium is also related to the osseous labyrinth shape (Muller, 1999). Thus, in highly derived dog breeds, such as the brachycephalic pug, the very reduced cranial space influences the orientation of the anterior and posterior canals, which depart much more from orthogonality than in dolichocephalic breeds (Smith & Laitman, 2020; Smith et al., 2020). Similarly, it has been suggested that the extremely enlarged cochlea of laryngeal echolocating bats spatially constrains the shape of the anterior canal, which is more vertically compressed than in Old World fruit bats (Davies et al., 2013).

It has also been hypothesized that semicircular canal morphology is related to the shape and size of the subarcuate fossa (Spoor, 1993; Spoor & Leakey, 1996; Jeffery & Spoor, 2006). The fossa is found in prenatal stages of all primates, but is secondarily obliterated after birth in hominids and in some large-bodied cercopithecoids (Spoor & Leakey, 1996) and lemurs (Gannon et al., 1988). When present in adult individuals, it expands within the petrosal bone from the endocranial cavity, being encircled by the bony encasing of the anterior canal. It houses the petrosal lobule of the cerebellar paraflocculus (Bolk, 1906; Gannon et al., 1988), a portion of the vestibulocerebellum,

which is involved in managing the vestibulo-ocular reflex (Leung et al., 2000; Xiong & Nagao, 2002). Using a phylogenetically informed multivariate regression, Jeffery et al. (2008) confirmed the size of the subarcuate fossa has a significant positive correlation with the overall size of the anterior canal and the width of the posterior canal. However, these results must be interpreted with caution, as the reciprocal influence between the paraflocculus and the subarcuate fossa is unclear. These authors were unable to discern whether there is a stretching action of the fossa on the canals, whether the fossa simply expands to fill the space made available by canal radius enlargement, or whether the size of the canals and of the fossa are independently determined by genetic factors (Jeffery et al., 2008).

Sexual dimorphism in semicircular canal shape. With the aim to find reliable proxies for sex estimations of immature individuals in archeological and forensic contexts, and in view of the encouraging results obtained for the external morphology of the temporal bone (Wahl & Graw, 2001), Osipov et al. (2013) identified a number of sexually dimorphic parameters in the semicircular canals of modern humans. In particular, these authors detected a significant sexual dimorphism in semicircular canal height, width, and radius of curvature. These variables were successfully used to classify the individuals by means of gender, both as single variables (with a 76% accuracy) and combined in a multivariate function (84% accuracy). However, the authors did not identify significant differences in cochlear shape, unlike Braga et al. (2019a), according to whom the human cochlea would be sexually dimorphic since early postnatal stages. Admittedly, the differences highlighted Osipov et al. (2013) were quite meager and the authors themselves warned about the possibility of being population-related. Indeed, the results obtained at the time of assessing the sex of two ancient populations of modern humans were unsatisfactory, with only about 60% of the specimens being correctly classified (Ward et al., 2020), thus suggesting that further exploration of sexual dimorphism in the labyrinth should be undertaken in collections of individuals of known sex.

Phylogenetic inferences. The vast majority of research efforts have focused on the functional significance of the mammalian semicircular canals (see Sections 1.2.2 and 1.2.3). However, the potential of labyrinthine morphology for phylogenetic reconstruction was already recognized during the 1990s (Spoor, 1993; Spoor & Zonneveld, 1994a, 1998; Spoor, et al., 1994; Hublin, et al., 1996). In the last two decades, characters derived from inner ear shape have contributed to phylogenetic reconstruction in several mammal groups such as marsupials (Schmelzle et al., 2007), xenarthrans (Billet et al., 2013), notungulates (Macrini et al., 2010, 2013), ruminants (Mennecart et al., 2016, 2017), or even early mammals (Luo et al., 2012). The inner ear

as a whole has also been proven as a very powerful tool to distinguish among placental mammal clades at a high taxonomical level (Ekdale, 2013, 2016).

Regarding primates, the work of Spoor and Zonneveld (1998) represented a milestone in our understanding of labyrinthine diversity, particularly for hominids. These authors first described semicircular canal morphology in a broad primate sample and identified several phylogenetically informative characters in the inner ear shape. The semicircular canal morphology of modern *H. sapiens* was most thoroughly inspected, leading to the identification of several distinctive traits from great apes and monkeys. In particular, modern humans were interpreted as more derived than great apes (except *P paniscus*) in possession of a larger vertical canal than the lateral one, and also more derived than other anthropoids as a whole in several other features. In turn, Spoor and Zonneveld (1998) showed that great apes possess smaller canals than what expected based on body mass and an anterior canal with a lower aspect ratio (shorter than wide) compared with anthropoids. For each great ape genus, Spoor and Zonneveld (1998) also identified some unique features and, based on their results—indicating an overall morphometric uniformity in non-hominid taxa in terms of canal radius size—these authors tentatively reconstructed the crown anthropoid LCA, and possibly that of crown primates as a whole, as most similar to the condition displayed by extant prosimians, ceboids, hylobatids, and *Macaca*. Furthermore, similarities among extant great apes and the Miocene dryopithecine *Rudapithecus* (Spoor & Zonneveld, 1994b) led Spoor and Zonneveld (1998) to support a great ape-like hominid LCA. While these inferences might appear oversimplified, the resolution then available from standard CT scans hardly allowed a proper characterization of the very complex semicircular canal shape in large species, let alone that of the much smaller taxa.

The use of linear measurements for studying inner ear morphology within a phylogenetic context became widespread in the following years, especially for assessing hominin taxonomic affinities (Spoor et al., 2003; Rook et al., 2004; Glantz et al., 2008; Bouchneb & Crevecoeur, 2009; Crevecoeur, 2012; Braga et al., 2013; Lee et al., 2013; Crevecoeur et al., 2016; Hill et al., 2014; Wu, et al., 2014; Gómez-Olivencia et al., 2015; Quam et al., 2016; Wu & Zhang, 2016; Conde-Valverde et al., 2018), yet with just minor improvements in the protocols and techniques employed. The first analysis relying on 3DGM methods with modern μCT data investigated semicircular canal variation in strepsirrhine primates (Lebrun et al., 2010). In addition to supporting inner ear shape as a taxonomic proxy, this study first ascertained the presence of phylogenetic signal in labyrinthine morphology. Lebrun et al. (2010) further suggested that a random walk model of evolution best describes inner ear phenotypic distribution through the morphospace and may be used to reconstruct ancestral morphotypes for the internal nodes of the phylogeny (Sidlauskas, 2008; Lebrun et al., 2010, 2012). Similar approaches have been used to investigate the inner ear

morphology from a phylogenetic perspective in different mammal groups (e.g., Billet et al., 2015; Grohé et al., 2014, 2016; Beaudet et al., 2016a, 2019; Le Maître et al., 2017; Boscaini et al., 2018; Ponce de León et al., 2018; Beaudet, 2019; Costeur et al., 2019). A significant phylogenetic signal has been recovered for different primate clades (del Río et al., 2020; Morimoto et al., 2020), carnivorans as a whole (Schwab et al., 2019), ruminants (Mennecart, et al., 2016), and diprodontian marsupials (Alloing-Séguier, et al., 2013). Somewhat surprisingly, it has been claimed that this would not be the case of extant hominoid vestibular morphology (Le Maître et al., 2017), although such a discrepancy might simply stem from methodological issues related to very small sample size.

The presence of phylogenetic signal in semicircular canal shape has allowed the use of phylogenetically informed methods in extant platyrrhines (del Río et al., 2020) and both extant and fossil anthropoids as a whole (Morimoto et al., 2020). The results obtained for New World monkeys indicate that subfamilies can be distinguished based on canal shape. The morphological disparity among closely related platyrrhine species was less than expected under a stochastic mode of evolution, supporting the view (e.g., Aristide et al., 2018) that disparity particularly increased during the early stages of platyrrhine radiation, being associated with their ecological diversification (del Río et al., 2020). In the latter study, del Río et al. (2020) also identified body size, rather than locomotion, as the main factor driving semicircular canal diversity in New World monkeys, in accordance with previous suggestions based on a small colobine sample (Rae et al., 2016). The results obtained for anthropoids as a whole were similar, with families and (to a lesser extent) subfamilies showing distinctive labyrinthine morphologies. Body mass and brain size were identified as the most influential factors driving semicircular canal shape, whereas no clear locomotion-related patterns could be identified (Morimoto et al., 2020). Considering the distribution of the taxa in their morphospace, the latter authors purportedly identified a 'typical monkey' morphology shared by platyrrhines, cercopithecoids, hylobatids, stem catarrhines (*Aegyptopithecus* and *Epipliopithecus*), and Miocene apes (*Nacholapithecus* and *Oreopithecus*), as opposed to a derived great ape condition (showing limited morphological variation), found also in Plio-Pleistocene hominins (Morimoto et al., 2020).

Overall, the results obtained by analyzing semicircular canal morphology appear very promising and have already shed some light on the phylogeny of multiple mammal clades. Nevertheless, methodologically modern studies have been lagging behind in primates, where more simplistic linear measurement-based protocols are still prevalent. The inspection of semicircular canal shape with adequate techniques, the definition of phylogenetically informative characters in a cladistic fashion, the quantification of intraspecific/interindividual variability, and the

morphological inspection of currently scarcely known species, all may substantially contribute to our knowledge on anthropoid primate evolutionary history.

1.3. Aims, scope, and structure

1.3.1. Scope and specific aims

During the Miocene, several catarrhine lineages of African origin dispersed into Eurasia and subsequently radiated there. In Europe, both pliopithecoids and hominoids have been recorded. However, despite intensive research efforts during the last decades, their phylogenetic relationships remain controversial, owing to pervasive homoplasy as well as the patchy and fragmentary nature of their available fossil record. A more in-depth investigation of anatomical areas not very prone to homoplasy is thus crucial to better resolve the phylogeny of fossil catarrhines. This dissertation focuses on the morphological study of the bony labyrinth semicircular canal and vestibule morphology, in search for phylogenetically informative morphological characters to help clarifying the phylogenetic relationships of European Miocene catarrhines.

As explained above, the potential suitability of this anatomical area for phylogenetic inference in fossil primates is a priori justified by the high fossilization potential of the petrosal bone, by the fact that its morphology is established in early ontogenetic stages and not remodeled thereafter, and by the promising results previously obtained for other mammalian groups. While previous studies have been performed on the primate inner ear, most have focused on hominins and relied on metrical variables. In contrast, this is the first study specifically devoted to the morphology of the semicircular canals in non-hominin catarrhines and the first one that applies to it an innovative 3DGM approach that is landmark-free and, as such, not biased by the subjective definition of a landmarking protocol. While previous studies generally relied on the entire inner ear, this dissertation focuses on the semicircular canals and vestibule. The cochlea was excluded because previous research has shown it to embed low phylogenetic signal, probably due to a functional link between cochlear morphology and hearing capabilities.

Three main specific aims were planned for this dissertation:

(1) To determine whether deformation-based 3DGM methods adequately capture semicircular canal and vestibule shape variation among anthropoid primates, as well as to evaluate if this method represents any advantages over traditional (landmark-based) 3DGM techniques.

(2) To quantify the amount of phylogenetic signal embedded in semicircular canal and vestibule morphology, as well as to compare it with its functional signal (presumably related to locomotor adaptation), in order to further evaluate the potential of this area for phylogenetic reconstruction among fossil catarrhines.
(3) To use the results of the 3DGM analyses to test competing phylogenetic hypotheses for specific Miocene European pliopithecoids and hominoids of debated affinities, using both discrete characters defined in a cladistic fashion and phenetic methods based on ancestral state reconstruction.

1.3.2. Structure of this work

This dissertation is structured into four main sections subdivided into various chapters. The first section includes the Introduction (Chapter 1) and the Materials and Methods (Chapter 2). The second section (Results) consists of three published papers (Chapters 3 to 5), which constitute the main corpus of this work. The third section, in turn, includes the Discussion (Chapter 6) and Conclusions (Chapter 7). Finally, the fourth section (Literature cited) provides the references cited in Chapters 1, 2, 6 and 7, as each of the published papers have their own citations.

The introductory chapter provides the necessary background to contextualize the more specific topics treated in the various published papers. It is divided into two main subsections: one devoted to the evolutionary history of catarrhines, and another that summarizes state-of-the-art knowledge on the inner ear. The Materials and Methods section, in turn, details the fossil sample studies, the composition of the extant and fossil comparative sample, and the various analytical and statistical techniques used in the framework of this dissertation.

The three papers included in the Results section have already been published in first quartile journals indexed by the Journal Citation Reports. They are the following:

- Urciuoli, A., Zanolli, C., Beaudet, A., Dumoncel, J., Santos, F., Moyà-Solà, S., Alba, D. M., 2020. The evolution of the vestibular apparatus in apes and humans. *eLife* 9, e51261. https://doi.org/10.7554/eLife.51261
- Urciuoli, A., Zanolli, C., Beaudet, A., Pina, M., Almécija, S., Moyà-Solà, S., Alba, D. M., 2021. A comparative analysis of the vestibular apparatus in *Epipliopithecus vindobonensis*: Phylogenetic implications. *J. Hum. Evol.* 151, 102930. https://doi.org/10.1016/j.jhevol.2020.102930
- Urciuoli, A., Zanolli, C., Almécija, S., Beaudet, A., Dumoncel, J., Morimoto, N., Nakatsukasa, M., Moyà-Solà, S., Begun, D. R., Alba, D. M., 2021. Reassessment of the phylogenetic relationships of the late Miocene apes *Hispanopithecus* and *Rudapithecus* based on vestibular morphology. *Proc. Natl. Acad. Sci. USA* 118, e2015215118. https://doi.org/10.1073/pnas.2015215118

In the Discussion, the results and conclusions of the three published papers are discussed together and in relation to the recently published literature to justify the main conclusions of this dissertation, which are succinctly provided in the final chapter. The Discussion and Conclusions are structured around three main topics, corresponding to the aforementioned specific aims: methodological advances in the morphological study of the primate inner ear; phylogenetic signal embedded in the semicircular canals and prospects for the future regarding morphology-based phylogenetic inferences; and insights on the phylogenetic relationships of selected Miocene European catarrhines (the pliopithecoid *Epipliopithecus* and the hominoids *Oreopithecus*, *Rudapithecus* and *Hispanopithecus*).

Chapter 2:
Materials and methods

Chapter 2. Materials and methods

2.1. Sample composition

2.1.1. Studied fossil sample

We studied the semicircular canal and vestibule morphology of three fossil catarrhines from the Miocene of Europe: the pliopithecoid *Epipliopithecus vindobonensis*, from the karstic infillings of Devínska Nová Ves (Slovakia), and the dryopithecines *Hispanopithecus laietanus* and *Rudapithecus hungaricus*, from Can Llobateres 2 (Spain) and Rudabánya (Hungary), respectively. The *E. vindobonensis* sample comprises three petrosal bones from two individuals (originally described by Zapfe, 1961): NMB OE 303a, b (individual III, left and right), housed at the Naturhistorisches Museum of Basel (Switzerland); and NHMW 1970/1397/0003 (individual II, right), housed at the Naturhistorisches Museum of Wien (Austria). *Hispanopithecus laietanus* is represented by a single petrosal from a male individual (IPS18000; Moyà-Solà & Köhler, 1993, 1995) housed at the Institut Català de Paleontologia Miquel Crusafont (Spain). The material of *R. hungaricus* includes the right petrosal of a female partial cranium (RUD 200; Kordos & Begun, 2001a; Gunz et al., 2020) and both petrosals of a male partial cranium (RUD 77; Kordos, 1987; Kordos & Begun, 1997), both housed in the Geological Museum of the Mining and Geological Survey of Hungary.

The *Epipliopithecus* NHMW 1970/1397/0003 specimen was scanned with a Viscom X8060 scan (Viscom XT9190-THP X-ray tube) at the Vienna μCT-Lab (Austria), obtaining a voxel size of 22 μm, while NMB OE 303 petrosals were scanned with a GE Phoenix Nanotom at the Biomaterials Science Centre of the University of Basel (Switzerland), achieving a voxel size of 25 μm. The petrosal of *Hispanopithecus* was scanned at the Centro Nacional de Investigación sobre la Evolución Humana (CENIEH) in Burgos (Spain), with a GE Phoenix V|Tome|x s 240 scanner, obtaining a voxel size of 29.5 μm. The μCTs of *Rudapithecus* were made available by David Begun and by the Max Plank Institute for Evolutionary Anthropology (Leipzig, Germany). They were scanned at the latter institution with a Skyscan 1172, obtaining a voxel of 13.6 μm. Additional scanning parameters are summarized in Table 2.1.

Table 2.1. Summary of the μCT parameters for the studied material

Family	Species	Catalog No.	Voltage	Current	Voxel size
Pliopithecidae	*Epipliopithecus vindobonensis*	NHMW 1970/1397/0003	120 kV	240 μA	22.0 μm
Pliopithecidae	*Epipliopithecus vindobonensis*	NMB OE 303a	180 kV	30 mA	25.0 μm
Pliopithecidae	*Epipliopithecus vindobonensis*	NMB OE 303b	180 Kv	30 mA	25.0 μm
Hominidae	*Hispanopithecus laietanus*	IPS18000	125 kV	120 μA	29.5 μm
Hominidae	*Rudapithecus hungaricus*	RUD 200	100 kV	100 μA	13.6 μm
Hominidae	*Rudapithecus hungaricus*	RUD 77 R	100 kV	100 μA	13.6 μm
Hominidae	*Rudapithecus hungaricus*	RUD 77 L	100 kV	100 μA	13.6 μm

2.1.2. Comparative material

Extant comparative sample. The extant comparative sample comprises a total of 198 μCT scans of dried crania and isolated petrosal bones, belonging to 31 species from 30 extant anthropoid genera, including all hominid genera and a selection of platyrrhines, cercopithecoids and hylobatids (Table 2.2). The voxel size for the comparative sample ranges from 10 μm to 130 μm. The majority of the μCT scans were downloaded from the MorphoSource digital repository (https://www.morphosource.org). The extant human sample includes specimens downloaded from FigShare digital repository (https://www.figshare.com) and μCT scans kindly provided by Jose Braga. Sergio Almécija also provided access to some hylobatid and bonobo scans. The μCT scans of some of the *Pan*, *Gorilla,* and *Pongo* individuals were downloaded from the European Synchrotron Radiation Facility "heritage database for palaeontology, evolutionary biology, and archaeology" (http://paleo.esrf.eu/). Even though some of the specimens belong to juvenile individuals, this should not influence the shape of their semicircular canals and vestibule, because the ossification of the bony labyrinth occurs during early prenatal stages and is not remodeled thereafter (Jeffery & Spoor, 2004; Perier et al., 2016).

Fossil comparative material. The fossil comparative sample comprises a total of seven anthropoid fossil taxa (Table 2.3). The μCT scans of crania of the stem anthropoid *Parapithecus grangeri* (Bush et al., 2004), the propliopithecoid *Aegyptopithecus zeuxis* (Simons et al., 2007), and of the stem platyrrhines *Dolichocebus gaimanensis* (Kay et al., 2009) and *Homunculus patagonicus* (Fulwood et al., 2016), together with the 3D surface of the inner ear of the hominin *Australopithecus* (Beaudet et al., 2019), were downloaded from Morphosource.org digital repository. The scan of *Oreopithecus bambolii* left petrosal (originally published by Rook et al., 2004) was kindly provided by Lorenzo Rook and downloaded from a digital repository (http://www.geo.unifi.it/ricerca/bambolii.htm). Masato Nakatsukasa and Naoki

Morimoto provided access to the slice stack of *Nacholapithecus kerioi* left isolated petrosal.

Table 2.2. Summary of extant anthropoids included as comparative sample. Sample size (*n*) is given for each species.

Family	Species	*n*
Aotidae	*Aotus trivirgatus*	5
Atelidae	*Alouatta Alouatta*	5
Atelidae	*Ateles geoffroyi*	5
Callitrichidae	*Callithrix argentata*	5
Cebidae	*Cebus apella*	5
Cebidae	*Saimiri sciureus*	5
Pithecidae	*Callicebus moloch*	5
Pithecidae	*Pithecia monachus*	5
Cercopithecidae	*Cercocebus torquatus*	5
Cercopithecidae	*Cercopithecus mitis*	5
Cercopithecidae	*Chlorocebus pygerythrus*	5
Cercopithecidae	*Colobus guereza*	5
Cercopithecidae	*Erythrocebus patas*	5
Cercopithecidae	*Lophocebus aterrimus*	5
Cercopithecidae	*Macaca fascicularis*	5
Cercopithecidae	*Mandrillus sphinx*	5
Cercopithecidae	*Miopithecus talapoin*	5
Cercopithecidae	*Nasalis larvatus*	5
Cercopithecidae	*Papio anubis*	5
Cercopithecidae	*Piliocolobus badius*	5
Cercopithecidae	*Presbytis hosei*	5
Cercopithecidae	*Presbytis rubicunda*	5
Cercopithecidae	*Theropithecus gelada*	5
Cercopithecidae	*Trachypithecus cristatus*	5
Hylobatidae	*Hoolock hoolock*	7
Hylobatidae	*Hylobates lar*	10
Hylobatidae	*Symphalangus syndactylus*	6
Hominidae	*Pongo* spp.	9
Hominidae	*Gorilla gorilla*	11
Hominidae	*Pan paniscus*	5
Hominidae	*Pan troglodytes*	12
Hominidae	*Pan* sp.	6
Hominidae	*Homo sapiens*	12

Table 2.3. Extinct anthropoid species included in the fossil comparative sample.

Species	Catalog No.	Voltage	Current	Voxel size
Parapithecus grangeri	DPC 18651	140 kV	200 µA	35.3 µm
Aegyptopithecus zeuxis	CGM 85785	160 kV	150 µA	56.0 x 56.0 x 63.8 µm
Dolichocebus gaimanensis	MACN 14128	150 kV	160 µA	47.0 µm
Homunculus patagonicus	MPM-PV 3501	165 kV	130 µA	40.0 µm
Homunculus patagonicus	MPM-PV 3502	165 kV	140 µA	39.0 µm
Homunculus patagonicus	MPM-PV 3503	165 kV	140 µA	44.0 µm
Oreopithecus bambolii	BAC 208	200 kV	3 mA	29.1 µm
Nacholapithecus kerioi	BG 42744	50 kV	50 µA	50.0 µm
Australopithecus sp.	StW 573			88.0 µm
Australopithecus sp.	StW 578			66.6 µm

2.1.3. Digital sample preparation

Prior to 3DGM analyses, the μCT slice stacks were segmented in Avizo 9.0.1 (FEI Visualization Sciences Group, Hillsboro, USA) to generate the 3D virtual models of the bony labyrinth cavities. When the canals were air filled, such as in the case of most extant specimens and some fossil remains (e.g., NMB OE 303, RUD 200 and RUD 77), the segmentation was performed using a semiautomatic procedure with the 'Watershed' module of Avizo. In several instances, the canals were partially or completely filled by sediments with poor contrast relative to fossilized bone, thus requiring a mostly manual segmentation. The 3D model of the entire bony labyrinth was generated in Avizo using a constant 'Constrained smoothing' (to prevent shrinkage of the surface volume) of 2.5. Afterwards, the 3D mesh of the semicircular canals and vestibule was separated from the cochlea to allow a direct comparison of

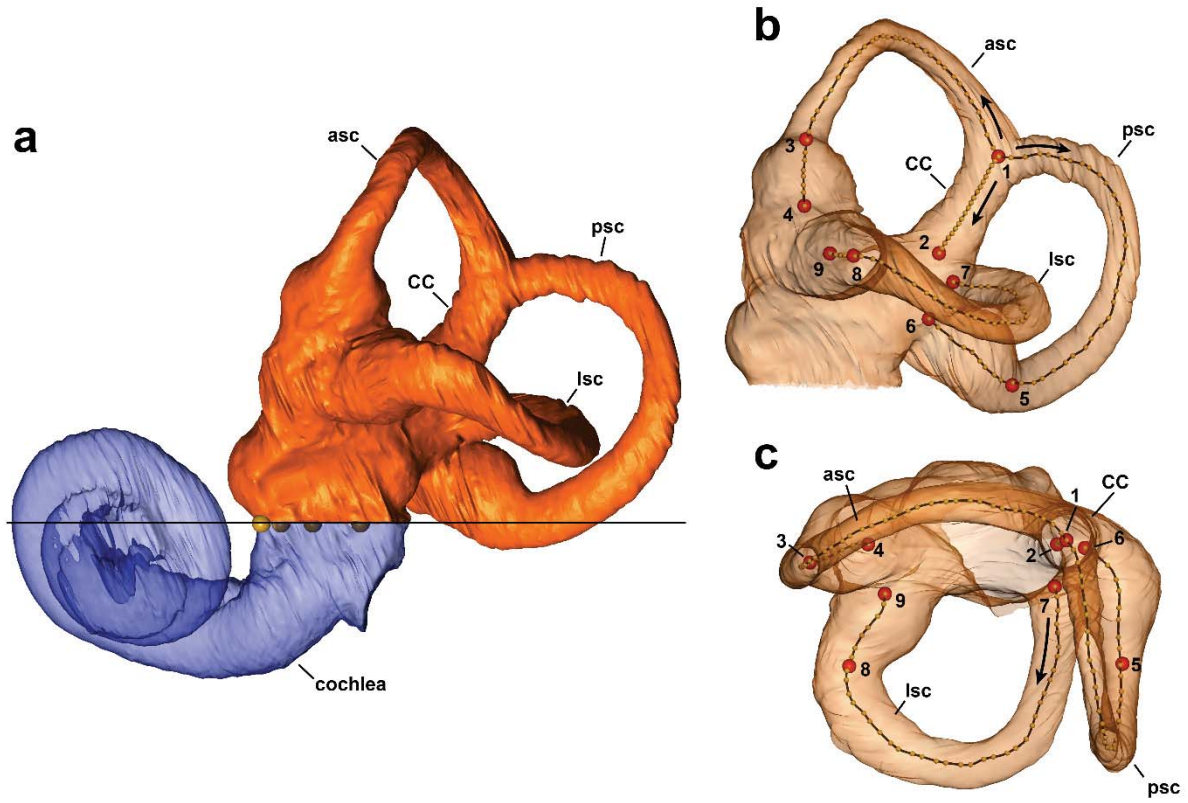

Figure 2.1. Renderings of the bony labyrinth (**a**) and of the semicircular canals and vestibule (**b, c**) of *Hispanopithecus laietanus* (right side, here mirrored). **a**) The semicircular canals and vestibule (orange) have been detached from the cochlea (blue) by cutting along a reference plane (in black) identified by lanmarkds (yellow spheres) placed below the oval window. **b**, **c**) lateral (b) and superior (**c**) views of the semicircular canals and vestibule. Landmarks (1–9, red spheres) have been placed at the starting/eding points of each canal and of the common crus, and at the connection between the slender and ampullary regions of each canal. Semilandmarks (small yellow spheres) have been placed along canal streamlines (black lines), always following the same direction (black arrows)

their shape with deformation-based 3DGM. To do so, we cut immediately inferior to the saccule and the oval window, using a set of landmarks, placed along the maximum curvature of the junction between the vestibule and the cochlea, as a reference for placing the cutting plane (Fig. 2.1a).

The holes derived from to the insertion of the vestibular nerves and the vestibular aqueduct on the bony encasing of the canals and vestibule, the separation from the cochlea, and the large aperture corresponding to the oval window, were filled in Geomagic Studio v. 2014.3.0 (3D Systems, Rock Hill, USA) using a flat patch of triangles. The artifacts derived from the 3D model generation (self-intersections and non-manifold edges) were removed with the 'Mesh Doctor' tool of the same software. Before shape analyses (see below), we used the refined 3D meshes to compute the streamline of the canals and of the common crus using the 'Auto Skeleton' module in Avizo. The obtained 3D lines were cut into four segments corresponding to each of the canals and to the common crus. For all the canals, the streamline was trimmed in correspondence of the connection between the canal ampulla and the vestibule. In the case of the lateral canal and of the common crus, an additional cut was performed along the junction between the slender portion of the canal and the vestibule. Finally, the anterior and posterior canals were separated from each other and from the common crus where they three streamlines connect in the common crus (Fig. 2.1b,c).

2.2. Semicircular canal shape analyses

2.2.1. Volumetric proportions

We inspected semicircular canal shape in terms of volumetric proportions by computing the allometric regression between canal length and volume. The total length (in mm) of the canals was obtained in Avizo as the sum of the lengths the of their streamlines and of that of the common crus. Semicircular canal volume (in mm^3) was computed in Geomagic: the canals and the common crus were separated from the vestibule using the starting/ending points of the streamlines as a reference, and holes produced by the cutting were filled with a flat surface to allow volume measurements. The relationship between canal length and volume was investigated using a bivariate ordinary least squares (OLS) linear regression of log-transformed (natural-logs, ln) cube root of the volume vs. log-transformed length of the canals for the whole anthropoid sample, as well as for hominids and non-hominid anthropoids separately. In the OLS method, the best fit line is computed by minimizing the sum of squared residuals (Warton et al., 2006), which are the deviations along the y-axis from the best-fit line. The regression line for non-hominid anthropoids was used as the baseline to

compute allometric residuals for extant and fossil specimens, as well as inferred ancestral morphotypes (see below). Allometric grade shifts between the two data subsets (i.e., similar scaling relationships at different intercepts) were inspected by means of analysis of covariance (ANCOVA). The latter may be used to test for significant differences between group intercepts when the null hypothesis of homogeneity in slopes cannot be rejected (Sokal & Rohlf, 1995).

2.2.2. Geometric morphometric analyses

Morphometrics is the quantitative study of form (size and shape) among living organism. Traditional morphometric methods rely on linear measurements, angles, and shape ratios, which provide a useful first approximation to both size (measured by scalar variables, i.e., those measured in units, such as length, area, volume, mass, etc.) and shape (measured by dimensionless variables, such as ratios and angles). Nevertheless, traditional morphometric methods are not particularly well suited to capture shape information on complex three-dimensional structures. This can be done more efficiently by means of geometric morphometric methods developed during the last two decades of the 20th century, which represented a huge revolution in morphometric analysis (Rohlf & Marcus, 1993; Adams, et al., 2004).

Standard two- and three-dimensional geometric morphometrics (2DGM and 3DGM, respectively) rely on the geometrical homology of biological structures identified in all the investigated specimens, generally by means of landmarks, (Bookstein, 1991; Dryden & Mardia, 1998), which are used to quantify differences in shape between them with a mathematical function (Bookstein, 1991). This landmark-based approach proved extremely powerful for the characterization of shape differences and soon became widespread across the life-sciences community (see reviews in Mitteroecker & Gunz, 2009; Lawing & Polly, 2010; Adams, et al., 2013). Three types of landmarks are used in geometric morphometrics (Bookstein, 1991; Dryden & Mardia, 1998). Type I landmarks correspond to homologous points that can readily be identified (e.g., foramina, ligament attachments on bones, etc.). Type II landmarks, in contrast, are defined by a local geometric property (e.g., maximum curvature). Finally, type III landmarks are found at the extremal point or at the centroid of a particular structure, and they are the least reliable because they largely depend on a subjective determination of their location (Bookstein, 1991). In addition to standard landmarks, curves and surfaces may also be described by means of semilandmarks (Bookstein, 1991; Gunz et al., 2005; Gunz & Mitteroecker, 2013), which rely on curve-to-curve and surface-to-surface geometric homology. The landmark configurations for a given sample are then aligned via Procrustes superimposition, which standardizes scale, position, and orientation of the landmark configurations. Also, it converts geometric distances into Procrustes distances (usually approximated

by the Euclidean distances between configuration coordinates), which is the natural measure of shape differences in Procrustes shape space (also known as Kendall space; Kendall, 1984).

This dissertation uses landmark-based 3DGM methods, previously shown to be more efficient than standard linear measurements in capturing the shape variation of the semicircular canals (e.g., Gunz et al., 2012). However, the performed analyses and interpretations mostly rely on a recently-described, alternative 3DGM method, based on deformation that is here applied for the first time to the study of semicircular canal and vestibule shape, and indeed the results provided by both methods for the anatomical structure under study are critically compared.

Landmark-based 3DGM analysis. On the basis of the streamlines obtained for the canals and common crus, we followed the simplified landmarking protocol defined by Gunz et al. (2012), which combines Type I landmarks with semilandmarks. This protocol was preferred over alternative ones, which rely exclusively on Type III landmarks, thus implying a higher uncertainty in landmark homology. A total of nine landmarks were located: three at the connection of the ampulla of each canal with the vestibule, one per canal at the transition between the canal ampullary and slender portions, one at the junction between the slender part of the lateral canal and the vestibule, one placed where the common crus merges with the vestibule, and one were the common crus meets with the anterior and posterior canals. In addition, we described the 3D trajectory of the streamlines with a total of 140 semilandmarks (40 for each of canal and 20 for the common crus), which were specifically designed to describe curved paths (Bookstein, 1991, 1997; Gunz & Mitteroecker, 2013). We then slid the semilandmarks in R, a procedure that optimizes semilandmark placement and removes the effects of an arbitrary spacing, using a customized script provided by Jean Dumoncel. The raw landmark coordinates were then converted into shape coordinates by means of generalized Procrustes alignment (Rohlf & Slice, 1990), via the 'procSym' function of the package *Morpho* v. 2.7 (Schlager, 2017) in RStudio v. 1.1.453 for R v. 3.6.1 (R Core Team, 2019). The obtained Procrustes aligned shape data was analyzed in R as explained below.

Deformation-based 3DGM analysis. Mainstream landmark-based geometric morphometrics methods are undoubtedly very powerful for describing shape variation, but there is an inherent subjectivity in the definition of landmarking protocols. For structures with a complex 3D shape (such as the bony labyrinth of the inner ear), finding a suitable landmarking protocol is not a trivial issue, as differences in the design of the landmarking protocol might potentially lead to different results. To circumvent these issue, some landmark-free and homology-free approaches have been developed (e.g., Chung et al., 2003; Reuter et al., 2006; Boyer et al., 2010;

Gorczowski et al., 2010). Nevertheless, these methods must make strong assumptions on the topology of the surfaces and have mathematical limitations, thus being problematic for meshes with irregularities (such as are those generated by the segmentation of fossil specimens). Deformation-based 3DGM methods have been designed as a response to these problems (Glaunès & Joshi, 2006; Durrleman et al., 2012a,b), being successfully applied to medical (Durrleman et al., 2014), developmental (Durrleman et al., 2012a), and paleoanthropological issues (Dumoncel et al., 2014; 2020; Beaudet et al., 2016a,b).

To describe the morphological variability of 3D continuous surfaces in a given sample, deformation analyses consider the meshes embedded in the 3D space and iteratively measure shape variation in terms of deformations of the underlying space to warp one to another. The deformations are then mapped using diffeomorphisms—i.e., mathematical functions characterized by being invertible (each input corresponds to a single output, and vice versa) and smooth (they are continuous and their derivatives are continuously differentiable). Diffeomorphisms are useful to link manifolds, i.e., differential geometry objects that allow to map the shape of an object without losing information about its topology. From an operational viewpoint, the first step computes an average model of the included surfaces (the template, representative of the sample) and identifies a set of control points (placed near the most variable parts of the template). Then, the template is warped to each specimen using the diffeomorphic function, in a way that preservers the topological constraints of the studied structures (preventing self-intersection of the vertices). Eventually, a set of momentum vectors are attached to the control points and used as deformation parameters for each included mesh (identifying the magnitude and direction of the displacement of the control points).

Similar to landmark-based 3DGM analyses—which rely on a Procrustes superimposition—deformation-based techniques require minimizing the distances between the faces composing each surface prior to the analysis. To meet this prerequisite, the surfaces are first decimated in Avizo to include the same number of faces, and then manually aligned to ensure that their anatomical orientation is correct. Subsequently, the 3D models are iteratively and automatically aligned to a reference model using the 'Align Surfaces' module of Avizo with the 'rigid + uniform scale' option, which minimizes the distances between the surface faces by scaling, translating and rotating the analyzed meshes. Shape analysis of the aligned surfaces was performed using the function 'estimate' of the Python-based software Deformetrica v. 3 (Durrleman et al., 2014) and v. 4 (Bône et al., 2018). Further technical information on the software can be found in the dedicated website (https://www.deformetrica.org/) and in the associated Wikia (https://gitlab.com/icm-institute/aramislab/deformetrica).

Due to the high computational requirements of this method, the calculations were performed in cluster computers. In the first and exploratory study, deformation analyses were conducted at the Calcul en Midi-Pyrénées (CALMIP; Toulouse, France) supercomputing center, using Deformetrica v. 3. This facility consists of a cluster supercomputer using CPUs for calculations and required ~10,000 core hours for each analysis attempt (used for the analysis described in Chapter 3). Following the advances of deformation methods (Bône et al., 2018), the remaining computations (Chapters 4 and 5) were performed on GPU chipsets at the Barcelona Supercomputing Center (BSC, Barcelona, Spain), using the MinoTauro cluster. The latter consists of a total of 39 nodes, each equipped with 2 K80 NVIDIA GPU cards, and it required a much reduced number (~100) of core hours per analysis.

Shape data analysis. The shape data generated by both analyses are highly multidimensional. Hence, to investigate the patterns of shape variation occurring in these data, we relied on principal components analysis (PCA) and on between-group principal components analysis (bgPCA), both allowing the projection of multivariate datasets in few dimensions while preserving as much variance as possible. In the case of the PCA, the dimensional reduction is achieved by computing composite variables (the components) that are a combination of the original variables and orthogonal one to the other by definition (Hotelling, 1933; Jolliffe, 1986; Jackson, 1991; Reyment & Jöreskog, 1993). A bgPCA is a type of PCA that allows to further reduce data dimensionality and enhances pre-existing differences between groups. To do so, a PCA is run on the covariance matrix of the group means and the original sample is plotted onto the newly generated morphospace a posteriori (Mitteroecker & Bookstein, 2011). While a PCA is mostly exploratory and allows a first inspection of shape data, a bgPCA allows to assess the distinctiveness of the groups defined a priori and may be used for classification. Both PCA and bgPCA were performed with the *ade4* 1.7-16 R package (Dray & Dufour, 2007).

In view of recent concerns on the use of bgPCA for 3DGM shape data (Bookstein, 2019; Cardini et al., 2019), we took multiple precautions to prevent spurious grouping, such as using a broad sample (Rohlf, 2020) with large groups (>>10 individuals). To ensure that grouping structure was not spurious, we compared the discrimination among groups in the configuration spaces and in the obtained morphospaces using different strategies. In Chapter 3, we computed a standard PCA, to visually inspect the presence of group separation not caused by the bgPCA. Similarly, a hierarchical clustering analysis, computed with the R packages *caret* v. 6.0–84 (Kuhn, 2008) and *Factominer* v. 1.34 (Lê et al., 2008) on the raw shape data, was used to ascertain the presence of a high percentage of correctly classified individuals according to the groups used in the bgPCA. Alternatively, in Chapters 4 and 5 we followed the recent suggestions by Polly and Cardini (2020). Thus, in addition to standard bgPCA, we

computed a cross-validated version of the analysis using a leave-one-out approach (Schlager, 2017; Cardini et al., 2019). This type of cross-validation consists in removing one individual at a time, using the remaining individuals from the sample to iteratively compute the analysis. The cross-validated scores were then visually compared to those of the original bgPCA to check for differences (Cardini & Polly, 2020). This analysis was computed using the 'groupPCA' function of *Morpho* v. 2.6 R package (Schlager, 2017; Cardini et al., 2019).

Additionally, Polly and Cardini (2020) suggested to test for group mean differences based on the raw shape data, the bgPCA, and the cross-validated bgPCA scores, by means of a permutational analysis of variance (PERMANOVA). Similar to regular analysis of variance (ANOVA), which enables the evaluation of differences among the mean values of predefined group, a PERMANOVA enables testing for differences in the ordination of group centroids, with equivalency in centroids and dispersion of the groups as the null hypothesis. Hence, a rejection of the null hypothesis ($p < 0.05$) implies differences in either the centroids and/or the group dispersions. This analysis is not performed on the actual ordination of the variables, but on the underlying distance matrices. In the case of null hypothesis rejection (that is, when the differences between group centroids and/or group dispersion are significant), it is also relevant ascertaining the amount of variance (R^2) explained by group differences for the raw shape space and for bgPCA and cross-validated bgPCA morphospaces, marked differences in R^2 (low in the raw data and higher for bgPC scores) are indicative of spurious grouping (Cardini & Polly, 2020). The PERMANOVA (1,000 permutations) was performed on the Euclidean distances between group means using the 'adonis' function of *Vegan* v. 2.6 R package (Oksanen et al., 2013), which also allows the computation of the R^2.

The correlation between semicircular canal shape and size (i.e., allometry) was assessed for both the raw shape data (deformation fields) and the bgPC scores (Chapter 3). For the raw shape data, we used a multivariate regression of deformation fields against the log-transformed cube root of the whole vestibular apparatus (canals and vestibule, in mm). The volume was measured in Geomagic prior to the alignment of the surfaces and used as a proxy of semicircular canal and vestibule size. Allometry in bgPCA results was tested by means of bivariate regressions computed for each bgPC against the log-transformed cube root of canal volume (in mm; excluding the vestibule, as described in Section 2.2.1). The multivariate and the bivariate regressions were computed for the whole anthropoid sample, as well as for two separate subsets (hominids and non-hominid anthropoids). We performed two different types of regressions, based on OLS (see above) and phylogenetic generalized least-squares (PGLS) methods. A generalized least-squares regression (GLS) derives from a generalization of the OLS approach and is used when some of the assumptions of the OLS are violated (such as, the regression is not linear in parameters, the mean of the

error terms is not zero, the errors are correlated with the independent variable; see review Kariya & Kurata, 2004). The PGLS constitutes a special case GLE, where the residuals covariate due to the shared phylogenetic history of the investigated taxa (Rohlf, 2001). Hence, a PGLS adjusts the independent variables using a covariance matrix computed on the basis of the branch lengths and topology of the phylogenetic tree employed.

Posterior probabilities. In addition to the classification done with bgPCA methods, we further assessed morphological affinities between fossil specimens and extant anthropoid clades based on their phenetic distance. To do so, we computed the posterior probability for the fossil specimens to pertain to the multivariate normal distribution of one or more predetermined groups (Wilson, 1981; Ambergen & Schaafsma, 1984; Albrecht, 1992). This approach relies on the distance between the subject and group centroids measured with Mahalanobis distances (D^2)—i.e., multivariate distances that take into account the variance and covariance of the population. Posterior probabilities fall within the 'unrestricted' methods of classification, meaning that they do not assume that the tested individuals must belong to one of the groups, and they reflect the likelihood of a specimen to belong to each defined group separately. A higher probability will be obtained in the case of a shorter distance from the group centroid, while a probability $p < 0.05$ informs us that the specimen does not fit into the group distribution. Please note that, unlike the group probabilities computed with bootstrap procedures, posterior probabilities do not sum to 100%. For the calculation of posterior probabilities, we used the 'typprobClass' function of *Morpho* v. 2.6 R package (Schlager, 2017).

Cluster analyses. The distribution of taxa in the morphospace can be used to ascertain their phenetic similarity by means of cluster analyses. This type of analysis groups the cases included in the sample (in this dissertation, genera) in a way that those pertaining to the same group (cluster) are more similar to each other than to those belonging to other groups. Different measures of phenetic distances and of clustering methods were used in this dissertation. In Chapter 4, Ward's minimum variance clustering method (Ward, 1963) on D^2 distances between pairs of species centroids bgPC scores was used. This hierarchical clustering method starts from an initial step in which all clusters are composed by a single element (agglomerative or bottom-up approach). Subsequently, Ward's method iteratively combines those elements that causes the minimum increase of within-cluster variance after merging. As an alternative approach, Chapter 5 employs neighbor-joining clustering analyses (Saitou & Nei, 1987) performed on Euclidean distances between species mean configurations in the raw shape data (i.e., the deformation fields) and on weighted Euclidean distances (similar to the former but using eigenvalues as a weighing

variable) between pairs of species centroids bgPC scores. Similar to Ward's, neighbor-joining is a bottom-up method that was designed for the creation of phylogenetic trees based on DNA or protein sequence data. Starting from an unresolved tree (with star topology), it iteratively adds nodes to the topology (based on the closest distance between pairs of taxa) and compute branch lengths, until the phylogeny is completely resolved. Hence, it differs from other clustering approaches for not being ultrametric (i.e., branch lengths for different lineages may vary). Different functions and packages were used for performing cluster analyses and computing distance matrices. Ward's cluster analysis was performed using the 'hclust' function of the *stats* R package, while we used the 'nj' function of *ape* v. 5.3 (Paradis & Schliep, 2019) R package to employ a neighbor joining approach. Standard Euclidean distances were measured using the 'dist' generic function included in R, while weighted Euclidean distances were calculated using the 'distances' function of the *distances* v. 0.1.8 package (Savje, 2019).

2.2.3. Phylogenetically informed analyses

Phylogenetic signal. Phylogenetic signal is a measure of the tendency of related species to resemble each other more than species drawn at random from the same phylogeny (Felsenstein, 1985; Harvey & Pagel, 1991; Blomberg & Garland, 2002; Blomberg et al., 2003). It has been used to investigate a plethora of different questions in several research areas, with a variety of proposed metrics to measure it in a quantitative way (e.g., Moran, 1950; Pagel, 1999; Blomberg et al., 2003; Pavoine et al., 2008; Revell et al., 2008). For our purposes, we will focus on two of them: Pagel's λ (Pagel, 1999) and Blomberg's K (Blomberg et al., 2003), as well as on the multivariate generalization of the latter (K_{mult}; Adams, 2014). These metrics relate to a Brownian motion (BM) model of evolution, which would imply that trait evolution follows a random walk along the branches of the phylogenetic tree and that the variance in the distribution of trait values increases proportionally with branch length (Martins, 1996; Pagel, 1999; Blomberg et al., 2003). In both Pagel's λ and Blomberg's K, the null hypothesis of lack of closer similarities among relatives (i.e., the absence of phylogenetic signal) is tested by comparing the observed value with those expected under random trait distribution via a randomization test ($p < 0.05$). However, even if they have been developed for the same scope, the two metrics are computed with different mathematical approaches and thus provide different information.

The statistic λ is a scaling parameter for the phylogeny and defines the influence of species phylogenetic relationships on the covariance matrix of the analyzed traits (Pagel, 1999; Freckleton et al., 2002). Hence, under a pure BM evolutionary model, the covariance of the traits is entirely driven by phylogenetic relatedness, and thus it does not require rescaling ($\lambda = 1$). However, when factors other than phylogeny influence

trait evolution, the weighting of phylogeny must be adjusted ($\lambda < 1$), until the extreme scenario of no phylogenetic correlation ($\lambda = 0$).

Blomberg's K, and its multivariate generalization K_{mult}, is the ratio between the mean squared error computed for the tip data (measured from a phylogenetic corrected mean) and the mean squared error for the variance-covariance matrix obtained for the analyzed phylogeny under BM model of evolution. This ratio is informative of how well a phylogenetic tree reflects the variance-covariance patterns found in the data. K is computed by comparing the obtained ratio with that expected given the topology of the phylogenetic tree, thus allowing the comparison of the results independently from the phylogenetic tree employed (Blomberg et al., 2003). In addition to information on the presence/absence of phylogenetic signal, the K and K_{mult} statistics are informative of the model of evolution that best describes the phylogenetic structure embedded in the shape data. Hence, as for Pagel's λ, a $K \approx 1$ is suggestive of model of evolution that closely resembles BM, while a $K \neq 1$ implies that the model of evolution is not aleatory; for $K < 1$, distantly related taxa resemble each other more than expected under BM (the variance accumulates within clades), possibly as a result of independent adaptation (i.e., homoplasy); in contrast, $K > 1$ is obtained when neighbor taxa are more similar than expected under random-walk model of evolution (the variance accumulates among clades), suggesting that stabilizing selection might have occurred (or else that shape is constrained by other factors).

To estimate phylogenetic signal, we relied on different molecular phylogenetic trees for the extant taxa, taken from Springer et al. (2012) or Arnold et al. (2010)—the latter downloaded from the 10kTrees Website v3 (https://10ktrees.fas.harvard.edu/). Pagel's λ and Blomberg's K were computed for the significant bgPCs using the 'phylosig' function of *phytools* v. 0.6–60 package for R (Revell, 2012), while K_{mult} was obtained in R via the 'physignal' function of the *geomorph* v. 3.1.0 package (Adams et al., 2019).

Phylomorphospace and ancestral state reconstructions. Major patterns of shape variation occurred along the branches of the phylogeny were identified using a phylomorphospace approach (Sidlauskas, 2008), which projects a phylogenetic tree onto a morphospace, and thus enables a straightforward visualization of the direction and magnitude of shape changes, expressed in terms of branch length and orientation. The position in the morphospace of the ancestral states was estimated using a maximum likelihood method for continuous characters (Felsenstein, 1988; Schluter et al., 1997) via the function 'fastAnc' of the R package *phytools*, while the tips of the tree correspond to the bgPC scores of species centroids. The aforementioned molecular-based phylogenetic trees were used as a backbone to add fossil species a posteriori, following different phylogenetic hypotheses for the studied fossil species (Chapters 4

& 5). The divergence of extinct taxa was arbitrary set 1 Myr before the estimated divergence date of the next derived node. Tip age estimates were based chronostratigraphic ages, as summarized in Table 2.4.

Table 2.4. Tip age estimations for the fossil species included in the analyses

Geological age	Species	Tip age	References
Late Oligocene	*Parapithecus grangeri*	29.85 Ma	Seiffer, 2006
Late Oligocene	*Aegyptopithecus zeuxis*	29.85 Ma	Seiffer, 2006
early Miocene	*Dolichocebus gaimanensis*	20.5 Ma	Kay, 2015
early Miocene	*Homunculus patagonicus*	17.2 Ma	Kay, 2015
middle Miocene	*Nacholapithecus kerioi*	14.77 Ma	Nakatsukasa & Kunimatsu, 2009
middle Miocene	*Epipliopithecus vindobonensis*	14.15 Ma	van der Meulen et al., 2011
late Miocene	*Rudapithecus hungaricus*	10.1 Ma	Casanovas-Vilar et al., 2011
late Miocene	*Hispanopithecus laietanus*	9.6 Ma	Alba et al., 2019
late Miocene	*Oreopithecus bambolii*	6.75 Ma	Rook et al., 2011
Early Pliocene	*Australopithecus* sp.	4.0 Ma	Wood & Boyle, 2016

The shape estimated for the internal nodes of the phylogeny (ancestral states) was used as a proxy for the LCA morphotype of several anthropoid clades. The bgPC scores of the LCAs were rotated and translated from the morphospace back into the configuration space, to generate a set of momentum vectors, used to warp the template model into the target LCA morphology in Deformetrica 3 and 4, using the 'shooting' function. The meshes used in deformation analyses lost their original size during the alignment process. However, the 'Transform Editor' module of Avizo provides information about the translation, rotation and scaling that each surface has undergone during alignment. Therefore, on the basis of species scale means, we estimated the scaling factors for the reconstructed LCAs using the 'anc.ML' function included in *phytools* (Revell, 2012). The rescaled LCA surfaces were then used to compute semicircular canal volume and length (see Section 2.1.1).

Cladistic methods. In addition to the phenetic analyses ran on the shape space obtained with 3DGM methods, we also relied on a cladistic approach based on the coding of a number of discrete characters (Chapters 3 and 4). Cladistics is both a systematic school and a method of phylogenetic inference originally devised by Hennig (1966). From the viewpoint of systematics, cladistics relies on the assumption that only clades (strictly monophyletic groups, i.e., those that include all the descendants from a common ancestor) should be defined as taxa. From the perspective of phylogenetic inference, cladistics stress that relatedness among taxa can only be discerned on the basis of shared-derived features (synapomorphies), whereas primitive similarities (symplesiomorphies) cannot evince phylogenetic proximity. Despite multiple problems, cladistics has been shown to be a powerful tool for morphology-based phylogenetic reconstruction and has become mainstream among paleontologists during the last decades.

Usually, to undertake a cladistic analysis, morphological variability is described in terms of characters that display two or more mutually exclusive states (Pimentcl & Riggins, 1987). Character states may be 'plesiomorphic' (primitive) or 'apomorphic' (derived), although these terms are relative to the clade of reference. Only shared-derived features (synapomorphies) are phylogenetically informative (i.e., useful to support a phylogenetic hypothesis), as opposed to symplesiomorphies (shared primitive features), constant characters, and autapomorphies (uniquely derived features). Cladistic analysis relies on the principle of maximum parsimony, which minimizes the number of changes in character states to find the simplest explanation of the character states distribution for a given taxon-character matrix. The resulting most parsimonious cladograms, depicting dichotomous sister-taxon relationships, but not ancestor-descendant hypotheses, are considered the hypothesis that has more explanatory power and, hence, the most likely hypothesis. Independently evolved character states (homoplasies), as opposed to homologies (those inherited from a common ancestor), introduce noise to phylogenetic reconstruction. However, from an epistemological viewpoint they cannot be identified a priori, but must be determined a posteriori based on the most parsimonious cladogram.

The characters and character states defined in the course of this dissertation for the semicircular canals could be integrated with pre-existing data matrices in the future to improve the phylogenetic analyses of extinct catarrhines. However, it makes no sense to perform a cladistic analysis based on a single anatomical area. Therefore, our approach relied on mapping such characters on multiple cladograms based on the molecular phylogeny of extinct taxa and several alternate hypotheses for the extinct taxa under consideration. First, we computed tree length (i.e., the sum of the number of changes occurring in all the considered characters for a given topology) to ascertain which hypothesis was the most parsimonious. Three indices customarily used in cladistics (Farris, 1989) were also computed to assess character congruence and hence evaluate the most parsimonious hypothesis: the consistency index (CI), the retention index (RI), and the rescaled consistency index (RC). The CI of a cladogram the minimum number of steps implied by a given taxon-character matrix independently from tree topology relative to the actual amount of change occurring in the most parsimonious cladogram (Kluge & Farris, 1969). The CI would equal 1 in the hypothetical case of no homoplasy, and is inversely proportional to the amount of homoplasy in the most parsimonious cladogram. The latter also applies to the RI, which further reflects how well the identified synapomorphies explain the tree. It is computed by dividing the difference between the maximum and observed amount of character change by the difference between the maximum and minimum amount of character change for a given topology. Finally, the RC is computed as the product of RI and CI; it stretches the range of the CI such that its minimum theoretically

attainable value is rescaled to 0, with its maximum remaining at 1 (Farris, 1989). These indices were computed with PAUP* v. 4.0a168 for Mac (Swofford, 2003).

Chapter 3:

The evolution of the vestibular apparatus in apes and humans

Reprinted from:

Urciuoli, A., Zanolli, C., Beaudet, A., Dumoncel, J., Santos, F., Moyà-Solà, S., Alba, D. M., 2020. The evolution of the vestibular apparatus in apes and humans. *eLife* 9, e51261. https://doi.org/10.7554/eLife.51261

eLIFE elifesciences.org

RESEARCH ARTICLE

The evolution of the vestibular apparatus in apes and humans

Alessandro Urciuoli[1]*, Clément Zanolli[2], Amélie Beaudet[3,4], Jean Dumoncel[5], Frédéric Santos[2], Salvador Moyà-Solà[1,6,7], David M Alba[1]*

[1]Institut Català de Paleontologia Miquel Crusafont, Universitat Autònoma de Barcelona, Cerdanyola del Vallès, Barcelona, Spain; [2]Laboratoire PACEA, UMR 5199 CNRS, Université de Bordeaux, Pessac, France; [3]School of Geography, Archaeology and Environmental Studies, University of the Witwatersrand, Johannesburg, South Africa; [4]Department of Anatomy, University of Pretoria, Pretoria, South Africa; [5]Laboratoire AMIS, UMR 5288 CNRS, Université de Toulouse, Toulouse, France; [6]Institució Catalana de Recerca i Estudis Avançats (ICREA), Barcelona, Spain; [7]Unitat d'Antropologia (Departament de Biologia Animal, Biologia Vegetal i Ecologia), Universitat Autònoma de Barcelona, Cerdanyola del Vallès, Barcelona, Spain

Abstract Phylogenetic relationships among extinct hominoids (apes and humans) are controversial due to pervasive homoplasy and the incompleteness of the fossil record. The bony labyrinth might contribute to this debate, as it displays strong phylogenetic signal among other mammals. However, the potential of the vestibular apparatus for phylogenetic reconstruction among fossil apes remains understudied. Here we test and quantify the phylogenetic signal embedded in the vestibular morphology of extant anthropoids (monkeys, apes and humans) and two extinct apes (*Oreopithecus* and *Australopithecus*) as captured by a deformation-based 3D geometric morphometric analysis. We also reconstruct the ancestral morphology of various hominoid clades based on phylogenetically-informed maximum likelihood methods. Besides revealing strong phylogenetic signal in the vestibule and enabling the proposal of potential synapomorphies for various hominoid clades, our results confirm the relevance of vestibular morphology for addressing the controversial phylogenetic relationships of fossil apes.

***For correspondence:**
alessandro.urciuoli@icp.cat (AU);
david.alba@icp.cat (DMA)

Competing interests: The authors declare that no competing interests exist.

Funding: See page 28

Received: 21 August 2019
Accepted: 18 January 2020
Published: 03 March 2020

Reviewing editor: Jessica C Thompson, Yale University, United States

Introduction

Catarrhine primates (Old World anthropoids) include two extant subclades: cercopithecoids (Old World monkeys) and hominoids (apes and humans). Based on molecular (e.g., ***Springer et al., 2012***) and paleontological (e.g., ***Harrison, 2013***; ***Stevens et al., 2013***) data, both groups diverged during the late Oligocene (≥25 Ma), but experienced very different evolutionary histories. Hominoids first radiated in the early Miocene of Africa (***Harrison, 2010***; ***Begun, 2013***; ***Begun, 2015***) and subsequently diversified into Eurasia during the middle and late Miocene (***Alba, 2012***; ***Begun, 2015***). Their diversity and geographic distribution (humans excluded) was much greater during the Miocene than at present, being currently restricted to a few genera in southeastern Asia and Africa. In contrast, extant cercopithecoid lineages started to diversify later and experienced a major radiation during the late Miocene (***Jablonski and Frost, 2010***), being currently much more diverse and widely distributed than hominoids in both Africa and Asia.

The decimated current diversity of hominoids, coupled with the fragmentary nature of their fossil record, abundant homoplasy (e.g., ***Larson, 1998***), and the lack of known fossil hylobatids prior to the latest Miocene (***Harrison, 2016***) make it difficult to confidently infer the phylogenetic relationships of extinct hominoids and thus reliably infer the morphotype of the last common ancestor (LCA)

eLife digest Humans, gorillas, chimpanzees, orangutans and gibbons all belong to a group known as the hominoids. This 'superfamily' also includes the immediate ancestors and close relatives of these species, however in many instances the evolutionary relationships between these extinct ape species remain controversial.

While DNA can help evolutionary biologists to work out how living species are related to one another, fossils are typically the principle source of information for extinct species. Inferring evolutionary relationships from fossils must be done with caution, but the bony cavity that houses the inner ear – which is involved in balance and hearing and fairly common in the fossil record – has proven useful for tracing the evolution of certain groups of mammals. However, no one had previously looked to see if this structure could give insights into the evolutionary relatedness among living and extinct hominoids.

Urciuoli et al. have now used a 3D imaging technique to capture the complex shapes of the inner ear cavities of 27 species of monkeys and apes, including humans and two extinct apes (*Oreopithecus* and *Australopithecus*). The results confirmed that the shape of these structures most closely reflected the evolutionary relationships between the species and not, for example, how the animals moved.

Urciuoli et al. went on to identify features of these bony chambers that were shared within several hominoid groups, and to estimate what the inner ears of the ancestors of these groups might have looked like. The results for *Australopithecus*, for example, were consistent with it being most closely related to modern humans than other apes, while those for the enigmatic *Oreopithecus* supported the view that it was a much older species of ape that converged in some respects with other apes still alive today.

The findings highlight the potential of the inner ear for reconstructing the early branches of our family tree. They also offer the prospect of refining the controversial evolutionary relationships within the impressive diversity of extinct ape species.

of various hominoid subclades. This is required not only to adequately understand the evolutionary history of the group as a whole, but also to reconstruct the LCA of chimpanzees and humans, from which the earliest hominins evolved during the late Miocene. The contribution of Miocene apes to debates about hominoid evolution is thus diminished by the numerous controversies about the phylogenetic position of the former.

For example, putative stem hominoids from the early Miocene of Africa (**Begun, 2013**; **Begun, 2015**), such as the proconsulid *Ekembo*, lack most of the synapomorphies of crown hominoids, such that some authors still contend that they might represent stem catarrhines instead (**Harrison, 2010**; **Harrison, 2013**). Even more uncertain is the position of dendropithecids (e.g., *Micropithecus*) and other small-bodied catarrhines from the early to middle Miocene of Africa, which are generally interpreted as stem catarrhines (**Harrison, 2010**; **Harrison, 2013**) but might include stem hominoids as well (**Alba et al., 2015**; **Begun, 2015**). The same controversy applies to the European middle to late Miocene *Pliobates*, recovered as a stem hominoid more derived than proconsulids (**Alba et al., 2015**) or alternatively as a member of the stem catarrhine pliopithecoid radiation (**Nengo et al., 2017**). Regarding undoubted hominoids, the distinction between stem and crown taxa is by no means less controversial, in part due to the virtual lack of fossil hylobatids since their origin in the early Miocene until the latest Miocene (**Harrison, 2016**). This is best exemplified by the late Miocene *Oreopithecus* from Italy, variously considered a hominid (**Moyà Solà and Köhler, 1997**; **Harrison and Rook, 1997**) or a stem hominoid (**Nengo et al., 2017**). Finally, the phylogenetic placement of Miocene apes from Eurasia is also controversial. For example, most Asian forms have been classically considered pongines (**Begun, 2013**), but most recently the late Miocene *Lufengpithecus* from China has been reinterpreted as a stem hominid (**Kelley and Gao, 2012**; **Begun, 2015**). Even more controversial is the position of the middle to late Miocene European dryopithecines, interpreted as either stem hominids (**Alba, 2012**; **Alba et al., 2015**) or hominines (**Begun, 2013**; **Begun, 2015**), and further controversies apply when trying to decipher the phylogenetic relationships among various members of this extinct group.

Deciding among phylogenetic hypotheses for Miocene apes has consequences for our current understanding of hominin origins, from calibrating molecular data to estimate their divergence time to the reconstruction of the ancestral locomotor repertoire from which the earliest bipeds arose. For example, the recently described dryopithecine *Danuvius* from Germany has been used to argue that bipedal and suspensory adaptations characterized the last common ancestor of crown hominids (**Böhme et al., 2019**). However, without a phylogenetic analysis supporting a more basal branching of *Danuvius* compared with the older dryopithecine *Pierolapithecus* (**Moyà-Solà et al., 2004**), which was orthograde but lacked adaptations to both bipedalism and suspension (**Alba et al., 2010**; **Alba, 2012**), the implications for the ancestral condition of the group remain moot.

The recent recovery of enamel proteome sequences from the early Pleistocene (1.9 Ma) fossil pongine *Gigantopithecus* (**Welker et al., 2019**) offers some hope that molecular data will become available for Miocene apes sometime in the future. In the meantime, to better resolve the phylogeny of Miocene hominoids, the search for morphological features not very prone to homoplasy is crucial. Anatomical structures that develop early during development and are not remodeled thereafter (such as the enamel-dentine junction of teeth) represent the best candidates (**Corruccini, 1987**; **Skinner et al., 2008**). In this regard, the inner ear is also a very promising anatomical area (**Spoor and Zonneveld, 1998**; **Spoor et al., 2003**), even if thus far its phylogenetic implications have been mostly explored for fossil hominins only (**Quam et al., 2016**; **Conde-Valverde et al., 2018**; **Ponce de León et al., 2018**; **Beaudet, 2019a**; **Beaudet et al., 2019b**), while its application to fossil apes has been mainly devoted to locomotor inferences (**David et al., 2010**; **Malinzak et al., 2012**; **Rook et al., 2004**; **Ryan et al., 2012**).

Housed in the highly mineralized petrosal bone, which is frequently preserved in the fossil record, the inner ear is composed of a series of endolymph-filled membranes (encased in the corresponding bony labyrinths), namely the cochlea or cochlear duct (involved in hearing) and the vestibular apparatus (devoted to balance and vision stability). The vestibule consists of three (anterior, posterior, and lateral) semicircular canals (SCs) and two macular organs (utricle and saccule). The approximately orthogonal SCs sense angular accelerations and decelerations of the head, while the maculae perceive linear accelerations and thus provide gravity reference (**Spoor and Zonneveld, 1998**; **Rabbitt et al., 2004**; **Johnson Chacko et al., 2018**; **Cheung and Ercoline, 2018**).

Differences in the relative size and morphology of the SCs have been correlated with locomotor agility (**Spoor et al., 1994**; **Spoor et al., 2007**; **Walker et al., 2008**; **Silcox et al., 2009**; **Ryan et al., 2012**; **Perier et al., 2016**) and positional behavior (**Le Maître et al., 2017**), albeit not without criticism (**Rae et al., 2016**; **Benson et al., 2017**; **Coutier et al., 2017**). On the other hand, the bony labyrinth morphology has been considered of great importance for phylogenetic reconstruction in various mammals including hominins (**Quam et al., 2016**; **Conde-Valverde et al., 2018**; **Ponce de León et al., 2018**; **Beaudet, 2019a**; **Beaudet et al., 2019b**) and nonhuman primates (**Lebrun et al., 2010**; **Lebrun et al., 2012**; **Grohé et al., 2016**; **Mennecart et al., 2017**; **Costeur et al., 2018**; **Schwab et al., 2019**). While previous research in hominoids has yielded encouraging results for phylogenetic reconstruction (**Spoor and Zonneveld, 1998**; **Spoor et al., 2003**; **Rook et al., 2004**; **Gunz et al., 2012**), according to some authors phylogeny may not be a major component of ape vestibular morphology (**Le Maître et al., 2017**).

Determining if and to what extent inner ear anatomy reflects phylogeny among extant hominoids is central for assessing the potential of this anatomical area to more confidently resolve the controversial phylogenetic relationships of fossil apes. To provide insight into this question, we use phylogenetically-informed statistical analyses to test the significance and quantify the amount of phylogenetic signal of vestibular shape captured by three-dimensional geometric morphometrics (3DGM) in living hominoids and a broader sample of extant anthropoids. To capture vestibular shape, we mostly rely on a landmark-free, deformation-based 3DGM approach that takes the whole surface into account (**Glaunès and Joshi, 2006**; **Durrleman et al., 2012b**; **Durrleman et al., 2012a**) and enables integrating the spatial trajectory of the semicircular canals with their thickness and volumetric variations, the latter two being more difficult to assess based on mainstream landmark-based 3DGM. Since our results reveal the presence of strong phylogenetic signal in the vestibular morphology, we also employ maximum likelihood methods (**Felsenstein, 1988**; **Schluter et al., 1997**) to reconstruct the ancestral vestibular morphology for the LCA of main hominoid subclades (crown hominoids, hominids, and hominines), with the aim to identify phylogenetically informative characters that can be used in formal cladistic analysis. To test the reliability and illustrate the usefulness of

our approach from a phylogenetic viewpoint, we also include two extinct hominoid taxa: the early hominin *Australopithecus* and the aforementioned controversial late Miocene ape *Oreopithecus*. The well-known phylogenetic placement of *Australopithecus* as the sister-taxon of humans predicts that its vestibular morphology will be somewhat derived towards the modern human condition. On the other hand, our analysis will enable testing the competing phylogenetic hypotheses for *Oreopithecus* (stem hominoid vs. hominid), thereby illustrating the potential of our method for clarifying the controversial affinities of extinct apes.

Results

Semicircular canal shape variation among anthropoids

In spite of a similar spatial configuration of the three SCs, their trajectory, stoutness and relative proportions are quite variable among anthropoids (***Figure 1***). A bgPCA performed among major anthropoid groups (platyrrhines, cercopithecoids, hylobatids, and hominids) enables their accurate distinction (***Figure 2***, ***Figure 2—figure supplement 1a***, ***Figure 2—source data 1***), as shown by classification results (more than 95% individuals correctly classified after cross-validation; ***Table 1***). In particular, bgPC1 discriminates hylobatids from hominids and all the remaining taxa (***Figure 2***, ***Figure 2—figure supplement 1c***). A landmark-based analysis applied to the same sample yields very similar results except for hylobatids, due to the reasons explained in the next section. Shape variation in the analyzed sample accounts for a strong phylogenetic signal (K_{mult} = 1.248, p<0.001), and this also holds for the first three bgPCs separately (see below).

When analyzed individually, we recover a similarly strong phylogenetic signal (λ = 1 and K = 1.15; ***Table 2***) for bgPC1 (68.8% of total variance). bgPC1 captures differences in thickness and cross-section of the SCs, and is also driven by the development of the macular organs relative to the canals. Great apes fall on positive values (***Figure 2***, ***Figure 2—figure supplement 1a***) due to their stout and flattened SCs combined with an extensive vertical compression of the anterior canal, a more anterosuperior insertion of the lateral canal into the vestibule, and a greater volume of the vestibular recesses relative to the canals (***Figures 3a–e***, ***4a–e*** and ***5a–e***). Hylobatids, as well as colobine and papionin cercopithecoids, showing slender and elongated canals but maintaining well developed ampullae, largely overlap on negative values, while cercopithecins and platyrrhines display intermediate values due to their slightly inflated SCs (***Figures 2***, ***3f–h***, ***4f–h*** and ***5f–h***). bgPC2 (19.6% of total variance) also bears strong phylogenetic signal (λ = 0.91; K = 1.51; ***Table 2***), with variance accumulating among rather than within clades (as indicated by K > 1). This axis separates platyrrhines—especially *Ateles* (***Figure 1i***)—from other anthropoids due to the more reduced lateral canal in the former, which is inversely proportional to anterior canal development and vertical elongation (***Figure 2a***). In contrast, *Gorilla* (***Figures 1a***, ***3a***, ***4a*** and ***5a***) occupies the opposite end of the distribution due to its large lateral canal and reduced anterior one, the latter being also vertically compressed, whereas the remaining hominoids show intermediate values along bgPC2. bgPC3 (11.6% of variance), which is driven by both trajectory and relative size of the SCs (***Figure 2b***), still displays a strong and significant phylogenetic signal (λ = 1 and K = 1.16; ***Table 2***). Hylobatids (***Figures 1f–h***, ***3f–h***, ***4f–h*** and ***5f–h***) display the highest scores for bgPC3, as a result of the right to acute angle formed by the apex of the common crus (CC), the latter being also shorter, a more anterosuperiorly projecting and long anterior canal, an obtuse angle between the planes identified by the anterior and lateral canals, and a more developed lateral canal relative to the posterior one, which is also posteriorly oriented. Most of the taxa fall within moderate positive and moderate negative values, with some cercopithecoids (*Cercopithecus*, *Macaca*, *Papio* and *Nasalis,* among others) and *Cebus* occupying the negative end of the distribution. African apes, cercopithecines, and *Nasalis* occupy an intermediate position, being characterized by a well-developed and anteriorly inclined posterior canal, an obtuse to right angle of the CC apex, and an obtuse angle between the vertical canals, combined with a larger lateral canal. Orangutans fall on moderately positive values and are distinguished from other great apes and humans by an anterosuperiorly projecting anterior canal (less than in hylobatids).

When fossil specimens are plotted a posteriori onto the tangent space identified by extant taxa, *Oreopithecus* (BAC 208; ***Figures 1n*** and ***6a***) falls on moderately positive scores for bgPC1 (where the distributions of hominids, cercopithecins, and platyrrhines overlap), while the two

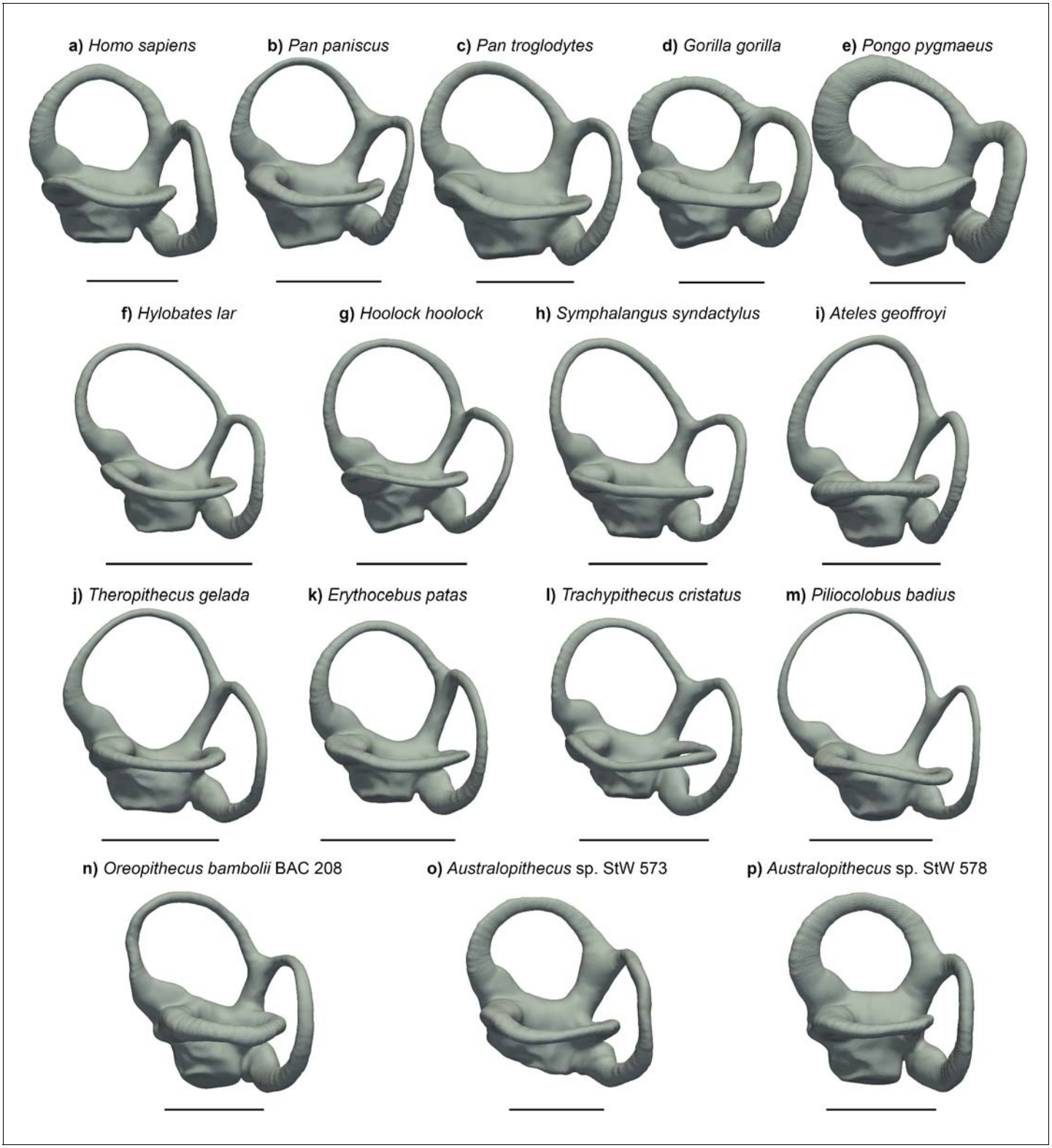

Figure 1. The vestibular apparatus of extant hominoids, other anthropoids, and some fossil hominoids, in lateral view. (**a**) *Homo sapiens* (EMBR 121); (**b**) *Pan paniscus* (MCZ 38019); (**c**) *Pan troglodytes* (AMNH.M 51204); (**d**) *Gorilla gorilla* (AMNH.M 167338); (**e**) *Pongo pygmaeus* (IPS 10647); (**f**) *Hylobates lar* (MCZ 41424); (**g**) *Hoolock hoolock* (AMNH.M 83425); (**h**) *Symphalangus syndactylus* (AMNH.M 106583); (**i**) *Ateles geoffroyi* (MCZ 29628); (**j**) *Theropithecus gelada* (AMNH.M 60568); (**k**) *Erythrocebus patas* (MCZ 47017); (**l**) *Trachypithecus cristatus* (MCZ 35597); (**m**) *Piliocolobus badius* (MCZ 24793); (**n**) *Oreopithecus bambolii* (BAC 208); (**o**) *Australopithecus* sp. (StW 573); (**p**) *Australopithecus* sp. (StW 578). Scale bars equal 5 mm.

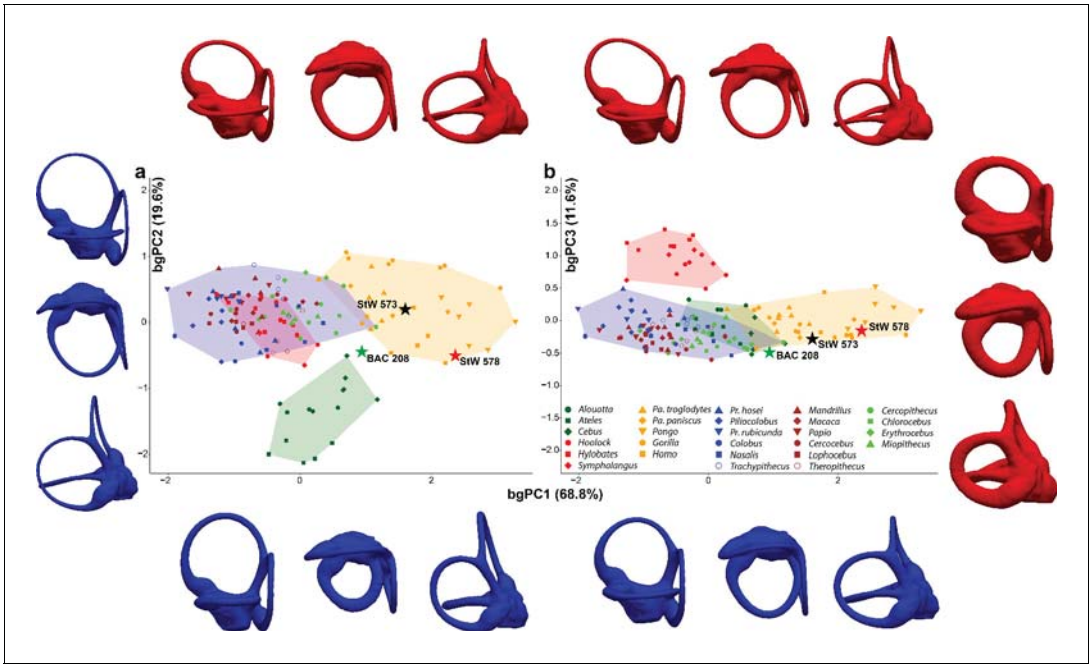

Figure 2. Main patterns of vestibular shape variation among the analyzed anthropoid sample as shown by bivariate plots of principal components from the between-group principal components analysis (bgPCA) using a few major clades (i.e., platyrrhines, cercopithecoids, hylobatids and hominids) as grouping factor. (**a**) bgPC2 vs. bgPC1. (**b**) bgPC3 vs. bgPC1. Variance explained by each bgPC is included within parentheses. Color code: dark green, platyrrhines; orange, hominids; red, hylobatids; brown, papionins; green, cercopithecins; blue, colobines. Colored stars correspond to: green, *Oreopithecus*; black, *Australopithecus* sp. (StW 573); red *Australopithecus* sp. (StW 578). Lateral (top/left), superior (middle), and posterior (bottom/right) views of deformation maximum (red) and minimum (blue) conformations for each bgPC are shown along each axis. Hominids are distinguished from hylobatids and cercopithecoids along bgPC1 (positive vs. mostly negative values, respectively), which is mainly driven by the volumetric proportions of the SCs and by their size relative to that of the vestibular recesses. bgPC2, driven by the size of the anterior and posterior SCs relative to the lateral one, distinguishes platyrrhines (more negative values) from catarrhines. Hylobatids (on positive values) differ from all other anthropoids along bgPC3 due to the reduced and posteriorly tilted posterior SC, as well as by the relative orientation among the canals. *Oreopithecus* does not match the variability of extant anthropoids as its morphology shows a mosaic of primitive and derived features. The two *Australopithecus* specimens match instead the range of extant hominids, with StW 573 being most similar to *Pan*, while StW 578 to *Homo*.
The online version of this article includes the following source data and figure supplement(s) for figure 2:

Source data 1. Individual scores for all the principal components (bgPC) yielded by the between-group principal components analysis (bgPCA) of deformation-based 3DGM of vestibular shape for anthropoids, using major taxa (i.e., hominids, hylobatids, cercopithecoids, and platyrrhines) as grouping factor.
Figure supplement 1. Box-and-whisker plots of the principal components (bgPCs) from the between-group principal components analyses (bgPCA) of vestibular shape for the anthropoid sample.

Australopithecus individuals (StW 573 and StW 578; ***Figures 1o,p*** and ***6b–c***) fall within the range of living great apes and humans (***Figure 2***, ***Figure 2—figure supplement 1a***). This is due to the volumetric proportions of their SCs and the possession of voluminous vestibular recesses (although the latter character is less pronounced in *Oreopithecus*). In BAC 208, SC volume is greater on the lateral

Table 1. Percentage of correctly classified individuals with cross-validation according to the groups (hominids, hylobatids, cercopithecoids, platyrrhines) used in the between-group principal components analysis based on group-centroid distances.

	Cercopithecoidea	Hominidae	Hylobatidae	Platyrrhini
Cercopithecoidea	96.3%	3.8%	0.0%	0.0%
Hominidae	3.3%	96.7%	0.0%	0.0%
Hylobatidae	5.9%	0.0%	94.1%	0.0%
Platyrrhini	0.0%	0.0%	0.0%	100.0%

Table 2. Phylogenetic signal results for a between-group principal components analysis (bgPCA) applied to vestibular shape deformation fields in the analyzed sample of extant anthropoids.

	bgPC1	bgPC2	bgPC3
Variance	68.79%	19.60%	11.61%
Eigenvalue	0.821	0.234	0.138
Pagel's λ	1.000 (p<0.001)	0.921 (p<0.001)	1.000 (p<0.001)
Blomberg's *K*	1.152 (p<0.001)	1.514 (p<0.001)	1.163 (p<0.001)

canal, while the two *Australopithecus* specimens possess stouter vertical canals. When the relative size of the SCs is taken into account, StW 573 shows more evenly developed canals than StW 578 and BAC 208, which both display a smaller lateral canal. Their position along the bgPC2 axis reflects these differences, with StW 573 falling on positive scores (close to the mean value for hominids and cercopithecoids; ***Figure 2a***, ***Figure 2—figure supplement 1b***) and the other two specimens occupying moderately negative values (within the range of extant catarrhines and approaching that of platyrrhines; ***Figure 2a***, ***Figure 2—figure supplement 1b***). This is caused by the comparatively smaller lateral canal and by the large vertical canal in StW 578 and in BAC 208. Due to the acute angles between the planes identified by the anterior and lateral canals and that between the planes of the posterior and anterior canals, *Oreopithecus* falls at the negative end of the extant anthropoid distribution for the bgPC3 (***Figure 2b***, ***Figure 2—figure supplement 1c***). On the other hand, the two *Australopithecus* specimens occupy more intermediate values because of the possession of a right angle between the planes of the aforementioned canals.

When the bgPCs are considered at the same time (***Figure 2***), the australopith specimens fall well within the great ape and human range. This is further supported by their posterior probabilities of

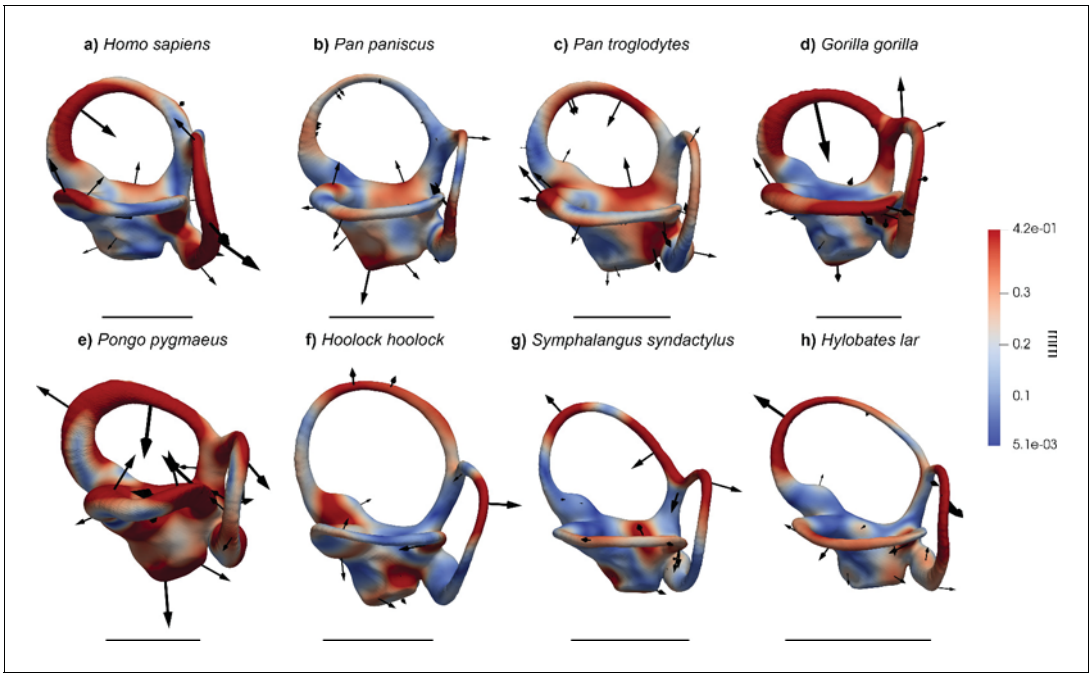

Figure 3. Results of the 3DGM deformation-based analysis superimposed on the vestibular apparatus of hominoids in lateral view. Cumulative displacement variations are rendered by pseudocolor scale ranging from dark blue (5.1 µm) to dark red (0.42 mm). Black arrows correspond to the vectors identifying the direction and amount of displacement. (**a**) *Homo sapiens* (EMBR 121); (**b**) *Pan paniscus* (MCZ 38019); (**c**) *Pan troglodytes* (AMNH. M 51204); (**d**) *Gorilla gorilla* (AMNH.M 167338); (**e**) *Pongo pygmaeus* (IPS10647); (**f**) *Hoolock hoolock* (AMNH.M 83425); (**g**) *Symphalangus syndactylus* (AMNH.M 106583); (**h**) *Hylobates lar* (MCZ 41424). Scale bars equal 5 mm. Hominids (**a–e**) differ from other anthropoids in the stouter semicircular canals and the vertically compressed (more eccentric) anterior semicircular canal, while hylobatids (**f–h**) possess slender canals more similar to those of cercopithecoids (**j–m**).

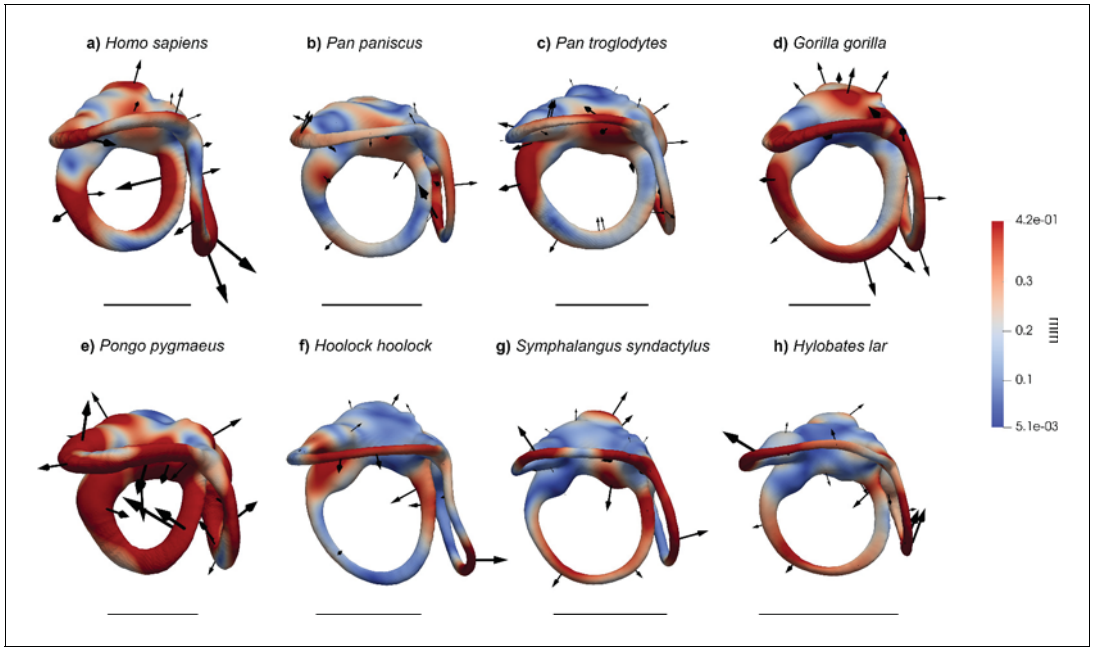

Figure 4. Results of the 3DGM deformation-based analysis superimposed on the vestibular apparatus of hominoids, in superior view. Cumulative displacement variations are rendered by pseudocolor scale ranging from dark blue (<5.1 µm) to dark red (0.42 mm). Black arrows correspond to the vectors identifying the direction and amount of displacement. (**a**) *Homo sapiens* (EMBR 121); (**b**) *Pan paniscus* (MCZ 38019); (**c**) *Pan troglodytes* (AMNH. M 51204); (**d**) *Gorilla gorilla* (AMNH.M 167338); (**e**) *Pongo pygmaeus* (IPS10647); (**f**) *Hoolock hoolock* (AMNH.M 83425); (**g**) *Symphalangus syndactylus* (AMNH.M 106583); (**h**) *Hylobates lar* (MCZ 41424). Scale bars equal 5 mm. Hominids (**a–e**) differ from other anthropoids in the stouter semicircular canals, except for the lateral canal of *Ateles*. Among great apes, *Pongo* (**e**) displays the most inflated canals and a uniquely displaced lateral semicircular canal, *Pan* (**b, c**) has the least derived morphology, and *Gorilla* (**e**) possesses a laterally protruding lateral canal. *Homo* (**a**) combines a slight (variable) reduction of the lateral canal with an enlarged posterior canal. Hylobatids (**f–h**) show an obtuse angle between the posterior and the anterior SCs.

group membership based on the proximity of fossil specimen scores to groups centroids, with StW 573 and 578 being classified as hominids with p=0.678 and p=0.190, respectively (***Table 3***). StW 573 falls close to *Pan* and *Homo*, whereas StW 578 occupies an intermediate position between humans and orangutans due to its stouter volumetric proportions. When the posterior probabilities are computed using the centroids of the hominoid genera, StW 573 is classified as *Pan* as first option (p=0.368) and as *Homo* as second (p=0.264), while StW 578 is more clearly classified as *Homo* with p=0.727 (***Table 4***). These results suggest that both australopith specimens show vestibular similarities with extant humans, but that StW 573 display a more plesiomorphic (chimpanzee-like) morphology. In turn, *Oreopithecus* shows a mosaic of vestibular features (*Pan*-like volumetric proportions, small lateral canal, and acute angles between the anterior and both the posterior and the lateral canals) that does not match the condition of any extant taxon (***Figure 2***). The posterior probabilities indicate closest similarities with cercopithecoids, followed by hominids and platyrrhines, although in all instances it falls outside the variability of the extant members of these groups (p<0.05; ***Table 3***). When comparisons are restricted to hominoid genera, *Oreopithecus* appears more similar to humans than to any ape genus, but again with a posterior probability that indicates significant differences with all of them (p<0.05; ***Table 4***).

The multivariate regression between shape (deformation fields) and size (log-transformed volume of the vestibule) shows a significant correlation (i.e., allometry) at p<0.001, but nevertheless explains only a limited portion of the variance (R^2 = 0.192). Bivariate regressions of the bgPCs against log-transformed cube root of vestibular volume reveal a significant correlation only for bgPC1 (R^2 = 0.635, p<0.001, ***Table 2***). A visual inspection of the scatter of points (***Figure 7a***) suggests that allometry for bgPC1 is more marked in hominids. This is confirmed when separate regressions are performed for hominids (R^2 = 0.480, p<0.001) and the rest of the sample (R^2 = 0.058, p<0.01), with the former displaying also a higher slope (***Table 5***). When phylogeny is considered by means of PGLS regression (***Table 5***), the correlation for the whole sample is still significant but explains much

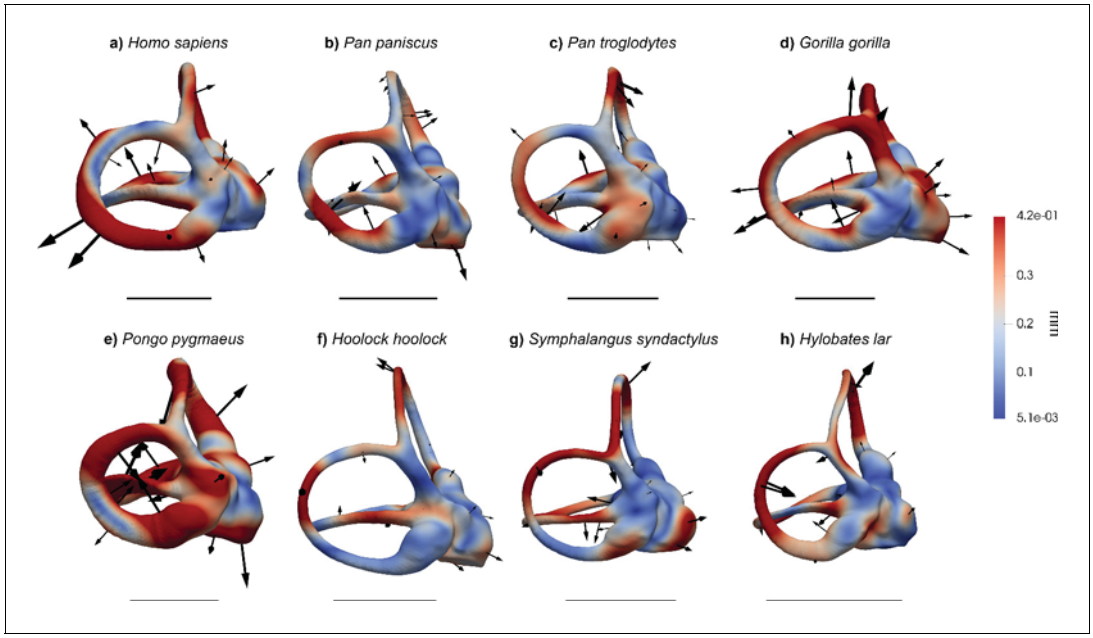

Figure 5. Results of the 3DGM deformation-based analysis superimposed on the vestibular apparatus of hominoids in posterior view. Cumulative displacement variations are rendered by pseudocolor scale ranging from dark blue (<5.1 µm) to dark red (0.42 mm). Black arrows correspond to the vectors identifying the direction and amount of displacement. (**a**) *Homo sapiens* (EMBR 121); (**b**) *Pan paniscus* (MCZ 38019); (**c**) *Pan troglodytes* (AMNH. M 51204); (**d**) *Gorilla gorilla* (AMNH.M 167338); (**e**) *Pongo pygmaeus* (IPS10647); (**f**) *Hoolock hoolock* (AMNH.M 83425); (**g**) *Symphalangus syndactylus* (AMNH.M 106583); (**h**) *Hylobates lar* (MCZ 41424). Scale bars equal 5 mm. *Homo* (**a**), together with *Gorilla* (**d**), displays a markedly posterolaterally protruding posterior canal. The two species of *Pan* (**b, c**) can be distinguished from one another for the orientation of the anterior canal (more medially inclined in *P. troglodytes*, (**c**). Hylobatids (**f–h**) display a small posterior canal relative to the size of the anterior and lateral ones.

less variance (R^2 = 0.261, p<0.01), becoming non-significant for hominids and the rest of the sample separately. bgPC3 shows a low yet significant correlation with volume for non-hominids, which becomes non-significant after PGLS correction (***Table 5***). Both *Australopithecus* and *Oreopithecus* overlap with the hominid scatter of points, with the two australopith specimens falling above the hominid regression line, whereas BAC 208 falls slightly below (although well above that of non-hominid anthropoids).

The bivariate regression between the log-transformed cube root of the SC volume and SC length shows in all instances a significant correlation that nevertheless only explains a limited (ca. 20–30%) amount of variance (***Table 5***, ***Figure 7b***). Isometry cannot be rejected for anthropoids as a whole, but a negatively allometric relationship emerges (revealing that length increases faster than volume) when hominids and other taxa are analyzed separately (***Table 5***). The latter is confirmed by PGLS regressions for the whole sample and the two groups separately, which further explain a higher proportion of variance (***Table 5***), although the hominid regression is not significant with all probability due to small sample size. The bivariate plot (***Figure 7b***) shows an allometric grade shift between hominids and the remaining anthropoid taxa, which is confirmed by ANCOVA results—indicating no significant differences (F = 0.705, p=0.403) between the allometric slopes but significantly different intercepts (F = 263.26, p<0.001) between the two groups. This indicates that hominids possess more voluminous (i.e., stouter) canals than other anthropoids at equal lengths, with only minimal overlap. All the fossil specimens display hominid-like volumetric proportions (***Figure 7b***): StW 573 and 578 fall slightly above the hominid regression line, whereas BAC 208, due to its slenderer semicircular canals, falls below (although much closer than to the non-hominid regression line).

Exploration of a preexisting group structure in the tangent space of the vestibular shape

Recently, caution has been advised regarding the use of between-group PCA (bgPCA) applied to 3D geometric morphometric (GM) data, as it could produce spurious grouping when there are fewer groups than variables (***Cardini et al., 2019***). However, the same study also highlighted that the

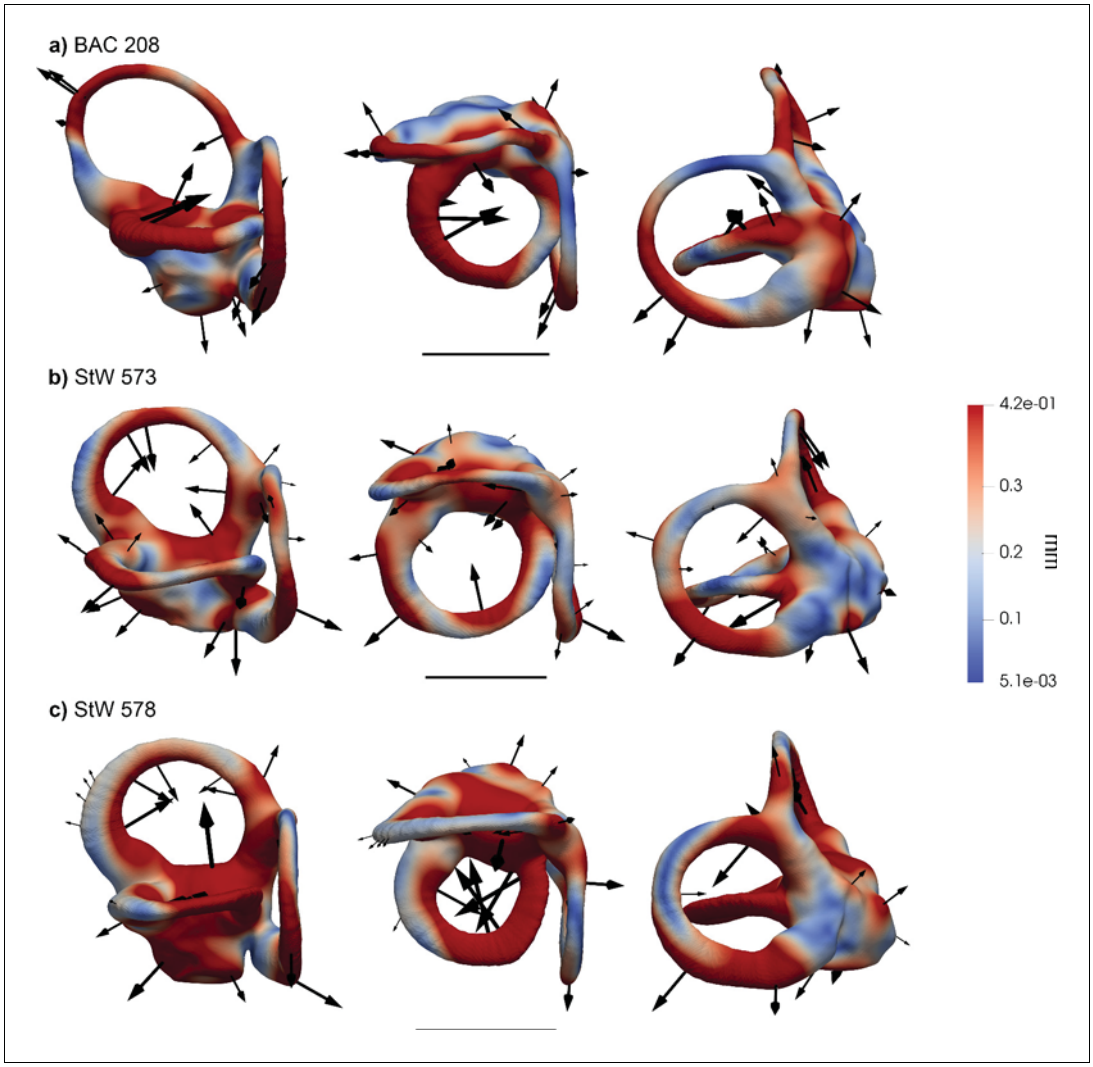

Figure 6. Results of the 3DGM deformation-based analysis superimposed on the vestibular apparatus of the fossil specimens included in the present study. Each vestibule is displayed in lateral (left), superior (middle), and posterior (right) views. Cumulative displacement variations are rendered by pseudocolor scale ranging from dark blue (<5.1 µm) to dark red (0.42 mm). Black arrows correspond to the vectors identifying the direction and amount of displacement. (**a**) *Oreopithecus bambolii* (BAC 208); (**b**) *Australopithecus* sp. (StW 573); (**c**) *Australopithecus* sp. (StW 578). Scale bars equal 5 mm. *Oreopithecus* (**a**) displays large vertical canals and a small, flat lateral one that intersect the plane of the posterior SC. The angle between the anterior and posterior SCs is one of the narrowest among the studied sample. StW 573 (**b**) and StW 578 (**c**) differ by means of a larger lateral canal in the previous and by the more rounded and developed anterior SC in the latter.

presence of a strong covariance among the variables (as found in many biological structures) largely reduces the magnitude of the problem. Interestingly, due to the properties of diffeomorphisms, the set of momenta is expected to be highly correlated, as close momenta tend to covary.

Prior to computing the bgPCA, we explored the principal components resulting from the vestibular shape GM analyses to investigate the presence of a preexisting group structure, which was found to be similar to that showed by bgPCA for both extant and fossil taxa (***Figure 8***). We used hierarchical clustering analysis (HCA) on the deformation fields for assessing the probability of correct classification of individuals according to the groups used in the bgPCA. The confusion matrix resulting from the HCA shows that most individuals are correctly identified in the corresponding groups (***Table 6***). Only in the deformation-based analyses hylobatids show a low percentage of classification

Table 3. Posterior probabilities of group membership based on the bgPC scores for fossil specimens in the analysis based on the anthropoid sample.
Note that these are probability estimates of having a particular score given membership in a particular group, not the likelihood of group membership in each of a priori defined groups given a particular score. Highest probability for each specimen in bold.

	Cercopithecoidea	Hominidae	Hylobatidae	Platyrrhini
BAC 208 (*Oreopithecus*)	**p=0.046**	p=0.013	p<0.001	p=0.012
StW 573 (*Australopithecus*)	p=0.005	**p=0.678**	p<0.001	p<0.001
StW 578 (*Australopithecus*)	p<0.001	**p=0.190**	p<0.001	p<0.001

(24% of the individuals), mostly due to the great similarity in the volumetric proportions and surface shape of the vestibule between this group and cercopithecoids.

Another way to ascertain that the group separation observed in our bgPCA is not the result of any bias is to compare different kind of analyses with a same data set and the same grouping factor. We thus compared our deformation-based results with those obtained from a configuration of 3D semilandmarks commonly used to investigate the vestibular shape (***Gunz et al., 2012***). Both analyses, based on the full primate sample, yielded a similar group separation (compare ***Figure 2*** with ***Figure 9***), as shown by the components resulting from the bgPCA. These results are also coherent with the biological reality, enabling the discrimination of major anthropoid clades in agreement with their phylogenetic relationships. In the landmark-based approach, hylobatids largely overlap with great apes in both bgPC1 (occupying an intermediate position) and bgPC2 (***Figure 9a***), but can be distinguished from them (and other anthropoids) to a large extent based on bgPC3 (***Figure 9b***). Shape variation in the analyzed sample, as captured by landmark-based 3DGM, accounts for a strong phylogenetic signal (K_{mult} = 0.973, p<0.001), and this also holds for the first three bgPCs separately (see below).

Shape differences along bgPC1 (53.3% of total variance) in the landmark-based approach embed a strong phylogenetic signal (λ = 1 and K = 1.26; ***Table 7***). This component correlates with the insertion of the lateral canal on the vestibule, the size and shape of the posterior canal, and the roundness of the SCs. Great apes and humans fall on negative values for the first axis (***Figure 9c***), as they are characterized by smaller canals compared to the size of the vestibular recesses and less rounded SCs (particularly the anterior one, which is vertically compressed). Hylobatids stand on intermediate scores that largely overlap with the hominid range (***Figure 9***) due to a combination of long SCs, a vertically compressed anterior canal, and well separated lateral and posterior canals (since posterior canal is posteriorly displaced and the lateral canal inserts anteriorly in the vestibule). In contrast, Old world monkeys tend to be located on positive values of bgPC1 and display a protruding lateral canal that intersects the plane defined by the posterior canal.

bgPC2 (29.3% of variance) separates platyrrhines—especially *Ateles* found in the most negative scores (***Figure 1i***)—from other anthropoids due to the more reduced lateral canal in the former, which is inversely proportional to anterior canal development and vertical elongation (***Figure 9d***). This pattern is shared, although to a lesser extent, by humans (***Figure 1d***) and *Theropithecus* (***Figure 1j***), which possess more developed anterior and posterior canals relative to the lateral one.

Table 4. Posterior probabilities of group membership based on the bgPC scores for fossil specimens in the analysis restricted to hominoid genera.
Note that these are probability estimates of having a particular score given membership in a particular group, not the likelihood of group membership in each of a priori defined groups given a particular score. The highest probability for each specimen in bold.

	Hoolock	*Hylobates*	*Symphalangus*	*Pongo*	*Gorilla*	*Pan*	*Homo*
BAC 208 (*Oreopithecus*)	p<0.001	p<0.001	p<0.001	p<0.001	p<0.001	p=0.002	**p=0.026**
StW 573 (*Australopithecus*)	p<0.001	p<0.001	p<0.001	p=0.019	p<0.001	**p=0.368**	p=0.264
StW 578 (*Australopithecus*)	p<0.001	p<0.001	p<0.001	p=0.062	p=0.077	p=0.030	**p=0.727**

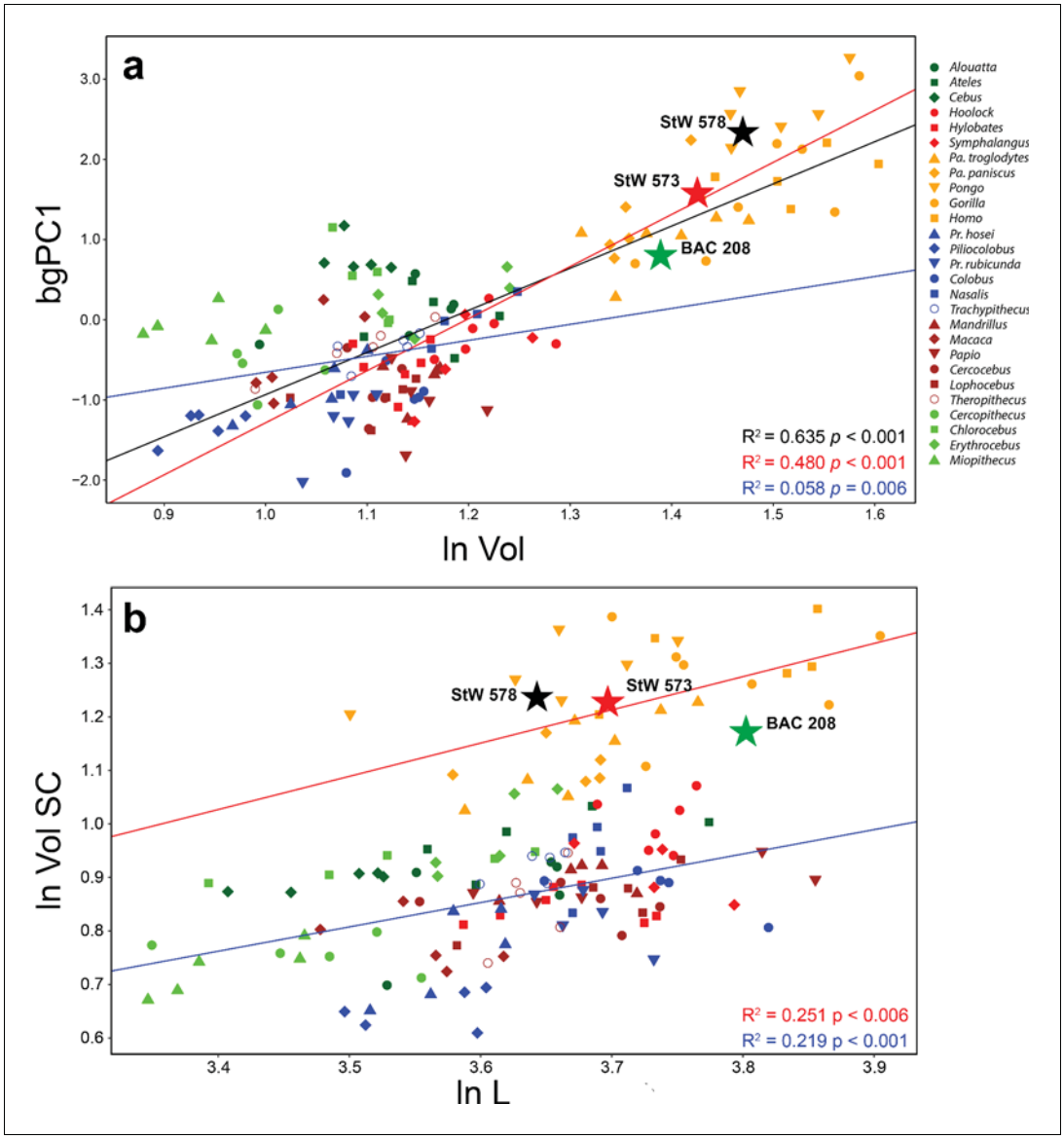

Figure 7. Bivariate regressions between (**a**) vestibular shape (as represented by bgPC1) and log-transformed cube root of vestibular volume (ln Vol), and (**b**) semicircular canal log-transformed cube root of volume (ln VolSC) vs.log-transformed length (ln L). Lines represent OLS best-fit lines for the whole anthropoid sample (black), hominids (red), and other anthropoid taxa (blue). Note that there is a significant correlation between bgPC1 (which captures differences in SC thickness and macular organ size) and vestibular volume, more marked in hominids than in the rest of the sample (see ***Table 3*** for further details). Note as well that hominids and other anthropoids show a similar negatively allometric relationship between the cube root of volume and length of the SCs, but with a marked allometric grade shift—such hominids possess stouter canals than other anthropoid taxa at comparable lengths once size-scaling effects have been taken into account (see ***Table 3*** for further details). Both australopiths fall above the regression line for hominids, while *Oreopithecus* is slightly below, yet well above the regression line for non-hominid taxa. Color code as in ***Figure 2***.

The online version of this article includes the following source data for figure 7:

Source data 1. Linear measurements for the analyzed specimens and used for computing the linear regressions.

In contrast, *Gorilla* (***Figure 1a***) occupies the positive end of the distribution due to its large lateral canal and reduced anterior one, the latter being also vertically compressed, whereas the remaining hominoids show intermediate values along bgPC2. The identified phylogenetic signal displayed by

Table 5. Bivariate regressions of vestibular shape vs. volume and of semicular canal volume vs. length.
Both ordinary least-square linear regressions (OLS) and phylogenetic generalized least-square regressions (PGLS) are provided for the whole anthropoid sample, as well as hominids and non-hominids separately. Vestibular shape is represented by the first three principal components (bgPC), while vestibular volume (Vol) is represented by its log-transformed cube root. Semicular canal volume (VolSC) and length (L) are represented by the log-transformed cube root and the log-transformed length, respectively, of the three semicircular canals together. For each regression, the coefficient of determination (R^2), the significance of the slope (p), and the slope and intercept values with their corresponding standard error (SE) and 95% confidence intervals (CI) are included. Regressions bolded when significant at p<0.05. For bgPCs vs. VOL regressions, a significant correlation denotes allometry, while for VOLSC vs. L regressions there is allometry when the correlation is significant and the 95% CI for the slope excludes unity.

	R^2	p	slope	SE	95% CI		intercept	SE	95% CI	
OLS										
Anthropoids (n = 142)										
bgPC1 vs. ln Vol	**0.635**	**<0.001**	**5.257**	**0.335**	**4.600**	**5.914**	**−6.191**	**0.399**	**−6.973**	**−5.409**
bgPC2 vs. ln Vol	0.008	0.146	0.453	0.309	−0.154	1.060	−0.533	0.368	−1.254	0.188
bgPC3 vs. ln Vol	0.000	0.385	0.192	0.220	−0.239	0.622	−0.226	0.261	−0.738	0.287
ln VolSC vs. ln L	**0.288**	**<0.001**	**0.897**	**0.118**	**0.666**	**1.128**	**−2.328**	**0.429**	**−3.169**	**−1.487**
Hominids (n = 30)										
bgPC1 vs. ln Vol	**0.480**	**<0.001**	**6.496**	**1.233**	**4.079**	**8.913**	**−7.781**	**1.797**	**−11.303**	**−4.259**
bgPC2 vs. ln Vol	0.026	0.195	−1.400	1.054	−3.466	0.666	2.307	1.538	−0.708	5.322
bgPC3 vs. ln Vol	0.039	0.153	−0.720	0.490	−1.681	0.240	1.036	0.714	−0.365	2.436
ln VolSC vs. ln L	**0.251**	**0.003**	**0.621**	**0.190**	**0.249**	**0.992**	**−1.084**	**0.705**	**−2.465**	**0.297**
Non-hominids (n = 112)										
bgPC1 vs. ln Vol	**0.058**	**0.006**	**1.990**	**0.709**	**0.601**	**3.380**	**−2.645**	**0.785**	**−4.183**	**−1.108**
bgPC2 vs. ln Vol	0.010	0.152	−1.027	0.712	−2.422	0.368	1.061	0.788	−0.482	2.605
bgPC3 vs. ln Vol	**0.046**	**0.013**	**1.332**	**0.529**	**0.295**	**2.368**	**−1.466**	**0.585**	**−2.613**	**−0.319**
ln VolSC vs. ln L	**0.219**	**<0.001**	**0.454**	**0.080**	**0.297**	**0.611**	**−0.783**	**0.291**	**−1.352**	**−0.213**
PGLS										
Anthropoids (n = 27)										
bgPC1 vs. ln Vol	**0.261**	**0.004**	**3.401**	**1.065**	**1.314**	**5.488**	**−3.719**	**1.376**	**−6.416**	**−1.022**
bgPC2 vs. ln Vol	0.003	0.416	0.625	0.756	−0.858	2.107	−1.27	0.962	−3.155	0.615
bgPC3 vs. ln Vol	0.063	0.111	−0.727	0.440	−1.589	0.135	0.879	0.570	−0.238	1.996
ln VolSC vs. ln L	**0.437**	**<0.001**	**0.502**	**0.109**	**0.288**	**0.716**	**3.144**	**0.124**	**2.901**	**3.388**
Hominids (n = 5)										
bgPC1 vs. ln Vol	0.221	0.240	4.440	3.042	−1.521	10.402	−4.627	4.499	−13.445	4.192
bgPC2 vs. ln Vol	0.036	0.760	−1.144	3.421	−7.850	5.561	1.892	4.990	−7.888	11.672
bgPC3 vs. ln Vol	0.062	0.687	−0.392	0.883	−2.122	1.338	0.596	1.309	−1.970	3.162
ln VolSC vs. ln L	0.553	0.093	0.631	0.259	0.124	1.138	2.920	0.327	2.279	3.561
Non-hominids (n = 22)										
bgPC1 vs. ln Vol	0.008	0.294	1.376	1.276	−1.125	3.877	−1.674	1.512	−4.639	1.290
bgPC2 vs. ln Vol	0.030	0.445	0.763	0.978	−1.154	2.679	−1.444	1.152	−3.701	0.814
bgPC3 vs. ln Vol	0.020	0.500	−0.419	0.610	−1.616	0.777	0.577	0.730	−0.854	2.008
ln VolSC vs. ln L	**0.504**	**<0.001**	**0.634**	**0.134**	**0.371**	**0.896**	**3.052**	**0.137**	**2.784**	**3.320**

bgPC2 is slightly reduced as compared to bgPC1, but still significant and very high (λ = 0.9 and K = 1.08;).

The bgPC3 (17.4% of variance) is driven by both trajectory and size of the SCs, especially of the posterior one (***Figure 9e***), and displays less phylogenetic signal than bgPC1 and bgPC2 (λ = 0.93 and K = 0.53, ***Table 7***). Along this axis *Homo*, *Ateles* and *Theropithecus* (***Figure 9b***) occupy the

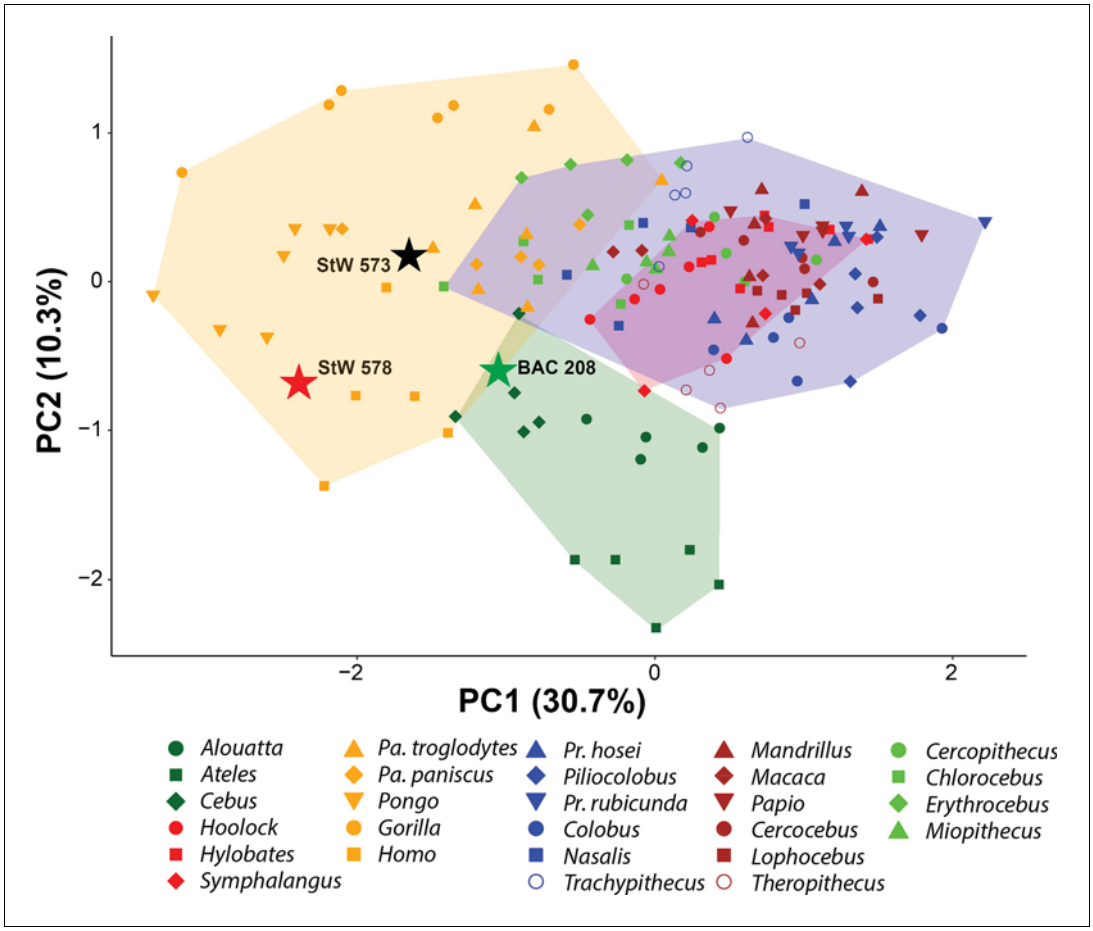

Figure 8. Tangent space of vestibular shape among the analyzed anthropoid sample as shown by bivariate plots of principal components from the PCA of deformation-based analysis. Variance explained by each PC is included within parentheses. Convex hulls correspond to: hominids (orange), hylobatids (red), cercopithecoids (blue), platyrrhines (green). Color code: dark green, platyrrhines; orange, hominids; red, hylobatids; brown, papionins; green, cercopithecins; blue, colobines. Hominids are distinguished from hylobatids and other anthropoids along PC1 (mostly negative vs. positive values, respectively), while PC2 tends to distinguish platyrrhines (more negative values) from catarrhines. Even if slightly more overlapping, the groups identified when observing the morphospace obtained with bgPCA are already present in the PCA.

The online version of this article includes the following source data for figure 8:

Source data 1. Individual scores for all the principal components (PC) yielded by the principal components analysis (PCA) of deformation-based 3DGM of vestibular shape for anthropoids.

positive end, as due to their large and anteriorly inclined posterior canal that protrudes laterally, an obtuse angle of the CC apex, large posterior canal, and an angle between the anterior and posterior canals that is close to 90˚. Great apes and the majority of non-hominoid taxa fall in an intermediate position (***Figure 9b***), differing from the aforementioned genera by the less obtuse angle in the CC apex and a larger lateral canal. Hylobatids and, to a lesser extent, *Trachypithecus* show the lowest scores for bgPC3, as the result of the right to acute angle formed by the apex of the CC, more

Table 6. Probability of correct classification of individuals from the hierarchical clustering analyses of deformation fields according to the groups (hominids, hylobatids, cercopithecoids, platyrrhines) used in the bgPCA.

Hominidae	Hylobatidae	Cercopithecoidae	Platyrrhini
90.0%	23.5%	65.0%	66.7%

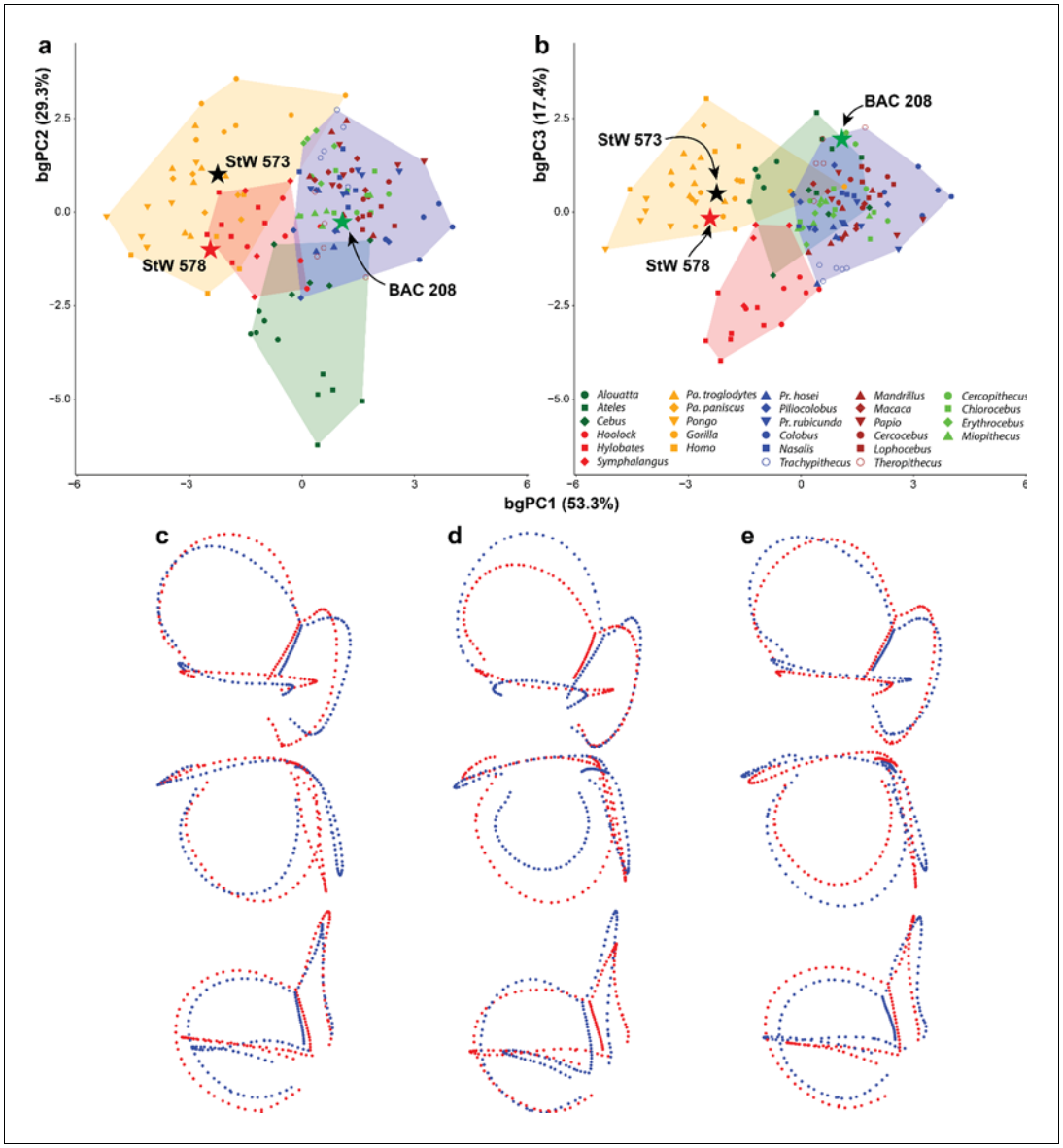

Figure 9. Main patterns of vestibular shape variation among the analyzed anthropoid sample as shown by bivariate plots of principal components from the landmark-based between-group principal components analysis (bgPCA) using major taxa as in ***Figure 2***. (**a**) bgPC2 vs. bgPC1. (**b**) bgPC3 vs. bgPC1. Variance explained by each bgPC is included within parentheses. Lateral (top), superior (middle), and anterior (bottom) views of landmarks and semilandmark maximum (red) and minimum (blue) conformations for (**c**) bgPC1, (**d**) bgPC2, and (**e**) bgPC3. Color code as in ***Figure 2***. Hominoids and cercopithecoids are distinguished along bgPC1 (mostly negative vs. positive values, respectively), which is mainly driven by the vertical compression of the anterior SC, as well as the position of the lateral (more anteriorly connecting with the vestibule) and the posterior (displaced posteromedially) canals. bgPC2, driven by the size of the anterior and posterior SCs relative to the lateral one, tends to distinguish platyrrhines (more negative values) from catarrhines, while bgPC3, driven by the size of the anterior and lateral SCs relative to that of the posterior canal, as well as by the relative orientation among the canals, tends to distinguish most hylobatids (more negative values) from great apes, humans, and cercopithecoids (more positive values). The two *Australopithecus* specimens fall within the hominid range, flanking that of hylobatids. Similarly to the deformation-based approach, StW 578 is more similar to humans (matching the distribution of *Homo*), while StW 573 is found within the scatter of points of *Pan* species. In the landmark-based analysis, *Oreopithecus* overlaps within cercopithecoids and also falls close to platyrrhines.

The online version of this article includes the following source data for figure 9:

Source data 1. Individual scores for all the principal components (bgPC) yielded by the between-group principal components analysis (bgPCA) of landmark-based 3DGM of vestibular shape for anthropoids, using major taxa (i.e., hominids, hylobatids, cercopithecoids, and platyrrhines) as grouping factor.

Table 7. Phylogenetic signal results for a between-group principal components analysis (bgPCA) applied to vestibular shape procrustes residuals in the analyzed sample of extant anthropoids.

	bgPC1	bgPC2	bgPC3
Variance	53.34%	29.29%	17.37%
Eigenvalue	2.462	1.352	0.802
Pagel's λ	1.000 (p<0.001)	0.902 (p<0.001)	0.932 (p=0.006)
Blomberg's *K*	1.226 (p=0.001)	1.081 (p=0.001)	0.528 (p=0.01)

developed anterior and lateral canals relative to the posterior one, and a posteriorly tilted posterior canal.

When plotted onto the tangent space of extant taxa, the two *Australopithecus* specimens overlap with the range of great apes and humans for all the bgPCs (***Figure 9***, ***Figure 9—source data 1***). They show a vertically compressed anterior canal together with well-separated lateral and posterior canals. The lateral canal is also moderately sinuous and its ampullar portion bends upwards, thus resulting in a negative score for bgPC1. The two specimens can be distinguished from one another by means of bgPC2 (***Figure 9a***), with StW 573 falling on positive values and StW 578 occupying negative ones. This is explained by the smaller lateral canal relative to the vertical SCs in StW 578, which therefore overlaps with extant human variation in both bgPC1 and bgPC2, whereas StW 573 overlaps instead with chimpanzees and bonobos (***Figure 9a***). Along bgPC3, both specimens display intermediate values due to the large posterior canal and for the almost right angle between the planes of the anterior and posterior SCs, overlapping with all extant anthropoids except hylobatids.

In turn, along bgPC1 *Oreopithecus* displays more positive values than hominoids and falls well within the range of non-hominoid anthropoids (it only slightly overlaps with the positive end of the hominoid distribution; ***Figure 9***) due to its more coplanar lateral canal that almost intersects the plane defined by the posterior canal. Furthermore, due to its small lateral canal and fairly short CC, BAC 208 displays an intermediate value for bgPC2, within the range of extant catarrhines and slightly above the positive end of platyrrhine distribution (***Figure 9a***). Finally, along bgPC3 *Oreopithecus* falls on a positive score, differing from hylobatids, as a result of the acute angles found between anterior canal plane and those defined by both the posterior and lateral canals (***Figure 9b***).

Overall, the two 3DGM techniques used in this paper generally yielded similar results except for hylobatids and *Oreopithecus* (along bgPC1 alone). This is attributable to differences in the underlying methodological assumptions of each method when computing shape variation. In particular, our 3DGM landmark protocol measures the spatial trajectory of SCs based on their midline skeleton (***Gunz et al., 2012***) and hence it does not capture differences in volumetric proportions. In contrast, by comparing surfaces as a whole (***Durrleman et al., 2012b***; ***Durrleman et al., 2012a***), the deformation analysis is particularly sensitive to volumetric differences. In addition, the amount of identified phylogenetic signal is very similar for both techniques, affecting the entire variance. Together with the results of the HCA, we confidently show that the separation found between the groups in the bgPCA of this study already exists in the shape data and that is not a spurious effect produced by the bgPCA method itself.

Hominoid phylomorphospace of the vestibule

The phylomorphospace approach applied to vestibular shape variation in hominoids infers different branch lengths for hominids and hylobatids from the ancestral morphology estimated for crown hominoids, which falls much closer to great apes and humans than to hylobatids for both bgPC1 and bgPC3 (***Figure 10***). According to our reconstructions based on the extant taxa (***Figure 10***), the crown hominoid LCA vestibular morphology (***Figure 11a***) would be characterized by equally developed and slightly inflated SCs, a fairly vertically compressed anterior canal, and by the slender portion of the lateral canal connecting more anteromedially with the vestibule. The estimated morphology for the LCA of hylobatids (***Figure 11b***) resembles to some extent that of the crown hominoid LCA (slightly vertically compressed anterior canal and lack of intersection between the lateral and posterior canals), combined with more monkey-like features (markedly slender canals with inflated ampullae), and others exclusive to hylobatids (an obtuse angle between a slightly anteriorly

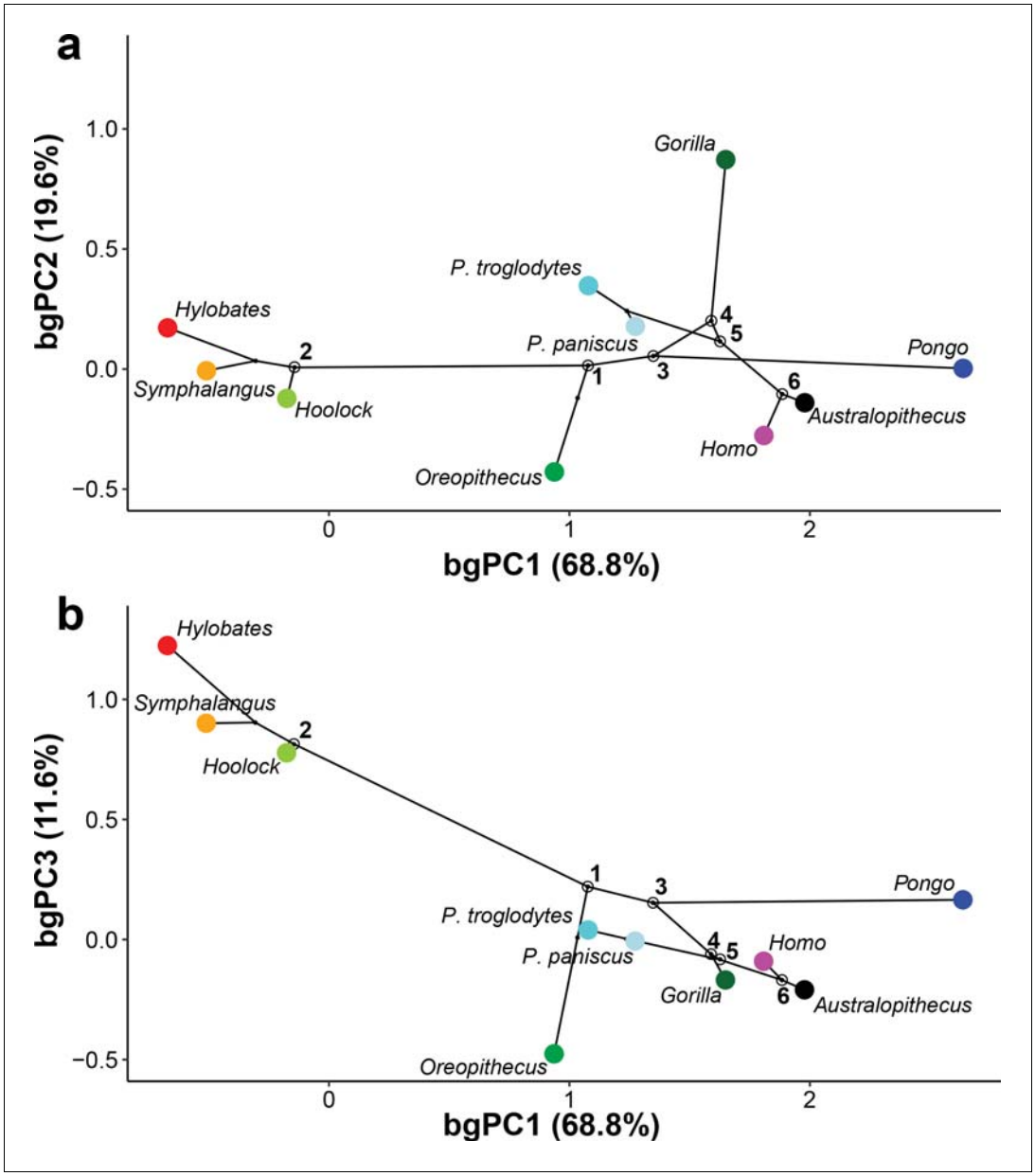

Figure 10. Reconstructed evolutionary history of the vestibular apparatus in the sample restricted to hominoids. The depicted phylomorphospaces are obtained by projecting the phylogeny displayed in ***Figure 13*** on the bivariate plots between principal components: (**a**) bgPC2 vs. bgPC1 (see ***Figure 2a***); (**b**) bgPC3 vs. bgPC1 (see ***Figure 2b***). Color code: red, *Hylobates lar*; orange, *Symphalangus syndactylus*; light green, *Hoolock hoolock*; blue, *Pongo pygmaeus*; dark green, *Gorilla gorilla*; cyan, *Pan troglodytes*; purple, *Pan paniscus*; fuchsia, *Homo sapiens*; chartreuse, *Oreopithecus bambolii*; black, *Australopithecus* sp. Key ancestral morphologies reconstructed using maximum likelihood for the last common ancestor of various clades are depicted as follows: 1, crown hominoids (hylobatids and hominids); 2, crown hylobatids (gibbons and siamangs); 3, crown hominids (great apes and humans); 4, crown hominines (African great apes and humans); 5, *Pan-Homo* clade; 6 *Australopithecus-Homo* clade.

protruding anterior canal and a small posterior canal relative to the others). Hylobatid genera are generally less diverging from one other than great apes and humans. *Hoolock* (***Figures 1f***, ***3f***, ***4f*** and ***5f***) apparently displays the most primitive morphology among hylobatids (with equally developed, rounded, almost orthogonal canals, and less anteriorly protruding anterior canal), while *Hylobates* (***Figures 1h***, ***3h***, ***4h*** and ***5h***) and, to a lesser extent, *Symphalangus* (***Figures 1g***,

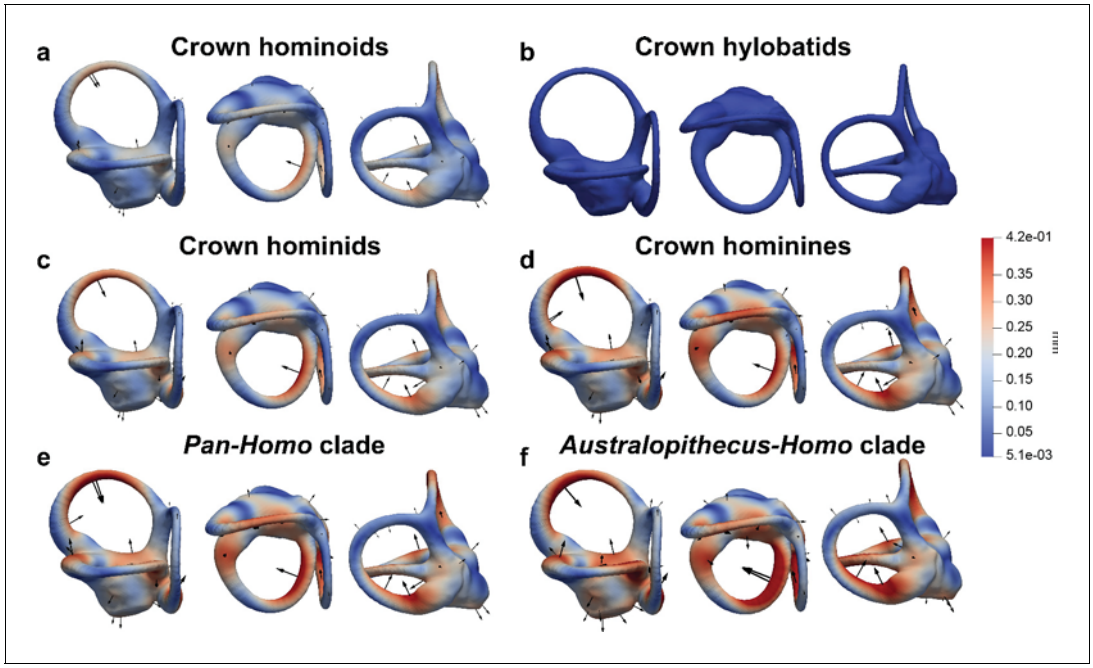

Figure 11. Reconstructed vestibular shape for the last common ancestors (LCA) of the main clades of interest as reconstructed using maximum likelihood methods for deformation-based 3DGM analyses applied to the anthropoid sample (***Figure 7***), in lateral (left), superior (middle), and posterior (right) views. Cumulative displacement variations are rendered by pseudocolor scale ranging from dark blue (<5.1 µm) to dark red (0.42 mm). Black arrows correspond to the vectors identifying the direction of displacement. The reconstructed LCAs depicted are the following: (**a**) crown hominoids; (**b**) crown hylobatids; (**c**) crown hominids; (**d**) crown hominines; (**e**) *Pan-Homo* clade; (**f**) *Australopithecus-Homo* clade.

3g, ***4g*** and ***5g***) show the slenderest SCs and an extremely anteriorly protruding anterior canal (as noted by ***Le Maître et al., 2017***).

The reconstructed morphologies for LCAs of crown hominids (***Figure 11c***) and, to a lesser extent, crown hominines (***Figure 11d***) and the *Pan-Homo* clade (***Figure 11e***) are not very far from the crown hominoid ancestral condition (***Figure 11a***) for any of the first three bgPCs. The crown hominid LCA is characterized by a lateral insertion of the slender portion of the lateral canal on the vestibule, a moderate medioventral displacement of the posterior canal, and an increased vertical compression of the anterior canal, in combination with thick and bulgy canals and well-developed vestibular recesses. The hominine and *Pan-Homo* clade LCAs possess stouter canals and are very similar to one another, distinguished only by the size of the lateral and anterior canals. The LCA of the *Pan-Homo* clade shows a larger and less vertically compressed anterior canal, and a smaller lateral one, which also connects more anteriorly with the vestibule. The hominin (*Australopithecus-Homo*) LCA (***Figure 11f***) is closer to *Homo*, being characterized by the stoutest volumetric proportions, with larger vertical canals relative to the *Pan-Homo* clade LCA, yet smaller than those found in humans. Its anterior canal is more vertically compressed than in *Homo*, rather resembling the morphology of *Pan*, while the posterior canal is rounded, thus being intermediate between the human (laterally projecting) and the chimpanzee (laterally compressed) morphology.

Among crown hominids, *Pan* (***Figures 1b–c***, ***3b–c***, ***4b–c*** and ***5b–c***) more closely resembles the morphology of the inferred LCAs of crown hominids and hominoids (***Figure 11a,c***) in the moderately inflated and equally developed SCs and in the degree of the vertical compression of the anterior canal. *Pongo* (***Figures 1e***, ***3e***, ***4e*** and ***5e***) occupies the positive end along bgPC1 (***Figure 10***) due to the possession of relatively small but extremely stout canals (especially the anterior one and the common crus). It also exhibits the most vertically compressed anterior canal and a 'triangular' lateral canal (i.e., showing straight slender portions of the bony labyrinth close to the ampulla and to the connection with the vestibule, as previously outlined by ***Spoor and Zonneveld, 1998***). Finally, *Gorilla* and *Homo* (***Figures 1a***, ***3d***, ***4d*** and ***5d***) are derived in opposite directions along bgPC2 (***Figure 10a***), as the former exhibits increased lateral canal radius with a flattened cross-section,

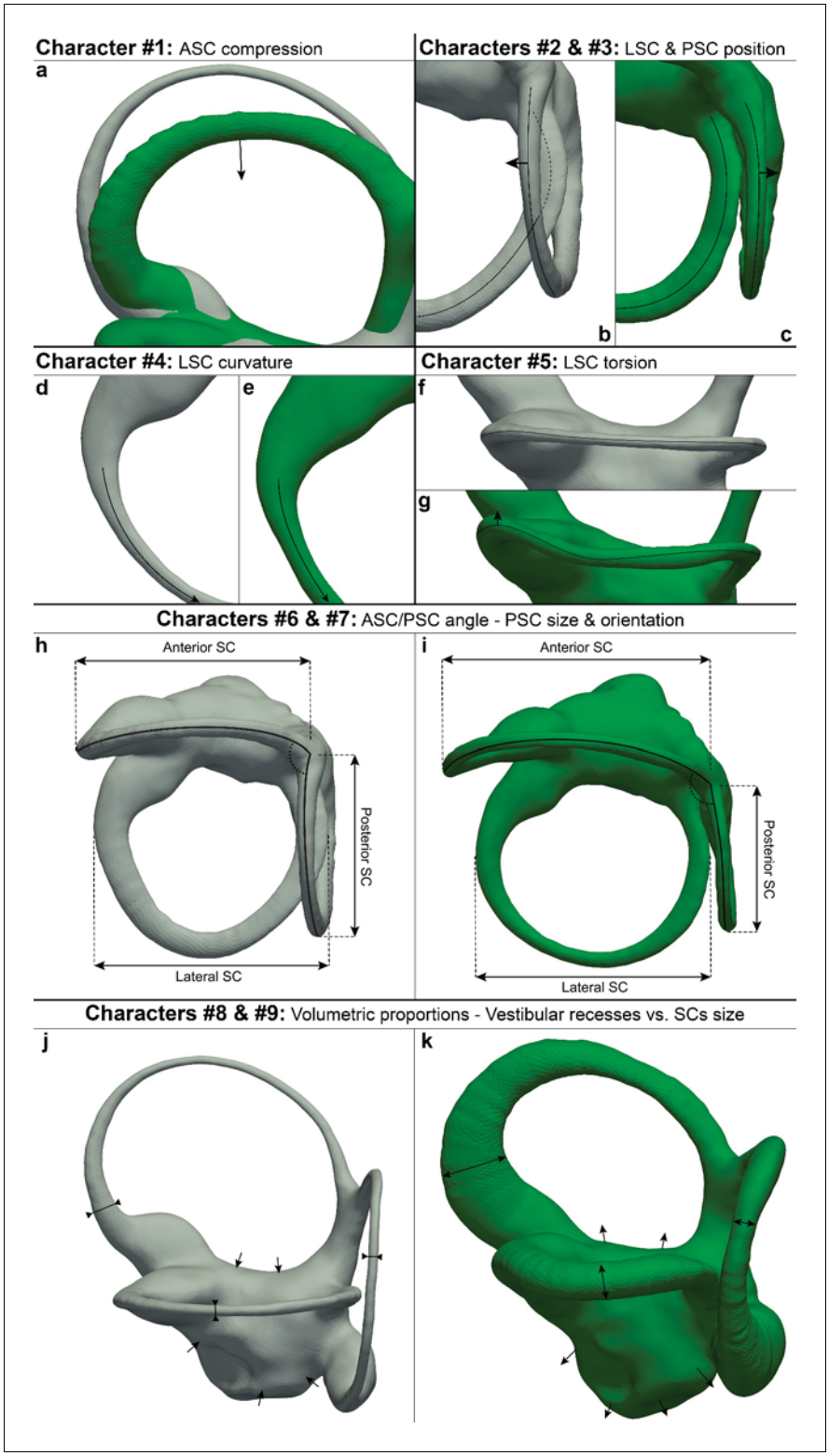

Figure 12. Illustration of hominoid, hominid and hylobatid synapormophies for the vestibular apparatus. See ***Table 8*** for further details. character #1: (**a**) rounded (gray) and compressed (green) anterior canal; character #2: (**b–c**) non-posteriorly displaced posterior canal (gray), posteriorly displaced posterior canal (green); character #3: (**b–c**) lateral canal intersecting(dashed line) the posterior one (gray), lateral canal non-intersecting the posterior one (in green); character #4: (**d-e**) curved (gray) and straight (green) medial portion of the lateral canal; character #5: (**f–g**) flat (gray) and bent upwards (green) trajectory of the lateral canal ampullar portion; character #6: (**h–i**) anterior

Figure 12 continued on next page

Figure 12 continued

and posterior SCs forming an angle (dotted arc) close to the right angle (gray), anterior and posterior canals forming an obtuse angle (green); character #7: (**h–i**) posterior canal equal in size to the other SCs and forming a right angle with the lateral canal (gray), small posterior canal relative the other SCs and inclined posteriorly respective to the lateral canal (green); character #8: (**j–k**) slender SCs (gray), stout canals (green); character #9: (**j–k**) small vestibular recesses (gray), enlarged vestibular recesses (green).

while humans retain quite rounded canals shape and cross-section, and show a reduction of the lateral canal, as opposed to more developed anterior and posterior canals.

Australopithecus is closer to humans than to any great ape, due to the possession of large vertical canals and stout volumetric proportions, being closest to the LCA of the *Australopithecus-Homo* clade and only slightly more derived in the same direction as *Pongo* due to the stouter canals (***Figure 10***). In contrast, *Oreopithecus* appears more plesiomorphic than humans and extant great apes in volumetric proportions, resembling those found in the LCA of crown hominoids. Nevertheless, *Oreopithecus* is clearly distinct from hylobatids in both SC stoutness and shape, being most clearly distinguished from gibbons and siamangs based on the acute angles defined the anterior canal with both the posterior and lateral canals (***Figure 10b***). *Oreopithecus* is also derived in terms of SC size (with the vertical canals much larger than the lateral one), similarly to humans albeit to a greater extent, and opposite to gorillas, due to the remarkably smaller lateral canal.

Discussion

Previous research on the morphology of the vestibular apparatus among extant mammals has focused on its relationship to positional behavior (***Spoor et al., 2007***; ***Perier et al., 2016***; ***Le Maître et al., 2017***), particularly in order to make locomotor inferences in extinct species (***Spoor et al., 1994***; ***Walker et al., 2008***; ***Silcox et al., 2009***; ***Ryan et al., 2012***). However, the phylogenetic signal embedded in vestibular morphology has not been adequately quantified among hominoids, because previous attempts were either exploratory (***Gunz et al., 2012***) or based on a restricted sample (***Le Maître et al., 2017***). Our results indicate that main anthropoid groups can be distinguished based on vestibular shape variation, and that there are important differences not only between hylobatids, great apes, and humans, but also among extant great ape genera. A significant phylogenetic signal is found to affect the entire variance of the anthropoid sample. Thus, the shape of the SCs is overall informative from a phylogenetic viewpoint—as hypothesized for strepsirrhine primates (***Lebrun et al., 2010***) and carnivorans (***Schwab et al., 2019***), but in contrast to previous results for hominoids (***Le Maître et al., 2017***) and some other mammals (***Grohé et al., 2016***; ***Costeur et al., 2018***).

Based on the analysis of the shape of the vestibular apparatus, we identify several potential hominoid synapomorphies (***Table 8***; ***Figure 12a–g***), including among others a posteromedially displaced posterior canal and a straight segment between the lateral-most point of the lateral canal and its anteromedially situated insertion on the vestibule. These features result in an anteromedially located lateral canal (i.e., the plane defined by the posterior canal is always separated from the trajectory of the lateral canal, even when the latter is well developed, as in *Gorilla* and *Hylobates*). This would imply an increased sensitivity for angular accelerations occurring along the coronal plane, which has been correlated with orthogrady in extant hominoids (***Le Maître et al., 2017***).

The most evident character shared by extant apes and humans (even if somewhat variable in the latter and in *Hoolock*), and further displayed by the extinct genera analyzed here, is the vertical compression of the anterior canal (***Figure 12a***), as noted for great apes only in a previous analysis (***Spoor and Zonneveld, 1998***). Since the subarcuate fossa arguably constrains the shape of the anterior canal (***Jeffery et al., 2008***), the hominoid morphology might be related to the absence of the fossa in great apes and siamangs (***Moyà-Solà and Köhler, 1993***; ***Gannon et al., 1988***; ***Spoor and Leakey, 1996***). However, the combination of a well-developed fossa and marked vertical compression of the anterior SC found in *Hylobates* argues against this hypothesis. The latter is further rejected by the cercopithecoid morphology, characterized by a rounded anterior SC even in the largest terrestrial genera (*Papio*, *Theropithecus*, and *Mandrillus*), which unlike other cercopithecoids

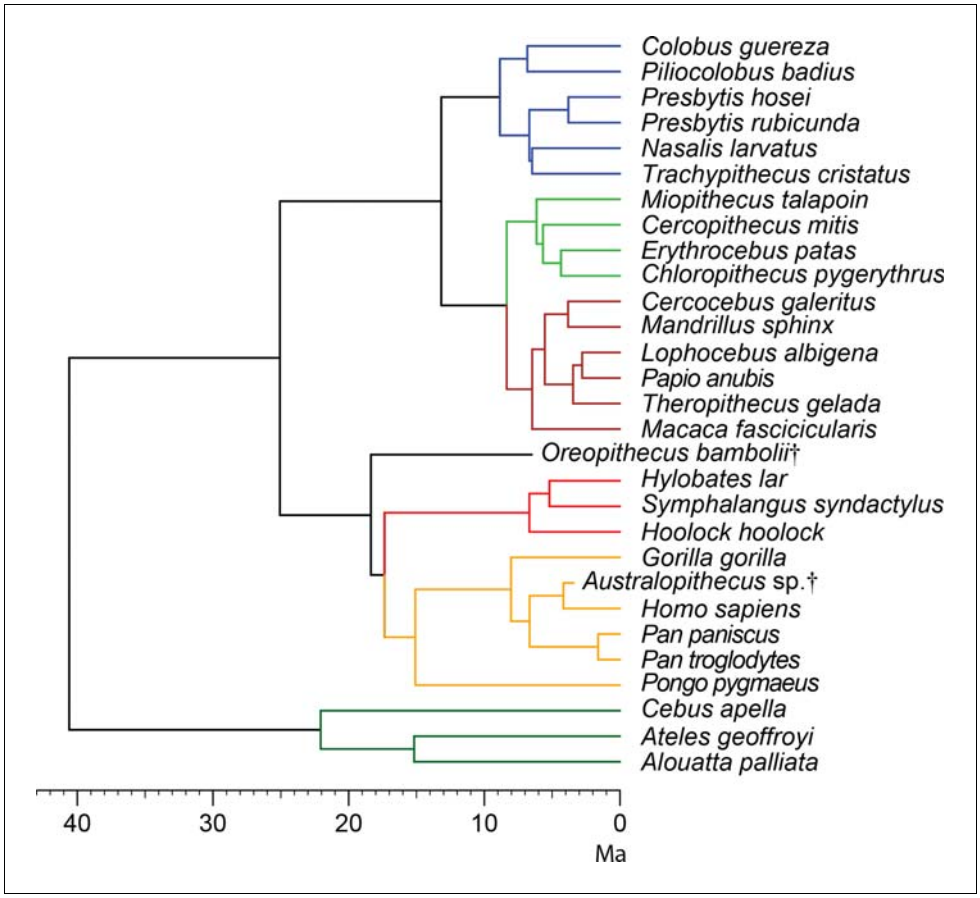

Figure 13. Time-calibrated molecular phylogeny of extant anthropoids used in the analyses of phylogenetic signal and PGLS regressions as inferred from a species supermatrix. Fossil taxa have been added a posteriori according to their phylogenetic position and their point estimates correspond to their last occurrence in the fossil record (***Rook et al., 2000***; ***Wood and Boyle, 2016***). *Oreopithecus* is here considered as a stem hominoid, predating the split between hominids and hylobatids, while *Australopithecus* has been added following the first appearance datum for *A. africanus* based on the Jacovec Cavern specimens. For the phylomorphospace the phylogenetic tree has been pruned to include extant and extinct hominoids only. Branches are color-coded: dark green, platyrrhines; brown, papionins; green, cercopithecins; blue, colobines; orange, hominids; red, hylobatids. Extinct taxa are denoted by a dagger.

display a much reduced (or even absent) subarcuate fossa (***Gannon et al., 1988***; ***Spoor and Leakey, 1996***).

As a result of vertical compression, all hominoids display the anterior canal projected anterosuperiorly to some extent (less accentuated in *Homo* and *Hoolock*). Such a projection of the anterior canal in *Hylobates* has been interpreted as a hylobatid synapomorphy (***Le Maître et al., 2017***). Our results raise doubts about the latter view and indicate instead that the anterior projection of this canal is variable within both hylobatids and hominids, and that the LCA of crown hylobatids might have not shown the patent elongation of the anterior canal that is found in *Hylobates* and *Symphalangus*. On the other hand, here we identify two potential synapomorphies for hylobatids (***Table 8***; ***Figure 12h,i***): an obtuse angle between the planes defined by the anterior and posterior canals, and a posteriorly-inclined posterior canal, which is smaller relative to the anterior and lateral ones.

In turn, bgPC1 clearly separates hominids (great apes and humans) from cercopithecoids and hylobatids and enables the identification of some potential hominid synapomorphies (***Table 8***; ***Figure 12j,k***). In particular, hominids differ from other anthropoids, including hylobatids, by derived volumetric proportions of the SCs (stouter canals relative to their length, or shorter canals relative to their volume) even when size-scaling considerations are taken into account, as well as by the possession of more extensive vestibular recess for a similar size of the SCs (***Table 8***; ***Figure 12j,k***), as

Table 8. Phylogenetically informative discrete characters of vestibular morphology that represent potential synapomorphies of either hominoids or hominids.

Character #	Character definition	Character states[a]	Synapomorphic for
#1	Anterior SC[b]	0 = rounded; 1 = vertically compressed	Hominoidea
#2	Posterior SC	0 = non posteromedially displaced; 1 = posteromedially displaced	Hominoidea
#3	Insertion of the lateral SC slender portion on the vestibule	0 = posterior (lateral SC intersecting the posterior SC plane); 1 = anterior (not intersecting)	Hominoidea
#4	Lateral SC medial portion	0 = curved; 1 = straight	Hominoidea
#5	Trajectory of the lateral SC ampullar portion	0 = flat; 1 = bent upwards	Hominoidea
#6	Angle between the planes identified by the anterior and posterior SCs	0 = close to right angle, 1 = obtuse	Hylobatidae
#7	Inclination and size of the posterior SC relative to the size of the anterior and lateral SCs	0 = forming a right angle and equal or larger in size, 1 = posteriorly tilted and smaller	Hylobatidae
#8	Robusticity of SCs	0 = slender; 1 = stout	Hominidae
#9	Extension of vestibular recesses relative to that of the SCs	0 = smaller; 1 = similar in size	Hominidae

Abbreviations: SC = semicircular canals.

[a] Character state 0 represents the primitive condition reconstructed for the last common ancestor of crown catarrhines.

[b] Some platyrrhines display a superior eccentricity of the anterior SC that might be apomorphic.

reflected in bgPC1. In particular, cercopithecoids and hylobatids completely overlap due to the possession of slender SCs, while hominids as a whole (even if more markedly orangutans) differ by their swollen and relatively shorter SCs (with only few cercopithecins falling within the hominid range). This might be related to the fact that hylobatids and cercopithecoids, unlike great apes, are swift moving animals that make fast and large head movements, thus requiring a limited duct sensitivity to avoid overstimulation and a quick response to angular displacement (***Spoor and Zonneveld, 1998***). This hypothesis is supported by biophysical models suggesting that the length of the membranous ducts is inversely proportional to their sensitivity and that a larger lumen of the ducts correlates with a reduced steadiness of the response to an external angular stimulus (i.e., the abrupt change of the position and/or posture) (***Muller, 1994***; ***Rabbitt et al., 2004***). Therefore, species with shorter and thicker ducts (such as hominids) require more time to perceive and react to sudden head displacements, while being more sensitive to fine movements. Nevertheless, caution must be used when inferring the lumen of the ducts from that of the bony canals, as the amount of the SC cross-section occupied by perilymphatic space is variable depending on the species (***Ramprashad et al., 1984***; ***Spoor and Zonneveld, 1998***).

Superimposed on the aforementioned hominoid and hominid synapomorphies (***Table 8***; ***Figure 12***), there are also marked differences among hominid genera. Such differences mainly relate the relative size among the SCs (which varies particularly along bgPC2 and bgPC3), while hylobatid genera are less diverse in this regard. Chimpanzees and bonobos are characterized by equally developed SCs and a moderately short CC. Similarly, orangutans possess evenly proportioned SCs and can be distinguished from *Pan* by a shorter CC, more inflated canals, and a greater vertical compression of the anterior SC. Gorillas display the largest intrageneric variability in the studied sample, especially with regard to SCs slenderness, coupled with some other distinctive traits (obtuse angle of the CC apex, and longer lateral SC and CC).

Humans differ from apes in the enlarged vertical canals, a laterally protruding and inferiorly displaced posterior canal, and a moderately smaller lateral canal. Relatively enlarged vertical canals are also found in *Theropithecus*. The human morphology has been linked to bipedalism (***Spoor et al., 1994***; ***Spoor et al., 2003***), as accelerations during bipedal walking mainly occur along the vertical axis, so that the broadly similar morphology of *Theropithecus* might be related to the bipedal

Table 9. Sample of extant anthropoid specimens analyzed in this paper based on µCT image stacks. See ***Supplementary file 1*** for further details on each specimen.

Family	Species	n	M	F	?
Atelidae	*Alouatta palliata*	5	3	2	0
Atelidae	*Ateles geoffroyi*	5	1	4	0
Cebidae	*Cebus apella*	5	3	2	0
Cercopithecidae	*Cercocebus galeritus*	5	3	2	0
Cercopithecidae	*Cercopithecus mitis*	5	0	5	0
Cercopithecidae	*Chlorocebus pygerythrus*	5	2	3	0
Cercopithecidae	*Colobus guereza*	5	2	3	0
Cercopithecidae	*Erythrocebus patas*	5	3	2	0
Cercopithecidae	*Lophocebus albigena*	5	2	3	0
Cercopithecidae	*Macaca fascicularis*	5	1	4	0
Cercopithecidae	*Mandrillus sphinx*	5	5	0	0
Cercopithecidae	*Miopithecus talapoin*	5	3	2	0
Cercopithecidae	*Nasalis larvatus*	5	0	5	0
Cercopithecidae	*Papio anubis*	5	3	2	0
Cercopithecidae	*Piliocolobus badius*	5	4	1	0
Cercopithecidae	*Presbytis hosei*	5	1	4	0
Cercopithecidae	*Presbytis rubicunda*	5	2	3	0
Cercopithecidae	*Theropithecus gelada*	5	4	1	0
Cercopithecidae	*Trachypithecus cristatus*	5	0	5	0
Hylobatidae	*Hoolock hoolock*	6	2	4	0
Hylobatidae	*Hylobates lar*	7	0	7	0
Hylobatidae	*Symphalangus syndactylus*	4	2	2	0
Hominidae	*Gorilla gorilla*	7	2	5	0
Hominidae	*Homo sapiens*	5	2	3	0
Hominidae	*Pan paniscus*	5	1	4	0
Hominidae	*Pan troglodytes*	7	4	3	0
Hominidae	*Pongo pygmaeus*	6	0	4	2

Abbreviations: n, total number of specimens; M, males; F, females; ?, unknown sex.

shuffling characteristic of this genus during foraging, causing them spend an extremely large amount of time with an erect trunk posture (***Wrangham, 1980***).

Irrespective of the functional implications of the variation in vestibular morphology among anthropoids, our analyses show that this variation bears strong phylogenetic signal and, hence, has potential for reconstructing the evolutionary history of the group—particularly hominoids, which in spite of their extant decimated diversity are more variable in this regard (particularly when size differences among the SCs are considered) (***Spoor and Zonneveld, 1998***; ***Le Maître et al., 2017***) than the taxonomically more diverse cercopithecoids. Although functional demands frequently lead to the independent evolution of similar morphologies (homoplasy), often function is not decoupled from—but superimposed on—phylogeny, with many clades being characterized by synapomorphic features linked to the adaptation for new functions. Therefore, to the extent that vestibular morphology appears to be linked to positional behavior (***Spoor et al., 1994***; ***Spoor et al., 2007***; ***Walker et al., 2008***; ***Silcox et al., 2009***; ***Ryan et al., 2012***; ***Le Maître et al., 2017***), the higher variation of vestibular morphology displayed by hominoids compared to cercopithecoids agrees with the more diverse and varied locomotor repertoires of the former. This is because cercopithecoids as a whole are largely pronograde terrestrial quadrupeds that mostly differ in the degree of arboreality vs. terrestriality (***Fleagle, 2013***; ***Gosselin-Ildari, 2013***), while crown hominoids are characterized by a derived

and versatile orthograde body plan and associated adaptations throughout the body that enable very different and very specialized antipronograde behaviors—vertical climbing (all apes), ricochetal brachiation (hylobatids), arboreal quadrumanous suspension and clambering (orangutans), below-branch arm-swinging as well as semiterrestrial knuckle-walking (African apes), and terrestrial bipedalism (humans) (**Hunt, 1991**; **Thorpe and Crompton, 2006**).

The fact that, in terms of positional behavior, extant hominoid lineages have more significantly diverged in different directions from their last common ancestor with cercopithecoids explains why extant hominoids more strongly differ in vestibular features—even if the functional link of some vestibular features remains to be better determined. Determining the order in which these features evolved is therefore required to use them for inferring the phylogenetic placement of extinct hominoids. Besides proposing various potential synapomorphies for the hominoid and hominid clades, we further reconstruct the evolution of the vestibular apparatus in this group by estimating ancestral vestibular morphotypes by means of maximum likelihood and a molecular phylogeny. From the LCA of crown hominoids, great apes and humans appear derived in the opposite direction of hylobatids with regard to their volumetric proportions (stout vs. slender SCs, respectively). According to our ancestral state reconstruction for crown hominoids, in this regard hylobatids appear secondarily convergent with cercopithecoids. However, this hypothesis (and the alternate one, that hylobatids merely reflect more closely the primitive condition for crown catarrhines as a whole) should be tested by means of adding extinct stem cercopithecoids and fossil hominoids of less controversial affinities than *Oreopithecus* to the analysis. It is noteworthy that *Hoolock*, in agreement with the basal position of this genus among extant hylobatids, apparently retains a more primitive morphology than other hominoids for various features. While the characters related to an anteromedial displacement of the lateral SC appear synapomorphic for hominoids, the only incipient vertical compression of the anterior canal SC morphology of *Hoolock* might be plesiomorphic for hylobatids, in which case the marked vertical compression of this canal would be a synapomorphy of hominids only, with the remaining hylobatid genera having also evolved it in parallel.

While various great ape lineages and humans further diverged from one another from the more derived condition of the reconstructed crown hominoid LCA, as noted above gibbons and siamangs might have secondarily converged to some extent with cercopithecoids by evolving slenderer SCs, presumably as a result of similar evolutionary pressures posed by fast-moving types of locomotion. Based on our reconstructed ancestral morphotypes, bonobos and (to a lesser extent) chimpanzees would be closer to the LCAs of hominids, hominines, and the *Pan-Homo* clade, than either humans or the remaining extant great apes (gorillas and orangutans). The latter would have diverged from the hominid LCA in markedly different directions both in terms of SC configuration and stoutness. Our results therefore support the view that not only hominins, but also gorillas and, to a large extent, the orangutan lineage diverged from ancestors with a largely *Pan*-like vestibular morphology. It would be tempting to interpret this pattern in locomotor terms (e.g., by suggesting a semiterrestrial ancestry not only for hominines, but also for crown hominids as a whole). However, caution is required as other selection pressures and/or non-adaptive factors could have potentially played an equally, if not more significant, role in determining vestibular shape variation in this group.

With regard to the fossil hominoids analyzed here, *Australopithecus* not only displays the various hominoid synapomorphies mentioned above, but also hominid-like volumetric proportions of the SCs and, as expected in a bipedal hominin, human-like vestibular features such as large anterior and posterior canals. This is in agreement with the large amount of habitual bipedal behaviors inferred for the almost complete skeleton (StW 573) to which one of the analyzed specimens belongs (**Heaton et al., 2019**), as well as previous analyses of the inner ear as a whole (**Beaudet et al., 2019b**). Following our ancestral state reconstruction, *Australopithecus* appears derived in the same direction as humans, although it more closely resembles the morphology of the *Australopithecus-Homo* clade LCA, which is derived from the reconstructed LCA of the *Pan-Homo* clade in the opposite direction as chimpanzees and bonobos are. The fact that the two analyzed specimens of *Australopithecus* are classified as humans with a moderately high probability reflects the fact that their vestibular morphology already approximates the human condition, although maintaining plesiomorphic characters, particularly in the specimen that more closely resembles chimpanzees. On the other hand, their similar classification probability with other extant great ape genera is consistent with a more primitive vestibular morphology. It is noteworthy that, although the two analyzed individuals are very similar to one another (**Beaudet et al., 2019b**), they display noticeable differences in

vestibular morphology, with StW 578 showing more human-like (even if stouter, approximating the orangutan morphology) canals and StW 573 retaining a more African great ape-like morphology. This could be related with diachronic changes within South African *Australopithecus* or to its previously noted heterogeneity (**Clarke, 2013**; **Grine, 2013**), and might help to discern, coupled with other features, the number of species represented among the current samples.

Unlike *Australopithecus*, *Oreopithecus* displays a mosaic vestibular morphology that defies a simple phylogenetic interpretation, as it does not fit well among the variation displayed by any extant hominoid genus. This is due to the combination of some hominoid and hominid synapomorphies with more plesiomorphic, cercopithecoid-like, or even platyrrhine-like, features. In particular, the hominid-like volumetric proportions of the *Oreopithecus* SCs would support the contention that this taxon is a great ape (**Begun et al., 1997**), or even a member of the European dryopithecine radiation, as previously argued by some authors (**Köhler and Moyà-Solà, 1997**; **Harrison and Rook, 1997**). However, other, apparently more plesiomorphic vestibular features, are at odds with such an interpretation, and even with the previous suggestion that *Oreopithecus* postcranium would be consistent with a giant hylobatid that emphasized cautious climbing (**Sarmiento, 1987**). In particular, the vestibular morphology of *Oreopithecus* does not overlap with that of extant hylobatids in any respect, particularly differing by the acute angle between the anterior and posterior canal planes and by the large posterior canal relative to the others. *Oreopithecus* also appears more primitive than crown hominoids in the shape of the lateral canal, which is flat (rather than displaying an upwards bent ampullar portion) and posteriorly displaced (especially in the junction between the ampulla and the vestibular recesses). In these regard, the *Oreopithecus* morphology more closely resembles that of cercopithecoids and platyrrhines, respectively, possibly reflecting a plesiomorphic condition that would be more consistent with a stem hominoid status, as recently supported by some other authors (**Nengo et al., 2017**).

If our interpretation above is correct, then the stout volumetric proportions of *Oreopithecus* would be homoplastic with those of great apes and humans, representing an independent acquisition that might be functionally related to the evolution of a slower mode of locomotion—in agreement with previous analysis of the inner ear of this taxon (**Rook et al., 2004**; **Ryan et al., 2012**) and the possession of an orthograde body plan with adaptations related to cautious vertical climbing and forelimb-dominated suspension (**Sarmiento, 1987**; **Harrison and Rook, 1997**). This is plausible given that hylobatids appear to some extent convergent in this regard to cercopithecoids, due to their agile locomotion. This suggests that volumetric proportions are quite labile in evolutionary terms, so that other features and functional considerations must also be considered when interpreting the vestibular morphology of extinct taxa in phylogenetic terms. Interestingly, *Oreopithecus* resembles australopiths and humans in the possession of a larger vertical and posterior canals relative to the lateral one, which apparently represents another homoplasy that would lend some support to the controversial claim that bipedalism featured prominently among the locomotor repertoire of this taxon (**Köhler and Moyà-Solà, 1997**; **Rook et al., 1999**). However, the SCs of *Oreopithecus* are clearly distinguishable from those present in *Homo* and *Australopithecus* regarding volumetric proportions, orientation, and shape. This rules out a hominin-like bipedalism for *Oreopithecus*—in further agreement with the lack of the lower torso features than in australopiths and humans are functionally linked to committed bipedalism (**Hammond et al., 2020**)—but would not be at odds with the possession of more varied orthograde positional behaviors combining climbing with a different type of bipedalism (more related to a stable bipedal stance and short distance shuffling instead of fast walking or running), as previously inferred based on the foot of this taxon (**Köhler and Moyà-Solà, 1997**).

In conclusion, our study provides new insight into the evolution of the vestibular apparatus in hominoids and confirms the potential of SC shape for investigating further the phylogenetic affinities of fossil apes, which are still controversial due to the inherent limitations of the fossil record. This is not to say that functional considerations must not be taken into account—rather the contrary, as several of the discussed vestibular features are arguably linked with the demands of particular positional behaviors, as noted by previous authors (**Spoor et al., 2007**; **Walker et al., 2008**; **Silcox et al., 2009**; **Ryan et al., 2012**; **Perier et al., 2016**; **Le Maître et al., 2017**). However, as exemplified by the analysis of the extinct hominin *Australopithecus*, the various characters identified as potentially synapomorphic for either crown hominoids or hominids offer the prospect of refining the phylogenetic placement of fossil apes for which their stem vs. crown hominoid status is controversial—as

these features can be easily scored from CTs of the petrosal bone and incorporated into formal cladistic analyses including information from other anatomical areas. On the other hand, our ancestral state reconstructions rely mainly on living taxa, which is potentially problematic in the case of hominoids, which were much more diverse in the Miocene and appear quite prone to homoplasy, particularly with regard to the locomotor adaptations of the few surviving lineages. Even if the quantification of phylogenetic signal based on the phylogeny of extant taxa indicates that vestibular morphology overall is not significantly affected by homoplasy, the evolutionary history of vestibular morphology presented here on the basis of ancestral morphotypes should be treated with caution as a set of working hypotheses that require further testing based on the information provided by a larger fossil sample. In particular, given the relationship between vestibular morphology and positional behavior, and the fact that the locomotor apparatus of extinct hominoids frequently displays a mosaic of primitive and derived features unknown among the surviving lineages (e.g., ***Moyà-Solà et al., 2004***; ***Alba, 2012***; ***Alba et al., 2015***; ***Böhme et al., 2019***), it may be predicted that the vestibular morphology of extinct hominoids will similarly display unique combinations of features. This is illustrated here by the condition of *Oreopithecus*, which is nevertheless most consistent with that of a stem hominoid somewhat convergent with hominids in terms of locomotion. In any case, our conclusions should be subjected to further scrutiny in the future by means of the inclusion of additional fossil taxa, with emphasis on Miocene hominoids as well as stem cercopithecoids.

Materials and methods

Sample composition and acquisition

The analyzed sample includes microcomputed tomography (µCT) scans of 142 dried anthropoid crania belonging to 27 species and 25 genera, including all extant great ape genera and a selection of hylobatids, cercopithecoids, and platyrrhines (***Table 9*** and ***Supplementary file 1***). A few specimens are juveniles instead of adults, but this should not affect their vestibular morphology as the bony labyrinth ossifies in early prenatal stages, bounding its shape and size (***Jeffery and Spoor, 2004***; ***Perier et al., 2016***). The hominoid subsample consists of 48 individuals belonging to 8 species and seven genera (***Supplementary file 1***). For each specimen, the bony labyrinth was virtually extracted (from the left side when possible, or otherwise from the right side and mirrored) by segmenting the µCT image stacks (voxel size reported in ***Supplementary file 1***). Virtual 3D models were generated using Avizo 9.0.1 software (FEI Visualization Sciences Group). The fossil sample consists of one left bony labyrinth belonging to the late Miocene stem-hominoid *Oreopithecus bambolii* (***Rook et al., 2004***) and of two right inner ear that have been virtually extracted from the *Australopithecus* specimens StW 573 and StW 578 from Sterkfontein (***Beaudet et al., 2019b***).The vestibular apparatus was separated from the cochlea by cutting right under the oval window and the saccule, and filling the resulting hole with a flat surface in Geomagic Studio 2014 software (3D Systems).

Shape analysis

Our 3DGM approach is based on deformation methods (***Durrleman et al., 2012b***; ***Durrleman et al., 2012a***), which do not rely on a priori defined landmarks but consider instead the geometrical correspondences between continuous surfaces, and are particularly convenient for comparing overall shape and complex 3D surface changes (***Durrleman et al., 2012b***; ***Dumoncel et al., 2014***; ***Beaudet et al., 2016a***). This method relies on the construction of a sample-average surface model (template) and its deformation to the investigated surfaces (***Durrleman et al., 2012b***; ***Durrleman et al., 2012a***; ***Beaudet et al., 2016b***). Unlike in classical landmark-based 3DGM analyses, the surfaces are represented by a set of oriented faces and the comparisons do not assume a point-to-point correspondence between samples (***Durrleman et al., 2012b***). Prior to the analysis, the unscaled vestibular surfaces were aligned and scaled using the 'Align Surface' module of Avizo 9.0. Then, deformations between surfaces were mathematically modeled as a diffeomorphism (i.e., a one-to-one deformation of the 3D space that is smooth, invertible, and with a smooth inverse), and a set of momenta (vectors representing the flow of deformations from the initial position of the control points on the template to the target shape) were estimated with Deformetrica 3 software. Due to its high-demanding computational power, analyses were run in the CALMIP supercomputing center (Toulouse, France).

We inspected interspecific major patterns of shape variation by means of between-group principal components analysis (bgPCA) of the deformation-based shape residuals, using major clades (i.e., platyrrhines, cercopithecoids, hylobatids and hominids) as grouping factor. The restricted platyrrhine sample included in this study is aimed to serve as an outgroup for catarrhines, since the description of the vestibular morphology variation among New World monkeys as a whole is beyond the scope of this paper. Each group has been designed to include a large number of individuals (>>10) in order to prevent spurious separation between the groups used in the analysis. We preferred bgPCA over linear discriminant analysis (LDA) because the latter produces overexaggerated separation among groups when the number of variables is close to the number of the analyzed individuals (**Mitteroecker and Bookstein, 2011**). Taking into account that some authors have recently recommended caution when interpreting bgPCA results, as they might present spurious grouping (**Cardini et al., 2019**), we compared our results with those of a landmark-based 3DGM analysis ran on the same sample and investigated the presence of a preexisting group structure (See '*Exploration of a preexisting group structure in the tangent space of the vestibular shape*' section for further details).

Correlation between SC shape and size (allometry) was assessed using multivariate regression of the deformation fields against log-transformed cube root of the entire vestibular volume (ln Vol, in mm^3), as well as bivariate regressions computed for each bgPC against ln Vol. We further inspected the correlation between log-transformed cube root of the SC volume (ln VolSC, in mm^3; including the SCs and the CC cut at their connection with the vestibular recesses) and log-transformed length (ln L, in mm; measured along the streamline of the SCs and of the CC). All these regressions were performed for the whole anthropoid sample, as well as for hominids and non-hominids separately, as we detected several differences for the former. In the case of the ln VolSC vs. ln L regression, we also checked the homogeneity of slopes and intercepts between hominoids and the rest of the sample via analysis of covariance (ANCOVA). Regressions were performed by means of ordinary least-square linear regression (OLS) as well as by taking into account the phylogenetic non-independence between data, that is by fitting our linear models via phylogenetic generalized least squares (PGLS). The data used to compute the regressions are given in **Figure 7—source data 1**.

The hierarchical clustering analysis (HCA) of the deformation fields (used to identify preexisting group structure embedded in our shape data) has been computed *caret* v6.0–84 (**Kuhn, 2008**) and *Factominer* v1.34 (**Le et al., 2008**) R packages. The discrimination and the amount of overlap among the groups defined a priori for the bgPCA has been quantified by computing the number of correctly classified individuals with cross-validation using the *Morpho* v2.6 (**Schlager, 2014**) R package. Finally, we estimated the posterior probabilities of group membership for the fossil specimens based on the Mahalanobis distances between their bgPC scores and group centroids using the '*typprobClass*' function of *Morpho* v2.6 (**Schlager, 2014**) R package. These probabilities, which were computed for both bgPCA (based on main anthropoid groups as well as on extant hominoid genera only) denote the likelihood of the specimens to belong to each group without assuming that it must belong to one of them (which is required when comparing the fossils with extant genera), so that the sum of probabilities for each specimen does not equal one. Probabilities < 0.05 indicate that the specimen falls outside the variability of that particular group. Further statistical analyses were carried out using different R packages in RStudio v.1.1.453 for R v.3.5.0: *ape* v5.1 (**Paradis, 2012**), *phytools* v0.6–60 (**Revell, 2012**), *Morpho* v2.6 (**Schlager, 2014**), *caper* v1.0.2 (**Orme et al., 2013**), and *geomorph* v3.1.1 (**Adams et al., 2019**).

Phylogenetic signal analysis

To assess phylogenetic signal, that is the degree to which related species resemble each other (**Felsenstein, 1985**; **Harvey and Pagel, 1991**), we used a phylogenetic tree (**Figure 13**) derived from a time-calibrated molecular phylogeny for the extant taxa (**Springer et al., 2012**). Estimated mean divergence dates for the various included extant clades are indicated in **Figure 13** (see **Table 1** and S1 in **Springer et al. (2012)** for 95% composite credibility intervals). The phylogenetic placement of *Oreopithecus* has been controversial; for our purposes here, we followed **Nengo et al. (2017)** in considering this taxon as a stem-hominoid, although other possibilities are discussed in the text. The node of the *Oreopithecus*-crown hominoid divergence has been placed 1 Ma older than the divergence of crown apes and humans and its tip corresponds to its last occurrence in the fossil record (7.0–6.5 Ma; **Rook et al., 2000**). For the South African *Australopithecus* sp., we used the published

first appearance datum for *Australopithecus africanus* (4.02 Ma) that includes the Jacovec specimens into the taxon (**Wood and Boyle, 2016**).

We computed Pagel's λ (**Pagel, 1999**), Blomberg's *K* (**Blomberg et al., 2003**) and K_{mult} (**Adams, 2014**) using *phytools* v.0.6–44 (**Revell, 2012**) and *geomorph* v3.1.1 (**Adams et al., 2019**) R packages. These metrics compare the variance in the phylogenetic tree tips relative to that expected under a Brownian motion evolutionary model. Pagel's λ is a scaling coefficient of the expected correlations between related species on the tree, and varies from 0 (no correlation due to absence of phylogenetic signal) to 1 (covariance proportional to phylogenetic distance, implying maximal phylogenetic signal). Blomberg's *K* and its multivariate generalization K_{mult} inform on how precisely the variance-covariance patterns found in the data are matched by the phylogenetic tree and where variance accumulates: $K \approx$ one implies that the mode of evolution closely resembles that expected under Brownian motion; when $K < 1$, close relatives resemble each other less than expected (variance is accumulated within clades), implying an evolutionary pattern that departs from a purely stochastic model (which could be caused by adaptation uncorrelated with phylogeny, that is homoplasy); finally, $K > 1$ is found when close relatives are more similar than expected under Brownian motion (variance is among clades), which could indicate stabilizing selection.

Phylomorphospace and ancestral states analysis

To quantify major patterns of vestibular shape variation along the branches of the phylogeny we relied on a phylomorphospace approach (**Sidlauskas, 2008**), which allows us to intuitively visualize the extent and direction of the inferred shape change by means of branch length and orientation. This method projects the phylogenetic tree (**Figure 13**) onto the tangent space computed from the bgPCA and estimates the position in the morphospace of the internal nodes (ancestral morphologies) via a maximum likelihood (ML) method for continuous characters (**Felsenstein, 1988**; **Schluter et al., 1997**) using the 'fastAnc' function of *phytools* v0.6–60 R package (**Revell, 2012**). Subsequently, the bgPC scores of the ancestral states are rotated and translated from the shape data back into the configuration space for interpolation and 3D visualization using Deformetrica 3 software.

Acknowledgements

Access to the HPC resources of CALMIP supercomputing center were granted under the allocation 2016-[P1440] attributed to the AMIS Laboratory, Toulouse (France). This work has been funded by the Agencia Estatal de Investigación and European Regional Development Fund of the European Union (projects CGL2016-76431-P and CGL2017-82654-P, AEI/FEDER, EU), by the Ministerio de Economía y Empresa (grant BES-2015–071318 to AU), the Generalitat de Catalunya (CERCA Programme, and consolidated research groups 2017 SGR 86 and 2017 SGR 116 GRC), and the French CNRS. We deeply thank Sergio Almécija for helpful advice and discussion during the elaboration of this paper and José Braga for valuable suggestions. We are grateful to Lorenzo Rook for giving access to the *Oreopithecus bambolii* petrosal bone originally published in **Rook et al. (2004)**. Lynn Copes, Lynn Lucas, and the MCZ provided access to a part of the scans used in the study, originally appearing in **Copes et al. (2016)**, funding for the collection of which was provided by NSF DDIG #0925793, and a Wenner-Gren Foundation Dissertation Grant #8102 (both to Lynn Copes). The Evolutionary Studies Institute provided access to the *Australopithecus* sp. data originally appearing in **Beaudet (2019a)**, the collection of which was funded by PAST, DST-NRF, CoE-Pal, Claude Leon Foundation, IFAS, French embassy, Leakey Foundation, Wits University. The scans for fossil and extant species were downloaded from MorphoSource.org, a web-accessible archive for 3D digital data housed by Duke University.

Additional information

Funding

Funder	Grant reference number	Author
Agencia Estatal de Investigación	CGL2016-76431-P	David M Alba

Agencia Estatal de Investigación	CGL2017-82654-P	Alessandro Urciuoli Salvador Moyà-Solà
Generalitat de Catalunya	2017 SGR 86	Alessandro Urciuoli Salvador Moyà-Solà
Generalitat de Catalunya	2017 SGR 116	David M Alba
Agencia Estatal de Investigación	BES-2015–071318	Alessandro Urciuoli

The funders had no role in study design, data collection and interpretation, or the decision to submit the work for publication.

Author contributions

Alessandro Urciuoli, Conceptualization, Data curation, Software, Formal analysis, Investigation, Visualization, Methodology, Writing - original draft, Writing - review and editing; Clément Zanolli, Conceptualization, Data curation, Software, Methodology, Writing - review and editing; Amélie Beaudet, Data curation, Software, Formal analysis, Methodology, Writing - review and editing; Jean Dumoncel, Software, Methodology; Frédéric Santos, Data curation, Software, Methodology; Salvador Moyà-Solà, Formal analysis, Supervision, Funding acquisition, Writing - review and editing; David M Alba, Conceptualization, Data curation, Formal analysis, Supervision, Investigation, Writing - original draft, Writing - review and editing

Author ORCIDs

Alessandro Urciuoli https://orcid.org/0000-0002-6265-8962
Clément Zanolli https://orcid.org/0000-0002-5617-1613
Amélie Beaudet https://orcid.org/0000-0002-9363-5966
Frédéric Santos https://orcid.org/0000-0003-1445-3871
David M Alba https://orcid.org/0000-0002-8886-5580

Decision letter and Author response

Decision letter https://doi.org/10.7554/eLife.51261.sa1
Author response https://doi.org/10.7554/eLife.51261.sa2

Additional files

Supplementary files

- Supplementary file 1. List of extant anthropoid specimens analyzed in this paper. µCT image stacks were downloaded from MorphoSource digital repository at https://www.MorphoSource.org (Duke University, Durham, NC, USA) or scanned at Paul Sabatier University (PSU, Toulouse, France), the American Museum of Natural History (AMNH; New York, NY, USA) and Centro Nacional de Investigación sobre la Evolución Humana (CENIEH; Burgos, Spain).
- Transparent reporting form

Data availability

All the results generated during this study are included as in the manuscript and as supporting files. Source data files are provided for Figures 2, 7, 8, and 9.

The following previously published datasets were used:

Author(s)	Year	Dataset title	Dataset URL	Database and Identifier
Beaudet A, Clarke RJ, Bruxelles L, Carlson KJ, Crompton R, de Beer F, Dhaene J, Heaton JL, Jakata K, Jashashvili T, Kuman K, McCly-	2019	Sterkfontein	https://www.morphosource.org/Detail/ProjectDetail/Show/project_id/632	MorphoSource, 632

mont J, Pickering TR, Stratford D				
Copes LE, Lucas LM, Thostenson JO, Hoekstra HE, Boyer DM	2016	A collection of non-human primate computed tomography scans housed in MorphoSource, a repository for 3D data	https://www.morphosource.org/Detail/ProjectDetail/Show/project_id/116	MorphoSource, 116

References

Adams DC. 2014. A generalized K statistic for estimating phylogenetic signal from shape and other high-dimensional multivariate data. *Systematic Biology* **63**:685–697. DOI: https://doi.org/10.1093/sysbio/syu030

Adams DC, Collyer ML, Kaliontzopoulou A. 2019. Geomorph: Software for geometric morphometric analyses. *R Package Version* .https://cran.rproject.org/package=geomorph

Alba DM, Almécija S, Moyà-Solà S. 2010. Locomotor inferences in *Pierolapithecus* and *Hispanopithecus*: reply to Deane and begun (2008). *Journal of Human Evolution* **59**:143–149. DOI: https://doi.org/10.1016/j.jhevol.2010.02.002, PMID: 20510436

Alba DM. 2012. Fossil apes from the Vallès-Penedès basin. *Evolutionary Anthropology* **21**:254–269. DOI: https://doi.org/10.1002/evan.21312, PMID: 23280922

Alba DM, Almécija S, DeMiguel D, Fortuny J, Pérez de los Ríos M, Pina M, Robles JM, Moyà-Solà S. 2015. Miocene small-bodied ape from eurasia sheds light on hominoid evolution. *Science* **350**:aab2625. DOI: https://doi.org/10.1126/science.aab2625, PMID: 26516285

Beaudet A, Dumoncel J, de Beer F, Duployer B, Durrleman S, Gilissen E, Hoffman J, Tenailleau C, Thackeray JF, Braga J. 2016a. Morphoarchitectural variation in South African fossil cercopithecoid endocasts. *Journal of Human Evolution* **101**:65–78. DOI: https://doi.org/10.1016/j.jhevol.2016.09.003, PMID: 27886811

Beaudet A, Dumoncel J, Thackeray JF, Bruxelles L, Duployer B, Tenailleau C, Bam L, Hoffman J, de Beer F, Braga J. 2016b. Upper third molar internal structural organization and semicircular canal morphology in Plio-Pleistocene South African cercopithecoids. *Journal of Human Evolution* **95**:104–120. DOI: https://doi.org/10.1016/j.jhevol.2016.04.004

Beaudet A. 2019a. The inner ear of the *Paranthropus* specimen DNH 22 from Drimolen, South Africa. *American Journal of Physical Anthropology* **170**:439–446. DOI: https://doi.org/10.1002/ajpa.23901, PMID: 31290572

Beaudet A, Clarke RJ, Bruxelles L, Carlson KJ, Crompton R, de Beer F, Dhaene J, Heaton JL, Jakata K, Jashashvili T, Kuman K, McClymont J, Pickering TR, Stratford D. 2019b. The bony labyrinth of StW 573 ("Little Foot"): Implications for early hominin evolution and paleobiology. *Journal of Human Evolution* **127**:67–80. DOI: https://doi.org/10.1016/j.jhevol.2018.12.002

Begun DR, Ward CV, Rose MD. 1997. Events in Hominoid Evolution. In: *Function, Phylogeny and Fossils: Miocene Hominoid Evolution and Adaptation*. New York: Plenum Press. p. 389–415. DOI: https://doi.org/10.1007/978-1-4899-0075-3_18

Begun DR. 2013. The Miocene Hominoid Radiations. In: *A Companion to Paleoanthropology*. Oxford: Blackwell. p. 398–416. DOI: https://doi.org/10.1002/9781118332344.ch21

Begun DR. 2015. Fossil Record of Miocene Hominoids. In: *Handbook of Paleoanthropology*. London: Springer. p. 1261–1332. DOI: https://doi.org/10.1007/978-3-642-39979-4_32

Benson RBJ, Starmer-Jones E, Close RA, Walsh SA. 2017. Comparative analysis of vestibular ecomorphology in birds. *Journal of Anatomy* **231**:990–1018. DOI: https://doi.org/10.1111/joa.12726, PMID: 29156494

Blomberg SP, Garland T, Ives AR. 2003. Testing for phylogenetic signal in comparative data: behavioral traits are more labile. *Evolution* **57**:717–745. DOI: https://doi.org/10.1111/j.0014-3820.2003.tb00285.x

Böhme M, Spassov N, Fuss J, Tröscher A, Deane AS, Prieto J, Kirscher U, Lechner T, Begun DR. 2019. A new Miocene ape and locomotion in the ancestor of great apes and humans. *Nature* **575**:489–493. DOI: https://doi.org/10.1038/s41586-019-1731-0

Cardini A, O'Higgins P, Rohlf FJ. 2019. Seeing distinct groups where there are none: spurious patterns from Between-Group PCA. *Evolutionary Biology* **46**:303–316. DOI: https://doi.org/10.1007/s11692-019-09487-5

Cheung B, Ercoline W. 2018. Semicircular canal size and shape influence on disorientation. *Aerospace Medicine and Human Performance* **89**:744–748. DOI: https://doi.org/10.3357/AMHP.5104.2018, PMID: 30020060

Clarke R. 2013. *Australopithecus* from Sterkfontein Caves, South Africa. In: Reed K, Fleagle J, Leakey R (Eds). *The Paleobiology Of Australopithecus*. Dordrecht: Springer. DOI: https://doi.org/10.1007/978-94-007-5919-0_7

Conde-Valverde M, Quam R, Martínez I, Arsuaga J-L, Daura J, Sanz M, Zilhão J. 2018. The bony labyrinth in the Aroeira 3 Middle Pleistocene cranium. *Journal of Human Evolution* **124**:105–116. DOI: https://doi.org/10.1016/j.jhevol.2018.08.003

Copes LE, Lucas LM, Thostenson JO, Hoekstra HE, Boyer DM. 2016. A collection of non-human primate computed tomography scans housed in MorphoSource, a repository for 3D data. *Scientific Data* **3**:160001. DOI: https://doi.org/10.1038/sdata.2016.1

Corruccini RS. 1987. The dentinoenamel junction in primates. *International Journal of Primatology* **8**:99–114. DOI: https://doi.org/10.1007/BF02735159

Costeur L, Grohé C, Aguirre-Fernández G, Ekdale E, Schulz G, Müller B, Mennecart B. 2018. The bony labyrinth of toothed whales reflects both phylogeny and habitat preferences. *Scientific Reports* **8**:7841. DOI: https://doi.org/10.1038/s41598-018-26094-0

Coutier F, Hautier L, Cornette R, Amson E, Billet G. 2017. Orientation of the lateral semicircular canal in Xenarthra and its links with head posture and phylogeny. *Journal of Morphology* **278**:704–717. DOI: https://doi.org/10.1002/jmor.20665

David R, Droulez J, Allain R, Berthoz A, Janvier P, Bennequin D. 2010. Motion from the past. A new method to infer vestibular capacities of extinct species. *Comptes Rendus Palevol* **9**:397–410. DOI: https://doi.org/10.1016/j.crpv.2010.07.012

Dumoncel J, Durrleman S, Braga J, Jessel JP, Subsol G. 2014. Landmark-free 3D method for comparison of fossil hominins and hominids based on endocranium and EDJ shapes. *American Journal of Physical Anthropology*: 153.

Durrleman S, Pennec X, Trouvé A, Ayache N, Braga J. 2012a. Comparison of the endocranial ontogenies between chimpanzees and bonobos via temporal regression and spatiotemporal registration. *Journal of Human Evolution* **62**:74–88. DOI: https://doi.org/10.1016/j.jhevol.2011.10.004

Durrleman S, Prastawa M, Korenberg JR, Joshi S, Trouvé A, Gerig G. 2012b. Topology Preserving Atlas Construction from Shape Data without Correspondence Using Sparse Parameters. In: Ayache N, Delingette H, Golland P, Mori K (Eds). *Proceedings of Medical Image Computing and Computer Aided Intervention*. Berlin: Springer-Verlag. p. 223–230. DOI: https://doi.org/10.1007/978-3-642-33454-2_28

Felsenstein J. 1985. Phylogenies and the comparative method. *The American Naturalist* **125**:1–15. DOI: https://doi.org/10.1086/284325

Felsenstein J. 1988. Phylogenies and quantitative characters. *Annual Review of Ecology and Systematics* **19**:445–471. DOI: https://doi.org/10.1146/annurev.es.19.110188.002305

Fleagle JG. 2013. *Primate Adaptation and Evolution*. San Diego. Academic press.

Gannon PJ, Eden AR, Laitman JT. 1988. The subarcuate Fossa and cerebellum of extant primates: comparative study of a skull-brain interface. *American Journal of Physical Anthropology* **77**:143–164. DOI: https://doi.org/10.1002/ajpa.1330770202, PMID: 3207165

Glaunés JA, Joshi S. 2006. Template Estimation Form Unlabeled Point Set Data and Surfaces for Computational Anatomy. In: Pennec X (Ed). *Proceedings of the International Workshop on the Mathematical Foundations of Computational Anatomy Sophia-Antipolis*. INRIA. p. 28–39.

Gosselin-Ildari AD. 2013. *The Evolution of Cercopithecoid Locomotion: A Morphometric, Phylogenetic, and Character Mapping Approach. Ph.D Dissertation*. Stony Brook University.

Grine FE. 2013. The Alpha Taxonomy of *Australopithecus africanus*. In: Delson E, Sargis EJ (Eds). *The Paleobiology of Australopithecus*. Dordrecht: Springer. p. 73–104. DOI: https://doi.org/10.1007/978-94-007-5919-0_6

Grohé C, Tseng ZJ, Lebrun R, Boistel R, Flynn JJ. 2016. Bony labyrinth shape variation in extant Carnivora: a case study of Musteloidea. *Journal of Anatomy* **228**:366–383. DOI: https://doi.org/10.1111/joa.12421

Gunz P, Ramsier M, Kuhrig M, Hublin JJ, Spoor F. 2012. The mammalian bony labyrinth reconsidered, introducing a comprehensive geometric morphometric approach. *Journal of Anatomy* **220**:529–543. DOI: https://doi.org/10.1111/j.1469-7580.2012.01493.x, PMID: 22404255

Hammond AS, Rook L, Anaya AD, Cioppi E, Costeur L, Moyà-Solà S, Almécija S. 2020. Insights into the lower torso in late miocene hominoid *Oreopithecus bambolii*. *PNAS* **117**:278–284. DOI: https://doi.org/10.1073/pnas.1911896116, PMID: 31871170

Harrison T. 2010. Anthropology. apes among the tangled branches of human origins. *Science* **327**:532–534. DOI: https://doi.org/10.1126/science.1184703, PMID: 20110491

Harrison T. 2013. Catarrhine Origins. In: Begun D. R (Ed). *A Companion to Paleoanthropology*. Oxford: Blackwell Publishing. p. 376–396. DOI: https://doi.org/10.1002/9781118332344

Harrison T. 2016. The Fossil Record and Evolutionary History of Hylobatids. Evolution of Gibbons and Siamang. In: Reichard UH, Hirai H, Barelli C (Eds). *Phylogeny, Morphology, and Cognition*. London: Springer. p. 90–110. DOI: https://doi.org/10.1007/978-1-4939-5614-2_4

Harrison T, Rook L. 1997. Enigmatic Anthropoid or Misunderstood Ape? In: Begun DR, Ward CV (Eds). *Function, Phylogeny, and Fossils*. Boston: Springer. p. 327–362. DOI: https://doi.org/10.1007/978-1-4899-0075-3_16

Harvey PH, Pagel MD. 1991. *The Comparative Method in Evolutionary Biology*. Oxford: Oxford University Press.

Heaton JL, Pickering TR, Carlson KJ, Crompton RH, Jashashvili T, Beaudet A, Bruxelles L, Kuman K, Heile AJ, Stratford D, Clarke RJ. 2019. The long limb bones of the StW 573 *Australopithecus* skeleton from Sterkfontein Member 2: Descriptions and proportions. *Journal of Human Evolution* **133**:167–197. DOI: https://doi.org/10.1016/j.jhevol.2019.05.015, PMID: 31358179

Hunt KD. 1991. Positional behavior in the Hominoidea. *International Journal of Primatology* **12**:95–118. DOI: https://doi.org/10.1007/BF02547576

Jablonski NG, Frost S. 2010. Cercopithecoidea. In: Werdelin L, Sanders WL (Eds). *Cenozoic Mammals of Africa*. London: University of California Press. p. 393–429. DOI: https://doi.org/10.1525/california/9780520257214.003.0023

Jeffery N, Ryan TM, Spoor F. 2008. The primate subarcuate fossa and its relationship to the semicircular canals part II: adult interspecific variation. *Journal of Human Evolution* **55**:326–339. DOI: https://doi.org/10.1016/j.jhevol.2008.02.010, PMID: 18395770

Jeffery N, Spoor F. 2004. Prenatal growth and development of the modern human labyrinth. *Journal of Anatomy* **204**:71–92. DOI: https://doi.org/10.1111/j.1469-7580.2004.00250.x, PMID: 15032915

Johnson Chacko L, Schmidbauer DT, Handschuh S, Reka A, Fritscher KD, Raudaschl P, Saba R, Handler M, Schier PP, Baumgarten D, Fischer N, Pechriggl EJ, Brenner E, Hoermann R, Glueckert R, Schrott-Fischer A. 2018.

Analysis of vestibular labyrinthine geometry and variation in the human temporal bone. *Frontiers in Neuroscience* **12**:107. DOI: https://doi.org/10.3389/fnins.2018.00107, PMID: 29535601

Kelley J, Gao F. 2012. Juvenile hominoid cranium from the late miocene of southern China and hominoid diversity in Asia. *PNAS* **109**:6882–6885. DOI: https://doi.org/10.1073/pnas.1201330109, PMID: 22511723

Köhler M, Moyà-Solà S. 1997. Ape-like or hominid-like? the positional behavior of*Oreopithecus bambolii* reconsidered. *PNAS* **94**:11747–11750. DOI: https://doi.org/10.1073/pnas.94.21.11747, PMID: 9326682

Kuhn M. 2008. Building predictive models in *R* using the caret package. *Journal of Statistical Software* **28**:1–26. DOI: https://doi.org/10.18637/jss.v028.i05

Larson SG. 1998. Parallel evolution in the hominoid trunk and forelimb. *Evolutionary Anthropology* **6**:87–99. DOI: https://doi.org/10.1002/(SICI)1520-6505(1998)6:3<87::AID-EVAN3>3.0.CO;2-T

Le S, Josse J, Husson F. 2008. FactoMineR: an R package for multivariate analysis. *Journal of Statistical Software* **25**. DOI: https://doi.org/10.18637/jss.v025.i01

Le Maître A, Schuetz P, Vignaud P, Brunet M. 2017. New data about semicircular canal morphology and locomotion in modern hominoids. *Journal of Anatomy* **231**:95–109. DOI: https://doi.org/10.1111/joa.12619

Lebrun R, de León MP, Tafforeau P, Zollikofer C. 2010. Deep evolutionary roots of strepsirrhine primate labyrinthine morphology. *Journal of Anatomy* **216**:368–380. DOI: https://doi.org/10.1111/j.1469-7580.2009.01177.x

Lebrun R, Godinot M, Couette S, Tafforeau P, Zollikofer C. 2012. The labyrinthine morphology of *Pronycticebus gaudryi* (Primates, Adapiformes). *Palaeobiodiversity and Palaeoenvironments* **92**:527–537. DOI: https://doi.org/10.1007/s12549-012-0099-z

Malinzak MD, Kay RF, Hullar TE. 2012. Locomotor head movements and semicircular canal morphology in primates. *PNAS* **109**:17914–17919. DOI: https://doi.org/10.1073/pnas.1206139109

Mennecart B, DeMiguel D, Bibi F, Rössner GE, Métais G, Neenan JM, Wang S, Schulz G, Müller B, Costeur L. 2017. Bony labyrinth morphology clarifies the origin and evolution of deer. *Scientific Reports* **7**:13176. DOI: https://doi.org/10.1038/s41598-017-12848-9

Mitteroecker P, Bookstein F. 2011. Linear discrimination, ordination, and the visualization of selection gradients in modern morphometrics. *Evolutionary Biology* **38**:100–114. DOI: https://doi.org/10.1007/s11692-011-9109-8

Moyà Solà S, Köhler M. 1997. The phylogenetic relationships of *Oreopithecus bambolii* Gervais, 1872. *Comptes Rendus de l'Académie des Sciences Paris* **324**:141–148.

Moyà-Solà S, Köhler M, Alba DM, Casanovas-Vilar I, Galindo J. 2004. *Pierolapithecus catalaunicus*, a new middle miocene great ape from Spain. *Science* **306**:1339–1344. DOI: https://doi.org/10.1126/science.1103094, PMID: 15550663

Moyà-Solà S, Köhler M. 1993. Recent discoveries of *Dryopithecus* shed new light on evolution of great apes. *Nature* **365**:543–545. DOI: https://doi.org/10.1038/365543a0

Muller M. 1994. Semicircular duct dimensions and sensitivity of the vertebrate vestibular system. *Journal of Theoretical Biology* **167**:239–256. DOI: https://doi.org/10.1006/jtbi.1994.1066

Nengo I, Tafforeau P, Gilbert CC, Fleagle JG, Miller ER, Feibel C, Fox DL, Feinberg J, Pugh KD, Berruyer C, Mana S, Engle Z, Spoor F. 2017. New infant cranium from the african Miocene sheds light on ape evolution. *Nature* **548**:169–174. DOI: https://doi.org/10.1038/nature23456, PMID: 28796200

Orme CDL, Freckleton RP, Thomas GH, Petzoldt T, Fritz SA, Isaac NJB, Pearse W. 2013. The Caper Package: Comparative Analysis of Phylogenetics and Evolution in R. *R Package Version*. https://cran.r-project.org/web/packages/caper/index.html

Pagel M. 1999. Inferring the historical patterns of biological evolution. *Nature* **401**:877–884. DOI: https://doi.org/10.1038/44766, PMID: 10553904

Paradis E. 2012. *Analysis of Phylogenetics and Evolution with R*. New York: Springer. DOI: https://doi.org/10.1007/978-1-4614-1743-9

Perier A, Lebrun R, Marivaux L. 2016. Different level of intraspecific variation of the bony labyrinth morphology in slow- versus fast-moving primates. *Journal of Mammalian Evolution* **23**:353–368. DOI: https://doi.org/10.1007/s10914-016-9323-3

Ponce de León MS, Koesbardiati T, Weissmann JD, Milella M, Reyna-Blanco CS, Suwa G, Kondo O, Malaspinas A-S, White TD, Zollikofer CPE. 2018. Human bony labyrinth is an Indicator of population history and dispersal from africa. *PNAS* **115**:4128–4133. DOI: https://doi.org/10.1073/pnas.1717873115

Quam R, Lorenzo C, Martínez I, Gracia-Téllez A, Arsuaga JL. 2016. The bony labyrinth of the Middle Pleistocene Sima de los Huesos hominins (Sierra de atapuerca, Spain). *Journal of Human Evolution* **90**:1–15. DOI: https://doi.org/10.1016/j.jhevol.2015.09.007, PMID: 26767955

Rabbitt RD, Damiano ER, Grant JW. 2004. Biomechanics of the Semicircular Canals and Otolith Organs. In: Highstein SM, Fay RR, Popper AN (Eds). *The Vestibular System*. New York: Springer. p. 153–201. DOI: https://doi.org/10.1007/0-387-21567-0_4

Rae TC, Johnson PM, Yano W, Hirasaki E. 2016. Semicircular canal size and locomotion in colobine monkeys: a cautionary tale. *Folia Primatologica* **87**:213–223. DOI: https://doi.org/10.1159/000449286

Ramprashad F, Landolt JP, Money KE, Laufer J. 1984. Dimensional analysis and dynamic response characterization of mammalian peripheral vestibular structures. *American Journal of Anatomy* **169**:295–313. DOI: https://doi.org/10.1002/aja.1001690306, PMID: 6609629

Revell LJ. 2012. *Phytools*: an R package for phylogenetic comparative biology (and other things). *Methods in Ecology and Evolution* **3**:217–223. DOI: https://doi.org/10.1111/j.2041-210X.2011.00169.x

Rook L, Bondioli L, Köhler M, Moyà-Solà S, Macchiarelli R. 1999. *Oreopithecus* was a bipedal ape after all: evidence from the iliac cancellous architecture. *PNAS* **96**:8795–8799. DOI: https://doi.org/10.1073/pnas.96.15.8795, PMID: 10411955

Rook L, Renne P, Benvenuti M, Papini M. 2000. Geochronology of *Oreopithecus*-bearing succession at Baccinello (Italy) and the extinction pattern of european miocene hominoids. *Journal of Human Evolution* **39**:577–582. DOI: https://doi.org/10.1006/jhev.2000.0432, PMID: 11102268

Rook L, Bondioli L, Casali F, Rossi M, Köhler M, Moyá Solá S, Macchiarelli R. 2004. The bony labyrinth of *Oreopithecus bambolii*. *Journal of Human Evolution* **46**:347–354. DOI: https://doi.org/10.1016/j.jhevol.2004.01.001

Ryan TM, Silcox MT, Walker A, Mao X, Begun DR, Benefit BR, Gingerich PD, Köhler M, Kordos L, McCrossin ML, Moyà-Solà S, Sanders WJ, Seiffert ER, Simons E, Zalmout IS, Spoor F. 2012. Evolution of locomotion in Anthropoidea: the semicircular canal evidence. *Proceedings of the Royal Society B: Biological Sciences* **279**:3467–3475. DOI: https://doi.org/10.1098/rspb.2012.0939

Sarmiento EE. 1987. The phylogenetic position of *Oreopithecus* and its significance in the origin of the Hominoidea. *American Museum Novitates* **2881**:1–44.

Schlager S. 2014. Morpho: calculations and visualisations related to geometric morphometrics. https://github.com/zarquon42b/Morpho

Schluter D, Price T, Mooers Arne Ø., Ludwig D. 1997. Likelihood of ancestor states in adaptive radiation. *Evolution* **51**:1699–1711. DOI: https://doi.org/10.1111/j.1558-5646.1997.tb05095.x

Schwab JA, Kriwet J, Weber GW, Pfaff C. 2019. Carnivoran hunting style and phylogeny reflected in bony labyrinth morphometry. *Scientific Reports* **9**:70. DOI: https://doi.org/10.1038/s41598-018-37106-4, PMID: 30635617

Sidlauskas B. 2008. Continuous and arrested morphological diversification in sister clades of characiform fishes: a phylomorphospace approach. *Evolution* **62**:3135–3156. DOI: https://doi.org/10.1111/j.1558-5646.2008.00519.x

Silcox MT, Bloch JI, Boyer DM, Godinot M, Ryan TM, Spoor F, Walker A. 2009. Semicircular canal system in early primates. *Journal of Human Evolution* **56**:315–327. DOI: https://doi.org/10.1016/j.jhevol.2008.10.007, PMID: 19185902

Skinner MM, Wood BA, Boesch C, Olejniczak AJ, Rosas A, Smith TM, Hublin JJ. 2008. Dental trait expression at the enamel-dentine junction of lower molars in extant and fossil hominoids. *Journal of Human Evolution* **54**:173–186. DOI: https://doi.org/10.1016/j.jhevol.2007.09.012, PMID: 18048081

Spoor F, Wood B, Zonneveld F. 1994. Implications of early hominid labyrinthine morphology for evolution of human bipedal locomotion. *Nature* **369**:645–648. DOI: https://doi.org/10.1038/369645a0, PMID: 8208290

Spoor F, Hublin JJ, Braun M, Zonneveld F. 2003. The bony labyrinth of Neanderthals. *Journal of Human Evolution* **44**:141–165. DOI: https://doi.org/10.1016/S0047-2484(02)00166-5, PMID: 12662940

Spoor F, Garland T, Krovitz G, Ryan TM, Silcox MT, Walker A. 2007. The primate semicircular canal system and locomotion. *PNAS* **104**:10808–10812. DOI: https://doi.org/10.1073/pnas.0704250104, PMID: 17576932

Spoor F, Leakey M. 1996. Absence of the subarcuate fossa in cercopithecids. *Journal of Human Evolution* **31**:569–575. DOI: https://doi.org/10.1006/jhev.1996.0081

Spoor F, Zonneveld F. 1998. Comparative review of the human bony labyrinth. *American Journal of Physical Anthropology* **107**:211–251. DOI: https://doi.org/10.1002/(SICI)1096-8644(1998)107:27+<211::AID-AJPA8>3.0.CO;2-V

Springer MS, Meredith RW, Gatesy J, Emerling CA, Park J, Rabosky DL, Stadler T, Steiner C, Ryder OA, Janečka JE, Fisher CA, Murphy WJ. 2012. Macroevolutionary dynamics and historical biogeography of primate diversification inferred from a species supermatrix. *PLOS ONE* **7**:e49521. DOI: https://doi.org/10.1371/journal.pone.0049521, PMID: 23166696

Stevens NJ, Seiffert ER, O'Connor PM, Roberts EM, Schmitz MD, Krause C, Gorscak E, Ngasala S, Hieronymus TL, Temu J. 2013. Palaeontological evidence for an Oligocene divergence between Old World monkeys and apes. *Nature* **497**:611–614. DOI: https://doi.org/10.1038/nature12161, PMID: 23676680

Thorpe SK, Crompton RH. 2006. Orangutan positional behavior and the nature of arboreal locomotion in Jominoidea. *American Journal of Physical Anthropology* **131**:384–401. DOI: https://doi.org/10.1002/ajpa.20422, PMID: 16617429

Walker A, Ryan TM, Silcox MT, Simons EL, Spoor F. 2008. The semicircular canal system and locomotion: the case of extinct lemuroids and lorisoids. *Evolutionary Anthropology* **17**:135–145. DOI: https://doi.org/10.1002/evan.20165

Welker F, Ramos-Madrigal J, Kuhlwilm M, Liao W, Gutenbrunner P, de Manuel M, Samodova D, Mackie M, Allentoft ME, Bacon AM, Collins MJ, Cox J, Lalueza-Fox C, Olsen JV, Demeter F, Wang W, Marques-Bonet T, Cappellini E. 2019. Enamel proteome shows that *Gigantopithecus* was an early diverging pongine. *Nature* **576**:262–265. DOI: https://doi.org/10.1038/s41586-019-1728-8, PMID: 31723270

Wood B, Boyle EK. 2016. Hominin taxic diversity: fact or fantasy? *American Journal of Physical Anthropology* **159**:37–78. DOI: https://doi.org/10.1002/ajpa.22902

Wrangham RW. 1980. Bipedal locomotion as a feeding adaptation in gelada baboons, and its implications for hominid evolution. *Journal of Human Evolution* **9**:329–331. DOI: https://doi.org/10.1016/0047-2484(80)90059-7

Species	ID	Source	Voxel size	Sex	DOI
Alouatta palliata	DUEALP 02	MorphoSource	0,06	M	-
Alouatta palliata	DUEALP 04	MorphoSource	0,05	M	-
Alouatta palliata	DUEALP 06	MorphoSource	0,07	M	-
Alouatta palliata	DUEALP 10	MorphoSource	0,05	F	-
Alouatta palliata	DUEALP 12	MorphoSource	0,06	F	-
Ateles geoffroyi	MCZ 10138	MorphoSource	0,06	F	http://dx.doi.org/10.17602/M2/M2917
Ateles geoffroyi	MCZ 29626	MorphoSource	0,06	F	http://dx.doi.org/10.17602/M2/M2918
Ateles geoffroyi	MCZ 29628	MorphoSource	0,06	F	http://dx.doi.org/10.17602/M2/M2919
Ateles geoffroyi	MCZ 29658	MorphoSource	0,06	F	http://dx.doi.org/10.17602/M2/M2920
Ateles geoffroyi	MCZ BOM 5351	MorphoSource	0,06	M	http://dx.doi.org/10.17602/M2/M2889
Cebus apella	MCZ 27891	MorphoSource	0,06	M	http://dx.doi.org/10.17602/M2/M5208
Cebus apella	MCZ 31063	MorphoSource	0,07	F	http://dx.doi.org/10.17602/M2/M5213
Cebus apella	MCZ 37833	MorphoSource	0,06	M	http://dx.doi.org/10.17602/M2/M5218
Cebus apella	MCZ 41090	MorphoSource	0,05	F	http://dx.doi.org/10.17602/M2/M5219
Cebus apella	MCZ 49635	MorphoSource	0,06	M	http://dx.doi.org/10.17602/M2/M5220
Cercocebus galeritus	AMNHM 52634	MorphoSource	0,06	M	-
Cercocebus galeritus	AMNHM 52635	MorphoSource	0,06	F	-
Cercocebus galeritus	AMNHM 52640	MorphoSource	0,06	F	-
Cercocebus galeritus	AMNHM 52641	MorphoSource	0,07	M	-
Cercocebus galeritus	AMNHM 52645	MorphoSource	0,08	M	-
Cercopithecus mitis	MCZ 22734	MorphoSource	0,08	F	http://dx.doi.org/10.17602/M2/M2928
Cercopithecus mitis	MCZ 25022	MorphoSource	0,08	F	http://dx.doi.org/10.17602/M2/M2929
Cercopithecus mitis	MCZ 26832	MorphoSource	0,08	F	http://dx.doi.org/10.17602/M2/M2930
Cercopithecus mitis	MCZ 39389	MorphoSource	0,08	F	http://dx.doi.org/10.17602/M2/M2933
Cercopithecus mitis	MCZ 44264	MorphoSource	0,08	F	http://dx.doi.org/10.17602/M2/M2935
Chlorocebus pygerythrus	SIU 4792	MorphoSource	0,05	F	-
Chlorocebus pygerythrus	SIU 4793	MorphoSource	0,05	F	-
Chlorocebus pygerythrus	SIU 4794	MorphoSource	0,05	F	-
Chlorocebus pygerythrus	SIU 4795	MorphoSource	0,05	M	-
Chlorocebus pygerythrus	SIU 4796	MorphoSource	0,05	M	-
Colobus guereza	AMNHM 52211	MorphoSource	0,07	M	-
Colobus guereza	AMNHM 52213	MorphoSource	0,07	F	-
Colobus guereza	AMNHM 52225	MorphoSource	0,05	F	-

Colobus guereza	AMNHM 52237	MorphoSource	0,07	M	-
Colobus guereza	AMNHM 52249	MorphoSource	0,07	F	-
Erythrocebus patas	MCZ 37280	MorphoSource	0,08	M	http://dx.doi.org/10.17602/M2/M2922
Erythrocebus patas	MCZ 47015	MorphoSource	0,08	M	http://dx.doi.org/10.17602/M2/M2923
Erythrocebus patas	MCZ 47016	MorphoSource	0,08	M	http://dx.doi.org/10.17602/M2/M2924
Erythrocebus patas	MCZ 47017	MorphoSource	0,06	F	http://dx.doi.org/10.17602/M2/M2925
Erythrocebus patas	MCZ 47018	MorphoSource	0,08	F	http://dx.doi.org/10.17602/M2/M2926
Gorilla gorilla	AMNHA 999686	MorphoSource	0,13	M	-
Gorilla gorilla	AMNHA 999687	MorphoSource	0,08	F	-
Gorilla gorilla	AMNHM 167338	MorphoSource	0,13	M	-
Gorilla gorilla	AMNHM 54356	MorphoSource	0,11	F	-
Gorilla gorilla	MCZ 17684	MorphoSource	0,13	F	http://dx.doi.org/10.17602/M2/M2943
Gorilla gorilla	MCZ 26850	MorphoSource	0,12	F	http://dx.doi.org/10.17602/M2/M2943
Gorilla gorilla	MCZ 37264	MorphoSource	0,13	F	http://dx.doi.org/10.17602/M2/M2949
Homo sapiens	EMBR 121	PSU	0,04	F	-
Homo sapiens	EMBR 179	PSU	0,04	M	-
Homo sapiens	EMBR 212	PSU	0,04	F	-
Homo sapiens	EMBR 215	PSU	0,04	M	-
Homo sapiens	EMBR 281	PSU	0,04	F	-
Hoolock hoolock	AMNHM 112673	MorphoSource	0,04	F	-
Hoolock hoolock	AMNHM 112720	MorphoSource	0,05	F	-
Hoolock hoolock	AMNHM 112983	MorphoSource	0,04	M	-
Hoolock hoolock	AMNHM 201742	MorphoSource	0,07	F	-
Hoolock hoolock	AMNHM 83421	MorphoSource	0,04	M	-
Hoolock hoolock	AMNHM 83425	AMNH	0,08	F	-
Hylobates lar	MCZ 41411	MorphoSource	0,07	F	http://dx.doi.org/10.17602/M2/M2959
Hylobates lar	MCZ 41412	MorphoSource	0,07	F	http://dx.doi.org/10.17602/M2/M2961
Hylobates lar	MCZ 41416	MorphoSource	0,07	F	http://dx.doi.org/10.17602/M2/M2965
Hylobates lar	MCZ 41418	MorphoSource	0,07	F	http://dx.doi.org/10.17602/M2/M2967
Hylobates lar	MCZ 41421	MorphoSource	0,07	F	http://dx.doi.org/10.17602/M2/M2969
Hylobates lar	MCZ 41424	MorphoSource	0,07	F	http://dx.doi.org/10.17602/M2/M3007
Hylobates lar	MCZ 41452	MorphoSource	0,07	F	http://dx.doi.org/10.17602/M2/M3011
Lophocebus albigena	AMNHM 52596	MorphoSource	0,07	M	-
Lophocebus albigena	AMNHM 52603	MorphoSource	0,06	F	-

Lophocebus albigena	AMNHM 52606	MorphoSource	0,07	M	-
Lophocebus albigena	AMNHM 52607	MorphoSource	0,09	F	-
Lophocebus albigena	AMNHM 52615	MorphoSource	0,07	F	-
Macaca fascicularis	MCZ 12758	MorphoSource	0,06	F	http://dx.doi.org/10.17602/M2/M3028
Macaca fascicularis	MCZ 22277	MorphoSource	0,06	F	http://dx.doi.org/10.17602/M2/M3029
Macaca fascicularis	MCZ 23812	MorphoSource	0,06	M	http://dx.doi.org/10.17602/M2/M3030
Macaca fascicularis	MCZ 23813	MorphoSource	0,06	F	http://dx.doi.org/10.17602/M2/M3031
Macaca fascicularis	MCZ 35765	MorphoSource	0,06	F	http://dx.doi.org/10.17602/M2/M3033
Mandrillus sphinx	AMNHA 9912049	MorphoSource	0,08	M	-
Mandrillus sphinx	AMNHA 9912056	MorphoSource	0,08	M	-
Mandrillus sphinx	AMNHM 89362	MorphoSource	0,08	M	-
Mandrillus sphinx	AMNHM 89364	MorphoSource	0,1	M	-
Mandrillus sphinx	AMNHM 89365	MorphoSource	0,06	M	-
Miopithecus talapoin	MCZ 19976	MorphoSource	0,05	M	http://dx.doi.org/10.17602/M2/M5095
Miopithecus talapoin	MCZ 23196	MorphoSource	0,05	M	http://dx.doi.org/10.17602/M2/M5094
Miopithecus talapoin	MCZ 23197	MorphoSource	0,05	M	http://dx.doi.org/10.17602/M2/M5093
Miopithecus talapoin	MCZ 34264	MorphoSource	0,05	F	http://dx.doi.org/10.17602/M2/M5092
Miopithecus talapoin	MCZ 37278	MorphoSource	0,05	F	http://dx.doi.org/10.17602/M2/M5086
Nasalis larvatus	MCZ 37342	MorphoSource	0,07	F	http://dx.doi.org/10.17602/M2/M5079
Nasalis larvatus	MCZ 41555	MorphoSource	0,07	F	http://dx.doi.org/10.17602/M2/M5059
Nasalis larvatus	MCZ 41559	MorphoSource	0,07	F	http://dx.doi.org/10.17602/M2/M5057
Nasalis larvatus	MCZ 41560	MorphoSource	0,07	F	http://dx.doi.org/10.17602/M2/M5056
Nasalis larvatus	MCZ 41562	MorphoSource	0,07	F	http://dx.doi.org/10.17602/M2/M5055
Pan paniscus	AMNHM 86857	AMNH	0,12	F	-
Pan paniscus	IPS9033	CENIEH	0,07	F	-
Pan paniscus	MCZ 38018	MorphoSource	0,09	M	http://dx.doi.org/10.17602/M2/M4399
Pan paniscus	MCZ 38019	MorphoSource	0,09	F	http://dx.doi.org/10.17602/M2/M4398
Pan paniscus	MCZ 38020	MorphoSource	0,1	F	http://dx.doi.org/10.17602/M2/M4397
Pan troglodytes	AMNHM 167342	MorphoSource	0,09	M	-
Pan troglodytes	AMNHM 167344	MorphoSource	0,11	M	-
Pan troglodytes	AMNHM 51204	MorphoSource	0,08	M	-
Pan troglodytes	IPS5698	CENIEH	0,08	M	-
Pan troglodytes	MCZ 17702	MorphoSource	0,1	F	http://dx.doi.org/10.17602/M2/M4395
Pan troglodytes	MCZ 23167	MorphoSource	0,11	F	http://dx.doi.org/10.17602/M2/M4390

Pan troglodytes	MCZ 26847	MorphoSource	0,1	F	http://dx.doi.org/10.17602/M2/M4389
Papio anubis	AMNHM 52677	MorphoSource	0,09	M	-
Papio anubis	MCZ 17342	MorphoSource	0,11	M	http://dx.doi.org/10.17602/M2/M4885
Papio anubis	MCZ 26473	MorphoSource	0,1	F	http://dx.doi.org/10.17602/M2/M4890
Papio anubis	MCZ 31619	MorphoSource	0,11	F	http://dx.doi.org/10.17602/M2/M4892
Papio anubis	MCZ BOM 8466	MorphoSource	0,08	M	http://dx.doi.org/10.17602/M2/M4889
Piliocolobus badius	MCZ 24080	MorphoSource	0,08	M	http://dx.doi.org/10.17602/M2/M2892
Piliocolobus badius	MCZ 24775	MorphoSource	0,09	M	http://dx.doi.org/10.17602/M2/M2893
Piliocolobus badius	MCZ 24793	MorphoSource	0,08	F	http://dx.doi.org/10.17602/M2/M2894
Piliocolobus badius	MCZ 25627	MorphoSource	0,08	M	http://dx.doi.org/10.17602/M2/M2895
Piliocolobus badius	MCZ 25631	MorphoSource	0,09	M	http://dx.doi.org/10.17602/M2/M2896
Pongo pygmaeus	IPS10647	CENIEH	0,08	F	-
Pongo pygmaeus	IPS10651	CENIEH	0,08	F	-
Pongo pygmaeus	IPS9031	CENIEH	0,08	F	-
Pongo pygmaeus	IPSSN	CENIEH	0,08	F	-
Pongo pygmaeus	MHNTZOO 201108	PSU	0,04	?	-
Pongo pygmaeus	SENCK 1576UU	PSU	0,01	?	-
Presbytis hosei	MCZ 35621	MorphoSource	0,08	F	http://dx.doi.org/10.17602/M2/M4611
Presbytis hosei	MCZ 37370	MorphoSource	0,08	F	http://dx.doi.org/10.17602/M2/M4610
Presbytis hosei	MCZ 37371	MorphoSource	0,08	M	http://dx.doi.org/10.17602/M2/M4609
Presbytis hosei	MCZ 37372	MorphoSource	0,08	F	http://dx.doi.org/10.17602/M2/M4608
Presbytis hosei	MCZ 37772	MorphoSource	0,08	F	http://dx.doi.org/10.17602/M2/M4607
Presbytis rubicunda	MCZ 22276	MorphoSource	0,08	M	http://dx.doi.org/10.17602/M2/M4557
Presbytis rubicunda	MCZ 35704	MorphoSource	0,08	F	http://dx.doi.org/10.17602/M2/M4552
Presbytis rubicunda	MCZ 35705	MorphoSource	0,08	F	http://dx.doi.org/10.17602/M2/M4551
Presbytis rubicunda	MCZ 35706	MorphoSource	0,08	F	http://dx.doi.org/10.17602/M2/M4556
Presbytis rubicunda	MCZ 35712	MorphoSource	0,08	M	http://dx.doi.org/10.17602/M2/M4555
Symphalangus syndactylus	AMNHM 102724	MorphoSource	0,06	M	-
Symphalangus syndactylus	AMNHM 106583	AMNH	0,08	F	-
Symphalangus syndactylus	MCZ 36031	MorphoSource	0,08	M	http://dx.doi.org/10.17602/M2/M4444
Symphalangus syndactylus	MCZ 36032	MorphoSource	0,07	F	http://dx.doi.org/10.17602/M2/M4443
Theropithecus gelada	AMNHM 19549	MorphoSource	0,08	M	-
Theropithecus gelada	AMNHM 238034	MorphoSource	0,12	F	-
Theropithecus gelada	AMNHM 60568	MorphoSource	0,08	M	-

Theropithecus gelada	AMNHM 80126	MorphoSource	0,09	M	-
Theropithecus gelada	AMNHM 90309	MorphoSource	0,09	M	-
Trachypithecus cristatus	MCZ 35567	MorphoSource	0,05	F	http://dx.doi.org/10.17602/M2/M4439
Trachypithecus cristatus	MCZ 35584	MorphoSource	0,05	F	http://dx.doi.org/10.17602/M2/M4436
Trachypithecus cristatus	MCZ 35586	MorphoSource	0,05	F	http://dx.doi.org/10.17602/M2/M4435
Trachypithecus cristatus	MCZ 35597	MorphoSource	0,05	F	http://dx.doi.org/10.17602/M2/M4433
Trachypithecus cristatus	MCZ 35603	MorphoSource	0,05	F	http://dx.doi.org/10.17602/M2/M4431
Oreopithecus bambolii	BAC 208	NMB	0,03	?	-
Australopithecus sp.	StW 573	DNMNH	0,09	F	-
Australopithecus sp.	StW 578	DNMNH	0,07	?	-

Chapter 4:

A comparative analysis of the vestibular apparatus in *Epipliopithecus vindobonensis*: Phylogenetic implications

Reprinted from:
Urciuoli, A., Zanolli, C., Beaudet, A., Pina, M., Almécija, S., Moyà-Solà, S., Alba, D. M., 2021. A comparative analysis of the vestibular apparatus in *Epipliopithecus vindobonensis*: Phylogenetic implications. *J. Hum. Evol*. 151, 102930. https://doi.org/10.1016/j.jhevol.2020.102930

Journal of Human Evolution 151 (2021) 102930

Contents lists available at ScienceDirect

Journal of Human Evolution

journal homepage: www.elsevier.com/locate/jhevol

A comparative analysis of the vestibular apparatus in *Epipliopithecus vindobonensis*: Phylogenetic implications

Alessandro Urciuoli [a, *], Clément Zanolli [b], Amélie Beaudet [a, c, d, 3], Marta Pina [a, e], Sergio Almécija [f, g, a], Salvador Moyà-Solà [a, h, i], David M. Alba [a, *]

[a] Institut Català de Paleontologia Miquel Crusafont, Universitat Autònoma de Barcelona, Edifici ICTA-ICP, c/ Columnes s/n, Campus de la UAB, 08193 Cerdanyola del Vallès, Barcelona, Spain
[b] Univ. Bordeaux, CNRS, MCC, PACEA, UMR 5199, F-33600, Pessac, France
[c] School of Geography, Archaeology and Environmental Studies, University of the Witwatersrand, Private Bag 3, Johannesburg, WITS 2050, South Africa
[d] Department of Anatomy, University of Pretoria, PO Box 2034, Pretoria, 0001, South Africa
[e] School of Earth and Environmental Sciences, Faculty of Science and Engineering, University of Manchester, 176 Oxford Road, Manchester, M13 9PL, UK
[f] Division of Anthropology, American Museum of Natural History, Central Park West at 79th Street, New York, NY 10024, USA
[g] New York Consortium in Evolutionary Primatology, New York, NY, USA
[h] Institució Catalana de Recerca i Estudis Avançats (ICREA), Passeig de Lluís Companys 23, 08010 Barcelona, Spain
[i] Unitat d'Antropologia (Departament de Biologia Animal, Biologia Vegetal i Ecologia), Universitat Autònoma de Barcelona, Campus de la UAB s/n, 08193 Cerdanyola del Vallès, Barcelona, Spain

ARTICLE INFO

Article history:
Received 1 April 2020
Accepted 6 December 2020
Available online xxx

Keywords:
Pliopithecidae
Catarrhini
Miocene
Inner ear
Phylogeny
Geometric morphometrics

ABSTRACT

Pliopithecoids are an extinct group of catarrhine primates from the Miocene of Eurasia. More than 50 years ago, they were linked to hylobatids due to some morphological similarities, but most subsequent studies have supported a stem catarrhine status, due to the retention of multiple plesiomorphic features (e.g., the ectotympanic morphology) relative to crown catarrhines. More recently, some morphological similarities to hominoids have been noted, raising the question of whether they could be stem members of this clade. To re-evaluate these competing hypotheses, we examine the morphology of the semicircular canals of the bony labyrinth of the middle Miocene pliopithecid *Epipliopithecus vindobonensis*. The semicircular canals are suitable to test between these hypotheses because (1) they have been shown to embed strong phylogenetic signal and reliably discriminate among major clades; (2) several potential hominoid synapomorphies have been identified previously in the semicircular canals; and (3) semicircular canal morphology has not been previously described for any pliopithecoid. We use a deformation-based (landmark-free) three-dimensional geometric morphometric approach to compare *Epipliopithecus* with a broad primate sample of extant and extinct anthropoids. We quantify similarities in semicircular canal morphology using multivariate analyses, reconstruct ancestral morphotypes by means of a phylomorphospace approach, and identify catarrhine and hominoid synapomorphies based on discrete characters. *Epipliopithecus* semicircular canal morphology most closely resembles that of platyrrhines and *Aegyptopithecus* due to the retention of multiple anthropoid symplesiomorphies. However, *Epipliopithecus* is most parsimoniously interpreted as a stem catarrhine more derived than *Aegyptopithecus* due to the possession of a crown catarrhine synapomorphy (i.e., the rounded anterior canal), combined with the lack of other catarrhine and any hominoid synapomorphies. Some similarities with hylobatids and atelids are interpreted as homoplasies likely related to positional behavior. The semicircular canal morphology of *Epipliopithecus* thus supports the common view that pliopithecoids are stem catarrhines.

* Corresponding authors.
E-mail addresses: alessandro.urciuoli@icp.cat (A. Urciuoli), david.alba@icp.cat (D.M. Alba).
[3] Department of Archaeology, University of Cambridge, Fitzwilliam St, Cambridge CB2 1QH, UK.

https://doi.org/10.1016/j.jhevol.2020.102930
0047-2484/

1. Introduction

1.1. The phylogenetic position of pliopithecoids

Pliopithecoids are an extinct superfamily of catarrhine primates, recorded in Eurasia from the early to the late Miocene (Andrews et al., 1996; Begun, 2002, 2017; Harrison, 2005, 2013). Their first occurrence, in the early Miocene of China (~18–17 Ma; Harrison and Gu, 1999; Begun, 2002; Harrison, 2013), slightly predates the oldest record of large-bodied apes in Eurasia (Heizmann and Begun, 2001; Casanovas-Vilar et al., 2011). In the absence of older (earliest Miocene) catarrhines in that continent, pliopithecoids are assumed to have an African origin (Harrison, 1987, 2013; Begun, 2017). Like apes, pliopithecoid ancestors probably dispersed into Eurasia before the Langhian transgression, which was possible due to the lowered sea level and tectonic events that led to the closure of the Tethys Seaway and the establishment of an intermittent terrestrial corridor beginning at ~19 Ma (Harzhauser et al., 2007; Harrison, 2013).

Decades ago, pliopithecoids were considered to be phylogenetically related to hylobatids due to some superficial resemblances in cranial morphology as well as body size and proportions (e.g., Hürzeler, 1954; Zapfe, 1958, 1961; Simons and Fleagle, 1973). Currently, they are generally considered a clade of stem catarrhines—as supported by the retention of several cranial and postcranial features that are plesiomorphic compared to the crown members of the group (Delson and Andrews, 1975; Ciochon and Corruccini, 1977; Fleagle, 1984; Harrison, 1987, 2005, 2013; Andrews et al., 1996; Begun, 2002, 2017). The divergence of pliopithecoids before the split of crown catarrhines is further supported by most recent cladistic analyses (Zalmout et al., 2010; Stevens et al., 2013; Nengo et al., 2017; Gilbert et al., 2020), implying a long ghost lineage of ca. 12–14 Myr for pliopithecoids (Begun, 2017). The exception is the cladistic analysis by Alba et al. (2015), which recovered pliopithecoids as a clade of stem hominoids—thereby eliminating the need to hypothesize a long gap in the pliopithecoid fossil record. Most recently, Almécija et al. (2019) further documented similarities in femoral morphology between pliopithecoids (*Epipliopithecus*) and extant hominoids, thereby casting additional doubts on the status of pliopithecoids as stem catarrhines. Further uncertainty in this regard stems from the fact that no tail vertebrae are known from pliopithecoids (Begun, 2017). Based on sacral morphology, Zapfe (1958, 1961) argued that no external tail would have been present, as in hominoids; although this has subsequently been rebutted (Ankel, 1965; Russo, 2016), available evidence in this regard remains uncertain.

There are multiple genera of pliopithecids (Harrison and Gu, 1999; Moyà-Solà et al., 2001; Begun, 2002, 2017; Harrison, 2005, 2013; Alba et al., 2010; Alba and Moyà-Solà, 2012; Alba and Berning, 2013; Sankhyan et al., 2017; Harrison et al., 2020), which, following Harrison et al. (2020), we provisionally group into four different families: dionysopithecids (*Dionysopithecus* and *Platodontopithecus*), krishnapithecids (*Krishnapithecus*), pliopithecids (*Pliopithecus* and *Epipliopithecus*), and crouzeliids (*Plesiopliopithecus*, *Barberapithecus*, *Anapithecus*, *Egarapithecus*, and *Laccopithecus*). However, it is noteworthy that the treatment of these genera at the family rank, and even the placing of some genera in one or another group, differs among authors (e.g., compare Alba and Moyà-Solà, 2012 with Begun, 2017). Such disagreements largely stem from the fact that the internal phylogeny of pliopithecoids is still unclear and that their affinities with fossil catarrhines from Africa remain uncertain (e.g., Harrison, 2013).

1.2. Evidence from Epipliopithecus

Deciphering the phylogenetic relationships of most pliopithecoids is hampered by the fact that they are mostly known by fragmentary dentognathic remains, with the exception of *Epipliopithecus vindobonensis*, whose craniodental and postcranial morphology is well documented by several skeletons from the middle Miocene (MN6, ~14.85–13.45 Ma[1]) karstic infillings of Devínska Nová Ves, Slovakia (Zapfe, 1958, 1961; Andrews et al., 1996; Begun, 2002; Harrison, 2013). *Epipliopithecus* was originally established as a subgenus of *Pliopithecus* by Zapfe and Hürzeler (1957), being subsequently considered a junior subjective synonym of the latter (e.g., Andrews et al., 1996; Harrison and Gu, 1999; Moyà-Solà et al., 2001; Harrison, 2005, 2013; Alba et al., 2010) or a distinct genus (e.g., Begun, 2002; Alba and Moyà-Solà, 2012; Arias-Martorell et al., 2015; Alba et al., 2015; this study). From a locomotor viewpoint, *E. vindobonensis* has been variously depicted as an arboreal or semiterrestrial generalized quadruped with varying degrees of climbing and suspensory abilities (see discussion in Arias-Martorell et al., 2015). From a phylogenetic perspective, its purported stem catarrhine status has been supported by features such as the short and only partially enclosed ectotympanic, the presence of entepicondylar foramen in the distal humerus, and single hinge-like carpometacarpal joint in the thumb (Zapfe, 1961; Szalay and Delson, 1979; Harrison, 1987, 2005; Andrews et al., 1996; Begun, 2002, 2017).

The external morphology of the petrosal bone of *E. vindobonensis* (Zapfe, 1961; Szalay, 1975; Fricano, 2018) has been of utmost significance in the discussion of its phylogenetic affinities, given that the presence of a tubular ectotympanic is considered synapomorphic of crown catarrhines (e.g., Szalay, 1975; Szalay and Delson, 1979; Harrison, 1987, 2005; Andrews et al., 1996; Begun, 2002; Zalmout et al., 2010; Alba et al., 2015; Nengo et al., 2017). The possibility remains that such ossification took place to some extent independently in cercopithecoids, hominoids and/or other anthropoids such as pliopithecoids (Begun, 2002, 2017; Alba et al., 2015). However, other features of *Epipliopithecus* also appear plesiomorphic as compared to crown catarrhines and show no particular similarities with hominoids, namely: the large postglenoid process separated from the acoustic meatus, as in platyrrhines (Zapfe, 1961); the lack of ossification in the tentorium cerebelli (unlike in most platyrrhines and stem anthropoids, but similar to *Aegyptopithecus* and crown catarrhines; Kay et al., 2009a); and the deep subarcuate fossa (Zapfe, 1961), as in platyrrhines and most anthropoids except hominids (Gannon et al., 1988; Kunimatsu et al., 2019). In contrast, the inner ear morphology of *Epipliopithecus* has not been described and therefore its potential phylogenetic implications remain unexplored.

1.3. The bony labyrinth of the inner ear

Among the inner cavities of the petrosal, the bony labyrinth of the inner ear is constituted by the semicircular canals (SCs) and the vestibule (which together host the soft-tissue structures linked with the sense of balance) plus the cochlea. Semicircular canal size (e.g., Spoor et al., 2007; Silcox et al., 2009; Ryan et al., 2012; Grohé et al., 2018) and orientation (David et al., 2010; Malinzak et al., 2012; Berlin et al., 2013; Perier et al., 2016; Gonzales et al., 2019) have been frequently used for inferring agility, while the shape of the canals as a whole has tentatively been linked to positional behavior (Le Maître et al., 2017). At the same time, recent studies

[1] Age uncertainly based on the boundaries recognized for MN6 (van der Meulen et al., 2011).

have demonstrated that the SCs bear strong phylogenetic signal among anthropoids (Lebrun et al., 2010, 2012; Urciuoli et al., 2019, 2020; del Rio et al., 2020; Morimoto et al., 2020) and other mammals (e.g., Grohé et al., 2015; Mennecart et al., 2016, 2017; Costeur et al., 2018).

Although adaptively relevant characters may constitute synapomorphies of particular clades, arguably their relationship with function makes them potentially more prone to homoplasy. However, the correlation between SC morphology and positional behavior has recently been questioned by some studies (i.e., Rae et al., 2016; del Rio et al., 2020; Morimoto et al., 2020), and SC shape variation has been shown to largely follow the expectations of a Brownian motion model of evolution in both platyrrhines (del Rio et al., 2020) and catarrhines (Urciuoli et al., 2020). These results are in accordance with those obtained for the bony labyrinth as a whole, showing that its morphology reflects phylogenetic relatedness as inferred from molecular data (Lebrun et al., 2010; Ekdale, 2013; Macrini et al., 2013; Billet et al., 2015). Cumulatively, this evidence suggests that bony labyrinth morphology is phylogenetically informative among mammals (Mennecart et al., 2017) and may thus potentially illuminate the phylogenetic relationships of extinct primates. Following Mennecart and Costeur (2016), who suggested that inner ear structures might be highly informative for large cladistics analyses, Urciuoli et al. (2020) explored catarrhine SC shape variation among catarrhines and proposed several potential synapomorphies for crown hominoids.

Here we test between two different phylogenetic hypotheses for *Epipliopithecus*, one hypothesis being that *Epipliopithecus* is a stem catarrhine, the other hypothesis that *Epipliopithecus* is a hominoid, based on the information provided by the shape of the SCs and vestibule. This morphology is described here for the first time using a three-dimensional geometric morphometric (3DGM) approach applied to a broad sample of extant and fossil anthropoids (Urciuoli et al., 2020). We refrained from analyzing the entire bony labyrinth (i.e., including also the cochlea) because its potential for phylogenetic reconstruction among primates is currently unclear. A recent analysis in platyrrhines suggested that cochlear shape departs from a Brownian motion model of evolution (Blomberg's $K < 1$; del Rio et al., 2020), thus potentially reflecting a greater influence of function (and likely homoplasy due to similar selection pressures) than is the case for the SCs and vestibule. This is in agreement with previous studies linking several macroscopic cochlear features to hearing capabilities (e.g., Manoussaki et al., 2006; Kirk and Gosselin-Ildari, 2009; Coleman and Colbert, 2010). More detailed morphometric analyses of this structure among anthropoids are thus required to determine whether cochlear morphology can be meaningfully used to decipher the phylogenetic relationships of extinct catarrhines such as *Epipliopithecus*.

2. Materials and methods

2.1. Described material

We inspected three petrosals of *E. vindobonensis* belonging to two individuals from Devínska Nová Ves, Slovakia (Zapfe, 1961): NMB OE 303a, b (individual III), left (a) and right (b), housed in the Naturhistorisches Museum of Basel, Switzerland[2]; and NHMW 1970/1397/0003 (individual II), right, housed in the Naturhistorisches Museum of Wien, Austria.

[2] Morimoto et al. (2020) included the bony labyrinth of NMB OE 303a in their comparative study but did not depict or specifically describe its morphology.

2.2. Comparative sample

The comparative sample includes μCT scans of 162 dried crania and temporal bones belonging to 31 extant anthropoid species (see Supplementary Online Material [SOM] Table S1 for the sample size of the extant species), plus five fossil anthropoids (SOM Table S2): the stem anthropoid *Parapithecus* (Bush et al., 2004), the stem catarrhine *Aegyptopithecus* (Simons et al., 2007), the stem platyrrhines *Dolichocebus* (Kay et al., 2009b) and *Homunculus* (Fulwood et al., 2016), and the hominoid *Oreopithecus* (Rook et al., 2004).

2.3. Sample preparation

NMB OE 303 was scanned with a Phoenix Nanotom, GE at the Biomaterials Science Centre of the University of Basel (Switzerland) obtaining a voxel size of 25 μm. NHMW 1970/1397/0003 was scanned at the Vienna μCT-Lab using a Viscom X8060 (Viscom XT9190-THP X-ray tube) obtaining a voxel size of 22 μm. The canals and vestibule of NMB OE 303a, b were filled with air, while in NHMW 1970/1397/0003 they were partially filled with sediment. In both cases we segmented the SCs and vestibule cavities using the 'watershed' tool of Avizo v. 9.0.1 (FEI Visualization Sciences Group, Houston), with additional manual corrections for NHMW 1970/1397/0003. The 3D surfaces of NMB OE 303b and NHMW 1970/1397/0003 were mirrored for comparison. The 3D meshes of the two individuals are available from MorphoSource (see Table 1).

The μCT scans of most extant comparative species and of fossil anthropoids were accessed from MorphoSource.org digital repository (https://www.morphosource.org) with the exception of *Oreopithecus bambolii* petrosal, which was kindly provided by Lorenzo Rook (see SOM Table S2 for voxel sizes). Further details about the μCT scans of the extant comparative sample (voxel sizes, exact source, DOI, etc.) can be found in Urciuoli et al. (2020: Supplementary File 1). The slice stacks of these crania were processed using Avizo v. 9.0.1., and the left bony labyrinth was segmented using the semiautomatic 'watershed' tool of Avizo (with additional manual corrections in the case of partially filled canals found in the fossil specimens) and digitally extracted; when the left bony labyrinth was unavailable, the right one was mirrored. As in Urciuoli et al. (2020), the SCs and the vestibule were separated from the cochlea by cutting the generated 3D meshes immediately inferior to the saccule and the oval window, using landmarks placed along the maximum curvature of the junction between the vestibule and the cochlea as reference for the cutting plane (Fig. 1). The resulting holes were filled with a flat surface using Geomagic Studio v. 2014.3.0 (3D Systems, Rock Hill, USA). Prior to the 3DGM analysis, the surfaces were first roughly prealigned by manually superimposing the meshes to ensure biological correspondence. Subsequently, the alignment was automatically refined using the Avizo module 'Align Surface' with the 'rigid + uniform' option. Similar to Procrustes superimposition, this module minimizes the distances between the faces of each surface by scaling, translating and rotating the analyzed meshes. The phylogenetic relationships of the extinct taxa included in the analyses, relative to extant anthropoids, are summarized in Figure 2.

2.4. Shape analysis

Differences in vestibule and SC shape were evaluated using a landmark-free 3DGM technique based on deformation, which relies on the geometrical correspondence of continuous surfaces and computes the magnitude and direction of deformation of the analyzed meshes from a group-average template (Glaunès and Joshi, 2006; Durrleman et al., 2012a, b; Dumoncel et al., 2014; Beaudet et al., 2016; Urciuoli et al., 2020). The deformations are

Table 1
Digital object identifiers (DOIs) of the 3D virtual models of the vestibule and semicircular canals of *Epipliopithecus vindobonensis* available from MorphoSource.org (https://www.morphosource.org).

Catalog No.	Museum	DOI
NMBOE 303a (individual III)	NMBOE	https://doi.org/10.17602/M2/M113935
NMBOE 303b (individual III)	NMBOE	https://doi.org/10.17602/M2/M113933
NHMW 1970/1397/0003 (individual II)	NHMW	https://doi.org/10.17602/M2/M113932

Abbreviations: NMB OE = Naturhistorisches Museum Basel, Switzerland; NHMW = Naturhistorisches Museum Wien, Austria.

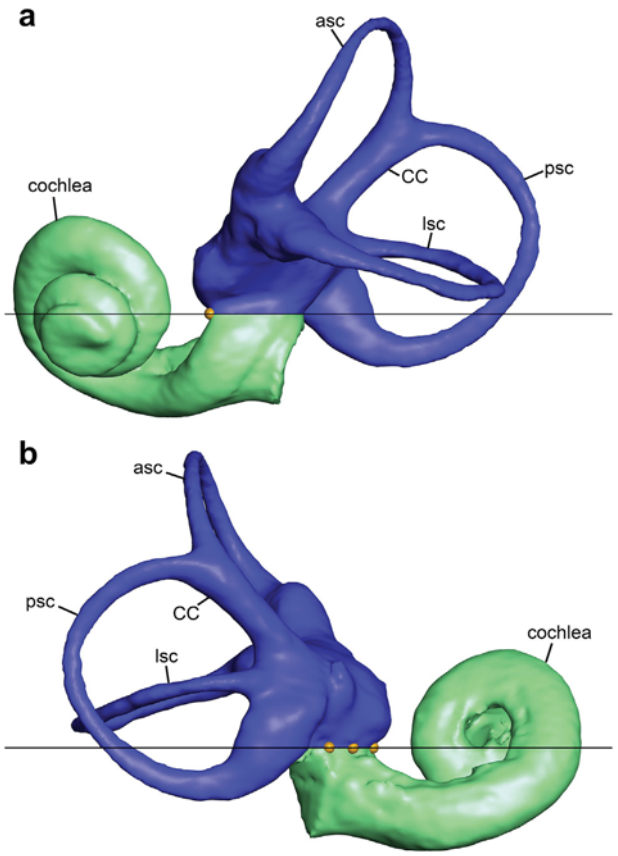

Figure 1. Illustration of the protocol used for digitally separating the cochlea (green) from the semicircular canals and the vestibule (blue). a) In anterior view, the first landmark (yellow filled circle) is placed anteriorly to the oval window, on the point of maximum surface curvature of the ridge-like morphology formed by the narrowing of the vestibule. b) In posterior view, three landmarks are placed along the junction between the bony vestibule and the cochlea, defined by the line of maximum surface curvature found immediately below the bulge formed by the saccular recess. A cutting plane (here perpendicular to the view and depicted by a black line) is best fitted to the identified landmarks using the 'Points To Fit' option of the 'Clipping Plane' module of Avizo v. 9.0.1 (FEI Visualization Sciences Group, Houston) via a customized script (available upon request to A.U.), and used as a reference for a straight cut. Abbreviations: asc = anterior semicircular canal; psc = posterior semicircular canal; lsc = lateral semicircular canal; CC = common crus. (For interpretation of the references to color in this figure legend, the reader is referred to the Web version of this article.)

mathematically modeled to obtain a one-to-one correspondence of the 3D space using the open-source software Deformetrica 4 (Bône et al., 2018). This technique yields results similar to landmark-based 3DGM methods while more easily tracking changes in volume (Urciuoli et al., 2020) and is less prone to biases introduced by the design of landmarking protocols, caused by the inherent difficulty to adequately capture complex 3D shapes based on a reduced number of homologous landmarks.

Due to the high computational power required, the sets of vectors, representing the flow of deformations from the initial position of the control points on the template to the target shape, were computed in the Barcelona Supercomputing Center (BSC) using the MinoTauro cluster (https://www.bsc.es/marenostrum/minotauro). To identify major patterns of shape variation across the sample, the resulting sets of vectors were inspected using between-group principal component analysis (bgPCA; Mitteroecker and Bookstein, 2011), using major clades (platyrrhines, cercopithecoids, hylobatids, and hominids) as the grouping factor (Urciuoli et al., 2020). To address recent concerns about the use of bgPCA based on highly multivariate data sets, such as those generated by 3DGM, and to rule out the presence of spurious groupings in our results (Bookstein, 2019; Cardini et al., 2019), we computed cross-validated bgPCA scores. These were obtained by iteratively repeating the bgPCA on a subset of the sample. The cross-validated bgPCA scores were then compared with those obtained with standard bgPCA (Cardini and Polly, 2020). The affinities of fossil specimens with the groups defined a priori in the bgPCA were evaluated using the 'typprobClass' function of the Morpho package v. 2.7 (Schlager, 2017) in R v. 3.6.1 (R Core Team, 2019). This function computes posterior probabilities of group membership based on the Mahalanobis distances between the bgPC scores of fossil specimens and group centroids. Null hypotheses of group membership were rejected at $p < 0.05$. Similarities among anthropoid species were also evaluated by running a cluster analysis (Ward's method) on the Mahalanobis distances between pairs of bgPCA species centroid scores using the 'ward.D2' method of the 'hclust' function of the 'stats' package in R. The cophenetic correlation coefficient, which allows one to evaluate how faithfully the obtained dendrogram preserves the pairwise distances between the original unmodeled datapoints, was calculated using the same package.

In addition, we inspected the volumetric proportions of *Epipliopithecus* and the remaining fossil taxa included in the analysis, and determined the correlation between log-transformed cube root canal volume (ln VolSC, mm) and log-transformed canal length (ln L, mm) by means of ordinary least-squares regression. Given that previous analyses identified an allometric grade shift between hominids and nonhominid anthropoids (Urciuoli et al., 2020), separate regression lines were computed for hominids and nonhominid anthropoid taxa using the 'stats' package in R.

2.5. Phylomorphospace, ancestral state estimation, and phylogenetic signal

To intuitively visualize the direction and magnitude of evolutionary change we relied on a phylomorphospace approach (Sidlauskas, 2008), by which a phylogenetic tree is projected onto the tangent space defined by the bgPCA of our shape data. Ancestral states for the internal nodes are estimated using a maximum likelihood method for continuous characters via the 'fastAnc' function of the 'phytools' v. 0.6–60 package for R (Revell, 2012), while the tips of the tree branches correspond to the centroid

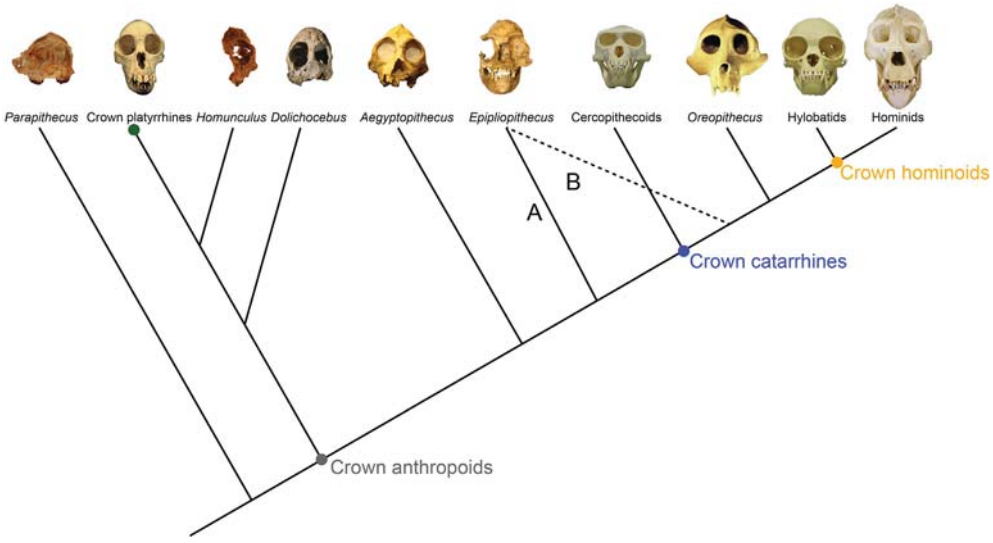

Figure 2. Cladogram of extant and fossil anthropoids showing the two phylogenetic hypotheses for *Epipliopithecus*. The solid line (A) denotes the most widely accepted phylogenetic position of *Epipliopithecus* as a stem catarrhine, whereas the dashed line (B) denotes the alternative hypothesis that *Epipliopithecus* would be more closely related to hominoids. Key nodes are highlighted as follows: gray circle = crown anthropoids; green circle = crown platyrrhines; blue circle = crown catarrhines; orange circle = crown hominoids. Skulls and crania (not to scale) were taken from the following sources for illustrative purposes only: extant skulls and *Aegyptopithecus*, Wikimedia Commons; *Dolichocebus*, Kay et al. (2009b: Fig. 1); *Homunculus*, Tejedor and Rosenberger (2008: Fig. 2); *Oreopithecus* (reconstruction), Moyà-Solà and Köhler (2000: Fig. 5); *Epipliopithecus*, photograph of a cast; *Parapithecus*, digital reconstruction with photographic texture made by Steven Heritage. (For interpretation of the references to color in this figure legend, the reader is referred to the Web version of this article.)

scores for the included taxa. We repeated the analyses using two composite phylogenetic trees, one with *Epipliopithecus* as a stem catarrhine and the other with this taxon as a stem hominoid (Figs. 2 and 3). For extant taxa we relied on a Bayesian phylogenetic analysis of eleven mitochondrial and six autosomal genes downloaded from the 10kTrees Website v. 3 (Arnold et al., 2010). Extinct species were added based on their phylogenetic position, their divergence being arbitrarily placed 1 Myr before the estimated divergence age of the next derived node, and tip ages based on their chronostratigraphic age. We used the following tip age estimates: *Epipliopithecus* 14.15 Ma (mean of 14.85 and 13.45 Ma, the maximum–minimum age range for MN6 in central Europe according to van der Meulen et al., 2011); *Aegyptopithecus* and *Parapithecus*, 29.85 Ma (mean of 30.2 and 29.5 Ma, based on the revised age range of the fauna of quarries I and M of the Jebel Qatrani Formation of the Fayum depression by Seiffert, 2006); *Dolichocebus*, 20.5 Ma (mean of 21.0 and 20.0 Ma age provided by Kay, 2015); *Homunculus*, 17.2 Ma (mean of 17.9 and 16.5 Ma age provided by Kay, 2015); and *Oreopithecus* 6.75 Ma (mean of 7.0 and 6.5 Ma for the last occurrence according to Rook et al., 2000).

The phylogenetic signal embedded in the shape data was measured using Pagel's λ (Pagel, 1999) and Blomberg's K (Blomberg et al., 2003), together with the multivariate version of Blomberg's K (K_{mult}; Adams, 2014). Pagel's λ and Blomberg's K were computed using the 'phylosig' function of the 'phytools' package in R, while K_{mult} was computed with the 'physignal' function of the 'geomorph' package v. 3.1.0 in R (Adams et al., 2019). These metrics were computed based on extant taxa only (Arnold et al., 2010).

Ancestral node morphologies were computed from the bgPC scores for the last common ancestors (LCAs) estimated by means of maximum likelihood, which were rotated and translated from the morphospace back into the deformation field space, generating a set of momentum vectors that were used in Deformetrica 4 to warp the template surface into the target LCA morphology. Volumetric proportions for the LCAs were computed based on the rescaled 3D models obtained from the phylomorphospace approach; the scaling factor for each LCA was estimated using the 'anc.ML' function of the R package 'phytools.' Morphological similarities between *Epipliopithecus* and the LCA centroids were assessed by means Euclidean distances between the *Epipliopithecus* centroid and the LCA bgPC scores, weighted on the basis of the percentage of variance explained by each bgPC and computed using the 'distances' function of the 'distances' package v. 0.1.8 in R (Savje, 2019).

The two phylogenetic hypotheses for *Epipliopithecus* depicted in Figure 3 were assessed further based on the coding of seven discrete characters that were deemed of phylogenetic significance based on shape comparisons and analyses. The resulting character-taxon matrix was analyzed for character congruence against a fixed topology consistent with the phylogenetic hypotheses depicted in Figure 3. For both cladograms, three indices customarily employed in cladistics (Farris, 1989) were computed in PAUP* v. 4.0a168 for Mac (Swofford, 2003) to assess the most parsimonious hypothesis: the consistency index (CI), the retention index (RI), and the rescaled consistency index (RC).

3. Results

3.1. Description and comparisons

The three bony labyrinths of *E. vindobonensis* are well preserved—except for the lateral canal of NMB OE 303b, which shows a small fracture in the bony encasing—and are not affected by diagenetic deformation, thereby permitting a straightforward extraction of the 3D surfaces of the vestibular apparatus bony labyrinth (Fig. 4a–c). Overall, the canals are fairly slender, as in platyrrhines and cercopithecins, falling within their variability as shown by a bivariate plot of SC volume vs. length (Fig. 5; Table 2; SOM Table S3). The bony vestibule is large, albeit less so than in hominids. The anterior and posterior canals are larger than the lateral canal, as in platyrrhines (Fig. 4e–i) and modern humans (Fig. 4u).

The *E. vindobonensis* common crus (CC) is long, as in extant platyrrhines (Fig. 4g–i) and in *Dolichocebus* (Fig. 4e), but unlike in most catarrhines. The trajectories of the anterior and posterior

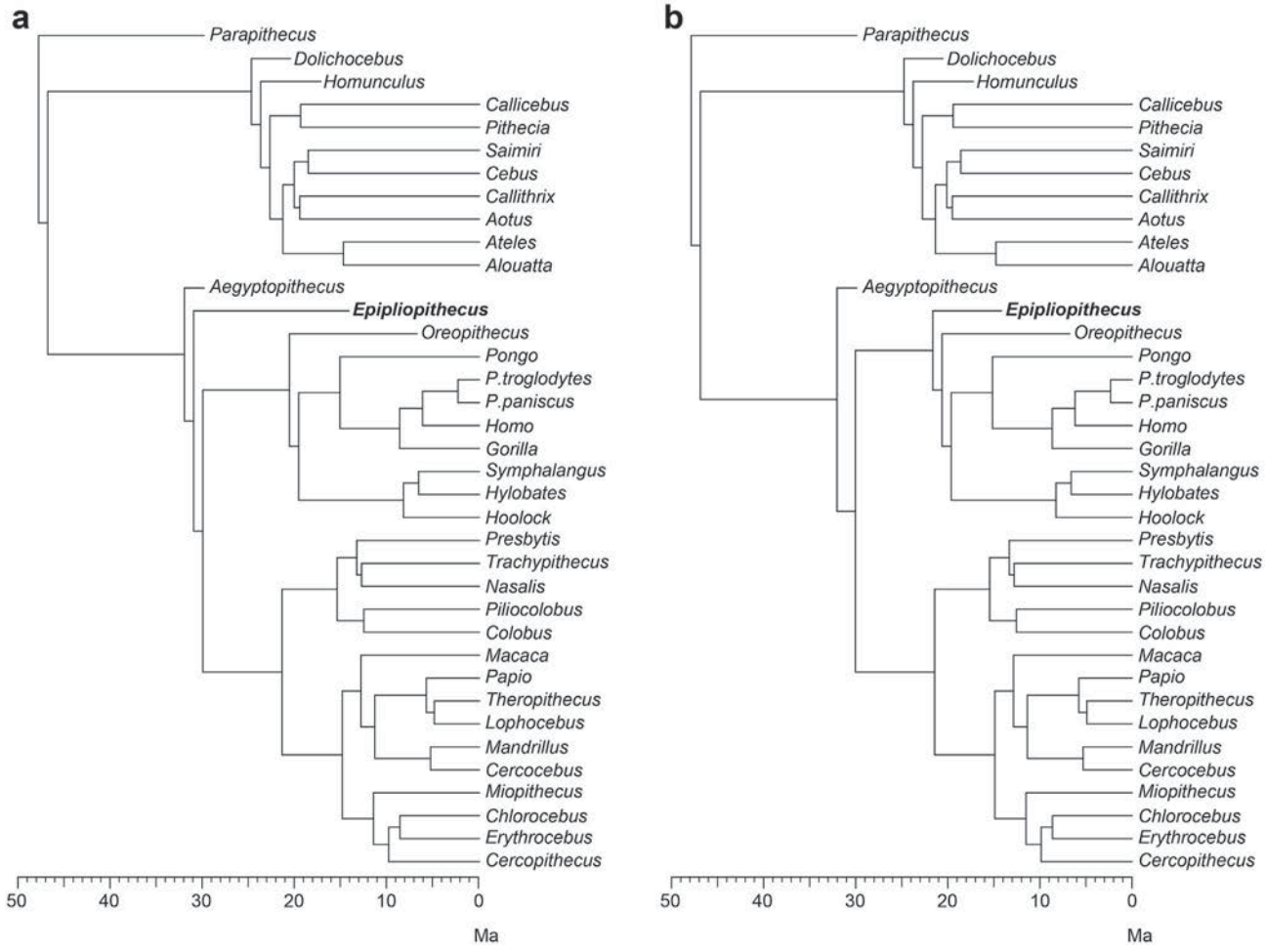

Figure 3. Phylogenetic trees used for the phylomorphospace approach. They differ in considering *Epipliopithecus* as a stem catarrhine (a) or a stem hominoid (b).

canal form a right angle when merging at the CC apex. Despite some similarities, the morphology of *Epipliopithecus* is clearly distinguishable from that of *Dolichocebus* and *Parapithecus* (Fig. 4d), as the CC is not posteromedially inclined and the anterior canal connection is placed more laterally.

The anterior canal of *E. vindobonensis* is slightly wider than tall (as in *Hoolock*; Fig. 4q), yet clearly rounded and lacking the vertical compression characteristic of extant hominoids (Fig. 4o–u), the anterosuperior elongation typical of hylobatids and *Pongo* (Fig. 4o–r; Urciuoli et al., 2020), and the extreme superior projection found in *Ateles* (Fig. 4g). The anterior canal of *Epipliopithecus* further differs from that of the stem anthropoid *Parapithecus* (Fig. 4d), the stem platyrrhine *Dolichocebus* (Fig. 4e), and the stem catarrhine *Aegyptopithecus* (Fig. 4j), characterized by an almost triangular morphology (albeit less so in the last genus). The superiormost portion of the anterior canal bends medially, causing a moderate torsion of the canal trajectory. This morphology is also found in the stem platyrrhine *Homunculus* (Fig. 4f) and, to a lesser extent, *Chlorocebus* (Fig. 4l) and *Dolichocebus* (Fig. 4e), while in most cercopithecoids it is much more bent (e.g., *Macaca*; Fig. 4m). A sinuous trajectory of the anterior canal, although with a different morphology, is also displayed by other taxa (e.g., *Cebus*; Fig. 4i) and thus is not very informative from a phylogenetic viewpoint. Despite the aforementioned similarities, *Epipliopithecus* differs from the stem platyrrhines *Homunculus* (Fig. 4f) and *Dolichocebus* (Fig. 4e), from most extant platyrrhines (particularly *Ateles*; Fig. 4g), and from the stem catarrhine *Aegyptopithecus* (Fig. 4j), in displaying a much less mediolaterally compressed anterior canal.

The posterior canal of *Epipliopithecus* is slightly taller than wide, similar to that of *Alouatta* (Fig. 4h) and *Symphalangus* (Fig. 4p), but differs from the latter by displaying a less arched connection with the CC. The orientation of the posterior canal relative to the plane defined by the anterior canal is different in the two individuals of *Epipliopithecus*: it forms an obtuse angle in NHMW 1970/1397/0003 (resembling the hylobatid condition), but forms a right angle in NMB OE 303 (as in other anthropoids; SOM Fig. S2).

The lateral canal is rounded and smaller than the other canals (more so in NMB OE 303), as in stem platyrrhines (Fig. 4e, f) and the stem catarrhine *Aegyptopithecus* (Fig. 4j), although in *Epipliopithecus* this canal is not strongly compressed mediolaterally as in the latter taxon (Fig. 4j). The trajectory of the ampullary portion of the lateral canal slightly bends superiorly (more so in NMB OE 303; Fig. 4b, c), while the insertion of its slender part is located anteriorly to the base of the CC (particularly in NHMW 1970/1397/0003; Fig. 4a), so that—as in extant hominoids but unlike cercopithecoids—the lateral canal does not intersect the plane defined by the posterior canal. The lateral canal also shows a wave-like shape, with its lateral-most tip pointing downward, superficially resembling some individuals of *Pongo* (Fig. 4r), while differing from the morphology of *Trachypithecus* (Fig. 4k) and *Macaca* (Fig. 4m), where the canal bends inferiorly right before the ampullary portion.

Figure 4. Rendered 3D models of the semicircular canals and vestibule of *Epipliopithecus vindobonensis* (all specimens depicted as from the left side) and selected extant anthropoids, in lateral (left), superior (middle), and posterior (right) views: a) *E. vindobonensis* (individual II, NHMW 1970/1397/0003, mirrored); b) *E. vindobonensis* (individual III, NMB OE 303a); c) *E. vindobonensis* (individual III, NMB OE 303b, mirrored); d) *Parapithecus grangeri* (DPC 18651); e) *Dolichocebus gaimanensis* (MACN 14128); f) *Homunculus patagonicus* (MPM-PV 3501); g) *Ateles geoffroyi* (MCZ 29628); h) *Alouatta palliata* (DU EA LP12); i) *Cebus apella* (MCZ27891); j) *Aegyptopithecus zeuxis* (CGM 85785); k) *Trachypithecus cristatus* (MCZ35603); l) *Chlorocebus pygerythrus* (SIU 4796); m) *Macaca fascicularis* (MCZ 35765); n) *Oreopithecus bambolii* (BAC 208); o) *Hylobates lar* (MCZ 41424); p) *Symphalangus syndactylus* (AMNH.M 106583); q) *Hoolock hoolock* (AMNH.M 83425); r) *Pongo pygmaeus* (IPS10647); s) *Gorilla gorilla* (AMNH.M 167338; t) *Pan paniscus* (MCZ 38019); u) *Homo sapiens* (EMBR 179). Scale bars equal 5 mm.

3.2. Shape analysis

The bgPCA discriminates major anthropoid clades with just minimal overlap when the three axes are considered simultaneously (Fig. 6), thus closely resembling the previous results by Urciuoli et al. (2020) despite the increased number of platyrrhine taxa included here. The bgPCA results reported in Figure 6 closely resemble those derived using a cross-validated bgPCA (SOM Fig. S1), indicating that group separation is not spurious (Cardini and Polly, 2020).

The first principal component (bgPC1, which explains 59% of the variance) mainly reflects differences in volumetric proportions among the SCs and the volume they occupy relative to that of the bony vestibule, separating hominids (stout canals; quite negative scores) from both cercopithecoids and hylobatids (slender canals; positive to slightly negative scores), while platyrrhines (including stem taxa), the stem anthropoid *Parapithecus*, the stem catarrhine *Aegyptopithecus*, the stem hominoid *Oreopithecus*, and *Epipliopithecus* occupy an intermediate position in the morphospace. In particular, the two *Epipliopithecus* individuals, due to their fairly slender canals (Fig. 4a–c), display similar intermediate scores along this axis, overlapping extensively with both extant and extinct platyrrhines in the overlap zone of cercopithecoids and hominoids (Fig. 6a, c).

In turn, bgPC2 (which explains 30% of the variance) accounts for differences in the size and shape of the anterior and posterior canals (Fig. 6a, d), in the position of the lateral canal ampullary insertion on the vestibule, and in CC length, separating most

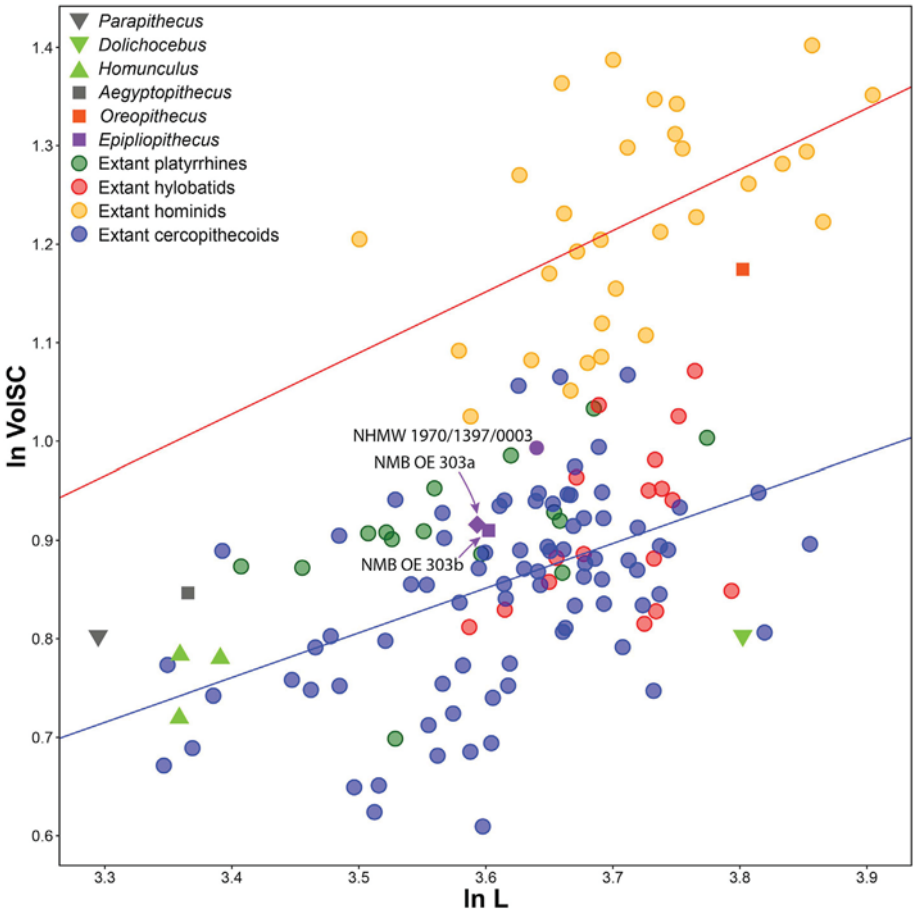

Figure 5. Bivariate plot of canal log-transformed cube root canal volume (mm; Ln VolSC) vs. log-transformed canal length (mm; ln L). Separate regression lines are depicted for hominids (red line) and for nonhominid anthropoids (blue line). *Epipliopithecus* (NHMW 1970/1397/0003 and NMB OE 303a, b) falls within the variability of nonhominid anthropoids, similar to all extinct taxa except *Oreopithecus*. Measurements for the included fossil taxa given in Table 6. (For interpretation of the references to color in this figure legend, the reader is referred to the Web version of this article.)

Table 2
Log-transformed cube root of canal volume (ln VolSC, mm^3) and log-transformed canal length (ln L, mm) measured for the fossil taxa included in the analysis.[a]

Catalog No.	Taxon	ln VolSC	ln L
NMBOE 303a	*Epipliopithecus vindobonensis*	3.640	0.993
NMBOE 303b	*Epipliopithecus vindobonensis*	3.602	0.910
NHMW 1970/1397/0003	*Epipliopithecus vindobonensis*	3.593	0.916
CGM 85785	*Aegyptopithecus zeuxis*	3.365	0.847
MPM-PV 30501	*Homunculus patagonicus*	3.391	0.780
MPM-PV 30502	*Homunculus patagonicus*	3.359	0.720
MPM-PV 30503	*Homunculus patagonicus*	3.359	0.784
MACN 14128	*Dolichocebus gaimanensis*	3.802	0.803
BAC 208	*Oreopithecus bambolii*	3.295	0.803
DPC 18651	*Parapithecus grangeri*	3.640	0.993

Abbreviations: BAC = Baccinello (field acronym; housed at Naturhistorisches Museum Basel, Switzerland); CGM = Egyptian Geological Museum, Cairo, Egypt; MPM-PV = Museo Regional Provincial Padre M.J. Molina, Río Gallegos, Argentina; MACN = Museo Argentino de Ciencias Naturales, Buenos Aires, Argentina; DPC = Duke Lemur Center, Durham, NC, USA.

[a] See SOM Table S1 for the specimens included in the extant comparative sample.

platyrrhines (positive scores) from catarrhines (moderately positive to negative scores). In particular, platyrrhines possess large and very superiorly elongated canals in the portion close to the CC apex, as well as a flat lateral canal, which also connects more inferiorly on the vestibule with its ampullary portion. Catarrhines are more variable in these features, showing rounded to vertically compressed anterior and posterior canals, a shorter CC, and a variably sinuous lateral canal with its ampullary portion connecting more superiorly. *Epipliopithecus* displays moderately positive scores, falling within the range of several extant platyrrhines (*Aotus*, *Alouatta*, *Callithrix* and *Callicebus*), due to their large anterior and posterior canals, coupled with a long CC and a small lateral canal. Both the stem platyrrhines and *Oreopithecus* show similar moderately positive scores, while *Aegyptopithecus* and *Parapithecus* show markedly positive values due to their superiorly elongated vertical canals (Fig. 6a).

Finally, bgPC3 (which explains 11% of the variance) is driven by the position of the lateral canal relative to the posterior one, by the size and orientation of the posterior canal, as well as the shape of the anterior canal and CC thickness (Fig. 6b, e), separating hylobatids (most positive values) from most extant and fossil anthropoids (intermediate to negative scores). Hylobatids have a much larger gap between the lateral and posterior canals than other anthropoids except some modern humans, and their posterior canal is also smaller than, and forms an obtuse angle with, the large and anteriorly protruding anterior canal. In contrast, in most cercopithecoids, *Aotus*, and *Callithrix,* the lateral canal broadly intersects with the posterior canal, while in the African great apes, *Theropithecus*, and *Cebus* the canals are only minimally separated. In addition, in all extant anthropoids except hylobatids, the plane of the posterior canal forms a right angle with the anterior canal, which does not project anteriorly. Both *Epipliopithecus* individuals display positive

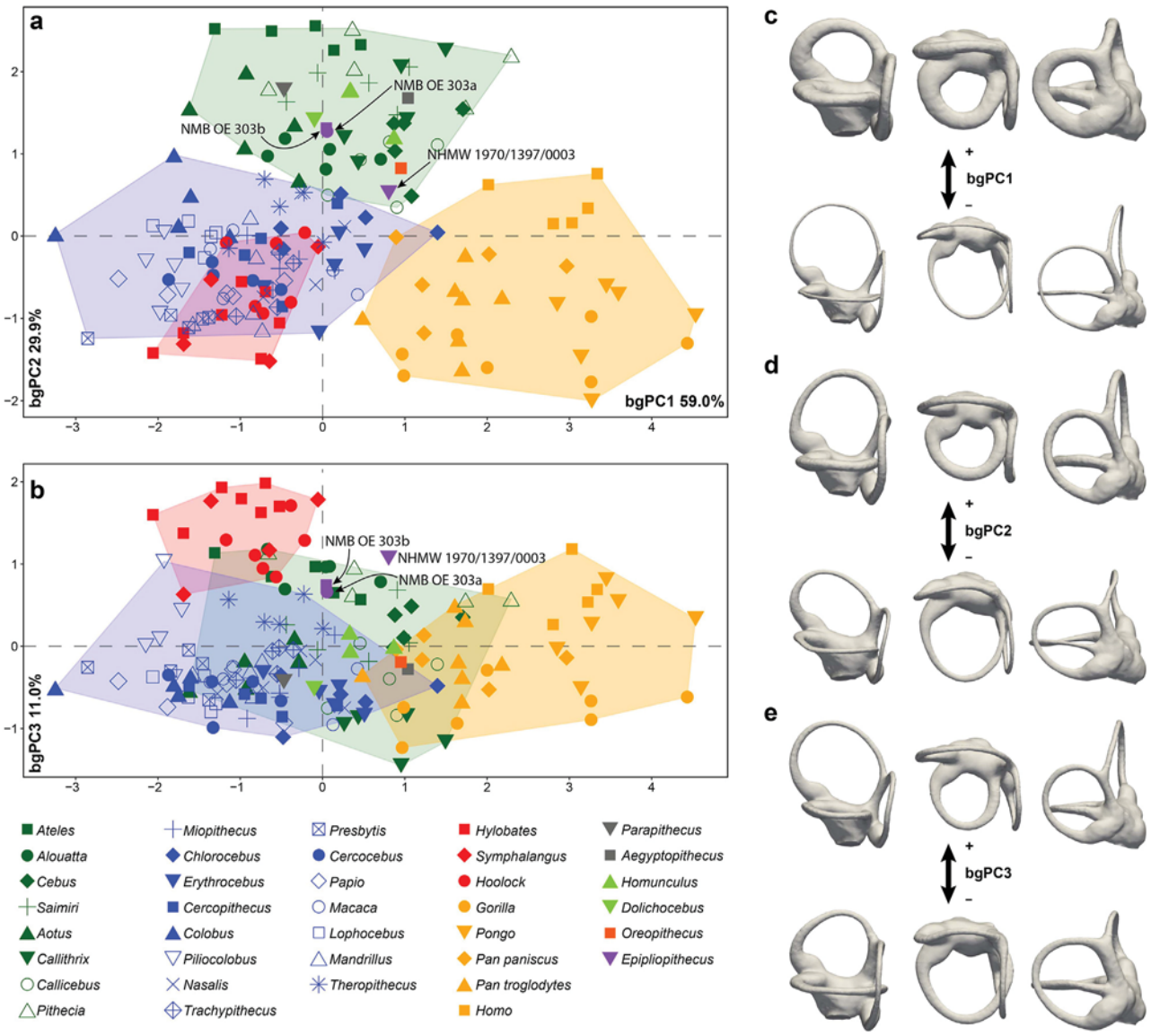

Figure 6. Patterns of vestibule and semicircular canal shape variation among major anthropoid clades based on the results of a between-group principal component analysis, as depicted by bivariate plots between principal components (bgPCs): a) bgPC2 vs. bgPC1; b) bgPC3 vs. bgPC1. Variance explained by each component is given along each axis. c–e) Extreme conformations of maximum (above) and minimum (below) bgPC scores: c) bgPC1; d) bgPC2; e) bgPC3. Four groups (platyrrhines, cercopithecoids, hylobatids, and hominids) were defined a priori, whereas specimens of *Epipliopithecus vindobonensis* were plotted post hoc onto the morphospace. Renderings in lateral (left), superior (middle), and posterior (right) views of warped 3D models representing the extreme conformations for each bgPC are placed close to the corresponding axis. Convex hulls depict the range of variation for a priori defined groups using the following color code: green = platyrrhines; blue = cercopithecoids; red = hylobatids; orange = hominids. (For interpretation of the references to color in this figure legend, the reader is referred to the Web version of this article.)

scores (NMB OE 303 with lower values), overlapping with some hylobatids (mainly *Hoolock*) and other extant anthropoids (particularly the hominids *Homo* and *Pongo*, the platyrrhines *Ateles* and *Alouatta*, and the cercopithecoids *Theropithecus* and *Piliocolobus*). The slightly dissimilar bgPC3 scores for the two *Epipliopithecus* individuals result from differences in orientation between the posterior and anterior canals (obtuse angle in NHMW 1970/1397/0003 vs. right angle in NMB OE 303; SOM Fig. S2), causing a wider separation between the lateral and posterior canals (Fig. 4a–c).

When the three bgPCs are considered together, the two *Epipliopithecus* individuals show the greatest morphological similarities with platyrrhines (less so in NHMW 1970/1397/0003), as demonstrated by Mahalanobis distances from group centroids and by their posterior probabilities of group membership (Table 3), leading us to reject close similarities to the remaining groups for NMB OE 303, and to all anthropoid groups for NHMW 1970/1397/0003 ($p < 0.05$). *Aegyptopithecus*, *Parapithecus*, *Oreopithecus*, and stem platyrrhines also closely resemble extant New World monkeys, with *Oreopithecus* also showing marginal affinities with cercopithecoids (Table 3). We obtain very similar results when considering all catarrhines as a single group, with all fossils being classified as platyrrhines (Table 4). For *Oreopithecus* and NHMW 1970/1397/0003, group membership for catarrhines cannot be rejected. However, both specimens show much lower Mahalanobis distances to the platyrrhine centroid (almost three times) than to that of catarrhines. The two *Epipliopithecus* individuals are closer to one another than they are to other fossil taxa (except for one individual of *Homunculus*, MPM-PV 3501), in turn showing similarities with stem platyrrhines, *Aegyptopithecus* and *Oreopithecus* (Table 5). A cluster analysis based on the momenta of the

Table 3
Mahalanobis distances (D^2) and posterior probabilities of group membership (p) based on the scores for fossil specimens in the between-group principal component analysis for the entire anthropoid sample.[a,b]

D^2	Cercopithecoidea	Hominidae	Hylobatidae	Platyrrhini
Epipliopithecus vindobonensis (NHMW 1970/1397/0003)	17.179	10.539	6.485	**3.437**
Epipliopithecus vindobonensis (NMB OE 303a)	12.190	14.262	6.588	**0.779**
Epipliopithecus vindobonensis (NMB OE 303b)	13.307	15.085	6.682	**1.056**
Oreopithecus bambolii (BAC 208)	8.083	5.450	11.574	**1.579**
Aegyptopithecus zeuxis (CGM 85785)	12.430	9.133	15.513	**0.990**
Homunculus patagonicus (MPM-PV 3501)	11.817	13.356	11.017	**0.073**
Homunculus patagonicus (MPM-PV 3502)	10.336	12.736	12.056	**0.165**
Homunculus patagonicus (MPM-PV 3503)	10.083	7.449	11.284	**0.590**
Dolichocebus gaimanensis (MACN 14128)	5.204	13.516	12.687	**1.935**
Parapithecus grangeri (DPC 18651)	6.533	17.859	13.047	**2.110**
P	Cercopithecoidea	Hominidae	Hylobatidae	Platyrrhini
Epipliopithecus vindobonensis (NHMW 1970/1397/0003)	0.006	0.007	0.018	**0.029**
Epipliopithecus vindobonensis (NMB OE 303a)	0.018	<0.001	<0.001	**0.678**
Epipliopithecus vindobonensis (NMB OE 303b)	0.013	<0.001	<0.001	**0.608**
Oreopithecus bambolii (BAC 208)	0.052	0.005	<0.001	**0.530**
Aegyptopithecus zeuxis (CGM 85785)	0.001	<0.001	<0.001	**0.688**
Homunculus patagonicus (MPM-PV 3501)	0.003	<0.001	<0.001	**0.980**
Homunculus patagonicus (MPM-PV 3502)	0.003	<0.001	<0.001	**0.919**
Homunculus patagonicus (MPM-PV 3503)	0.019	0.001	<0.001	**0.848**
Dolichocebus gaimanensis (MACN 14128)	0.013	<0.001	<0.001	**0.612**
Parapithecus grangeri (DPC 18651)	0.002	<0.001	<0.001	**0.411**

Abbreviations: NHMW = Naturhistorisches Museum of Wien, Austria; NMB = Naturhistorisches Museum of Basel, Switzerland; BAC = NMB accession number for *Oreopithecus bambolii* specimens; CGM = Egyptian Geological Museum, Cairo, Egypt; MPM-PV = Museo Regional Provincial Padre M.J. Molina, Río Gallegos, Argentina; MACN = Museo Argentino de Ciencias Naturales, Buenos Aires, Argentina; DPC = Duke Lemur Center, Durham, NC, USA.

[a] Note that these are probability estimates of having a particular score given membership in a particular group, not the likelihood of group membership in each of the a priori defined groups given a particular score (the greater the number, the higher the probability).

[b] The lowest distance (D^2) and highest posterior probability of group membership (p) for each specimen are bolded.

Table 4
Mahalanobis distances (D^2) and posterior probabilities of group membership (p) based on the scores for fossil specimens in the between-group principal component analysis for the entire anthropoid sample and considering all catarrhines as a single group.[a,b]

D^2	Catarrhini	Platyrrhini
Epipliopithecus vindobonensis (NHMW 1970/1397/0003)	13.016	**5.341**
Epipliopithecus vindobonensis (NMB OE 303a)	11.837	**1.654**
Epipliopithecus vindobonensis (NMB OE 303b)	13.040	**2.098**
Oreopithecus bambolii (BAC 208)	9.085	**3.890**
Aegyptopithecus zeuxis (CGM 85785)	16.900	**3.204**
Homunculus patagonicus (MPM-PV 3501)	13.814	**0.135**
Homunculus patagonicus (MPM-PV 3502)	13.057	**0.284**
Homunculus patagonicus (MPM-PV 3503)	10.989	**1.806**
Dolichocebus gaimanensis (MACN 14128)	8.645	**2.417**
Parapithecus grangeri (DPC 18651)	12.592	**3.670**
P	Catarrhini	Platyrrhini
Epipliopithecus vindobonensis (NHMW 1970/1397/0003)	0.109	**0.241**
Epipliopithecus vindobonensis (NMB OE 303a)	0.022	**0.876**
Epipliopithecus vindobonensis (NMB OE 303b)	0.017	**0.847**
Oreopithecus bambolii (BAC 208)	0.124	**0.673**
Aegyptopithecus zeuxis (CGM 85785)	0.002	**0.886**
Homunculus patagonicus (MPM-PV 3501)	0.002	**0.985**
Homunculus patagonicus (MPM-PV 3502)	0.002	**0.968**
Homunculus patagonicus (MPM-PV 3503)	0.034	**0.935**
Dolichocebus gaimanensis (MACN 14128)	0.013	**0.841**
Parapithecus grangeri (DPC 18651)	0.002	**0.795**

Abbreviations: NHMW = Naturhistorisches Museum of Wien, Austria; NMB = Naturhistorisches Museum of Basel, Switzerland; BAC = NMB accession number for *Oreopithecus bambolii* specimens; CGM = Egyptian Geological Museum, Cairo, Egypt; MPM-PV = Museo Regional Provincial Padre M.J. Molina, Río Gallegos, Argentina; MACN = Museo Argentino de Ciencias Naturales, Buenos Aires, Argentina; DPC = Duke Lemur Center, Durham, NC, USA.

[a] Note that these are probability estimates of having a particular score given membership in a particular group, not the likelihood of group membership in each of the a priori defined groups given a particular score (the greater the number, the higher the probability).

[b] The lowest distance and highest probability for each specimen are bolded.

deformation fields confirms these results (Fig. 7). *Epipliopithecus* clusters with *Alouatta* and *Ateles* (large and rounded vertical canals and a large gap between the lateral and posterior canals), as well as *Pithecia* (obtuse angle formed by the anterior and posterior canals), within a larger cluster that includes the remaining extant platyrrhines and the other fossil taxa included in the analysis. In particular, *Aegyptopithecus* and *Homunculus* cluster with *Saimiri* and *Cebus* (flat lateral canal and similarities in the anterior canal morphology), while *Oreopithecus* clusters with *Callicebus* (orientation of the anterior and posterior canals). Hylobatids cluster within

Table 5
Mahalanobis distances (D^2) between specimens of *Epipliopithecus* and other fossils based on between group principal component analysis scores.

D^2	NHMW 1970/1397/0003	NMB OE 303a	NMB OE 303b
Epipliopithecus vindobonensis (NHMW 1970/1397/0003)	–	1.332	1.285
Epipliopithecus vindobonensis (NMB OE 303a)	1.332	–	0.176
Epipliopithecus vindobonensis (NMB OE 303b)	1.285	0.176	–
Oreopithecus bambolii (BAC 208)	2.244	1.901	2.055
Aegyptopithecus zeuxis (CGM 85785)	2.360	1.804	1.927
Homunculus patagonicus (MPM-PV 3501)	1.943	0.919	1.033
Homunculus patagonicus (MPM-PV 3502)	2.246	1.251	1.388
Homunculus patagonicus (MPM-PV 3503)	1.914	1.450	1.592
Dolichocebus gaimanensis (MACN 14128)	3.081	2.077	2.243
Parapithecus grangeri (DPC18651)	3.201	2.017	2.161

Abbreviations: NHMW = Naturhistorisches Museum Wien, Austria; NMB OE = Naturhistorisches Museum Basel, Switzerland; BAC = Baccinello (housed at NMB); CGM = Egyptian Geological Museum, Cairo, Egypt; MPM-PV = Museo Regional Provincial Padre M.J. Molina, Río Gallegos, Argentina; MACN = Museo Argentino de Ciencias Naturales, Buenos Aires, Argentina; DPC = Duke Lemur Center, Durham, NC, USA.

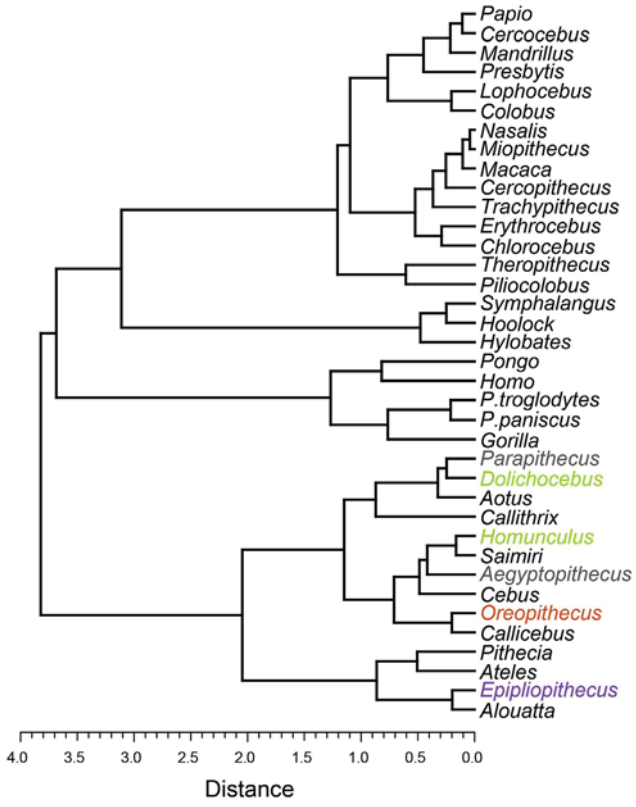

Figure 7. Dendrogram resulting from a cluster analysis (Ward's method) based on Mahalanobis distances computed between the species centroids of the between-group principal component analysis (bgPCA) of shape data. The cophenetic correlation coefficient is 0.703.

a larger group that also includes most cercopithecoids, and extant great apes cluster together due to their distinctive stout volumetric proportions (Urciuoli et al., 2020).

3.3. Phylogenetic signal and phylomorphospace

Like previous analyses (Urciuoli et al., 2020; del Rio et al., 2020; Morimoto et al., 2020), our results indicate that the vestibule and SCs embed significant phylogenetic signal ($K_{mult} = 1.134$, $p < 0.001$), suggesting these traits conform to a Brownian motion model of evolution, with closely related taxa resembling one another slightly more than expected ($K_{mult} > 1$). The phylogenetic signal computed for each bgPC separately is significant in all instances (Table 6), with bgPC1 and bgPC2 suggesting the same evolutionary mode as K_{mult} ($K > 1$). Conversely, we observe that the variance accumulates within clades for bgPC3 ($K < 1$), thus suggesting that changes along this axis might be more strongly affected by homoplasy.

The phylogenetic signal detected justifies the application of the phylomorphospace approach (Fig. 8). The results indicate that the reconstructed LCAs of crown anthropoids (Fig. 9a) and crown catarrhines (Fig. 9c) fall within the variability of extant New World monkeys, being very close to the platyrrhine LCA (Fig. 9b)—irrespective of the phylogenetic hypothesis used in the analysis for *Epipliopithecus* (i.e., stem catarrhine vs. stem hominoid, Figs. 3 and 8; SOM Fig. S3). Cercopithecoids and hominoids appear much more derived in SC morphology than platyrrhines, but in different directions. The crown anthropoid, crown platyrrhine and crown catarrhine LCAs are reconstructed as possessing large and slightly vertically-elongated canals (more so in the crown anthropoid and crown platyrrhine LCAs; Fig. 9a, b) coupled with a long CC (shorter in the crown catarrhine LCA; Fig. 9c), intermediate volumetric proportions (similar to those found in New World monkeys and cercopithecins; Fig. 10), and a coplanar lateral canal that does not intersect the plane of the posterior one (Fig. 9a–c). The LCA of crown catarrhines also shows a slightly more superiorly bent ampullary portion, more so than in *Epipliopithecus* (Fig. 9c). In contrast, the reconstructed crown hominoid LCA (Fig. 9d) is found in an area of the morphospace devoid of extant taxa and, according to our estimation, it already displayed some derived characters that are not found in *Epipliopithecus* (i.e., moderately vertically-compressed anterior canal, stouter canal proportions, lateral ampulla connecting more superiorly with the vestibule).

From a phenetic viewpoint, based on weighted Euclidean distances between *Epipliopithecus* and the bgPC scores for the reconstructed LCAs (Table 7), the former taxon is most similar to the crown catarrhine ancestral condition, and also closer to the crown anthropoid and platyrrhine LCAs, than to the ancestral conditions reconstructed for either hominoids or cercopithecoids.

We further synthesized the information provided by the phylomorphospace approach by defining seven discrete characters coded in a cladistic fashion (Table 8; Fig. 11). Their coding for the reconstructed LCAs as well as both extant and extinct anthropoids

Table 6
Phylogenetic signal computed for the between-group principal analysis applied to the deformation fields of the extant anthropoid comparative sample. The variance explained by each principal component (bgPC) and the *p*-value for the statistics are given within parentheses.

	bgPC1 (59%)	bgPC2 (30%)	bgPC3 (11%)
Pagel's λ	1.000 ($p < 0.0001$)	0.843 ($p < 0.0001$)	0.925 ($p < 0.0001$)
Blomberg's K	1.148 ($p < 0.0001$)	1.446 ($p < 0.001$)	0.732 ($p < 0.001$)

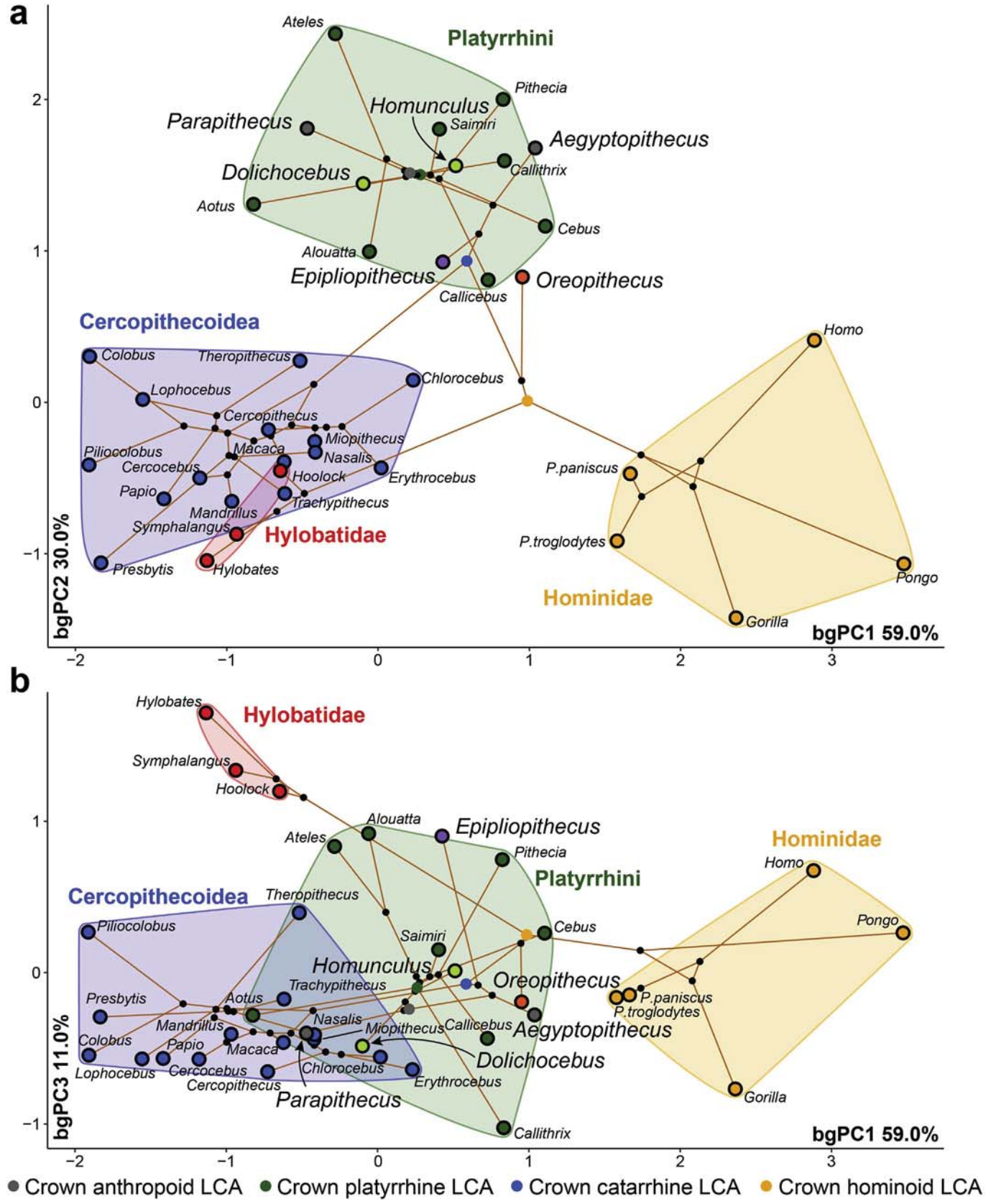

Figure 8. Phylomorphospace of the anthropoid semicircular canals. The phylogenetic tree (with *Epipliopithecus* included as a stem catarrhine; Fig. 3a) is projected onto the tangent space defined by the between-group principal components (bgPCs) as shown in Figure 6. The internal nodes (i.e., the ancestral states) were estimated using maximum likelihood: a) bgPC2 vs. bgPC1; b) bgPC3 vs. bgPC1. Variance explained by each component is given along each axis. Convex hulls depict the range of variation for a priori defined groups using the following color code: green = platyrrhines; blue = cercopithecoids; red = hylobatids; orange = hominids. The ancestral nodes discussed for assessing *Epipliopithecus* phylogenetic affinities do not change consistently in their position in the morphospace irrespective of the phylogenetic hypothesis used for their estimation (see SOM Fig. S3 for the alternative phylogenetic tree including *Epipliopithecus* as a stem hominoid). Key nodes are highlighted as follows: gray circle = crown anthropoids; green circle = crown platyrrhines; blue circle = crown catarrhines; orange circle = crown hominoids. (For interpretation of the references to color in this figure legend, the reader is referred to the Web version of this article.)

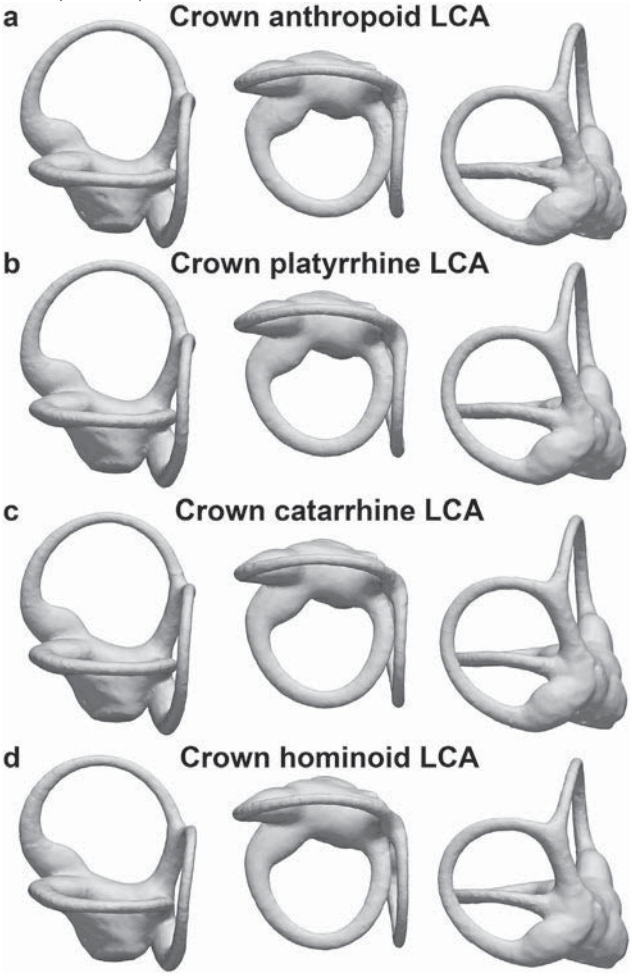

Figure 9. Reconstruction of the semicircular canals and vestibule for the last common ancestors of the following clades: a) crown anthropoids; b) crown platyrrhines; c) crown catarrhines; d) crown hominoids. The renderings of each 3D model are depicted in lateral (left), superior (middle), and posterior (right) views.

included in the analyses is reported in Table 9 and SOM Table S4. When the character states for extinct and extant taxa are analyzed against the two phylogenetic hypotheses by considering parsimony as a criterion (Table 10), *Epipliopithecus* is more parsimoniously interpreted as a stem catarrhine (Fig. 3a) than as a stem hominoid (Fig. 3b). The phylogenetic implications of the seven coded characters (Fig. 11; Tables 8 and 9; SOM Table S4) are discussed below and illustrated in Figure 12.

Size of the vestibule relative to the semicircular canals Extant hominids differ from all the remaining extant taxa in possessing a relatively larger vestibule, which may be thus interpreted as a synapomorphy of at least crown hominids. Among the extinct taxa, only the purported stem hominoid *Oreopithecus* displays the derived hominid condition, indicating either an independent acquisition of this feature in this taxon (as supported by our LCA reconstructions) or a secondary reversal in hylobatids. *Epipliopithecus*, in any case, retains the plesiomorphic condition of nonhominoid anthropoids.

Robusticity of the semicircular canals This character has the same distribution as the size of the vestibule relative to the SCs. Extant hominids and *Oreopithecus* differ from the remaining taxa by displaying stouter proportions. Accordingly, such proportions might be interpreted either as convergent between *Oreopithecus* and hominids, or as a hominoid synapomorphy with subsequent reversal in hylobatids. Our LCA reconstructions do not provide clear support for either possibility, as they suggest an intermediate ancestral condition in the overlap zone between hominoids and nonhominoid catarrhines. In either case, for this character

Table 7
Weighted Euclidean distances computed between the between-group principal component scores of the reconstructed last common ancestors (LCAs) and the *Epipliopithecus* centroid.

LCA	Distance
Crown anthropoids	1.304
Crown platyrrhines	1.141
Crown catarrhines	0.989
Crown cercopithecoids	1.646
Crown hominoids	1.256

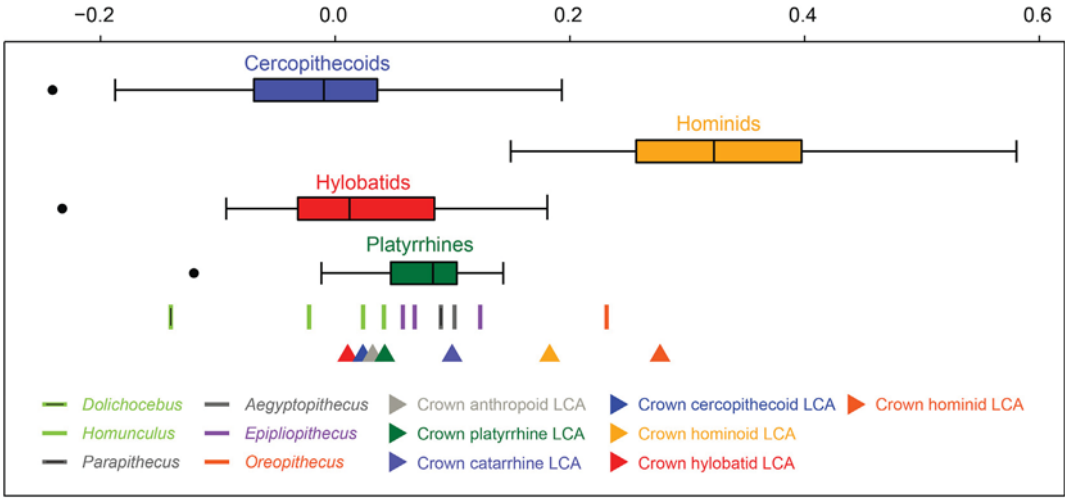

Figure 10. Box-and-whisker plot of allometric residuals based on best-fit line of the nonhominid anthropoid regression of log-transformed cube root of canal volume and log-transformed canal length (as depicted in Fig. 5). Vertical lines correspond to the median, boxes depict interquartile range, whiskers represent maximum and minimum values within 1.5 times the interquartile range, and black dots are outliers. Sample sizes for extant groups are the following: Platyrrhini ($n = 40$), Cercopithecoidea ($n = 75$), Hylobatidae ($n = 17$), Hominidae ($n = 30$).

Table 8
Definition of the discrete characters of semicircular canal (SC) and vestibule morphology used in this paper.

Character No.	Character statements (characters + character states)[a]
#1	Size of the vestibule relative to the SCs: 0 = small; 1 = large.
#2	Robusticity of the SCs: 0 = slender; 1 = stout.
#3	Shape of the anterior SC: 0 = vertically compressed; 1 = rounded; 2 = elongated superiorly.
#4	Shape of the anterior portion of the anterior SC: 0 = non-projecting anterosuperiorly; 1 = anterosuperiorly projecting.
#5	Shape of the posterior SC: 0 = vertically compressed; 1 = rounded; 2 = elongated superiorly.
#6	Shape of the lateral SC ampullary portion: 0 = flat or only slightly bent superiorly; 1 = markedly bent superiorly.
#7	Length of the CC: 0 = long; 1 = intermediate; 2 = short.

[a] See Figure 11 for an illustration of the character states.

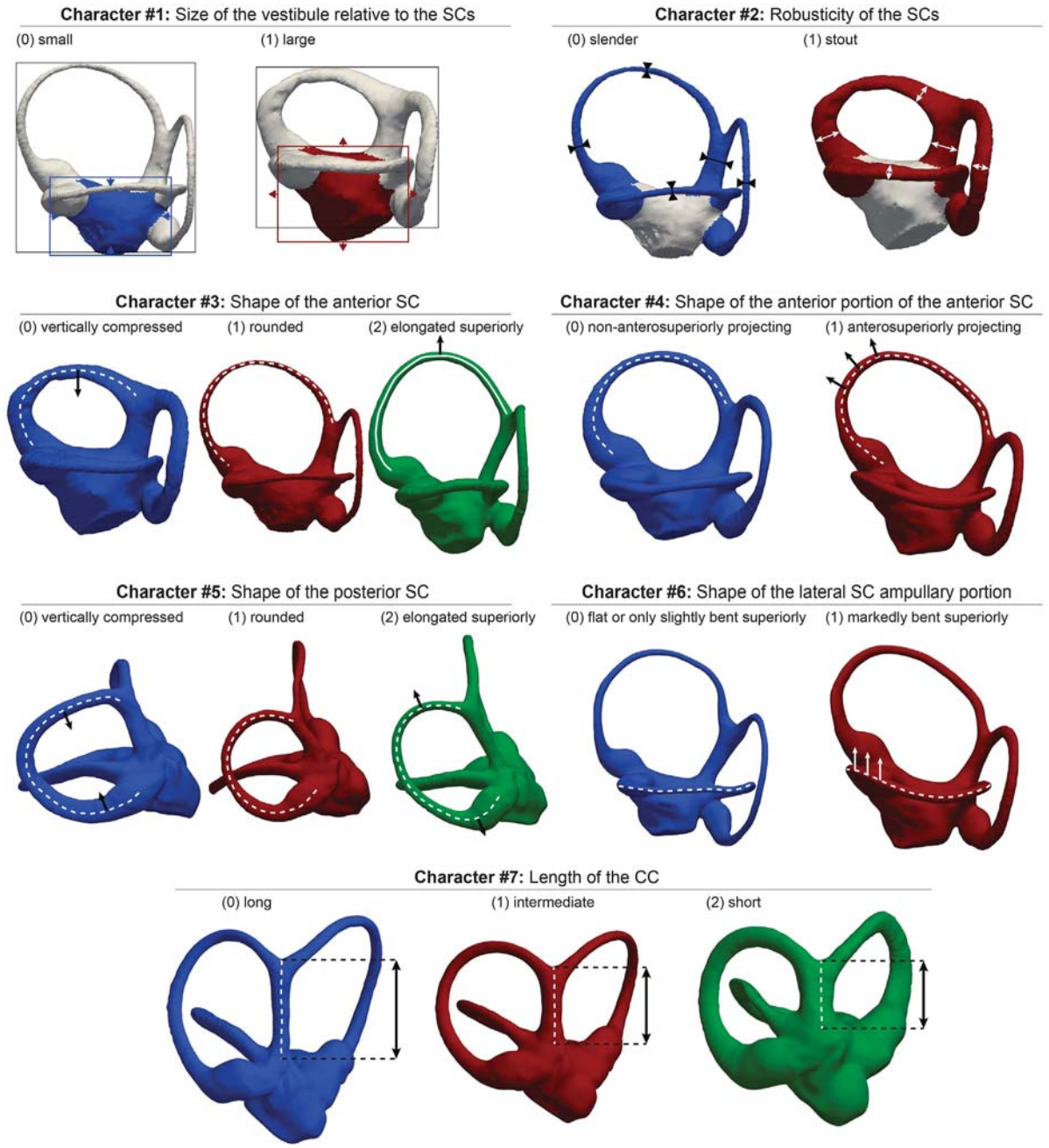

Figure 11. Illustration of the discrete characters of semicircular canal and vestibule morphology used in this paper. Numbers preceding each state (0, 1, 2) correspond to character states numbered in Tables 8 and 9, and SOM Table S4.

Table 9
Character states coded for the estimated last common ancestors (LCAs) and for the fossil taxa included in the analysis.[a].

Species/LCAs	#1	#2	#3	#4	#5	#6	#7
Epipliopithecus vindobonensis	0	0	1	0	2	0	0
Aegyptopithecus zeuxis	0	0	2	0	2	0	0
Dolichocebus gaimanensis	0	0	2	0	2	0	0
Homunculus patagonicus	0	0	2	0	0, 2	0	0
Oreopithecus bambolii	1	1	0	1	1	0	2
Parapithecus grangeri	0	0	2	0	2	0	0
Crown anthropoid LCA	0	0	2	0	2	0	0
Crown platyrrhine LCA	0	0	2	0	2	0	0
Crown catarrhine LCA	0	0	1	0	1	0	1
Crown cercopithecoid LCA	0	0	1	0	1	0	1
Crown hominoid LCA	0	0	0	0	1	1	2
Crown hylobatid LCA	0	0	0	1	1	1	2
Crown hominid LCA	1	1	0	0	1	1	2

[a] See character definitions in Table 7 and SOM Table S2 for the coding of extant species.

Table 10
Measures of character congruence for the two main phylogenetic hypotheses (i.e., stem catarrhine vs. stem hominoid) discussed in this paper for *Epipliopithecus*. The higher the index, the more parsimonious the hypothesis.[a].

Metrics	Stem catarrhine (Fig. 3a)	Stem hominoid (Fig. 3b)
Tree length	22	24
CI	0.455	0.417
RI	0.826	0.797
RC	0.376	0.332

Abbreviations: CI = consistency index; RI = retention index; RC = rescaled consistency index.
[a] See also Figure 3 and SOM Table 2 for character descriptions.

Epipliopithecus displays the more plesiomorphic condition of nonhominoid anthropoids.

Shape of the anterior semicircular canal This character is more variable than the preceding ones, both within anthropoid subclades, and sometimes even within the same species. However, extant catarrhines generally differ from platyrrhines by possessing an anterior canal that is not superiorly elongated, being instead either rounded (as in humans and most cercopithecoids) or vertically compressed (as in great apes and generally hylobatids, although in the latter it varies intraspecifically between rounded and vertically compressed). Our LCA reconstructions suggest that the ancestral anthropoid condition—a superiorly elongated anterior canal—is symplesiomorphic not only for platyrrhines but also for the stem catarrhine *Aegyptopithecus*. They further support the view that a rounded anterior SC is synapomorphic of crown catarrhines, while a vertically compressed anterior SC would be synapomorphic for crown hominoids + *Oreopithecus*. In this regard, *Epipliopithecus* is more derived than *Aegyptopithecus* but less so than *Oreopithecus*. This character, therefore, unambiguously supports for *Epipliopithecus* a catarrhine status more derived than in *Aegyptopithecus*, although it would be consistent with either a stem catarrhine or a stem hominoid status.

Shape of the anterior portion of the semicircular canal Hylobatids and orangutans differ from the rest of the sample by displaying an anterosuperiorly projecting anterior portion of the anterior canal. This condition may be interpreted as a crown hominoid synapomorphy subsequently reversed in hominines, as further supported by the fact that *Oreopithecus* displays the derived condition for hominoids. Alternatively, this feature might have been independently acquired in *Oreopithecus*, as suggested by our LCA reconstructions, which only recover it as a hylobatid synapomorphy. Given the possession of other SC hominoid synapomorphies in *Oreopithecus*, we tend to favor the former interpretation, even if both are equally parsimonious. In any case, *Epipliopithecus* retains the more plesiomorphic condition of nonhominoid anthropoids.

Shape of the posterior semicircular canal Although this character is somewhat variable within anthropoid subclades and sometimes even within species, some generalities can be drawn. In platyrrhines, the posterior canal is generally elongated superiorly to some extent, whereas most cercopithecoids have a rounded posterior canal, and hominoids generally vary between a rounded and a vertically compressed morphology (only sometimes superiorly elongated in *Pan*). Our LCA reconstructions indicate that platyrrhines and *Aegyptopithecus* retain the ancestral anthropoid condition (superiorly elongated posterior canal), whereas the rounded morphology would be synapomorphic for crown hominoids. *Epipliopithecus* displays the plesiomorphic anthropoid condition and thus differs from *Oreopithecus*, which displays the derived catarrhine morphology.

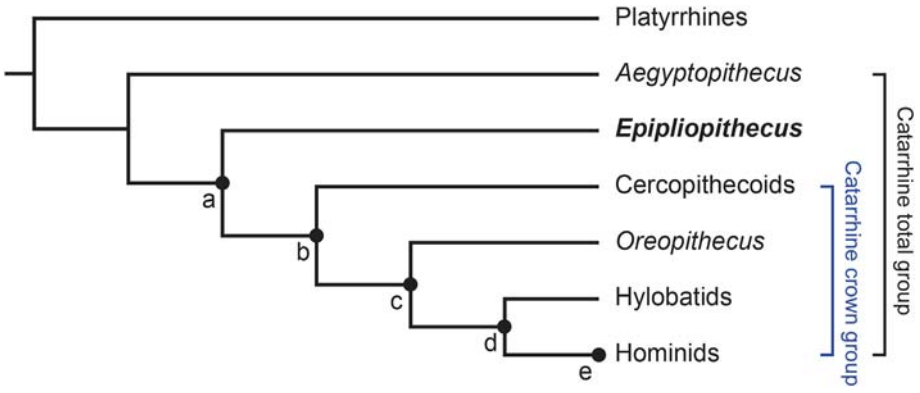

Figure 12. Simplified cladogram of crown anthropoids and selected extinct catarrhines (*Epipliopithecus* and *Oreopithecus*) summarizing the main synapomorphies inferred for the various clades in semicircular canal and vestibule morphology. The four extant anthropoid clades distinguished (platyrrhines, cercopithecoids, hylobatids and hominids) are depicted as terminal nodes. The synapomorphies inferred for each node are summarized below; character number (preceded by a hash) and character state (within parentheses) are provided after each synapomorphy within brackets. a) *Epipliopithecus* + crown catarrhines: rounded anterior canal [#3(1)]; b) Crown catarrhines: rounded posterior canal [#5(1)], moderately short CC [#7(1)]; c) *Oreopithecus* + crown hominoids: vertically compressed anterior canal [#3(0)], anterosuperiorly projecting anterior portion of the anterior canal [#4(1)], short CC [#7(2)]; d) Crown hominoids: markedly superiorly bent ampullary portion of the lateral canal [#6(1)]; e) Crown hominids (unless *Oreopithecus* + crown hominoid synapomorphies [node c] with reversal in hylobatids): large vestibule relative to the SCs [#1(1)], stout SCs [#2(1)]. Abbreviations: CC = common crus; SC = semicircular canals. See Figure 11 for an illustration of the various character states and Table 9 and SOM Table S4 for the scoring of reconstructed last common ancestors and individual taxa, respectively.

Shape of the lateral semicircular canal ampullary portion Extant hominoids differ from the remaining extant taxa and all the analyzed extinct genera by displaying a markedly superiorly-bent ampullary portion of the lateral canal. Both *Epipliopithecus* and *Oreopithecus* thus display a more plesiomorphic condition than crown hominoids, as further confirmed by our LCA reconstructions. Length of the common crus This character is also variable to some extent, but platyrrhines generally display a longer CC than extant catarrhines, with hominoids having an even shorter CC than most cercopithecoids. Our LCA reconstructions support an intermediate length of the CC as synapomorphic of crown catarrhines, with a short CC being synapomorphic for hominoids. *Epipliopithecus* resembles *Aegyptopithecus* and platyrrhines by retaining the ancestral anthropoid condition, whereas *Oreopithecus* displays the derived hominoid morphology.

4. Discussion

Our analysis of the SC and vestibule morphology of *Epipliopithecus* allows us to refine our understanding of the evolution of this anatomical region in anthropoid primates and to refine previous hypotheses proposed by Urciuoli et al. (2020). The results of our deformation-based 3DGM analysis and the reconstruction of ancestral morphotypes for main anthropoid clades indicate that, like the stem catarrhine *Aegyptopithecus*, *Epipliopithecus* displays a platyrrhine-like morphology most similar to that reconstructed for the crown catarrhine LCA. This might be compatible with *Epipliopithecus* being either a stem catarrhine, or a crown catarrhine only slightly postdating the cercopithecoid-hominoid split. However, the fact that *Epipliopithecus* most closely resembles the crown anthropoid (and platyrrhine) LCAs (Table 7) suggests that the semicircular morphology of this taxon is most consistent with its status as a stem catarrhine. This conclusion is further supported by the analysis of seven discrete characters coded for this anatomical area—which indicate that this is the most parsimonious hypothesis, for reasons discussed in greater detail below.

4.1. Epipliopithecus *as a hominoid*

Based on the morphology of the SCs and vestibule, *Epipliopithecus* lacks multiple hominoid synapomorphies, including a large vestibule relative to the canals, stout SCs, vertically compressed anterior canal, anterosuperiorly projecting anterior portion of the anterior canal, markedly superiorly bent ampullary portion of the lateral canal, and short CC. Urciuoli et al. (2020) already interpreted some of these features (vertically compressed anterior canal and markedly superiorly bent ampullary portion of the lateral canal) as potential crown hominoid synapomorphies, whereas they interpreted others (large vestibule and stout canals) as hominid synapomorphies. Urciuoli et al. (2020) interpreted a superiorly bent ampullary portion of the lateral canal as a hominoid synapomorphy. However, hominoids are, in fact, characterized by the possession of a markedly bent trajectory, whereas other catarrhines display a flat to slightly superiorly-bent ampullary portion of the lateral canal. This is the case for *Epipliopithecus*, which displays much less bending of the lateral canal than in *Oreopithecus* or any extant hominoid.

The possession of a large vestibule and stout canals was previously interpreted as being synapomorphic for hominids (Urciuoli et al., 2020) because hylobatids display a different ('monkey-like') condition. The differences in volumetric proportions between *Epipliopithecus* and hominids are particularly clear (Fig. 10), with the former closely resembling platyrrhines, *Aegyptopithecus*, and the inferred ancestral catarrhine condition. Given that both features are present in *Oreopithecus*, they may be interpreted as hominoid synapomorphies subsequently reversed in hylobatids—thereby supporting a more basal branching for *Epipliopithecus*. However, their interpretation as hominid synapomorphies is equally parsimonious, as it would only imply their independent acquisition in *Oreopithecus*. Therefore, neither a large vestibule nor stout canals can be used to unambiguously discount a hominoid status for *Epipliopithecus*. A similar caveat applies to the lack of an anterosuperiorly projecting anterior canal in *Epipliopithecus*. This condition was previously interpreted as an autapomorphy of *Hylobates* (Le Maître et al., 2017) or as a hylobatid synapomorphy (Spoor and Zonneveld, 1998; Urciuoli et al., 2020). However, given its presence in orangutans and *Oreopithecus*, it is more readily interpreted as a hominoid synapomorphy subsequently reversed in hominines. The interpretation of some of the potential hominoid synapomorphies lacking in *Epipliopithecus* is ambiguous due to homoplasy (convergence and/or reversal). However, it is worth noting that, except for the markedly superiorly bent ampullary portion of the lateral canal, *Oreopithecus* further displays two more unambiguous hominoid synapomorphies (vertically compressed anterior canal and short CC). The absence of these features in *Epipliopithecus* thus conclusively excludes a more derived hominoid status for the latter as compared with *Oreopithecus*.

Epipliopithecus also displays some hylobatid-like features in the spatial configuration between the lateral and posterior canals, as well as in the orientation between the anterior and posterior canals. According to Urciuoli et al. (2020), the lack of intersection between the lateral and posterior canals and the presence of an obtuse angle between the anterior and posterior canals would be synapomorphic for hominoids and hylobatids, respectively. However, only *Hylobates* consistently displays both features, while most anthropoid taxa, as well as the two *Epipliopithecus* individuals, show a considerable amount of intraspecific variation. Hence, we refrained from coding these features in a cladistic manner, especially in view of the low phylogenetic signal ($K < 1$) recovered for bgPC3 (accounting for the variation in the configuration of these features), which suggests a substantial degree of homoplasy. Indeed, previous analyses hypothesized that suspensory species possess more obtuse angles between the vertical canals (Gonzales et al., 2019), as this configuration provides an increased sensitivity for pitch (at the expense of roll) head movements (Muller and Verhagen, 2002a,b,c). The similarities between NHMW 1970/1397/0003, hylobatids, and some atelids (Spoor and Zonneveld, 1998; Gonzales et al., 2019) would thus agree with previous inferences about the locomotor repertoire of this taxon including some degree of suspensory behaviors (Zapfe, 1958; Fleagle, 1983; Langdon, 1986; Rose, 1994; Arias Martorell et al., 2015). In contrast, the more plesiomorphic condition of NBM OE 303III (characterized by tangent lateral and posterior canals, and vertical canals approximating a right angle), also found in *Aegyptopithecus* and some non-suspensory platyrrhine species, suggests caution when using SC orientation alone for inferring positional behaviors (Perier et al., 2016; contra; Malinzak et al., 2012; Berlin et al., 2013).

4.2. *Epipliopithecus* as a stem catarrhine

Epipliopithecus resembles both stem platyrrhines and the stem catarrhine *Aegyptopithecus* in lacking all of the aforementioned hominoid synapomorphies, thereby retaining the plesiomorphic anthropoid condition—a relatively small vestibule, slender SCs, anterosuperiorly nonprojecting anterior portion of the anterior canal, superiorly elongated posterior canal, ampullary portion of the lateral canal not markedly bent superiorly, and long CC. The fact that *Epipliopithecus* lacks hominoid synapomorphies displayed by *Oreopithecus* could still be consistent with a more basal stem hominoid status. However, such an interpretation is contradicted

by the retention in *Epipliopithecus* of a superiorly elongated posterior canal and a long CC—contrasting with the rounded posterior canal and moderately short CC that are synapomorphic of crown catarrhines. The catarrhine status of *Epipliopithecus* and other pliopithecoids is well established based on multiple features, such as the loss of the second premolars and the presence of a C^1/P_3 honing complex (e.g., Harrison, 2013). The catarrhine status of *Epipliopithecus* is further supported by the possession of a rounded anterior canal, which is intermediate between the primitive morphology (superiorly elongated anterior canal) retained by platyrrhines and *Aegyptopithecus*, and the more derived (vertically compressed) morphology synapomorphic of hominoids. In this regard, *Epipliopithecus* is more derived toward crown catarrhines than the propliopithecoid *Aegyptopithecus*, in agreement with other cranial features such as the possession of a partially enclosed tubular ectotympanic in *Epipliopithecus* (e.g., Harrison, 2013).

In summary, based on the morphology of the SCs and vestibule, *Epipliopithecus* is most parsimoniously interpreted as a stem catarrhine more derived than *Aegyptopithecus*, due to its possession of a crown catarrhine synapomorphy—rounded anterior canal—coupled with the lack of two additional crown catarrhine synapomorphies (superiorly elongated posterior canal and long CC) and multiple hominoid and/or hominid synapomorphies as described above. The shapes of the anterior and posterior canals and CC should be considered with caution in light of the intraspecific variability displayed by these characters in some taxa (SOM Table S4). Previous analyses noted a structural relationship between the morphology of these canals and the extension of the subarcuate fossa (Jeffery and Spoor, 2006; Jeffery et al., 2008), and this relationship has been uncritically assumed in some studies (Spoor et al., 2007; Silcox et al., 2009; Gonzales et al., 2019). However, in most cases the fossa simply expands within the space left available from the ossification of the canals, with little or no influence on their shape (Jeffery et al., 2008; see also Urciuoli et al., 2020). In support of the latter hypothesis, we observe meager dissimilarities in the anterior canal morphology of NHMW 1970/1397/0003 and NBM OE 303III—except for the angle, as discussed above—irrespective of the marked differences in the morphology of the fossa between the two individuals (Zapfe, 1961). While a large amount of morphological variation has been documented within ruminant genera (Mennecart and Costeur, 2016), variation in CC length and shape has not been exhaustively analyzed in primates (Spoor and Zonneveld, 1998; Ekdale 2013; Lee et al., 2013). In the present study, we found considerable intraspecific variation in CC length for some species of monkeys and apes. Nevertheless, our results support a clear morphocline from the ancestral condition (long CC) retained by platyrrhines, *Aegyptopithecus*, and *Epipliopithecus*, to the most derived condition (short CC) characteristic of hominoids, with cercopithecoids displaying an intermediate condition that is likely synapomorphic for crown catarrhines as a whole. Therefore, *Epipliopithecus* SC morphology supports its interpretation as more derived than *Aegyptopithecus* toward crown catarrhines but excludes a crown catarrhine status and, in particular, a closer relationship with hominoids (unlike in the case of *Oreopithecus*).

5. Conclusions

Our results are in broad agreement with previous analyses suggesting that *Epipliopithecus* displays a 'typical monkey' inner ear morphology (Morimoto et al., 2020), while *Oreopithecus* possesses SC and vestibule features derived toward the crown hominoid condition (Urciuoli et al., 2020). At the same time, our study further refines previous comparisons of SC and vestibule morphology between *Epipliopithecus* and other anthropoids, enabling us to test competing hypotheses about the phylogenetic position of this taxon (i.e., stem catarrhine vs. stem hominoid).

From a phenetic viewpoint, for this anatomical area *Epipliopithecus* more closely resembles platyrrhines and the stem catarrhine *Aegyptopithecus*, as well as the reconstructed ancestral catarrhine morphotype. The fact that *Epipliopithecus* shows greater similarities with the platyrrhine and anthropoid ancestral morphotypes, rather than with those of cercopithecoids or hominoids, supports the view that *Epipliopithecus* is a stem catarrhine instead of a stem hominoid. From a cladistic perspective, this interpretation is confirmed based on a series of crown catarrhine and crown hominoid synapomorphies. *Epipliopithecus* is more parsimoniously interpreted as a stem catarrhine than as a stem hominoid based on the vestibular morphology analyzed here because it lacks several catarrhine and all hominoid synapomorphies. Specifically, the possession of a rounded posterior canal reinforces the view that *Epipliopithecus* is more derived than *Aegyptopithecus* among stem catarrhines.

The information provided by the SCs and vestibule is thus congruent with the ectotympanic morphology of *Epipliopithecus* (see review in Fricano, 2018), which is more plesiomorphic than in crown catarrhines but more derived than in propliopithecoids. Some similarities between *Epipliopithecus* and hylobatids are based on characters that are too variable within species to be of use for phylogenetic assessment. Such features might have evolved independently between some atelids and hylobatids, due to similar locomotor-related selection pressures, and do not support the close phylogenetic link classically hypothesized between pliopithecoids and hylobatids (Hürzeler, 1954; Zapfe, 1961; Simons and Fleagle, 1973), particularly given that *Epipliopithecus* displays no crown hominoid synapomorphies. We therefore conclude that the SC and vestibular morphology reinforces the most commonly held view that, in accordance with most (Zalmout et al., 2010; Stevens et al., 2013; Nengo et al., 2017) but not all (Alba et al., 2015) recent cladistic analyses, *Epipliopithecus* is best interpreted as a stem catarrhine rather than a stem hominoid.

Declaration of competing interest

The authors declare no conflict of interest.

Acknowledgments

This research has been funded by the Agencia Estatal de Investigación (CGL2016-76431-P and CGL2017-82654-P, AEI/FEDER EU; and BES-2015-071318 to A.U.), the Generalitat de Catalunya (CERCA Programme, and consolidated research groups 2017 SGR 86 and 2017 SGR 116 GRC), the French Centre National de la Recherche Scientifique, the Leakey Foundation (research grant), and the Synthesys Project (AT-TAF-4689; http://synthesys3.myspecies.info/), which is financed by the European Community Research Infrastructure Action under the FP7. Part of the analyses were performed using High Performance Computing resources from BSC (BCV-2020-1-0008). We are grateful to Jose Torres for the technical help provided in the setup of the analysis. We thank the following people for providing or permitting access to CT scans: Ursula Göhlich (*Epipliopithecus* NHMW 1970/1397/0003), Martin Dockner, Loïc Costeur (*Epipliopithecus* NMBOE 303), Lorenzo Rook (*Oreopithecus*), José Braga (human specimens), Lynn Copes, Lynn Lucas, and the MCZ (part of the scans used in the study, funded by NSF DDIG #0925793 and Wenner-Gren Foundation Dissertation Grant #8102 to Lynn Copes), Richard Kay (*Homunculus* and *Dolichocebus*), Timothy Ryan (*Aegyptopithecus*; funded by NSF BCS-0416164 to Timothy Ryan and the Leakey Foundation), and the Division of Fossil Primates of the Duke Lemur Center (*Parapithecus*). We also

thank Erik Seiffert and Steven Heritage for providing a digital rendering of *Parapithecus*. Finally, we thank the Editor (Andrea Taylor), the Associate Editor, and three anonymous reviewers for useful comments that helped us to improve a previous version of this paper.

Supplementary Online Material

Supplementary Online Material to this article can be found online at https://doi.org/10.1016/j.jhevol.2020.102930.

References

Adams, D.C., 2014. A generalized K statistic for estimating phylogenetic signal from shape and other high-dimensional multivariate data. Syst. Biol. 63, 685–697.
Adams, D.C., Collyer, M.L., Kaliontzopoulou, A., 2019. Geomorph: Software for geometric morphometric analyses. R Package Version. https://cran.rproject.org/package=geomorph.
Alba, D.M., Berning, B., 2013. On the holotype and original description of the pliopithecid *Plesiopliopithecus lockeri* (Zapfe, 1960). J. Hum. Evol. 65, 338–340.
Alba, D.M., Moyà-Solà, S., 2012. A new pliopithecid genus (Primates: Pliopithecoidea) from Castell de Barberà (Vallès-Penedès Basin, Catalonia, Spain). Am. J. Phys. Anthropol. 147, 88–112.
Alba, D.M., Moyà-Solà, S., Malgosa, A., Casanovas-Vilar, I., Robles, J.M., Almécija, S., Galindo, J., Rotgers, C., Bertó Mengual, J.V., 2010. A new species of *Pliopithecus* Gervais, 1849 (Primates: Pliopithecidae) from the Middle Miocene (MN8) of Abocador de Can Mata (els Hostalets de Pierola, Catalonia, Spain). Am. J. Phys. Anthropol. 141, 52–75.
Alba, D.M., Almécija, S., DeMiguel, D., Fortuny, J., Pérez de los Ríos, M., Pina, M., Robles, J.M., Moyà-Solà, S., 2015. Miocene small-bodied ape from Eurasia sheds light on hominoid evolution. Science 350, aab2625.
Almécija, S., Tallman, L., Sallam, H.M., Fleagle, J.G., Hammond, A.S., Seiffert, E.R., 2019. Early anthropoid femora reveal divergent adaptive trajectories in catarrhine hind-limb evolution. Nat. Commun. 10, 4778.
Andrews, P.J., Harrison, T., Delson, E., Bernor, R.L., Martin, L., 1996. Distribution and biochronology of European and Southwest Asian Miocene catarrhines. In: Bernor, R.L., Fahlbusch, V., Mittmann, H. (Eds.), The Evolution of Western Eurasian Neogene Mammalian Faunas. Columbia University Press, New York, pp. 168–207.
Ankel, F., 1965. Der Canalis Sacralis als Indikator für die Länge der Caudalregion der Primaten. Folia Primatol. 3, 263–276.
Arias-Martorell, J., Alba, D.M., Potau, J.M., Bello-Hellegouarch, G., Pérez-Pérez, A., 2015. Morphological affinities of the proximal humerus of *Epipliopithecus vindobonensis* and *Pliopithecus antiquus*: Suspensory inferences based on a 3D geometric morphometrics approach. J. Hum. Evol. 80, 83–95.
Arnold, C., Matthews, L.J., Nunn, C.L., 2010. The 10kTrees website: A new online resource for primate phylogeny. Evol. Anthropol. 19, 114–118.
Beaudet, A., Dumoncel, J., Thackeray, J.F., Bruxelles, L., Duployer, B., Tenailleau, C., Bam, L., Hoffman, J., de Beer, F., Braga, J., 2016. Upper third molar internal structural organization and semicircular canal morphology in Plio-Pleistocene South African cercopithecoids. J. Hum. Evol. 95, 104–120.
Begun, D.R., 2002. The Pliopithecoidea. In: Hartwig, W.C. (Ed.), 2002. The Primate Fossil Record. Cambridge University Press, Cambridge, pp. 221–240.
Begun, D.R., 2017. Evolution of the Pliopithecoidea. In: Fuentes, A. (Ed.), The International Encyclopedia of Primatology. John Wiley & Sons. https://doi.org/10.1002/9781119179313.wbprim0165.
Berlin, J.C., Kirk, E.C., Rowe, T.B., 2013. Functional implications of ubiquitous semicircular canal non-orthogonality in mammals. PLoS One 8, e79585.
Billet, G., Hautier, L., Lebrun, R., 2015. Morphological diversity of the bony labyrinth (inner ear) in extant xenarthrans and its relation to phylogeny. J. Mammal. 96, 658–672.
Blomberg, S.P., Garland, T., Ives, A.R., 2003. Testing for phylogenetic signal in comparative data: behavioral traits are more labile. Evolution 57, 717–745.
Bône, A., Louis, M., Martin, B., Durrleman, S., 2018. Deformetrica 4: an open-source software for statistical shape analysis. In: Reuter, M., Wachinger, C., Lombaert, H., Paniagua, B., Lüthi, M., Egger, B. (Eds.), Shape in Medical Imaging. Shape MI 2018. Springer, Cham, pp. 3–13.
Bookstein, F.L., 2019. Pathologies of between-groups principal components analysis in geometric morphometrics. Evol. Biol. 46, 271–302.
Bush, E.C., Simons, E.L., Dubowitz, D.J., Allman, J.M., 2004. Endocranial volume and optic foramen size in *Parapithecus grangeri*. In: Ross, C.F., Kay, R.F. (Eds.), Anthropoid Origins: New Visions. Kluwer/Plenum, New York, pp. 603–614.
Cardini, A., O'Higgins, P., Rohlf, F.J., 2019. Seeing distinct groups where there are none: Spurious patterns from between-group PCA. Evol. Biol. 46, 303–316.
Cardini, A., Polly, P.D., 2020. Cross-validated between-group PCA scatterplots: A solution to spurious group separation? Evol. Biol. 47, 85–95.
Casanovas-Vilar, I., Alba, D.M., Garcés, M., Robles, J.M., Moyà-Solà, S., 2011. Updated chronology for the Miocene hominoid radiation in Western Eurasia. Proc. Natl. Acad. Sci. USA 108, 5554–5559.
Ciochon, R.L., Corruccini, R.S., 1977. The phenetic position of *Pliopithecus* and its phylogenetic relationship to the Hominoidea. Syst. Zool. 26, 290–299.
Coleman, M.N., Colbert, M.W., 2010. Correlations between auditory structures and hearing sensitivity in non-human primates. J. Morphol. 271, 511–532.
Costeur, L., Grohé, C., Aguirre-Fernández, G., Ekdale, E., Schulz, G., Müller, B., Mennecart, B., 2018. The bony labyrinth of toothed whales reflects both phylogeny and habitat preferences. Sci. Rep. 8, 7841.
David, R., Droulez, J., Allain, R., Berthoz, A., Janvier, P., Bennequin, D., 2010. Motion from the past. A new method to infer vestibular capacities of extinct species. C. R. Palevol 9, 397–410.
del Rio, J., Aristide, L., dos Reis, S.F., dos Santos, T.M.P., Lopes, R.T., Perez, S.I., 2020. Allometry, function and shape diversification in the inner ear of platyrrhine primates. J. Mamm. Evol. https://doi.org/10.1007/s10914-019-09490-9.
Delson, E., Andrews, P.J., 1975. Evolution and interrelationships of the catarrhine primates. In: Luckett, W.P., Szalay, F.S. (Eds.), Phylogeny of the Primates: A Multidisciplinary Approach. Plenum Press, New York, pp. 405–446.
Dumoncel, J., Durrleman, S., Braga, J., Jessel, J.P., Subsol, G., 2014. Landmark-free 3D method for comparison of fossil hominins and hominids based on endocranium and EDJ shapes. Am. J. Phys. Anthropol. 153 (S58), 110.
Durrleman, S., Pennec, X., Trouvé, A., Ayache, N., Braga, J., 2012a. Comparison of the endocranial ontogenies between chimpanzees and bonobos via temporal regression and spatiotemporal registration. J. Hum. Evol. 62, 74–88.
Durrleman, S., Prastawa, M., Korenberg, J.R., Joshi, S., Trouvé, A., Gerig, G., 2012b. Topology preserving atlas construction from shape data without correspondence using sparse parameters. In: Ayache, N., Delingette, H., Golland, P., Mori, K. (Eds.), Medical Image Computing and Computer-Assisted Intervention – MICCAI 2012. Springer, Berlin, pp. 223–230.
Ekdale, E.G., 2013. Comparative anatomy of the bony labyrinth (inner ear) of placental mammals. PLoS One 8, e66624.
Farris, J.S., 1989. The retention index and the rescaled consistency index. Cladistics 5, 417–419.
Fleagle, J.G., 1983. Locomotor adaptations of Oligocene and Miocene hominoids and their phyletic implications. In: Ciochon, R.L., Corruccini, R.S. (Eds.), New Interpretations of Ape and Human Ancestry. Plenum Press, New York, pp. 301–324.
Fleagle, J.G., 1984. Are there any fossil gibbons? In: Preuschoft, H., Chivers, D.J., Brockelman, W.Y., Creel, N. (Eds.), The Lesser Apes: Evolutionary and Behavioral Biology. Edinburgh University Press, Edinburgh, pp. 431–447.
Fricano, E.E.I., 2018. The primate ectotympanic tube: correlates of structure, function, and development. Ph.D. Dissertation. Johns Hopkins University.
Fulwood, E.L., Boyer, D.M., Kay, R.F., 2016. Stem members of Platyrrhini are distinct from catarrhines in at least one derived cranial feature. J. Hum. Evol. 100, 16–24.
Gilbert, C.C., Ortiz, A., Pugh, K.D., Campisano, C.J., Patel, B.A., Singh, N.P., Fleagle, J.G., Patnaik, R., 2020. New middle Miocene ape (Primates: Hylobatidae) from Ramnagar, India fills major gaps in the hominoid fossil record. Proc. R. Soc. B 287, 20201655.
Glaunès, J.A., Joshi, S., 2006. Template estimation form unlabeled point set data and surfaces for Computational Anatomy. In: Pennec, X., Joshi, S. (Eds.), MICCAI 2006 Workshop Proceedings. MFCA'06 Workshop. Mathematical Foundations of Computational Anatomy: Geometrical and Statistical Methods for Modelling Biological Shape Variability. INRIA/MICCAI, Conpenhagen, pp. 29–39.
Gonzales, L.A., Malinzak, M.D., Kay, R.F., 2019. Intraspecific variation in semicircular canal morphology—A missing element in adaptive scenarios? Am. J. Phys. Anthropol. 168, 10–24.
Grohé, C., Tseng, Z.J., Lebrun, R., Boistel, R., Flynn, J.J., 2015. Bony labyrinth shape variation in extant Carnivora: a case study of Musteloidea. J. Anat. 228, 366–383.
Grohé, C., Lee, B., Flynn, J.J., 2018. Recent inner ear specialization for high-speed hunting in cheetahs. Sci. Rep. 8, 2301.
Gannon, P.J., Eden, A.R., Laitman, J.T., 1988. The subarcuate fossa and cerebellum of extant primates: comparative study of a skull-brain interface. Am. J. Phys. Anthropol. 77, 143–164.
Harrison, T., 1987. The phylogenetic relationships of the early catarrhine primates: a review of the current evidence. J. Hum. Evol. 16, 41–80.
Harrison, T., 2005. The zoogeographic and phylogenetic relationships of early catarrhine primates in Asia. Anthropol. Sci. 113, 43–51.
Heizmann, E.P.J., Begun, D.R., 2001. The oldest Eurasian hominoid. J. Hum. Evol. 41, 463–481.
Harrison, T., 2013. Catarrhine origins. In: Begun, D.R. (Ed.), A Companion to Paleoanthropology. Blackwell Publishing, Oxford, pp. 376–396.
Harrison, T., Gu, Y., 1999. Taxonomy and phylogenetic relationships of early Miocene catarrhines from Sihong, China. J. Hum. Evol. 37, 225–277.
Harrison, T., Zhang, Y., Wei, G., Sun, C., Wang, Y., Liu, J., Tong, H., Huang, B., Xu, F., 2020. A new genus of pliopithecoid from the late Early Miocene of China and its implications for understanding the paleozoogeography of the Pliopithecoidea. J. Hum. Evol. 145, 102838.
Harzhauser, M., Kroh, A., Mandic, O., Piller, W.E., Göhlich, U., Reuter, M., Berning, B., 2007. Biogeographic responses to geodynamics: A key study all around the Oligo–Miocene Tethyan Seaway. Zool. Anz. 246, 241–256.
Hürzeler, J., 1954. Contribution a l'odontologie et a la phylogénèse du genre *Pliopithecus* Gervais. Ann. Paleontol. 40, 5–63.
Jeffery, N., Spoor, F., 2006. The primate subarcuate fossa and its relationship to the semicircular canals part I: prenatal growth. J. Hum. Evol. 51, 537–549.
Jeffery, N., Ryan, T.M., Spoor, F., 2008. The primate subarcuate fossa and its relationship to the semicircular canals part II: adult interspecific variation. J. Hum. Evol. 55, 326–339.

Kay, R.F., Simons, E., Ross, J.L., 2009a. The basicranial anatomy of African Eocene/Oligocene anthropoids. Are there any clues for platyrrhine origins? In: Fleagle, J.G., Gilbert, C.C. (Eds.), Elwyin Simons: A Search for Origins. Springer, New York, pp. 125–158.
Kay, R.F., Fleagle, J.G., Mitchell, T.R.T., Colbert, M., Bown, T., Powers, D.W., 2009b. The anatomy of *Dolichocebus gaimanensis*, a stem platyrrhine monkey from Argentina. J. Hum. Evol. 54, 323–382.
Kay, R.F., 2015. Biogeography in deep time – what do phylogenetics, geology, and paleoclimate tell us about early platyrrhine evolution? Mol. Phylogenet. Evol. 82, 358–374.
Kirk, E.C., Gosselin-Ildari, A.D., 2009. Cochlear labyrinth volume and hearing abilities in primates. Anat. Rec. 292, 765–776.
Kunimatsu, Y., Nakatsukasa, M., Shimizu, D., Nakano, Y., Ishida, H., 2019. Loss of the subarcuate fossa and the phylogeny of *Nacholapithecus*. J. Hum. Evol. 131, 22–27.
Langdon, J.H., 1986. Functional morphology of the Miocene hominoid foot. Contrib. Primatol. 22, 239–257.
Lebrun, R., P de León, M., Tafforeau, P., Zollikofer, C., 2010. Deep evolutionary roots of strepsirrhine primate labyrinthine morphology. J. Anat. 216, 368–380.
Lebrun, R., Godinot, M., Couette, S., Tafforeau, P., Zollikofer, C., 2012. The labyrinthine morphology of *Pronycticebus gaudryi* (Primates, Adapiformes). Palaeobiodivers. Palaeoenviron. 92, 527–537.
Lee, J.Y., Shin, K.J., Kim, J.N., Yoo, J.Y., Song, W.C., Koh, K.S., 2013. A morphometric study of the semicircular canals using micro-CT images in three-dimensional reconstruction. Anat. Rec. 269, 834–839.
Le Maître, A., Schuetz, P., Vignaud, P., Brunet, M., 2017. New data about semicircular canal morphology and locomotion in modern hominoids. J. Anat. 231, 95–109.
Macrini, T.E., Flynn, J.J., Ni, X., Croft, D.A., Wyss, A.R., 2013. Comparative study of notoungulate (Placentalia, Mammalia) bony labyrinths and new phylogenetically informative inner ear characters. J. Anat. 223, 442–461.
Malinzak, M.D., Kay, R.F., Hullar, T.E., 2012. Locomotor head movements and semicircular canal morphology in primates. Proc. Natl. Acad. Sci. USA 109, 17914–17919.
Manoussaki, D., Dimitriadis, E.K., Chadwick, R.S., 2006. Cochlea's graded curvature effect on low frequency waves. Phys. Rev. Lett. 96, 088701.
Mennecart, B., Costeur, L., 2016. Shape variation and ontogeny of the ruminant bony labyrinth, an example in Tragulidae. J. Anat. 229, 422–435.
Mennecart, B., Rössner, G.E., Métais, G., DeMiguel, D., Schulz, G., Müller, B., Costeur, L., 2016. The petrosal bone and bony labyrinth of early to middle Miocene European deer (Mammalia, Cervidae) reveal their phylogeny. J. Morphol. 277, 1329–1338.
Mennecart, B., DeMiguel, D., Bibi, F., Rössner, G.E., Métais, G., Neenan, J.M., Wang, S., Schulz, G., Müller, B., Costeur, L., 2017. Bony labyrinth morphology clarifies the origin and evolution of deer. Sci. Rep. 7, 13176.
Mitteroecker, P., Bookstein, F., 2011. Linear discrimination, ordination, and the visualization of selection gradients in modern morphometrics. Evol. Biol. 38, 100–114.
Moyà-Solà, S., Köhler, M., 2000. Comprendere *Oreopithecus bambolii*, un ominoide fossile enigmatico. Atti Mus. St. Nat. Maremma 18, 39–65.
Moyà-Solà, S., Köhler, M., Alba, D.M., 2001. *Egarapithecus narcisoi*, a new genus of Pliopithecidae (Primates, Catarrhini) from the late Miocene of Spain. Am. J. Phys. Anthropol. 114, 312–324.
Morimoto, N., Kunimatsu, Y., Nakatsukasa, M., Ponce de León, M.S., Zollikofer, C.P., Ishida, H., Sasaki, T., Suwa, G., 2020. Variation of bony labyrinthine morphology in Mio–Plio–Pleistocene and modern anthropoids. Am. J. Phys. Anthropol. 173, 276–292.
Muller, M., Verhagen, J.H.G., 2002a. Optimization of the mechanical performance of a two-duct semicircular duct system—Part 1: dynamics and duct dimensions. J. Theor. Biol. 216, 409–424.
Muller, M., Verhagen, J.H.G., 2002b. Optimization of the mechanical performance of a two-duct semicircular duct system—Part 2: excitation of endolymph movements. J. Theor. Biol. 216, 425–442.
Muller, M., Verhagen, J.H.G., 2002c. Optimization of the mechanical performance of a two-duct semicircular duct system—Part 3: the positioning of the ducts in the head. J. Theor. Biol. 216, 443–459.
Nengo, I., Tafforeau, P., Gilbert, C.C., Fleagle, J.G., Miller, E.R., Feibel, C., Fox, D.L., Feinberg, J., Pugh, K.D., Berruyer, C., Mana, S., Engle, Z., Spoor, F., 2017. New infant cranium from the African Miocene sheds light on ape evolution. Nature 548, 169–174.
Pagel, M., 1999. Inferring the historical patterns of biological evolution. Nature 401, 877–884.
Perier, A., Lebrun, R., Marivaux, L., 2016. Different level of intraspecific variation of the bony labyrinth morphology in slow- versus fast-moving Primates. J. Mamm. Evol. 23, 353–368.
R Core Team, 2019. R: A language and environment for statistical computing. R Foundation for Statistical Computing, Vienna.
Rae, T.C., Johnson, P.M., Yano, W., Hirasaki, E., 2016. Semicircular canal size and locomotion in colobine monkeys: a cautionary tale. Folia Primatol. 87, 213–223.
Revell, L.J., 2012. Phytools: an R package for phylogenetic comparative biology (and other things). Methods Ecol. Evol. 3, 217–223.
Rook, L., Renne, P., Benvenuti, M., Papini, M., 2000. Geochronology of *Oreopithecus*-bearing succession at Baccinello (Italy) and the extinction pattern of european miocene hominoids. J. Hum. Evol. 39, 577–582.
Rook, L., Bondioli, L., Casali, F., Rossi, M., Köhler, M., Moyá Solá, S., Macchiarelli, R., 2004. The bony labyrinth of *Oreopithecus bambolii*. J. Hum. Evol. 46, 347–354.
Rose, M.D., 1994. Quadrupedalism in some Miocene catarrhines. J. Hum. Evol. 26, 387–411.
Russo, G.A., 2016. Comparative sacral morphology and the reconstructed tail lengths of five extinct primates: *Proconsul heseloni, Epipliopithecus vindobonensis, Archaeolemur edwardsi, Megaladapis grandidieri*, and *Palaeopropithecus kelyus*. J. Hum. Evol. 90, 135–162.
Ryan, T.M., Silcox, M.T., Walker, A., Mao, X., Begun, D.R., Benefit, B.R., Gingerich, P.D., Köhler, M., Kordos, L., McCrossin, M.L., Moyà-Solà, S., Sanders, W.J., Seiffert, E.R., Simons, E., Zalmout, I.S., Spoor, F., 2012. Evolution of locomotion in Anthropoidea: the semicircular canal evidence. Proc. R. Soc. B 279, 3467–3475.
Sankhyan, A.R., Kelley, J., Harrison, T., 2017. A highly derived pliopithecoid from the Late Miocene of Haritalyangar, India. J. Hum. Evol. 105, 1–12.
Savje, F., 2019. Distances: tools for distance metrics. https://cran.r-project.org/web/packages/distances/index.html.
Schlager, S., 2017. Morpho and Rvcg – shape analysis in R: R-packages for geometric morphometrics, shape analysis and surface manipulations. In: Zheng, G., Li, S., Székely, G. (Eds.), Statistical Shape and Deformation Analysis. Methods, Implementation and Applications. Academic Press, London, pp. 217–256.
Seiffert, E.R., 2006. Revised age estimates for the later Paleogene mammal faunas of Egypt and Oman. Proc. Natl. Acad. Sci. USA 103, 5000–5005.
Sidlauskas, B., 2008. Continuous and arrested morphological diversification in sister clades of characiform fishes: a phylomorphospace approach. Evolution 62, 3135–3156.
Silcox, M.T., Bloch, J.I., Boyer, D.M., Godinot, M., Ryan, T.M., Spoor, F., Walker, A., 2009. Semicircular canal system in early primates. J. Hum. Evol. 56, 315–327.
Simons, E.L., Fleagle, J.G., 1973. The history of extinct gibbon-like primates. In: Rumbaugh, D.M. (Ed.), Gibbon and Siamang Vol. 2. Anatomy, Dentition, Taxonomy, Molecular Evolution and Behavior. Karger, Basel, pp. 121–148.
Simons, E.L., Seiffert, E.R., Ryan, T.M., Attia, Y., 2007. A remarkable female cranium of the early Oligocene anthropoid *Aegyptopithecus zeuxis* (Catarrhini, Propliopithecidae). Proc. Natl. Acad. Sci. USA 104, 8731–8736.
Spoor, F., Zonneveld, F., 1998. Comparative review of the human bony labyrinth. Yearbk. Phys. Anthropol. 41, 211–251.
Spoor, F., Garland, T., Krovitz, G., Ryan, T.M., Silcox, M.T., Walker, A., 2007. The primate semicircular canal system and locomotion. Proc. Natl. Acad. Sci. USA 104, 10808–10812.
Stevens, N.J., Seiffert, E.R., O'Connor, P.M., Roberts, E.M., Schmitz, M.D., Krause, C., Gorscak, E., Ngasala, S., Hieronymus, T.L., Temu, J., 2013. Palaeontological evidence for an Oligocene divergence between Old World monkeys and apes. Nature 497, 611–614.
Swofford, D., 2003. PAUP*. Phylogenetic Analysis Using Parsimony (*and Other Methods). Version 4. Sinauer Associates, Sunderland.
Szalay, F.S., 1975. Phylogeny of primate higher taxa: the basicranial evidence. In: Luckett, W.P., Szalay, F.S. (Eds.), Phylogeny of the Primates: A Multidisciplinary Approach. Plenum Press, New York, pp. 91–125.
Szalay, F.S., Delson, E., 1979. Evolutionary History of the Primates. Academic Press, New York.
Tejedor, M.F., Rosenberger, A.L., 2008. A neotype for *Homunculus patagonicus* Ameghino, 1891, and a new interpretation of the taxon. PaleoAnthropology 68–82.
Urciuoli, A., Zanolli, C., Begun, D.R., Almécija, S., Dumoncel, J., Moyà-Solà, S., Alba, D.M., 2019. A deformation-based geometric morphometric analysis of the vestibular apparatus in the Miocene apes *Hispanopithecus laietanus* and *Rudapithecus hungaricus*. Am. J. Phys. Anthropol. 168 (S68), 253.
Urciuoli, A., Zanolli, C., Beaudet, A., Dumoncel, J., Santos, F., Moyà-Solà, S., Alba, D.M., 2020. The evolution of the vestibular apparatus in apes and humans. eLife 9, e51261.
van der Meulen, A.J., García-Paredes, I., Álvarez-Sierra, M.Á., van den Hoek Ostende, L.W., Hordijk, K., Oliver, A., López-Guerrero, P., Hernández-Ballarín, V., Peláez-Campomanes, P., 2011. Biostratigraphy or biochronology? Lessons from the Early and Middle Miocene small Mammal Events in Europe. Geobios 44, 309–321.
Zalmout, I.S., Sanders, W.J., MacLatchy, L., Gunnell, G., Al-Mufarreh, Y.A., Ali, M.A., Nasser, A.-A.H., Al-Masary, A.M., Al-Sobhi, S.A., Nadhra, A.O., Matari, A.H., Wilson, J.A., Gingerich, P.D., 2010. New Oligocene primate from Saudi Arabia and the divergence of apes and Old World monkeys. Nature 466, 360–365.
Zapfe, H., 1958. The skeleton of *Pliopithecus* (*Epipliopithecus*) *vindobonensis* Zapfe and Hürzeler. Am. J. Phys. Anthropol. 16, 441–457.
Zapfe, H., 1961. Die Primatenfunde aus der miozänen Spaltenfüllung von Neudorf an der March (Děvínská Nová Ves), Tschechoslowakei. Schweizer. palaeontol. Abh. 78, 1–293.
Zapfe, H., Hürzeler, J., 1957. Die Fauna der miozänen Spaltenfüllung von Neudorf an der March (ČSR.). Primates. Sitzungsber. Öst. Akad. Wiss. Math. Naturwiss. Kl. 166, 113–123.

Supplementary Online Material (SOM):

A comparative analysis of the vestibular apparatus in *Epipliopithecus vindobonensis*: Phylogenetic implications

Alessandro Urciuoli [a,*], Clément Zanolli [b], Amélie Beaudet [c,d], Marta Pina [a,e], Sergio Almécija [f,g,a], Salvador Moyà-Solà [a,h,i], David M. Alba [a,*]

[a] *Institut Català de Paleontologia Miquel Crusafont, Universitat Autònoma de Barcelona, Edifici ICTA-ICP, c/ Columnes s/n, Campus de la UAB, 08193 Cerdanyola del Vallès, Barcelona, Spain*

[b] *Univ. Bordeaux, CNRS, MCC, PACEA, UMR 5199, F-33600 Pessac, France*

[c] *School of Geography, Archaeology and Environmental Studies, University of the Witwatersrand, Private Bag 3, Johannesburg, WITS 2050, South Africa*

[d] *Department of Anatomy, University of Pretoria, PO Box 2034, Pretoria, 0001, South Africa*

[e] *School of Earth and Environmental Sciences, Faculty of Science and Engineering, University of Manchester, 176 Oxford Road, Manchester M13 9PL, UK*

[f] *Division of Anthropology, American Museum of Natural History, Central Park West at 79th Street, New York, NY 10024, USA*

[g] *New York Consortium in Evolutionary Primatology, New York, NY, USA*

[h] *Institució Catalana de Recerca i Estudis Avançats (ICREA), Passeig de Lluís Companys 23, 08010 Barcelona, Spain*

[i] *Unitat d'Antropologia (Departament de Biologia Animal, Biologia Vegetal i Ecologia), Universitat Autònoma de Barcelona, Campus de la UAB s/n, 08193 Cerdanyola del Vallès, Barcelona, Spain*

*Corresponding authors.

E-mail address: alessandro.urciuoli@icp.cat (A. Urciuoli); david.alba@icp.cat (D.M. Alba).

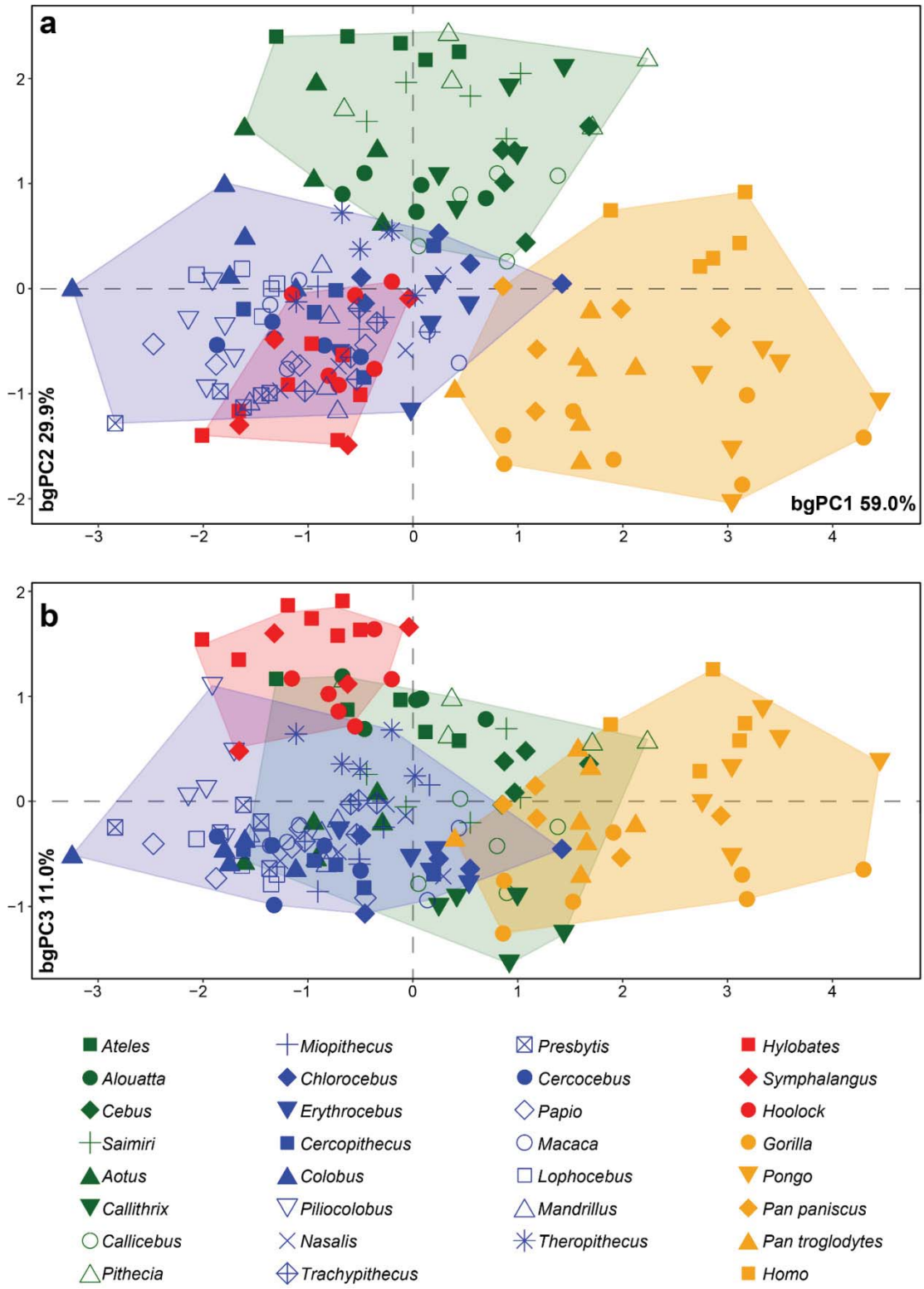

SOM Figure S1. Bivariate plots of cross-validated between-group principal component analysis (bgPCA) scores. a) bgPC2 vs. bgPC1; b) bgPC3 vs bgPC1. Variance explained by each component is given along each axis. The striking similarities (only a very slight rotation of the morphospace can be observed) between cross-validated bgPCA scores and standard ones (as shown in Fig. 6) allow us to discount spurious grouping caused by the bgPCA itself and demonstrate the presence of a grouping structure within our shape data.

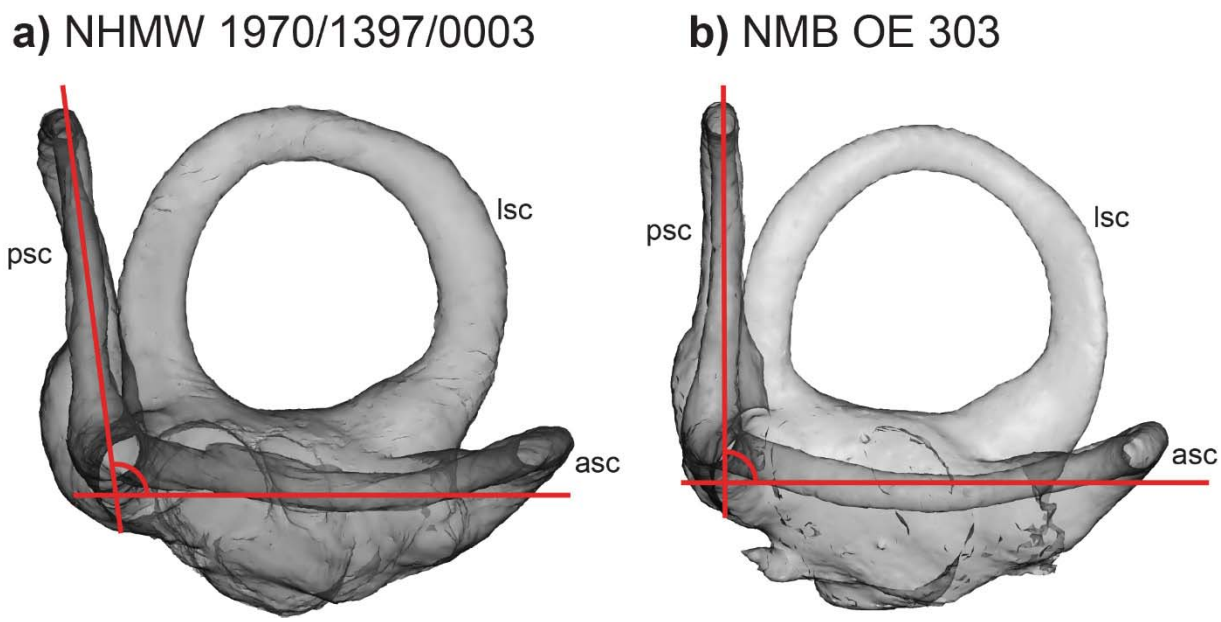

SOM Figure S2. Differences in the relative orientation of the anterior and posterior canals displayed by the two *Epipliopithecus* individuals as observed from a view perpendicular to the best fit planes (represented by the red lines) of each canal. In NHMW 1970/1397/0003 (a) the planes identify an obtuse angle, while in NMB OE 303 (b) the canals form a right angle. Abbreviations: asc = anterior canal; psc = posterior canal; lsc = lateral canal.

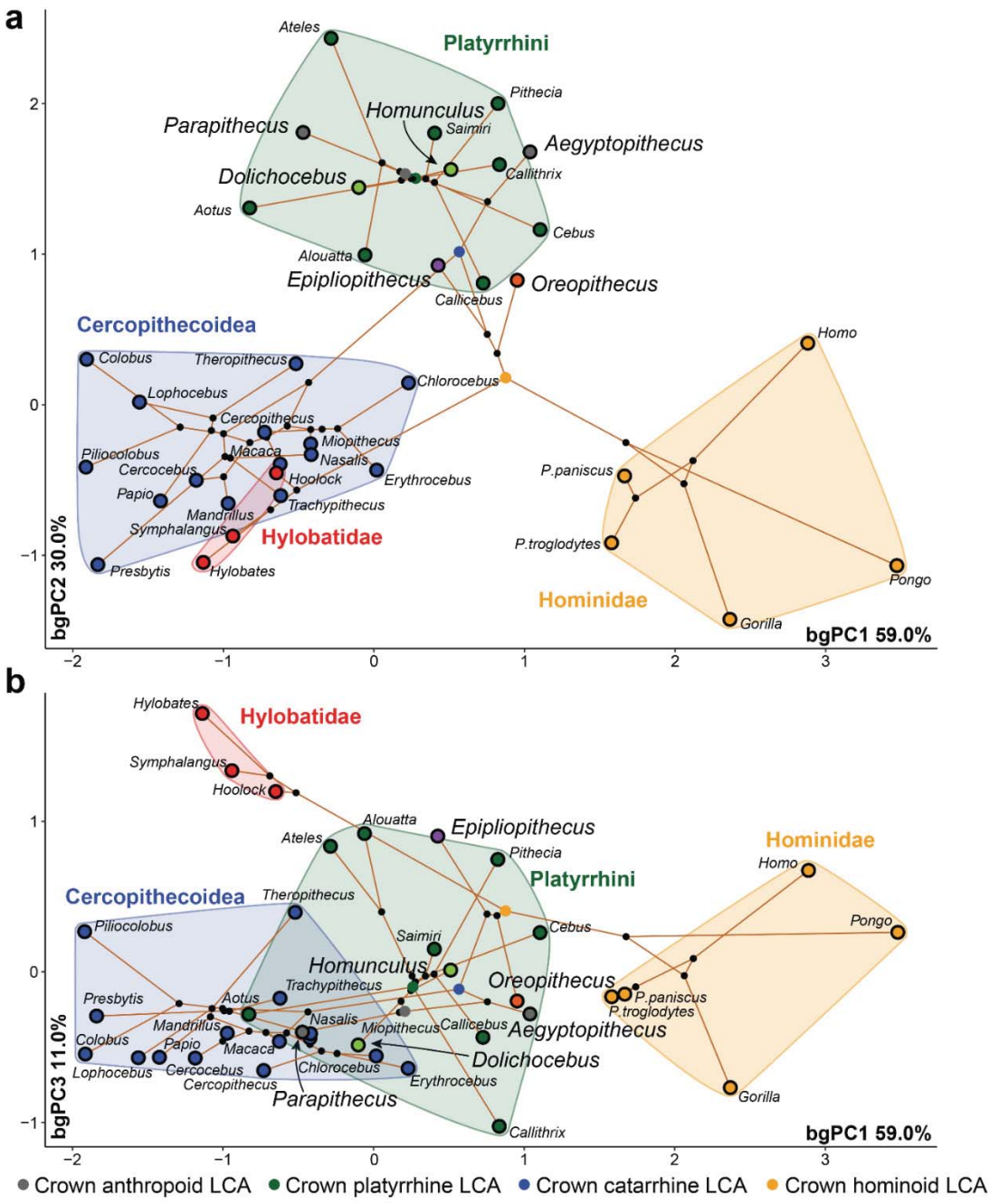

SOM Figure S3. Reconstruction of the evolutionary history of vestibule and semicircular canal morphology in anthropoids as obtained using a phylomorphospace approach based on species centroids and considering *Epipliopithecus* as a stem hominoid (Fig. 3b): a) bgPC2 vs. bgPC1; b) bgPC3 vs. bgPC1. Variance explained by each component is given along each axis. Convex hulls depict the range of variation for a priori defined groups using the following color code: green = platyrrhines; blue = cercopithecoids; red = hylobatids; orange = hominids. The ancestral nodes discussed for assessing *Epipliopithecus* phylogenetic affinities have been marked as in Figure 1. Abbreviation: bgPCA = between-group principal component.

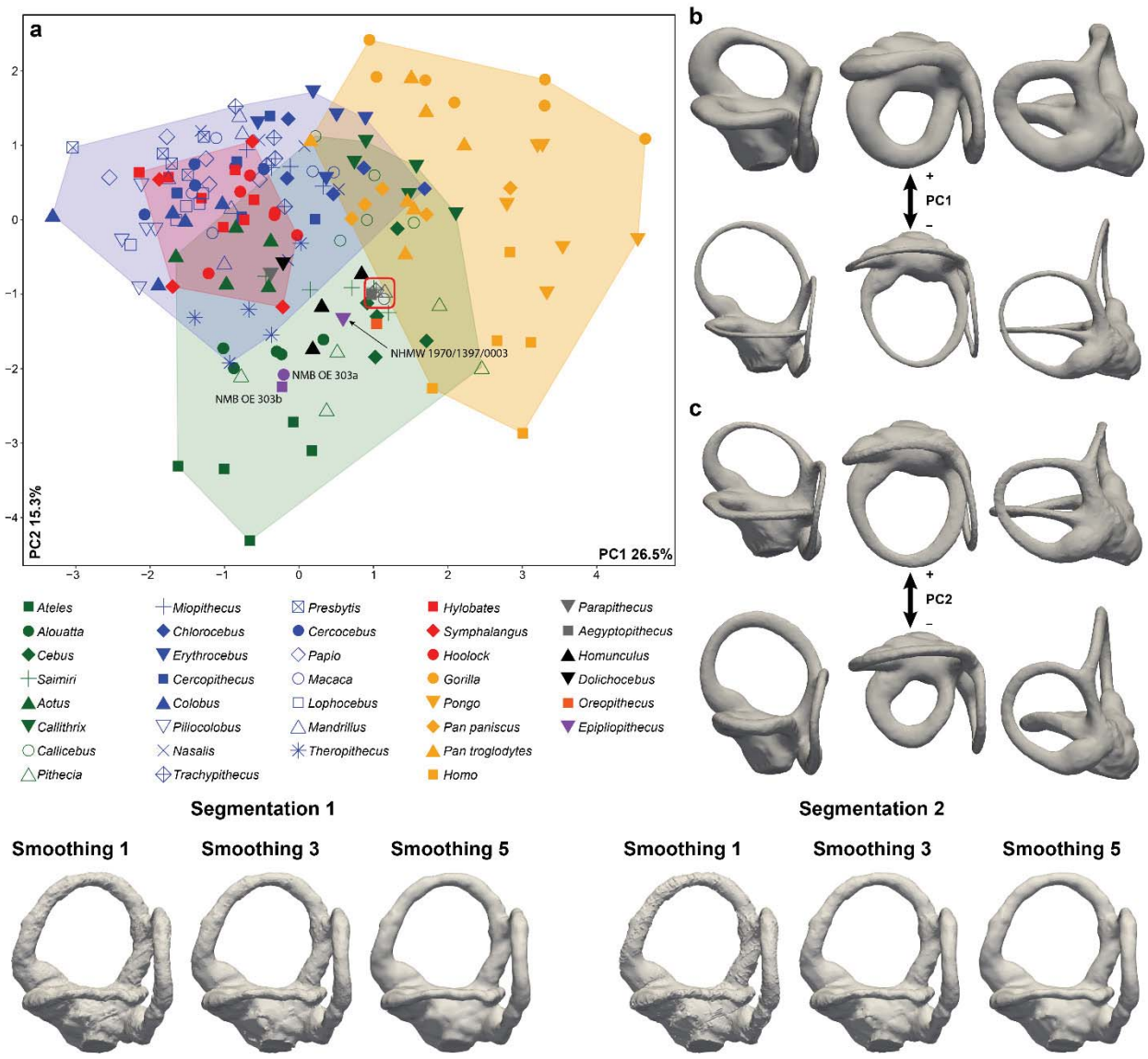

SOM Figure S4. Effects of manual segmentation and smoothing. Bivariate plot of the principal component analysis applied to the deformation fields of the semicircular canal and vestibule analysis. a) PC2 vs. PC1 (the variance explained by each component is given along the axis); maximum and minimum extreme conformations for PC1 (b) and PC2 (c) in lateral (left), superior (middle), and posterior (right) views. To test the effects of manual segmentation and smoothing, the *Aegyptopithecus* specimen was segmented independently by two different users. We then applied to the two resulting models three different degrees of smoothing (kernel 1, 3 and 5), and included the six resulting models in our PCA analysis to check the distance between the different versions of the same specimen. The visual inspection of the scatter of points, together with the observed relative error (3.8%), discounts a significant effect of the segmentation on the results of our analyses.

SOM Table S1

Sample sizes of the extant species included in the comparative sample.

Species	*n*	M	F	?
Alouatta palliata	5	3	2	0
Aotus trivirgatus	5	1	4	0
Ateles geoffroyi	5	1	4	0
Callicebus moloch	5	5	0	0
Callithrix argentata	5	4	1	0
Cebus apella	5	3	2	0
Cercocebus galeritus	5	0	5	0
Cercopithecus mitis	5	2	3	0
Chlorocebus pygerythrus	5	2	3	0
Colobus guereza	5	3	2	0
Erythrocebus patas	5	3	2	0
Gorilla gorilla	7	2	5	0
Homo sapiens	5	2	3	0
Hoolock hoolock	6	2	4	0
Hylobates lar	7	0	7	0
Lophocebus albigena	5	2	3	0
Macaca fascicularis	5	1	4	0
Mandrillus sphinx	5	5	0	0
Miopithecus talapoin	5	3	2	0
Nasalis larvatus	5	0	5	0
Pan paniscus	5	1	4	0
Pan troglodytes	7	4	3	0
Papio Anubis	5	3	2	0
Piliocolobus badius	5	4	1	0
Pithecia monachus	5	1	1	3
Pongo pygmaeus	6	0	4	2
Presbytis rubicunda	5	2	3	0
Saimiri sciureus	5	3	2	0
Symphalangus syndactylus	4	2	2	0
Theropithecus gelada	5	4	1	0
Trachypithecus cristatus	5	0	5	0

Abbreviations: M = male; F = female; ? = unknown sex.

SOM Table S2

List of µCT image stacks of the fossil comparative sample.

Catalog No.	Taxon	MorphoSource ID[a]	Voxel size (mm)[b]
CGM 85785	*Aegyptopithecus zeuxis*	M2377	0.05600 × 0.05600 × 0.06379
MPM-PV 30501	*Homunculus patagonicus*	M7940	0.040
MPM-PV 30502	*Homunculus patagonicus*	M7941	0.039
MPM-PV 30503	*Homunculus patagonicus*	M7942	0.044
MACN 14128	*Dolichocebus gaimanensis*	M7978	0.047
BAC 208	*Oreopithecus bambolii*[c]	—	0.02905
DPC 18651	*Parapithecus grangeri*	M90	0.0353

Abbreviations: BAC = Baccinello (field acronym; housed at Naturhistorisches Museum Basel, Switzerland); CGM = Egyptian Geological Museum, Cairo, Egypt; MPM-PV = Museo Regional Provincial Padre M.J. Molina, Río Gallegos, Argentina; MACN = Museo Argentino de Ciencias Naturales, Buenos Aires, Argentina; DPC = Duke Lemur Center, Durham, NC, USA.

[a] All the stacks available from MorphoSource can be accessed by searching their ID number ('M' excluded) at https://www.morphosource.org.

[b] Voxel size for isometric µCT image stacks repeated just once.

[c] The µCT scan was kindly provided by Lorenzo Rook.

SOM Table S3

Source data for Figure 5 consisting of log-transformed canal length (ln L, in mm) and log-transformed cube root of canal volume (ln VolSC, in mm) for extant species.

ID	Species	ln L	ln VolSC
DU LP 02	*Alouatta palliata*	3.654	0.929
DU LP 04	*Alouatta palliata*	3.529	0.699
DU LP 06	*Alouatta palliata*	3.658	0.920
DU LP 10	*Alouatta palliata*	3.551	0.909
DU LP 12	*Alouatta palliata*	3.660	0.867
MCZ 19801	*Aotus trivirgatus*	3.220	0.614
MCZ 19802	*Aotus trivirgatus*	3.322	0.590
MCZ 19805	*Aotus trivirgatus*	3.279	0.648
MCZ 27214	*Aotus trivirgatus*	3.314	0.651
MCZ 30562	*Aotus trivirgatus*	3.213	0.627
MCZ 10138	*Ateles geoffroyi*	3.685	1.033
MCZ 29626	*Ateles geoffroyi*	3.596	0.886
MCZ 29628	*Ateles geoffroyi*	3.620	0.985
MCZ 29658	*Ateles geoffroyi*	3.559	0.953
MCZ BOM 5351	*Ateles geoffroyi*	3.774	1.003
MCZ 20186	*Callicebus moloch*	3.096	0.634
MCZ 20188	*Callicebus moloch*	3.109	0.713
MCZ 26922	*Callicebus moloch*	3.098	0.688
MCZ 30559	*Callicebus moloch*	3.109	0.632
MCZ 30564	*Callicebus moloch*	3.116	0.776
MCZ 30579	*Callithrix argentata*	3.294	0.757
MCZ 30580	*Callithrix argentata*	3.301	0.787
MCZ 30582	*Callithrix argentata*	3.291	0.760
MCZ 30583	*Callithrix argentata*	3.394	0.787
MCZ 32164	*Callithrix argentata*	3.277	0.838
MCZ 27891	*Cebus apella*	3.407	0.873
MCZ 31063	*Cebus apella*	3.455	0.872
MCZ 37833	*Cebus apella*	3.522	0.908
MCZ 41090	*Cebus apella*	3.507	0.907
MCZ 49635	*Cebus apella*	3.526	0.901
AMNH-M 52634	*Cercocebus galeritus*	3.661	0.891
AMNH-M 52635	*Cercocebus galeritus*	3.737	0.845
AMNH-M 52640	*Cercocebus galeritus*	3.708	0.791
AMNH-M 52641	*Cercocebus galeritus*	3.691	0.860
AMNH-M 52645	*Cercocebus galeritus*	3.553	0.855
MCZ 22734	*Cercopithecus mitis*	3.447	0.758
MCZ 25022	*Cercopithecus mitis*	3.349	0.773

MCZ 26832	*Cercopithecus mitis*	3.521	0.798
MCZ 39389	*Cercopithecus mitis*	3.485	0.752
MCZ 44264	*Cercopithecus mitis*	3.555	0.712
SIU 4792	*Chlorocebus pygerythrus*	3.393	0.889
SIU 4793	*Chlorocebus pygerythrus*	3.529	0.941
SIU 4794	*Chlorocebus pygerythrus*	3.642	0.948
SIU 4795	*Chlorocebus pygerythrus*	3.484	0.905
SIU 4796	*Chlorocebus pygerythrus*	3.611	0.935
AMNH-M 52211	*Colobus guereza*	3.737	0.894
AMNH-M 52213	*Colobus guereza*	3.720	0.913
AMNH-M 52225	*Colobus guereza*	3.649	0.893
AMNH-M 52237	*Colobus guereza*	3.743	0.890
AMNH-M 52249	*Colobus guereza*	3.819	0.806
MCZ 37280	*Erythrocebus patas*	3.615	0.941
MCZ 47015	*Erythrocebus patas*	3.626	1.056
MCZ 47016	*Erythrocebus patas*	3.659	1.065
MCZ 47017	*Erythrocebus patas*	3.566	0.928
MCZ 47018	*Erythrocebus patas*	3.567	0.902
AMNH-A 999686	*Gorilla gorilla*	3.807	1.261
AMNH-A 999687	*Gorilla gorilla*	3.755	1.297
AMNH-M 167338	*Gorilla gorilla*	3.905	1.351
AMNH-M 54356	*Gorilla gorilla*	3.700	1.387
MCZ 17684	*Gorilla gorilla*	3.866	1.223
MCZ 26850	*Gorilla gorilla*	3.749	1.312
MCZ 37264	*Gorilla gorilla*	3.726	1.108
EMBR 121	*Homo sapiens*	3.834	1.282
EMBR 179	*Homo sapiens*	3.853	1.294
EMBR 212	*Homo sapiens*	3.690	1.204
EMBR 215	*Homo sapiens*	3.733	1.347
EMBR 281	*Homo sapiens*	3.857	1.402
AMNH-M 112673	*Hoolock hoolock*	3.733	0.981
AMNH-M 112720	*Hoolock hoolock*	3.728	0.951
AMNH-M 112983	*Hoolock hoolock*	3.689	1.037
AMNH-M 201742	*Hoolock hoolock*	3.765	1.071
AMNH-M 83421	*Hoolock hoolock*	3.752	1.025
AMNH-M 83425	*Hoolock hoolock*	3.747	0.941
MCZ 41411	*Hylobates lar*	3.587	0.812
MCZ 41412	*Hylobates lar*	3.677	0.886
MCZ 41416	*Hylobates lar*	3.725	0.815
MCZ 41418	*Hylobates lar*	3.734	0.828
MCZ 41421	*Hylobates lar*	3.650	0.858

MCZ 41424	*Hylobates lar*	3.656	0.882
MCZ 41452	*Hylobates lar*	3.615	0.829
AMNH-M 52596	*Lophocebus albigena*	3.686	0.881
AMNH-M 52603	*Lophocebus albigena*	3.753	0.933
AMNH-M 52606	*Lophocebus albigena*	3.582	0.773
AMNH-M 52607	*Lophocebus albigena*	3.724	0.834
AMNH-M 52615	*Lophocebus albigena*	3.712	0.880
MCZ 12758	*Macaca fascicularis*	3.541	0.855
MCZ 22277	*Macaca fascicularis*	3.618	0.752
MCZ 23812	*Macaca fascicularis*	3.478	0.803
MCZ 23813	*Macaca fascicularis*	3.574	0.724
MCZ 35765	*Macaca fascicularis*	3.566	0.754
AMNH-A 9912049	*Mandrillus sphinx*	3.677	0.923
AMNH-A 9912056	*Mandrillus sphinx*	3.693	0.922
AMNH-M 89362	*Mandrillus sphinx*	3.669	0.915
AMNH-M 89364	*Mandrillus sphinx*	3.719	0.870
AMNH-M 89365	*Mandrillus sphinx*	3.614	0.856
MCZ 19976	*Miopithecus talapoin*	3.385	0.742
MCZ 23196	*Miopithecus talapoin*	3.466	0.791
MCZ 23197	*Miopithecus talapoin*	3.346	0.671
MCZ 34264	*Miopithecus talapoin*	3.369	0.689
MCZ 37278	*Miopithecus talapoin*	3.462	0.748
MCZ 37342	*Nasalis larvatus*	3.692	0.949
MCZ 41555	*Nasalis larvatus*	3.670	0.834
MCZ 41559	*Nasalis larvatus*	3.670	0.974
MCZ 41560	*Nasalis larvatus*	3.689	0.994
MCZ 41562	*Nasalis larvatus*	3.712	1.067
AMNH-M 86857	*Pan paniscus*	3.691	1.120
IPS9033	*Pan paniscus*	3.680	1.079
MCZ 38018	*Pan paniscus*	3.691	1.086
MCZ 38019	*Pan paniscus*	3.579	1.092
MCZ 38020	*Pan paniscus*	3.650	1.170
AMNH-M 167342	*Pan troglodytes*	3.672	1.193
AMNH-M 167344	*Pan troglodytes*	3.702	1.155
AMNH-M 51204	*Pan troglodytes*	3.737	1.212
IPS5698	*Pan troglodytes*	3.766	1.227
MCZ 17702	*Pan troglodytes*	3.667	1.051
MCZ 23167	*Pan troglodytes*	3.588	1.025
MCZ 26847	*Pan troglodytes*	3.636	1.082
AMNH-M 52677	*Papio anubis*	3.815	0.948
MCZ 17342	*Papio anubis*	3.643	0.855

MCZ 26473	*Papio anubis*	3.677	0.863
MCZ 31619	*Papio anubis*	3.855	0.896
MCZ BOM 8466	*Papio anubis*	3.594	0.872
MCZ 24080	*Piliocolobus badius*	3.496	0.649
MCZ 24775	*Piliocolobus badius*	3.598	0.609
MCZ 24793	*Piliocolobus badius*	3.588	0.685
MCZ 25627	*Piliocolobus badius*	3.512	0.624
MCZ 25631	*Piliocolobus badius*	3.604	0.694
MCZ 20265	*Pithecia monachus*	3.431	0.766
MCZ 20266	*Pithecia monachus*	3.321	0.909
MCZ 27124	*Pithecia monachus*	3.473	0.950
MCZ 30720	*Pithecia monachus*	3.315	0.995
MCZ BOM 5057	*Pithecia monachus*	3.471	0.943
IPS10647	*Pongo pygmaeus*	3.660	1.363
IPS10651	*Pongo pygmaeus*	3.750	1.342
IPS9031	*Pongo pygmaeus*	3.500	1.205
IPSSN	*Pongo pygmaeus*	3.662	1.231
MHNTZOO 201108	*Pongo pygmaeus*	3.626	1.270
SENCK 1576UU	*Pongo pygmaeus*	3.712	1.298
MCZ 35712	*Presbytis rubicunda*	3.678	0.877
MCZ 37370	*Presbytis rubicunda*	3.579	0.837
MCZ 37371	*Presbytis rubicunda*	3.619	0.775
MCZ 37372	*Presbytis rubicunda*	3.516	0.651
MCZ 37772	*Presbytis rubicunda*	3.616	0.841
AMNH-M 33875	*Saimiri sciureus*	3.350	0.788
AMNH-M 72068	*Saimiri sciureus*	3.284	0.832
AMNH-M 72074	*Saimiri sciureus*	3.280	0.785
AMNH-M 72078	*Saimiri sciureus*	3.411	0.775
AMNH-M 72079	*Saimiri sciureus*	3.270	0.766
AMNH-M 102724	*Symphalangus syndactylus*	3.671	0.964
AMNH-M 106583	*Symphalangus syndactylus*	3.739	0.952
MCZ 36031	*Symphalangus syndactylus*	3.732	0.881
MCZ 36032	*Symphalangus syndactylus*	3.793	0.849
AMNH-M 19549	*Theropithecus gelada*	3.667	0.946
AMNH-M 238034	*Theropithecus gelada*	3.606	0.740
AMNH-M 60568	*Theropithecus gelada*	3.627	0.890
AMNH-M 80126	*Theropithecus gelada*	3.661	0.807
AMNH-M 90309	*Theropithecus gelada*	3.630	0.871
MCZ 35567	*Trachypithecus cristatus*	3.599	0.888
MCZ 35584	*Trachypithecus cristatus*	3.639	0.940
MCZ 35586	*Trachypithecus cristatus*	3.653	0.937

MCZ 35597	*Trachypithecus cristatus*	3.651	0.889
MCZ 35603	*Trachypithecus cristatus*	3.664	0.947

Abbreviations: ID = catalog number; ln L = log-transformed canal length; ln VolSC = log-transformed cube root of canal volume; DU EA LP = Duke University, Evolutionary Anthropology, Durham, NC, USA; MCZ = Museum of Comparative Zoology, Harvard University, Cambridge, MA, USA; MCZ BOM = Museum of Comparative Zoology ("Bone of Mammals"), Harvard University, Cambridge, MA, USA; AMNH-M = American Museum of Natural History (Mammalogy collection), New York, NY, USA; AMNH-A = American Museum of Natural History (Anthropology collection), New York, NY, USA; SENCK = Senckenberg Naturmuseum, Frankfurt, Germany; MHNTZOO = Muséum d'histoire naturelle de Toulouse (Zoologie), Toulouse, France; IPS = collections of the ICP, Sabadell, Spain; SIU = Southern Illinois University, Carbondale, IL, USA.

SOM Table S4

Matrix of character states coded for the extant and fossil species included in the analysis.[a]

Species	#1	#2	#3	#4	#5	#6	#7
Aegyptopithecus zeuxis	0	0	2	0	2	0	0
Alouatta palliata	0	0	B	0	2	0	0
Aotus trivirgatus	0	0	2	0	2	0	A
Ateles geoffroyi	0	0	2	0	2	0	0
Callicebus moloch	0	0	2	0	2	0	0
Callithrix argentata	0	0	2	0	2	0	0
Cebus apella	0	0	B	0	2	0	0
Cercocebus galeritus	0	0	1	0	1	0	1
Cercopithecus mitis	0	0	1	0	B	0	1
Chlorocebus pygerythrus	0	0	1	0	1	0	1
Colobus guereza	0	0	1	0	1	0	1
Dolichocebus gaimanensis	0	0	2	0	2	0	0
Epipliopithecus vindobonensis	0	0	1	0	2	0	0
Erythrocebus patas	0	0	1	0	1	0	1
Gorilla gorilla	1	1	0	0	A	1	B
Homo sapiens	1	1	1	0	0	0	2
Homunculus patagonicus	0	0	2	0	B	0	0
Hoolock hoolock	0	0	A	1	1	1	2
Hylobates lar	0	0	0	1	1	1	2
Lophocebus albigena	0	0	1	0	B	0	1
Macaca fascicularis	0	0	1	0	1	0	1
Mandrillus sphinx	0	0	1	0	1	0	1
Miopithecus talapoin	0	0	1	0	1	0	A
Nasalis larvatus	0	0	1	0	A	0	2
Oreopithecus bambolii	1	1	0	1	1	0	2
Pan paniscus	1	1	0	0	2	1	1
Pan troglodytes	1	1	0	0	B	1	B
Papio anubis	0	0	1	0	1	0	1
Parapithecus grangeri	0	0	2	0	2	0	0
Piliocolobus badius	0	0	1	0	1	0	B
Pithecia monachus	0	0	1	0	2	0	A
Pongo ssp	1	1	0	1	A	1	2
Presbytis rubicunda	0	0	1	0	1	0	2
Saimiri sciureus	0	0	2	0	2	0	0
Symphalangus syndactylus	0	0	A	1	A	A	2

Theropithecus gelada	0	0	1	0	0	0	1
Trachypithecus cristatus	0	0	1	0	A	0	1

[a]Abbreviations for variable characters: A = (0,1); B = (0,2). See Table 7 for character definitions and Table 8 for coding of extinct taxa and the last common ancestors of main anthropoid clades.

Chapter 5:

Reassessment of the phylogenetic relationships of the late Miocene apes *Hispanopithecus* and *Rudapithecus* based on vestibular morphology

Reprinted from:

Urciuoli, A., Zanolli, C., Almécija, S., Beaudet, A., Dumoncel, J., Morimoto, N., Nakatsukasa, M., Moyà-Solà, S., Begun, D. R., Alba, D. M., 2021. Reassessment of the phylogenetic relationships of the late Miocene apes *Hispanopithecus* and *Rudapithecus* based on vestibular morphology. *Proc. Natl. Acad. Sci. USA* 118, e2015215118. https://doi.org/10.1073/pnas.2015215118

Reassessment of the phylogenetic relationships of the late Miocene apes *Hispanopithecus* and *Rudapithecus* based on vestibular morphology

Alessandro Urciuoli[a,1], Clément Zanolli[b], Sergio Almécija[a,c,d], Amélie Beaudet[a,e,f,g], Jean Dumoncel[h], Naoki Morimoto[i], Masato Nakatsukasa[i], Salvador Moyà-Solà[a,j,k], David R. Begun[l], and David M. Alba[a,1]

[a]Institut Català de Paleontologia Miquel Crusafont, Universitat Autònoma de Barcelona, 08193 Barcelona, Spain; [b]Univ. Bordeaux, CNRS, MCC, PACEA, UMR 5199, F-33600 Pessac, France; [c]Division of Anthropology, American Museum of Natural History, New York, NY 10024; [d]New York Consortium in Evolutionary Primatology, New York, NY 10016; [e]Department of Archaeology, University of Cambridge, Cambridge CB2 1QH, United Kingdom; [f]School of Geography, Archaeology, and Environmental Studies, University of the Witwatersrand, Johannesburg, WITS 2050, South Africa; [g]Department of Anatomy, University of Pretoria, Pretoria 0001, South Africa; [h]Laboratoire Anthropology and Image Synthesis, UMR 5288 CNRS, Université de Toulouse, 31073 Toulouse, France; [i]Laboratory of Physical Anthropology, Graduate School of Science, Kyoto University, 606 8502 Kyoto, Japan; [j]Institució Catalana de Recerca i Estudis Avançats, 08010 Barcelona, Spain; [k]Unitat d'Antropologia, Departament de Biologia Animal, Biologia Vegetal i Ecologia, Universitat Autònoma de Barcelona, 08193 Barcelona, Spain; and [l]Department of Anthropology, University of Toronto, Toronto, ON M5S 2S2, Canada

Edited by Justin S. Sipla, University of Iowa, Iowa City, IA, and accepted by Editorial Board Member C. O. Lovejoy December 3, 2020 (received for review July 19, 2020)

Late Miocene great apes are key to reconstructing the ancestral morphotype from which earliest hominins evolved. Despite consensus that the late Miocene dryopith great apes *Hispanopithecus laietanus* (Spain) and *Rudapithecus hungaricus* (Hungary) are closely related (Hominidae), ongoing debate on their phylogenetic relationships with extant apes (stem hominids, hominines, or pongines) complicates our understanding of great ape and human evolution. To clarify this question, we rely on the morphology of the inner ear semicircular canals, which has been shown to be phylogenetically informative. Based on microcomputed tomography scans, we describe the vestibular morphology of *Hispanopithecus* and *Rudapithecus*, and compare them with extant hominoids using landmark-free deformation-based three-dimensional geometric morphometric analyses. We also provide critical evidence about the evolutionary patterns of the vestibular apparatus in living and fossil hominoids under different phylogenetic assumptions for dryopiths. Our results are consistent with the distinction of *Rudapithecus* and *Hispanopithecus* at the genus rank, and further support their allocation to the Hominidae based on their derived semicircular canal volumetric proportions. Compared with extant hominids, the vestibular morphology of *Hispanopithecus* and *Rudapithecus* most closely resembles that of African apes, and differs from the derived condition of orangutans. However, the vestibular morphologies reconstructed for the last common ancestors of dryopiths, crown hominines, and crown hominids are very similar, indicating that hominines are plesiomorphic in this regard. Therefore, our results do not conclusively favor a hominine or stem hominid status for the investigated dryopiths.

inner ear | semicircular canals | evolution | fossil apes | Hominidae

Hominoids (apes and humans) originated in Africa during the Oligocene (1) but subsequently dispersed into Eurasia, giving rise to an impressive radiation during the middle and late Miocene (2, 3). Thus, while extant hominoids include only two moderately diverse families—hylobatids (gibbons and siamangs) and hominids (great apes and humans)—the panoply of extinct genera recorded during the Miocene still defies classification into a coherent systematic scheme. Other than the late Miocene *Oreopithecus*—which might be a late-occurring stem hominoid (4, 5)—there is consensus that most Eurasian large-bodied hominoids are members of the great-ape-and-human clade (Hominidae) (2, 3, 6). While most Asian extinct great apes, such as *Sivapithecus*, are considered to be more closely related to the orangutan clade (Ponginae) than to African apes and humans (Homininae) (2, 6–8), the phylogenetic affinities of European *Dryopithecus* and allied forms have long been debated. Until a decade ago, several species of European apes from the middle and late Miocene were included within this genus (9–16). However, discoveries at the middle Miocene composite section of Abocador de Can Mata (6, 17–20) prompted the recognition that the late Miocene species belong to one or more different genera distinct from *Dryopithecus* (2, 3, 6, 7, 18, 21–26): *Hispanopithecus* from Spain and *Rudapithecus* from Hungary, the latter formerly considered a subgenus of the former by some authors (6, 18, 22).

Together with *Dryopithecus* and other middle to late Miocene taxa (17, 19, 27), *Hispanopithecus* and *Rudapithecus* are currently classified in a subfamily (Dryopithecinae) (6, 20, 26) or tribe (Dryopithecini) (3, 7, 21) of their own, distinct from pongines. Both taxa possess a hominid-like cranial morphology (6, 11–13, 21, 25, 28, 29), as shown by the high zygomatic root, reduced midfacial prognathism, lack of subarcuate fossa, deep glenoid

Significance

Reconstructing the phylogenetic relationships of extinct apes is challenging due to their fragmentary fossil record and the recurrent independent evolution of morphological features. Given the relevance of the phylogenetic signal of the bony labyrinth, here we assess the phylogenetic affinities of the late Miocene great apes *Hispanopithecus* and *Rudapithecus* by studying their inner ear morphology. Our results are consistent with the distinct generic status of these dryopiths, which further differ from the derived condition of orangutans and most closely resemble African apes. However, the latter appear largely primitive (similar to the last common ancestor of great apes and humans). Hence, our results do not conclusively favor a closer relationship with African apes as opposed to great apes as a whole.

Author contributions: A.U., S.M.-S., D.R.B., and D.M.A. designed research; A.U. and C.Z. performed research; A.U., C.Z., A.B., J.D., N.M., M.N., and D.R.B. contributed new reagents/analytic tools; A.U., C.Z., S.A., A.B., J.D., and D.M.A. analyzed data; and A.U., C.Z., and D.M.A. wrote the paper.

The authors declare no competing interest.

This article is a PNAS Direct Submission. J.S.S. is a guest editor invited by the Editorial Board.

[1]To whom correspondence may be addressed. Email: alessandro.urciuoli@icp.cat or david.alba@icp.cat.

This article contains supporting information online at https://www.pnas.org/lookup/suppl/doi:10.1073/pnas.2015215118/-/DCSupplemental.

Published January 25, 2021.

fossa, and prominent entoglenoid process. However, there is no consensus regarding the phylogenetic position of this group—being either considered stem hominids (6, 19, 30), stem hominines (2, 3, 14, 16, 25), or even pongines (10, 28, 29)—which may be informally referred to as "dryopiths." Resolving the phylogenetic position of dryopiths has important implications for the evolution of the great ape and human clade, since their purported hominine status has led to paleobiogeographic scenarios favoring a European origin and subsequent back-to-Africa dispersal for the African and human clade (2, 3, 15, 24, 25). Disagreements and uncertainties about the phylogenetic position of extinct apes are persistent, and stem from a combination of factors, including the incomplete and fragmentary hominoid fossil record, the decimated current diversity of the group, and pervasive homoplasy coupled with mosaic evolution (6, 23, 31–35).

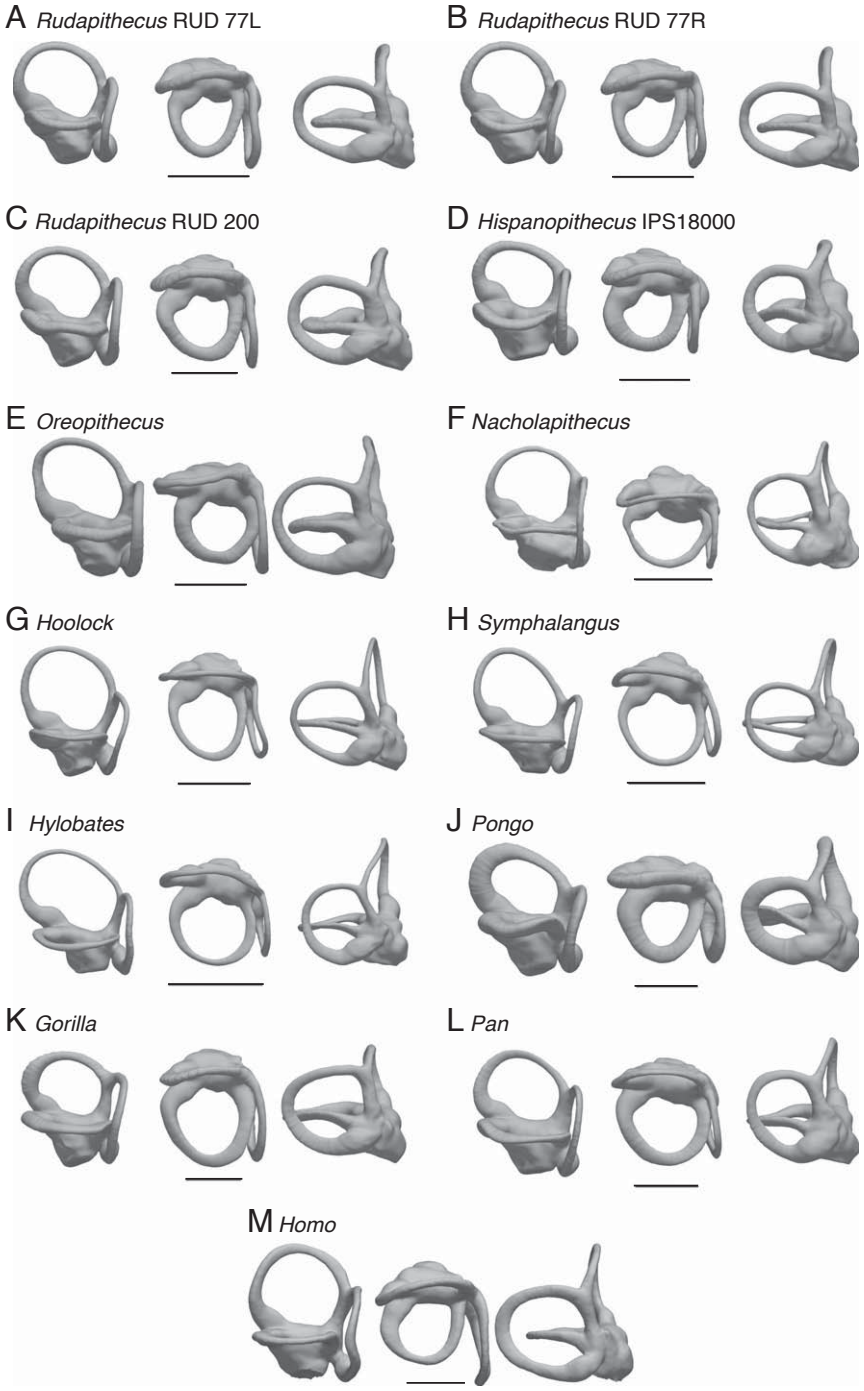

Fig. 1. The vestibular apparatus morphology of *R. hungaricus* (*A–C*), *H. laietanus* (*D*), fossil hominoids (*E* and *F*), and individuals from extant hominoid genera (*G–M*) as depicted by renderings of the 3D models. From left to right, in posterolateral, superior, and posteromedial views: (*A*) *R. hungaricus* (RUD 77L); (*B*) *R. hungaricus* (RUD 77R); (*C*) *R. hungaricus* (RUD 200); (*D*) *H. laietanus* (IPS18000); (*E*) *Oreopithecus bambolii* (BAC 208); (*F*) *N. kerioi* (BG 42744); (*G*) *Hoolock hoolock* (AMNH.M 83425); (*H*) *Symphalangus syndactylus* (AMNH.M 106583); (*I*) *Hylobates lar* (MCZ 41424); (*J*) *Pongo* sp.(IPS10647); (*K*) *Gorilla gorilla* (AMNH.M 167338); (*I*) *Pan troglodytes* (AMNH.M 51204); (*M*) *Homo sapiens* (F 04). (Scale bars, 5 mm.)

The morphology of the semicircular canals (SCs), which partly constitute the inner ear's bony labyrinth, has been classically related to locomotion (36–42). However, several studies have highlighted the possibility of inferring phylogenetic relatedness based on this portion of the inner ear morphology (43–47). Recently, it has been shown that this anatomical structure also embeds a strong phylogenetic signal among catarrhine primates by means of three-dimensional geometric morphometric (3DGM) analyses (5, 47–49), thus being potentially useful to test phylogenetic hypotheses for extinct hominoids. Previous studies relied on the SC radius of *Rudapithecus hungaricus* and *Hispanopithecus laietanus* to infer slow and deliberate arboreal locomotion for these species (41). However, recent analyses raised doubts about the reliability of locomotor behavior predictions based on the SC radius only (50, 51). In contrast, here we rely on microcomputed tomography (μCT) scans of the same specimens and a deformation-based (landmark-free) 3DGM approach to assess their closest affinities in SC morphology with extant hominoids and interpret them from an evolutionary viewpoint. First, we describe the fossil remains and qualitatively compare them with extant hominoids. Second, we assess if the volumetric proportions of their SCs more closely resemble those of hominids than those of other anthropoids. Third, we quantitatively evaluate changes in SC and vestibule morphology by means of a between-group principal component analysis (bgPCA) applied to a sample of extant and extinct hominoids. The affinities of the investigated fossil taxa are further assessed by means of cluster analyses and group membership probabilities based bgPCA results. Finally, we reconstruct the evolutionary history of the hominoid SCs using a phylomorphospace approach (including reconstructed ancestral morphotypes) under various phylogenetic assumptions for dryopiths.

Results

Descriptions and Comparisons. Three-dimensional renderings of the vestibular apparatus of fossil and extant hominoids investigated here are illustrated in the Fig. 1. The vestibular apparatus of *R. hungaricus* is well preserved in the three available specimens (Fig. 1 *A*–*C*). As in extant hominids, the SCs are stout—although less so than in orangutans (Fig. 1*J*), most humans (Fig. 1*M*), and gorillas (Fig. 1*K*)—and the vestibule is large relative to the volume occupied by SCs. The anterior and posterior canals are large and similar in size (Fig. 1 *A* and *B*). The anterior canal is slightly vertically compressed, as in extant hominoids and the fossil apes *Nyanzapithecus alesi* (4) and *Nacholapithecus kerioi* (Fig. 1*F*), and somewhat larger in RUD 77 than in RUD 200. The anterior canal is somewhat anterosuperiorly projecting, albeit much less so than in *Pongo* (Fig. 1*J*) and *Oreopithecus* (Fig. 1*E*). The lateral and posterior canals are slightly different between the two individuals. In RUD 77, the lateral canal is noticeably smaller than the other SCs (Fig. 1 *A* and *B*), slightly compressed horizontally, and slenderer than in RUD 200. The lateral canal of RUD 200 is stout and large, almost reaching the size of the vertical SCs (similar to the condition in African apes, yet smaller than in gorillas) (Fig. 1*C*), and its slender portion connects with the vestibule somewhat more inferiorly than in RUD 77. The junction of the slender portion of the lateral canal and the ampulla further differs between the two individuals, as it protrudes anteriorly in RUD 200, while it is posterolaterally oriented in RUD 77. In both individuals, the ampullary portion bends superiorly and the slender segment between the connection with the vestibule and the posterolateral tip of the lateral canal is straight, as in *Hoolock* (Fig. 1*G*) and in most hominids (Fig. 1 *J*–*M*), except for some *Gorilla* and *Pan* specimens that show some curvature. However, this section of the canal is more laterally oriented in RUD 77, while it is almost parallel to the posterior canal in RUD 200. The posterior canal is elongated posterolaterally in RUD 77, as in gorillas (Fig. 1*K*) and some humans (Fig. 1*M*), while it is slightly more rounded in RUD 200 (Fig. 1*C*). In both RUD 77 and RUD 200, the posterior and lateral canals approximately define a right angle (slightly more obtuse in RUD 77) and the trajectory of the lateral canal does not intersect the plane identified by the posterior canal. The common crus (CC) is short and slender, with the slender portions of the anterior and posterior canals almost forming right angle at the CC apex. The SCs are almost coplanar, with a slight amount of torsion in the upper portion of the anterior one (the tip slightly bending medially), in the medial-most part of the posterior one (displaced anteriorly), and in the tip of the lateral canal (pointing inferiorly).

The vestibular apparatus of *H. laietanus* (Fig. 1*D*) differs from that of *Rudapithecus* (especially RUD 77) (Fig. 1 *A* and *B*) by being more voluminous and displaying more equally developed SCs. The larger volume is particularly appreciable on the vestibular recesses (which are more voluminous than the SCs, as in orangutans) (Fig. 1*J*) and in the much more inflated ampullae. The anterior canal is more vertically compressed than in *Rudapithecus*, showing an almost rectangular shape. This canal is also much slenderer than in orangutans (Fig. 1*J*) and gorillas (Fig. 1*K*), most closely resembling chimpanzees (Fig. 1*L*). The lateral canal is stouter than the others, especially in the ampullary portion. Its posterolateral-most tip slightly bends inferiorly, resulting in a moderate torsion of the canal. The slender segment between the connection with the vestibule and the posterolateral tip of the lateral canal is straight, as in *Rudapithecus* (Fig. 1 *A*–*C*), *Hoolock* (Fig. 1*G*), and most hominids (Fig. 1 *J*–*M*), and laterally oriented, as in *Pongo* (Fig. 1*J*), some humans (Fig. 1*M*), and RUD 77 (Fig. 1 *A* and *B*). The ampullary portion of the lateral canal is bent superiorly, as in *Rudapithecus* (Fig. 1 *A*–*C*) and extant hominoids (Fig. 1 *G*–*M*). However, unlike extant great apes (Fig. 1 *J*–*L*) and *Rudapithecus* (Fig. 1 *A*–*C*), the portion between the ampulla and the tip of the lateral canal is inflated. The posterior canal is small and rounded, with a large ampulla. The CC is longer than in *Rudapithecus* (Fig. 1 *A*–*C*) and in most extant great apes (with *Pongo* showing the shortest), yet more inflated (even if much less so that in orangutans) (Fig. 1*J*), and the CC apex forms an obtuse angle. As in *Rudapithecus* and extant hominids, the planes identified by the lateral and posterior canals form a right angle and their trajectories do not intersect.

Volumetric Proportions. Allometric regressions of SC volume vs. length were performed separately for hominoids and the rest of anthropoids included in the sample (Fig. 2*A*; measurements for the dryopiths are given in *SI Appendix*, Table S1), because it has been previously shown that the former display an allometric grade shift toward relatively higher volumes at a comparable length once size-scaling effects have been taken into account (5), with only minimal overlap. *Hispanopithecus* falls above the hominid regression line, while *Rudapithecus* is situated more (RUD 77) or less (RUD 200) below the line, close to *Nacholapithecus*, but in all cases within the range of extant hominids and well above the regression line of other anthropoids (Fig. 2*A*). Gorillas are variable in this regard, while humans and orangutans display stouter proportions than chimpanzees and bonobos (Fig. 2*B*). The SCs of *Hispanopithecus* appear intermediate between these aforementioned taxa (closer to humans and orangutans), while those of *Rudapithecus*, *Oreopithecus*, and *Nacholapithecus* are slenderer and more comparable to those of chimpanzees and bonobos. Overall, given their range of variation, all the extinct apes analyzed here display extant hominid-like volumetric proportions of the vestibular apparatus.

Shape Analysis. The bgPCA (Fig. 3), based on the deformation fields computed for the hominoid sample, allows us to discriminate extant hominoid species, as shown by classification results

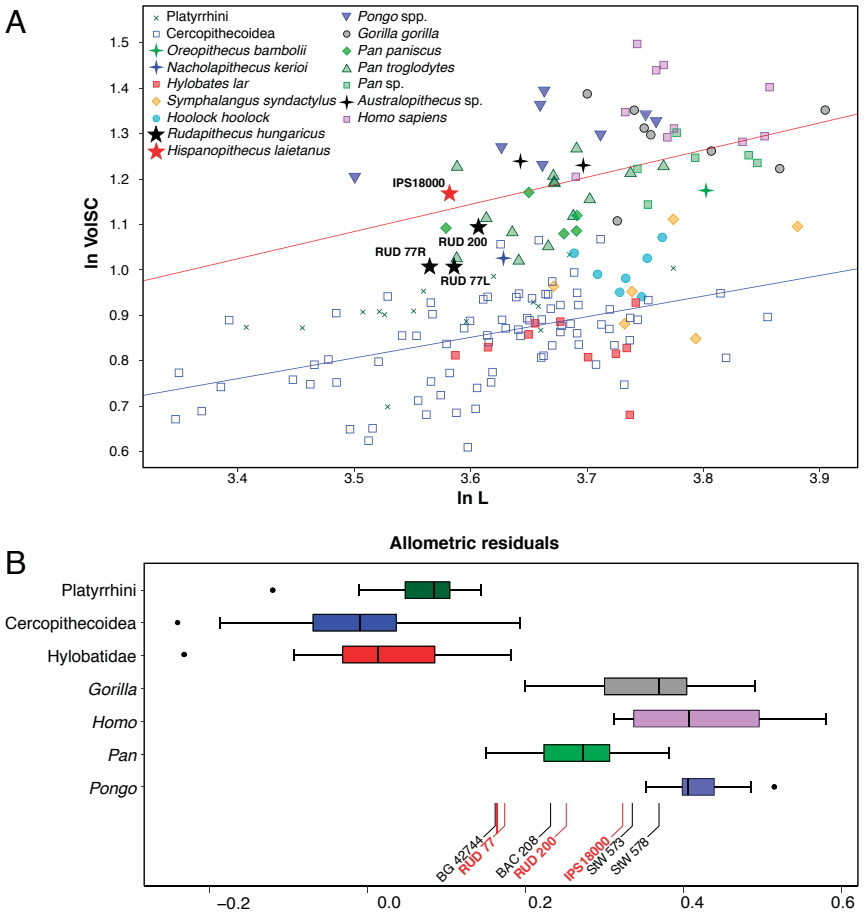

Fig. 2. (*A*) Allometric regressions of cube root of SC volume (ln VolSC, in millimeters) vs. SC length (ln L, in millimeters) in anthropoids. Lines represent ordinary least-squares best-fit lines for extant hominids (red) and other extant anthropoids (blue). Both hominids and other anthropoids show a negatively allometric relationship between VolSC and L, but with a marked allometric grade shift, such that hominids possess stouter canals than other anthropoid taxa at comparable lengths (see *SI Appendix*, Table S1 for comparative sample measurements). (*B*) Boxplots of allometric residuals computed using the best-fit line of the nonhominid anthropoid regression as baseline. Horizontal line is the median, boxes represent the interquartile range, whiskers represent maximum and minimum excluding outliers (beyond 1.5 times the upper and lower quartiles), and black dots are outliers. Samples for each boxplot are: Platyrrhini (n = 15), Cercopithecoidea (n = 80), Hylobatidae (n = 23), *Gorilla* (n = 8), *Pongo* (n = 8), *Pan* (n = 25), and *Homo* (n = 10). Note that all the fossils overlap with extant hominoids. However, while *Australopithecus* (StW 573 and StW 578) and *Hispanopithecus* (IPS18000) approach the human and orangutan condition, *Rudapithecus* RUD 200 and *Oreopithecus* (BAC 208) only overlap with African apes, while *Nacholapithecus* (BG 42744) and *Rudapithecus* RUD 77 only overlap with chimpanzees and bonobos, and marginally also with the upper range of hylobatids and cercopithecoids.

(99% of correctly classified individuals before and after cross-validation). These results closely resemble those computed using a cross-validated bgPCA (*SI Appendix*, Fig. S1). We also recover very significant group mean differences ($P < 0.001$) for the raw shape data (*SI Appendix*, Table S2), confirming that group structure does not artifactually result from the bgPCA (52). Indeed, group differences account for a substantial amount of variance (R^2) in the raw shape data, indicating that group separation is not spurious (52), although intergroup variance is increased to a similar extent by the standard bgPCA space and the cross-validated bgPCA (*SI Appendix*, Table S2).

bgPC1 (40.7% of the total variance) pulls apart hominids (mostly positive values) from hylobatids (negative values), with no overlap. Positive values along this axis indicate short and bulgy SCs, together with a right angle between the anterior and posterior SCs. Orangutans and humans display the most extreme condition due to the stoutness of their SCs. Chimpanzees, bonobos, and gorillas show a broad range of variation, with some individuals close to the origin due to their somewhat slenderer SCs (albeit less so than in hylobatids, which display negative values), and others overlapping with *Pongo* and *Homo*. Along bgPC1, *Hispanopithecus* overlaps with australopiths, extant great apes, and humans, while the *Rudapithecus* specimens fall within the African great ape range. Both RUD 77 and RUD 200 closely approach the origin, with the latter showing slightly more positive values. *Oreopithecus* and *Nacholapithecus* are found on moderate negative values, within the lower range of *Pan* and *Gorilla*, due to their quite slender SCs (albeit clearly stouter than in hylobatids).

The patterns of shape variation captured by bgPC2 (33.4% of total variance) (Fig. 3*A*) reflect changes in the shape of three canals as well as their relative proportions. In particular, bgPC2 clearly discriminates *Homo* (with most negative values) from the rest of the sample, due to the presence in the former of a large and rounded (sometimes even slightly superiorly elongated) anterior canal, a posterolaterally displaced inferior portion of the posterior canal, and a small, fairly anterolaterally elongated lateral canal, whose slender portion connects to the vestibule more superiorly and anterolaterally than in apes. The latter fall on intermediate and positive values, with hylobatids considerably overlapping with *Pan* spp. (Fig. 3*A*). To a large extent, this is due to their anterior canal shape, which appears intermediate

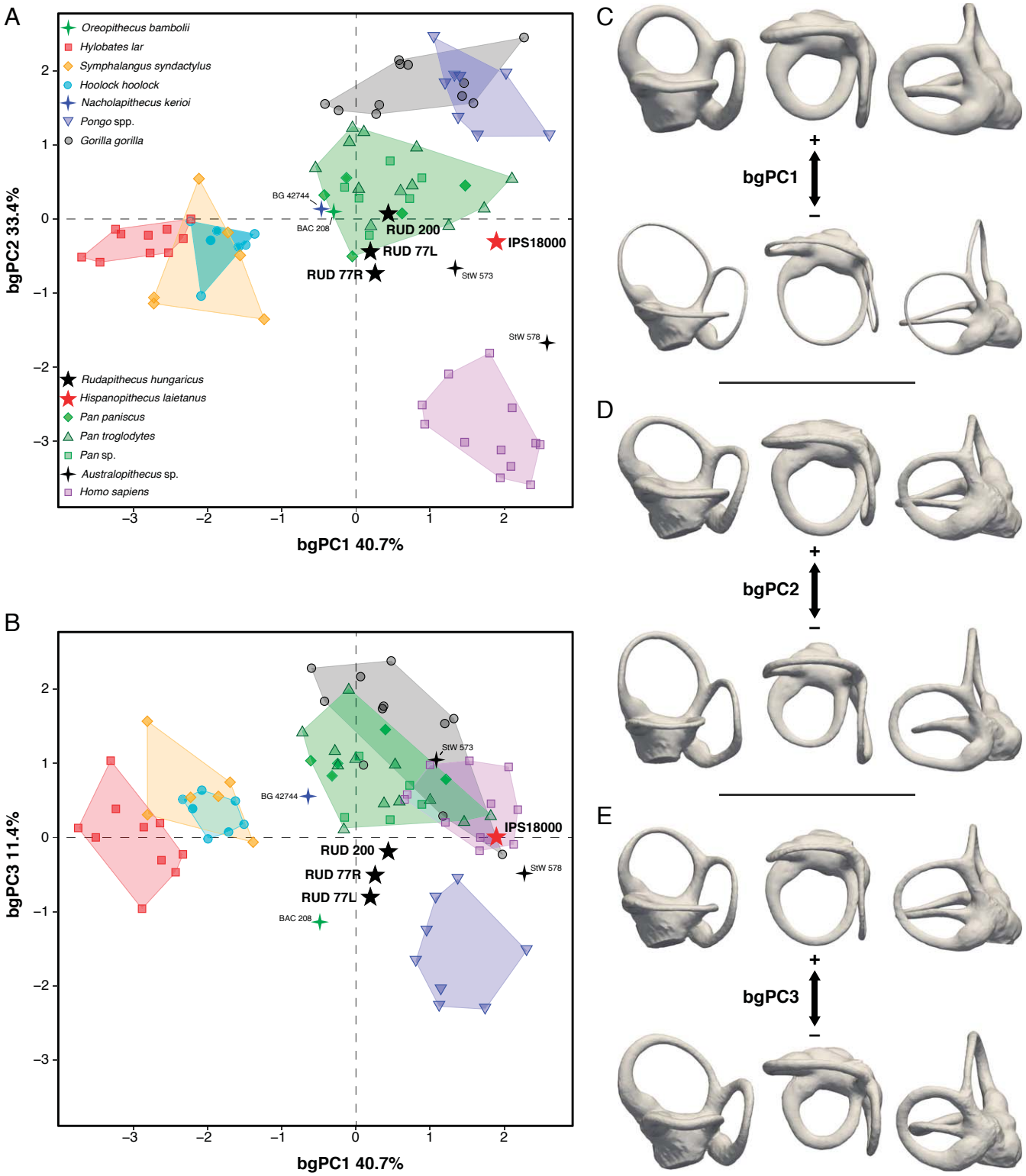

Fig. 3. Results of the bgPCA based on vestibular shape (as reflected by deformation data) in hominoids using genera as grouping factor (variance explained by each bgPC is included within parentheses): (*A*) bgPC2 vs. bgPC1; (*B*) bgPC3 vs. bgPC1. Extreme conformations for each bgPC are displayed: (*C*) bgPC1; (*D*) bgPC2; (*E*) bgPC3. Convex hulls are drawn for each hominoid genus and colored as follows: blue, *Pongo*; black, *Gorilla*; green, *Pan*; lilac, *Homo*; red, *Hylobates*; orange, *Symphalangus*; cyan, *Hoolock*.

between the rounded morphology of humans and the marked vertical compression of *Pongo* and *Gorilla* (the latter taxa occupying more positive values with only very slight overlap with *Pan* and hylobatids). Both *Rudapithecus* and *Hispanopithecus*, like *Oreopithecus* and *Nacholapithecus*, show intermediate values along this axis, overlapping with hylobatids and *Pan* spp. (as well as the *Australopithecus* specimen StW 573), but not with *Pongo* and *Gorilla*. Conversely, the other australopith (StW 578) more closely approaches humans due to its larger vertical SCs.

bgPC3 (11.4% of variance) (Fig. 3*B*) is driven by the shape of the anterior canal, its relative size relative compared with that of the lateral one, the length of the CC, and the amount of torsion of the lateral canal. Thus, negative values reflect a large and anterosuperiorly projecting anterior canal, coupled with a small lateral one, and a short CC. This axis discriminates *Pongo* (most negative values) from the rest of the sample, only minimally overlapping with some *Hylobates*. One individual of *Rudapithecus* (RUD 77) and *Oreopithecus* overlap with the range of orangutans due to their anterosuperiorly projecting anterior canal (albeit less so in RUD 77), short CC, and markedly small lateral canal. A similar morphology of the anterior canal is also found in some *Hylobates* and in one of the *Australopithecus* specimens (StW 573), resulting in moderately negative scores. *Hispanopithecus* and the other individual of *Rudapithecus* (RUD 200) fall at the negative end of the gorilla and human variation, due to their intermediate anterior canal morphology, longer CC (yet less so than in most *Pan* and *Gorilla* individuals), and a larger lateral canal. *Nacholapithecus* and the other australopith specimen (StW 578) fall among moderate positive values, overlapping with gorillas, chimpanzees, bonobos, humans, and hylobatids, due to their long CC and more vertically aligned (i.e., superiorly directed) connection of the anterior canal with the CC.

When the inspected bgPCs are considered simultaneously to compute posterior probabilities of group membership (Table 1), the *Rudapithecus* RUD 77 individual occupies a position in the morphospace that does not fit well with most extant hominoid genera ($P < 0.05$), rather approaching the position of *Nacholapithecus* and *Oreopithecus* in the morphospace (Table 2). Conversely, RUD 200 shows considerable similarities with *Pan* ($P = 0.549$) and *Nacholapithecus*. The three *Rudapithecus* specimens fall closer to one another than either approaches the single specimen of *Hispanopithecus* (Table 2), which is also more distant than *Nacholapithecus* from all the considered specimens (Table 2). *Hispanopithecus* mostly differs along bgPC1, sharing similarities in the volumetric proportions of the SCs and in the vertically compressed anterior canal morphology with *Australopithecus* individual StW 573 (Table 2). IPS18000 marginally differs from *Pan* ($P = 0.053$) and is clearly an outlier compared to the remaining extant genera.

The cluster analyses based on the significant bgPCs (Fig. 4*A*) and raw shape data (Fig. 4*B*) further support the aforementioned results, since *Rudapithecus* and *Hispanopithecus* do not cluster with one another and show affinities with different taxa. In particular, the cluster based on the bgPCA results (Fig. 4*A*) indicates that *Rudapithecus* is most similar to both *Pan* and *Nacholapithecus*, while *Hispanopithecus* approaches hominins. This is further supported by the raw shape data cluster (Fig. 4*B*), which mainly differs by recovering a great ape cluster.

Phylomorphospace and Reconstruction of Ancestral Morphologies. The shape data, as captured by the bgPCA performed on the extant hominoid sample, approaches the Brownian motion model of evolution, as supported by the phylogenetic signal computed for the bgPCs ($K_{mult} = 0.864$, $P = 0.019$) and for the raw data (i.e., the deformation fields; $K_{mult} = 0.863$, $P = 0.017$). We used phylogenetically informed techniques on the shape data to visualize the direction and magnitude of vestibular shape change during hominoid evolution as well as to depict the internal nodes of the phylogeny—that is, the inferred vestibular morphology of the last common ancestors (LCAs) of major groups—as reconstructed by maximum likelihood. The results are very similar irrespective of the precise phylogenetic placement of dryopiths as stem hominines (Fig. 5 and *SI Appendix*, Fig. S2*B*), stem hominids (*SI Appendix*, Figs. S2*A* and S3 *A* and *C*), or stem pongines (*SI Appendix*, Figs. S2*C* and S3 *B* and *D*). The crown hominoid LCA (Figs. 5 and 6*A*) is reconstructed as possessing evenly sized and moderately inflated SCs, a moderately long and not inflated CC, a fairly vertically compressed, yet not anterosuperiorly projecting anterior canal, an almost rounded posterior canal, an obtuse angle between the planes identified by the anterior and posterior canals (close to the right angle), and a right angle among the SCs merging at the CC apex

Table 1. Mahalanobis squared distances (D^2) between fossil scores and extant hominoid group centroids and associated posterior probabilities (P) of group membership for all fossil individuals

D^2 or P	*Hoolock*	*Symphalangus*	*Hylobates*	*Pongo*	*Gorilla*	*Pan*	*Homo*
D^2							
IPS18000 (*Hispanopithecus laietanus*)	6.086	6.861	10.532	9.229	5.329	**1.407**	5.076
RUD 77R (*Rudapithecus hungaricus*)	**2.044**	2.776	4.233	8.831	9.809	2.736	4.063
RUD 77L (*Rudapithecus hungaricus*)	**2.252**	3.325	4.104	6.735	10.091	3.132	5.621
RUD 200 (*Rudapithecus hungaricus*)	2.478	3.312	5.338	7.475	5.174	**0.745**	6.566
BAC 208 (*Oreopithecus bambolii*)	4.359	6.261	4.809	**4.087**	15.042	7.218	11.210
BG 42744 (*Nacholapithecus kerioi*)	1.200	1.662	3.546	10.016	4.942	**0.683**	7.673
StW 573 (*Australopithecus* sp.)	5.323	5.367	9.865	14.341	5.192	**1.246**	4.182
StW 578 (*Australopithecus* sp.)	9.400	10.538	13.134	10.554	16.362	7.661	**2.552**
P							
IPS18000 (*Hispanopithecus laietanus*)	<0.001	<0.001	<0.001	<0.001	<0.001	**0.053**	<0.001
RUD 77R (*Rudapithecus hungaricus*)	0.006	0.003	<0.001	<0.001	<0.001	**0.011**	<0.001
RUD 77L (*Rudapithecus hungaricus*)	**0.015**	0.005	<0.001	<0.001	<0.001	0.012	<0.001
RUD 200 (*Rudapithecus hungaricus*)	<0.001	<0.001	<0.001	<0.001	<0.001	**0.549**	<0.001
BAC 208 (*Oreopithecus bambolii*)	**0.016**	0.001	<0.001	<0.001	<0.001	<0.001	<0.001
BG 42744 (*Nacholapithecus kerioi*)	0.035	0.012	<0.001	<0.001	<0.001	**0.184**	<0.001
StW 573 (*Australopithecus* sp.)	<0.001	<0.001	<0.001	<0.001	<0.001	**0.026**	<0.001
StW 578 (*Australopithecus* sp.)	<0.001	<0.001	<0.001	<0.001	<0.001	<0.001	**0.013**

Note that these are probability estimates of having a particular score given membership in a particular group, not the likelihood of group membership in each of a priori defined groups given a particular score. The lowest D^2 and the highest probability for each specimen are in bold.

Table 2. Mahalanobis distances (D^2) between dryopiths and other fossils

D^2	IPS18000	RUD 77R	RUD 77L	RUD 200
IPS18000 (*Hispanopithecus laietanus*)	—	2.037	2.504	1.012
RUD 77R (*Rudapithecus hungaricus*)	2.037	—	0.179	0.772
RUD 77L (*Rudapithecus hungaricus*)	2.504	0.179	—	0.848
RUD 200 (*Rudapithecus hungaricus*)	1.012	0.772	0.848	—
BAC 208 (*Oreopithecus bambolii*)	6.678	2.495	1.385	3.571
BG 42744 (*Nacholapithecus kerioi*)	2.286	1.270	1.505	0.416
StW 573 (*Australopithecus* sp.)	0.703	2.587	3.657	1.637
StW 578 (*Australopithecus* sp.)	3.080	2.745	3.087	4.479

These distances are based on the scores of the significant bgPCs (bgPC1 – bgPC3).

(Fig. 6*A*). Irrespective of the phylogenetic assumptions for dryopiths, the reconstructed LCA for crown hominoids is closer to hominids (especially *Nacholapithecus*, *Rudapithecus* and, among extant taxa, *Pan*) than to hylobatids (Fig. 5), in terms of their intermediate volumetric proportions, contrasting with the markedly slenderer SCs of gibbons and siamangs. In turn, the LCAs of crown hominines and dryopiths (*Rudapithecus* + *Hispanopithecus*) closely resemble one another irrespective of the underlying phylogenetic assumptions for the fossil species (Fig. 5 and *SI Appendix*, Fig. S3), being extant hominid-like in volumetric proportions but otherwise showing a more plesiomorphic morphology in the evenly sized and fairly rounded SCs.

The inferred LCA of crown hominids, in particular, closely resembles that of crown hominoids, except for the stouter volumetric proportions, more derived toward the extant hominid condition (Figs. 5 and 6*B*). It displays equally sized SCs, an obtuse to right angle in the apex of a moderately long CC, and a slightly laterally elongated posterior canal (Fig. 6*B*). Orangutans appear derived from the LCA by displaying more inflated SCs (especially the anterior one) (Figs. 1*J* and 6*B*), further diverging in the opposite direction from African great apes and humans because its short and extremely stout CC, as well as its anterosuperiorly projecting anterior canal and marked torsion of the lateral canal (Fig. 5*B*). The LCA of hominines (Fig. 6*C*) appears somewhat more derived than the LCAs of hominoids and hominids for both volumetric proportions and SC shape. It displays moderately stout SCs and medium/large vestibular recesses, equally developed SCs (with a slightly smaller lateral one), a vertically compressed anterior canal (more so than in any other LCA), a slightly laterally projecting posterior canal, and a long CC with an obtuse angle in its apex (Fig. 6*C*). *Homo* and *Gorilla* would have evolved in opposite directions from this ancestral morphology in terms of SC relative size, with humans showing the largest vertical canals (Figs. 1*M* and 5*A*) and gorillas displaying a larger lateral canal (Figs. 1*K* and 5*A*). Chimpanzees and bonobos, due to their equally sized SCs and fairly elongated CC (Figs. 1*L* and 5*A*), are closer to the hominine LCA morphology, while *Australopithecus* appears derived toward the human condition, due to the moderate increase in the size of the anterior and posterior canals (Fig. 5). The reconstructed morphotype for the LCA of the investigated dryopiths (Fig. 6*D*) closely resembles those of hominines and hominids by displaying moderately stout and evenly sized SCs (with a slightly smaller lateral one), an obtuse angle at the CC apex, and a not anterosuperiorly projecting anterior canal, differing from the hominid LCA by the somewhat less vertically compressed anterior canal (Fig. 6 *B* and *D*).

Hispanopithecus and *Rudapithecus* appear to have diverged in opposite directions from their LCA (Fig. 5). The former seems derived in the volumetric proportions (similarly to *Pongo*, *Australopithecus*, and *Homo*), whereas the *Rudapithecus* condition in this regard is very similar to that of *Pan* as well as the reconstructed hominid LCA, and (to a lesser extent) to those of *Nacholapithecus* and *Oreopithecus* (Figs. 5 and 6*B*). Similarly, the fairly short CC and a somewhat anterosuperiorly projecting anterior canal found in *Rudapithecus* (less so than in orangutans and *Oreopithecus*) contrast with the longer CC and the rectangular-shaped anterior canal found in *Hispanopithecus* (Fig. 1*D*). In these regards, *Hispanopithecus* more closely resembles the members of the African ape and human clade (Fig. 1 *A*–*C*).

In summary, each extant hominid genus is derived in a particular direction from the ancestral morphology, with *Pan* remaining close to the hominid and hominine LCAs;

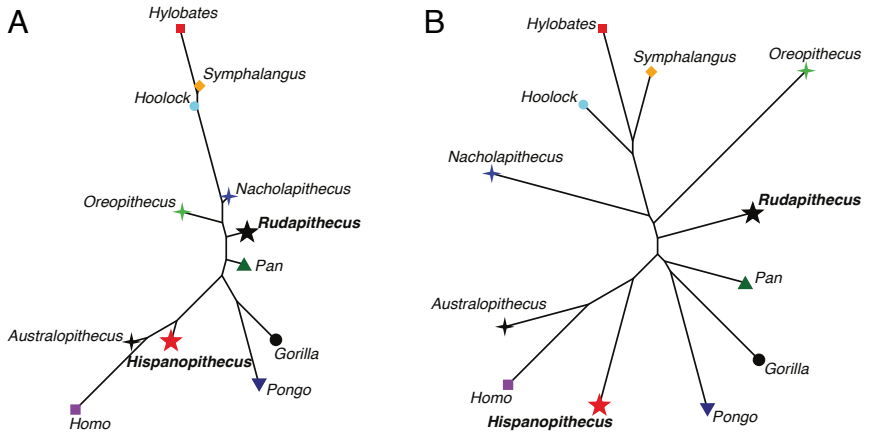

Fig. 4. Dendrograms resulting from neighbor joining cluster analyses based on: (*A*) The weighted Euclidean distances computed for the bgPCs (cophenetic correlation: 0.98); (*B*) the Euclidean distances computed for the raw shape data (i.e., the deformation fields) obtained from the deformation-based 3DGM analysis (cophenetic correlation: 0.96).

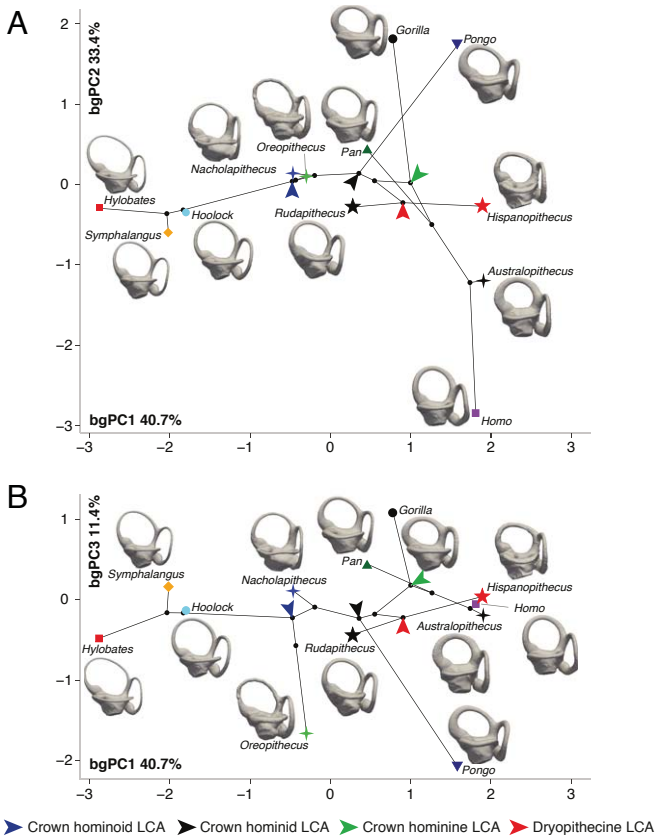

Fig. 5. Phylomorphospaces of the vestibular apparatus in hominoids, obtained by projecting the phylogenetic tree that considers dryopithecines a clade of stem hominines (*SI Appendix*, Fig. S1*B*) on bivariate plots between bgPCs. The tips correspond to genus bgPCA score centroids: (*A*) bgPC2 vs. bgPC1; (*B*) bgPC3 vs. bgPC1. Key ancestral morphologies reconstructed using maximum likelihood for the LCAs of various clades are depicted by means of arrowheads. See *SI Appendix*, Fig. S2 for the results based on alternative phylogenetic hypotheses (*SI Appendix*, Fig. S1 *A* and *C*).

Nacholapithecus appears as the least derived among both extant and fossil hominid taxa, together with *Oreopithecus.* The latter taxon also shows similarities with *Pongo* in the anterosuperiorly projecting anterior canal (Fig. 1 *E* and *J*), despite being much slenderer in *Oreopithecus*. Overall, the dryopiths appear less derived than most extant genera relative to either the crown hominid or the crown hominine LCA, irrespective of their preferred phylogenetic placement. *Rudapithecus* appears more primitive than *Hispanopithecus*, being closer than the latter to both *Nacholapithecus* and *Oreopithecus,* and closely approaching both the reconstructed crown hominid LCA and *Pan* (Figs. 1, 5, and 6). In contrast, *Hispanopithecus* is in some respects more derived than *Rudapithecus*, particularly toward orangutans, australopiths, and humans in the large vestibular recesses and in the stout SC volumetric proportions, and toward orangutans alone in the rounded posterior canal morphology (Fig. 5). Despite *Hispanopithecus* sharing its CC apex morphology (intermediate between African great apes and orangutans) and anterior canal shape (not anterosuperiorly projecting, yet not as squared as in gorillas) with *Homo* and *Australopithecus*, this condition could be plesiomorphic for hominids as a whole, as it is also found in the stem hominid *Nacholapithecus* (Fig. 5). Overall, the two dryopiths share with African great apes and humans some features (moderately stout SCs, not anterosuperiorly projecting the anterior canal, fairly long CC), but according to our analyses these features appear primitive (being likely present in the hominid LCA and, to a lesser extent, *Nacholapithecus*), with hominines (particularly gorillas) and especially orangutans having subsequently derived in opposite directions.

Discussion

Our results show that the vestibular morphology of both *Hispanopithecus* and *Rudapithecus* more closely resembles that of extant great apes and humans than that of hylobatids, in agreement with the current consensus that they belong to the great-ape-and-human clade (2, 3, 6, 26). These similarities particularly concern the volumetric proportions of the SCs as well as the size of the latter relative to the vestibular recesses. Volumetric proportions, as reflected by the ratio between the volume and the length of the SCs, appear particularly relevant given that an allometric grade shift has been previously identified to characterize all extant hominids, so that they display relatively more voluminous SCs than other anthropoids (including hylobatids) at comparable

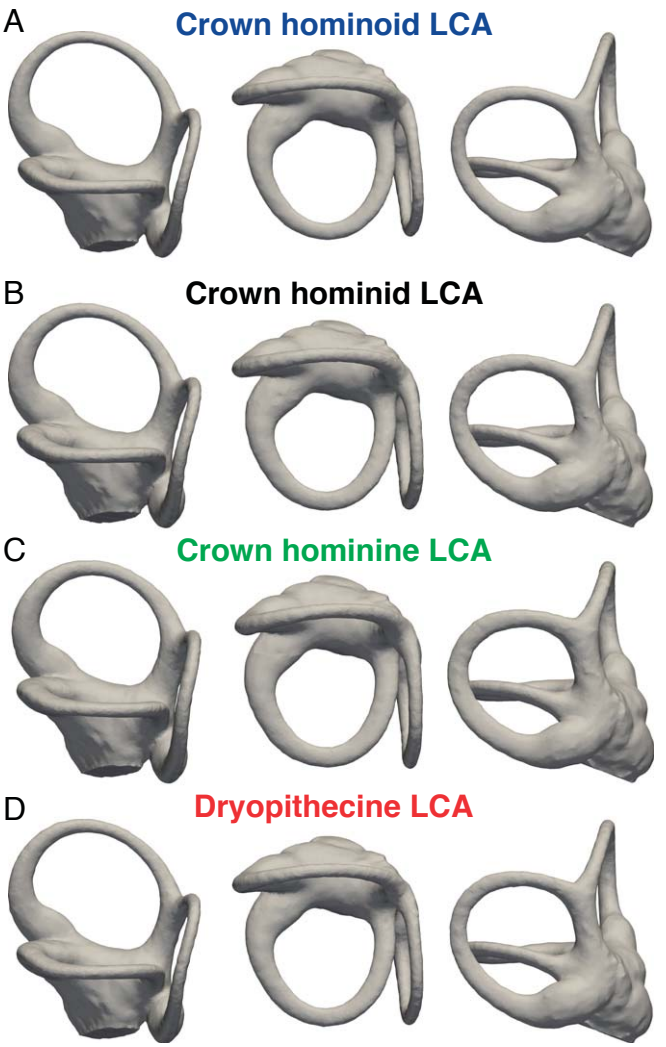

Fig. 6. Reconstructed vestibular shape for the LCA of the main clades of interest as inferred using maximum-likelihood methods for deformation-based 3DGM analyses applied to the hominoid sample under the stem-hominine phylogenetic hypothesis for dryopiths (*SI Appendix*, Fig. S1*B*), in posterolateral (*Left*), superior (*Center*), and posteromedial (*Right*) views. The reconstructed LCAs depicted are the following: (*A*) Crown hominoids; (*B*) crown hominids; (*C*) crown hominines; (*D*) dryopithecines (*Hispanopithecus* + *Rudapithecus*). The results for the other phylogenetic hypotheses (not shown) are virtually identical.

lengths (5). The derived condition of hominids has been linked with locomotion (5), but is noteworthy that chimpanzees, bonobos, and gorillas are slightly more variable in SC volumetric proportions than orangutans and humans. Given the relationship between SC shape variation and locomotion noted by some authors (53, 54), our results might reflect stronger locomotor-related selection pressures in orangutans and humans.

The classification results based on the bgPCA as well as the cluster analyses indicate that the two investigated dryopiths are distinguishable from one another, with the three specimens (two individuals) of *Rudapithecus* being more similar to one another than to the single specimen of *Hispanopithecus*. This result, together with other cranial differences (e.g., morphology of the frontal squama, premaxilla, and zygomatic), supports the distinction of these taxa at the genus rank (2, 3, 7, 21, 25, 35). *Rudapithecus* generally displays a somewhat more primitive morphology, closer to the one inferred for the crown hominid LCA. It shows some similarities with the fossil hominoids *Oreopithecus* and *Nacholapithecus*. The latter taxon appears more primitive than other hominids, in agreement with a previous study based on the entire inner ear morphology (49). However, both the hominid-like volumetric proportions of *Nacholapithecus* and the lack of a subarcuate fossa (55) support its stem hominid status, closely resembling the morphotype reconstructed for the crown hominid LCA. The morphology of *Rudapithecus* also resembles that of crown hominids, such as *Pan* (volumetric proportions and the relative size of the SCs) and, to a lesser extent, orangutans (the somewhat anterosuperiorly projecting anterior canal and the short CC). As previously noted (5), chimpanzees and bonobos appear least derived than other extant hominids. This is shown by the possession of similarly sized SCs (shared with the reconstructed crown hominid and crown hominine LCAs, while the dryopith LCA displays a slightly smaller lateral canal) and, especially, by the fairly slender volumetric proportions (intermediate between the hominine and hominid LCAs, yet closer to the latter). This is also supported by the similarities between *Pan* species and Miocene apes, especially *Nacholapithecus*. Nonetheless, chimpanzees and bonobos appear derived in some features (the small and rounded posterior canal as well as the obtuse angle of the CC apex), just like gorillas and humans are derived in other directions (largest lateral canal relative to the other SCs and markedly enlarged vertical canals, respectively).

Among hominids, orangutans and humans show the most extreme condition in the volumetric proportions of the SCs. Orangutans further diverge from the hominid LCA by the anterosuperiorly projecting anterior canal (even more so than in hylobatids). *Hispanopithecus* appears more derived than the other Miocene taxa, especially by the stouter SCs, while it does not fit well within the variation of any extant genus. More clearly than *Rudapithecus*, *Hispanopithecus* displays a mosaic of features that is unknown among extant hominids, including similarities with chimpanzees and bonobos (in the long CC), humans (the obtuse angle of the CC apex and the right angle between the planes of the posterior and lateral canals), and orangutans (the stout CC and the voluminous vestibular recesses, the latter also shared with humans) coupled with some unique features (the swollen area between the ampulla and the tip of the lateral canal, and the markedly inflated ampullae).

Interpreting the similarities of the investigated dryopiths in evolutionary terms is not straightforward. The results of the phylomorphospace approach and the reconstructed ancestral vestibular morphologies suggest that modern hominid-like volumetric proportions of the SCs would have been present in the LCA of crown hominids, while that of crown hominoids as a whole would have displayed somewhat intermediate proportions between hylobatids and hominids (yet closer to the latter). Differences in volumetric proportions of the SCs have been related to locomotor adaptations, because they directly affect the sensitivity and steadiness of the SCs in response to angular accelerations (5, 56). Hence, the moderately stout SCs of the LCA of crown hominids indicate that it showed a slow type of locomotion, which was present, to a large extent, also in the LCA of crown hominoids, as previously inferred based on the size of the SC radius alone (41). Both *Rudapithecus* and *Hispanopithecus* show a wide gap between the lateral and posterior canals (the planes defined by them are well separated and do not intersect), caused by the anterolateral location of the lateral canal. This trait has been linked to orthograde behaviors (42), in agreement with the fossil evidence available for these taxa (6, 11, 23, 25, 35, 57–61). However, from a phylogenetic viewpoint, the presence of the aforementioned feature in the investigated dryopiths is less informative than their hominid-like volumetric proportions, since the former have been identified as a synapomorphy of crown hominoids as a whole (5).

We conclude that, with differences that are consistent with their distinction at the genus rank, both *Hispanopithecus* and *Rudapithecus* display a unique hominid-like vestibular morphology that differs from that of any extant hominid genera but that appears quite close to that ancestral for crown hominids and crown hominines, mainly diverging from that of hylobatids by the stouter volumetric proportions of the SCs that are uniquely characteristic of great apes and humans among anthropoids. Orangutans appear most derived from such an ancestral vestibular morphology, whereas the investigated dryopiths lack most orangutan-like derived features, except for the slightly anterosuperiorly projecting anterior canal in *Rudapithecus* (also found in *Hylobates*) and some torsion in the shape of the lateral canal (a character that appears to be quite variable within hominoids). The lack of orangutan-derived features in dryopithecines does not completely rule out a stem pongine status, as previously supported by some authors (10, 28, 29), as it represents a more primitive morphology that probably precedes the subsequent evolution of the orangutan-like features in the pongine lineage. However, our results are more consistent with a stem hominid (6, 30) or a stem hominine (2, 3, 14, 16, 25) status for the investigated dryopiths. Our results suggest that African apes and hominin genera evolved in different directions from an ancestral morphology that more closely resembles that of *Pan* among extant hominines, and which is largely plesiomorphic for hominids, as further supported by similarities with the stem hominid *Nacholapithecus* (except for the slenderer volumetric proportions of the latter). Therefore, similarities between the SC morphology of the studied dryopiths and that of African apes do not necessarily imply a hominine status, but overall support the previous claim (5), based on extant taxa alone, that extant hominines evolved from an ancestral condition quite similar to that of the crown hominid LCA, and that the latter was characterized by derived volumetric proportions of the SCs. Pending the analysis of other Miocene apes, *Pan* among the extant taxa and *Rudapithecus* among extinct apes constitute the best available proxies for such ancestral morphologies, being already somewhat more derived from the crown hominoid condition that is best approximated by *Nacholapithecus*. In the future, the inclusion in the analyses of additional extinct hominoids will hopefully clarify further the evolutionary history of these hominoids during the Miocene.

Materials and Methods

Sample Composition and Acquisition. We inspected three petrosals from two individuals of *R. hungaricus* from Rudabánya, Hungary (RUD 77, left [RUD 77L] and right [RUD 77R]; and RUD 200, right) (12, 13) and the single available petrosal of *H. laietanus* from Can Llobateres 2, Spain (IPS18000, right) (10, 28, 29). The specimens of *Rudapithecus* are housed at the Geological Museum of the Mining and Geological Survey of Hungary and were scanned with a Skyscan 1172 (obtaining a resolution of 0.0136 mm) at the

Max Plank Institute for Evolutionary Anthropology (Leipzig, Germany), with the following parameters: 100-kV voltage and 100 mA. In turn, IPS18000 is housed at the Institut Català de Paleontologia Miquel Crusafont in Sabadell (Spain) and was scanned with a GE Phoenix V|Tome|X s 240 (obtaining a resolution of 0.0295 mm) at the Centro Nacional de Investigación sobre la Evolución Humana (Burgos, Spain), with the following parameters: 125-kV voltage and 120 mA. The three-dimensional (3D) virtual models of IPS18000, RUD 200 and RUD 77R were mirrored to enable the comparison with extant species. The segmented surfaces of the SCs of these fossils are available from MorphoSource (https://www.morphosource.org) (*SI Appendix*, Table S3).

The comparative sample for the volumetric proportion evaluation has been taken from a previous analysis that evaluated the phylogenetic signal embedded in the vestibule morphology (5), and integrated with recently published material of extant hominoids (4) and humans (62), together with the stem hominid *N. kerioi* (49). Overall, it consists of μCT scans of 169 dried crania and petrosals belonging to 27 extant anthropoid species, including all hominid genera and a selection of hylobatids, cercopithecoids, and platyrrhines, together with fossil taxa (*SI Appendix*, Table S3). The 3D meshes of the inner ear bony labyrinth of StW 573 and StW 578 were downloaded from the Sterkfontein project of the digital repository http://MorphoSource.org. The juvenile status of a few specimens should not affect their vestibular morphology since the bony labyrinth ossifies in early prenatal stages and does not change subsequently (63). The analysis of the patterns of shape variation was focused on hominoids alone and was based on a subsample of 77 individuals representing all extant hominoid genera (*SI Appendix*, Table S4). Part of the scans used in the study originally appeared in refs. 64 and 65.

The μCT scans (voxel size for the extant and fossil specimens added in the present analysis to those originally published in ref. 5 can be found in *SI Appendix*, Table S4) were segmented using Avizo 9.0.1 (FEI Visualization Sciences Group) to digitally extract the left bony labyrinth, when available, or that from the right side (mirrored before the surface alignment). The vestibular apparatus was separated from the cochlea by cutting the generated 3D surfaces right under the saccule and the oval window and filling the resulting holes with Geomagic Studio 2014 (3D Systems) using a flat surface (5).

The anatomical axes used for describing SC morphology corresponds to those employed in the vast majority of inner ear analysis focusing on primates (36, 37, 42, 49), which conventionally follow the same orientation as in humans (i.e., superior/inferior and anterior/posterior).

Shape Analysis. Shape was analyzed using a deformation-based 3DGM technique that does not rely on a priori defined landmarks and examines the geometrical correspondences between continuous surfaces (5, 48, 66–68). This method quantifies the deformation from the analyzed surfaces from a constructed sample-average surface (template) (66, 68), mathematically models them as a diffeomorphism, and computes a set of vectors (momenta) that describe the direction and magnitude of deformation from the average template. The unscaled 3D models were aligned with Avizo 9.0.1 using the "Align Surface" module before running the analyses. The diffeomorphisms and the momenta were computed in the Barcelona Supercomputing Center (Barcelona, Spain) with Deformetrica 4 software. The 3D models of the fossils were projected a posteriori in the tangent space generated by means of bgPCA ran on the set of momenta for the hominoid-only sample using genera as grouping factor. The bgPCA was computed in R Studio v1.1.453 for R v3.5.0 using the *ade4* package (69), while the cross-validated bgPCA was derived using the "groupPCA" function of the *Morpho* v2.6 (70) library. Group mean differences were tested by computing a permutational ANOVA (1,000 permutations) based on the Euclidean distance between the means using the "adonis" function of the *Vegan* package (71). The amount of variance (R^2) explained by group differences in the raw shape data, and in the scores of both standard and cross-validated bgPCA results, was estimated with the same function as for the permutation test. To further assess similarities between the analyzed fossil taxa and extant hominoid genera in terms of vestibular morphology, we computed Mahalanobis squared distances (D^2) between the bgPC scores of fossils and group centroids used in the bgPCA. The distances were also used to compute the posterior probabilities of group membership for the fossil specimens by means of the "typprobClass" function of the *Morpho* v2.6 (70) package, on the basis of the multivariate normal distribution of extant groups defined a priori in the bgPCA analyses. The similarities between extant and fossil hominoids were further investigated by means of a cluster analysis (neighbor joining) computed using the "nj" function of the *ape v5.3* package in R (72) on the basis of species mean configurations for the raw data and of weighted Euclidean distances between pairs of species bgPC centroid scores, obtained using the "distances" function of the *distances* v0.1.8 package in R (73)

Additionally, the correlation between the log-transformed cube root of SC volume (ln VolSC, in millimeters) and log-transformed SC length (ln L, in millimeters) was assessed means of ordinary least-squares linear regression, as the relationship between these variables has previously been shown to display an allometric grade shift between hominids and other anthropoids (5). Two separate regressions were computed for the nonhominid anthropoids and for great apes and humans using SPSS Statistics v. 17.0 for Windows (see figure 7b in ref. 5). The regression for the nonhominid sample was used as a baseline for computing the allometric residuals (*SI Appendix*, Table S1) (see table 5 in ref. 5) for the extant and extinct species. Comparisons between the latter and extant groups are depicted by means of box-and-whisker plots.

Phylomorphospace and Phylogenetic Signal. Major patterns of vestibular shape variation were quantified using a phylomorphospace approach (74), obtained by projecting a phylogeny on to the tangent space derived from the bgPCA of a 3DGM shape analysis. In this method, the tips of the phylogeny correspond to the genus bgPC centroid, while the internal nodes (i.e., the ancestral states) of the tree are estimated using a maximum-likelihood method for continuous characters, assuming that the reconstructed nodes approximate the true morphology of the ancestors. Thus, when a time-calibrated phylogeny is used, its two-dimensional representation enables the intuitive interpretation of the magnitude and direction of evolution, based on branch length and orientation. The molecular-based phylogenetic tree for extant hominoids used in this analysis was downloaded from the 10kTrees Website (v3; https://10ktrees.fas.harvard.edu/), while *Hispanopithecus* and *Rudapithecus* were added based on the assumption that they are closely related and constitute a clade, with the tips corresponding to 9.6 Ma and 10.1 Ma, respectively (20), and diverging at 11.1 Ma, but considering three different phylogenetic placements for these taxa as discussed in the literature during the last two decades (see above): stem hominids, stem hominines, and stem pongines (*SI Appendix*, Fig. S2). Analyses were repeated based on the resulting three different cladograms and their results compared to evaluate the effect of phylogenetic uncertainties surrounding these taxa. *Oreopithecus* is here considered as a stem hominoid as indicated by most recent cladistic analyses (4). *Nacholapithecus* has been included in a stem hominid position, 2 Myr older than the divergence between pongines and hominines (crown hominids), thus always preceding the divergence of dryopiths in all the phylogenetic hypotheses, and its tip corresponds to 14.77 Ma (55, 75). The divergence between crown hominoids and *Oreopithecus* has been placed 1 Myr older than the divergence between hylobatids and hominids and its tip corresponds to its last occurrence in the fossil record (7.0 to 6.5 Ma) (76). For the South African *Australopithecus* sp., we used the published first appearance datum for *Australopithecus africanus* (4.02 Ma) that includes the Jacovec specimens into the species (77).

The position in the morphospace of the internal nodes of the phylogeny (ancestral morphologies) was estimated via a maximum-likelihood method for continuous characters (78) using the "fastAnc" function of *phytools* v0.6-60 R package (79). Subsequently, the bgPC scores of the ancestral states were rotated and translated from the shape data back into the configuration space for interpolation and 3D visualization using Deformetrica 3 software.

The phylogenetic signal embedded in vestibular shape, as captured by all the bgPCs, was quantified by means of the multivariate phylogenetic index K_{mult} (80) using *geomorph* v3.1.1 (81) R package. The K_{mult} statistic, like its univariate counterpart (82), assesses the amount of phylogenetic signal relative to that expected for character undergoing Brownian motion and reflects the accuracy with which the phylogenetic tree describes the variance–covariance pattern found in the shape data. It is also informative about the accumulation of the variance in the phylogeny. Thus, $K_{mult} \sim 1$ is obtained when the inspected mode of evolution can adequately be described using a stochastic Brownian motion model. For $K_{mult} < 1$, the majority of the variance is found within clades, thus implying that neighbor taxa resemble one another less than expected and that the mode of evolution is not aleatory, possibly as the results of homoplastic adaptations (i.e., related to function rather than phylogeny). Values of $K_{mult} > 1$ indicate that variance is mostly found among different clades, being obtained when close taxa are less diverse that expected under Brownian motion (suggesting that phenomena of stabilizing selection might have occurred).

Data Availability. The 3D mesh data have been deposited in MorphoSource, https://morphosource.org/ (Rudapithecus hungaricus: RUD:77 R: https://doi.org/10.17602/M2/M126214; RUD:77 L: https://doi.org/10.17602/M2/M126215; RUD:200: https://doi.org/10.17602/M2/M126216; Hispanopithecus laietanus: IPS:18000: https://doi.org/10.17602/M2/M126217; Nacholapithecus kerioi:

KNM:BG:42744: https://doi.org/10.17602/M2/M166427; Oreopithecus bambolii: NMB:BAC:208: https://doi.org/10.17602/M2/M166428).

ACKNOWLEDGMENTS. We thank Jose Braga for allowing us to use the CT scans of the human specimens; the Max Plank Institute for providing access to the microCT scans of RUD 77 and RUD 200; the European Synchrotron Radiation Facility heritage database for palaeontology, evolutionary biology, and archaeology, for providing access to a part of the hominoid scans used in the present analysis; and Lynn Copes, Lynn Lucas, and the Museum of Comparative Zoology (Cambridge, MA) for providing access to a part of the scans used in the study, and funded by NSF DDIG #0925793, and a Wenner-Gren Foundation Dissertation Grant #8102 (both to Lynn Copes). These scans were downloaded from MorphoSource.org, a web-accessible archive for three-dimensional digital data housed by Duke University. This research has been funded by the Agencia Estatal de Investigación CGL2016-76431-P and CGL2017-82654-P, AEI/FEDER EU; and BES-2015-071318 (to A.U.); the Generalitat de Catalunya (CERCA Programme); the consolidated research groups 2017 SGR 86 and 2017 SGR 116 GRC; and the French Centre National de la Recherche Scientifique. Part of the analyses were performed using Barcelona Supercomputing Center resources (BCV-2020-1-0008). A.B. was funded by the University of the Witwatersrand.

1. N. J. Stevens *et al*., Palaeontological evidence for an Oligocene divergence between Old World monkeys and apes. *Nature* **497**, 611–614 (2013).
2. D. R. Begun, "The Miocene hominoid radiation" in *A Companion to Paleoanthropology*, D. R. Begun, Ed. (Blackwell Publishing, 2013), pp. 398–416.
3. D. R. Begun, "Fossil record of Miocene hominoids" in *Handbook of Paleoanthropology*, W. Henke, I. Tattersall, Eds. (Springer, ed. 2, 2015), pp. 1261–1332.
4. I. Nengo *et al*., New infant cranium from the African Miocene sheds light on ape evolution. *Nature* **548**, 169–174 (2017).
5. A. Urciuoli *et al*., The evolution of the vestibular apparatus in apes and humans. *eLife* **9**, e51261 (2020).
6. D. M. Alba, Fossil apes from the Vallès-Penedès Basin. *Evol. Anthropol.* **21**, 254–269 (2012).
7. D. R. Begun, Miocene hominids and the origins of the African apes and humans. *Annu. Rev. Anthropol.* **39**, 67–84 (2010).
8. J. Kelley, "The hominoid radiation in Asia" in *The Primate Fossil Record*, W. C. Hartwig, Ed. (Cambridge University Press, 2002), pp. 369–384.
9. P. Andrews, T. Harrison, E. Delson, R. L. Bernor, L. Martin, "Distribution and biochronology of European and Southwest Asian Miocene catarrhines" in *The Evolution of Western Eurasian Neogene Mammal Faunas*, R. L. Bernor, V. Fahlbusch, H.-W. Mittmann, Eds. (Columbia University Press, 1996), pp. 168–207.
10. S. M. Solà, M. Köhler, Recent discoveries of *Dryopithecus* shed new light on evolution of great apes. *Nature* **365**, 543–545 (1993).
11. S. Moyà-Solà, M. Köhler, A *Dryopithecus* skeleton and the origins of great-ape locomotion. *Nature* **379**, 156–159 (1996).
12. L. Kordos, D. R. Begun, A new reconstruction of RUD 77, a partial cranium of *Dryopithecus brancoi* from Rudabánya, Hungary. *Am. J. Phys. Anthropol.* **103**, 277–294 (1997).
13. L. Kordos, D. R. Begun, A new cranium of *Dryopithecus* from Rudabánya, Hungary. *J. Hum. Evol.* **41**, 689–700 (2001).
14. D. R. Begun, C. V. Ward, M. D. Rose, "Events in hominoid evolution" in *Function, Phylogeny and Fossils: Miocene Hominoid Evolution and Adaptation*, D. R. Begun, C. V. Ward, M. D. Rose, Eds. (Plenum Press, 1997), pp. 389–415.
15. D. R. Begun, "African and Eurasian Miocene hominoids and the origins of the Hominidae" in *Hominoid Evolution and Environmental Change in the Neogene of Europe, Vol 2. Phylogeny of the Neogene Hominoid Primates of Eurasia*, L. D. Bonis, G. Koufos, P. Andrews, Eds. (Cambridge University Press, 2001), pp. 231–253.
16. D. R. Begun, "European hominoids" in *The Primate Fossil Record*, W. Hartwig, Ed. (Cambridge University Press, 2002), pp. 339–368.
17. S. Moyà-Solà, M. Köhler, D. M. Alba, I. Casanovas-Vilar, J. Galindo, *Pierolapithecus catalaunicus*, a new Middle Miocene great ape from Spain. *Science* **306**, 1339–1344 (2004).
18. S. Moyà-Solà *et al*., First partial face and upper dentition of the middle Miocene hominoid *Dryopithecus fontani* from Abocador de Can Mata (Vallès-Penedès Basin, Catalonia, NE Spain): Taxonomic and phylogenetic implications. *Am. J. Phys. Anthropol.* **139**, 126–145 (2009).
19. S. Moyà-Solà *et al*., A unique Middle Miocene European hominoid and the origins of the great ape and human clade. *Proc. Natl. Acad. Sci. U.S.A.* **106**, 9601–9606 (2009).
20. I. Casanovas-Vilar, D. M. Alba, M. Garcés, J. M. Robles, S. Moyà-Solà, Updated chronology for the Miocene hominoid radiation in Western Eurasia. *Proc. Natl. Acad. Sci. U.S.A.* **108**, 5554–5559 (2011).
21. D. R. Begun, Dryopithecins, Darwin, de Bonis, and the European origin of the African apes and human clade. *Geodiversitas* **31**, 789–816 (2009).
22. D. M. Alba *et al*., New dental remains of *Hispanopithecus laietanus* (primates: Hominidae) from Can Llobateres 1 and the taxonomy of late Miocene hominoids from the Vallès-Penedès Basin (NE Iberian Peninsula). *J. Hum. Evol.* **63**, 231–246 (2012).
23. D. M. Alba, S. Almécija, I. Casanovas-Vilar, J. M. Méndez, S. Moyà-Solà, A partial skeleton of the fossil great ape *Hispanopithecus laietanus* from Can Feu and the mosaic evolution of crown-hominoid positional behaviors. *PLoS One* **7**, e39617 (2012).
24. D. R. Begun, *Sivapithecus* is east and *Dryopithecus* is west, and never the twain shall meet. *Anthropol. Sci.* **113**, 53–64 (2005).
25. D. R. Begun, M. C. Nargolwalla, L. Kordos, European Miocene hominids and the origin of the African ape and human clade. *Evol. Anthropol.* **21**, 10–23 (2012).
26. P. Andrews, Last common ancestor of apes and humans: Morphology and environment. *Folia Primatol. (Basel)* **91**, 122–148 (2020).
27. M. Böhme *et al*., A new Miocene ape and locomotion in the ancestor of great apes and humans. *Nature* **575**, 489–493 (2019).
28. M. Köhler, S. Moyà-Solà, D. M. Alba, "Eurasian hominoid evolution in the light of recent *Dryopithecus* findings" in *Hominoid Evolution and Environmental Change in the Neogene of Europe, Vol 2. Phylogeny of the Neogene Hominoid Primates of Eurasia*, L. D. Bonis, G. Koufos, P. Andrews, Eds. (Cambridge University Press, 2001), pp. 192–212.
29. S. Moyà-Solà, M. Köhler, New partial cranium of *Dryopithecus* Lartet, 1863 (Hominoidea, primates) from the upper Miocene of Can Llobateres, Barcelona, Spain. *J. Hum. Evol.* **29**, 101–139 (1995).
30. D. M. Alba *et al*., Miocene small-bodied ape from Eurasia sheds light on hominoid evolution. *Science* **350**, aab2625 (2015).
31. D. R. Begun, L. Kordos, "Phyletic affinities and functional convergence in *Dryopithecus* and other Miocene and living hominids." in *Function, Phylogeny, and Fossils: Miocene Hominoid Evolution and Adaptions*, D.R. Begun, C.V. Ward, M.D. Rose, Eds. (Plenum Press, 1997), pp. 291–316.
32. D. R. Begun, How to identify (as opposed to define) a homoplasy: Examples from fossil and living great apes. *J. Hum. Evol.* **52**, 559–572 (2007).
33. S. G. Larson, Parallel evolution in the hominoid trunk and forelimb. *Evol. Anthropol.* **6**, 87–99 (1998).
34. T. C. Rae, Mosaic evolution in the origin of the Hominoidea. *Folia Primatol. (Basel)* **70**, 125–135 (1999).
35. C. V. Ward, "Postcranial and locomotor adaptations of hominoids" in *Handbook of Paleoanthropology*, W. Henke, I. Tattersall, Eds. (Springer, 2015), pp. 1363–1386.
36. F. Spoor, B. Wood, F. Zonneveld, Implications of early hominid labyrinthine morphology for evolution of human bipedal locomotion. *Nature* **369**, 645–648 (1994).
37. F. Spoor, F. Zonneveld, Comparative review of the human bony labyrinth. *Am. J. Phys. Anthropol.* **41**, 211–251 (1998).
38. F. Spoor *et al*., The primate semicircular canal system and locomotion. *Proc. Natl. Acad. Sci. U.S.A.* **104**, 10808–10812 (2007).
39. R. David *et al*., Motion from the past. A new method to infer vestibular apparatus capacities of extinct species. *C. R. Palevol* **9**, 397–410 (2010).
40. R. David, A. Stoessel, A. Berthoz, F. Spoor, D. Bennequin, Assessing morphology and function of the semicircular duct system: Introducing new in-situ visualization and software toolbox. *Sci. Rep.* **6**, 32772 (2016).
41. T. M. Ryan *et al*., Evolution of locomotion in Anthropoidea: The semicircular canal evidence. *Proc. Biol. Sci.* **279**, 3467–3475 (2012).
42. A. Le Maître, P. Schuetz, P. Vignaud, M. Brunet, New data about semicircular canal morphology and locomotion in modern hominoids. *J. Anat.* **231**, 95–109 (2017).
43. L. Rook *et al*., The bony labyrinth of *Oreopithecus bambolii*. *J. Hum. Evol.* **46**, 349–356 (2004).
44. M. S. Ponce de León *et al*., Human bony labyrinth is an indicator of population history and dispersal from Africa. *Proc. Natl. Acad. Sci. U.S.A.* **115**, 4128–4133 (2018).
45. A. Beaudet, The inner ear of the *Paranthropus* specimen DNH 22 from Drimolen, South Africa. *Am. J. Phys. Anthropol.* **170**, 439–446 (2019).
46. A. Beaudet *et al*., The bony labyrinth of StW 573 ("Little Foot"): Implications for early hominin evolution and paleobiology. *J. Hum. Evol.* **127**, 67–80 (2019).
47. J. del Rio *et al*., Allometry, function and shape diversification in the inner ear of platyrrhine primates. *J. Mammal. Evol.*, 10.1007/s10914-019-09490-9 (2020).
48. A. Urciuoli, C. Zanolli, S. Almécija, S. Moyà-Solà, D. M. Alba, Analysis of the primate vestibular apparatus: A comparison of landmark-based and deformation-based 3D geometric morphometric approaches. *Proc. Eur. Soc. Stud. Hum. Evol.* **7**, 193 (2018).
49. N. Morimoto *et al*., Variation of bony labyrinthine morphology in Mio-Plio-Pleistocene and modern anthropoids. *Am. J. Phys. Anthropol.* **173**, 276–292 (2020).
50. T. C. Rae, P. M. Johnson, W. Yano, E. Hirasaki, Semicircular canal size and locomotion in colobine monkeys: A cautionary tale. *Folia Primatol. (Basel)* **87**, 213–223 (2016).
51. M. D. Malinzak, R. F. Kay, T. E. Hullar, Locomotor head movements and semicircular canal morphology in primates. *Proc. Natl. Acad. Sci. U.S.A.* **109**, 17914–17919 (2012).
52. A. Cardini, P. D. Polly, Cross-validated between-group PCA scatterplots: A solution to spurious group separation? *Evol. Biol.* **47**, 85–95 (2020).
53. A. Perier, R. Lebrun, L. Marivaux, Different level of intraspecific variation of the bony labyrinth morphology in slow- versus fast-moving Primates. *J. Mamm. Evol.* **23**, 353–368 (2016).
54. L. A. Gonzales, M. D. Malinzak, R. F. Kay, Intraspecific variation in semicircular canal morphology—A missing element in adaptive scenarios? *Am. J. Phys. Anthropol.* **168**, 10–24 (2019).
55. Y. Kunimatsu, M. Nakatsukasa, D. Shimizu, Y. Nakano, H. Ishida, Loss of the subarcuate fossa and the phylogeny of *Nacholapithecus*. *J. Hum. Evol.* **131**, 22–27 (2019).
56. R. D. Rabbitt, E. R. Damiano, J. W. Grant, "Biomechanics of the semicircular canals and otolith organs" in *The Vestibular System*, S. M. Highstein, R. R. Fay, A. N. Popper, Eds. (Springer, 2004), pp. 153–201.
57. D. R. Begun, Phyletic diversity and locomotion in primitive European hominids. *Am. J. Phys. Anthropol.* **87**, 311–340 (1992).

58. D. R. Begun, New catarrhine phalanges from Rudabánya (Northeastern Hungary) and the problem of parallelism and convergence in hominoid postcranial morphology. *J. Hum. Evol.* **24**, 373–402 (1993).
59. S. Almécija, D. Alba, S. Moyà-Solà, M. Köhler, Orang-like manual adaptations in the fossil hominoid *Hispanopithecus laietanus*: First steps towards great ape suspensory behaviours. *Proc. Biol. Sci.* **274**, 2375–2384 (2007).
60. D. M. Alba, S. Almécija, S. Moyà-Solà, Locomotor inferences in *Pierolapithecus* and *Hispanopithecus*: Reply to Deane and Begun (2008). *J. Hum. Evol.* **59**, 143–149, discussion 150–154 (2010).
61. M. Pina, D. M. Alba, S. Almécija, J. Fortuny, S. Moyà-Solà, Brief communication: Paleobiological inferences on the locomotor repertoire of extinct hominoids based on femoral neck cortical thickness: The fossil great ape *hispanopithecus laietanus* as a test-case study. *Am. J. Phys. Anthropol.* **149**, 142–148 (2012).
62. W. Wimmer, C. Vandersteen, N. Guevara, M. Caversaccio, H. Delingette, "Robust cochlear modiolar axis detection in CT" in *Medical Image Computing and Computer Assisted Intervention–MICCAI 2019*, D. Shen *et al*., Eds. (Springer, 2019), pp. 3–10.
63. N. Jeffery, F. Spoor, Prenatal growth and development of the modern human labyrinth. *J. Anat.* **204**, 71–92 (2004).
64. L. E. Copes, W. H. Kimbel, Cranial vault thickness in primates: *Homo erectus* does not have uniquely thick vault bones. *J. Hum. Evol.* **90**, 120–134 (2016).
65. L. E. Copes, L. M. Lucas, J. O. Thostenson, H. E. Hoekstra, D. M. Boyer, A collection of non-human primate computed tomography scans housed in MorphoSource, a repository for 3D data. *Sci. Data* **3**, 160001 (2016).
66. S. Durrleman *et al*., "Topology preserving atlas construction from shape data without correspondence using sparse parameters" in *Proceedings of Medical Image Computing and Computer Aided Intervention*, N. Ayache, H. Delingette, P. Golland, K. Mori, Eds. (Springer, 2012), pp. 223–230.
67. J. Dumoncel, S. Durrleman, J. Braga, J. P. Jessel, G. Subsol, Landmark-free 3D method for comparison of fossil hominins and hominids based on endocranium and EDJ shapes. *Am. J. Phys. Anthropol.* **153**, 114 (2014).
68. A. Beaudet *et al*., Upper third molar internal structural organization and semicircular canal morphology in Plio-Pleistocene South African cercopithecoids. *J. Hum. Evol.* **95**, 104–120 (2016).
69. S. Dray, A. Dufour, The ade4 Package: Implementing the duality diagram for ecologists. *J. Stat. Softw.* **22**, 10.18637/jss.v022.i04 (2007).
70. S. Schlager, "Morpho and Rvcg—Shape analysis in R" in *Statistical Shape and Deformation Analysis*, G. Zheng, S. Li, G. Szekely, Eds. (Academic Press, 2017), pp. 217–256.
71. J. Oksanen *et al*., vegan: Community ecology package (R package version 2.5-6, 2019). https://CRAN.R-project.org/package=vegan. Accessed 12 January 2021.
72. E. Paradis, K. Schliep, Ape 5.0: An environment for modern phylogenetics and evolutionary analyses in R. *Bioinformatics* **35**, 526–528 (2019).
73. F. Savje, distances: Tools for distance metrics (R package version 0.1.8, 2019). https://CRAN.R-project.org/package=distances. Accessed 12 January 2021.
74. B. Sidlauskas, Continuous and arrested morphological diversification in sister clades of characiform fishes: A phylomorphospace approach. *Evolution* **62**, 3135–3156 (2008).
75. M. Nakatsukasa, Y. Kunimatsu, *Nacholapithecus* and its importance for understanding hominoid evolution. *Evol. Anthropol.* **18**, 103–119 (2009).
76. L. Rook, L. Bondioli, M. Köhler, S. Moyà-Solà, R. Macchiarelli, *Oreopithecus* was a bipedal ape after all: Evidence from the iliac cancellous architecture. *Proc. Natl. Acad. Sci. U.S.A.* **96**, 8795–8799 (1999).
77. B. Wood, E. K Boyle, Hominin taxic diversity: Fact or fantasy? *Am. J. Phys. Anthropol.* **159**, S37–S78 (2016).
78. D. Schluter, T. Price, A. Ø. Mooers, D. Ludwig, Likelihood of ancestor states in adaptive radiation. *Evolution* **51**, 1699–1711 (1997).
79. L. J. Revell, phytools: An R package for phylogenetic comparative biology (and other things). *Methods Ecol. Evol.* **3**, 217–223 (2012).
80. D. C. Adams, A generalized K statistic for estimating phylogenetic signal from shape and other high-dimensional multivariate data. *Syst. Biol.* **63**, 685–697 (2014).
81. D. C. Adams, M. L. Collyer, A. Kaliontzopoulou, Geomorph: Software for geometric morphometric analyses (R package version 3.1.0, 2019). https://cran.r-project.org/package=geomorph. Accessed 12 January 2021.
82. S. P. Blomberg, T. Garland Jr, A. R. Ives, Testing for phylogenetic signal in comparative data: Behavioral traits are more labile. *Evolution* **57**, 717–745 (2003).

PNAS
www.pnas.org

Supplementary Information for

Reassessment of the phylogenetic relationships of the late Miocene apes Hispanopithecus and Rudapithecus based on vestibular morphology

Alessandro Urciuoli, Clément Zanolli, Sergio Almécija, Amélie Beaudet, Jean Dumoncel, Naoki Morimoto, Masato Nakatsukasa, Salvador Moyà-Solà, David R. Begun, David M. Alba
Corresponding authors: Alessandro Urciuoli and David M. Alba
Email: alessandro.urciuoli@icp.cat; david.alba@icp.cat

This PDF file includes:

Figures S1 to S3
Tables S1 to S5

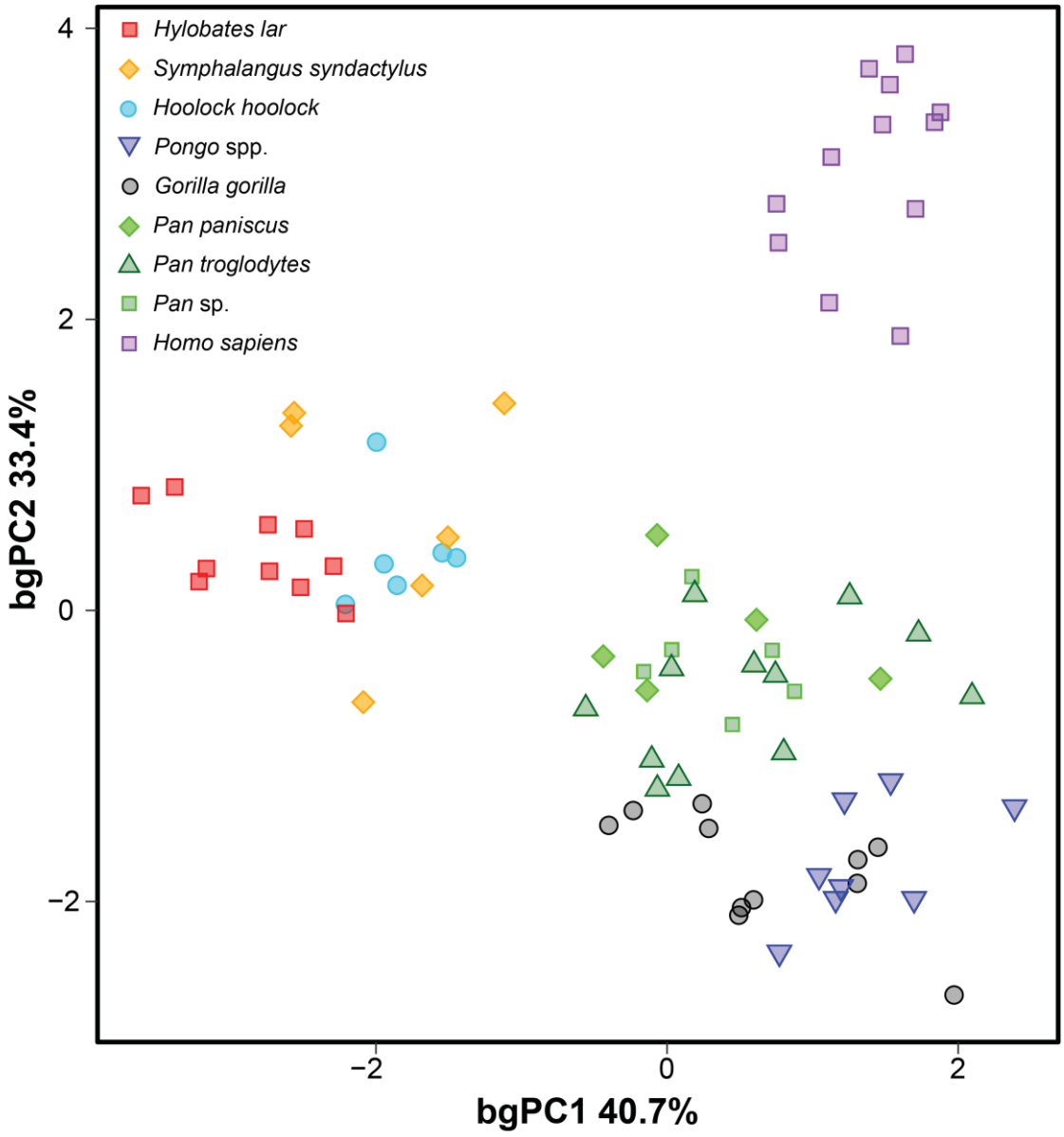

Fig. S1. Results of the cross-validated between-group principal component analysis (bgPCA). Scatterplot of bgPC2 vs. bgPC1 scores. The clear similarities between cross-validated bgPCA scores and regular ones (as shown in Fig. 3), except from a mirroring along the bgPC2 axis (which does affect the relative positioning of the clouds of points) and a very slight rotation of the morphospace, allow us to discount spurious grouping and prove the presence of a grouping structure embedded in our shape data.

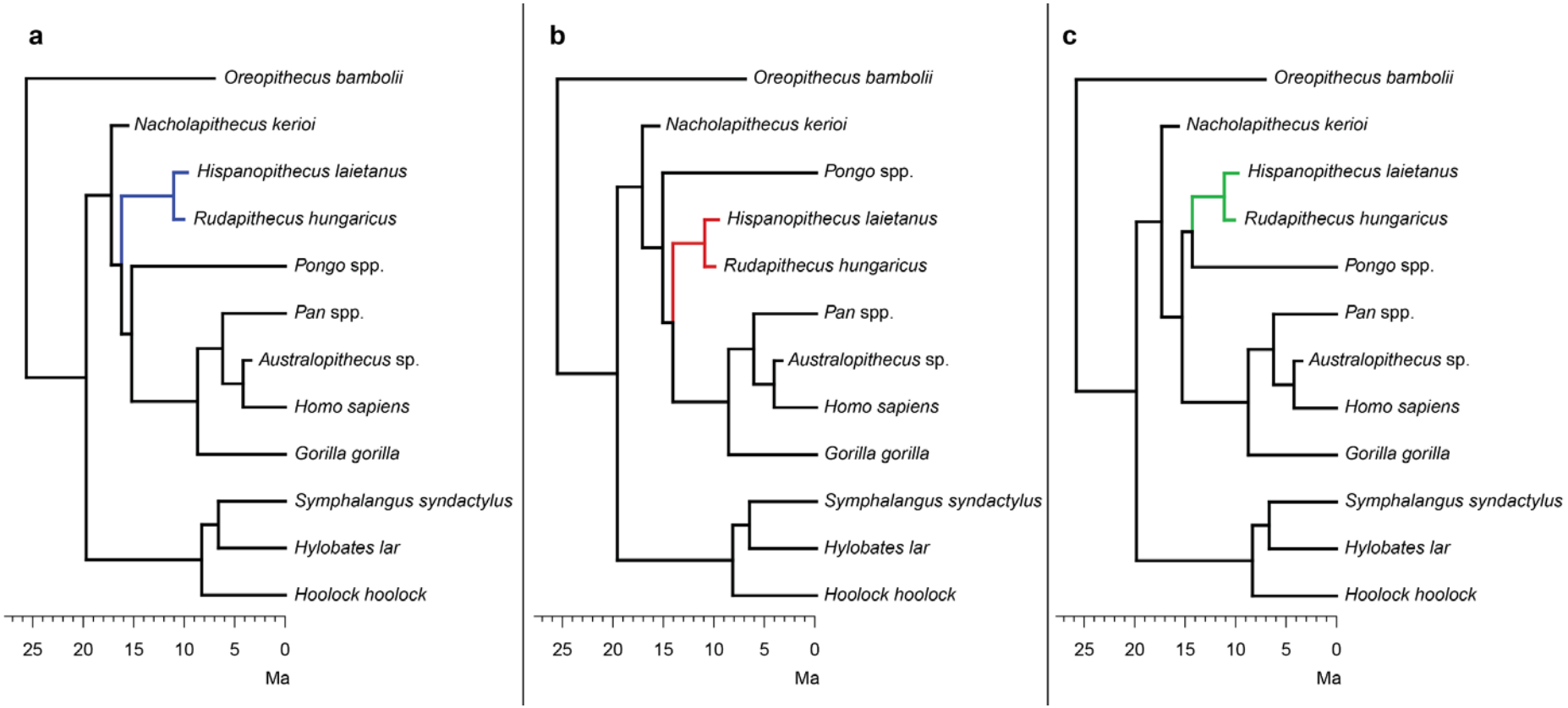

Fig. S2. Composite phylogenetic trees with the investigated Miocene dryopithecines as (**a**) stem hominids (blue), (**b**) stem hominines (red), and (**c**) stem pongines (green). The corresponding phylomorphospace results are depicted in Fig. 6 of the main text for (b) and in SI Appendix, Fig. S3 for (a, c).

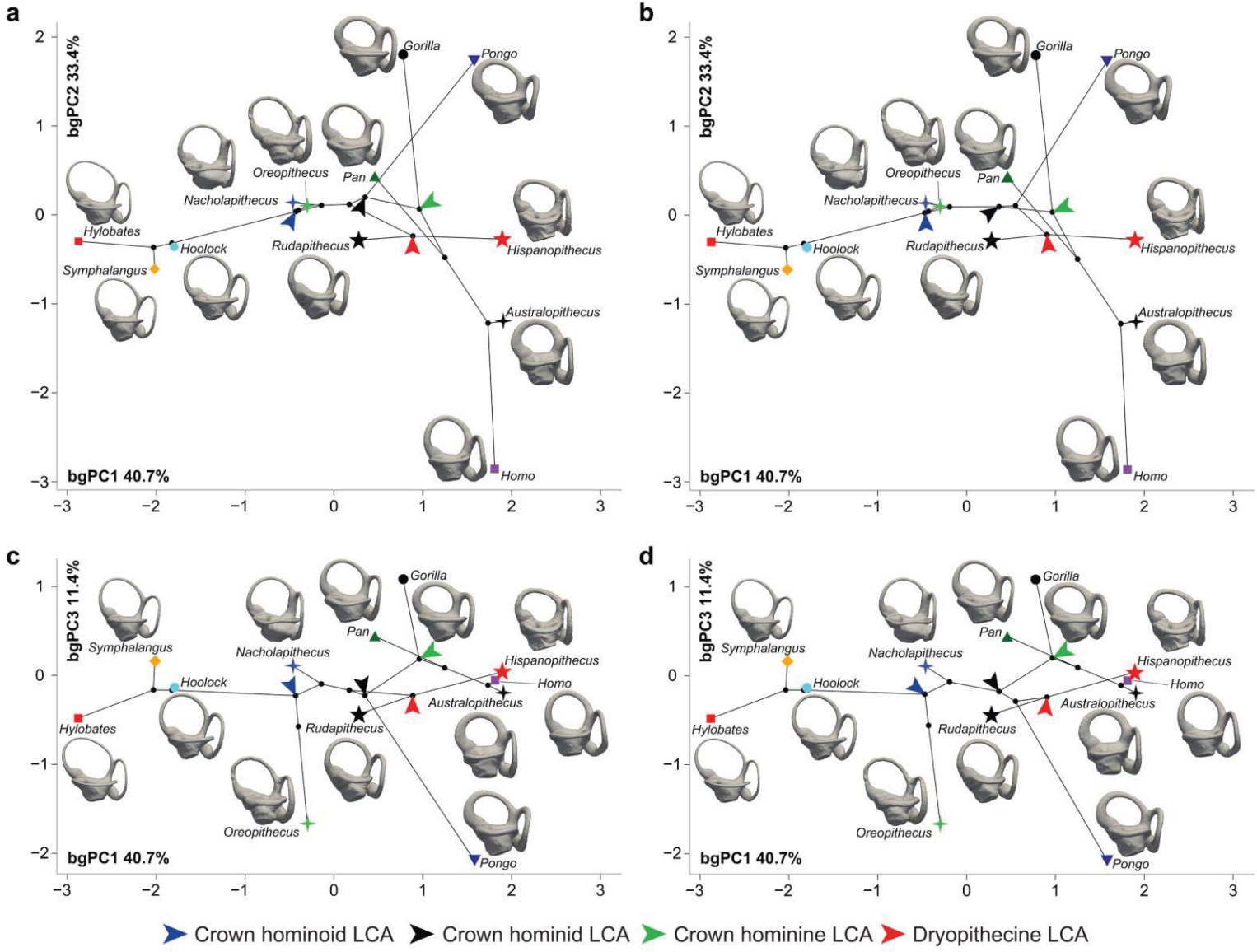

Fig. S3. Phylomorphospaces of the vestibular apparatus in hominoids, obtained by projecting the phylogenetic tree that considers dryopithecines a clade of stem hominids (a, c; see SI Appendix, Fig. S2a) and of stem pongines (b, d; see SI Appendix, Fig. S2c) on bivariate plots between bgPCs. The tips correspond to genus bgPCA score centroids: (**a, c**) bgPC2 vs. bgPC1; (**b, d**) bgPC3 vs. bgPC1. Key ancestral morphologies reconstructed using maximum likelihood for the last common ancestors (LCAs) of various clades are depicted by means of arrowheads.

Table S1. Log-transformed length (ln L, in mm) and volume cube root (ln VolSC, in mm) of the semicircular canals used for computing the allometric residuals using the non-hominid anthropoid regression as a baseline.

ID	Taxon	log L	log Vol	Residuals
DUEALP 02	*Alouatta palliata*	3.654	0.929	0.053
DUEALP 04	*Alouatta palliata*	3.529	0.699	-0.120
DUEALP 06	*Alouatta palliata*	3.658	0.920	0.042
DUEALP 10	*Alouatta palliata*	3.551	0.909	0.080
DUEALP 12	*Alouatta palliata*	3.660	0.867	-0.012
MCZ 10138	*Ateles geoffroyi*	3.685	1.033	0.143
MCZ 29626	*Ateles geoffroyi*	3.596	0.886	0.036
MCZ 29628	*Ateles geoffroyi*	3.620	0.985	0.125
MCZ 29658	*Ateles geoffroyi*	3.559	0.953	0.120
MCZ BOM 5351	*Ateles geoffroyi*	3.774	1.003	0.073
MCZ 27891	*Cebus apella*	3.407	0.873	0.110
MCZ 31063	*Cebus apella*	3.455	0.872	0.086
MCZ 37833	*Cebus apella*	3.522	0.908	0.092
MCZ 41090	*Cebus apella*	3.507	0.907	0.098
MCZ 49635	*Cebus apella*	3.526	0.901	0.083
AMNHM 52634	*Cercocebus galeritus*	3.661	0.891	0.011
AMNHM 52635	*Cercocebus galeritus*	3.737	0.845	-0.068
AMNHM 52640	*Cercocebus galeritus*	3.708	0.791	-0.109
AMNHM 52641	*Cercocebus galeritus*	3.691	0.860	-0.032
AMNHM 52645	*Cercocebus galeritus*	3.553	0.855	0.024
MCZ 22734	*Cercopithecus mitis*	3.447	0.758	-0.024
MCZ 25022	*Cercopithecus mitis*	3.349	0.773	0.036
MCZ 26832	*Cercopithecus mitis*	3.521	0.798	-0.018
MCZ 39389	*Cercopithecus mitis*	3.485	0.752	-0.047
MCZ 44264	*Cercopithecus mitis*	3.555	0.712	-0.119
SIU 4792	*Chlorocebus pygerythrus*	3.393	0.889	0.132
SIU 4793	*Chlorocebus pygerythrus*	3.529	0.941	0.122
SIU 4794	*Chlorocebus pygerythrus*	3.642	0.948	0.077
SIU 4795	*Chlorocebus pygerythrus*	3.484	0.905	0.106
SIU 4796	*Chlorocebus pygerythrus*	3.611	0.935	0.079
AMNHM 52211	*Colobus guereza*	3.737	0.894	-0.019
AMNHM 52213	*Colobus guereza*	3.720	0.913	0.007
AMNHM 52225	*Colobus guereza*	3.649	0.893	0.020
AMNHM 52237	*Colobus guereza*	3.743	0.890	-0.026
AMNHM 52249	*Colobus guereza*	3.819	0.806	-0.145
MCZ 37280	*Erythrocebus patas*	3.615	0.941	0.082
MCZ 47015	*Erythrocebus patas*	3.626	1.056	0.193
MCZ 47016	*Erythrocebus patas*	3.659	1.065	0.187
MCZ 47017	*Erythrocebus patas*	3.566	0.928	0.092
MCZ 47018	*Erythrocebus patas*	3.567	0.902	0.066
AMNHA 999686	*Gorilla gorilla*	3.807	1.261	0.316

AMNHA 999687	*Gorilla gorilla*	3.755	1.297	0.375
AMNHM 167338	*Gorilla gorilla*	3.905	1.351	0.362
AMNHM 54356	*Gorilla gorilla*	3.700	1.387	0.490
MCZ 17684	*Gorilla gorilla*	3.866	1.223	0.251
MCZ 26850	*Gorilla gorilla*	3.749	1.312	0.393
MCZ 37264	*Gorilla gorilla*	3.726	1.108	0.199
ESFR 50001994	*Gorilla gorilla*	3.741	1.351	0.436
EMBR 121	*Homo sapiens*	3.834	1.282	0.324
EMBR 179	*Homo sapiens*	3.853	1.294	0.328
EMBR 212	*Homo sapiens*	3.690	1.204	0.312
EMBR 215	*Homo sapiens*	3.733	1.347	0.435
EMBR 281	*Homo sapiens*	3.857	1.402	0.434
F01	*Homo sapiens*	3.775	1.311	0.380
F03	*Homo sapiens*	3.743	1.497	0.581
F04	*Homo sapiens*	3.769	1.291	0.363
F05	*Homo sapiens*	3.759	1.439	0.515
F06	*Homo sapiens*	3.766	1.451	0.524
AMNHM 112673	*Hoolock hoolock*	3.733	0.981	0.069
AMNHM 112720	*Hoolock hoolock*	3.728	0.951	0.041
AMNHM 112983	*Hoolock hoolock*	3.689	1.037	0.145
AMNHM 201742	*Hoolock hoolock*	3.765	1.071	0.145
AMNHM 83421	*Hoolock hoolock*	3.752	1.025	0.105
AMNHM 83425	*Hoolock hoolock*	3.747	0.941	0.023
AMNHM 201743	*Hoolock hoolock*	3.709	0.990	0.089
MCZ 41411	*Hylobates lar*	3.587	0.812	-0.034
MCZ 41412	*Hylobates lar*	3.677	0.886	0.000
MCZ 41416	*Hylobates lar*	3.725	0.815	-0.093
MCZ 41418	*Hylobates lar*	3.734	0.828	-0.084
MCZ 41421	*Hylobates lar*	3.650	0.858	-0.016
MCZ 41424	*Hylobates lar*	3.656	0.882	0.006
MCZ 41452	*Hylobates lar*	3.615	0.829	-0.029
AMNHM 184598	*Hylobates lar*	3.742	0.928	0.012
MCZ 41455	*Hylobates lar*	3.737	0.681	-0.233
MCZ 41469	*Hylobates lar*	3.701	0.808	-0.090
AMNHM 52596	*Lophocebus albigena*	3.686	0.881	-0.009
AMNHM 52603	*Lophocebus albigena*	3.753	0.933	0.013
AMNHM 52606	*Lophocebus albigena*	3.582	0.773	-0.070
AMNHM 52607	*Lophocebus albigena*	3.724	0.834	-0.073
AMNHM 52615	*Lophocebus albigena*	3.712	0.880	-0.023
MCZ 12758	*Macaca fascicularis*	3.541	0.855	0.031
MCZ 22277	*Macaca fascicularis*	3.618	0.752	-0.107
MCZ 23812	*Macaca fascicularis*	3.478	0.803	0.007
MCZ 23813	*Macaca fascicularis*	3.574	0.724	-0.116
MCZ 35765	*Macaca fascicularis*	3.566	0.754	-0.082
AMNHA 9912049	*Mandrillus sphinx*	3.677	0.923	0.036
AMNHA 9912056	*Mandrillus sphinx*	3.693	0.922	0.029

AMNHM 89362	*Mandrillus sphinx*	3.669	0.915	0.032
AMNHM 89364	*Mandrillus sphinx*	3.719	0.870	-0.036
AMNHM 89365	*Mandrillus sphinx*	3.614	0.856	-0.002
MCZ 19976	*Miopithecus talapoin*	3.385	0.742	-0.012
MCZ 23196	*Miopithecus talapoin*	3.466	0.791	0.001
MCZ 23197	*Miopithecus talapoin*	3.346	0.671	-0.065
MCZ 34264	*Miopithecus talapoin*	3.369	0.689	-0.057
MCZ 37278	*Miopithecus talapoin*	3.462	0.748	-0.041
MCZ 37342	*Nasalis larvatus*	3.692	0.949	0.056
MCZ 41555	*Nasalis larvatus*	3.670	0.834	-0.050
MCZ 41559	*Nasalis larvatus*	3.670	0.974	0.091
MCZ 41560	*Nasalis larvatus*	3.689	0.994	0.102
MCZ 41562	*Nasalis larvatus*	3.712	1.067	0.165
AMNHM 86857	*Pan paniscus*	3.691	1.120	0.227
IPS9033	*Pan paniscus*	3.680	1.079	0.192
MCZ 38018	*Pan paniscus*	3.691	1.086	0.193
MCZ 38019	*Pan paniscus*	3.579	1.092	0.250
MCZ 38020	*Pan paniscus*	3.650	1.170	0.296
ESFR 50001988	*Pan* spp.	3.846	1.235	0.272
ESFR 50001759	*Pan* spp.	3.743	1.222	0.306
ESFR 50001797	*Pan* spp.	3.777	1.302	0.370
ESFR 50002604	*Pan* spp.	3.752	1.144	0.223
ESFR 50001738	*Pan* spp.	3.839	1.252	0.292
ESFR 50001754	*Pan* spp.	3.793	1.246	0.307
AMNHM 167342	*Pan troglodytes*	3.672	1.193	0.309
AMNHM 167344	*Pan troglodytes*	3.702	1.155	0.257
AMNHM 51204	*Pan troglodytes*	3.737	1.212	0.299
IPS5698	*Pan troglodytes*	3.766	1.227	0.301
MCZ 17702	*Pan troglodytes*	3.667	1.051	0.170
MCZ 23167	*Pan troglodytes*	3.588	1.025	0.179
MCZ 26847	*Pan troglodytes*	3.636	1.082	0.215
ESFR 50001793	*Pan troglodytes*	3.691	1.266	0.374
ESFR 50001795	*Pan troglodytes*	3.672	1.190	0.306
ESFR 50001796	*Pan troglodytes*	3.588	1.226	0.380
ESFR 50001799	*Pan troglodytes*	3.671	1.207	0.323
MCZ 37260	*Pan troglodytes*	3.688	1.118	0.227
MCZ 46414	*Pan troglodytes*	3.641	1.020	0.150
MCZ 46415	*Pan troglodytes*	3.613	1.113	0.256
AMNHM 52677	*Papio anubis*	3.815	0.948	0.000
MCZ 17342	*Papio anubis*	3.643	0.855	-0.016
MCZ 26473	*Papio anubis*	3.677	0.863	-0.023
MCZ 31619	*Papio anubis*	3.855	0.896	-0.071
MCZ BOM 8466	*Papio anubis*	3.594	0.872	0.023
MCZ 24080	*Piliocolobus badius*	3.496	0.649	-0.155
MCZ 24775	*Piliocolobus badius*	3.598	0.609	-0.241
MCZ 24793	*Piliocolobus badius*	3.588	0.685	-0.161

MCZ 25627	*Piliocolobus badius*	3.512	0.624	-0.188
MCZ 25631	*Piliocolobus badius*	3.604	0.694	-0.159
IPS10647	*Pongo* sp.	3.660	1.363	0.485
IPS10651	*Pongo* sp.	3.750	1.342	0.423
IPS9031	*Pongo* sp.	3.500	1.205	0.399
IPSSN	*Pongo* sp.	3.662	1.231	0.352
MHNTZOO 201108	*Pongo* sp.	3.626	1.270	0.407
SENCK 1576UU	*Pongo* sp.	3.712	1.298	0.396
ESRF 50001801	*Pongo* sp.	3.663	1.395	0.515
SENCK 6782	*Pongo* sp.	3.759	1.327	0.404
MCZ 35621	*Presbytis hosei*	3.562	0.681	-0.153
MCZ 37370	*Presbytis hosei*	3.579	0.837	-0.005
MCZ 37371	*Presbytis hosei*	3.619	0.775	-0.085
MCZ 37372	*Presbytis hosei*	3.516	0.651	-0.162
MCZ 37772	*Presbytis hosei*	3.616	0.841	-0.018
MCZ 22276	*Presbytis rubicunda*	3.732	0.747	-0.164
MCZ 35704	*Presbytis rubicunda*	3.663	0.811	-0.069
MCZ 35705	*Presbytis rubicunda*	3.693	0.836	-0.058
MCZ 35706	*Presbytis rubicunda*	3.641	0.868	-0.002
MCZ 35712	*Presbytis rubicunda*	3.678	0.877	-0.010
AMNHM 102724	*Symphalangus syndactylus*	3.671	0.964	0.080
AMNHM 106583	*Symphalangus syndactylus*	3.739	0.952	0.038
MCZ 36031	*Symphalangus syndactylus*	3.732	0.881	-0.030
MCZ 36032	*Symphalangus syndactylus*	3.793	0.849	-0.091
EA 258	*Symphalangus syndactylus*	3.774	1.111	0.181
ESFR 50001912	*Symphalangus syndactylus*	3.881	1.095	0.116
AMNHM 19549	*Theropithecus gelada*	3.667	0.946	0.064
AMNHM 238034	*Theropithecus gelada*	3.606	0.740	-0.114
AMNHM 60568	*Theropithecus gelada*	3.627	0.890	0.026
AMNHM 80126	*Theropithecus gelada*	3.661	0.807	-0.072
AMNHM 90309	*Theropithecus gelada*	3.630	0.871	0.006
MCZ 35567	*Trachypithecus cristatus*	3.599	0.888	0.036
MCZ 35584	*Trachypithecus cristatus*	3.639	0.940	0.071
MCZ 35586	*Trachypithecus cristatus*	3.653	0.937	0.062
MCZ 35597	*Trachypithecus cristatus*	3.651	0.889	0.015
MCZ 35603	*Trachypithecus cristatus*	3.664	0.947	0.066
RUD 77L	*Rudapithecus hungaricus*	3.586	1.008	0.163
RUD 77R	*Rudapithecus hungaricus*	3.565	1.009	0.173
RUD 200	*Rudapithecus hungaricus*	3.607	1.096	0.241
IPS18000	*Hispanopithecus laietanus*	3.582	1.166	0.323
BAC 208	*Oreopithecus bambolii*	3.802	1.175	0.231
BG 42744	*Nacholapithecus kerioi*	3.629	1.026	0.161
StW 573	*Australopithecus* sp.	3.697	1.230	0.335
StW 578	*Australopithecus* sp.	3.643	1.239	0.368

Table S2. Results of group mean differences tests computed for the raw shape data, the standard between-group principal components analysis (bgpCA) scores, and cross-validated bgPCA scores. Significant differences are recovered in all instances. The amount of variance (R^2) explained by group differences increases slightly between the raw data and bgPCA scores (both standard and cross-validated). The difference in R^2 between standard bgPCA and cross-validated bgPCA are minimal.

Shape data	p	R^2
Full dataspace	< 0.001	0.624
bgPCA scores	< 0.001	0.852
Cross-validated bgPCA scores	< 0.001	0.836

Table S3. Voxel size for the sample used in this paper, indicating those used in ref. 1 and those newly added in this study.

Species	ID	Source	Voxel size	Sex	DOI	MorphoSource ID	Source
Alouatta palliata	DUEALP 02	MorphoSource	0.06	M	-	S1923	Urciuoli et al., 2020
Alouatta palliata	DUEALP 04	MorphoSource	0.05	M	-	S1924	Urciuoli et al., 2020
Alouatta palliata	DUEALP 06	MorphoSource	0.07	M	-	S78	Urciuoli et al., 2020
Alouatta palliata	DUEALP 10	MorphoSource	0.05	F	-	S1926	Urciuoli et al., 2020
Alouatta palliata	DUEALP 12	MorphoSource	0.06	F	-	S79	Urciuoli et al., 2020
Ateles geoffroyi	MCZ 10138	MorphoSource	0.06	F	http://dx.doi.org/10.17602/M2/M2917	S971	Urciuoli et al., 2020
Ateles geoffroyi	MCZ 29626	MorphoSource	0.06	F	http://dx.doi.org/10.17602/M2/M2918	S972	Urciuoli et al., 2020
Ateles geoffroyi	MCZ 29628	MorphoSource	0.06	F	http://dx.doi.org/10.17602/M2/M2919	S973	Urciuoli et al., 2020
Ateles geoffroyi	MCZ 29658	MorphoSource	0.06	F	http://dx.doi.org/10.17602/M2/M2920	S974	Urciuoli et al., 2020
Ateles geoffroyi	MCZ BOM 5351	MorphoSource	0.06	M	http://dx.doi.org/10.17602/M2/M2889	S943	Urciuoli et al., 2020
Cebus apella	MCZ 27891	MorphoSource	0.06	M	http://dx.doi.org/10.17602/M2/M5208	S1725	Urciuoli et al., 2020
Cebus apella	MCZ 31063	MorphoSource	0.07	F	http://dx.doi.org/10.17602/M2/M5213	S1730	Urciuoli et al., 2020
Cebus apella	MCZ 37833	MorphoSource	0.06	M	http://dx.doi.org/10.17602/M2/M5218	S1736	Urciuoli et al., 2020
Cebus apella	MCZ 41090	MorphoSource	0.05	F	http://dx.doi.org/10.17602/M2/M5219	S1737	Urciuoli et al., 2020
Cebus apella	MCZ 49635	MorphoSource	0.06	M	http://dx.doi.org/10.17602/M2/M5220	S1738	Urciuoli et al., 2020
Cercocebus galeritus	AMNHM 52634	MorphoSource	0.06	M	-	S4019	Urciuoli et al., 2020
Cercocebus galeritus	AMNHM 52635	MorphoSource	0.06	F	-	S4024	Urciuoli et al., 2020
Cercocebus galeritus	AMNHM 52640	MorphoSource	0.06	F	-	S4025	Urciuoli et al., 2020
Cercocebus galeritus	AMNHM 52641	MorphoSource	0.07	M	-	S1513	Urciuoli et al., 2020
Cercocebus galeritus	AMNHM 52645	MorphoSource	0.08	M	-	S4026	Urciuoli et al., 2020
Cercopithecus mitis	MCZ 22734	MorphoSource	0.08	F	http://dx.doi.org/10.17602/M2/M2928	S982	Urciuoli et al., 2020
Cercopithecus mitis	MCZ 25022	MorphoSource	0.08	F	http://dx.doi.org/10.17602/M2/M2929	S983	Urciuoli et al., 2020
Cercopithecus mitis	MCZ 26832	MorphoSource	0.08	F	http://dx.doi.org/10.17602/M2/M2930	S984	Urciuoli et al., 2020
Cercopithecus mitis	MCZ 39389	MorphoSource	0.08	F	http://dx.doi.org/10.17602/M2/M2933	S988	Urciuoli et al., 2020
Cercopithecus mitis	MCZ 44264	MorphoSource	0.08	F	http://dx.doi.org/10.17602/M2/M2935	S990	Urciuoli et al., 2020
Chlorocebus pygerythrus	SIU 4792	MorphoSource	0.05	F	-	S4036	Urciuoli et al., 2020
Chlorocebus pygerythrus	SIU 4793	MorphoSource	0.05	F	-	S4037	Urciuoli et al., 2020

Chlorocebus pygerythrus	SIU 4794	MorphoSource	0.05	F	-	S4038	Urciuoli et al., 2020
Chlorocebus pygerythrus	SIU 4795	MorphoSource	0.05	M	-	S4039	Urciuoli et al., 2020
Chlorocebus pygerythrus	SIU 4796	MorphoSource	0.05	M	-	S4040	Urciuoli et al., 2020
Colobus guereza	AMNHM 52211	MorphoSource	0.07	M	-	S1143	Urciuoli et al., 2020
Colobus guereza	AMNHM 52213	MorphoSource	0.07	F	-	S3768	Urciuoli et al., 2020
Colobus guereza	AMNHM 52225	MorphoSource	0.05	F	-	S1147	Urciuoli et al., 2020
Colobus guereza	AMNHM 52237	MorphoSource	0.07	M	-	S1148	Urciuoli et al., 2020
Colobus guereza	AMNHM 52249	MorphoSource	0.07	F	-	S3770	Urciuoli et al., 2020
Erythrocebus patas	MCZ 37280	MorphoSource	0.08	M	http://dx.doi.org/10.17602/M2/M2922	S976	Urciuoli et al., 2020
Erythrocebus patas	MCZ 47015	MorphoSource	0.08	M	http://dx.doi.org/10.17602/M2/M2923	S977	Urciuoli et al., 2020
Erythrocebus patas	MCZ 47016	MorphoSource	0.08	M	http://dx.doi.org/10.17602/M2/M2924	S978	Urciuoli et al., 2020
Erythrocebus patas	MCZ 47017	MorphoSource	0.06	F	http://dx.doi.org/10.17602/M2/M2925	S979	Urciuoli et al., 2020
Erythrocebus patas	MCZ 47018	MorphoSource	0.08	F	http://dx.doi.org/10.17602/M2/M2926	S980	Urciuoli et al., 2020
Gorilla gorilla	AMNHA 999686	MorphoSource	0.13	M	-	S5189	Urciuoli et al., 2020
Gorilla gorilla	AMNHA 999687	MorphoSource	0.08	F	-	S5186	Urciuoli et al., 2020
Gorilla gorilla	AMNHM 167338	MorphoSource	0.13	M	-	S5128	Urciuoli et al., 2020
Gorilla gorilla	AMNHM 54356	MorphoSource	0.11	F	-	S5125	Urciuoli et al., 2020
Gorilla gorilla	MCZ 17684	MorphoSource	0.13	F	http://dx.doi.org/10.17602/M2/M2943	S644	Urciuoli et al., 2020
Gorilla gorilla	MCZ 26850	MorphoSource	0.12	F	http://dx.doi.org/10.17602/M2/M2947	S995	Urciuoli et al., 2020
Gorilla gorilla	MCZ 37264	MorphoSource	0.13	F	http://dx.doi.org/10.17602/M2/M2949	S997	Urciuoli et al., 2020
Gorilla gorilla	MCZ 14750	MorphoSource	0.13	F	-	S993	This study
Gorilla gorilla	MCZ 37625	MorphoSource	0.12	F	-	S998	This study
Gorilla gorilla	MCZ 49006	MorphoSource	0.13	F	-	S1002	This study
Gorilla gorilla	ESFR 50001994	ESFR	0.05	F	-	-	This study
Homo sapiens	EMBR 121	PSU	0.04	F	-	-	Urciuoli et al., 2020
Homo sapiens	EMBR 179	PSU	0.04	M	-	-	Urciuoli et al., 2020
Homo sapiens	EMBR 212	PSU	0.04	F	-	-	Urciuoli et al., 2020
Homo sapiens	EMBR 215	PSU	0.04	M	-	-	Urciuoli et al., 2020
Homo sapiens	EMBR 281	PSU	0.04	F	-	-	Urciuoli et al., 2020
Homo sapiens	EMBR 473	PSU	0.04	M	-	-	This study

Homo sapiens	EMBR 479	PSU	0.04	M	-	-	This study
Homo sapiens	EMBR 583	PSU	0.04	F	-	-	This study
Homo sapiens	F01	Wimmer et al., 2019	0.06	?	-	-	This study
Homo sapiens	F03	Wimmer et al., 2019	0.06	?	-	-	This study
Homo sapiens	F04	Wimmer et al., 2019	0.06	?	-	-	This study
Homo sapiens	F05	Wimmer et al., 2019	0.06	?	-	-	This study
Homo sapiens	F06	Wimmer et al., 2019	0.06	?	-	-	This study
Hoolock hoolock	AMNHM 112673	MorphoSource	0.04	F	-	S6216	Urciuoli et al., 2020
Hoolock hoolock	AMNHM 112720	MorphoSource	0.05	F	-	S1206	Urciuoli et al., 2020
Hoolock hoolock	AMNHM 112983	MorphoSource	0.04	M	-	S6213	Urciuoli et al., 2020
Hoolock hoolock	AMNHM 201742	MorphoSource	0.07	F	-	S8066	Urciuoli et al., 2020
Hoolock hoolock	AMNHM 83421	MorphoSource	0.04	M	-	S6217	Urciuoli et al., 2020
Hoolock hoolock	AMNHM 83425	AMNH	0.08	F	-	S1209	Urciuoli et al., 2020
Hoolock hoolock	AMNHM 201743	AMNH	0.06	F	-	S12604	This study
Hylobates lar	MCZ 41411	MorphoSource	0.07	F	http://dx.doi.org/10.17602/M2/M2959	S1004	Urciuoli et al., 2020
Hylobates lar	MCZ 41412	MorphoSource	0.07	F	http://dx.doi.org/10.17602/M2/M2961	S1005	Urciuoli et al., 2020
Hylobates lar	MCZ 41416	MorphoSource	0.07	F	http://dx.doi.org/10.17602/M2/M2965	S1007	Urciuoli et al., 2020
Hylobates lar	MCZ 41418	MorphoSource	0.07	F	http://dx.doi.org/10.17602/M2/M2967	S1008	Urciuoli et al., 2020
Hylobates lar	MCZ 41421	MorphoSource	0.07	F	http://dx.doi.org/10.17602/M2/M2969	S1009	Urciuoli et al., 2020
Hylobates lar	MCZ 41424	MorphoSource	0.07	F	http://dx.doi.org/10.17602/M2/M3007	S1017	Urciuoli et al., 2020
Hylobates lar	MCZ 41452	MorphoSource	0.07	F	http://dx.doi.org/10.17602/M2/M3011	S1022	Urciuoli et al., 2020
Hylobates lar	AMNHM 184598	MorphoSource	0.04	M	-	S6214	This study
Hylobates lar	MCZ 41455	MorphoSource	0.07	F	-	S1024	This study
Hylobates lar	MCZ 41469	MorphoSource	0.07	F	-	S1029	This study
Lophocebus albigena	AMNHM 52596	MorphoSource	0.07	M	-	S4015	Urciuoli et al., 2020
Lophocebus albigena	AMNHM 52603	MorphoSource	0.06	F	-	S694	Urciuoli et al., 2020
Lophocebus albigena	AMNHM 52606	MorphoSource	0.07	M	-	S4005	Urciuoli et al., 2020
Lophocebus albigena	AMNHM 52607	MorphoSource	0.09	F	-	S4016	Urciuoli et al., 2020
Lophocebus albigena	AMNHM 52615	MorphoSource	0.07	F	-	S3767	Urciuoli et al., 2020
Macaca fascicularis	MCZ 12758	MorphoSource	0.06	F	http://dx.doi.org/10.17602/M2/M3028	S1032	Urciuoli et al., 2020

Macaca fascicularis	MCZ 22277	MorphoSource	0.06	F	http://dx.doi.org/10.17602/M2/M3029	S1033	Urciuoli et al., 2020
Macaca fascicularis	MCZ 23812	MorphoSource	0.06	M	http://dx.doi.org/10.17602/M2/M3030	S1034	Urciuoli et al., 2020
Macaca fascicularis	MCZ 23813	MorphoSource	0.06	F	http://dx.doi.org/10.17602/M2/M3031	S1035	Urciuoli et al., 2020
Macaca fascicularis	MCZ 35765	MorphoSource	0.06	F	http://dx.doi.org/10.17602/M2/M3033	S1037	Urciuoli et al., 2020
Mandrillus sphinx	AMNHA 9912049	MorphoSource	0.08	M	-	S5815	Urciuoli et al., 2020
Mandrillus sphinx	AMNHA 9912056	MorphoSource	0.08	M	-	S5816	Urciuoli et al., 2020
Mandrillus sphinx	AMNHM 89362	MorphoSource	0.08	M	-	S4595	Urciuoli et al., 2020
Mandrillus sphinx	AMNHM 89364	MorphoSource	0.10	M	-	S4596	Urciuoli et al., 2020
Mandrillus sphinx	AMNHM 89365	MorphoSource	0.06	M	-	S4213	Urciuoli et al., 2020
Miopithecus talapoin	MCZ 19976	MorphoSource	0.05	M	http://dx.doi.org/10.17602/M2/M5095	S1666	Urciuoli et al., 2020
Miopithecus talapoin	MCZ 23196	MorphoSource	0.05	M	http://dx.doi.org/10.17602/M2/M5094	S1665	Urciuoli et al., 2020
Miopithecus talapoin	MCZ 23197	MorphoSource	0.05	M	http://dx.doi.org/10.17602/M2/M5093	S1664	Urciuoli et al., 2020
Miopithecus talapoin	MCZ 34264	MorphoSource	0.05	F	http://dx.doi.org/10.17602/M2/M5092	S1663	Urciuoli et al., 2020
Miopithecus talapoin	MCZ 37278	MorphoSource	0.05	F	http://dx.doi.org/10.17602/M2/M5086	S1657	Urciuoli et al., 2020
Nasalis larvatus	MCZ 37342	MorphoSource	0.07	F	http://dx.doi.org/10.17602/M2/M5079	S1653	Urciuoli et al., 2020
Nasalis larvatus	MCZ 41555	MorphoSource	0.07	F	http://dx.doi.org/10.17602/M2/M5059	S1644	Urciuoli et al., 2020
Nasalis larvatus	MCZ 41559	MorphoSource	0.07	F	http://dx.doi.org/10.17602/M2/M5057	S1577	Urciuoli et al., 2020
Nasalis larvatus	MCZ 41560	MorphoSource	0.07	F	http://dx.doi.org/10.17602/M2/M5056	S1642	Urciuoli et al., 2020
Nasalis larvatus	MCZ 41562	MorphoSource	0.07	F	http://dx.doi.org/10.17602/M2/M5055	S1641	Urciuoli et al., 2020
Pan paniscus	AMNHM 86857	AMNH	0.12	F	-	-	Urciuoli et al., 2020
Pan paniscus	IPS9033	CENIEH	0.07	F	-	-	Urciuoli et al., 2020
Pan paniscus	MCZ 38018	MorphoSource	0.09	M	http://dx.doi.org/10.17602/M2/M4399	S1333	Urciuoli et al., 2020
Pan paniscus	MCZ 38019	MorphoSource	0.09	F	http://dx.doi.org/10.17602/M2/M4398	S1332	Urciuoli et al., 2020
Pan paniscus	MCZ 38020	MorphoSource	0.10	F	http://dx.doi.org/10.17602/M2/M4397	S1331	Urciuoli et al., 2020
Pan sp.	ESFR 50001988	ESFR	0.05	?	-	-	This study
Pan sp.	ESFR 50001759	ESFR	0.05	?	-	-	This study
Pan sp.	ESFR 50001797	ESFR	0.02	?	-	-	This study
Pan sp.	ESFR 50002604	ESFR	0.05	?	-	-	This study
Pan sp.	ESFR 50001738	ESFR	0.05	?	-	-	This study
Pan sp.	ESFR 50001754	ESFR	0.05	M	-	-	This study

Pan troglodytes	AMNHM 167342	MorphoSource	0.09	M	-	S5129	Urciuoli et al., 2020
Pan troglodytes	AMNHM 167344	MorphoSource	0.11	M	-	S5313	Urciuoli et al., 2020
Pan troglodytes	AMNHM 51204	MorphoSource	0.08	M	-	S4610	Urciuoli et al., 2020
Pan troglodytes	IPS5698	CENIEH	0.08	M	-	-	Urciuoli et al., 2020
Pan troglodytes	MCZ 17702	MorphoSource	0.10	F	http://dx.doi.org/10.17602/M2/M4395	S1330	Urciuoli et al., 2020
Pan troglodytes	MCZ 23167	MorphoSource	0.11	F	http://dx.doi.org/10.17602/M2/M4390	S1326	Urciuoli et al., 2020
Pan troglodytes	MCZ 26847	MorphoSource	0.10	F	http://dx.doi.org/10.17602/M2/M4389	S1325	Urciuoli et al., 2020
Pan troglodytes	ESFR 50001793	ESFR	0.05	F	-	-	This study
Pan troglodytes	ESFR 50001795	ESFR	0.05	?	-	-	This study
Pan troglodytes	ESFR 50001796	ESFR	0.05	?	-	-	This study
Pan troglodytes	ESFR 50001799	ESFR	0.05	M	-	-	This study
Pan troglodytes	MCZ 37260	MCZ	0.10	F	-	S1323	This study
Pan troglodytes	MCZ 46414	MCZ	0.08	F	-	S1322	This study
Pan troglodytes	MCZ 46415	MCZ	0.09	F	-		This study
Papio anubis	AMNHM 52677	MorphoSource	0.09	M	-	S4027	Urciuoli et al., 2020
Papio anubis	MCZ 17342	MorphoSource	0.11	M	http://dx.doi.org/10.17602/M2/M4885	S1615	Urciuoli et al., 2020
Papio anubis	MCZ 26473	MorphoSource	0.10	F	http://dx.doi.org/10.17602/M2/M4890	S1618	Urciuoli et al., 2020
Papio anubis	MCZ 31619	MorphoSource	0.11	F	http://dx.doi.org/10.17602/M2/M4892	S1620	Urciuoli et al., 2020
Papio anubis	MCZ BOM 8466	MorphoSource	0.08	M	http://dx.doi.org/10.17602/M2/M4889	S1617	Urciuoli et al., 2020
Piliocolobus badius	MCZ 24080	MorphoSource	0.08	M	http://dx.doi.org/10.17602/M2/M2892	S947	Urciuoli et al., 2020
Piliocolobus badius	MCZ 24775	MorphoSource	0.09	M	http://dx.doi.org/10.17602/M2/M2893	S948	Urciuoli et al., 2020
Piliocolobus badius	MCZ 24793	MorphoSource	0.08	F	http://dx.doi.org/10.17602/M2/M2894	S949	Urciuoli et al., 2020
Piliocolobus badius	MCZ 25627	MorphoSource	0.08	M	http://dx.doi.org/10.17602/M2/M2895	S950	Urciuoli et al., 2020
Piliocolobus badius	MCZ 25631	MorphoSource	0.09	M	http://dx.doi.org/10.17602/M2/M2896	S951	Urciuoli et al., 2020
Pongo sp.	IPS10647	CENIEH	0.08	F	-	-	Urciuoli et al., 2020
Pongo sp.	IPS10651	CENIEH	0.08	F	-	-	Urciuoli et al., 2020
Pongo sp.	IPS9031	CENIEH	0.08	F	-	-	Urciuoli et al., 2020
Pongo sp.	IPSSN	CENIEH	0.08	F	-	-	Urciuoli et al., 2020
Pongo sp.	MHNTZOO 201108	PSU	0.04	?	-	-	Urciuoli et al., 2020

Pongo sp.	SENCK 1576UU	PSU	0.01	?	-	-	Urciuoli et al., 2020
Pongo sp.	ESRF 50001801	ESFR	0.05	M	-	-	This study
Pongo sp.	SENCK 6782	PSU	0.01	?	-	-	This study
Presbytis hosei	MCZ 35621	MorphoSource	0.08	F	http://dx.doi.org/10.17602/M2/M4611	S1455	Urciuoli et al., 2020
Presbytis hosei	MCZ 37370	MorphoSource	0.08	F	http://dx.doi.org/10.17602/M2/M4610	S1454	Urciuoli et al., 2020
Presbytis hosei	MCZ 37371	MorphoSource	0.08	M	http://dx.doi.org/10.17602/M2/M4609	S1453	Urciuoli et al., 2020
Presbytis hosei	MCZ 37372	MorphoSource	0.08	F	http://dx.doi.org/10.17602/M2/M4608	S1452	Urciuoli et al., 2020
Presbytis hosei	MCZ 37772	MorphoSource	0.08	F	http://dx.doi.org/10.17602/M2/M4607	S1451	Urciuoli et al., 2020
Presbytis rubicunda	MCZ 22276	MorphoSource	0.08	M	http://dx.doi.org/10.17602/M2/M4557	S1423	Urciuoli et al., 2020
Presbytis rubicunda	MCZ 35704	MorphoSource	0.08	F	http://dx.doi.org/10.17602/M2/M4552	S1419	Urciuoli et al., 2020
Presbytis rubicunda	MCZ 35705	MorphoSource	0.08	F	http://dx.doi.org/10.17602/M2/M4551	S1418	Urciuoli et al., 2020
Presbytis rubicunda	MCZ 35706	MorphoSource	0.08	F	http://dx.doi.org/10.17602/M2/M4556	S1422	Urciuoli et al., 2020
Presbytis rubicunda	MCZ 35712	MorphoSource	0.08	M	http://dx.doi.org/10.17602/M2/M4555	S1421	Urciuoli et al., 2020
Symphalangus syndactylus	AMNHM 102724	MorphoSource	0.06	M	-	S5810	Urciuoli et al., 2020
Symphalangus syndactylus	AMNHM 106583	AMNH	0.08	F	-	-	Urciuoli et al., 2020
Symphalangus syndactylus	MCZ 36031	MorphoSource	0.08	M	http://dx.doi.org/10.17602/M2/M4444	S1359	Urciuoli et al., 2020
Symphalangus syndactylus	MCZ 36032	MorphoSource	0.07	F	http://dx.doi.org/10.17602/M2/M4443	S1358	Urciuoli et al., 2020
Symphalangus syndactylus	EA 258	MorphoSource	0.11	?	-	S15647	This study
Symphalangus syndactylus	ESFR 50001912	ESFR	0.02	?	-	-	This study
Theropithecus gelada	AMNHM 19549	MorphoSource	0.08	M	-	S4588	Urciuoli et al., 2020
Theropithecus gelada	AMNHM 238034	MorphoSource	0.12	F	-	S4589	Urciuoli et al., 2020
Theropithecus gelada	AMNHM 60568	MorphoSource	0.08	M	-	S4042	Urciuoli et al., 2020
Theropithecus gelada	AMNHM 80126	MorphoSource	0.09	M	-	S4065	Urciuoli et al., 2020
Theropithecus gelada	AMNHM 90309	MorphoSource	0.09	M	-	S4075	Urciuoli et al., 2020
Trachypithecus cristatus	MCZ 35567	MorphoSource	0.05	F	http://dx.doi.org/10.17602/M2/M4439	S1355	Urciuoli et al., 2020
Trachypithecus cristatus	MCZ 35584	MorphoSource	0.05	F	http://dx.doi.org/10.17602/M2/M4436	S1353	Urciuoli et al., 2020
Trachypithecus cristatus	MCZ 35586	MorphoSource	0.05	F	http://dx.doi.org/10.17602/M2/M4435	S1352	Urciuoli et al., 2020
Trachypithecus cristatus	MCZ 35597	MorphoSource	0.05	F	http://dx.doi.org/10.17602/M2/M4433	S1351	Urciuoli et al., 2020
Trachypithecus cristatus	MCZ 35603	MorphoSource	0.05	F	http://dx.doi.org/10.17602/M2/M4431	S1350	Urciuoli et al., 2020
Oreopithecus bambolii	BAC 208	NMB	0.03	?	http://dx.doi.org/10.17602/M2/M1664	S45464	Urciuoli et al., 2020

Australopithecus sp.	StW 573	DNMNH	0.09	F	pending	S20126	Urciuoli et al., 2020
Australopithecus sp.	StW 578	DNMNH	0.07	?	pending	S20125	Urciuoli et al., 2020
Nacholapithecus kerioi	BG 42744	NMK	0.05	?	http://dx.doi.org/10.17602/M2/M166427	S45493	This study
Hispanopithecus laietanus	IPS18000	CENIEH	0.03	?	http://dx.doi.org/10.17602/M2/M126217	S32817	This study
Rudapithecus hungaricus	RUD 77R	MPIEV	0.01	F	http://dx.doi.org/10.17602/M2/M126214	S32814	This study
Rudapithecus hungaricus	RUD 77L	MPIEV	0.01	F	http://dx.doi.org/10.17602/M2/M126215	S32814	This study
Rudapithecus hungaricus	RUD 200	MPIEV	0.01	F	http://dx.doi.org/10.17602/M2/M126216	S32816	This study

Table S4. Individual scores for all the principal components (bgPC) yielded by the between-group principal components analysis (bgPCA) of deformation-based 3DGM of vestibular shape for hominoids, using extant hominoid genera (i.e., *Homo*, *Gorilla*, *Pongo*, *Pan*, *Hylobates*, *Symphalangus*, and *Hoolock*) as grouping factor. The variance explained by each bgPC is reported within parentheses. Composition of the extant (n = 77) and fossil (n = 8) sample used for the analysis restricted to hominoid taxa.

ID	Taxon	bgPC1 (40.76%)	bgPC2 (33.74%)	bgPC3 (11.07%)	bgPC4 (8.5%)	bgPC5 (3.66%)	bgPC6 (2.27%)
StW573	*Australopithecus* sp.	1.3382732	-0.6634555	0.6212176	-0.3267709	0.2880409	-0.7897531
StW578	*Australopithecus* sp.	2.5763640	-1.6707594	-0.9761788	-0.1106569	0.0130315	-0.0855152
AMNHA999686	*Gorilla gorilla*	0.3137984	1.5395531	0.5476009	-1.1685954	0.3772195	-0.3420127
AMNHA999687	*Gorilla gorilla*	1.4569229	1.8336002	1.1308304	-1.1804031	0.5454415	-0.1286459
AMNHM167338	*Gorilla gorilla*	0.2726503	1.4155719	1.7905287	-1.1587084	-0.1816552	0.3381696
AMNHM54356	*Gorilla gorilla*	2.2663033	2.4482984	-0.7093243	-0.4792158	0.4292925	-0.5571369
ESFR50001994	*Gorilla gorilla*	1.4309570	1.6591508	-0.1699655	-1.0162740	0.3417946	-0.1622657
MCZ14750	*Gorilla gorilla*	0.5972012	2.0898448	1.3754468	-0.9625735	0.8538613	0.2444910
MCZ17684	*Gorilla gorilla*	-0.2344109	1.4640772	1.4447730	-1.5305631	0.2435803	-0.0169845
MCZ26850	*Gorilla gorilla*	1.5832453	1.5628506	1.2004216	-0.7940395	0.6535348	-0.1539377
MCZ37264	*Gorilla gorilla*	-0.4177107	1.5510936	1.9099210	-0.6656547	0.6288634	-0.1264012
MCZ37625	*Gorilla gorilla*	0.5801500	2.1427338	1.3400916	-0.9938100	0.8444579	0.2596263
MCZ49006	*Gorilla gorilla*	0.7030849	2.0788497	2.0123121	-0.5636038	0.3146633	-0.0797444
IPS18000	*Hispanopithecus laietanus*	1.8936129	-0.2719603	0.0411819	0.6268859	-0.0845936	0.3771966
EMBR121	*Homo sapiens*	1.8027346	-1.8085839	0.6070075	-0.6522354	0.6194173	-0.4809867
EMBR179	*Homo sapiens*	1.4650783	-3.0109084	-0.2586061	-0.2613913	0.0224463	0.3156086
EMBR212	*Homo sapiens*	2.3546135	-3.5844536	0.5211053	0.6460556	0.9045449	0.2465241
EMBR281	*Homo sapiens*	2.4830380	-3.0436689	-0.0800687	-0.5388172	0.4544495	-0.1842686
EMBR473	*Homo sapiens*	2.0893947	-3.3359158	-0.5027434	-0.0145984	0.1486939	-0.3173582
EMBR479	*Homo sapiens*	1.2494006	-2.0906183	0.5502618	-0.5851786	0.2333492	-0.2791741
EMBR583	*Homo sapiens*	1.9568233	-3.1148782	-0.4715052	-0.2888287	-0.2292497	0.0670015
F01	*Homo sapiens*	0.8925617	-2.5079848	0.0640081	-0.3641263	-0.1998405	0.2844841
F03	*Homo sapiens*	1.9459691	-3.4910926	-0.6573660	-0.5122909	0.0614192	-0.0413988
F04	*Homo sapiens*	0.9273597	-2.7668340	0.1332824	-0.1619039	-0.1646234	0.5419049
F05	*Homo sapiens*	2.1064765	-2.5466356	0.0036455	-0.2869690	0.3254311	-0.2639593

F06	*Homo sapiens*	2.4252385	-3.0222423	-0.5675022	-0.2450268	0.4642186	-0.4224578
AMNH201743	*Hoolock hoolock*	-1.5827514	-0.3761531	-0.3940247	-0.9472469	-1.2512374	-0.8348292
AMNHM112673	*Hoolock hoolock*	-1.8726856	-0.1598028	-0.4912032	-0.7345257	-0.4375065	-0.7603535
AMNHM112720	*Hoolock hoolock*	-1.9588243	-0.2875319	0.1935174	-0.4589063	-0.2223387	-0.7418477
AMNHM112983	*Hoolock hoolock*	-1.3656768	-0.2010666	-0.2860088	-1.0989523	-1.2589159	-1.0487105
AMNHM201742	*Hoolock hoolock*	-2.2283294	-0.0314326	0.0646998	-0.9394124	-0.8067232	-0.1960586
AMNHM83421	*Hoolock hoolock*	-1.4870402	-0.3487819	0.0420548	-1.1135738	-1.3618881	-1.0502255
AMNHM83425	*Hoolock hoolock*	-2.0876545	-1.0382619	-0.0656396	-0.9056551	-1.2467934	-0.3141687
AMNHM184598	*Hylobates lar*	-2.7998407	-0.2192540	-1.4737985	-0.3011830	0.5300182	-0.4166405
MCZ41411	*Hylobates lar*	-2.2250244	0.0002347	-0.7090184	0.6049438	0.9406985	-0.1187557
MCZ41412	*Hylobates lar*	-2.5266859	-0.4553475	-0.7905596	0.4252711	0.4995864	-0.4965751
MCZ41416	*Hylobates lar*	-3.6975970	-0.5139974	-0.3379045	0.6942158	0.8875791	0.0057917
MCZ41418	*Hylobates lar*	-3.1676492	-0.2029184	-0.0692441	0.2760012	0.5208797	-0.1671867
MCZ41421	*Hylobates lar*	-2.7757573	-0.4584324	-0.3267795	0.4557397	0.9461023	-0.2417524
MCZ41424	*Hylobates lar*	-2.3277271	-0.2637354	-0.9606589	0.2866966	1.0583153	-0.4359539
MCZ41452	*Hylobates lar*	-2.5470117	-0.1386758	-0.2696538	0.7369511	0.9803932	0.0686923
MCZ41455	*Hylobates lar*	-3.4504785	-0.5824691	-0.4703190	0.5072662	0.6112690	0.1155685
MCZ41469	*Hylobates lar*	-3.2409270	-0.1375783	0.6087417	0.6935175	0.8757233	0.1482708
BG42744	*Nacholapithecus kerioi*	-0.4642447	0.1359874	0.1076864	0.3255132	-0.3597446	0.0559937
BAC208	*Oreopithecus bambolii*	-0.2997381	0.0992835	-1.6603925	-1.0422202	-0.9970555	-0.1077210
AMNHM86857	*Pan paniscus*	0.6219677	0.0751903	1.0457679	0.7286966	-0.5199285	0.4155006
IPS9033	*Pan paniscus*	-0.0488700	-0.5035698	0.5699902	1.3347924	-0.0107562	0.5513203
MCZ38018	*Pan paniscus*	-0.4272007	0.3216974	0.6081783	0.5445969	-0.6332861	-0.0351403
MCZ38019	*Pan paniscus*	-0.1278585	0.5547184	0.3958990	0.5483718	-0.6500677	0.0403460
MCZ38020	*Pan paniscus*	1.4736445	0.4511601	0.3466141	0.7955150	-0.1223949	-0.4878229
ESFR50001988	*Pan* sp.	0.1798163	-0.2188625	0.0496762	0.7770419	-0.9321070	0.2670706
ESFR50001759	*Pan* sp.	0.7249979	0.2756223	0.7037410	0.2872531	-0.2327579	0.0274602
ESFR50001797	*Pan* sp.	0.8883331	0.5550743	0.4471127	1.0565885	-0.3216910	-0.6279794
ESFR50002604	*Pan* sp.	-0.1528878	0.4270550	0.2720372	1.2337790	-0.1295036	0.1708049
ESFR50001738	*Pan* sp.	0.0416432	0.2807808	1.0984640	0.7016937	-0.2966199	-0.0804702

ESFR50001754	*Pan* sp.	0.4607356	0.7827394	0.2403353	0.8727077	-0.2631552	-0.6415749
AMNHM167342	*Pan troglodytes*	0.7583596	0.4513930	0.5521876	1.2565171	0.0053606	-0.9014392
AMNHM167344	*Pan troglodytes*	0.2007911	-0.0976055	0.6292290	1.6630391	-0.0094563	0.1923988
AMNHM51204	*Pan troglodytes*	-0.0468513	1.2272948	0.5385163	0.6147403	-0.2509026	-0.4775304
ESFR50001793	*Pan troglodytes*	1.7287895	0.1397799	-0.2556778	1.0994647	-0.7619089	0.4469822
ESFR50001795	*Pan troglodytes*	0.8174869	0.9630190	0.0314446	0.8466524	-0.0789189	0.4357785
ESFR50001796	*Pan troglodytes*	2.1027219	0.5392616	-0.1731636	0.8772582	0.0235053	-0.0340047
ESFR50001799	*Pan troglodytes*	1.2512361	-0.0943425	0.0549321	0.6209725	-0.1257386	0.1548743
IPS5698	*Pan troglodytes*	0.0375824	0.4039856	-0.3606590	0.9928748	-0.3554733	-0.2075464
MCZ23167	*Pan troglodytes*	0.1064227	1.1707078	1.6035775	1.2783395	0.0196043	0.1684895
MCZ37260	*Pan troglodytes*	-0.0883370	1.0366506	0.7424941	1.3207423	0.0315792	0.0234912
MCZ46414	*Pan troglodytes*	-0.5454593	0.6858963	1.0035701	1.0256316	-0.3949361	0.7238880
MCZ46415	*Pan troglodytes*	0.6021587	0.3746121	0.0049062	1.0406770	0.0009213	0.1318657
ESRF50001801	*Pongo* sp.	2.0235351	1.9759838	-2.8626699	-0.8276244	-0.0814874	-0.1284787
IPS10647	*Pongo* sp.	2.6059094	1.1422423	-2.0399729	-0.0076384	-0.1448368	0.2994378
IPS10651	*Pongo* sp.	1.3771335	1.3794436	-2.8231520	-0.4959235	-0.1633515	0.1785825
IPS9031	*Pongo* sp.	1.0489164	2.4688540	-2.1901255	0.1525544	0.5469639	0.5177789
IPSSN	*Pongo* sp.	1.3275634	1.9492827	-1.3002212	-0.0324717	0.1108408	-0.2275310
MHNTZOO201108	*Pongo* sp.	1.4011301	1.9326695	-2.5913898	-0.0161196	-0.2795580	-0.0651892
SENCK1576	*Pongo* sp.	1.2013025	1.8433926	-1.7647592	0.1653941	-0.2196811	-0.0703733
SENCK6782	*Pongo* sp.	1.6381174	1.1397677	-1.0363457	-0.6856401	-0.0872838	0.3819519
RUD200	*Rudapithecus hungaricus*	0.4360545	0.0825615	-0.1778371	-0.7312362	-0.2272576	-0.1377664
RUD77L	*Rudapithecus hungaricus*	0.1943000	-0.4290993	-0.7934884	-0.7418348	-0.7369641	0.7086102
RUD77R	*Rudapithecus hungaricus*	0.2584431	-0.7458323	-0.5197980	-0.6046092	-0.9355201	0.9187386
AMNHM102724	*Symphalangus syndactylus*	-1.2378044	-1.3517852	-0.5378909	-0.6381418	-0.4315750	1.0004973
AMNHM106583	*Symphalangus syndactylus*	-2.1167431	0.5430253	0.0930548	-0.6285219	-0.2313290	0.6435202
EA258	*Symphalangus syndactylus*	-1.5619680	-0.4898104	0.3057531	-0.8624782	-0.5674299	1.4292011
ESFR50001912	*Symphalangus syndactylus*	-1.7267945	-0.1824883	0.1079608	-1.3928622	-0.5421532	0.7087465
MCZ36031	*Symphalangus syndactylus*	-2.7230455	-1.0591925	-0.1513939	-0.3936643	-0.5639739	1.5367528
MCZ36032	*Symphalangus syndactylus*	-2.7256941	-1.1402468	1.1636228	-0.2572034	-0.2929850	1.2819981

SI References

1. A. Urciuoli *et al.*, The evolution of the vestibular apparatus in apes and humans. *eLife* **9**, e51261 (2020).

Chapter 6:
Discussion

Chapter 6. Discussion

6.1. Geometric morphometric analyses of semicircular canal shape

6.1.1. Landmark-based approaches

The technological advances achieved at the end of the 20th century in computed tomography have enabled the analysis of inner anatomy in a way that was previously precluded for fossils. This is the case of the inner ear bony labyrinth. During the late 1990s and throughout the 2000s, a great amount of attention was devoted to the inner ear morphology in mammals, especially primates (see Section 1.3). Early morphometric analyses defined a number of linear measurements and angles to describe the three-dimensional labyrinthine morphology (Spoor,1993; Spoor & Zonneveld, 1998; Spoor et al., 2003). Such analyses were originally limited to the plane of scanning (XY plane) due to inaccuracy in the third dimension caused by the anisotropic voxel size (always larger along the Z-axis; Spoor & Zonneveld, 1995) characteristic of early medical CT scans. Traditional morphometric analyses (based on linear measurements and shape ratios) have the advantage of permitting a relatively straightforward statistical treatment of the obtained shape data. However, such approaches do not describe the complex shape of inner ear structures in sufficient detail. In addition, further inaccuracies might result from interobserver error in the measurement of metrical variables and angles, due to difficulties to standardize the orientation of inner ear structures relative to one another, as well as relative to the cranium as a whole. In spite of these caveats and the increased resolution available from modern medical CT and μCT scans—which currently enable 3D analyses even for small species—linear measurements are still largely used for convenience (see Section 1.3.3), given the availability of comparative results from the literature. As a result, more refined methods for shape analysis have remained underused in the case of the inner ear, and have only become more widespread during the last decade.

Several landmarking protocols for 3DGM analysis have been developed and successfully applied to the study of labyrinthine morphology during the last decade (Lebrun, et al., 2010; Gunz, et al., 2012; Mennecart & Costeur, 2016; Ponce de León, et al., 2018). However, determining the optimal setup to adequately capture inner ear shape variation without being overly complex is not a trivial task. The landmark set designed by Lebrun et al. (2010), which gave rise to a number derivative protocols

(e.g., Boistel et al., 2011; Billet, et al., 2012; Lebrun et al., 2012; Alloing-Séguier et al., 2013; Schutz et al., 2014; Benoit et al., 2015; Grohé, et al., 2015; Ponce de León, et al., 2018; Morimoto et al., 2020), rely on a very limited number of landmarks (ten for the cochlea and twelve for the semicircular canals), which hardly match the complex morphology of the bony labyrinth. As a direct result, the potential for discriminating among taxa based on labyrinthine shape is restricted. In addition to the number of landmarks defined, their type is also relevant. In the case of the aforementioned protocols, they rely on Type III landmarks (sensu Bookstein, 1991). Landmarks of this type are defined on the basis of the relative orientation of bony labyrinth structures (e.g., the anterior-most point of a canal) and, thus, very affected by uncertainties related to the researcher's subjective perception of landmark position. Hence, these landmarks are affected by the same reliability issues (related to interobserver error) as linear measurements and angles.

Gunz et al. (2012) partially circumvented them by combining landmarks and semilandmarks—the latter being specifically designed for capturing curves (Gunz et al., 2005; Mitteroecker & Gunz, 2009; Gunz & Mitteroecker, 2013). This approach allows one to increase, almost at will, the number of landmarks used to capture the shape of a given 3D curve (or a patch to capture a 3D surface). Such procedures provide an increased accuracy for describing the 3D shape of complex objects (such as the semicircular canals and the cochlea). Gunz et al. (2012) defined two protocols: restricted and extended. Their restricted protocol relies on semilandmarks placed along the streamline and on the outermost margin of the canals and cochlea, plus a few additional standard landmarks identifying the starting/ending points of the canals and the ampullae. In turn, their extended protocol adds a second set of landmarks placed along the outer margin of the canals (Gunz et al., 2012). The placement of landmarks along the outermost margin of the canals is based on a rule (being 'furthest away from the vestibule') that implies the use of type III landmarks.

In a further elaboration that built on the Gunz et al.'s (2012) protocol, Mennecart and Costeur (2016) relied on both the external and internal canal courses of the canals, instead that on streamlines alone, as the latter do not provide information on the thickness of the semicircular canals. Canal thickness is certainly important for a detailed semicircular canal shape analysis (see below). However, Mennecart and Costeur's (2016) protocol (see also Mennecart et al., 2017; Costeur et al., 2018) only captures differences in thickness along a single axis of the elliptical canal cross section. Hence, it can only provide a crude proxy for differences in overall canal volume. Any methodological choice on the protocol to use should be determined by the research aims of each study, but their limitations should be explicitly considered. Gunz et al.'s (2012) simplified protocol, used in this dissertation, appears well suited to describe canal size and orientation because it is not computationally demanding and is consistently repeatable (as the streamline following the lumen centroid is computed

automatically). However, such advantages are at the expense of information on canal volume. It has been hypothesized that more complex protocols (i.e., including more landmarks) could describe semicircular canal shape in greater detail, and thus enhance the accuracy of the analysis from a taxonomic viewpoint (Mennecart & Costeur, 2016; Goswami et al., 2019; but see Cardini, 2020). A denser distribution of semilandmarks along the canals would, in all probability, enable to capture finer details of shape, but it is uncertain whether the latter would compensate for the concomitant increase in time devoted to sample preparation. Be that as it may, it is likely that, in the near future, some researchers will start using landmark patches to better describe inner ear morphology, thereby increasing to some extent the accuracy of landmark-based 3DGM methods for capturing inner ear shape differences. However, this will require the definition of homologous surfaces on the complex shape of the semicircular canals. Furthermore, the landmarking process itself will be inevitably complicated by the abundant irregularities (e.g., those caused by the connection of the nerves and vessels or by the junction with the vestibular aqueduct) on the 3D model surface.

6.1.2. Landmark- vs. deformation-based geometric morphometrics

Technical and operational considerations. Within the framework of the constantly evolving field of 3DGM, the present dissertation aimed to evaluate the viability of a recently developed deformation-based 3DGM method for studying shape variation occurring in the semicircular canals among catarrhines. In addition to comparing the reliability of this method relative to mainstream, landmark-based 3DGM for describing semicircular canal shape, both methods were also compared from an operational perspective—especially in terms of the time required by data collection and computational processing, which should carefully be considered by researchers when planning their analyses.

Both techniques have a number of preliminary steps in common, regarding the virtual extraction and preparation of semicircular canal and vestibule 3D models (see Chapter 2). However, they consistently differ in preprocessing operations and in computational time. On the one hand, most of the time required by a landmark-based 3DGM protocol precedes the analysis in a strict sense, being devoted to the computation of the canal streamlines, landmark placement, and semilandmark sliding. In contrast, the computational time required by the actual 3DGM statistical analysis (Procrustes alignment, principal components analysis, etc.) is almost negligible. In contrast, deformation analyses only require a prealignment of the surfaces with a reference mesh, which is much less time demanding—although the time required increases proportionally to the number of faces of the analyzed meshes. As a down side, deformation-based 3DGM is much more demanding in terms of

computational time and power, even though both have been largely reduced with the latest version of the Deformetrica software (Bône, et al., 2018). The first computations ran in the framework of this dissertation (using cores with a CPU architecture) lasted approximately a week using Deformetrica 3 software in the CALMIP (Toulouse, France) facility. In contrast, time was greatly reduced (to about one hour) by running the analysis (using cores with a GPU architecture) with Deformetrica 4 in the MinoTauro cluster at the Barcelona Supercomputing Center (BSC, Barcelona, Spain). This huge difference in computational time was caused both by the use of different types of processor architectures (it has been ascertained that GPU represents the best option of computations with Deformetrica; Bône et al., 2018) and by the code optimization implemented in Deformetrica 4 relative to previous versions of the same software. Nevertheless, landmark-based 3DGM is still much faster and has the advantage of being readily computable on most present-day personal computers. In contrast, the use of Deformetrica (even in workstation-level computers) is currently restricted to computations with a very limited number of surfaces.

In terms of shape data topology, the output obtained using both techniques can be structured in either a $k \times n \times d$ array—where k is the number of points, d is the number of dimensions (three in three-dimensional analyses), and n is the sample size—or a $n \times m$ matrix, where n is the sample size and m the number of variables. This topology enables the use of the same type of statistical analysis that are currently available for landmark-based 3DGM for inspecting patterns of shape variation based on deformation data. It is noteworthy that the number of variables analyzed for deformation-based shape data is, as a general rule, considerably larger than that of landmark-based 3DGM, hence implying a greater amount of computational time. While this could be negligible for running most analyses (as they can be concluded within seconds/minutes for both techniques), the difference for some recursive tests (such as cross-validated bgPCA scores; Cardini & Polly, 2020) vary considerably (more than 24 h for deformation-based analyses, generally less than five minutes for landmark-based ones).

Results of landmark- and deformation-based analyses. The results of this dissertation confirm that deformation-based 3DGM is a viable option for semicircular canal and vestibule morphology, as it has already been shown for other anatomical areas (e.g., Durrleman et al., 2012a; Beaudet et al., 2016a; Zanolli et al., 2018; Braga et al., 2019b; Pan et al., 2019). Furthermore, this methodological approach has proven particularly useful for capturing differences in volumetric proportions and the relative size of the canals, as well as their shape and orientation. At the same time, deformation techniques appear less prone to interobserver biases than standard landmark-based 3DGM, since most of the preprocessing required is done automatically and thus prevents possible inaccuracies arising from the identification of homologous

landmarks. However, given the much longer time required to perform the computations, deformation-based analyses should be carefully planned—particularly because the use of GPU cluster computers is highly recommended for increasing the speed of the analyses.

Based on the results of this dissertation for the semicircular canals, reported in Chapter 3, both landmark- and deformation-based 3DGM provide a satisfactory discrimination among a priori defined groups, confirming that both approaches are suitable, in general terms, for the study of this anatomical area. However, the results are not entirely comparable between the two approaches in terms of morphospace. Differences mostly relate to the position of hylobatids and *Oreopithecus* relative to hominids (they overlap with hominids only in the case of landmark-based 3DGM). This discrepancy is caused by the particular landmarking design employed for landmark-based analysis in this dissertation, following Gunz et al. (2012), as explained above. Since this protocol only uses semilandmarks to describe the canal streamlines, the analysis is more sensitive to differences in canal trajectory and relative positioning, but it does not capture differences related to canal width. The bivariate analyses performed in Chapters 3 and 5 confirm that the volumetric proportions of the semicircular canals readily distinguish extant hominids from other anthropoids, thus being of utmost importance for evaluating the phylogenetic position of extinct taxa. This is not to say that such differences could not be captured with a suitable landmarking protocol, which would nevertheless require using surface patches for each canal and for the common crus. The problem is that, by directly applying the mainstream landmarking protocol, such differences remained unnoticed in previous works. In contrast, the direct comparison of continuous surfaces (Durrleman et al., 2012a,b, 2014; Beaudet et al., 2016a; Zanolli et al., 2018; Braga et al., 2019b; Pan et al., 2019), as allowed by the deformation-based approach, automatically integrates such an aspect of shape variation, thereby eliminating the biases related to the particular design of the landmarking protocol selected by each researcher.

6.2. Semicircular canal shape: Phylogenetic implications

6.2.1. Phylogenetic signal

To the best of my knowledge, this is the first comprehensive study on the phylogenetic signal embedded in semicircular canal and vestibule shape among anthropoids. Several studies hypothesized that characters of the inner ear morphology, such as those of the surrounding temporal bone (Lockwood, et al., 2004), could be used for assessing phylogenetic relationships among primates (Spoor, 1993; Spoor & Zonneveld, 1998; Hublin, et al., 1996; Rook et al., 2004) and other mammals

(Ekdale, 2013; Grohé, et al., 2015; Mennecart & Costeur, 2016; Mennecart, et. al., 2017; Boscaini, et. al., 2018). However, during the last decades the analysis of semicircular canal shape has been mainly focused on providing locomotor inferences (e.g., Spoor, et al., 2007; see also Section 1.3). The few previous phylogenetically-oriented analyses of canal morphology (e.g., Lebrun, et al., 2010; Gunz, et al., 2012; Le Maître, et al., 2017; Schwab et al., 2019) were exploratory and did not included enough taxa for a proper assessment of phylogenetic signal. In addition, the use and the interpretation of the Blomberg's K statistics (and its multivariate expression, K_{mult}) in some of these studies has been inaccurate. Previous analyses aimed to track the variation of phylogenetic signal at different taxonomic ranks, and accordingly K was iteratively computed for a number of subsets of the total sample (Grohé, et al., 2016, 2017; Coutier, et al., 2017; Le Maître, et al., 2017; Schwab, et al., 2019; Morimoto, et al., 2020). This practice should be discouraged because the statistical power of the K statistic rapidly drops as the number of included taxa is reduced, with a suggested minimum threshold of $n \geq 20$ for obtaining reliable results (Blomberg et al., 2003).

The results reported in Chapters 3 and 4 demonstrate that major anthropoid taxa can be distinguished by means of semicircular canal morphology, with clear differences not only among platyrrhines, cercopithecoids, hylobatids, and hominids, but also among New World monkey and, particularly, great ape genera. The computed phylogenetic signal is significant for the entire variance, irrespective of the 3DGM approach used. This confirms previous results obtained for the entire inner ear (i.e., including the cochlea) in strepsirrhines (Lebrun, et al., 2010), anthropoids (Morimoto, et al., 2020), and platyrrhines (del Río et al., 2020), but is at odds with previous results for hominoids (Le Maître, et al., 2017). The phylogenetic signal results obtained in this dissertation match a model of evolution that, in most cases, closely adheres to a random-walk (i.e., Brownian motion), in accordance with recent results retrieved for the semicircular canals of platyrrhines (del Río, et al., 2020). This pattern does not hold for other mammalian groups such as cetaceans (Costeur, et al., 2018) and various carnivorans (Grohé, et al., 2016; 2018; Schwab, et al., 2019), where a value of $K < 1$ might reflect homoplasy. As explained in Chapter 4, a figure of $K < 1$ was obtained for differences in relative canal orientation (particularly, for the angle between the anterior and posterior canals), thus suggesting a possible relationship with function. Based on canal mechanics (Muller & Verhagen, 2002a-c), Gonzales et al. (2019) proposed a link between the amplitude of the angle formed by the vertical canals and locomotion, such that species with a more obtuse angle would display increased amounts of suspensory behaviors. However, the amount of variance related to such a morphology is very small. All in all, the results for phylogenetic signal suggest that the shape of the semicircular canals represents a fruitful source of phylogenetically informative characters that may be used in formal cladistic analysis.

6.2.2. The evolution of semicircular canals in anthropoids

Previous studies on inner ear morphology in mammals demonstrated that higher taxa can be distinguished on the basis of shared derived characters of the bony labyrinth (e.g., Ekdale, 2013). Following these encouraging results, more detailed studies investigated inner ear shape in search of synapomorphies for a number of mammalian clades (Macrini et al., 2013; Billet et al., 2015; Ekdale, 2016; Mennecart & Costeur 2016; Racicot et al., 2016; Mennecart et al., 2017). Within the context of this dissertation, an exploratory analysis based on a sample of anthropoid species was performed, in which anthropoid semicircular canal variation was inspected to ascertain the presence of a phylogenetic signal (Chapter 3). In the same analysis, a number of discrete characters (Chapter 3, Table 8) were proposed as potential synapomorphies of various hominoid clades, based on the condition of the analyzed taxa as well as the reconstructed LCAs for these clades. These characters were subsequently refined based on additional extant and fossil anthropoids (Chapter 4). According to the results of the latter chapter, a total of seven characters of the semicircular canals and vestibule are formally defined in a cladistic fashion to summarize phylogenetically-informative differences among anthropoid primates (Table 6.1).

Table 6.1. Discrete characters of semicircular canal (SC) and vestibule morphology as coded in Chapter 4. See Chapter 4 Figure 11 for an illustration of the states.

#	Character statements (characters + character states)
#1	Size of the vestibule relative to the SCs: 0 = small; 1 = large.
#2	Robusticity of the SCs: 0 = slender; 1 = stout.
#3	Shape of the anterior SC: 0 = vertically compressed; 1 = rounded; 2 = elongated superiorly.
#4	Shape of the anterior portion of the anterior SC: 0 = non-projecting anterosuperiorly; 1 = anterosuperiorly projecting.
#5	Shape of the posterior SC: 0 = vertically compressed; 1 = rounded; 2 = elongated superiorly.
#6	Shape of the lateral SC ampullary portion: 0 = flat or only slightly bent superiorly; 1 = markedly bent superiorly.
#7	Length of the CC: 0 = long; 1 = intermediate; 2 = short.

Abbreviations: # = character number; SC = semicircular canals; CC = common crus.

Catarrhine synapomorphies. Only a few previous papers have analyzed the semicircular canal morphology of catarrhine primates (both extant and fossil). Such studies have been based on a very limited sample of non-hominin catarrhine species and focused on the correlation between canal size and locomotion (e.g., Spoor et al., 2007; Ryan et al., 2012) or the evolution of a single catarrhine subclade (e.g., hominins: Spoor & Zonneveld, 1998; hominoids: Le Maître et al., 2017; cercopithecoids: Beaudet et al., 2016b). From an evolutionary perspective, Spoor & Zonneveld (1998) and, more recently, Morimoto et al. (2020) concluded that monkeys (platyrrhines and cercopithecoids) and lesser apes share a rather generalized semicircular canal morphology, which most likely closely resembles the ancestral anthropoid condition.

The results of this dissertation (Chapters 3 and 5) confirm that great apes and humans are derived in semicircular canal morphology (see below), but further show that monkeys and lesser apes display a much greater variation, which cannot be simply epitomized as "generalized monkey-like shape". Indeed, among anthropoids, at least three characters (Table 6.1) broadly separate platyrrhines from catarrhines and are interpreted in this dissertation as catarrhine synapomorphies: a rounded or vertically compressed anterior canal; a rounded or posterolaterally projecting posterior canal; and a moderately long or short common crus.

Although Spoor and Zonneveld (1998) provided some data on SC shape variation among anthropoids, they were limited to a number of shape indices (ratios between canal length and width) for a relatively small number of anthropoid species. Furthermore, these authors did not linger over their interpretation. The analyses provided in this dissertation, albeit overall in accordance with Spoor & Zonneveld's (1998) preliminary results, go one step beyond and enable a more refined evolutionary interpretation. In particular, the results of Chapters 3 and 4 indicate that, despite some variation within anthropoid subclades (particularly at lower taxonomic ranks), platyrrhines retain the plesiomorphic anthropoid condition (a vertically elongated anterior canal). In contrast, catarrhines are derived in morphology of the anterior canal, which is rounded in cercopithecoids (plus humans and a few *Hoolock* individuals) and vertically compressed in apes (see also below). Platyrrhines are also primitive in the possession of a vertically elongated posterior canal (both superiorly and inferiorly). Conversely, crown catarrhines generally have a rounded or even posterolaterally elongated posterior canal. There is some variability below the family rank, so that a few catarrhine species possess a slightly vertically stretched posterior canal, albeit different in shape from that of platyrrhines (the elongation is found inferiorly). The factors that might affect the shape of anterior and posterior canal are unclear. Since the subarcuate fossa—housing the petrosal lobe of the paraflocculus—opens inside the arc of the anterior canal (and sometimes partly protrudes also into that of the posterior canal), some studies have suggested a possible relationship between canal shape (especially that of the anterior canal) and the extension of the subarcuate fossa (Jeffery & Spoor, 2006; Jeffery et al., 2008). Indeed, catarrhines are characterized by a generally smaller fossa—even absent in hominids and in some siamang and large cercopithecoids—as compared with platyrrhines (Gannon et al., 1988; Spoor & Leakey, 1996). Although this relationship between canal shape and subarcuate fossa development has been uncritically taken for granted (Spoor et al., 2007; Silcox et al., 2009; Gonzales et al., 2019), it remains to be clarified whether the fossa would stretch the canal or merely expand into the space left available by the opening of the canal (Jeffery & Spoor, 2006; Jeffery et al., 2008). The information currently available for adult anthropoids tentatively favors the latter interpretation, since conspecific adult individuals with markedly different fossa shapes display in

contrast canals very similar in shape (Chapters 3 and 4). Further analyses quantifying the correlation between subarcuate fossa and canal shape in a large number of anthropoid species at different ontogenetic stages would be required to test the relationship between both structures.

In addition to differences in canal shape, the results reported in Chapter 4 identify a clear morphocline in the length of the common crus, from the very long common crus of platyrrhines (the plesiomorphic condition for anthropoids) to the moderately long condition of cercopithecoids, to the shortest length in hominoids. Unfortunately, unlike the shape of the canals, the length of the common crus has been largely overlooked by studies on the primate bony labyrinth (Spoor & Zonneveld, 1998; Ekdale, 2013; Lee et al., 2013). In ruminants, previous analyses recovered a relatively high amount of intraspecific variability (Mennecart & Costeur, 2016). This is partly confirmed by the results obtained in Chapter 4, especially within hominoid and cercopithecoid species—which, nonetheless, always show a shorter common crus than platyrrhines. Future analyses devoted to the variation of common crus length among anthropoid primates will hopefully clarify further this issue.

Hominoid synapomorphies. As for catarrhines as a whole, the results reported in Chapters 3 and 4 allow to pinpoint some semicircular canal features that distinguish hominoids from other anthropoids. Although the first analysis of semicircular canal morphology among anthropoids led to the definition of five potential hominoid synapomorphies (Chapter 3), a more in-depth analysis based on a larger sample indicated a considerable amount of intraspecific variation for two of these characters, which were thus considered unreliable from a phylogenetic viewpoint. At the same time, an additional character (#4 in Table 6.1) synapomorphic for hominoids was defined (Chapter 4). According to currently available data, the semicircular canal features synapomorphic of hominoids would include the following: a vertically compressed anterior canal; a superiorly bent ampullary portion of the lateral canal; and possibly an anterosuperiorly projecting anterior portion of the anterior canal.

The presence of a vertically compressed anterior canal is the feature that most clearly distinguishes hominoids from other anthropoids. This morphology, here proposed as a hominoid synapomorphy, was already noted (but not interpreted) by Spoor & Zonneveld (1998, Table 5) on the basis of a smaller sample (mostly including hominoids). Modern humans differ from apes in this regard and show instead a more rounded anterior canal, similar to that of cercopithecoids. Therefore, the human condition is here interpreted as a reversal to the ancestral catarrhine condition. This agrees with previous conclusions, based on linear measurements, that the morphology of *H. sapiens* is largely primitive and closer to that of large cercopithecoids (Spoor & Zonneveld, 1998).

In turn, an anterosuperiorly very projecting anterior portion of the anterior canal was also considered synapomorphic of hylobatids by Le Maître et al. (2017). These authors further suggested that the ancestral crown hominoid condition would have been characterized by a slightly anterosuperiorly projecting anterior canal, intermediate between the condition of hylobatids (very anterosuperiorly projecting) and that of great apes (non-anterosuperiorly projecting) and, thus, more closely resembling other taxa such as macaques. These conclusions are at odds with the results reported in Chapters 3–5. First, Le Maître et al. (2017) missed the fact that a hylobatid-like morphology of the anterior portion of the anterior canal is also found in orangutans (Chapter 4). Such discrepancy is likely attributable to the very reduced number of landmarks used by Le Maître et al. (2017; see Chapter 6). In addition, the anterior canal is not anterosuperiorly projecting (not even slightly) in *Macaca* (contra Le Maître et al., 2017), but rather rounded (Chapter 4). In spite of this, the morphology proposed by Le Maître et al. (2017) for the crown hominoid LCA is not at odds with the results of this dissertation. Indeed, the presence of an anterosuperiorly projecting anterior canal in both *Pongo* and hylobatids suggests that this feature might be a synapomorphy of crown hominoids as a whole, subsequently lost in hominines.

The results reported in Chapters 3 and 4 further suggest that hominoids are distinctive in the morphology of the ampullary portion of the lateral canal. Initially, this character was coded with only two states (Chapter 3): bent superiorly (in hominoids) vs. flat (in other anthropoids). However, a more refined analysis of anthropoid variation required the definition of an additional (intermediate) state, which describes the condition found in several cercopithecoid species (Chapter 4). This character did not previously receive attention in the literature, being first described in this dissertation. It should not be mistaken for the overall sinuosity of canal. Canal sinuosity—termed "canal torsion" (Spoor & Zonneveld, 1998) or "total linear deviation" (Ekdale ,2013)—refers to the deviation of a canal from a best-fit plane along its entire trajectory, which has been reported to be very variable within primate species (Spoor & Zonneveld, 1998; Ekdale, 2013). In contrast, the character as defined here only refers to the local geometry of the ampullary portion.

Hominid synapomorphies. The visual inspection of semicircular canal and vestibule morphology in anthropoids readily denotes that great apes (especially *Pongo*) and humans display stouter canals and a larger vestibule (relative to the volume of the canals) than other anthropoids (including gibbons and siamangs). These differences hold even when size-scaling is considered by means of allometric regressions between canal length and volume, which show a marked allometric grade shift in volumetric proportions between hominids and other extant anthropoids (Chapter 3). The functional interpretation of the derived hominoid condition is unclear. Spoor and Zonneveld (1998) proposed that species with fast and ample head

movements during locomotion require limited duct sensitivity (to avoid overstimulation) and a very small fast time constant (allowing a swift response to angular accelerations). Based on the biophysical models that describe how ducts perceive angular accelerations (see Chapter 1), a reduction in the sensitivity and the time required to perceive an external stimulus could be achieved by possessing long and narrow ducts (as found in the swift-moving monkeys and gibbons)—because duct length is inversely proportional to duct sensitivity, and a smaller duct lumen corresponds to a faster response (Muller, 1994; Rabbitt et al., 2004; Rabbit, 2019; see Chapter 1). Conversely, species with short ducts and large lumen would be less reactive to abrupt changes in position and posture, but more sensitive to fine movements. Although this explanation is very reasonable, caution is required when inferring duct lumen size from that of the bony canals, as previous analyses have demonstrated that the volume occupied by the ducts within the canals might be very variable (Ramprashad et al., 1984; Spoor & Zonneveld, 1998). Leaving aside functional interpretations, the evidence available for extant anthropoids suggests that the small vestibule and slender canals of hylobatids may be interpreted as a symplesiomorphy of catarrhines, with hominids being apomorphic.

The results reported in Chapter 5 indicate that extant hominid genera are quite distinctive from one another in semicircular canal morphology. The autapomorphic features that characterize each genus were not coded in a cladistic fashion because they are not phylogenetically informative when only extant genera are considered. However, some of them might prove in the future to be useful for interpreting the phylogenetic position of extinct crown great apes, such as fossil pongines. Orangutans possess a very anterosuperiorly projecting anterior canal (similar to that of hylobatids) and extremely stout canal proportions (also found, albeit to a lesser extent, in some gorillas and modern humans). Orangutans are even more distinctive owing to the possession of a very short and stout common crus, as noted previously (Spoor & Zonneveld, 1998; Le Maître et al., 2017), as well as a very deep V-shaped junction between the slender portion of the anterior and posterior canals at the common crus apex. While these features appear autapomorphic of orangutans, they might eventually prove to be synapomorphies of some of all pongines once the inner ear anatomy of orangutan's extinct relatives becomes available. For example, these features might help clarifying if *Lufengpithecus* is a very basal pongine instead of a dryopithecine, or determining what pongine genus is more closely related to orangutans. Unfortunately, no inner ears of fossil pongines are current available.

With regard to hominines, previous research based on linear measurements, shape indices, and angles suggested that extant great apes are rather homogenous in inner ear morphology (Spoor & Zonneveld, 1998). In contrast, the results reported in Chapter 5 on the basis of deformation 3DGM indicate that gorillas and chimpanzees are quite different from one another, as well as relative to humans. In particular,

modern humans appear markedly derived, not only from the condition displayed by the hominid and hominin reconstructed LCAs, but the *Pan-Homo* LCA, especially in their very large and rounded vertical canals and the more coronally oriented lateral canal. These features were previously identified as modern human autapomorphies (Spoor & Zonneveld, 1998). Gorillas display approximately the opposite condition to humans, being characterized by very small anterior and posterior canals, as well as a large laterally elongated lateral canal similar to that of some cercopithecoids. Chimpanzees and bonobos, in contrast, are very similar to one another, and display a more generalized morphology characterized by fairly stout and evenly sized canals. Interestingly, a *Pan*-like morphology is recovered not only for the hominine, but also the crown hominid LCAs, suggesting that while gorillas and hominins diverge in opposite directions, chimpanzees and bonobos retain a very plesiomorphic semicircular canal morphology among great apes and humans. As it will be discussed below, this has important implications for the interpretation of the semicircular canal morphology of extinct hominids.

6.2.3. Phylogenetic implications for Miocene catarrhines

In addition to the inspection of semicircular canal shape variation among extant anthropoids (Chapter 3), the analyses reported in Chapters 4 and 5 also include several fossil anthropoids, which enable more refined inferences about the polarity of evolutionary change. In particular, the analyzed fossils permitted a more accurate calibration of the internal nodes of the phylogeny (the ancestral states), which were used to test contrasting phylogenetic hypotheses for the studied fossil taxa. To do so, different phylogenetically informed methods were employed (see Chapter 2). In Chapter 4, indices customarily used in cladistic analyses were used to discern the most parsimonious phylogenetic hypothesis among those discussed in the previous in literature. Furthermore, the ancestral morphotypes for main crown catarrhine clades were estimated using a maximum likelihood approach applied to the shape data (Chapters 3–5). Based on these results, it was possible to reach several different conclusions for specific extinct taxa, which are discussed below.

Oreopithecus. Since its discovery at the end of the 19th century, the insular ape *Oreopithecus* has attracted a lot of attention, due to the conflicting phylogenetic signals provided by its cranial and postcranial morphology. This has led to the proposition of very disparate phylogenetic interpretations, ranging from being considered a cercopithecoid to a hominid, or even a hominin (see Section 1.1.3). In contrast, recent cladistic analyses have recovered *Oreopithecus* as a stem hominoid related to nyanzapithecids from the early and middle Miocene of Africa (Nengo et al., 2017; Gilbert et al., 2020a). The results reported in Chapters 3–5 for *Oreopithecus*

semicircular canal shape indicate a mixture of monkey-like, hominoid-like, and even great ape-like features. In particular, the flat lateral canal of *Oreopithecus* resembles the platyrrhine condition, whereas the intersection between lateral canal trajectory and posterior canal plane is closer to that of cercopithecoids. In turn, the vertically compressed anterior canal is a hominoid synapomorphy, while the stout volumetric proportions are interpreted as a synapomorphy of hominids. These results do not completely agree with those from a pioneering study of the whole bony labyrinth shape of *Oreopithecus* by Rook et al. (2004). Based on linear measurements, canal angles, and shape indices previously defined by Spoor & Zonneveld (1998), Rook et al. (2004) concluded that this taxon possessed an overall extant great ape-like morphology. The results of this dissertation indicate that *Oreopithecus* displays volumetric proportions comparable to those of great apes but that, in other aspects, it does not fit well with the variation of extant hominids, or even that of extant hominoids as a whole (Chapters 3–5).

The hominid-like volumetric proportions of the canals and the large vestibule of *Oreopithecus* have different interpretations from a phylogenetic perspective. Given that extant hominids share stout semicircular canals and an extensive vestibule, on the basis of these features *Oreopithecus* could be interpreted as a great ape, as previously argued (e.g., Moyà-Solà & Köhler, 1997; Harrison & Rook, 1997). However, the retention of more plesiomorphic (monkey-like) semicircular canal features (a flat lateral canal, whose trajectory intersects the plane of the posterior canal) suggests instead that *Oreopithecus* is not a crown hominoid. Two different explanations are possible: either the stout semicircular canals and large vestibule are a synapomorphy of *Oreopithecus* + crown hominoids that was subsequently reversed in hyobatids; or the similarities between *Oreopithecus* and hominids are homoplastic. The former possibility cannot be completely ruled out, but based on the results of recent cladistic analyses (Nengo et al., 2017; Gibert et al., 2020a) and the possession of an (apparently) independently evolved orthograde body plan, the second hypothesis is more likely. The similarities in volumetric proportions between *Oreopithecus* and extant hominids might have independently evolved due to the acquisition of a slower mode of locomotion, as suggested by its semicircular canal radius (Ryan et al., 2012). This would be in agreement with previous locomotor inferences based on the postcranial morphology that *Oreopithecus* was adapted to cautious vertical climbing (Hammond et al., 2020) and below-branch suspensory behaviors (Jungers, 1987; Sarmiento 1987; Harrison, 1991; Harrison & Rook, 1997; Russo & Shapiro, 2013). In this regard, it is also noteworthy that in some respects (large anterior and posterior canals relative to a very small lateral canal) *Oreopithecus* resembles the condition of modern humans and australopiths (Chapter 3). Given that the human condition in this regard has been interpreted as an adaptation to bipedalism (e.g., Spoor et al., 1994; Spoor & Zonneveld, 1998), the semicircular canals of *Oreopithecus* might lend some support to the

contention that this species possessed adaptations to terrestrial bipedalism (Köhler & Moyà-Solà, 1997; Rook et al., 1999). All in all, the semicircular canal morphology of *Oreopithecus* should be subjected to further scrutiny in the future, both from a phylogenetic and functional viewpoint, ideally on the basis to the as yet unpublished data available for stem hominoids such as *Ekembo* and *Nyanzapithecus*.

Epipliopithecus. The pliopithecoid *Epipliopithecus* is possibly the best represented fossil catarrhine in the European Miocene fossil record, with several partial skeletons available (Zapfe, 1958, 1961). While there is consensus that pliopithecoids are stem catarrhines (e.g., Harrison, 1987, 2013; Andrews et al., 1996; Begun, 2002, 2017; Nengo et al., 2017; Gilbert et al., 2020a), a recent cladistic analysis based on cranial and postcranial characters recovered *Epipliopithecus* as a stem hominoid, sister taxon to the dentropithecids (Alba et a.., 2015a). The analysis reported in Chapter 4 thus seeks to provide additional evidence, based on semicircular morphology, to test between these competing hypotheses. The results indicate that *Epipliopithecus* displays an overall plesiomorphic morphology relative to hominoids (as previously suggested by Morimoto et al., 2020) and lacks specific similarities with hominids, hylobatids, or hominoids as a whole Instead, *Epipliopithecus* more closely resembles extant and fossil platyrrhines, the stem anthropoid *Parapithecus*, and the stem catarrhine *Aegyptopithecus*. None of the crown hominoid synapomorphies identified for the semicircular canal morphology of hominoid are present in *Epipliopithecus* (Chapter 4), which rather resembles the reconstructed crown catarrhine LCA and appears less derived than the *Oreopithecus* in lacking a vertically compressed and anterosuperiorly projecting anterior canal and a short common crus, among others.

Epipliopithecus displays some similarities with hylobatids in the spatial arrangement of the lateral and posterior canals, as well as the angle between the latter and the anterior canal. These similarities, however, cannot be used to support a closer link with hylobatids, as proposed many decades ago (Hürzeler, 1954; Zapfe, 1958, 1961; Simons & Fleagle, 1973). The presence of a similar morphology in atelids (Spoor & Zonneveld, 1998) suggests instead that these features might have independently evolved in relation to locomotion (Gonzales et al., 2019), in agreement with previous locomotor inferences suggesting some amount of suspensory behaviors for *Epipliopithecus* (Zapfe, 1958; Fleagle, 1983; Langdon,1986; Rose, 1994; Arias-Martorell et al., 2015). Together with the lack of hominoid synapomorphies, the retention of several anthropoid symplesiomorphies (a vertically elongated posterior canal and a long common crus) supports the common view that *Epipliopithecus* precedes the cercopithecoid-hominoid divergence (e.g., Fleagle, 1984; Harrison, 1987, 2013; Andrews et al., 1996; Begun, 2002a, 2017). Interestingly, however, *Epipliopithecus* appears more derived than the propliopithecoid *Aegyptopithecus* in the possession

of a rounded anterior canal, which is otherwise synapomorphic of crown catarrhines (Chapter 4). The results of this dissertation thus lend additional support to the common view that pliopithecoids are stem catarrhines more derived than propliopithecoids, in agreement with the somewhat more derived ectotympanic morphology of *Epipliopithecus* (e.g., Harrison, 2013; Fricano, 2019).

Hispanopithecus* and *Rudapithecus. The results of the analysis of semicircular canal and vestibule morphology in the dryopithecines *Hispanopithecus* and *Rudapithecus* (Chapter 5) indicate that, despite being similar to one another, the semicircular morphology of *Hispanopithecus* and *Rudapithecus* is different enough to support, together with other anatomical differences in cranial morphology, their distinct genus status (Begun, 2009, 2013, 2015; Begun et al., 2012; Ward, 2015; contra Alba, 2012). Relative to extant hominid genera, the semicircular canal morphology of *Rudapithecus* most closely resembles that of *Pan*, even if one of the specimens analyzed falls outside the range of the latter. In contrast, the stouter canals and the relatively large anterior and posterior canals of *Hispanopithecus* appear intermediate between those of *Pan* and of *Australopithecus*, while in other respects this genus displays a combination of features that does not fill well with that of any other extant or extinct hominoid genus.

From a phylogenetic perspective, the two investigated dryopithecines display several hominid synapomorphies, in agreement with the current consensus that they are members of the great ape and human clade (Alba, 2012; Begun, 2013, 2015; Andrews, 2019). In particular, both genera appear more derived than *Nacholapithecus* from the middle Miocene of Africa—variously interpreted as a stem hominoid (Harrison, 2010; Begun, 2015; Nengo et al., 2017; Gilbert et al., 2020a) or a stem hominid (Cameron, 2004; Begun, 2010; Alba, 2012; Kunimatsu et al., 2019)—in the possession of stout canal proportions of the canals and a large vestibule. According to the results reported in Chapter 5, *Nacholapithecus* appears quite plesiomorphic as compared with extant great apes (in agreement with a previous analysis of the whole bony labyrinth; Morimoto et al., 2020), and much closer (together with *Oreopithecus*) to the inferred crown hominoid LCA. Among hominids, *Rudapithecus* appears somewhat less derived than *Hispanopithecus*, more closely resembling the crown hominid LCA. Neither *Rudapithecus* nor *Hispanopithecus* appear derived toward the orangutan condition, so that the pongine status previously advocated for these taxa by some authors (Moyà-Solà & Köhler, 1993, 1995; Köhler et al., 2001a) is not supported. However, it would be preliminary to completely rule out this hypothesis—at least, until the semicircular morphology of extinct pongines becomes available—because the extant orangutan's condition appears very autapomorphic. Be that as it may, the results reported in Chapter 5 are more consistent with dryopithecines being either stem hominids (Moyà-Solà et al., 2004, 2009b; Alba, 2012; Alba et al., 2015a) or

stem hominines (Begun et al., 1997, 2012; Begun, 2001, 2002b, 2009, 2010, 2013, 2015). This notwithstanding, as explained above the semicircular canal morphology of *Pan* is the most plesiomorphic among extant hominids—even reminiscent of that of *Nacholapithecus*, and closer to the ancestral morphotypes reconstructed for both hominids and hominines. Therefore, the similarities between dryopithecines and extant African great apes (particularly *Pan*) do not unambiguously favor a stem hominine status over a stem hominid status for *Hispanopithecus* and *Rudapithecus.* Future analyses focused on other extinct hominoids, such as *Lufengpithecus* and *Ekembo*, might help refining further ancestral state reconstructions and thus contribute to a better evaluation of the phylogenetic position of dryopithecines based on semicircular canal morphology.

Chapter 7:
Conclusions

7. Conclusions

The main conclusions of this dissertation are summarized below:

1. Deformation-based three-dimensional geometric morphometrics (3DGM) adequately captures the complex 3D shape variation of the semicircular canals (SCs). As compared with standard landmark-based 3DGM it has two advantages: it is less prone to interobserver errors; and the results are not dependent on subjective decisions taking during the design of the landmarking protocol. In particular, deformation-based 3DGM proved intrinsically more efficient in capturing differences in canal stoutness, which could only be captured by means of more complex landmarking protocols than that customarily used.
2. Both landmark- and deformation-based 3DGM results indicate that SC shape embeds strong phylogenetic signal among anthropoids and is useful to distinguish major clades and even extant hominoid genera, thus being potentially useful to test phylogenetic hypotheses for extinct taxa.
3. Combined with the SC morphology of extant taxa, the reconstruction of ancestral morphotypes for various catarrhine clades enables to determine several potentially synapomorphic characters for crown catarrhines (rounded to vertically-compressed canals; intermediate to short common crus), crown hominoids (shape of the anterior and lateral canals), and crown hominids (stout volumetric proportions of the canals and large vestibular recesses).
4. The semicircular canal and vestibule morphology of the pliopithecoid *Epipliopithecus vindobonensis* confirms the widely held view that—in agreement with evidence from other anatomical regions—this taxon is most parsimoniously interpreted as a stem catarrhine more derived than propliopithecoids, yet lacking other catarrhine and any hominoid synapomorphies. Some similarities (gap between the lateral SC trajectory and the posterior SC plane, angle between the vertical SCs) with hylobatids and atelids may be convergences related to locomotion.
5. The semicircular canals (SCs) of the enigmatic fossil ape *Oreopithecus* display a unique mosaic of plesiomorphic (platyrrhine- and stem catarrhine-like) and derived (hominoid- and even cercopithecoid-like) features. This evidence is here interpreted as indicating a likely stem hominoid status, with its stout SC volumetric proportions being independently acquired from those of hominids. However, additional information on Miocene stem hominoids would be required to conclusively discount a great ape status for *Oreopithecus*.

6. The SC morphology of the dryopithecines *Hispanopithecus* and *Rudapithecus* is consistent with their distinction at the genus rank and characterized by much stouter canals than in *Nacholapithecus*, clearly confirming their great ape status—in accordance with other anatomical areas. Although both genera more closely resemble African apes in SC morphology, the latter are largely plesiomorphic and much less derived than orangutans. Therefore, SC morphology does not conclusively favor a stem hominine vs. a stem hominid status for dryopithecines.
7. As a general conclusion, this dissertation is the first study devoted to the study of SC morphology among anthropoids by means of deformation-based 3DGM techniques. The results confirm the potential of this anatomical area for phylogenetic inference in Miocene catarrhines, by providing informative characters that can be incorporated to formal morphology-based cladistic analyses including multiple anatomical areas. Future lines of research should focus on extending this kind of research to other internal structures (cochlea and middle ear ossicles) to further contribute with additional synapomorphies that might help disentangling the still controversial phylogenetic relationships of most Miocene catarrhines.

References

References

Adams, D. C., 2014. A generalized K statistic for estimating phylogenetic signal from shape and other high-dimensional multivariate data. Syst. Biol. 63, 685–697.

Adams, D. C., Rohlf, F. J., Slice, D. E., 2004. Geometric morphometrics: ten years of progress following the "revolution". It. J. Zool. 71, 5–16.

Adams, D. C., Rohlf, F. J., Slice, D. E., 2013. A field comes of age: geometric morphometrics in the 21st century. Hystrix 24, 7–14.

Adams, D. C., Collyer, M. L., Kaliontzopoulou, A., 2019. Geomorph: Software for geometric morphometric analyses. R Package Version. https://cran.rproject.org/package=geomorph

Agustí, J., Oms, O., Piñero, P., Chochisvili, G., Bukhsianidze, M., Lordkipanidze, D., 2020. Late survival of dryopithecine hominoids in Southern Caucasus. J. Hum. Evol. 138, 102690.

Alba, D. M., 2010. Cognitive inferences in fossil apes (Primates: Hominoidea): does encephalization reflect intelligence? J. Anthropol. Sci. 88, 11–48.

Alba, D. M., 2012. Fossil apes from the vallès-penedès basin. Evol. Anthropol. 21, 254–269.

Alba, D. M., Berning, B., 2013. On the holotype and original description of the pliopithecid *Plesiopliopithecus lockeri* (Zapfe, 1960). J. Hum. Evol. 65, 338–340.

Alba, D. M., Moyà-Solà, S., 2012. A new pliopithecid genus (Primates: Pliopithecoidea) from Castell de Barberà (Vallès-Penedès Basin, Catalonia, Spain). Am. J. Phys. Anthropol. 147, 88–112.

Alba, D. M., Moyà-Solà, S., Köhler, M., Rook, L., 2001. Heterochrony and the cranial anatomy of *Oreopithecus*: some cladistic fallacies and the significance of developmental constraints in phylogenetic analysis. In: de Bonis, L., Koufos, G. D., Andrews, P. (Eds), *Hominoid Evolution and Climatic Change in Europe, Vol. 2. Phylogeny of the Neogene Hominoid Primates of Eurasia*. Cambridge: Cambridge University Press, pp. 284–315.

Alba, D. M., Moyà-Solà, S., Malgosa, A., Casanovas-Vilar, I., Robles, J. M., Almécija, S., Galindo, J., Rotgers, C., Bertó Mengual, J. V., 2010a. A new species of *Pliopithecus* Gervais, 1849 (Primates: Pliopithecidae) from the Middle Miocene (MN8) of Abocador de Can Mata (els Hostalets de Pierola, Catalonia, Spain). Am. J. Phys. Anthropol. 141, 52–75.

Alba, D. M., Fortuny, J., Moyà-Solà, S., 2010b. Enamel thickness in the Middle Miocene great apes *Anoiapithecus*, *Pierolapithecus* and *Dryopithecus*. Proc. R. Soc. B 277, 2237–2245.

Alba, D. M., Almécija S., Moyà-Solà, S., 2010c. Locomotor inferences in *Pierolapithecus* and *Hispanopithecus*: Reply to Deane and Begun (2008). J. Hum. Evol. 59, 143–149.

Alba, D. M., Moyà-Solà S, Almécija S., 2011. A partial hominoid humerus from the middle Miocene of Castell de Barberà (Vallès-Penedès Basin, Catalonia, Spain). Am. J. Phys. Anthropol. 144, 365–381.

Alba, D. M., Moyà-Solà, S., Robles, J. M., Galindo, J., 2012a. Brief communication: The oldest pliopithecid record in the Iberian Peninsula based on new material from the Vallès-Penedès Basin. Am. J. Phys. Anthropol. 147, 135–140.

Alba, D. M., Casanovas-Vilar, I., Almécija, S., Robles, J. M., Arias-Martorell, J., Moyà-Solà, S., 2012b. New dental remains of *Hispanopithecus laietanus* (Primates: Hominidae) from Can Llobateres 1 and the taxonomy of Late Miocene hominoids from the Vallès-Penedès Basin (NE Iberian Peninsula). J. Hum. Evol. 63, 231–246.

Alba, D. M., Almécija, S., Casanovas-Vilar, I., Mendez, J. M., Moyà-Solà, S., 2012c. A partial skeleton of the fossil great ape *Hispanopithecus laietanus* from Can Feu and the mosaic evolution of crown-hominoid positional behaviors. PLoS One 7, e39617.

Alba, D. M., Fortuny, J., Pérez de los Ríos, M., Zanolli, C., Almécija, S., Casanovas-Vilar, I., Robles, J. M., Moyà-Solà, S., 2013. New dental remains of *Anoiapithecus* and the first appearance datum of hominoids in the Iberian Peninsula. J. Hum. Evol. 65, 573–584.

Alba, D. M., Delson, E., Carnevale, G., Colombero, S., Delfino, M., Giuntelli, P., Pavia, M., Pavia, G., 2014. First joint record of *Mesopithecus* and cf. *Macaca* in the Miocene of Europe. J. Hum. Evol. 67, 1–18.

Alba, D. M., Almécija, S., DeMiguel, D., Fortuny, J., Pérez de los Ríos, M., Pina, M., Robles, J. M., Moyà-Solà, S., 2015a. Miocene small-bodied ape from Eurasia sheds light on hominoid evolution. Science 350, aab2625.

Alba, D. M., Montoya, P., Pina, M., Rook, L., Abella, J., Morales, J., Delson, E., 2015b. First record of *Mesopithecus* (Cercopithecidae, Colobinae) from the Miocene of the Iberian Peninsula. J. Hum. Evol. 88, 1–14.

Alba, D. M., Casanovas-Vilar, I., Garcés, M., Robles, J. M., 2017. Ten years in the dump: An updated review of the Miocene primate-bearing localities from Abocador de Can Mata (NE Iberian Peninsula). J. Hum. Evol. 102, 12–20.

Alba, D. M., Garcés, M., Casanovas-Vilar, I., Robles, J. M., Pina, M., Moyà-Solà, S., Almécija, S., 2019. Bio-and magnetostratigraphic correlation of the Miocene primate-bearing site of Castell de Barberà to the earliest Vallesian. J. Hum. Evol. 132, 32–46.

Albrecht, G. H., 1992. Assessing the affinities of fossils using canonical variates and generalized distances. Hum. Evol. 7, 49–69.

Allen, K. L., McCrossin, M. L. Functional morphology of the *Kenyapithecus* hand from Maboko Island (Kenya). Am. J. Phys. Anthropol. 132(S44), 62.

Alloing-Séguier, L., Sánchez-Villagra, M. R., Lee, M. S. Y., Lebrun, R., 2013. The bony labyrinth in diprotodontian marsupial mammals: diversity in extant and extinct forms and relationships with size and phylogeny. J. Mammal. Evol. 20, 191–198.

Allum, J. H., Bloem, B. R., Carpenter, M. G., Hulliger, M., Hadders-Algra, M., 1998. Proprioceptive control of posture: a review of new concepts. Gait Posture 8, 214–242.

Almécija, S., Alba, D. M., 2014. On manual proportions and pad-to-pad precision grasping in *Australopithecus afarensis*. J. Hum. Evol. 73, 88–92.

Almécija, S., Sherwood, C. C., 2017. Hands, brains, and precision grips: Origins of tool use behaviors. In: Kaas, J. (Ed), *Evolution of Nervous Systems*. Amsterdam: Academic Press, pp. 299–315.

Almécija, S., Alba, D. M., Moyà -Solà, S., Köhler, M., 2007. Orang-like manual adaptations in the fossil hominoid *Hispanopithecus laietanus*: first steps towards great ape suspensory behaviours. Proc. R. Soc. B 274, 2375–2384.

Almécija, S., Alba, D. M., Moyà -Solà, S., 2009. *Pierolapithecus* and the functional morphology of Miocene ape hand phalanges: paleobiological and evolutionary implications. J. Hum. Evol. 57, 284–297.

Almécija, S., Alba, D. M., Moyà-Solà, S., 2012. The thumb of Miocene apes: new insights from Castell de Barberà (Catalonia, Spain). Am. J. Phys. Anthropol. 148, 436–450.

Almécija, S., Tallman, M., Alba, D. M., Pina, M., Moyà-Solà, S., Jungers, W. L., 2013. The femur of *Orrorin tugenensis* exhibits morphometric affinities with both Miocene apes and later hominins. Nat. Commun. 4, 2888.

Almécija, S., Shrewsbury, M., Rook, L., Moyà-Solà, S., 2014. The morphology of *Oreopithecus bambolii* pollical distal phalanx. Am. J. Phys. Anthropol. 153, 582–597.

Almécija, S., Smaers, J., Jungers, W., 2015. The evolution of human and ape hand proportions. Nat. Commun. 6, 7717.

Almécija, S., Tallman, L., Sallam, H. M., Fleagle, J. G., Hammond, A. S., Seiffert, E. R., 2019. Early anthropoid femora reveal divergent adaptive trajectories in catarrhine hind-limb evolution. Nat. Commun. 10, 4778.

Alpagut, B., Andrews, P., Martin, L., 1990. New hominoid specimens from the Middle Miocene site at Paçalar, Turkey. J. Hum. Evol. 19, 397–422.

Altmann, F., Vermes, E., 1933. Zur Kenntnis des feineren Baues des Schläfenbeines der Menschaffen. Mschr. Ohrenheilk. 67, 1199–1246.

Ambergen, A. W., Schaafsma, W., 1984. Interval estimates for posterior probabilities, applications to Border Cave. In: van Vark G. N., Howells, W. W. (Eds), *Multivariate Statistical Methods in Physical Anthropology*. Boston: D. Reidel Publishing, pp. 115–134.

Andrews P., 1985. Family group systematics and evolution among catarrhine primates. In: Delson, E. (Ed), *Ancestors: The Hard Evidence*. New York: Alan R. Liss, pp. 14–22.

Andrews, P., 1992. Evolution and environment in the Hominoidea. Nature 360, 641–647

Andrews, P., 1996. Paleoecology and hominoid paleoenvironments. Biol. Rev. 71, 257–300.

Andrews, P., 2019. Last common ancestor of apes and humans: Morphology and environment. Folia Primatol. 91, 122–148.

Andrews, P., Cronin, J. E., 1982. The relationships of *Sivapithecus* and *Ramapithecus* and the evolution of the orang-utan. Nature 297, 541–546.

Andrews, P., Kelley, J., 2007. Middle Miocene dispersals of apes. Folia Primatol. 78, 328–343.

Andrews, P., Martin, L. B., 1987. The phyletic position of the Ad Dabtiyah hominoid. Bull. Br. Mus. Nat. Hist. Geol. 41, 383–393.

Andrews, P., Tekkaya, I., 1980. A revision of the Turkish Miocene hominoid *Sivapthecus meteai*. Paleontology 23, 85–95.

Andrews, P., Walker, A., 1976. The primate and other fauna from Fort Ternan, Kenya. In: Isaac, G. L., McCown, E. R. (Eds), *Human Origins*. Menlo Park: Benjamin, pp. 279–304.

Andrews, P., Hamilton, W. R., Whybrow, P. J., 1978. Dryopithecines from the Miocene of Saudi Arabia. Nature 274, 249–250.

Andrews, P. J., Harrison, T., Delson, E., Bernor, R. L., Martin, L., 1996. Distribution and biochronology of European and Southwest Asian Miocene catarrhines. In: Bernor, R. L., Fahlbusch, V., Mittmann, H. (Eds), *The Evolution of Western Eurasian Neogene Mammalian Faunas*. New York: Columbia University Press, pp. 168–207.

Angelaki, D. E., Cullen, K. E., 2008. Vestibular system: The many facets of a multimodal sense. Annu. Rev. Neurosci. 31, 125–150.

Antón, S. C., 2003. Natural history of *Homo erectus*. Am. J. Phys. Anthropol. 122, 126–170.

Antón, S. C., Potts, R., Aiello, L. C., 2014. Evolution of early *Homo*: An integrated biological perspective. Science 345, 1236828.

Anyonge, W., 1991. Fauna from a new lower Miocene locality west of Lake Turkana, Kenya. J. Vert. Paleontol. 11, 378–390.

Araújo, R., Fernandez, V., Polcyn, M. J., Fröbisch, J., Martins, R. M. S., 2017. Aspects of gorgonopsian paleobiology and evolution: insights from the basicranium, occiput, osseous labyrinth, vasculature, and neuroanatomy. PeerJ 5, e3119.

Arias-Martorell, J., Alba, D. M., Potau, J. M., Bello-Hellegouarch, G., Pérez-Pérez, A., 2015. Morphological affinities of the proximal humerus of *Epipliopithecus vindobonensis* and *Pliopithecus antiquus*: Suspensory inferences based on a 3D geometric morphometrics approach. J. Hum. Evol. 80, 83–95.

Aristide, L., Bastide, P., dos Reis, S. F., dos Santos, T. M. P., Lopes, R. T, Perez, P. I., 2018. Multiple factors behind early diversification of skull morphology in the continental radiation of New World monkeys. Evolution 72, 2697–2711.

Arnold, C., Matthews, L. J., Nunn, C. L., 2010. The 10kTrees website: A new online resource for primate phylogeny. Evol. Anthropol. 19, 114–118.

Asfaw, B., White, T., Lovejoy, O., Latimer, B., Simpson, S., Suwa, G., 1999. *Australopithecus garhi*: a new species of early hominid from Ethiopia. Science 284, 629–635.

Balzeau, A., Crevecoeur, I., Rougier, H, Froment, A., Gilissen, E, Grimaud-Hervé, D., Mennecier, P., Sema, P., 2010. A pplications of imaging methodologies to paleoanthropology: Beneficial results relating to the preservation, management and development of collections. C. R. Palevol. 9, 265–275.

Barry, J. C., Morgan, M. E., Flynn, L. J., Pilbeam, D., Jacobs, L. L., Lindsay, E. H., Raza, S. M., Solounias, N., 1995. Patterns of faunal turnover and diversity in Neogene Siwaliks of Northern Pakistan. Palaeogeogr. Palaeoclimatol. Palaeoecol. 115, 209–226.

Barry, J. C., Morgan, M. E., Flynn, L. J., Pilbeam, D., Behrensmeyer, A. K., Raza, S. M., Khan, I. A., Badgley, C., Hicks, J., Kelley, J., 2002. Faunal and environmental change in the Late Miocene Siwaliks of Northern Pakistan. Paleobiol. Mem. 28, 1–72.

Barry, J., Behrensmeyer, A., Badgley, C., Flynn, L., Peltonen, H., Cheema, I., Pilbeam, D., Lindsay, E., Raza, S., Rajpar, A., Morgan, M., 2013. The Neogene Siwaliks of the Potwar Plateau, Pakistan. In: Wang, X., Fortelius, M., Flynn, L. J. (Eds), *Fossil Mammals of Asia: Neogene Biostratigraphy and Chronology*. Columbia University Press, pp. 373–399.

Bast, T. H., 1942. XXXII Development of the otic capsule: VI. Histological changes and variations in the growing bony capsule of the vestibule and cochlea. Ann. Otol. Rhinol. 51, 343–357.

Beaudet, A., 2019. The inner ear of the *Paranthropus* specimen DNH 22 from Drimolen, South Africa. Am. J. Phys. Anthropol. 170, 439–446.

Beaudet, A., Dumoncel, J., de Beer, F., Duployer, B., Durrleman, S., Gilissen, E., Hoffman, J., Tenailleau, C., Thackeray, J. F., Braga, J., 2016a. Morphoarchitectural variation in South African fossil cercopithecoid endocasts. J. Hum. Evol. 101, 65–78.

Beaudet, A., Dumoncel, J., Thackeray, J. F., Bruxelles, L., Duployer, B., Tenailleau, C., Bam, L., Hoffman, J., de Beer, F., Braga, J., 2016b. Upper third molar internal structural organization and semicircular canal morphology in Plio-Pleistocene South African cercopithecoids. J. Hum. Evol. 95, 104–120

Beaudet, A., Clarke, R. J., Bruxelles, L., Carlson, K. J., Crompton, R., de Beer, F., Dhaene, J., Heaton, J. L., Jakata, K., Jashashvili, T., Kuman, K., McClymont, J., Pickering, T. R., Stratford, D., 2019. The bony labyrinth of StW 573 ("Little Foot"): Implications for early hominin evolution and paleobiology. J. Hum. Evol. 127, 67–80.

Begun, D. R., 1988. Catarrhine phalanges from the Late Miocene (Vallesian) of Rudabánya. J. Hum. Evol. 17, 413–438.

Begun, D. R., 1989. A large pliopithecine molar from Germany and some notes on the Pliopithecinae. Folia Primatol. 52, 156–166.

Begun, D. R., 1992a. Phyletic diversity and locomotion in primitive European hominids. Am. J. Phys. Anthropol. 87, 311–340.

Begun, D. R., 1992b. *Dryopithecus crusafonti* sp. nov., a new Miocene hominoid species from Can Ponsic (northeastern Spain). Am. J. Phys. Anthropol. 87, 291–309.

Begun, D. R., 1993. New catarrhine phalanges from Rudabánya (Northeastern Hungary) and the problem of parallelism and convergence in hominoid postcranial morphology. J. Hum. Evol. 24, 373–402.

Begun, D. R., 1994. Relations among the great apes and humans: New interpretations based on the fossil great ape *Dryopithecus*. Am. J. Phys. Anthropol., 37, 11–63.

Begun, D. R., 1995. Late Miocene European orang-utans, gorillas, humans, or none of the above? J. Hum. Evol. 29, 169–180.

Begun, D. R., 2000. Middle Miocene hominoid origins. Science 287, 2375a.

Begun, D. R., 2001. African and Eurasian Miocene hominoids and the origins of the Hominidae. In: de Bonis, L., Koufos, G., Andrews, P. (Eds), *Hominoid Evolution and Climate Change in Europe: Volume 2. Phylogeny of the Neogene Hominoid primates of Eurasia*. Cambridge: Cambridge University Press, pp. 231–253.

Begun, D. R., 2002a. The Pliopithecoidea. In: Hartwig, W. C. (Ed), *The Primate Fossil Record*. Cambridge: Cambridge University Press, pp. 221–240.

Begun, D. R., 2002b. European hominoids. In: Hartwig, W. C. (Ed), *The Primate Fossil Record.* Cambridge: Cambridge University Press, pp. 339–368.

Begun, D. R., 2005. *Sivapithecus* is east and *Dryopithecus* is west, and never the twain shall meet. Anthropol. Sci. 113, 53–64.

Begun, D. R., 2007. How to identify (as opposed to define) a homoplasy: Examples from fossil and living great apes. J. Hum. Evol. 52, 559–572.

Begun, D. R., 2009. Dryopithecins, Darwin, de Bonis, and the European origin of the African apes and human clade. Geodiversitas 31, 789–816.

Begun, D. R., 2010. Miocene hominids and the origins of the African apes and humans. Ann. Rev. Anthropol. 39, 67–84.

Begun, D. R., 2013. The Miocene hominoid radiations. In: Begun, D. R. (Ed.), *A Companion to Paleoanthropology.* Oxford: Blackwell Publishing, pp. 398–416.

Begun, D. R., 2015. Fossil record of Miocene hominoids. In: Henke, W., Tattersall, I., (Eds) *Handbook of Paleoanthropology*. Heidelberg: Springer Verlag, pp. 921–977.

Begun, D. R., 2017. Evolution of the Pliopithecoidea. In: Fuentes, A. (Ed), *The International Encyclopedia of Primatology,* Chichester: John Wiley & Sons. https://doi.org/10.1002/9781119179313.wbprim0165

Begun, D. R., Güleç, E., 1998. Restoration of the type and palate of *Ankarapithecus meteai*: Taxonomic and phylogenetic implications. Am. J. Phys. Anthropol. 105, 279–314.

Begun, D. R., Kordos, L., 2004. Cranial evidence of the evolution of intelligence in fossil apes. In: Russon, A. E., Begun, D. R. (Eds), *The Evolution of Thought: Evolutionary Origins of Great Ape Intelligence*. Cambridge: Cambridge University Press, pp. 260–279.

Begun, D. R., Nargolwalla, M. C., 2004. Late Miocene hominid biogeography: some recent perspectives. Evol. Anthropol. 13, 234–238.

Begun, D. R., Ward, C. V., 2005. Comment on "*Pierolapithecus catalaunicus*, a new Middle Miocene great ape from Spain". Science 208, 203c.

Begun, D. R., Moyà-Solà, S., Köhler, M., 1990. New Miocene hominoid specimens from Can Llobateres (Vallès Penedès, Spain) and their geological and paleoecological context. J. Hum. Evol. 3, 255–268.

Begun, D. R., Ward, C. V., Rose, M. D., 1997. Events in hominoid evolution. In: Begun, D. R., Ward, C. V., Rose, M. D. (Eds), *Function, Phylogeny and Fossils: Miocene Hominoid Evolution and Adaptation.* New York: Plenum Press, pp. 389–415.

Begun, D. R., Güleç, E., Geraads, D., 2003. The Çandir hominoid locality: Implications for the timing and pattern of hominoid dispersal events. Cour. Forsch. Inst. Senckenberg 240, 240–265.

Begun, D. R., Nargolwalla, M. C., Kordos, L., 2012. European Miocene hominids and the origin of the African Ape and human clade. Evol. Anthropol. 21, 10–23.

Belmaker, M., 2010. The presence of a large cercopithecine (cf. *Theropithecus* sp.) in the 'Ubeidiya formation (Early Pleistocene, Israel). J. Hum. Evol. 58, 79–89.

Benefit, B., 1987. *The molar morphology, natural history, and phylogenetic position of the middle Miocene monkey* Victoriapithecus. Ph.D. Dissertation, New York University.

Benefit, B., 1993. The permanent dentition and phylogenetic position of *Victoriapithecus* from Maboko Island, Kenya. J. Hum. Evol. 25, 83–172.

Benefit, B., 1994. Phylogenetic, paleodemographic, and taphonomic implications of *Victoriapithecus* deciduous teeth from Maboko, Kenya. Am. J. Phys. Anthropol. 95, 277–331.

Benefit, B., 1999. *Victoriapithecus*: The key to Old World monkey and catarrhine origins. Evol. Anthropol. 7, 155–174.

Benefit, B., 2000. Old World monkey origins and diversification: an evolutionary study of diet and dentition. In: Whitehead, P. F., Jolly, C. J. (Eds), *Old World Monkeys*. Cambridge: Cambridge University Press, pp. 133–169.

Benefit, B., McCrossin, M., 1997. Earliest known Old World monkey skull. Nature 388, 368–371.

Benefit, B., McCrossin, M. L., 2000. Middle Miocene hominoid origins. Science 287, 2375a.

Benefit, B., McCrossin, M., 2002. The Victoriapithecidae, Cercopithecoidea. In: Hartwig, W. C. (Ed), *The Primate Fossil Record*. Cambridge, Cambridge University Press, pp. 241–253.

Benefit, B., McCrossin, M., 2015. A window into ape evolution. Science 350, 515–516.

Benefit, B., Pickford, M., 1986. Miocene fossil cercopithecoids from Kenya. Am. J. Phys. Anthropol. 69, 441–464.

Benefit, B. R., McCrossin, M., Boaz, N. T., Pavlakis, P., 2008. New fossil cercopithecoids from the Late Miocene of As Sahabi, Libya. Garyounis Sci. Bull. 5, 265–282.

Benoit, J., Thackeray, F. J., 2017. A cladistic analysis of *Graecopithecus*. Afr. J. Sci. 113, 1–2.

Benoit, J., Marzougui, W., Ammar, H. K., Lebrun, R., Tabuce, R., Marivaux, L., 2013. New insights into the ear region anatomy and cranial blood supply of advanced stem Strepsirhini: evidence from three primate petrosals from the Eocene of Chambi, Tunisia. J. Hum. Evol. 65, 551–572.

Benoit, J., Lehmann, T., Vatter, M., Lebrun, R., Merigeaud, S., Costeur, L., Tabuce, R., 2015. Comparative anatomy and three-dimensional geometric-morphometric study of the bony labyrinth of *Bibymalagasia* (Mammalia, Afrotheria). J. Vert. Paleontol. 35, e930043.

Benoit, J., Manger, P. R., Norton, L., Fernandez, V., Rubidge, B. S., 2017. Synchrotron scanning reveals the palaeoneurology of the head-butting *Moschops capensis* (Therapsida, Dinocephalia). PeerJ 5, e3496.

Benoit-Gonin, L. & Lafite-Dupont, P., 1907. Destinée du canal semi-circulaire externe dans le passage de la station quadrupède à la station bipède. C. R. Soc. Biol. Paris 62, 98–99.

Benson, R. B. J., Starmer-Jones, E., Close, R. A., Walsh, S. A., 2017. Comparative analysis of vestibular ecomorphology in birds. J. Anat. 231, 990–1018.

Berg, W. 1903. Zur Corrosionanatomie des Schläfenbein der Affen. Z. Morphol. Anthropol. 5, 315–345.

Berger, L. R., de Ruiter, D. J., Churchill, S. E., Schmid, P., Carlson, K. J., Dirks, P. H., Kibii, J. M., 2010. *Australopithecus sediba*: a new species of *Homo*-like australopith from South Africa. Science 328, 195–204.

Berger, L. R., Hawks, J., de Ruiter, D. J., Churchill, S. E., Schmid, P., Delezene, L. K., Kivell, T. L., Garvin, H. M., Williams, S. A., DeSilva, J. M., Skinner, M. M., 2015. *Homo naledi*, a new species of the genus *Homo* from the Dinaledi Chamber, South Africa. eLife 4, e09560.

Berlin, J. C., Kirk, E. C., Rowe, T. B., 2013. Functional implications of ubiquitous semicircular canal non-orthogonality in mammals. PLoS One 8, e79585.

Berthoz, A., 1991. Reference frames for the perception and control of movement. In: Paillard, J. (Ed), *Brain and Space*. Oxford: Oxford University Press, pp. 81–111.

Berthoz, A., Pozzo, T., 1988. Intermittent head stabilization during postural and locomotory tasks in humans. In: Amblard, B., Berthoz, A., Clarac, F. (Eds), *Posture and Gait: Development, Adaptation and Modulation*. Amsterdam: Excerpta medica, pp. 189–198.

Bhagat, R., Bertrand, O. C., Silcox, M. T., 2020. Evolution of arboreality and fossoriality in squirrels and aplodontid rodents: Insights from the semicircular canals of fossil rodents. J. Anat. https://doi.org/10.1111/joa.13296.

Billet, G., Hautier, L., Asher, R. J., Schwarz, C., Crumpton, C., Martin, T., Ruf, I., 2012. High morphological variation of vestibular system accompanies slow and infrequent locomotion in three-toed sloths. Proc. R. Soc. B 279, 3932–3939.

Billet, G., Germain, D., Ruf, I., de Muizon, C., Hautier, L., 2013. The inner ear of *Megatherium* and the evolution of the vestibular system in sloths. J. Anat. 223, 557–567.

Billet, G., Hautier, L., Lebrun, R., 2015. Morphological diversity of the bony labyrinth (inner ear) in extant Xenarthrans and its relation to phylogeny. J. Mammal. 96 658–672.

Blanks, R. H. I., Curthoys, I. S., Markham, C. H., 1975. Planar relationships of the semicircular canals in man. Acta Otolaryngol. 80, 185–196.

Bloch, J. I., Silcox, M. T. Boyer, D. M., Sargis, E. J., 2007. New Paleocene skeletons and the relationship of plesiadapiforms to crown-clade primates. Proc. Natl. Acad. Sci. USA 104, 1159–1164.

Blomberg, S. P., Garland, T. Jr., 2002. Tempo and mode in evolution: phylogenetic inertia, adaptation and comparative methods. J. Evol. Biol. 15, 899–910.

Blomberg, S. P., Garland, T. Jr., Ives, A. R., 2003. Testing for phylogenetic signal in comparative data: behavioral traits are more labile. Evolution 57, 717–745.

Böhme, M., Spassov, N., Ebner, M., Geraads, D., Hristova, L., Kirscher, U., Kötter, S., Linnemann, U., Prieto, J., Roussiakis, S., Theodorou, G., 2017. Messinian age and savannah environment of the possible hominin *Graecopithecus* from Europe. PloS One 12, e0177347.

Böhme, M., Spassov, N., Fuss, J., Tröscher, A., Dean, A. S., Prieto, J., Kirscher, U., Lechner, T., Begun, D. R., 2019. A new Miocene ape and locomotion in the ancestor of great apes and humans. Nature 575, 489–493.

Boistel, R., Herrel, A., Lebrun, R., Daghfous, G., Tafforeau, P., Losos, J. B., Vanhooydonck, B., 2011. Shake rattle and roll: The bony labyrinth and aerial descent in squamates. Integr. Comp. Biol. 51, 957–968.

Bolk, L., 1906. Das Cerebellum der Säugetiere. F. Bohn, Haarlem.

Bône, A., Louis, M., Martin, B., Durrleman, S., 2018. Deformetrica 4: an open-source software for statistical shape analysis. In: Reuter, M., Wachinger, C., Lombaert, H., Paniagua, B., Lüthi, M., Egger, B. (Eds), *Shape in Medical Imaging. Shape MI 2018*. Cham: Springer, pp. 3–13.

Bookstein, F. L., 1991. *Morphometric Tools for Landmark Data: Geometry and Biology*. New York: Cambridge University Press.

Bookstein, F. L., 1997. Landmark methods for forms without landmarks: morphometrics of group differences in outline shape. Med. Image Anal. 1, 225–243.

Boscaini, A., Iurino, D.A., Billet, G., Hautier, L., Sardella, R., Tirao, G., Gaudin, T. J., Pujos, F., 2018. Phylogenetic and functional implications of the ear region anatomy of *Glossotherium robustum* (Xenarthra, Mylodontidae) from the Late Pleistocene of Argentina. Sci. Nat. 105, 28.

Bouchneb, L., Crevecoeur, I., 2009. The inner ear of Nazlet Khater 2 (Upper Paleolithic, Egypt). J. Hum. Evol. 56, 257–262.

Boyer, D. M., Lipman, Y., Clair, E. S., Puente, J., Patel, B. A., Funkhauser, T., Jernvall, J., Daubechies, I., 2010. Algorithms to automatically quantify the geometric similarity of anatomical surfaces. Proc. Natl. Acad. Sci. USA 108, 18221–18226.

Boyle, E. K., Wood, B., 2020. Human evolutionary history. In: Kaas, J. H. (Ed), *Evolutionary Neuroscience*. London: Academic Press, pp. 733–752.

Braga, J., Thackeray, J. F., Dumoncel, J., Descouens, D., Bruxelles, L., Loubes, J. M., Kahn, J. L., Stampanoni, M., Bam, L., Hoffman, J., de Beer, F., 2013. A new partial temporal bone of a juvenile hominin from the site of Kromdraai B (South Africa). J. Hum. Evol. 65, 447–456.

Braga, J., Samir, C., Risser, L., Dumoncel, J., Descouens, D., Thackeray, J. F., Balaresque, P., Oettlé, A., Loubes, J.-M., Fradi, A., 2019a. Cochlear shape reveals that the human organ of hearing is sex-typed from birth. Sci. Rep. 9, 10889.

Braga, J., Zimmer, V., Dumoncel, J., Samir, C., De Beer, F., Zanolli, C., Pinto, D., Rohlf, F.J. and Grine, F.E., 2019b. Efficacy of diffeomorphic surface matching and 3D geometric morphometrics for taxonomic discrimination of Early Pleistocene hominin mandibular molars. J. Hum. Evol. 130, 21–35.

Bramble, D. M., Lieberman, D. E., 2004. Endurance running and the evolution of *Homo*. Nature 432, 345–352.

Bronstein, A. M., 1988. Evidence for a vestibular input contributing to dynamic head stabilization in man. Acta Otolaryngol. 105, 1–6.

Brown, B., Ward, S., 1988. Basicranial and facial topography in *Pongo* and *Sivapithecus*. In: Schwartz, J. H. (Ed), *Orang-utan Biology*. London: Oxford University Press, pp. 247–260.

Brunet, M., Beauvilain, A., Coppens, Y., Heintz, E., Moutaye, A.E., 1996. *Australopithecus bahrelghazali*, une nouvelle espece d'Hominide ancien de la region de Koro Toro (Tchad). C. R. Acad. Sci. Paris 322, 907–913.

Brunet, M., Guy, F., Pilbeam, D., Mackaye, H. T., Likius, A., Ahounta, D., Beauvilain, A., Blondel, C., Bocherens, H., Boisserie, J. -R., de Bonis, L., Coppens, Y., Dejax, J., Denys, C., Duringer, P., Eisenmann, V., Gongdibe, F., Fronty, P., Geraads, D., Lehmann, T., Lihoreau, F., Louchart, A., Mahamat, A., Merceron, G., Mouchelin, G., Otero, O., Pelàez-Campomanes, P., Ponce de León, M. S., Rage, J.- C., Sapanet, M., Schuster, M., Sudre, J., Tassy, P., Valentin, X., Vignaud, P., Viriot, L., Zazzo, A., Zollikofer, C., 2002. A new hominid from the Upper Miocene of Chad, Central Africa. Nature 418, 145–151.

Brunet, M., Guy, F., Pilbeam, D., Lieberman, D. E., Likius, A., Mackaye, H. T., Ponce de León, M. S., Zollikofer, C., Vignaud, P., 2005. New material of the earliest hominid from the Upper Miocene of Chad. Nature 434, 752–755.

Bush, E. C., Simons, E. L., Dubowitz, D. J., Allman, J. M., 2004. Endocranial volume and optic foramen size in *Parapithecus grangeri*. In: Ross, C. F., Kay, R. F. (Eds), *Anthropoid Origins: New Visions*. New York: Kluwer/Plenum, pp. 603–614.

Cameron, D. W., 2003. A functional and phylogenetic interpretation of the Late Miocene Siwalik hominid *Indopithecus* and the Chinese Pleistocene hominid *Gigantopithecus*. Himal. Geol. 24, 19–28.

Cameron, D. W., 2004. *Hominid Adaptations and Extinctions*. Sydney: University of New South Wales Press.

Capshaw, G., Soares, D., Carr, C. E., 2019. Bony labyrinth morphometry reveals hidden diversity in lungless salamanders (Family Plethodontidae): Structural correlates of ecology, development, and vision in the inner ear. Evolution, 73, 2135–2150.

Carbone, L., Harris, R. A., Gnerre, S., Veeramah, K. R., Lorente-Galdos, B., Huddleston, J., Meyer, T. J., Herrero, J., Roos, C., Aken, R., Anaclerio, F.,

Archidiacono, N., Baker, C., Barrell, D., Batzer, M. A., Beal, K., Blancher, A., Bohrson, C. L., Brameier, M., Campbell, M. S., Capozzi, O., Casola, C., Chiatante, G., Cree, A., Damert, A., de Jong, P. J., Dumas, L., Fernandez-Callejo, M., Flicek, P., Fuchs, N. V., Gut, I., Gut, M., Hahn, M. W., Hernandez-Rodriguez, J., Hillier, L. W., Hubley, R., Ianc, B., Izsvák, Z., Jablonski, N. G., Johnstone, L. M., Karimpour-Fard, A., Konkel, M. K., Kostka, D., Lazar, N. H., Lee, S. L., Lewis, L. R., Liu, Y., Locke, D. P., Mallick, S., Mendez, F. L., Muffato, M., Nazareth, L. V., Nevonen, K. A., O'Bleness, M., Ochis, C., Odom, D. T., Pollard, K. S., Quilez, J., Reich, D., Rocchi, M., Schumann, G. G., Searle, S., Sikela, J. M., Skollar, G., Smit, A., Sonmez, K., ten Hallers, B., Terhune, E., Thomas, G. W. C., Ullmer, B., Ventura, M., Walker, J. A., Wall, J. D., Walter, L., Ward, M. C., Wheelan, S. J., Whelan, C. W., White, S., Wilhelm, L. J., Woerner, A. E., Yandell, M., Zhu, B., Hammer, M. F., Marques-Bonet, T., Eichler, E. E., Fulton, L., Fronick, C., Muzny, D. M., Warren, W. C., Worley, K. C., Rogers, J., Wilson, R. K., Gibbs, R. A., 2014. The gibbon genome provides a novel perspective on the accelerated karyotype evolution of small apes. Nature 513, 195–201

Cardini, A., 2020. Less tautology, more biology? A comment on "high-density" morphometrics. Zoomorphology 139, 513–529.

Cardini, A., O'Higgins, P., Rohlf, F. J., 2019. Seeing distinct groups where there are none: Spurious patterns from between-group PCA. Evol. Biol. 46, 303–316.

Cardini, A., Polly, P. D., 2020. Cross-validated between-group PCA scatterplots: A solution to spurious group separation? Evol. Biol. 47, 85–95.

Casanovas-Vilar, I., Alba, D. M., Garcés, M., Robles, J. M., Moyà-Solà, S., 2011a. Updated chronology for the Miocene hominoid radiation in Western Eurasia. Proc. Natl. Acad. Sci. USA 108, 5554–5559.

Clarke, A. H., 2005. On the vestibular labyrinth of *Brachiosaurus brancai*. J. Vestibul. Res.-Equil. 15, 65–71.

Clarke, R. J., 1997. First complete restoration of the *Oreopithecus* skull. Hum. Evol. 12, 221–232.

Chaimanee, Y., Suteethorn, V., Jintasakul, P., Vidthayanon, C., Marandat, B., Jaeger, J-. J., 2004. A new orang-utan relative from the Late Miocene of Thailand. Nature 427, 439–441.

Chaimanee, Y., Lazzari, V., Chaivanich, K., Jaeger, J-. J., 2019. First maxilla of a late Miocene hominid from Thailand and the evolution of pongine derived characters. J. Hum. Evol. 134, 102636.

Chang, W:, Cole, L., Cantos, R., Wu, D. K., 2004. Molecular genetics of vestibular organ development. In: Highstein, S. M., Fay, R. R., Popper, A. N. (Eds), *The Vestibular System*. New York: Springer, pp. 11–56.

Chatterjee, H. J., Ho, S. Y. W., Barnes, I., Groves, C., 2009. Estimating the phylogeny and divergence times of primates using a supermatrix approach. BMC Evol. Biol.9, 259.

Chung, M. K., Worsley, K. J., Robbins, S., Paus, T., Taylor, J., Giedd, J. N., Rapoport, J. L., Evans, A. C., 2003. Deformation-based surface morphometry applied to gray matter deformation. NeuroImage 18, 198–213.

Ciochon, R. L., Corruccini, R. S., 1977. The phenetic position of *Pliopithecus* and its phylogenetic relationship to the Hominoidea. Syst. Zool. 26, 290–299.

Collard, M., Wood, B., 2015. Defining the genus *Homo*. In: Henke, W., Tattersall, I. (Eds), *Handbook of Paleoanthropology*. Heidelberg: Springer Verlag. pp. 2107–2144.

Conde-Valverde, M., Quam, R., Martínez, I., Arsuaga, J.-L., Daura, J., Sanz, M., Zilhão, J., 2018. The bony labyrinth in the Aroeira 3 Middle Pleistocene cranium. J. Hum. Evol. 124, 105–116.

Conroy, G. C., Pickford, M., Senut, B., Couvering, V. J., 1992. *Otavipithecus namibiensis*, first Miocene hominid from southern Africa. Nature 356, 144–148.

Coster, P., Benammi, M., Chaimanee, Y., Yamee, C., Chavasseau, O., Emonet, E-. G., Jaeger; J- J., 2010. A complete magnetic-polarity stratigraphy of the Miocene continental deposits of Mae Moh Basin, northern Thailand, and a reassessment of the age of hominoid-bearing localities in northern Thailand. GSA Bull. 122 , 1180–1191.

Costeur, L., Grohé, C., Aguirre-Fernández, G., Ekdale, E., Schulz, G., Müller, B., Mennecart, B., 2018. The bony labyrinth of toothed whales reflects both phylogeny and habitat preferences. Sci. Rep. 8, 7841.

Cote, S., McNulty, K. P., Stevens, N. J., Nengo, I. O., 2016. A detailed assessment of the maxillary morphology of *Limnopithecus evansi* with implications for the taxonomy of the genus. J. Hum. Evol. 94, 83–91.

Coutier, F., Hautier, L., Cornette, R., Amson, E., Billet, G., 2017. Orientation of the lateral semicircular canal in Xenarthra and its links with head posture and phylogeny. J. Morphol. 278, 704–717.

Cox, P. G., Jeffery, N., 2008. Geometry of the semicircular canals and extraocular muscles in rodents, lagomorphs, felids and modern humans. J. Anat. 213, 583–596.

Creath, R., Kiemel, T., Horak, F., Jeka, J. J., 2008. The role of vestibular and somatosensory systems in intersegmental control of upright stance. J. Vestibul. Res.-Equil. 18, 39–49.

Crevecoeur, I., 2012. The Upper Paleolithic human remains of Nazlet Khater 2 (Egypt) and past modern human diversity. In: Hublin, J. J., McPherron, S. (Eds.) *Modern Origins*. Dordrecht: Springer, pp. 205–219.

Crevecoeur, I., Brooks, A., Ribot, I., Cornelissen, E., Semal, P., 2016. Late Stone Age human remains from Ishango (Democratic Republic of Congo): New insights on Late Pleistocene modern human diversity in Africa. J. Hum. Evol. 96, 35–57.

Crusafont Pairó, M., Hürzeler, J., 1969. Catálogo comentado de los póngidos fósiles de España. Acta Geol. Hisp. 4, 44–48.

Cunningham, J. A., Imran, A. R., Lautenschlager, S., Rayfield, E. J., Donoghue, P. C. J., 2014. A virtual world of paleontology. Trends Ecol. Evol. 29, 347–357.

Curthoys, I., 1982. Postnatal development changes in the response of rat primary horizontal semicircular canal neurons to sinusoidal angular accelerations. Exp. Brain Res. 47, 295–300.

Curthoys, I. S., Markham, C. H., Curthoys, E. J., 1977. Semicircular canal duct and ampulla dimensions in cat, guinea pig and man. J. Morphol. 151, 17–34.

Damiano, E. R., Rabbitt, R. D., 1996. A singular perturbation model for fluid dynamics in the vestibular semicircular canal and ampulla. J. Fluid. Mech. 307, 333–372.

Daver, G., Nakatsukasa, M., 2015. *Proconsul heseloni* distal radial and ulnar epiphyses from the Kaswanga Primate Site, Rusinga Island, Kenya. J. Hum. Evol. 80, 17–33.

David, R., Droulez, J., Allain, R., Berthoz, A., Janvier, P., Bennequin, D., 2010. Motion from the past. A new method to infer vestibular capacities of extinct species. C. R. Palevol. 9, 397–410.

David, R., Stoessel, A., Berthoz, A., Spoor, F., Bennequin, D., 2016. Assessing morphology and function of the semicircular duct system: introducing new in-situ visualization and software toolbox. Sci. Rep. 6, 32772.

David, R., Gunz, P., Stoessel, A., Spoor, F., 2019. Accurately predicting head motion in fossil primates using soft-tissue information. Proc. Eur. Soc. Study Hum. Evol. 8, 44.

Davies, A. G., Oates, J. F., 1995. *Colobine Monkeys: their Ecology, Behavior and Evolution*. New York: Cambridge University Press.

Davies, K. T. J., Bates, P. J. J., Maryanto, I., Cotton, J. A., Rossiter, S. J., 2013. The evolution of bat vestibular systems in the face of potential antagonistic selection pressures for flight and echolocation. PLoS One 8, e61998.

Dean, M. C., 1988. Growth processes in the cranial base of hominoids and their bearing on morphological similarities that exist in the cranial base of *Homo* and *Paranthropus*. In: Grine, F. E. (Ed), *Evolutionary History of the "Robust" Australopithecines*. New York: A. de Gruyter, pp. 107–112.

Deane, A. S., 2017. Re-evaluating the diets of *Morotopithecus bishopi* and *Afropithecus turkanensis*: An anterior dentognathic perspective. J. Hum. Evol. 112, 1–14.

Deane, A. S., Begun, D. R., 2008. Broken fingers: retesting locomotor hypotheses for fossil hominoids using fragmentary proximal phalanges and high-resolution polynomial curve fitting (HR-PCF). J. Hum. Evol. 55, 691–701.

Deane, A. S., Begun, D. R., 2010. *Pierolapithecus* locomotor adaptations: a reply to Alba et al.'s comment on Deane and Begun (2008). J. Hum. Evol. 59, 150–154.

de Beer, G. R., 1947. How animals hold their heads. Proc. Linn Soc. Lond. 159, 125–139.

de Bonis, L., Koufos, G. D., 1993. The face and the mandible of *Ouranopithecus macedoniensis*: description of new specimens and comparisons. J. Hum. Evol. 24, 469–491.

de Bonis, L., Koufos, G. D., 1994. Our ancestors' ancestor: *Ouranopithecus* is a Greek link in human ancestry. Evol. Anthropol. 3, 75–84.

de Bonis, L., Melentis, J., 1977. Les primates hominoïdes du Vallésien de Macédoine (Grèce). Étude de la machoire inférieure. Geobios 10, 849–885.

de Bonis, L., Melentis, J., 1978. Les Primates hominoïdes du Miocène supérieur de Macédoine. Étude de la machoire supérieure. Ann. Paléontol. 64, 185–202.

de Bonis, L., Koufos, G. D., Guy, F., Peigne, S., Sylvestrou, I., 1998. Nouveaux restes du primate hominoïde *Ouranopithecus* dans les dépôts du Miocène supérieur de Macédoine (Grèce). C. R. Acad. Sci. Paris 327, 141–146.

Dechesne, C., Mbiene, J. P., Sans, A., 1986. Postnatal development of vestibular receptor surfaces in the rat. Acta Otolaryngol. 101, 11–18.

Delattre, A., 1951. La rotation vestibulaire. C. R. Acad. Sci. 233, 978–980.

del Rio, J., Aristide, L., dos Reis, S. F., dos Santos, T. M. P., Lopes, R. T., Perez, S. I., 2020. Allometry, function and shape diversification in the inner ear of platyrrhine primates. J. Mammal. Evol. https://doi.org/10.1007/s10914-019-09490-9.

Delson, E., 1974. Preliminary review of cercopithecid distribution in the Circum Mediterranean region. Mém. Bureau Recher. Géol. Min. Fr. 78, 131–135.

Delson, E., 1975. Evolutionary history of the Cercopithecidae. Contrib. Primatol. 5, 167–217.

Delson, E., 1980. Fossil macaques, phyletic relationships and a scenario of development. In: Lindburg, D. G. (Ed), *The Macaques: Studies in Ecology, Behaviour and Evolution*. New York: Van Nostrand Reinhold Co., pp. 10–30.

Delson, E., 1986. An anthropoid enigma: historical introduction to the study of *Oreopithecus bambolii*. J. Hum. Evol. 15, 523–531.

Delson, E., 1993. *Theropithecus* fossils from Africa and India and the taxonomy of the genus. In Jablonski, N. G. (Ed), Theropithecus: *The Rise and Fall of a Primate Genus*. Cambridge: Cambridge University Press, pp. 157–189.

Delson, E., Andrews, P. J., 1975. Evolution and interrelationships of the catarrhine primates. In: Luckett, W. P., Szalay, F. S. (Eds), *Phylogeny of the Primates: A Multidisciplinary Approach*. New York: Plenum Press, pp. 405–446.

DeMiguel, D., Alba, D. M., Moyà-Solà, S., 2014. Dietary specialization during the evolution of western Eurasian hominoids and the extinction of European great apes. PLoS One 9, e97442.

Denker, A. 1899a. Zur vergleichenden Anatomie des Gehörorgans der Säugetiere. Ergebn. Anat. Entw. Gesch. 9, 297–325.

Denker, A. 1899b. *Vergleichend-anatomische Untersuchungen über das Gehörorgan der Säugethiere nach Corrosionspräparaten und Knochenschnitten*. Leipzig: Von Veit.

Depéret, C., 1911. Sur la découverte d'un grand Singe anthropoïde du genre *Dryopithecus* dans le Miocène moyen de La Grive-Saint-Alban (Isère). C. R. Acad. Sci. Paris 153, 32–35.

Dickson B. V., Sherratt E., Losos J. B., Pierce S. E., 2017. Semicircular canals in Anolis lizards: ecomorphological convergence and ecomorph affinities of fossil species. R. Soc. Open Sci. 4, 170058

Dray, S., Dufour, A., 2007. The *ade4* package: Implementing the duality diagram for ecologists. J. Stat. Softw. 22, 1–20.

Dryden, I. L., Mardia, K. V., 1998. *Statistical Shape Analysis*. New York: John Wiley & Sons.

Dujim, M. J., 1951. On the head posture in birds and its relation features. Proc. K. Ned. Akad. Wet. C 54, 202–271.

Dunbar, D. C., Badam, G. L., Hallgrímsson, B., Vieilledent, S., 2004. Stabilization and mobility of the head and trunk in wild monkeys during terrestrial and flat-surface walks and gallops. J. Exp. Biol. 207, 1027–1042.

Dunbar, D. C., Macpherson, J. M., Simmons, R. W., Zarcades A., 2008. Stabilization and mobility of the head, neck and trunk in horses during overground locomotion: comparisons with humans and other primates. J. Exp. Biol. 211, 3889–3907.

Dunsworth, H. M., 2006. Proconsul heseloni *Feet from Rusinga Island, Kenya*. Ph.D. Dissertation, Pennsylvania State University.

Durrleman, S., Pennec, X., Trouvé, A., Ayache, N., Braga, J., 2012a. Comparison of the endocranial ontogenies between chimpanzees and bonobos via temporal regression and spatiotemporal registration. J. Hum. Evol. 62, 74–88.

Durrleman, S., Prastawa, M., Korenberg, J.R., Joshi, S., Trouvé, A., Gerig, G., 2012b. Topology preserving atlas construction from shape data without correspondence using sparse parameters. In: Ayache, N., Delingette, H., Golland, P., Mori, K. (Eds), *Medical Image Computing and Computer-Assisted Intervention – MICCAI 2012*. Berlin: Springer, pp. 223–230.

Durrleman, S., Prastawa, M., Charon, N., Korenberg, J. R., Joshi, S., Gerig, G., Trouvé, A., 2014. Morphometry of anatomical shape complexes with dense deformations and sparse parameters. NeuroImage 101, 35–49.

Ekdale, E. G., 2013. Comparative anatomy of the bony labyrinth (inner ear) of placental mammals. PLoS One 10, e0137149.

Ekdale, E. G., 2016. Form and function of the mammalian inner ear. J. Anat., 228, 324–337.

Engström, H., Lindeman, H. H., Ades, H. W., 1966. Anatomical features of the auricular sensory organs. In: *Second Symposium on the Role of the Vestibular Organs in Space Exploration, SP-115*. Moffett Field: NASA Ames Research Center, pp. 33–46.

Farris, J. S., 1989. The retention index and homoplasy excess. Syst. Biol. 38, 406–407.

Felsenstein, J., 1985. Phylogenies and the comparative method. Am. Nat. 125, 1–15.

Felsenstein, J.,1988. Phylogenies and quantitative characters. Annu. Rev. Ecol. Syst. 19, 445–471.

Fenart, R., Deblock, R., 1973. *Pan paniscus* et *Pan troglodytes* craniométrie: Étude comparative et ontogénique selon les méthodes classiques et vestibulaire. Tome I. Ann. Mus. Roy. Afrique Centr. 204, 1–507.

Finstermeier, K., Zinner, D., Brameier, M., Meyer, M., Kreuz, E., Hofreiter, M., Roos, C., 2013. A mitogenomic phylogeny of living primates. PLoS One, 8, e69504.

Fitzpatrick, R. C., Butler, J. E., Day, B. L., 2006. Resolving head rotation for human bipedalism. Curr. Biol. 16, 1509–1514.

Fleagle, J. G., 1984. Are there any fossil gibbons? In: Preuschoft, H., Chivers, D. J., Brockelman, W. Y., Creel, N. (Eds), *The Lesser Apes: Evolutionary and Behavioral Biology*. Edinburgh: Edinburgh University Press, pp. 431–447.

Fleagle, J. G., 2013. *Primate Adaptation and Evolution*. Boston: Academic press.

Fleagle J. G., Kay R. F., 1983. New interpretations of the phyletic position of Oligocene hominoids. In: Ciochon, R. L., Corruccini, R. S. (Eds), *New Interpretations of Ape and Human Ancestry. Advances in Primatology*. Boston: Springer, pp. 181–210.

Foley, R., 2001. The evolutionary consequences of increased carnivory in hominids. In: Stanford, C. B., Bunn, H. T. (Eds), *Meat-eating and Human Evolution*. Oxford: Oxford University Press, pp. 305–331.

Freckleton, R. P., Harvey, P. H., Pagel, M., 2002. Phylogenetic analysis and comparative data: a test and review of evidence. Am. Nat. 160, 712–726.

Fricano, E. E. I., 2018. *The Primate Ectotympanic Tube: Correlates of Structure, Function, and Development*. Ph.D. Dissertation. Johns Hopkins University.

Frost, S. R., Gilbert, C. C., Pugh, K. D., Guthrie, E. H., Delson, E., 2015. The hand of *Cercopithecoides williamsi* (Mammalia, Primates): Earliest evidence for thumb reduction among colobine monkeys. PLoS One 10, e0125030.

Fulwood, E. L., Boyer, D. M., Kay, R. F., 2016. Stem members of Platyrrhini are distinct from catarrhines in at least one derived cranial feature. J. Hum. Evol. 100, 16–24.

Fuss, J., Spassov, N., Begun, D.R., Böhme, M., 2017. Potential hominin affinities of *Graecopithecus* from the Late Miocene of Europe. PloS One, 12, e0177127.

Gabunia, L., Lordkipanidze, D., Vekua, A., 2001. Late Miocene hominoid *Udabnopithecus* from Georgia. In: de Bonis, L., Koufos, G., Andrews, P. (Eds), *Phylogeny of the Neogene Hominoid Primates of Eurasia*. London: Cambridge University Press, pp. 2–18.

Galik, K., Senut, B., Pickford, M., Gommery, D., Treil, J., Kuperavage, A. J., Eckhardt, R. B., 2004. External and internal morphology of the BAR 10020'00 *Orrorin tugenensis* femur. Science 305, 1450–1453.

Gannon, P. J., Eden, A. R., Laitman, J. T., 1988. The subarcuate fossa and cerebellum of extant primates: comparative study of a skull-brain interface. Am. J. Phys. Anthropol. 77, 143–164.

Gaudry, A., 1890. Le Dryopithèque. Mem. Soc. Géol. Fr. 1, 1–11.

Gebo, D. L., MacLatchy, L., Kityo, R., Deino, A., Kingston, J., Pilbeam, D., 1997. A hominoid genus from the early Miocene of Uganda. Science 276, 401–404.

Gervais, P., 1872. Sur un singe fossile, d'une espèce non encore décrite, qui a été découverte au monte Bamboli. C. R. Acad. Sci. Paris 74, 1217–1223.

Gibert, J., Ribot, F., Gibert, L., Leakey, M., Arribas, A., Martinez, B., 1995. Presence of the cercopithecid genus *Theropithecus* in Cueva Victoria (Murcia, Spain). J. Hum. Evol. 28, 487–493.

Gilbert, C.C., Bibi, F., Hill, A., Beech, M.J., 2014. Early guenon from the late Miocene Baynunah Formation, Abu Dhabi, with implications for cercopithecoid biogeography and evolution. Proc. Natl. Acad. Sci. USA 111, 10119–10124.

Gilbert, C. C., Ortiz, A., Pugh, K. D., Campisano, C. J., Patel, B. A., Singh, N. P., Fleage, J. G., Patnaik, R., 2020a. New middle Miocene ape (Primates: Hylobatidae) from Ramnagar, India fills major gaps in the hominoid fossil record. Proc. R. Soc. B 287, 20201655.

Gilbert, C. C., Pugh, K. D., Fleagle, J. G., 2020b. Dispersal of Miocene hominoids (and pliopithecoids) from Africa to Eurasia in light of changing tectonics and climate. In: Prasad, G. V. R., Patnaik, R. (Eds.), *Biological Consequences of Plate Tectonics: New Perspectives on Post-Gondwana Break-up*. Cham: Springer, pp. 393–412.

Girard, L. L., 1923. Plan des canaux semi-circulaires horizontaux considéré comme plan horizontal de la tête. Bull. Mem. Soc. Anthropol. Paris 4, 14–33.

Glantz, M., Viola, B., Wrinn, P., Chikisheva, T., Derevianko, A., Krivoshapkin, A., Islamov, U., Suleimanov, R., Ritzman, T., 2008. New hominin remains from Uzbekistan. J. Hum. Evol. 55, 223–237.

Glaunès, J. A., Joshi, S., 2006. Template estimation form unlabeled point set data and surfaces for Computational Anatomy. In: Pennec, X., Joshi, S. (Eds), *MICCAI 2006 Workshop Proceedings. MFCA'06 Workshop. Mathematical Foundations of Computational Anatomy: Geometrical and Statistical Methods for Modelling Biological Shape Variability*. Conpenhagen: INRIA/MICCAI, pp. 29–39.

Golpe Posse, J. M., 1993. Los hispanopitecos (Primates, Pongidae) de los yacimientos del Vallès-Penedès (Cataluña, España). II: Descripción del material existente en el Instituto de Paleontología de Sabadell. Paleontol. Evol. 26–27, 151–224.

Gómez-Olivencia, A., Crevecoeur, I., Balzeau, A., 2015. La Ferrassie 8 Neandertal child reloaded: New remains and re-assessment of the original collection. J. Hum. Evol. 82, 107–126.

Gonzales, L. A., Malinzak, M. D., Kay, R. F., 2019. Intraspecific variation in semicircular canal morphology—A missing element in adaptive scenarios? Am. J. Phys. Anthropol. 168, 10–24.

Gorczowski, K., Styner,M., Jeong, J. Y.,Marron, J. S., Piven, J., Hazlett, H. C., Pizer, S. M., Gerig, G., 2010. Multi-object analysis of volume, pose, and shape using statistical discrimination. IEEE Trans. Pattern Anal. Mach. Intell. 32, 652–661.

Goswami, A., Watanabe, A., Felice, R. N., Bardua, C., Fabre, A. C., Polly, P. D., 2019. High-density morphometric analysis of shape and integration: the good, the bad, and the not-really-a-problem. Integr. Comp. Biol. 59, 669–683.

Grabowski, M., Jungers, W. L., 2017. Evidence of a chimpanzee-sized ancestor of humans but a gibbon-sized ancestor of apes. Nat. Commun. 8, 880.

Graf, W., Vidal, P. -P., 1996. Semicircular canal size and upright stance are not interrelated. J. Hum. Evol. 30, 175–181.

Graf, W., Klam, F. L., 2006. Système vestibulaire : anatomie fonctionnelle et comparée, évolution et développement. C. R. Palevol 5, 637–655.

Gray, A. A., 1907. *The Labyrinth of Animals, Vol. 1*. London: Churchill.

Gray, A. A., 1908. *The Labyrinth of Animals: Including Mammals, Birds, Reptiles, and Amphibians*. London: Churchill.

Grohé, C., Tseng, Z. J., Lebrun, R., Boistel, R., Flynn, J. J., 2016. Bony labyrinth shape variation in extant Carnivora: a case study of Musteloidea. J. Anat. 228, 366–383.

Grohé, C., Lee, B., Flynn, J.J., 2018. Recent inner ear specialization for high-speed hunting in cheetahs. Sci. Rep. 8, 1–8.

Groves, C., 2001. *Primate Taxonomy*. Washington DC: Smithsonian Institution Press.

Güleç, E. S., Sevim, A., Pehlevan, C., Kaya, F., 2007. A new great ape from the late Miocene of Turkey. Anthropol. Sci. 115, 153–158.

Gunz, P., Mitteroecker, P. 2013. Semilandmarks: a method for quantifying curves and surfaces. Hystrix 24, 103–109.

Gunz, P., Mitteroecker, P., Bookstein, F. L., 2005. Semilandmarks in three dimensions. In: Slice, D. E. (Ed), *Modern Morphometrics in Physical Anthropology*. New York: Klewer Academic/Plenum, pp. 73–98.

Gunz, P., Ramsier, M., Kuhrig, M., Hublin, J. J., Spoor, F., 2012. The mammalian bony labyrinth reconsidered, introducing a comprehensive geometric morphometric approach. J. Anat. 220, 529–543.

Gunz, P., Kozakowski, S., Neubauer, S., Le Cabec, A., Kullmer, O., Benazzi, S., Hublin, J-. J., Begun, D. R., 2020. Skull reconstruction of the late Miocene ape *Rudapithecus hungaricus* from Rudabánya, Hungary. J. Hum. Evol. 138, 102687.

Guy, F., Lieberman, D. E., Pilbeam, D., Ponce de León, M., Likius, A., Mackaye, H. T., Vignaud, P., Zollikofer, C., Brunet, M., 2005. Morphological affinities of the *Sahelanthropus tchadensis* (Late Miocene hominid from Chad) cranium. Proc. Natl. Acad. Sci. USA 102, 18836–18841.

Hadziselimovic, H., Savkovic, L., 1964. Appearance of semicircular canals in birds in relation to mode of life. Acta Anat. 57, 306–315.

Haile-Selassie, Y., 2001. Late Miocene hominids from the Middle Awash, Ethiopia. Nature 412, 178–181.

Haile-Selassie, Y., Suwa, G., White, T. D., Late Miocene teeth from middle Awash, Ethiopia, and early hominid dental evolution. Science, 303, 1503–1505.

Hammond, A. S., Foecke, K. K., Kelley, J., 2019. Hominoid anterior teeth from the late Oligocene site of Losodok, Kenya. J. Hum. Evol. 59–75.

Hammond, A. S., Rook, L., Anaya, A. D., Cioppi, E., Costeur, L., Moyà-Solà, S., Almécija, S., 2020. Insights into the lower torso in late Miocene hominoid *Oreopithecus bambolii*. Proc. Natl. Acad. Sci. USA 117, 278–284.

Harcourt-Smith, W. E. H., 2015. Origin of bipedal locomotion. In: Henke, W., Tattersall, I. (Eds), *Handbook of Paleoanthropology*. Heidelberg: Springer Verlag. pp. 1919–1960.

Harlé, É. 1898. Une machoire de dryopitheque. Bull. Soc. Géol. Fr. 26, 377–383.

Harlé, É., 1899. Nouvelles pieces de Dryopitheque et quelques conquilles, de Saint Gaudens (Haute-Garonne). Bull. Soc. Géol. Fr. 27, 304–310.

Harrison, T., 1986. New fossil anthropoids from the middle Miocene of East Africa and their bearing on the origin of the Oreopithecidae. Am. J. Phys. Anthropol. 71, 265–284.

Harrison, T., 1987. The phylogenetic relationships of the early catarrhine primates: a review of the current evidence. J. Hum. Evol. 16, 41–80.

Harrison, T., 1988. A taxonomic revision of the small catarrhine primates from the Early Miocene of East Africa. Folia Primatol. 50, 59–108.

Harrison, T., 1989. A new species of *Micropithecus* from the middle Miocene of Kenya. J. Hum. Evol. 18, 537–557.

Harrison, T., 1991. Some observations on the Miocene hominoids from Spain. J. Hum. Evol. 19, 515–520.

Harrison, T., 1992. A reassessment of the taxonomic and phylogenetic affinities of the fossil catarrhines from Fort Ternan, Kenya. Primates 33, 501–522.

Harrison, T., 2002. Late Oligocene to middle Miocene catarrhines from Afro-Arabia. In: Hartwig, W. C. (Ed), *The Primate Fossil Record*. Cambridge: Cambridge University Press, pp. 311–338.

Harrison, T., 2005. The zoogeographic and phylogenetic relationships of early catarrhine primates in Asia. Anthropol. Sci. 113, 43–51.

Harrison, T., 2010. Dendropithecoidea, Proconsuloidea, and Hominoidea (Catarrhini, Primates). In: Werdelin, L. (Ed), *Cenozoic Mammals of Africa*. Berkeley: University of California Press, pp. 429–469.

Harrison, T., 2011. Cercopithecids (Cercopithecidae, Primates). In: Harrison, T. (Ed), *Paleontology and Geology of Laetoli: Human Evolution in Context*. Dordrecht: Springer, pp. 83–139.

Harrison, T., 2013. Catarrhine origins. In: Begun, D. R. (Ed), *A Companion to Paleoanthropology*. Oxford: Blackwell Publishing, pp. 376–396.

Harrison, T., 2016. The fossil record and evolutionary history of hylobatids. In: Reichard, U. H., Hirohisa, H., Barelli, C. (Eds), *Evolution of Gibbons and Siamang: Phylogeny, Morphology and Cognition*. New York: Springer, pp. 91–110.

Harrison, T., Andrews, P., 2009. The anatomy and systematic position of the early w

Harrison, T., Gu, Y., 1999. Taxonomy and phylogenetic relationships of early Miocene catarrhines from Sihong, China. J. Hum. Evol. 37, 225–277.

Harrison, T., Rook, L., 1997. Enigmatic anthropoid or misunderstood ape? The phylogenetic status of *Oreopithecus bambolii* reconsidered. In: Begun, D. R., Ward, C. V., Rose, M. D. (Eds), *Function, Phylogeny, and Fossils: Miocene Hominoid Evolution and Adaptations*. New York: Plenum Press, pp. 327–362.

Harrison, T., Zhang, Y., Wei, G., Sun, C., Wang, Y., Liu, J., Tong, H., Huang, B., Xu, F., 2020. A new genus of pliopithecoid from the late Early Miocene of China and its implications for understanding the paleozoogeography of the Pliopithecoidea. J. Hum. Evol. 145, 102838.

Harvey, P. H., Pagel, M. D., 1991. *The Comparative Method in Evolutionary Biology*. Oxford: Oxford Univ. Press.

Harzhauser, M., Kroh, A., Mandic, O., Piller, W. E., Göhlich, U., Reuter, M., Berning, B., 2007. Biogeographic responses to geodynamics: A key study all around the Oligo–Miocene Tethyan Seaway. Zool. Anz. 246, 241–256.

Hashimoto S, Naganuma H, Tokumasu K, Itoh A, and Okamoto M. 2005. Threedimensional reconstruction of the human semicircular canals and measurement of each membranous canal plane defined by Reid's stereotactic coordinates. Ann. Otol. Rhinol. 114, 934–938.

Heizmann, E., Begun, D. R., 2001. The oldest European hominoid. J. Hum. Evol. 41, 465–481.

Hennig, W., 1966. Anthomyiidae. In: Lindner, E. (Ed), *Die Fliegen der Palaearktischen Region*. Stuttgart, 145–192.

Hershkovitz, I., Weber, G. W., Quam, R., Duval, M., Grün, R., Kinsley, L., Ayalon, A., Bar-Matthews, M., Valladas, H., Mercier, N., J.L., A., Martinón-Torres, M., Bermúdez de Castro, J. M., Fornai, C., Martín-Francés, L., Sarig, R., May, H., Krenn, V. A., Slon, V., Rodríguez, L., García, R., Lorenzo, C., Carretero, J. M., Frumkin, A., Shahack-Gross, R., Bar-Yosef Mayer, D. E., Cui, Y., Wu, X., Peled, N., Groman-Yarolavski, I., Weissbrod, L., Yeshurun, R., Tsatskin, A., Zaidner, Y., Weinstein-Evron, M., 2018. The earliest modern humans outside Africa. Science 359, 456–459.

Highstein, S. M., 2004. Anatomy and physiology of the central and peripheral vestibular system: overview. In: Highstein, S. M., Fay, R. R., Popper, A. N. (Eds), *The Vestibular System*. New York: Springer, pp. 1–10.

Hill, C. A., Radovčić, J., Frayer, D.W., 2014. Brief communication: Investigation of the semicircular canal variation in the Krapina Neandertals. Am. J. Phys. Anthropol. 154, 302–306.

Holloway, R. L., 2008. The human brain evolving: A personal retrospective. Annu. Rev. Anthropol. 37, 1–19.

Holloway, R., 2015. The evolution of the hominid brain. In: Henke, W., Tattersall, I., (Eds) *Handbook of Paleoanthropology*. Heidelberg: Springer Verlag, pp. 1961–1987.

Hopkins, M., 1906. On the relative dimensions of the osseous semicircular canals of birds. Biol. Bull. 11, 253–264.

Hotelling, H., 1933. Analysis of a complex of statistical variables into principal components. J. Educ. Psychol. 24, 417–441.

Howland, H., 1973. The role of the semicircular canals in the angular orientation of fish. Ann. N. Y. Acad. Sci. 188, 202–216.

Hublin, J.- J., Spoor, F., Braun, M., Zonneveld, F,. Condemi, S., 1996. A late Neanderthal associated with Upper Palaeolithic artefacts. Nature, 381, 224–226.

Hublin, J.- J., Ben-Ncer, A., Bailey, S.E., Freidline, S.E., Neubauer, S., Skinner, M.M. Bergmann, I., Le Cabec, A., Benazzi, S., Harvati, K., Gunz, P., 2017. New fossils from Jebel Irhoud, Morocco and the pan-African origin of *Homo sapiens*. Nature 546, 289–292.

Hughes, J. K., Elton, S., O'Regan, H. J., 2008. *Theropithecus* and 'Out of Africa' dispersal in the Plio-Pleistocene J. Hum. Evol. 54, 43–77.

Hullar, T. E., 2006. Semicircular canal geometry, afferent sensitivity, and animal behaviour. Anat. Rec. A 288, 466–472.

Hunt, K.D., 2016. Why are there apes? Evidence for the co-evolution of ape and monkey ecomorphology. J. Anat. 228, 630–685.

Hunt, K.D., 2018. Arboreal locomotion. In: Trevathan, W., Cartmill, M., Dufour, D., Larsen, C., O'Rourke, D., Rosenberg, K., Strier K. (Eds), *The International Encyclopedia of Biological Anthropology*. https://doi.org/10.1002/9781118584538. ieba0033

Hürzeler, J., 1951. Contribution à l'étude de la dentition de lait d'*Oreopithecus bambolii* Gervais 1872. Ecl. Geol. Helv. 44, 404–411.

Hürzeler, J., 1954. Contribution a l'odontologie et a la phylogénèse du genre *Pliopithecus* Gervais. Ann. Paleontol. 40, 5–63.

Hürzeler, J., 1958. *Oreopithecus bambolii* Gervais: a preliminary report. Verhandl. Naturforch. Gesell. Basel 69, 1–48.

Hyrtl, J., 1845. Vergleichend-anatomische Untersuchungen über das innere Gehörorgan des Menschen und der Säugethiere, 3. Prague: F. Ehrlich.

Ifediba, M. A., Rajguru, S. M., Hullar, T. E., Rabbitt, R. D., 2007. The role of 3-canal biomechanics in angular motion transduction by the human vestibular labyrinth. Ann. Biomed. Eng. 35, 1247–1263.

Igarashi, M., O-Uchi, T., Alford, B. R., 1981. Volumetric and dimensional measurements of vestibular structures in the squirrel monkey. Acta Otolaryngol. 91, 437–444.

Igarashi, M., Ohashi, K., Ishi, M., 1986. Morphometric comparison of endolymphatic and perilymphatic spaces in human temporal bones. Acta Otolaryngol. 91, 161–164.

Ishida, H., Pickford, M., 1997. A new late Miocene hominoid from Kenya: *Samburupithecus kiptalami* gen. et sp. nov. C. R. Acad. Sci. Paris 325, 823–829.

Ishida, H., Pickford, M., Nakaya, H., Nakano, Y., 1984. Fossil anthropoids from Nachola and Samburu Hills, Samburu District, Kenya. Afr. Stud. Monogr. 2, 73–85.

Ishida, H., Kunimatsu, Y., Takano, T., Nakano, Y., Nakatsukasa, M., 2004. *Nacholapithecus* skeleton from the Middle Miocene of Kenya. J. Hum. Evol. 46, 69–103.

Jablonski, N. G., 2002. Fossil Old World monkeys: The late Neogene radiation. In: Hartwig, W. C. (Ed), *The Primate Fossil Record*. Cambridge: Cambridge University Press, pp. 255–299.

Jablonski, N. G., Frost, S., 2010. Cercopithecoidea. In: Werdelin, L., Sanders, W.L. (Eds), *Cenozoic Mammals of Africa.* Berkeley: University of California Press, pp. 393–429.

Jackson, J. E. 1991. *A User's Guide to Principal Components*. New York: John Wiley.

Jaeger, J-. J., Soe, A. N., Chavasseau, O., Coster, P., Emonet, E. G., Guy, F., Lebrun, R., Maung, A., Khyaw, A. A., Shwe, H., Tun, S. T., 2011. First hominoid from the late Miocene of the Irrawaddy Formation (Myanmar). PLoS One, 6, e17065.

Jeffery, N., Spoor, F., 2002. Brain size and the human cranial base: A prenatal perspective. Am. J. Phys. Anthropol. 118, 324–340.

Jeffery, N., Spoor, F., 2004. Prenatal growth and development of the modern human labyrinth. J. Anat. 204, 71–92.

Jeffery, N., Spoor, F., 2006. The primate subarcuate fossa and its relationship to the semicircular canals part I: prenatal growth. J. Hum. Evol. 51, 537–549.

Jeffery, N., Ryan, T. M., Spoor, F., 2008. The primate subarcuate fossa and its relationship to the semicircular canals part II: Adult interspecific variation. J. Hum. Evol. 55, 325–339.

Ji, X., Jablonski, N. G., Su, D. F., Deng, C., Flynn, L. J., You, Y., Kelley, J., 2013. Juvenile hominoid cranium from the terminal Miocene of Yunnan, China. Chinese Sci. Bull. 58, 3771–3779.

Jolliffe, I., T., 1986. *Principal Component Analysis*. New York: Springer Verlag.

Jones, G., Spells, K., 1963. A theoretical and comparative study of the functional dependence of the semicircular canal upon its physical dimensions. Proc. R. Soc. B 157, 403–419.

Jungers, W. L., 1987. Body size and morphometric affinities of the appendicular skeleton in *Oreopithecus bambolii* (IGF 11778). J. Hum. Evol. 16, 445–456.

Kappelman, J., Kelley, J., Pilbeam, D., Sheikh, K. A., Ward, S., Anwar, M., Barry, J. C., Brown, B., Hake, P., Johnson, N. M., Raza, S. M., Shah, S. M. I., 1991. The earliest occurrence of *Sivapithecus* from the middle Miocene Chinji Formation of Pakistan. J. Hum. Evol. 21, 61–73.

Kappelman, J., Richmond, B. G., Seiffert, E. R., Ryan, T. M., 2003. Fortelius, M., Kappelman, J., Sen, S., Bernor, R. L. (Eds), *Geology and Paleontology of the Miocene Sinap Formation, Turkey*. New York: Columbia Univ. Press, pp. 90–124.

Kariya, T., Kurata, H., 2004. *Generalized Least Squares*. New York: John Wiley & Sons.

Katoh, S., Beyene, Y., Itaya, T., Hyodo, H., Hyodo, M., Yagi, K., Gouzu, C., WoldeGabriel, G., Hart, W. H., Ambrose, S. H., Nakaya, H., Bernor, R. L., Boisserie, J.-R., Bibi, F., Saegusa, H., Sasaki, T., Sano, K., Asfaw, B., Suwa, G., 2016. New geological and palaeontological age constraint for the gorilla–human lineage split. Nature 530, 215–218.

Kay, R. F., Hylander, W. L., 1978. The dental structure of mammalian folivores with special reference to primates and phalangeroids (Marsupialia). In: Montgomery, G. G., (Ed), *The Ecology of Arboreal Folivores*. Washington DC: Smithsonian Institution Press, pp. 173–192.

Kay, R. F., Fleagle, J. G., Mitchell, T. R. T., Colbert, M., Bown, T., Powers, D. W., 2009. The anatomy of *Dolichocebus gaimanensis*, a stem platyrrhine monkey from Argentina. J. Hum. Evol. 54, 323–382.

Kelley, J., 1997. Paleobiological and phylogenetic significance of life history in Miocene hominoids. In: Begun, D. R., Ward, C. V., Rose, M. D. (Eds.), *Function, Phylogeny and Fossils: Miocene Hominoid Evolution and Adaptation.* New York: Plenum Press, pp. 173–208.

Kelley, J., 1988. A new large species of *Sivapithecus* from the Siwaliks of Pakistan. J. Hum. Evol. 17, 305–324.

Kelley, J., 2002. The hominoid radiation in Asia. In: Hartwig, W. C. (Ed), *The Primate Fossil Record*. Cambridge: Cambridge University Press, pp. 369–384.

Kelley, J., 2004. Life history and cognitive evolution in the apes. In: Russon, A. E., Begun, D. R. (Eds) *The Evolution of Thought: Evolutionary Origins of Great Ape Intelligence*. Cambridge: Cambridge University Press, pp. 280–297.

Kelley, J., Gao, F., 2012. Juvenile hominoid cranium from the late Miocene of southern China and hominoid diversity in Asia. Proc. Natl. Acad. Sci. USA 109, 6882–6885.

Kelley, J., Smith, T. M., 2004. Age at first molar emergence in early Miocene *Afropithecus turkanensis* and life-history evolution in the Hominoidea. J. Hum. Evol. 44, 307–329.

Kelley, J., Ward, S., Brown, B., Hill, A., Downs, W., 2000. Middle Miocene hominoid origins. Science 287, 2375a.

Kelley, J., Andrews, P., Alpagut, B., 2008a. A new hominoid species from the middle Miocene site of Paçalar, Turkey. J. Hum. Evol. 54, 455–479.

Kelley, J., Andrews, P., Alpagut, B., 2008b. The hominoid remains from the middle Miocene site of Pasalar, Turkey. J. Hum. Evol. 54, 453–454.

Kendall, D. G., 1984. Shape-manifolds, Procrustean metrics and complex projective spaces. Bull. Lond. Math. Soc. 16, 81–121.

Ketten, D. R., 1992. The marine mammal ear: specializations for aquatic audition and echolocation. In: Thomas, J., (Ed.) *Marine Mammals Sensory Systems.* New York: Plenum, pp. 53–57.

Kimbel, W. H., 2009. The origin of *Homo*. In: Grine, F. E., Fleagle, J. G., Leakey, R. E. (Eds), *The First Humans*. New York: Springer, pp. 31–37.

Kimbel, W. H., 2015. The species and diversity of australopiths. In: Henke, W., Tattersall, I. (Eds), *Handbook of Paleoanthropology*. Heidelberg: Springer Verlag. pp. 2071–2106.

Kimbel, W. H., Villmoare, B., 2016. From *Australopithecus* to *Homo*: the transition that wasn't. Phil. Trans. R. Soc. B 371, 20150248.

Kimbel, W. H., Suwa, G., Asfaw, B., Rak, Y., White, T. D., 2014. *Ardipithecus ramidus* and the evolution of the human cranial base. Proc. Natl. Acad. Sci. USA 111, 948–953.

Kluge, A. G., Farris, J. S., 1969. Quantitative phyletics and the evolution of anurans. Syst. Biol. 18, 1–32.

Köhler, M., Moyà-Solà, S., 1997. Ape-like or hominid-like? The positional behavior of *Oreopithecus bambolii* reconsidered. Proc. Natl. Acad. Sci. USA 94, 11747-11750.

Köhler, M., Moyà -Solà, S., Alba, D. M., 2000. *Macaca* (Primates, Cercopithecidae) from the Late Miocene of Spain. J. Hum. Evol. 38, 447–452.

Köhler, M., Moyà-Solà, S., Alba, D. M., 2001a. Cranial reconstruction of *Dryopithecus*. Am. J. Phys. Anthropol. 115, 284–288.

Köhler, M., Moyà-Solà, S., Alba, D. M., 2001b. Eurasian hominoid evolution in the light of recent *Dryopithecus* findings. In: de Bonis, L., Koufos, G. D., Andrews, P. (Eds), *Phylogeny of the Neogene Hominoid Primates of Eurasia*. Cambridge: Cambridge University Press, pp. 192–212.

Kordos, L., 1987. Description and reconstruction of the skull of *Rudapithecus hungaricus* Kretzoi (Mammalia). Annls. Hist. Nat. Mus. Nat. Hung. 79, 77–88.

Kordos, L., Begun, D. R., 1997. A new reconstruction of RUD 77, a partial cranium of *Dryopithecus brancoi* from Rudabánya, Hungary. Am. J. Phys. Anthropol. 103, 277–294.

Kordos, L., Begun, D. R., 2001a. A new cranium of *Dryopithecus* from Rudabánya, Hungary. J. Hum. Evol. 41, 689–700.

Kordos, L., Begun, D. R., 2001b. Primates from Rudabánya: allocation of specimens to individuals, sex and age categories. J. Hum. Evol. 40, 17–39.

Koufos, G. D., 2006. Palaeoecology and chronology of the Vallesian (late Miocene) in the Eastern Mediterranean region. Palaeogeogr. Palaeoclimatol. Palaeoecol. 234, 127–145.

Koufos, G. D., de Bonis, L., 2004. The deciduous lower dentition of *Ouranopithecus macedoniensis* (Primates, Hominoidea) from the late Miocene deposits of Macedonia, Greece. J. Hum. Evol. 46, 699–718.

Koufos, G. D., de Bonis, L., 2005. The Late Miocene hominoids *Ouranopithecus* and *Graecopithecus*. Implications about their relationships and taxonomy. Ann. Paleontol. 91, 227–40.

Koufos, G. D., de Bonis, L., Kugiumtzis, D., 2016. New material of the hominoid *Ouranopithecus macedoniensis* from the late Miocene of the Axios valley (Macedonia, Greece) with some remarks on its sexual dimorphism. Folia Primatol. 87, 94–122.

Kuhn, M., 2008. Building predictive models in R using the *caret* package. J. Stat. Softw. 28. https://doi.org/10.18637/jss.v028.i05

Kunimatsu, Y., Ishida, H., Nakatsukasa, M., Nakano, Y., Sawada, Y., 2004. Maxillae and associated gnathodental specimens of *Nacholapithecus kerioi*, a large-bodied hominoid from Nachola, northern Kenya. J. Hum. Evol. 46, 365–400.

Kunimatsu, Y., Nakatsukasa, M., Sawada, Y., Sakai, T., Hyodo, M., Hyodo, H., Itaya, T., Nakaya, H., Saegusa, H., Mazurier, A., Saneyoshi, M., Tsujikawa, H., Yamamoto, A., Mbua, E., 2007. A new Late Miocene great ape from Kenya and its implications for the origins of African great apes and humans. Proc. Natl. Acad. Sci. USA 104, 19220–19225.

Kunimatsu, Y., Sawada, Y., Sakai, T., Saneyoshi, M., Nakaya, H., Yamamoto, A., Nakatsukasa, M., 2017. The latest occurrence of the nyanzapithecines from the early Late Miocene Nakali Formation in Kenya, East Africa. Anthropol. Sci. 125, 45–51.

Kunimatsu, Y., Nakatsukasa, M., Shimizu, D., Nakano, Y., Ishida, H., 2019. Loss of the subarcuate fossa and the phylogeny of *Nacholapithecus*. J. Hum. Evol. 131, 22–27.

Langdon, J., 1986. Functional morphology of the Miocene hominoid foot. Contrib. Primatol. 22, 1–225.

Lartet, E., 1856. Note sur un grand singe fossile qui se rattache au groupe des singes supérieurs. C. R. Acad. Sci. 43, 219–223.

Lawing, A. M., Polly, P. D., 2009. Geometric morphometrics: recent applications to the study of evolution and development. J. Zool. 280, 1–7.

Lê, S., Josse, J., Husson, F., 2008. FactoMineR: an R package for multivariate analysis. J. Stat. Softw. 25. https://doi.org/10.18637/jss.v025.i01

Leakey, M., Walker, A., 1997. *Afropithecus*: function and phylogeny. In: Begun, D. R., Ward, C. V., Rose, M. D. (Eds), *Function, Phylogeny and Fossils: Miocene Hominoid Evolution and Adaptations*. New York: Plenum, pp. 225–239.

Leakey, M. G., Ungar, P. S., Walker, A., 1995a. A new genus of large primate from the Late Oligocene of Lothidok, Turkana district, Kenya. J. Hum. Evol. 28, 519–531.

Leakey, M. G., Feibel, C. S., McDougall, I., Walker, A., 1995b. New four million year old hominid species from Kanapoi and Allia Bay, Kenya. Nature 376, 565–571.

Leakey, M. G., Teaford, M. F., Ward, C. V., 2003. Cercopithecidae from Lothagam. In: Leakey, M. G., Harris, J. M. (Eds), *Lothagam: The Dawn of Humanity in Eastern Africa*. New York: Columbia University Press, pp. 201–248.

Leakey, R. E., Leakey, M. G., 1986. A new Miocene hominoid from Kenya. Nature 324, 143–146.

Leakey, R. E., Leakey, M. G., 1986. A second new Miocene hominoid from Kenya. Nature 324, 146–148.

Leakey, R. E., Leakey, M. G., 1987. A new Miocene small-bodied ape from Kenya. J. Hum. Evol. 16, 369–387.

Lebrun, R., P. de León, M., Tafforeau, P., Zollikofer, C., 2010. Deep evolutionary roots of strepsirrhine primate labyrinthine morphology. J. Anat 216, 368–380.

Lebrun, R., Godinot, M., Couette, S., Tafforeau, P., Zollikofer, C., 2012. The labyrinthine morphology of *Pronycticebus gaudryi* (Primates, Adapiformes). Palaeobiodiv. Palaeoenvir. 92, 527–537.

Ledebkin, L., 1924. Über die Lage des Canalis semicircularis lateralis bei Säugern. Anat. Anz. 58, 449–460.

Lee, J.-Y., Shin, K.-J., Kim, J.-N., Yoo, J.-Y., Song, W.-C., Koh, K.-S., 2013. A morphometric study of the semicircular canals using micro-CT images in three-dimensional reconstruction. Anat. Rec. 296, 834–839.

Le Gros Clark, W. E., Thomas, D. P., 1951. Associated jaws and limb bones of *Limnopithecus macinnesi*. Foss. Mamm. Afr. 3, 1–40.

Le Maître, A., Schuetz, P., Vignaud, P., Brunet, M., 2017. New data about semicircular canal morphology and locomotion in modern hominoids. J. Anat. 231, 95–109.

Leung, H. C., Suh, M., Kettner, R. E., 2000. Cerebellar flocculus and paraflocculus Purkinje cell activity during circular pursuit in monkey. J. Neurophysiol. 83, 13–30.

Locke, E. M., Benefit, B., Kimock, C. M., Miller, E. R., Nengo, I., 2020. New dentognathic fossils of *Noropithecus bulukensis* (Primates, Victoriapithecidae) from the late Early Miocene of Buluk, Kenya. J. Hum. Evol. 148, 102886.

Lockwood, C. A., Kimbel, W. H., Lynch, J. M., 2004. Morphometrics and hominoid phylogeny: support for a chimpanzee–human clade and differentiation among great ape subspecies. Proc. Natl. Acad. Sci. USA 101, 4356–4360.

Lordkipanidze, D., Ponce de León, M. S., Margvelashvili, A., Rak, Y., Rightmire, G. P., Vekua, A., Zollikofer, C. P. E., 2013. A complete skull from Dmanisi, Georgia, and the evolutionary biology of Early *Homo*. Science 342, 326–331.

Lovejoy, C. O., 2009. Reexamining human origins in light of *Ardipithecus ramidus* Science 326, 74e1–74e8.

Lovejoy, C. O., Suwa, G., Simpson, S. W., Matternes, J. H., White, T. D., 2009a. The great divides: *Ardipithecus ramidus* reveals the postcrania of our last common ancestors with African apes. Science 326, 101–106.

Lovejoy, C. O., Suwa, G., Spurlock, L., Asfaw, B., White, T. D., 2009b. The pelvis and femur of *Ardipithecus ramidus*: the emergence of upright walking. Science 326, 71e1–71e6.

Lovejoy, C. O., Latimer, B., Suwa, G., Asfaw, B., White, T. D., 2009c. Combining prehension and propulsion: the foot of *Ardipithecus ramidus*. Science 326, 72e1–72e8.

Lovejoy, C. O., Simpson, S. W., White, T. D., Asfaw, B., Suwa, G., 2009d. Careful climbing in the Miocene: the forelimbs of *Ardipithecus ramidus* and humans are primitive. Science 326, 70e1–70e8.

Lowenstein, O., Saunders, R. D., 1975. Otolith-controlled response from the first order neurons of the labyrinth of the bullfrog to changes in linear acceleration. Proc. R. Soc. Lond. B 191, 475–505.

Luo, Z.-X., Ruf, I., Martin, T., 2012. The petrosal and inner ear of the Late Jurassic cladotherian mammal *Dryolestes leiriensis* and implications for ear evolution in therian mammals. Zool. J. Linn. Soc. 166, 433–463.

Macchiarelli, R., Bergeret-Medina, A., Marchi, D., Wood, B., 2020. Nature and relationships of *Sahelanthropus tchadensis*. J. Hum. Evol. 149, 102898.

MacLatchy, L., 2004. The oldest ape. Evol. Anthropol. 13, 90–103.

MacLatchy, L. M., Gebo, D., Kityo, R., Pilbeam, D., 2000. Postcranial functional morphology of *Morotopithecus bishopi*, with implications for the evolution of modern ape locomotion. J. Hum. Evol. 39, 159–183.

MacLatchy, L. M., Rossie, J., Houssaye, A., Olejniczak, A. J., Smith, T. M. 2019. New hominoid fossils from Moroto II, Uganda and their bearing on the taxonomic and adaptive status of *Morotopithecus bishopi*. J. Hum. Evol. 132, 227–246.

MacPhee, R. D. E., 1981. Auditory regions of primates and eutherian insectivores: morphology, ontogeny, and character analysis. Contrib. Primatol. 18, 1–282.

Macrini, T. E., Flynn, J. J., Croft, D. A., Wyss, A. R., 2010. Inner ear of a notoungulate placental mammal: anatomical description and examination of potentially phylogenetically informative characters. J. Anat. 216, 600–610.

Macrini, T. E., Flynn, J. J., Ni, X., Croft, D. A., Wyss, A. R., 2013. Comparative study of notoungulate (Placentalia, Mammalia) bony labyrinths and new phylogenetically informative inner ear characters. J. Anat. 223, 442–461.

Madar, S. I., Rose, M. D., Kelley, J., MacLatchy, L., Pilbeam, D., 2002. New *Sivapithecus* postcranial specimens from the Siwaliks of Pakistan. J. Hum. Evol. 42, 705–752.

Maddin, H. C., Sherratt, E., 2014. Influence of fossoriality on inner ear morphology: insights from caecilian amphibians. J. Anat., 225, 83–93.

Malinzak, M. D., 2010. *Experimental Analyses of the Relationship Between Semicircular Canal Morphology and Locomotor Head Rotations in Primates*. Ph.D. Dissertation, Duke University.

Malinzak, M.D., Kay, R.F., Hullar, T.E., 2012. Locomotor head movements and semicircular canal morphology in primates. Proc. Natl. Acad. Sci. USA 109, 17914–17919.

Marigó, J., Susanna, I., Minwer-Barakat, R., Madurell-Malapeira, J., Moyà-Solà, S., Casanovas-Vilar, I., Robles, J. M., Alba, D. M., 2014. The primate fossil record in the Iberian Peninsula. J. Iber. Geol. 40, 179–211.

Martins, E. P., 1996. Phylogenies, spatial autoregression, and the comparative method: a computer simulation test. Evolution 50, 1750–1765.

Marugán-Lobáón, J., Chiappe, L. M., Farke, A. A., 2013. The variability of inner ear orientation in saurischian dinosaur: testing the use of semicircular canals as a reference system for comparative anatomy. PeerJ 1, e124.

Matano, S., Kubo, T., Gunther, M., 1985. Semicircular canal organ in three primate species and behavioral correlations. Fortschr. Zool. 30, 677–680.

Matano, S., Kubo, T., Matsunaga, T., Niemitz, C., Günther, M., 1986. On the size of the semicircular canals organ in *Tarsius bancanus*. In: Taub, D. M., King, F. A., (Eds), *Current Perspectives in Primate Biology*. New York: Van Nostrand Reinhold.

McBrearty, S., Jablonski, N., 2005. First fossil chimpanzee. Nature 437, 105–108.

McCrossin, M. L., Benefit, B. R., 1997. On the relationships and adaptations of *Kenyapithecus*, a largebodied hominoid from the middle Miocene of eastern Africa. In: Begun, D. R., Ward, C. V., Rose, M. D. (Eds) *Function, Phylogeny and Fossils: Miocene Hominoid Origins and Adaptations*. New York: Plenum, pp. 241–267.

McNulty, K. P., Begun, D. R., Kelley, J., Manthi, F. K., Mbua, E. N., 2015. A systematic revision of *Proconsul* with the description of a new genus of early Miocene hominoid. J. Hum. Evol. 84, 42–61.

Mein, P., 1986. Chronological succession of hominoids in the European Neogene. In: Else, J. C., Lee, P. C. (Eds), *Primate evolution*. Cambridge: Cambridge University Press, pp. 59–70.

Mennecart., B., Costeur, L., 2016. Shape variation and ontogeny of the ruminant bony labyrinth, an example in Tragulidae. J. Anat. 229, 422–435.

Mennecart, B., Rössner, G. E., Métais, G., DeMiguel, D., Schulz, G., Müller, B., Costeur, L., 2016. The petrosal bone and bony labyrinth of early to middle Miocene European deer (Mammalia, Cervidae) reveal their phylogeny. J. Morphol. 277, 1329–1338.

Mennecart, B., DeMiguel, D., Bibi, F., Rössner, G. E., Métais, G., Neenan, J. M., Wang, S., Schulz, G., Müller, B., Costeur, L., 2017. Bony labyrinth morphology clarifies the origin and evolution of deer. Sci. Rep. 7, 13176.

Mergner, T., Huber, W., Becker, W., 1997. Vestibular-neck interaction and transformation of sensory coordinates. J. Vestibul. Res. 7, 347–367.

Metscher, B. D., 2009. MicroCT for comparative morphology: simple staining methods allow high-contrast 3D imaging of diverse nonmineralized animal tissues. BMC Physiol. 9, 11.

Miller, E. R., Benefit, B., McCrossin, M. L., Plavcan, J. M., Leakey, M. G., El-Barkooky, A. N., Hamdan, M. A., Gawad, M. A., Hassan, S. M., Simons, E. L., 2009. Systematics of early and middle Miocene Old World monkeys. J. Hum. Evol. 57, 195–211.

Milton, K., 1999. A hypothesis to explain the role of meat-eating in human evolution. Evol. Anthropol. 8, 11–21.

Mitteroecker, P., Bookstein, F., 2011. Linear discrimination, ordination, and the visualization of selection gradients in modern morphometrics. Evol. Biol. 38, 100–114.

Mitteroecker, P., Gunz P., 2009. Advances in geometric morphometrics. Evol. Biol. 36, 235–247.

Money, K., Correia, J., 1972. The vestibular system of the owl. Comp. Biochem. Physiol. 42A, 353–358.

Mongle, C. S., Strait, D. S., Grine, F. E., 2019. Expanded character sampling underscores phylogenetic stability of *Ardipithecus ramidus* as a basal hominin. J. Hum. Evol. 131, 28–39.

Moorjani, P., Amorim, C. E. G., Arndt, P. F., Przeworski, M., 2016. Variation in the molecular clock of primates. Proc. Natl. Acad. Sci. USA 113, 10607–10612.

Moran, P. A. P., 1950. Notes on continuous stochastic phenomena. Biometrika 37, 17–23.

Morgan, M. E., Lewton, K. L., Kelley, J., Otárola-Castillo, E., Barry, J. C., Flynn, L. J., Pilbeam, D., 2015. A partial hominoid innominate from the Miocene of Pakistan: Description and preliminary analyses. Proc. Natl. Acad. Sci. USA 112, 82–87.

Morimoto, N., Kunimatsu, Y., Nakatsukasa, M., Ponce de León, M. S., Zollikofer, C. P., Ishida, H., Sasaki, T., Suwa, G., 2020. Variation of bony labyrinthine morphology in Mio–Plio–Pleistocene and modern anthropoids. Am. J. Phys. Anthropol. 173, 276–292.

Morita, W., Morimoto, N., Kunimatsu, Y., Mazurier, A., Zanolli, C., Nakatsukasa, M., 2017. A morphometric mapping analysis of lower fourth deciduous premolar in hominoids: Implications for phylogenetic relationship between *Nakalipithecus* and *Ouranopithecus*. C. R. Palevol. 16, 655–669.

Motani, R., 2009. The evolution of marine reptiles. Evol. Educ. Outreach 2, 224–235.

Mottl, M., 1957. Bericht über die neuen Menschenaffenfunde aus Österreich, von St. Stefan im Lavanttral, Kärnten. Carinthia II 67, 39–76.

Moyà-Solà, S., Köhler, M., 1993. Recent discoveries of *Dryopithecus* shed new light on evolution of great apes. Nature 365, 543–545.

Moyà-Solà, S., Köhler, M., 1995. New partial cranium of *Dryopithecus* Lartet, 1863 (Hominoidea, Primates) from the upper Miocene of Can Llobateres, Barcelona, Spain. J. Hum. Evol. 29, 101–139.

Moyà-Solà, S., Köhler, M., 1997. The phylogenetic relationships of *Oreopithecus bambolii* Gervais, 1872. C. R. Acad. Sci. Paris 324, 141–148.

Moyà-Solà, S., Köhler, M., Rook, L., 1999. Evidence of hominid-like precision grip capability in the hand of the Miocene ape *Oreopithecus*. Proc. Natl. Acad. Sci. USA 96, 313–317.

Moyà-Solà, S., Köhler, M., Alba, D. M., 2001. *Egarapithecus narcisoi*, a new genus of Pliopithecidae (Primates, Catarrhini) from the late Miocene of Spain. Am. J. Phys. Anthropol. 114, 312–324.

Moyà-Solà, S., Köhler, M., Alba, D. M., Casanovas-Vilar, I., Galindo, J., 2004. *Pierolapithecus catalaunicus*, a new middle Miocene great ape from Spain. Science, 306, 1339–1344.

Moyà-Solà, S., Köhler, M., Rook, L., 2005a. The *Oreopithecus* thumb: a strange case in hominoid evolution. J. Hum. Evol. 49, 395–404.

Moyà-Solà, S., Köhler, M., Alba, D. M., Casanovas-Vilar, I., Galindo, J., 2005b. Response to comment on "*Pierolapithecus catalaunicus*, a new Middle Miocene great ape from Spain". Science, 308, 203d.

Moyà-Solà, S., Köhler, M., Alba, D. M., Casanovas-Vilar, I., Galindo, J., Robles, J. M., Cabrera, L., Garces, M., Almécija, S., Beamud, E., 2009a First partial face and upper dentition of the Middle Miocene hominoid *Dryopithecus fontani* from Abocador de Can Mata (Vallès–Penedès Basin, Catalonia, NE Spain): Taxonomic and phylogenetic implications. Am. J. Phys. Anthropol. 139, 126–145.

Moyà-Solà, S., Alba, D. M., Almécija, S., Casanovas-Vilar, I., Köhler, M., De Esteban-Trivigno, S., Robles, J. M., Galindo, J., Robles, J. M., Fortuny, J., 2009b. A unique

Middle Miocene European hominoid and the origins of the great ape and human clade. Proc. Natl. Acad. Sci. USA 106, 9601–9606.
Muller, M., 1994. Semicircular duct dimensions and sensitivity of the vertebrate vestibular system. J. Theor. Biol. 167, 239–256.
Muller, M., 1999. Size limitations in semicircular duct systems. J. Theor. Biol. 198, 405–437.
Muller, M., Verhagen, J.H.G., 2002a. Optimization of the mechanical performance of a two-duct semicircular duct system – part 1: dynamics and duct dimensions. J. Theor. Biol. 216, 409–424.
Muller, M., Verhagen, J.H.G., 2002b. Optimization of the mechanical performance of a two-duct semicircular duct system – Part 2: excitation of endolymph movements. J. Theor. Biol. 216, 425–442.
Muller, M., Verhagen, J.H.G., 2002c. Optimization of the mechanical performance of a two-duct semicircular duct system – part 3: the positioning of the ducts in the head. J. Theor. Biol. 216, 443–459.
Nakatsukasa, M., 2008. Comparative study of Moroto vertebral specimens. J. Hum. Evol. 55, 581–588.
Nakatsukasa, M., Kunimatsu, Y., 2009. *Nacholapithecus* and its importance for understanding hominoid evolution. Evol. Anthropol. 18, 103–119.
Nakatsukasa, M., Tsujikawa, H., Shimizu, D., Takano, T., Kunimatsu, Y., Nakano, Y., Ishida, H., 2003. Definitive evidence of tail loss in *Nacholapithecus*, an East African Miocene hominoid. J. Hum. Evol. 45, 179–186.
Nakatsukasa, M., Ward, C. V., Walker, A., Teaford, M. F., Kunimatsu, Y., Ogihara, N., 2004. Tail loss in *Proconsul heseloni*. J. Hum. Evol. 46, 777–784.
Napier, J. R., David, P. R., 1959. The fore-limb skeleton and associated remains of *Proconsul africanus*. Foss. Mamm. Afr. 16, 1–69.
Napier, J. R., Napier, P. H., 1967. *A Handbook of Living Primates*. London: Academic Press.
Nater, A., Mattle-Greminger, M.P., Nurchayo, A., Nowak, M.G., de Manuel, M., Desai, T., Groves, C., Pybus, M., Sonay, T.B., Roos, C., Lameira, A.R., Wich, S.A., Askew, J., Davila-Ross, M., Fredriksson, G., de Valles, G., Casals, F., Prado-Martinez, J., Goossens, B., Verschoor, E.J., Warren, K.S., Singleton, I., Marques, D.A., Pamungkas, J., Perwitasari-Farajallah, D., Rianti, P., Tuuga, A., Gut, I.G., Gut, M., Orozco-terWengel, P., van Schaik, C.P., Bertranpetit, J., Anisimova, M., Scally, A., Marques-Bonet, T., Meijaard, E., Krützen, M., 2017. Morphometric, behavioral, and genomic evidence for a new orangutan species. Curr. Biol. 27, 3487–3498.
Nengo, I. O., Rae, T. C., 1992. New hominoid fossils from the early Miocene site of Songhor, Kenya. J. Hum. Evol. 23, 423–429.
Nengo, I., Tafforeau, P., Gilbert, C. C., Fleagle, J. G., Miller, E. R., Feibel, C., Fox, D. L., Feinberg, J., Pugh, K. D., Berruyer, C., Mana, S., Engle, Z., Spoor, F., 2017. New infant cranium from the African Miocene sheds light on ape evolution. Nature 548, 169–174.
Ni, X., Flynn, J. J., Wyss, A. R., 2010. The bony labyrinth of the early platyrrhine primate *Chilecebus*. J. Hum. Evol. 59, 595–607.
Oksanen, J., Blanchet, F. G., Friendly, M., Kindt, R., Legendre, P., McGlinn, D., Minchin, P. R., O'Hara, R. B., Simpson, G. L., Solymos, P., Stevens, M. H. H.,

Szoecs, E., Wagner, H., *vegan*: Community ecology package (R package version 2.5-6, 2019). https://CRAN.R-project.org/package=vegan

Oman, C. M., Marcus, E. N., Curthoys, I. S., 1987. The influence of semicircular canal morphology on endolymph flow dynamics. Acta Otolaryngol. 103, 1–13.

Ortiz, A., Pilbrow, V., Villamil, C. I., Korsgaard, J. G., Bailey, S. E., Harrison, T., 2015. The taxonomic and phylogenetic affinities of *Bunopithecus sericus*, a fossil hylobatid from the Pleistocene of China. PLoS One 10, e0131206.

Osipov, B., Harvati, K., Nathena, D., Spanakis, K., Karantanas, A., Kranioti, E. F., 2013. Sexual dimorphism of the bony labyrinth: A new age-independent method. Am. J. Phys. Anthropol. 151, 290–301.

Owen, B., Lee, D., 1986. Establishing a frame of reference for action. In: Wade, M., Whiting, H. (Eds), *Motor Development in Children: Aspect of Coordination and Control*. Dordrecht: Martinus Nijhoff, pp. 341–360

Ozansoy, F., 1965. Study of the continental sites and the mammals from the Cenozoic of Turkey. Mem. Soc. Geol. Fr. 44, 1–92.

Pagel, M., 1999. Inferring the historical patterns of biological evolution. Nature 401, 877–884.

Palci, A., Hutchinson, M. N., Caldwell, M. W., Lee, M. S. Y., 2017. The morphology of the inner ear of squamate reptiles and its bearing on the origin of snakes. R. Soc. Open Sci. 4, 170685

Pan, L., Dumoncel, J., Mazurier, A., Zanolli, C., 2019. Structural analysis of premolar roots in Middle Pleistocene hominins from China. J. Hum. Evol. 136, 102669.

Pan, Y., 2006. Primates Linnaeus, 1758. In: Qi, G., Dong, W. (Eds.) Lufengpithecus hudienensis *site*. Beijing: Science Press, pp. 131–148.

Paradis, E., Schliep, K., 2019. *ape* 5.0: an environment for modern phylogenetics and evolutionary analyses in R. Bioinformatics 35, 526–528.

Patel, B. A., Grossman, A., 2006. Dental metric comparisons of *Morotopithecus* and *Afropithecus*: Implications for the validity of the genus *Morotopithecus*. J. Hum. Evol. 51, 506–512.

Pavoine, S., Ollier, S., Pontier,D., Chessel, D., 2008. Testing for phylogenetic signal in phenotypic traits: new matrices of phylogenetic proximities. Theor. Popul. Biol. 73, 79–91.

Peppe, D. J., McNulty, K. P., Cote, S. M., Harcourt-Smith, W. E., Dunsworth, H. M., Van Couvering, J. A., 2009. Stratigraphic interpretation of the Kulu Formation (Early Miocene, Rusinga Island, Kenya) and its implications for primate evolution. J. Hum. Evol. 56, 447–461.

Perelman, P., Johnson, W. E., Roos, C., Seuánez, H. N., Horvath, J. E., Moreira, M. A. M., Kessing, B., Pontius, J., Roelke, M., Rumpler, Y., Schneider, M. P. C., Silva, A., O'Brien, S. J., Pecon-Slattery, J., 2011. A molecular phylogeny of living primates. PLoS Genetics 7, e1001342.

Pérez de los Ríos, M., Moyà-Solà, S., Alba, D. M., 2012. The nasal and paranasal architecture of the middle Miocene ape *Pierolapithecus catalaunicus* (Primates: Hominidae): phylogenetic implications. J. Hum. Evol. 63, 497–506.

Pérez de los Ríos, M., Alba, D. M., Moyà-Solà, S., 2013. Taxonomic attribution of the La Grive hominoid teeth. Am. J. Phys. Anthropol. 151, 558–565.

Perier, A., Lebrun, R., Marivaux, L., 2016. Different level of intraspecific variation of the bony labyrinth morphology in slow- versus fast-moving primates. J. Mammal. Evol. 23, 353–368.

Pfaff, C., Martin, T., Ruf, I., 2015. Bony labyrinth morphometry indicates locomotor adaptations in the squirrel-related clade (Rodentia, Mammalia). Proc. R. Soc. B. 282, 20150744.

Pfaff, C., Nagel, D., Gunnell, G., Weber, G.W., Kriwet, J., Morlo, M., Bastl, K., 2017. Palaeobiology of *Hyaenodon exiguus* (Hyaenodonta, Mammalia) based on morphometric analysis of the bony labyrinth. J. Anat. 230, 282–289.

Pickford, M., 1986. Hominoids from the Miocene of East Africa and the phyletic position of *Kenyapithecus*. Z. Morph. Anthropol. 76, 117–130.

Pickford, M., 2002. New reconstruction of the Moroto hominoid snout and a reassessment of its affinities to *Afropithecus turkanensis*. Hum. Evol. 17, 1–19.

Pickford, M., Kunimatsu, Y., 2005. Catarrhines from the middle Miocene (ca. 14.5 Ma) of Kipsaraman, Tugen Hills, Kenya. Anthropol. Scie. 113, 189–224.

Pickford, M., Ishida, H., Nakano, Y., Nakaya, H., 1984. Fossiliferous localities of the Nachola-Samburu Hills area, northern Kenya. Afr. Stud. Monogr. 2, 45–56.

Pickford, M., Senut, B., Gommery, D., Treil, J., 2002. Bipedalism in *Orrorin tugenensis* revealed by its femora. C. R. Palevol. 1, 1–13.

Pickford, M., Senut, B., Gommery, D., Musiime, E., 2003. New catarrhine fossils from Moroto II, Early Middle Miocene (ca 17.5 Ma) Uganda. C. R. Palevol 2, 649–662.

Pickford, M., Senut, B., Gommery, D., Musiime, E., 2009. Distinctiveness of *Ugandapithecus* from *Proconsul*. Estud. Geol. 65, 183–241.

Pickford, M., Musalizi, S., Senut, B., Gommery, D., Musiime, E., 2010. Small apes from the Early Miocene of Napak, Uganda. Geo.-Pal. Uganda 3, 1–111.

Pickford, M., Senut, B., Musalizi, S., Gommery, D., Ssebuyungo, C., 2019. Early Miocene victoriapithecid monkey from Napak, Uganda. Geo-Pal Uganda 12, 1–17.

Pilbeam, D. R., 1969. Tertiary Pongidae of East Africa: Evolutionary relationships and taxonomy. Bull. Peabody Mus. Nat. Hist. 31, 1–185.

Pilbeam, D. R., 1982. New hominoid skull material from the Miocene of Pakistan. Nature 295, 232–234.

Pilbeam, D. R., Simons, E. L., 1971. Humerus of *Dryopithecus* from Saint Gaudens, France. Nature 229, 406–407.

Pilbeam, D., Walker A., 1968. Fossil monkeys from the Miocene of Napak, north-east Uganda. Nature, 220, 657–660.

Pilbeam, D. R., Rose, M. D., Barry, J. C., Shah, S. M. I., 1990. New *Sivapithecus* humeri from Pakistan and the relationship of *Sivapithecus* and *Pongo*. Nature 348, 237–239.

Pillans, B., Williams, M., Cameron, D. W., Patnaik, R., Hogarth, J., Sahni, A., Sharma, J. C., Williams, F., Bernor, R. L., 2005. Revised correlation of the Haritalyangar magnetostratigraphy, Indian Siwaliks: Implications for the age of the Miocene hominids *Indopithecus* and *Sivapithecus*, with a note on a new hominid tooth. J. Hum. Evol. 48, 507–515.

Pimentcl, R. A., Riggins, R., 1987. The nature of cladistic data. Cladistics 3, 201–209.

Pina, M., Alba, D. M., Almécija, S., Fortuny, J., Moyè-Solè, S., 2012. Brief communication: Paleobiological inferences on the locomotor repertoire of extinct hominoids based on femoral neck cortical thickness: The fossil great ape *Hispanopithecus laietanus* as a test-case study. Am. J. Phys. Anthropol. 149, 142–148.

Pina, M., Almécija, S., Alba, D. M., O'Neill, M. C., Moyà-Solà, S., 2014. The Middle Miocene ape *Pierolapithecus catalaunicus* exhibits extant great ape-like morphometric affinities on its patella: inferences on knee function and evolution. PLoS One 9, e91944.

Pina, M., Alba, D. M., Moyà-Solà, S., Almécija, S., 2019. Femoral neck cortical bone distribution of dryopithecin apes and the evolution of hominid locomotion. J. Hum. Evol. 136, 102651.

Ponce de León, M. S., Koesbardiati, T., Weissmann, J. D., Milella, M., Reyna-Blanco, C. S., Suwa, G., Kondo, O., Malaspinas, A.-S., White, T. D., Zollikofer, C. P. E., 2018. Human bony labyrinth is an indicator of population history and dispersal from Africa. Proc. Natl. Acad. Sci. USA, 115, 4128–4133.

Pozzi, L., Hodgson, J. A., Burrell, A. S., Sterner, K. N., Raaum, R. L., Disotell, T. D., 2014. Primate phylogenetic relationships and divergence dates inferred from complete mitochondrial genomes. Mol. Phyl. Evol. 75, 165–183.

Pozzo, T., Berthoz, A., Lefort, L., 1990. Head stabilization during various locomotor tasks in humans. 1. Normal subjects. Exp. Brain Res. 82, 97–106.

Pugh, K. D., 2020. *The Phylogenetic Relationships of Middle-Late Miocene Apes: Implications for Early Human Evolution*. Ph.D. Dissertation, City University of New York.

Quam, R., Lorenzo, C., Martínez, I., Gracie-Téllez, A., Arsuaga, J. L., 2016. The bony labyrinth of the middle Pleistocene Sima de los Huesos hominins (Sierra de Atapuerca, Spain). J. Hum. Evol. 90, 1–15.

Qi, G., Dong, W., Zheng, L., Zhao, L., Gao, F., Yue, L., Zhang, Y., 2006. Taxonomy, age and environment status of the Yuanmou hominoids. Chinese Sci. Bull. 51, 704–712.

R Core Team, 2019. R: A language and environment for statistical computing. R Foundation for Statistical Computing, Vienna.

Raaum, R. L., Sterner, K. N., Noviello, C. M., Stewart, C.-B., Disotell, T. R., 2005. Catarrhine primate divergence dates estimated from complete mitochondrial genomes: concordance with fossil and nuclear DNA evidence. J. Hum. Evol. 48, 237–257.

Rabbitt, R. D., 2019. Semicircular canal biomechanics in health and disease. J. Neurophysiol. 121, 732–755.

Rabbitt, R. D., Damiano, E. R., Grant, J.W., 2004. Biomechanics of the semicircular canals and otolith organs. In: Highstein, S. M., Fay, R. R., Popper, A. N. (Eds), *The Vestibular System*. New York: Springer, pp. 153–201.

Racicot, R. A., Gearty, W., Kohno, N., Flyn, J. J., 2016. Comparative anatomy of the bony labyrinth of extant and extinct porpoises (Cetacea: Phocoenidae). Biol. J. Linn. Soc. 119, 831–846.

Rae, T. C., 1997. The early evolution of the hominoid face. In: Begun, D., Ward, C., Rose, M. (Eds), *Function, Phylogeny, and Fossils: Miocene Hominoid Evolution and Adaptations*. New York: Plenum, pp.59–77.

Rae, T. C., 1999. Mosaic evolution in the origin of the Hominoidea. Folia Primatol. 70, 125–135.

Rae, T. C., Johnson, P. M., Yano, W., Hirasaki, E., 2016. Semicircular canal size and locomotion in colobine monkeys: a cautionary taleRamprashad, F., Landolt, J. P., Money, K. E., Laufer, J., 1984. Dimensional analysis and dynamic response

characterization of mammalian peripheral vestibular structures. Am. J. Anat. 169, 295–313.

Rafferty, K. L., Walker, A., Ruff, C. B., Rose, M. D., Andrews, P. J., 1995. Postcranial estimates of body weight in *Proconsul*, with a note on a distal tibia of *P. major* from Napak, Uganda. Am. J. Phys. Anthropol. 97, 391–402.

Ramprashad, F., Landolt, J., Money, K., Laufer, J., 1986. Comparative morphometric study of the vestibular system of the vertebrata: Reptilia, Aves, Amphibia, and Pisces. Acta Otolaryngol. Supp. 1986, 1–42.

Rasmussen, D. T., 2002. Early catarrhines of the African Eocene and Oligocene. In: Hartwig, W. C. (Ed.), *The Primate Fossil Record*. Cambridge: Cambridge University Press, pp. 203–220.

Rasmussen, D. T., Friscia, A. R., Gutierrez, M., Kappelman, J., Miller, E. R., Muteti, S., Reynoso, D., Rossie, J. B., Spell, T. L., Tabor, N. J., Gierlowski-Kordesch, E., Jacobs, B. F., Kyongo, B., Macharwas, M., Muchemi, F., 2019. Primitive Old World monkey from the earliest Miocene of Kenya and the evolution of cercopithecoid bilophodonty. Proc. Natl. Acad. Sci. U.S.A. 116, 6051–6056 (2019).

Reichard, U. H., Barelli, C., Hirai, H., Nowak, M. G., 2016. The evolution of gibbons and siamang. In: Reichard, U., Hirai, H., Barelli, C. (Eds), *Evolution of Gibbons and Siamang*. New York: Springer, pp. 3–41.

Retzius, G., 1881. *Das Gehörorgan der Wirbeltiere. I. Das Gehörorgan der Fische und Amphibien*. Stockholm: Centraldruckerei.

Retzius, G., 1884. *Das Gehörorgan der Wirbeltiere. II. Das Gehörorgan der Reptilien, der Vögel und der Säugetiere*. Stockholm: Centraldruckerei.

Reuter, M., Wolter, F. E., Peinecke, N., 2006. Laplace-Beltrami spectra as 'Shape-DNA' of surfaces and solids. Comput. Aided Des. 38, 342–366.

Revell, L. J., 2012. Phytools: an R package for phylogenetic comparative biology (and other things). Methods Ecol. Evol. 3, 217–223.

Revell, L. J., Harmon, L. J., Collar, D. C., 2008. Phylogenetic signal, evolutionary process, and rate. Syst. Biol. 57, 591–601.

Reyment, R. A., Jöreskog, K., G., 1993. *Applied Factor Analysis in the Natural Sciences*. Cambridge: Cambridge University Press.

Rightmire, G. P., 2004. Brain size and encephalization in early to Mid-Pleistocene *Homo*. Am. J. Phys. Anthropol. 124, 109-123.

Rightmire, G. P., 2013. *Homo erectus* and Middle Pleistocene hominins: Brain size, skull form, and species recognition. J. Hum. Evol. 65, 223–252.

Rohlf, F. J., 2001. Comparative methods for the analysis of continuous variables: Geometric interpretations. Evolution 55, 2143–2160.

Rohlf, F. J., 2020. Why clusters and other patterns can seem to be found in analyses of high-dimensional data. Evol. Biol. https://doi.org/10.1007/s11692-020-09518-6

Rohlf, F. J., Marcus, L. F., 1993. A revolution in morphometrics. Trends Ecol. Evol. 8, 129–132.

Rohlf F. J., Slice D. E., 1990. Extensions of the Procrustes method for the optimal superimposition of landmarks. Syst. Zool. 39, 40–59.

Rook, L., Bondioli, L., Köhler, M., Moyà Solà, S., Macchiarelli, R., 1999. *Oreopithecus* was a bipedal ape after all: Evidence from the iliac cancellous architecture. Proc. Natl. Acad. Sci. 96, 8795–8799.

Rook, L., Bondioli, L., Casali, F., Rossi, M., Köhler, M., Moyá-Solá, S., Macchiarelli, R., 2004. The bony labyrinth of *Oreopithecus bambolii.* J. Hum. Evol. 46, 349–356.

Rook, L., Oms, O., Benvenuti, M., Papini, M., 2011. Magnetostratigraphy of the Late Miocene Baccinello–Cinigiano basin (Tuscany, Italy) and the age of *Oreopithecus bambolii* faunal assemblages. Palaeogeogr. Palaeoclimatol. Palaeoecol. 305, 286–294.

Roberts, P., Delson, E., Miracle, P., Ditchfield, P., Roberts, R. G., Jacobs, Z., Blinkhorn, J., Ciochon, R. L., Fleagle, J. G., Frost, S. R., Gilbert, C. C., Gunnell, G. F., Harrison, T., Korisettar, R., Petraglia, M. D., 2014. Continuity of mammalian fauna over the last 200,000 y in the Indian subcontinent. Proc. Natl. Acad. Sci. USA 111, 5848–5853.

Roos, C., Kothe, M., Alba, D. M., Delson, E., Zinner, D., 2019. The radiation of macaques out of Africa: Evidence from mitogenome divergence times and the fossil record. J. Hum. Evol. 114–132.

Rose, M. D., 1983. Miocene hominoid postcranial morphology: monkey-like, ape-like, neither, or both? In: Ciochon, R. L., Corruccini, R. S. (Eds), *New Interpretations of Ape and Human Ancestry*. New York: Plenum, pp. 405–417.

Rose, M. D., 1993. Locomotor anatomy of Miocene hominoids. In: Gebo, D. L. (Ed), *Postcranial Adaptation in Nonhuman Primates*. DeKalb: Northern Illinois University Press, pp. 252–272.

Rose, M. D., 1994. Quadrupedalism in some Miocene catarrhines. J. Hum. Evol. 26, 387–411.

Rose, M. D., 1997. Functional and phylogenetic features of the forelimb in Miocene hominoids. In: Begun, D. R., Ward, C. V., Rose, M. D. (Eds), *Function, Phylogeny and Fossils: Miocene Hominoid Evolution and Adaptations*. New York: Plenum, pp. 79–100.

Rose, M. D., Leakey, M. G., Leakey, R. E. F., Walker, A. C., 1992. Postcranial specimens of *Simiolus enjiessi* and other primitive catarrhines from the early Miocene of Lake Turkana, Kenya. J. Hum. Evol. 22, 171–237.

Ross, C. F., Ravosa, M. J., 1993. Basicranial flexion, relative brain size, and facial kyphosis in nonhuman primates. Am. J. Phys. Anthropol. 91, 305–324.

Rossie, J. B., MacLatchy, L., 2006. A new pliopithecoid genus from the Early Miocene of Uganda. J. Hum. Evol. 50, 568 – 586.

Rossie, J. B., Seiffert, E. R., 2006. Continental paleobiogeography as phylogenetic evidence. In: Lehman, S. M., Fleagle, J. G. (Eds), *Primate Biogeography. Developments in Primatology: Progress and Prospects*. Boston: Springer, pp. 469–522.

Rossie, J. B., Hill, A., 2018. A new species of *Simiolus* from the middle Miocene of the Tugen Hills, Kenya. J. Hum. Evol. 125, 50–58.

Rossie, J. B., Gilbert, C. C., Hill, A., 2013. Early cercopithecid monkeys from the Tugen Hills, Kenya. Proc. Natl. Acad. Sci. USA 110, 5818–5822.

Ruff, C. B., Walker, A., Teafor, M. F., 1989. Body mass, sexual dimorphism and femoral proportions of *Proconsul* from Rusinga and Mfangano Islands, Kenya. J. Hum. Evol. 18, 515–536.

Russo, G. A., Shapiro, L. J., 2013. Reevaluation of the lumbosacral region of *Oreopithecus bambolii*. J. Hum. Evol. 65, 253–265.

Ryan, T. M., Silcox, T. M., Walker, A., M., Xianyun, Begun, D. R., Benefit, B. R., Gingerich, D. D., Köhler, M., Kordos, L., McCrossin, M. L., Moyà-Solà, S., Sanders, W. J., Seiffert, E. R., Simons, E., Zalmout, I. S., Spoor, F., 2012. Proc. R.

Soc. B 279, 3467–3475. Evolution of locomotion in Anthropoidea: the semicircular canal evidence. Proc. R. Soc. B 279, 3467–3475.

Saitou, N., Nei, M., 1987. The neighbor-joining method: a new method for reconstructing phylogenetic trees. Mol. Biol. Evol. 4, 406–425.

Sánchez-Villagra, M. R., Schmelzle, T., 2007. Anatomy and development of the bony inner ear in the woolly opossum, *Caluromys philander* (Didelphimorphia, Marsupialia). Mastozool. Neotrop. 14, 53–60.

Sanders, W. J., Bodenbender, B. E., 1994. Morphometric analysis of lumbar vertebra UMP 67-28: Implications for spinal function and phylogeny of the Miocene Moroto hominoid. J. Hum. Evol. 26, 203–237.

Sankhyan, A. R., Kelley, J., Harrison, T., 2017. A highly derived pliopithecoid from the Late Miocene of Haritalyangar, India. J. Hum. Evol. 105, 1–12.

Sarmiento, E. E. 1987. The phylogenetic position of *Oreopithecus* and its significance in the origin of the Hominoidea. Am. Mus. Novit. 2881, 1–44.

Savje, F., 2019. Distances: tools for distance metrics. https://cran.r-project.org/web/packages/distances/index.html

Schellhorn, R. A, 2018. Potential link between lateral semicircular canal orientation, head posture, and dietary habits in extant rhinos (Perissodactyla, Rhinocerotidae). J. Morphol. 279, 50–61.

Schlager, S., 2017. Morpho and Rvcg e shape analysis in R: R-packages for geometric morphometrics, shape analysis and surface manipulations. In: Zheng, G., Li, S., Székely, G. (Eds), *Statistical Shape and Deformation Analysis*. *Methods, Implementation and Applications*. London: Academic Press, pp. 217–256.

Schluter, D., Price, T., Mooers, A. Ø., Ludwig, D., 1997. Likelihood of ancestor states in adaptive radiation. Evolution 51, 1699–1711.

Schmelzle, T., Maier, W., Sanchez-Villagra, M.R., 2007. Vestibular labyrinth diversity in diprotodontian marsupial mammals. Mammal Study 32, 83–97.

Schönemann, A., 1906. Schläfenbein und Schädelbasis, eine anatomisch-otiatrische Studie.Neue Denkschriften Allg. Schweiz. Gesellsch. Naturwissensch. 40, 95–160.

Schrenk, F., Kullmer, O., Bromage, T., 2015. The earliest putative *Homo* fossils. In: Henke, W., Tattersall, I. (Eds), *Handbook of Paleoanthropology*. Heidelberg: Springer Verlag. pp. 2145–2166.

Schutz, H., Jamniczky, H. A., Hallgrímsson, B., Garland, T., Jr., 2014. Shape-shift: Semicircular canal morphology responds to selective breeding for increased locomotor activity. Evolution 68, 3184–3198.

Schwab, J. A., Kriwet, J., Weber, G. W., Pfaff, C., 2019. Carnivoran hunting style and phylogeny reflected in bony labyrinth morphometry. Sci. Rep. 9, 70.

Schwab, J. A., Young, M. T., Neenan, J. M., Walsh, S. A., Witmer, L. M., Herrerae, Y., Allain, R., Brochu, C. A., Choiniere, J. N., Clark, J. M., Dollman, K. N., Etches, S., Fritsch, G., Gignac, P. M., Ruebenstahl, A., Sachs, S., Turner, A. H., Vignaud, P., Wilberg, E. W., Xu, X., Zanno, L. E., Brusatte, S. L., 2020. Inner ear sensory system changes as extinct crocodylomorphs transitioned from land to water. Proc. Natl. Acad. Sci. USA 117, 10422–10428.

Schwartz, J. H., 1997. *Lufengpithecus* and hominoid phylogeny: problems in delineating and evaluating phylogenetically relevant characters. In: Begun, D. R., Ward, C. V., Rose, M. D. (Eds), *Function, Phylogeny and Fossils: Miocene Hominoid Evolution and Adaptations*. New York: Plenum, pp. 363–388.

Seiffert, E. R., 2006. Revised age estimates for the later Paleogene mammal faunas of Egypt and Oman. Proc. Natl. Acad. Sci. USA, 103, 5000–50005.

Seiffert, E. R., 2012. Early primate evolution in Afro-Arabia. Evol. Anthropol. 21, 239–253.

Seiffert, E. R., Simons, E. L., Clyde, W. C., Rossie, J. B., Attia, Y., Bown, T. M., Chatrath, P., Mathison, M. E., 2005. Basal anthropoids from Egypt and the antiquity of Africa's higher primate radiation. Science, 310, 300–304.

Seiffert, E. R., Simons, E. L., Fleagle, J. G., Godinot, M., 2010. Paleogene anthropoids. In: Werdelin, L., Sanders, W. J. (Eds), *Cenozoic Mammals of Africa*. Berkeley: University of California Press, pp. 369–391.

Senut, B., 2011. Origin of hominids: European or African origin, neither or both? Estud. Geol. 67, 395–409.

Senut, B., Pickford, M., Gommery, D., Kunimatsu, Y., 2000. A new genus of Early Miocene hominoid from East Africa: *Ugandapithecus major* (Le Gros Clark & Leakey, 1950). C. R. Acad. Sci. Paris 3, 227–233.

Sereno, P. C., Jeffery, A. W., Witmer, L. M., Whitlock, J. A., Maga, A., Ide, O., Rowe, T. A., 2007. Structural extremes in a cretaceous dinosaur. PLoS One 2, e1230.

Shea, B. T., 2013. Cranial evolution in the apes. In: Begun, D. R. (Ed), *A Companion to Paleoanthropology*. Oxford: Blackwell Publishing, pp. 119–13.

Sidlauskas, B., 2008. Continuous and arrested morphological diversification in sister clades of characiform fishes: a phylomorphospace approach. Evolution 62, 3135–3156.

Silcox, T. M., 2008. The biogeographic origins of Primates and Euprimates: east, west, north, or south of Eden? In: Sargis, E. J., Dagosto, M. (Eds). *Mammalian Evolutionary Morphology: a Tribute to Frederick S. Szalay.* Dordrecht: Springer, pp. 199–231.

Silcox, T. M., Bloch, J. I., Boyer, D. M., Godinot, M., Ryan, T. M., Spoor, F., Walker, A., 2009. Semicircular canal system in early primates. J. Hum. Evol. 56, 315–327.

Simons, E. L., 1987. New faces of Aegyptopithecus from the Oligocene of Egypt. J. Hum. Evol. 16, 273–289.

Simons, E. L., 1995. Egyptian Oligocene primates: a review. Am. J. Phys. Anthropol. 38, 199–238.

Simons, E. L., Fleagle, J. G., 1973. The history of extinct gibbon-like primates. In: Rumbaugh, D. M. (Ed), *Gibbon and Siamang Vol. 2. Anatomy, Dentition, Taxonomy, Molecular Evolution and Behavior*. Basel: Karger, pp. 121–148.

Simons, E. L., Pilbeam, D. R., 1965. Preliminary revision of the Dryopithecinae (Pongidae, Anthropoidea). Folia Primatol. 3, 81–152.

Simons, E. L., Seiffert, E. R., Ryan, T. M., Attia, Y., 2007. A remarkable female cranium of the Early Oligocene anthropoid *Aegyptopithecus zeuxis* (Catarrhini, Propliopithecidae). Proc. Natl. Acad. Sci. USA, 104, 8731–8736.

Simpson, S. W., Levin, N. E., Quade, J., Rogers, M., Semaw, S., 2019. *Ardipithecus ramidus* postcrania from Gona Project area, Afar Regional State, Ethiopia. J. Hum. Evol. 129, 1–45.

Singleton, M., 2000. The phylogenetic affinities of *Otavipithecus namibiensis*. J. Hum. Evol. 38, 537–573.

Smith, C. M., Laitman, J.T., 2020. Alterations to vestibular morphology in highly bred domestic dogs may affect balance. Anat. Rec. https://doi.org/10.1002/ar.24423.

Smith, C. M., Tang, C. Y., Laitman, J. T., 2020. Visualizing the unbalanced world of domestic dogs: An interactive examination of the canid vestibular system. FASEB J. 34 (S1), https://doi.org/10.1096/fasebj.2020.34.s1.05859.

Smith, T. M., Martin, L. B., Reid, D. J., de Bonis, L., Koufos, G. D., 2004. An examination of dental development in *Graecopithecus freybergi* (= *Ouranopithecus macedoniensis*). J. Hum. Evol. 46. 551–77.

Smith, T. M., Dean, M. C., Kelley, J., Martin, L. B., Reid, D. J., Schwartz, G. T., 2003. Molar crown formation in Miocene hominoids; a preliminary synthesis. Am. J. Phys. Anthropol. S36, 196.

Sokal, R. R., Rohlf, F. J., 1995. *Biometry: The Principles and Practice of Statistics in Biological Research*. New York: W. H. Freeman and Company.

Spassov, N., Geraads, D., Hristova, L., Markov, G. N., Merceron, G., Tzankov, T., Stoyanov, K., Böhme, M., Dimitrova, A., 2012. A hominid tooth from Bulgaria: the last pre-human hominid of continental Europe. J. Hum. Evol. 68, 138–145.

Spoor, F., 1993. *The Comparative Morphology and Phylogeny of the Human Bony Labyrinth*. Ph.D. Dissertation, University of Utrecht.

Spoor, F., 1997. Basicranial architecture and relative brain size of Sts 5 (*Australopithecus africanus*) and other Plio-Pleistocene hominids. S. Afr. J. Sci. 93, 182–187.

Spoor, F., Leakey, M., 1996. Absence of the subarcuate fossa in cercopithecids. J. Hum. Evol. 31, 569–575.

Spoor, F., Zonneveld, F., 1994a. The bony labyrinth in *Homo erectus*: A preliminary report. Cour. Forsch.-Inst. Senckenberg. 171, 251–256.

Spoor, F., Zonneveld, F., 1994b. The bony labyrinth of Pio-Pleistocene hominids. Am. J. Phys. Anthropol. 37(S18), 185.

Spoor, F., Zonneveld, F, 1995. Morphometry of the primate bony labyrinth: a new method based on high-resolution computed tomography. J. Anat. 186, 271–286.

Spoor, F., Zonneveld., F., 1998. Comparative review of the human bony labyrinth. Yearb. Phys. Anthropol. 41, 211–251.

Spoor, F., Wood, B., Zonneveld, F., 1994. Implications of early hominid labyrinthine morphology for evolution of human bipedal locomotion. Nature 369, 645.

Spoor, F., Bajpai, S., Hussain, S. T., Kumar, K., Thewissen, J. G. M., 2002. Vestibular evidence for the evolution of aquatic behaviour in early cetaceans. Nature 417, 163–165.

Spoor, F., Hublin, J., Braun, M., Zonneveld, F., 2003. The bony labyrinth of Neanderthals. J. Hum. Evol. 44, 141–165.

Spoor, F., Garland, T., Krovitz, G., Ryan, T.M., Silcox, M.T., Walker, A., 2007. The primate semicircular canal system and locomotion. Proc. Natl. Acad. Sci. USA 104, 10808–10812.

Springer, M. S., Meredith, R. W., Gatesy, J., Emerling, C. A., Park, J., Rabosky, D. L., Stadler, T., Steiner, C., Ryder, O. A., Janečka, J. E., Fisher, C. A., Murphy, W. J., 2012. Macroevolutionary dynamics and historical biogeography of primate diversification inferred from a species supermatrix. PLoS One 7, e49521.

Stanyon, R., 2013. Cytogenetic studies of small ape (Hylobatidae) chromosomes. Tsitologiia 55, 167–171.

Steiper, M. E., Young, N. M., 2008. Timing primate evolution: Lessons from the discordance between molecular and paleontological estimates. Evol. Anthropol. 17, 179–188.

Stevens, N. J., Seiffert, E. R., O'Connor, P. M., Roberts, E. M., Schmitz, M. D., Krause, C., Gorscak, E., Ngasala, S., Hieronymus, T. L., Temu, J., 2013. Palaeontological evidence for an Oligocene divergence between Old World monkeys and apes. Nature 497, 611–614.

Strait, D. S., Grine, F. E., Moniz, M. A., 1997. A reappraisal of early hominid phylogeny. J. Hum. Evol. 32, 17–82.

Straus, W. L., 1963. The classification of *Oreopithecus*. In: Washburn, S. L. (Ed), *Classification and Human Evolution.* Chicago: Aldine, pp. 146–177.

Stringer, C., 2002. Modern human origins: progress and prospects. Phil. Trans. R. Soc. Lond. B 357, 563–579.

Susanna, I., Alba, D. M., Almécija, S., Moyà-Solà, S., 2014. The vertebral remains of the late Miocene great ape *Hispanopithecus laietanus* from Can Llobateres 2 (Vallès-Penedès Basin, NE Iberian Peninsula). J. Hum. Evol. 73, 15–34.

Susman, R. L., 2004. *Oreopithecus bambolii*: an unlikely case of hominid-like grip capability in a Miocene ape. J. Hum. Evol. 46, 105–117.

Sutton, M. D., Rahman, I. A., Garwood, R., 2016. Virtual paleontology – An overview. Paleontol. Soc. Pap. 22, 1–20.

Suwa, G., Kono, R. T., Katoh, S., Asfaw, B., Beyene, Y., 2007. A new species of great ape from the Late Miocene epoch in Ethiopia. Nature 488, 921–924.

Suwa, G., Asfaw, B., Kono, R. T., Kubo, D., Lovejoy, C. O., White, T. D., 2009a. The *Ardipithecus ramidus* skull and its implications for hominid origins Science 326, 68e1–68e7.

Suwa, G., Kono, R. T., Simpson, S. W., Asfaw, B., Lovejoy, C. O., White, T. D., 2009b. Paleobiological implications of the *Ardipithecus ramidus* dentition. Science 326, 94–99.

Suwa, G., Beyene, Y., Nakaya, H., Bernor, R. L., Boisserie, J. R., Bibi, F., Ambrose, A. H., Sano, K., Katoh, S., Asfaw, B., 2015. Newly discovered cercopithecid, equid and other mammalian fossils from the Chorora Formation, Ethiopia. Anthropol. Sci. 123, 19–39.

Swofford, D., 2003. PAUP*. Phylogenetic Analysis Using Parsimony (*and Other Methods). Version 4. Sinauer Associates, Sunderland

Szalay, F. S., Delson, E., 1979. *Evolutionary History of the Primates*. New York: Academic Press.

Szalay, F. S., Langdon, J. H., 1986. The foot of *Oreopithecus*: An evolutionary assessment. J. Hum. Evol. 15, 585–621.

Takahashi, H., 1976. Comparative anatomical study of the bony labyrinth of the inner ear of primates. Kaibogaku Zasshi 51, 366–387.

Takano, T., Nakatsukasa, M., Pina, M., Kunimatsu, Y., Nakano, Y., Morimoto, N., Ogihara, N., Ishida, H., 2020. New forelimb long bone specimens of *Nacholapithecus kerioi* from the Middle Miocene of northern Kenya. Anthropol. Sci. 128, 27–40.

Tanturri, V., 1933. Zur Anatomie und Physiologie des Labyrinthes der Voegel. Mschr. Ohrenh. 67, 1–27.

Tattersall, I., Schwartz, J. H., 2009. Evolution of the genus *Homo*. Ann. Rev. Earth Planet. Sci. 37, 67–92.

Temerin L. A., Cant, J. G. H., 1983. The evolutionary divergence of Old World monkeys and apes. Am. Nat. 122, 335–351.

Thewissen, J. G. M., Williams, E. M., Hussain, S. T., 2001. Skeletons of terrestrial cetaceans and the relationship of whales to artiodactyls. Nature 413, 277–281.

Thompson, J. C., Carvalho, S., Marean, C. W., Alemseged, Z., 2019. Origins of the human predatory pattern. The transition to large-animal exploitation by early hominins. Curr. Anthropol. 60, 1–23.

Turkewitsch, B., 1934. Zur Anatomie des Gehororgans der Vogel (Canals semicirculares). Zschr. Anat. Entw. 103, 551–585.

Turvey, S. T., Bruun, K., Ortiz, A., Hansford, J., Hu, S., Ding, Y., Zhang, T., Chatterjee, H. J., 2018. New genus of extinct Holocene gibbon associated with humans in Imperial China. Science, 360, 6395, 1346–1349.

Ungar, P. S., Kay, R. F., 1995. The dietary adaptations of European Miocene catarrhines. Proc. Natl. Acad. Sci. USA 92, 5479–5481.

Ungar, P. S., 1996. Dental microwear of European Miocene catarrhines: evidence for diets and tooth use. J. Hum. Evol. 31, 335–366.

Valerio, S., Taube, J. S., 2016. Head direction cell activity is absent in mice without the horizontal semicircular canals. J. Neurosci. 36, 741–754.

Van Buskirk, W., 1987. Vestibular mechanics. In: Skalak, R., Chien, S. (Eds) *Handbook of Bioengineering*. New York: New York Academy of Sciences, pp. 31.1–31.17.

Van Der Klaauw, C. J., 1947. Size and position of the functional components of the skull: a contribution to the knowledge of the architecture of the skull, based on data in the literature. Arch. Néerl. Zool. 9, 1–556.

Van Der Klaauw, C. J., 1931. The auditory bulla in some fossil mammals: with a general introduction to this region of the skull. Bull. Am. Mus. Nat. Hist. 67, 1–352.

Van Kampen, P. N. 1904. *De Tympanaalstreek van den Zoogdierschedel.* Amsterdam: P. N. Van Kampen and Zoon.

Vasilopoulou-Kampitsi, M., Goyens, J., Baeckens, S., Van Damme, R., Aerts, P., 2019. Habitat use and vestibular system's dimensions in lacertid lizards. J. Anat., 235, 1–14.

Vidal, P. P., Graf, W., Berthoz, A., 1986. The orientation of the cervical vertebral column in unrestrained awake animals I. Resting position. Exp. Brain Res. 61, 549–559.

Villalta de Comella, J. F., Crusafont Pairó, M., 1944. Dos nuevos antropomorfos del Mioceno español y su situación dentro de la moderna sistemática de los símidos. Not. Com. Inst. Geol. Min. España 13, 1–51.

Villemin, F., Beauvieux, J., 1934. Recherche sur la topographie des canaux semi-circulaires et leurs ampoules chez les vertebres. C. R. Soc. Biol. (Bordeaux) 117, 553–555.

Villmoare, B., Kimbel, W. H., Seyoum, C., Campisano, C. J., DiMaggio, E. N., Rowan, J., Braun, D. R., Arrowsmith, J. R., Reed, K. E., 2015. Early *Homo* at 2.8 Ma from Ledi-Geraru, Afar, Ethiopia. Science 347, 1352–1355.

von Koenigswald, G. H. R., 1969. Miocene Cercopithecoidea and Oreopithecoidea from the Miocene of East Africa. Foss. Vert. Afr. 1, 39–51.

von Koenigswald, G. H. R., 1972. Ein Unterkiefer eines fossilen Hominoiden aus dem Unterpliozan Griechenlands. Proc. K. Ned. Akad. Wet. B 75, 385–394.

Wahl, J., Graw, M., 2001. Metric sex differentiation of the pars petrosa ossis temporalis. Int. J. Legal. Med. 114, 4–5.

Walker, A., 1997.*Proconsul* function and phylogeny. In: Begun, D. R., Ward, C. V., Rose, M. D. (Eds), *Function, Phylogeny, and Fossils: Miocene Hominoid Evolution and Adaptation*. New York: Plenum Press, pp. 209–224.

Walker, A., 1997. *Proconsul*. Function and phylogeny. In: D. R., Begun, C. V., Ward, M. D., Rose (Eds), *Function, Phylogeny and Fossils: Miocene Hominoid Evolution and Adaptation*. New York: Plenum Press, pp. 209–224.

Walker, A., Falk, D., Smith, R., Pickford, M., 1983. The skull of *Proconsul africanus*: reconstruction and cranial capacity. Nature 305, 525–527.

Walker, A., Ryan, T. M., Silcox, M. T., Simons, E. L., Spoor, F., 2008. The semicircular canal system and locomotion: The case of extinct lemuroids and lorisoids. Evol. Anthropol. 17, 135–145.

Ward, C. V., 1993. Torso morphology and locomotion in *Proconsul nyanzae*. Am. J. Phys. Anthropol. 92, 291–328.

Ward, C. V. 1997. Functional anatomy and phyletic implications of the hominoid trunk and hindlimb. In: Begun, D. R., Ward, C. V., Rose, M. D. (Eds), *Function, Phylogeny and Fossils: Miocene Hominoid Evolution and Adaptations*. New York: Plenum, pp. 101–130.

Ward, C. V., 2013. Postural and locomotor adaptations of *Australopithecus* species. In: Reed, K., Fleagle, J., Leakey, R. (Eds), *The Paleobiology of Australopithecus. Vertebrate Paleobiology and Paleoanthropology*. Dordrecht: Springer, pp. 235–246.

Ward, C. V., 2015a. Postcranial and locomotor adaptations of hominoids. In: Henke, W., Tattersall, I., (Eds) *Handbook of Paleoanthropology*. Heidelberg: Springer Verlag. pp. 1363–1386.

Ward, C. V., 2015b. Australopithecines. In: Muehlenbein, M. P. (Ed), *Basics in Human Evolution*. London: Academic Press, pp. 129–142.

Ward, C. V., Walker, A., Teaford, M. F., 1991. *Proconsul* did not have a tail. J. Hum. Evol. 21, 215–220.

Ward, C. V., Walker, A., Teaford, M. F., Odhiambo, L., 1993. Partial skeleton of *Proconsul nyanzae* from Mfangano Island, Kenya. Am. J. Phys. Anthropol. 90, 77–111.

Ward, D. L., Pomeroy, E., Schroeder, L., Viola, T. B., Silcox, M. T., Stock, J. T., 2020. Can bony labyrinth dimensions predict biological sex in archaeological samples? J. Archaeol. Sci. Rep. 31, 102354.

Ward, J. H., 1963. Hierarchical grouping to optimize an objective function. J. Am. Stat. Ass. 58, 236–44.

Ward, S. C., 1997b. The taxonomy and phylogenetic relationships of *Sivapithecus* revisited. In: Begun, D. R., Ward, C. V., Rose, M. D. (Eds), *Function, Phylogeny and Fossils: Miocene Hominoid Evolution and Adaptations*. New York: Plenum, pp. 269–290.

Ward, S. C., Brown, B., 1986. The facial skeleton of *Sivapithecus indicus*. In: Swindler, D., Erwin, J. (Eds), *Comparative Primate Biology, Vol. 1: Systematics, Evolution, and Anatomy*. New York: Liss, pp. 413–452.

Ward, S. C., Duren, D. L., 2002. Middle and late Miocene African hominoids. In: Hartwig, W. C. (Ed), *The Primate Fossil Record*. Cambridge: Cambridge University Press, pp 385–397.

Ward, S. C., Pilbeam, D., 1983. Maxillofacial morphology of Miocene hominoids from Africa and Indo-Pakistan. In: Ciochon, R. L., Corruccini, R. S. (Eds), *New*

Interpretations of Ape and Human Ancestry. New York: Plenum Press, pp. 211–238.

Ward, S., Brown, B., Hill, A., Kelley, J., Downs, W., 1999. *Equatorius*: A new hominoid genus from the middle Miocene of Kenya. Science 285, 1382–1386.

Warton, D. I., Wright, I. J., Falster, D. S., Westoby, M., 2006. Bivariate line-fitting methods for allometry. Biol. Rev. 81, 259–291.

Watkins, R. T., 1989. The Buluk Member, a fossil hominoid-bearing sedimentary sequence of Miocene age from Northern Kenya. J. Afr. Earth Sci. 8, 107–112.

Weber, G. W., Bookstein, F. L., 2011. *Virtual Anthropology*. Wien: Springer-Verlag.

Welker, F., Ramos-Madrigal, J., Kuhlwilm, M., Liao, W., Gutenbrunner, P., de Manuel, M., Samodova, D., Mackie, M., Allentoft, M. E., Bacon, A. M., Collins, M. J., Cox, J., Lalueza-Fox, C., Olsen, J. V., Demeter, F., Wang, W., Marques-Bonet, T., Cappellini, E., 2019. Enamel proteome shows that *Gigantopithecus* was an early diverging pongine. Nature 576, 262–265.

Wersäll, J., Bagger-Sjöbäck, D., 1974. Morphology of the vestibular sense organ. In: Kornhuber, H. H. (Ed), *Handbook of Sensory Physiology: Vestibular System*. New York: Springer-Verlag, pp. 123–170.

White, T. D., Suwa, G., Asfaw, B., 1994. *Australopithecus ramidus*, a new species of early hominid from Aramis, Ethiopia. Nature 375, 88.

White, T. D., Asfaw, B., Beyene, Y., Haile-Selassie, Y., Lovejoy, C. O., Suwa, G., WoldeGabriel, G., 2009. *Ardipithecus ramidus* and the paleobiology of early hominids. Science 326, 75–86.

Wilkinson, R. D., Steiper, M. E., Soligo, C., Martin, R. D., Yang, Z., Tavaré, S., 2011. Dating primate divergences through an integrated analysis of paleontological and molecular data. Syst. Biol. 60, 16–31.

Williams, S. A., Prang, T. C., Meyer, M. R., Russo, G. A., Shapiro, L. J., 2020. Reevaluating bipedalism in *Danuvius*. Nature 586, E1–E3.

Wilson, S. R., 1981. On comparing fossil specimens with populations samples. J. Hum. Evol. 10, 207–214.

Witmer, L. M., Chatterjee, S., Franzosa, J., Rowe, T., 2003. Neuroanatomy of flying reptiles and implications for flight, posture and behaviour. Nature 425, 950–953.

Witmer, L. M., Ridgely, R. C., Dufeau, D. L., Semones, M. C., 2008. Using CT to peer into the past: 3D visualization of the brain and ear regions of birds, crocodiles, and nonavian dinosaurs. In: Endo, H., Frey, R. (Eds), *Anatomical Imaging.* Japan, Springer, pp. 67–87.

Wolpoff, M. H., Senut, B., Hawks, J., 2002. *Sahelanthropus* or *'Sahelpithecus* ?. Nature 419, 581–582.

Wood, B., Collard, M., 1999. The human genus. Science 284, 65–71.

Wood, B. A., Constantino, P., 2007. *Paranthropus boisei*: fifty years of evidence and analysis. Yearb. Phys. Anthropol. 50, 106–132.

Wood, B., Schroer, K., 2013. *Paranthropus*. In: Begun, D. R. (Ed), *A Companion to Paleoanthropology*. Malden: Wiley–Blackwell, pp. 457–478.

Wu, X.-J., Crevecoeur, I., Liu, W., Xing, S., Trinkaus, E., 2014. Temporal labyrinths of eastern Pleistocene humans. Proc. Natl. Acad. Sci. USA, 111, 10509–10513.

Wu, X., Zhang, Y., 2016. The temporal bony labyrinthine morphology of lantian *Homo erectus* from Gongwangling, Shaanxi province. Acta Anthropol. Sin. 35, 14–23.

Xiong, G., Nagao, S., 2002. The lobulus petrosus of the paraflocculus relays cortical visual inputs to the posterior interposed and lateral cerebellar nuclei: an

anterograde and retrograde tracing study in the monkey. Exp. Brain Res. 147, 252–263.

Yamauchi, A. M., Rabbitt, R. D., Boyle, R., Highstein, S. M., 2002. Relationship between inner-ear fluid pressure and semicircular canal afferent nerve discharge. J. Assoc. Res. Otolaryngol. 3, 26–44.

Zalmout, I. S., Sanders, W. J., MacLatchy, L., Gunnell, G., Al-Mufarreh, Y. A., Ali, M. A., Nasser, A. -A. H., Al-Masary, A. M., Al-Sobhi, S. A., Nadhra, A. O., Matari, A. H., Wilson, J. A., Gingerich, P. D., 2010. New Oligocene primate from Saudi Arabia and the divergence of apes and Old World monkeys. Nature 466, 360–365.

Zanolli, C., Pan, L., Dumoncel, J., Kullmer, O., Kundrat, M., Liu, W., Macchiarelli, R., Mancini, L., Schrenk, F., Tuniz, C., 2018. Inner tooth morphology of *Homo erectus* from Zhoukoudian. New evidence from an old collection housed at Uppsala University, Sweden. J. Hum. Evol. 116, 1–13.

Zapfe, H., 1958. The skeleton of *Pliopithecus* (*Epipliopithecus*) *vindobonensis* Zapfe and Hürzeler. Am. J. Phys. Anthropol. 16, 441–457.

Zapfe, H., 1961. Die Primatenfunde aus der miozänen Spaltenfüllung von Neudorf an der March (Děvínská Nová Ves), Tschechoslowakei. Schweizer. Palaeontol. Abh. 78, 1–293.

Zhang, Y., Harrison, T., 2017. *Gigantopithecus blacki*: a giant ape from the Pleistocene of Asia revisited. Am. J. Phys. Anthropol. 162, 153–177.

Zhang, Y., Kono, R. T., Jin, C., Wang, W., Harrison, T., 2014. Possible change in dental morphology in *Gigantopithecus blacki* just prior to its extinction: Evidence from the upper premolar enamel-dentine junction. J. Hum. Evol. 75, 166–171.

Zollikofer, C. P. E., Ponce de León, M. S., Lieberman, D. E., Guy, F., Pilbeam, D., Likius, A., Mackaye, H. T., Vignaud, P., Brunet, M., 2005. Virtual cranial reconstruction of *Sahelanthropus tchadensis*. Nature 434, 755–759.